University of Alberta

Geotechnical Applications of Crumbed Tire Rubber

by

Hanh N. Hong ©

A thesis submitted to the Faculty of Graduate Studies and Research in partial
fulfilment of the requirements for the degree of Masters of Science

In

Geotechnical Engineering
Department of Civil and Environmental Engineering

Edmonton, Alberta
Fall 2000

National Library
of Canada

Acquisitions and
Bibliographic Services

395 Wellington Street
Ottawa ON K1A 0N4
Canada

Bibliothèque nationale
du Canada

Acquisitions et
services bibliographiques

395, rue Wellington
Ottawa ON K1A 0N4
Canada

Your file Votre référence

Our file Notre référence

The author has granted a non-exclusive licence allowing the National Library of Canada to reproduce, loan, distribute or sell copies of this thesis in microform, paper or electronic formats.

L'auteur a accordé une licence non exclusive permettant à la Bibliothèque nationale du Canada de reproduire, prêter, distribuer ou vendre des copies de cette thèse sous la forme de microfiche/film, de reproduction sur papier ou sur format électronique.

The author retains ownership of the copyright in this thesis. Neither the thesis nor substantial extracts from it may be printed or otherwise reproduced without the author's permission.

L'auteur conserve la propriété du droit d'auteur qui protège cette thèse. Ni la thèse ni des extraits substantiels de celle-ci ne doivent être imprimés ou autrement reproduits sans son autorisation.

0-612-59818-7

Canada

UNIVERSITY OF ALBERTA

LIBRARY RELEASE FORM

NAME OF AUTHOR:	Hanh Nong Hong
TITLE OF THESIS:	Geotechnical Applications of Crumbed Tire Rubber
DEGREE:	Master of Science
YEAR THIS DEGREE GRANTED:	2000

Permission is hereby granted to the University of Alberta Library to reproduce single copies of this thesis and to lend or sell such copies for private, scholarly, or scientific research purposes only.

The author reserves all other publication and other rights in association with the copyright in the thesis, and except as hereinbefore provided, neither the thesis nor any substantial portion thereof may be printed or otherwise reproduced in any material from whatever without the author's prior written permission.

18415 - 95 A Avenue NW
Edmonton, AB
T5T 3V7

June 21, 2000

ABSTRACT

It is estimated that over 300 million used automobile and truck tires are discarded annually in North America. Until recently, scrap tires have generally been disposed of in landfills and stockpiles; approximately 2 billion remain, making them a significant solid waste management and disposal problem. An enormous potential exists in recycling these scrap tires into crumbed tire rubber and potentially using them in geotechnical engineering applications. To investigate this potential, it was necessary to first understand the general behaviour and engineering properties. Therefore, the first goal of this research was to conduct a thorough literature review. Special focus was also given to material property testing and analysis. The findings from the literature review later provided a basis to proceed with laboratory testing. Therefore, the second objective was primarily to focus on characterizing the geotechnical properties including particle size and gradation, specific gravity, compaction characteristics, compressibility, shear strength behaviour, thermal properties and dynamic properties. The geotechnical properties were then compared to that of conventional construction materials including sands and gravels. The geotechnical properties of crumbed tire rubber can be summarized as uniformly graded, lightweight, highly compressible, high strength, free draining, a good thermal insulator, and an excellent vibration dampener.

UNIVERSITY OF ALBERTA

FACULTY OF GRADUATE STUDIES AND RESEARCH

The undersigned certify that they have read, and recommend to the Faculty of Graduate Studies and Research for acceptance, a thesis entitled **Geotechnical Applications of Crumbed Tire Rubber** submitted by **Hanh Nong Hong** in partial fulfillment of the requirements for the degree of **Master of Science** in **Geotechnical Engineering.**

D Sego

Dr. D.C. Sego (Supervisor)

Kevin Biggar

Dr. K.W. Biggar (Co-Supervisor)

Dr. D. H. Chan (Internal Examiner)

Dr. D. Rogowsky (Internal Examiner)

Dr. P.-Y. B. Jar (External Examiner)

June 14, 2000

Date thesis approved by committee.

AKNOWLEDGEMENTS

The research for this thesis was undertaken for the Geotechnical Group, Department of Civil and Environmental Engineering, University of Alberta, Edmonton, Alberta, under the guidance and supervision of Dr. Dave C. Sego and Dr. Kevin W. Biggar.

I would like thank both Dr. Sego and Dr. Biggar for their guidance and input as supervisors. I am especially grateful for their limitless expertise in both the geotechnical and geo-environmental engineering fields. I consider both of my supervisors as not only mentors, but as colleagues and friends. I am especially grateful for their encouragement and have enjoyed working with them on this research project.

I would also like to thank the geotechnical group support staff for their assistance. Mr. Gerry Cyre provided invaluable technical assistance in designing and producing the thermal conductivity probes and bender element system. Mr. Steve Gamble and Ms. Christine Hereygers were also invaluable in setting up and maintaining the laboratory testing equipment.

Tire crumbs used in the laboratory experiments were provided by: Alberta Environmental Rubber Products, Tire Recyclers of Calgary, and Midwest Tire Processors of Vulcan. Funding for this research was provided by the Tire Research Management Association of Alberta (TRMA) and NSERC. I would like to thank TRMA for their financial support, which allowed me achieved my goals and to complete this research.

I would especially like to thank my parents, Thinh and Anh, both of whom provided me with moral support and encouragement throughout my years as a student. I am indebted to them always.

Finally, thanks to all my friends in the Geotechnical graduate office who provided me with such a pleasurable working and social environment; especially on Friday afternoons at the Power Plant.

TABLE OF CONTENTS

CHAPTER 1 INTRODUCTION **1**

1.1 Purpose of Investigation 1

1.2 Objective of this Research 2

1.3 Organization of the Thesis 4

CHAPTER 2 LITERATURE REVIEW **5**

2.1 Introduction 5

2.2 General Tire Characteristics 5

2.3 Common Scrap Tire Disposal Methods 6

2.3.1 Energy Recovery 6

2.3.2 Landfilling and Stockpiling 8

2.3.3 Recycling and Reuse 8

2.4 Crumbed Tire Rubber Production 9

2.4.1 Ambient Grinding 10

2.4.1.1 Granulator Process 10

2.4.1.2 Crackermill Process 10

2.4.1.3 Micromill Process 11

2.4.2 Cryogenic Grinding 12

2.4.3 Retreading Process 14

2.5 Geotechnical Properties of Recycled Tire Rubber 15

2.5.1 Particle Size and Gradation 15

2.5.2 Specific Gravity 16

2.5.3 Compaction Characteristics 16

2.5.4 Compressibility 18

2.5.4.1 Elastic Parameters.. 20

2.5.5 Hydraulic Conductivity..22

2.5.6 Strength..24

2.5.6.1 Direct Shear.. 25

2.5.6.2 Triaxial Compression.. 27

2.5.7 Dynamic Properties..29

2.5.8 Thermal Properties..31

2.6 Civil and Geotechnical Applications of Recycled Tire Rubber..........................31

2.6.1 Introduction..31

2.6.2 Highway Construction..32

2.6.2.1 Light Weight Embankment.. 32

2.6.2.2 Asphalt Road Pavement.. 34

2.6.3 Landfill Uses..36

2.6.4 Leachate Drainage Media..36

2.6.5 Daily Landfill Cover..37

2.6.6 On-Site Sewage Disposal System..37

2.6.7 Soil Amendment..38

2.7 Environmental Considerations..38

CHAPTER 3 SORPTION PROPERTIES..73

3.1 Introduction..73

3.2 Background Information..73

3.3 Sorption Properties..74

3.3.1 Sorption of Organic Compounds..74

3.3.2 Sorption of Inorganic Compounds..82

3.4 Summary..85

CHAPTER 4 LEACHING PROPERTIES 107
4.1 Introduction 107
4.2 Leaching Properties 107
4.3 Summary 114
CHAPTER 5 LABORATORY TESTING PROCEDURES 124
5.1 Introduction 124
5.2 Testing Material 124
5.3 Particle Size and Gradation 124
5.4 Specific Gravity 125
5.5 Compaction Characteristics 126
5.6 Compressibility 126
5.7 Hydraulic Conductivity 128
5.8 Strength 129
  5.8.1 Direct Shear Test 129
  5.8.2 Triaxial Compression 130
5.9 Thermal Properties 130
  5.9.1 General Theory 130
  5.9.2 Thermal Testing Apparatus 132
  5.9.3 RTD Calibration 132
  5.9.4 Sample Preparation 132
  5.9.5 Thermal Conductivity Measurement 133
  5.9.6 Analysis of Results 133
5.10 Dynamic Properties 135
  5.10.1 General Theory 135

5.10.2 Free Vibration with Viscous Damping 136
5.10.3 Critical Damping Constant and the Damping Ratio 137
5.10.4 Experimental Determination of Material Damping 139
5.10.5 Dynamic Testing Apparatus 142
5.10.6 Dynamic Test Procedures 144
  5.10.6.1 Comparison of Bender Elements 144
  5.10.6.2 Shear Wave Velocity and Shear Modulus 144
  5.10.6.3 Material Damping 146

CHAPTER 6 EXPERIMENTAL RESULTS AND DISCUSSION 169

6.1 Particle Size and Gradation 169
6.2 Specific Gravity 171
6.3 Compaction Characteristics 172
  6.3.1 Loose Dry Unit Weight 172
  6.3.2 Compacted Dry Unit Weight 172
6.4 Compressibility 174
  6.4.1 Stress-Strain Response 174
  6.4.2 Effect of Grain-Size Distribution 175
  6.4.3 Effect of Pore Fluid 176
  6.4.4 Compressibility Parameters 177
6.5 Hydraulic Conductivity 178
  6.5.1 Influence of Overburden Pressure 178
  6.5.2 Effect of Grain-Size Distribution 179
6.6 Thermal Properties 180
  6.6.1 Thermal Needle and Aluminum Cells 180
    6.6.1.1 Influence of Pore Fluid on Thermal Conductivity 180

6.6.1.2 Influence of Temperature on Thermal Conductivity 181
6.6.1.3 Influence of Compaction on Thermal Conductivity 182
6.6.2 Combined Thermal Needle and Large-Strain Apparatus 183
6.6.2.1 Influence of Dry Unit Weight on Dry Samples 183
6.6.2.2 Influence of Dry Unit Weight on Saturated Samples 184
6.6.3 Comparisons Between Methods 184
6.6.4 Comparisons of Measured Thermal Conductivities 185
6.7 Shear Strength 186
6.7.1 Direct Shear 186
6.7.1.1 Shear and Deformation Behaviour 186
6.7.1.2 Analysis of Data 188
6.7.1.3 Shear Strength Parameters 189
6.7.1.4 Influence of Grain-Size Distribution 191
6.7.1.5 Influence of Water 191
6.7.2 Triaxial Compression 192
6.7.2.1 Shear Behaviour of Tire Crumbs 192
6.7.2.2 Deformation Behaviour of Tire Crumbs 193
6.7.2.3 Analysis of Data 194
6.7.2.4 Shear Strength Parameters 196
6.8 Dynamic Properties 198
6.8.1 Damping Measurements for Ottawa Sand 198
6.8.1.1 Large-Strain Apparatus and Bender Elements 198
6.8.1.2 Triaxial Cell and Bender Elements 199
6.8.2 Damping Measurements for Tire Crumbs 200
6.8.2.1 Shear Wave Velocity and Shear Modulus 200
6.8.2.2 Material Damping 202
CHAPTER 7 CONCLUSIONS, AND RECOMENDATIONS 282
7.1 General 282

7.2 Summary and Conclusions 282
7.3 Recommendations for Future Research 292
7.3.1 Thermal Insulation Applications 292
7.3.2 Vibration Damping Applications 292
7.3.3 Re-evaluation of Shear Strength Behaviour 293
REFERENCES **294**
APPENDIX A - PARTICLE SIZE AND GRADATION **306**
APPENDIX B - SPECIFIC GRAVITY **325**
APPENDIX C - COMPACTION **329**
APPENDIX D - COMPRESSIBILITY **332**
APPENDIX E - HYDRAULIC CONDUCTIVITY **347**
APPENDIX F - THERMAL CONDUCTIVITY **356**
APPENDIX G - SHEAR STRENGTH **366**
APPENDIX H - DYNAMIC PROPERTIES **399**

LIST OF TABLES

Table 2.1 Typical composition of rubber tire (after Dods et al., 1983) 40

Table 2.2 Typical crumb rubber pricing (after Kohler, 1996) 40

Table 2.3 Summary of particle size, shape and distribution of tire crumbs and shreds... 41

Table 2.4 Specific gravities of scrap tires and select materials 42

Table 2.5 Summary of compaction results for recycled tire rubber and granular soils.... 43

Table 2.6 Summary of Compressibility results for tire crumbs, shreds, and select materials 45

Table 2.7 Elastic parameters of tire crumbs and shreds 46

Table 2.8 Summary of hydraulic conductivities of recycled tire rubber 47

Table 2.9 Summary of shear strength parameters for tire crumbs and shreds measured in direct shear 48

Table 2.10 Summary of shear strength parameters for tire crumbs and shreds measured in triaxial compression 49

Table 2.11 Shear modulus for Ottawa sand-CRM mixture determined from resonant column testing (after Romero and Pamukcu, 1997) 51

Table 2.12 Measured thermal conductivities of tire rubber and selected materials........ 52

Table 3.1 Summary of sorption results on tire shreds (6 to 25 mm nominal size) for single-solute experiment (after Park et al., 1996) 88

Table 3.2 Summary of sorption results on tire shreds (6 to 25 mm nominal size) for multi-solute experiment (after Park et al., 1996) 89

Table 3.3 Summary of sorption results on ground tire rubber (0.6 to 1.18 mm nominal size) for single-solute and multi-solute experiments (after Kershaw and Pamukcu, 1996) 89

Table 3.4 Adsorption coefficients for ground tire rubber (after Kim et al., 1997) 89

Table 3.5 Comparison of partition coefficients between single-solute and multi-solute sorption tests (after Kim et al., 1997) 90

Table 3.6 Effect of inorganic substances and pH on organic sorption (reproduced from Kim et al., 1994) 90

Table 3.7 Sorption results on carbon black and comparisons with GAC and ground tire (after Kim et al., 1997) 90
Table 3.8 Breakthrough time to reach 10% of the influent concentration for ground tire rubber in soil-bentonite wall (after Park et al., 1997) 91
Table 3.9 Porosity and surface area of three commercial activated carbons (after San Miguel et al., 1998) 91
Table 3.10 Freundlich Adsorption Parameters from Phenol, Methylene Blue, Procion Red, and Procion Turquoise (reproduced from San Miguel et al., 1998) 92
Table 3.11 Sorption rate constant and sorption capacity of Hg (II) on to tire crumbs of varying particle sizes (after Knocke and Hemphill, 1981) 93
Table 3.12 Sorption property of Hg (II) on to tire rubber at various temperatures (after Knocke and Hemphill, 1981) 93
Table 3.13 Summary of adsorption isotherm parameters for various organic and inorganic compounds for recycled tire rubber and other sorbents (single-solute solutions) 94
Table 4.1 Summary of tire leachate studies from Vermont Department of Environmental Conservation (reproduced from Envirologic, Inc., 1990) 115
Table 4.2 Concentration of iron and zinc in leachate samples (after Al-abbaa et al., 1997) 118
Table 4.3 Concentrations (pg/g) of PCDD and PCDF in soil collected in the vicinity of Hagersville tire fire site (after Steer et al., 1995) 119
Table 4.4 PCDD/PCDF concentrations (ppt) in water runoff from Hagersville tire fire site (after Steer et al., 1995) 119
Table 4.5 PCDD/PCDF concentrations (ppt) in oil runoff from Hagersville tire fire site (after Steer et al., 1995) 120
Table 4.6 Water quality results on filtered samples for Richmond Field Trial (after Humphrey et al., 1997) 121
Table 5.1 Crumbed tire rubber used in laboratory experiments 147
Table 5.2 Sequence of tests for thermal conductivity measurements 147
Table 6.1 Visual examination and sieve analysis of tire crumbs 205
Table 6.2 Apparent specific gravity, G_s, of tire crumbs 206

Table 6.3 Apparent specific gravities, G_s, of scrap tires and select materials from other investigators 206
Table 6.4 Laboratory dry unit weights of tire crumbs 207
Table 6.5 Compressibility tests on tire crumbs 208
Table 6.6 Compressibility indices and coefficient of volume compressibility of tire crumbs 208
Table 6.7 Hydraulic conductivity, k_{20}, for tire crumbs 209
Table 6.8 Average measured thermal conductivity, λ_{avg}, from thermal needle method. 210
Table 6.9 Measured thermal conductivity, λ, from combined thermal needle and consolidation apparatus 210
Table 6.10 Comparisons of measured thermal conductivity, λ 211
Table 6.11 Shear strength parameters from direct shear tests under dry conditions 212
Table 6.12 Shear strength parameters from direct shear testing under saturated conditions 213
Table 6.13 Shear strength parameters from consolidated-drained triaxial compression tests 214
Table 6.14 Comparison of triaxial strength parameters for tire crumbs and shreds 216
Table 6.15 Logarithmic decrement and damping ratio from large-strain apparatus and bender element tests of Ottawa, $\sigma_v = 0$ kPa 217
Table 6.16 Logarithmic decrement and damping ratio from triaxial cell and bender element tests of Ottawa sand 217
Table 6.17 Dynamic results from bender element tests of tire crumbs 218

LIST OF FIGURES

Figure 2.1 Scrap tire utilization in the United States for the year, 1995 (modified from Bernal et al., 1996) 53
Figure 2.2 Crackermill, Midwest Tire Processors of Vulcan, AB. (photo by Hong, 998) 54
Figure 2.3 Schematic of a typical tire grinding system using the cryogenic process for producing tire crumbs (modified from Kohler, 1996) 54
Figure 2.4 Particle-size distribution of tire crumbs and shreds as determined by various authors 55
Figure 2.5 Triaxial consolidation response of recycled tire rubber with different grain sizes under isotropic stress conditions (modified from Benda, 1995) 56
Figure 2.6 Confined stress-strain response of 50 x 70 mm tire shreds (modified from Edil and Bosscher, 1994) 57
Figure 2.7 Confined initial loading stress-strain curve for 3 in minus tire shreds (modified from Manion and Humphrey, 1992) 58
Figure 2.8 Void ratio versus vertical stress for shredded tires and wood chips (modified from Newcomb and Drescher, 1994) 59
Figure 2.9 Hydraulic conductivity of tire shreds and clean sands at under various overburden pressures (modified from Edil and Bosscher, 1994) 60
Figure 2.10 Direct shear stress and deformation behavior of samples containing both tire crumbs and shreds (0.85 to 12.5 mm) (modified from Cecich et al., 1996) 61
Figure 2.11 Direct shear strength envelope for tire crumbs/shreds with particle size ranging from 0.85 to 12.5 mm (modified from Cecich et al., 1996) 62
Figure 2.12 Direct stress and deformation behavior of 50 mm x 50 mm tire shreds in direct shear (modified from Bernal et al., 1997) 63
Figure 2.13 Horizontal deformation versus mobilized friction angle for tire shreds with maximum nominal size of 50 x 50 mm from direct shear tests (modified from Bernal et al., 1997) 64

Figure 2.14 Direct stress and deformation behavior of tire shreds (50 to 75 mm, Pine State Recycling) tested in 300 mm (12 in) shear box (modified from Humphrey et al., 1992) 65

Figure 2.15 Direct shear strength envelopes for tire shreds (50 to 75 mm) (modified from Humphrey et al., 1997) 66

Figure 2.16 CD triaxial stress and volumetric strain behaviour for No. 4 minus tire crumbs (modified from Masad et al., 1996) 67

Figure 2.17 Triaxial stress and volumetric strain behavior for 9.5 mm tire shreds (modified from Benda, 1995) 68

Figure 2.18 Triaxial stress and volumetric strain behavior for 25 mm (1 in) tire shreds (modified and reproduced from Bernal et al., 1996) 69

Figure 2.19 Triaxial stress-strain behaviour to tire shreds prepared at different compaction efforts under various confining pressures (modified from Ahmed, 1996) 70

Figure 2.20 Triaxial stress and volumetric strain behaviour for tire shreds (9.5 mm) conducted under constant σ_1 stress path (modified from Benda, 1995) 72

Figure 3.1 Thickness of a layer of tire shreds for 90% organic chemical removal (modified from Park et al., 1996) 97

Figure 3.2 Conceptual schematic of a reactive permeable barrier system (modified from Kershaw and Pamukcu, 1997) 98

Figure 3.3 Product yields derived from the pyrolysis of tire rubber at different temperatures (modified from San Miguel et al., 1998) 99

Figure 3.4 Surface area, micropore volume and mesopore volume from pyrolytic chars produced at different temperatures (modified from San Miguel et al., 1998) 99

Figure 3.5 Relative aqueous adsorption efficiencies of tire rubber chars at different temperatures (modified from San Miguel et al., 1998) 100

Figure 3.6 Adsorption isotherms of methylene blue, phenol, Procion red and Procion Turquoise on to tire rubber chars (modified from San Miguel et al., 1998) 101

Figure 3.7 Effect of Hg (II) concentration on the observed rate of sorption (modified from Knocke and Hemphill, 1981) 103

Figure 3.8 Comparative Hg (II) sorption capacity of tire rubber from various authors (modified from Knocke and Hemphill, 1981) 104
Figure 3.9 Relationship between available sorbent surface area and observed sorption capacity for Hg (II) (modified from Knocke and Hemphill, 1981) 105
Figure 3.10 Adsorption of Hg (II) by ground tire rubber as a function of pH (modified from Meng et al., 1998) 106
Figure 3.11 Hg (II) adsorption isotherm by ground tire rubber (modified from Meng et al., 1999) 106
Figure 4.1 Zinc concentrations in DTPA extracts of the potting media as affected by pH and rubber content (modified from Handreck, 1996) 122
Figure 4.2 Zinc concentrations in H_2O extracts of the media as affected by pH and rubber content (modified from Handreck, 1996) 123
Figure 5.1 Large-strain consolidation apparatus set-up under dry conditions (photo by H. Hong, 1998) 148
Figure 5.2 Large-strain consolidation apparatus set-up under saturated conditions (photo by H. Hong, 1998) 149
Figure 5.3 Schematic of large-strain consolidation apparatus (modified from Qiu and Sego, 1998) 150
Figure 5.4 Compaction of tire crumbs in vacuum split mold 151
Figure 5.5 Applying vacuum to top cap of vacuum split mold 152
Figure 5.6 Triaxial specimens after removing vacuum split mold 152
Figure 5.7 Thermal needle, top cap, and aluminum cell 153
Figure 5.8 Schematic of thermal needle 154
Figure 5.9 Thermoconductivity cells in portable cooler 155
Figure 5.10 Apparatus set-up for thermal testing (Not to scale) 156
Figure 5.11 Single degree of freedom system with viscous damping (modified from Rao, 1995) 157
Figure 5.12 Vibration decay with time for an underdamped system with one-degree-of-freedom (modified from Hall and Richart, 1963) 158
Figure 5.13 Comparison of motion with different types of damping (modified from Rao, 1995) 159

Figure 5.14 Amplitude versus cycle number plot for Ottawa sand (modified from Hall, 1963) 160
Figure 5.15 Amplitude-frequency curve for a constant force type of excitation (modified from Brocanelli and Rinaldi, 1998) 161
Figure 5.16 The Nyquist diagram (modified from Brocanelli and Rinaldi, 1998) 162
Figure 5.17 Protuding bender element system in triaxial cell head and base (modified from Cunning, 1994) 163
Figure 5.18 Photo of dynamic testing apparatus set-up 164
Figure 5.19 Apparatus set-up for dynamic testing 165
Figure 5.20 Schematic of piezoceramic bender elements: (A) series connected, (B) parallel connected (modified from Dyvik and Madshus, 1985) 166
Figure 5.21 Typical bender element output trace for a square input wave in tire crumbs 167
Figure 5.22 (a) Amplitude and phase angle in the resonant mode; (b) Corresponding Nyquist diagram and plot of the circle that best fits the results (modified from Brocanelli and Rinaldi, 1998) 168
Figure 6.1 Grain-size distribution of tire crumbs 219
Figure 6.2 Typical stress-strain response of tire crumbs tested under dry conditions ... 220
Figure 6.3 Hysterisis stress-strain response of 1 in uncompacted tire shreds under dry conditions from one-dimensional confined compressibility tests (modified from Ahmed, 1993) 221
Figure 6.4 Initial loading stress-strain response of tire crumbs with different grain-size distribution under dry conditions 222
Figure 6.5 e versus logσ_v plot for No. 20 Minus tire crumbs (Tire Recyclers of Calgary) 223
Figure 6.6 e versus logσ_v plot for 1/4 in tire crumbs (Midwest Tire Processors of Vulcan) 224
Figure 6.7 Initial loading stress-strain response of tire crumbs with different grain-size distribution under water-saturated conditions 225
Figure 6.8 Discharge velocity versus hydraulic gradient for No. 20 Minus tire crumbs226

Figure 6.9 Discharge velocity versus hydraulic gradient for 1/4 in tire crumbs (Midwest Tire Processors of Vulcan) 227

Figure 6.10 Hydraulic conductivity versus overburden pressure for all tire crumbs tested 228

Figure 6.11 $\lambda_{sat}/\lambda_{dry}$ for unfrozen, compacted and loose tire crumbs using thermal needle method 229

Figure 6.12 Measured thermal conductivity as a function of temperature under different degrees of saturation and compaction 230

Figure 6.13 Measured thermal conductivity, λ, as a function of unit weight for tire crumbs, frozen or unfrozen, and dry or saturated 231

Figure 6.14 Measured thermal conductivity, λ, versus dry unit weight for dry tire crumbs using combined thermal needle and consolidation apparatus 232

Figure 6.15 Measured thermal conductivity, λ, versus dry unit weight for saturated tire crumbs, combined thermal needle and consolidation apparatus 233

Figure 6.16 Comparison of measured thermal conductivities versus dry unit weight between thermal cells and large-strain apparatus 234

Figure 6.17 Stress and deformation response under direct shear, dry, $\sigma_N = 25$ kPa 235

Figure 6.18 Stress and deformation response under direct shear, dry, $\sigma_N = 50$ kPa 236

Figure 6.19 Stress and deformation response under direct shear, dry, $\sigma_N = 100$ kPa 237

Figure 6.20 Comparison of direct shear stress and deformation behaviour, saturated and dry, No. 20 minus (Tire Recyclers of Calgary) 238

Figure 6.21 Comparison of direct shear stress and deformation behaviour, saturated and dry, 1/4 in (Midwest Tire Processors of Vulcan) 239

Figure 6.22 Comparison of direct shear stress and deformation behaviour, saturated and dry, 1/4 in (Alberta Environmental Rubber Products) 240

Figure 6.23 Direct shear strength envelopes, dry, 1/4 in (Alberta Environmental Rubber Products), Method A 241

Figure 6.24 Direct shear strength envelopes, dry, 1/4 in (Alberta Environmental Rubber Products), Method B 242

Figure 6.25 Direct shear strength envelopes, dry, 1/4 in (Alberta Environmental Rubber Products), Method C 243

Figure 6.26 Direct shear mobilized friction angle, ϕ_{mob}, versus shear deformation, average values for all crumb sizes tested under dry conditions 244

Figure 6.27 Direct shear mobilized friction angle, ϕ_{mob}, versus horizontal displacement for all grain-sizes tested dry, Method C 245

Figure 6.28 ϕ_{sat}/ϕ_{dry} for tire crumbs under direct shear, No. 20 minus and 1/4-in crumbs only 246

Figure 6.29 Triaxial stress and volumetric strain behaviour of tire crumbs, all grain-size distribution, $\sigma_3 = 25$ kPa 247

Figure 6.30 Triaxial stress and volumetric strain behaviour of tire crumbs, all grain-size distribution, $\sigma_3 = 50$ kPa 248

Figure 6.31 Triaxial stress and volumetric strain behaviour of tire crumbs, all grain-size distribution, $\sigma_3 = 100$ kPa 249

Figure 6.32 Lateral bulging at low confining pressure for 1/4 in tire crumbs (Midwest Tire Processors of Vulcan) 250

Figure 6.33 Modified shear strength envelopes from CD triaxial tests, 1/4 in (Alberta Environmental Rubber Products), Method A' ($c \neq 0$) 251

Figure 6.34 Modified CD triaxial shear strength envelopes from CD triaxial tests, 1/4 in (Alberta Environmental Rubber Products), Method B' ($c = 0$) 252

Figure 6.35 Modified non-linear shear strength envelopes from CD triaxial tests, 1/4 in (Environmental Rubber Products), Method C' 253

Figure 6.36 Triaxial mobilized friction angle, ϕ'_{mob}, versus axial strain, all grain-size distribution, Method A' ($c \neq 0$) 254

Figure 6.37 Comparison of triaxial mobilized friction angle, ϕ'_{mob}, of tire crumb at respective strain levels with others, Method A' ($c \neq 0$) 255

Figure 6.38 Triaxial mobilized friction angle, ϕ'_{mob}, versus axial strain, all grain-size distribution, Method B' ($c = 0$) 256

Figure 6.39 Comparison of the triaxial mobilized friction angle, ϕ'_{mob}, of tire crumbs with others, Method B' ($c = 0$) 257

Figure 6.40 Triaxial mobilized friction angle, ϕ'_{mob}, versus axial strain from secant tangents taken over 25 to 50 kPa stress range, Method C' (non-linear) 258

Figure 6.41 Triaxial mobilized friction angle, ϕ'_{mob}, versus axial strain from secant tangents taken over 50 to 100 kPa stress range, Method C' (non-linear)............ 259
Figure 6.42 Amplitude-frequency curve obtained from large-strain apparatus and bender element tests of Ottawa sand.. 260
Figure 6.43 Dynamic properties obtained from large-strain apparatus and bender element tests of Ottawa sand. 261
Figure 6.44 Typical amplitude-frequency curve obtained from triaxial cell apparatus and bender element tests of Ottawa sand, $\sigma_3 = 0$ kPa... 263
Figure 6.45 Typical amplitude-frequency curve obtained from triaxial cell apparatus and bender element tests of Ottawa sand, $\sigma_3 = 100$ kPa... 264
Figure 6.46 Dynamic properties obtained from triaxial cell apparatus and bender element tests of Ottawa sand, $\sigma_3 = 0$ kPa. (a) Amplitude-time decay curves. (b) Amplitude versus cycle number plot.. 265
Figure 6.47 Dynamic properties obtained from triaxial cell apparatus and bender element tests of Ottawa sand, $\sigma_3 = 100$ kPa. (a) Amplitude-time decay curves. (b) Amplitude versus cycle number plot.. 266
Figure 6.48 Comparisons of damping ratios of Ottawa sand under different confining pressures... 267
Figure 6.49 Typical oscilloscope signals from a bender element test with a square wave pulse excitation on boulder clay (modified from Viggiani and Atkinson, 1995) 268
Figure 6.50 Typical oscilloscope signals from a bender element test on tire crumbs with a square wave excitation 269
Figure 6.51 Times of arrival, t, versus dry unit weight.. 270
Figure 6.52 Shear wave velocity, V_s, as a function of dry unit weight.......................... 271
Figure 6.53 Shear modulus, G_{max}, as a function of dry unit weight.............................. 272
Figure 6.54 Shear wave velocity, V_s, as a function of void ratio, e.............................. 273
Figure 6.55 Shear wave velocities through quartz sands (after Hardin and Richart, 1963) 274
Figure 6.56 Amplitude-frequency curve for No. 20 minus tire crumbs, $\sigma_v = 10$ kPa ... 275
Figure 6.57 Amplitude-frequency curve for No. 20 minus tire crumbs, $\sigma_v = 50$ kPa ... 276

Figure 6.58 Variation of damping ratio, D, with dry unit weight, γ_d, for all tire crumb sizes tested 277

Figure 6.59 Variation of damping ratio, D, with void ratio, e, for all tire crumb sizes tested 278

Figure 6.60 Variation of damping ratio, D, with vertical stress, σ_v, for all tire crumb sizes tested 279

Figure 6.61 Comparison of the damping ratio with ampltidue for dry and saturated Ottawa sand in longitudinal oscillation, dense samples (modified from Hall and Richart, 1963) 280

Figure 6.62 Comparison of the damping ratio with amplitude for dry and saturated Ottawa sand in longitudinal oscillation, loose samples (modified from Hall and Richart, 1963) 281

LIST OF SYMBOL

Symbol	Meaning	Units
ν	Poisson's ratio	dimensionless
A	amplitude	mV
AASHTO	American Association of State Highway and Transportation Officials	-
ASTM	American Standards for Testing and Materials	-
BTEX	benzene, toluene, ethylene, x-lyene	-
btu	British thermal units	-
c	damping constant	dimensionless
c, c'	apparent cohesion	kPa
C_c	compression index	dimensionless
C_c	coefficient of concavity	-
c_{cr}	critical damping constant	dimensionless
CD	consolidated-drained	-
C_e	solution concentration at equilibrium after sorption	mg/L
CF	chloroform	-
cm	centimeter	-
C_r	recompression index	dimensionless
CRM	crumb rubber modifier	-
C_s	swelling index	dimensionless
C_u	coefficient of uniformity	-
D	damping ratio	%
e	void ratio	dimensionless
E	elastic Young's modulus	kPa
EB	ethylbenzene	-
e_{max}	maximum void ratio	dimensionless
e_{min}	minimum void ratio	dimensionless
EPA	Environmental Protection Agency	-
f	frequency	Hz
ft	feet	-
ft	feet	-
G	shear modulus	MPa
GAC	granular activated carbon	-
G_{max}	maximum shear modulus	MPa
G_s	specific gravity	dimensionless
Hz	hertz	-
i	hydraulic conductivity	dimensionless

in	inch	-
K	linear isotherm partition coefficient	
k	hydraulic conductivity	cm/s
k_{20}	hydraulic conductivity corrected to temperature at 20°C	cm/s
K_f	Freundlich sorption equilibrium constant	mg/g
kg	kilogram	-
K_L	linear sorption equilibrium constant	L/g
kN	kilo-Newtons	-
K_o	lateral earth pressure at rest	dimensionless
K_{ow}	octanol-water partition coefficient	-
lb	pounds	-
m	meter	-
m	mass	kg or g
MC	methylene	-
mg	milligram	-
MJ	mega Joules	-
mm	millimeter	-
MW	molecular weight	g/mol
n	porosity	%
n_f	constant indicative of sorptive capacity	dimensionless
°C	degrees Celsius	-
PCDD	polychlorinated dibenzo-p-dioxins	-
PCDF	polychlorinated dibenzofurans	
ppb	parts per billion	-
ppq	parts per quadrillion	-
ppt	parts per trillion	-
RUMAC	Rubber-Modified Asphalt Concrete	-
T	temperature	oC
t	time	s or ms
$t_{1/2}$	half sorption time	hrs
TCA	1,1,1-trichlorethane	-
TCE	trichlorethylene	-
TDF	tire derived fuel	-
TOL	toluene	-
v	discharge velocity	cm/s

VDOT	Virginia Department of Transportation	-
W	watts	-
X	mass of adsorbate sorbed	mg
yd	yard	
ΔH	horizontal deformations	mm
δ	logarithmic decrement	dimensionless
ε	shear strain	%
ε_1	axial strains	%
ε_3	lateral strains	%
ε_v	volumetric strains	%
ϕ'_{mob}	mobilized angle of shearing resistance	degrees
ϕ, ϕ'	angle of shearing resistance	degrees
γ_d	dry unit weight	kN/m^3
γ_w	unit weight of water	9.81 kN/m^3
λ	thermal conductivity	W/m-°C
μm	micro meter	-
°	degrees	-
ρ_d	dry density	kg/m^3
ρ_s	solids density	kg/m^3
σ_1	axial stress	kPa
σ_3	confining stress	kPa
σ_N	normal stress	kPa
σ_v	vertical or overburden stress	kPa
ω_n	undamped natural frequency	Hz

CHAPTER 1 INTRODUCTION

1.1 Purpose of Investigation

The scrap tire generation in the industrialized countries is approximately one passenger car tire per capita per year. This figure amounts to approximately 300 million passenger car tires per year in North America (T.A.G. Resource Recovery, 1996). In addition, it is estimated that approximately 2 billion waste tires have accumulated in stockpiles and illegal tire dumps across the United States (U.S. EPA, 1991). Clearly, scrap tires have historically represented a significant solid waste management and disposal problem, even though the volume of scrap tires represents less than 2% of the total solid waste stream in North America. The problem is evident in the large stockpiles that have accumulated over the years. These stockpiles have become public health hazards and pose serious risks to the environment (Park et al., 1997; Humphrey, 1996; Masad et al., 1996, Manion and Humphrey, 1992; Matthews and Silverman, 1991).

Stockpiled tires provide an excellent breeding ground for mosquitoes, which have been identified to carry various types of encephalitis and yellow fever (Manion and Humphrey, 1992; Matthews and Silverman, 1991). Furthermore, the mosquitoes are reported to reproduce 4,000 times faster in tires than in their natural environment (Matthews and Silverman, 1991). The U. S. EPA estimated that in 1986, the health care costs for scrap tire related to encephalitis alone totaled US $5.4 million.

Fire is a particularly important environmental and public health concern. Once ignited, tire fires are extremely difficult to contain and extinguish. When stockpiles of tires burn, a thick black smoke is produced and toxic pollutants are emitted. Burning tires also produce a run-off of petroleum products. Synthetic crude oil, which is produced in the fire, enables the fire to spread quickly, making its control extremely difficult. To make matters worse, oil and other chemical contaminants combined with water that is used to fight the fire seeps into the ground, and contaminate the soil and possibly the groundwater supply. In the last decade, tire fires have become notorious for gaining media attention. One of the largest tire fires ever in North America occurred on February

1990 in the town of Hagersville, Ontario (Waste Age, 1990). The fire, which involved 14 million scrap tires, burned for more than 17 days and caused the evacuation of more than 1,000 nearby residents. Ontario officials estimated that the fire clean-up costs to the Ontario provincial government may have exceeded $14 million. Another costly tire fire disaster occurred in Catskill, New York on February 1989. The fire, which involved 2 million scrap tires, forced the evacuation of people living within a 4 km radius from the site (Matthews and Silverman, 1991). It took the combined efforts of fire departments from at least five counties one week to contain the blaze. It is therefore, extremely important that alternative tire disposal methods, besides stockpiling, are found.

An enormous potential exists in recycling these scrap tires, including potentially using them in civil engineering applications. Currently, only about 3% of those discarded annually in Alberta are used in civil projects, and that market is exclusively for tire shreds. In most cases, the shreds are used as a replacement for traditional construction material such as gravel and sand. Some of the civil applications of tire shreds include using them as road subgrades, backfill behind retaining walls, and drainage media in leachate collection systems. Another great potential is realized in reducing the tire shreds into crumbed tire rubber, and using the crumbs in high-value geotechnical applications. This may include using tire crumbs as a sorption media or in reactive permeable barriers to mitigate and possibly remediate contaminated groundwater, as a thermal insulator to prevent frost penetration behind retaining walls and in road subgrades, and even in foundation vibration control.

1.2 Objective of this Research

In order to investigate the potential geotechnical applications of crumbed tire rubber, it was necessary to first understand its general behavior and engineering properties. The research was divided into two phases. Phases I was a detailed review of the literature, and Phase II consisted of laboratory material testing.

In Phase I, the literature review examined the following:

- The general behaviour and basic engineering properties;
- Sorption capacity and leachability;
- The available and new laboratory testing procedures for evaluating the engineering properties;
- Are modifications required to the accepted material testing procedures; and
- The successful and unsuccessful uses of this material.

The information gathered in Phase I of the research would provide guidance to carry out the study in Phase II. The goal of Phase II, hence, was to conduct laboratory experiments to characterize the following engineering properties of crumbed tire rubber produced from a number of different suppliers in Alberta:

(1) Particle size and gradation;
(2) Specific gravity;
(3) Compaction characteristics
(4) Hydraulic conductivity;
(5) Compressibility;
(6) Thermal properties;
(7) Strength; and
(8) Dynamic properties.

Another very important objective of this research is to introduce new high-value geotechnical applications.

A site visit to two crumb rubber-manufacturing plants in Alberta was also undertaken in June of 1998. The plants visited were Tire Recyclers of Calgary (TROC) and Midwest Tire Processor of Vulcan. The trip provided an opportunity to collect samples of different crumb rubber sizes for use in the laboratory testing, and to become familiar with the processes used to make the crumb from shredded tires. Samples of tire crumbs were also collected from Alberta Environmental Rubber Products, Edmonton, however, a site visit to their plant was not permitted.

1.3 Organization of the Thesis

The research is presented in the following six chapters. Chapter 2 of this thesis provides background information and comparisons on the general behaviour and engineering properties of both tire crumbs and shreds. Comparisons to conventional geo-materials are also presented. The chapter also discusses the current practice in scrap tire disposal including incineration, land filling/stockpiling, and recycling. The available and new laboratory testing procedures relevant to characterizing the engineering properties of tire crumbs will also be discussed.

The sorption properties and leaching experiments were omitted because of the available information in the literature. Hence, the sorption properties and leachability of tire crumbs are discussed in detail in Chapter 3 and Chapter 4 respectively.

Chapter 5 describes the laboratory apparatus that were used and testing procedures that followed through out this research. A detailed discussion on the thermal and dynamic property testing is also presented.

Chapter 6 presents the test results and analyses and compares them to those reported in the literature.

The conclusions and summary of all the work done, and recommendations for future research are presented in Chapter 7.

All relevant data, figures, and graphs are contained in a CD-ROM that is included with this thesis.

CHAPTER 2 LITERATURE REVIEW

2.1 Introduction

In this chapter, a summary of the published literature by various authors, organizations and institutions is discussed. The literature that was relevant to this research included information such as general tire characteristics, common scrap tire disposal methods, crumbed rubber production technology, civil/geotechnical applications of recycled tire rubber, material property testing, and geotechnical properties.

2.2 General Tire Characteristics

Modern tires are principally composed of a combination of synthetic and natural rubber elastomers derived from oil and gas (T.A.G. Resource Recovery, 1996). Although natural rubber is still used in tires, synthetic rubbers have become an essential part of the modern tire manufacturing process. Styrene-butadiene rubber (SBR) is the most important synthetic rubber used by the tire industry because of its good mechanical and physical properties combined with its favorable cost. Steel and/or fabric reinforcement is added throughout a tire to improve strength. Other additives such as carbon blacks, extender oils, waxes, and other chemical compounds are also used in tires in varying amounts. A typical composition of tire rubber is shown in Table 2.1. Carbon black is used to strengthen the rubber and aid abrasion resistance (Park et al., 1996). Waxes are added to enhance performance characteristics and manufacturing efficiency (T.A.G. Resource Recovery, 1996). Extender oil, which is a mixture of aromatic hydrocarbons, helps to soften the rubber and improve workability, and sulfur is used to cross-link the polymer chains within the rubber and to harden and prevent excessive deformation at elevated temperatures (Park et al., 1996). The accelerator is typically an organo-sulfur compound that acts as a catalyst for the vulcanization process. Zinc oxide and stearic acid also act to control the vulcanization process and to enhance the physical properties of the rubber.

2.3 Common Scrap Tire Disposal Methods

Figure 2.1 shows the estimated scrap tire designation for the United States in 1995. Of the 253 million scrap tires generated during that year, about 31% were illegally dumped, land filled, and/or stockpiled, 6.0% were exported, 52% were used in energy recovery as a fuel source, and the remaining 11% were either reused or recycled. The three major disposal options of scrap tires can be categorize as: (1) energy recovery, (2) land filling and stockpiling, and (3) recycling and reuse (Bernal et al., 1996). A brief explanation of each disposal method is described below

2.3.1 Energy Recovery

The most common tire disposal method currently used in the United States is the incineration of tire shreds and whole tires as fuel. There are four main markets for scrap rubber fuel: (1) dedicated tire-to-energy plants, (2) cement kilns, (3) electric utilities, and (4) pulp and paper mills. Scrap tires, either shredded or whole and used as fuels are commonly known as tire-derived fuel or TDF. The incineration of tires as a means of disposal has significantly increased over the past decade. It was reported that in 1990, the United States consumed approximately 11% of its annual scrap tire generation as fuel (U.S. EPA, 1991). However, that figure has increased about 5 times in 1995 to approximately 52%. The reason for the increase is that burning scrap tires is a way to reduce energy costs and become more competitive. In fact, tires are reported to have a higher energy value than most coals and are cleaner burning. Scrap tires have a heat value of 32.6 MJ/kg (14,000 btu/lb), compared with coal values of 18.6 to 27.9 MJ/kg (8,000 to 12,000 Btu/lb) (Borchardt, 1991).

The most economical way to use tires for fuel is to burn them whole. In 1992, there were only two dedicated whole-tire-to-energy plants operating in the United States: the Modesto Energy project in Westley, California and the Exeter Energy project in Sterling, Connecticut (Hughes, 1993). The Modesto Energy project was designed to burn whole scrap tires as its sole fuel source. The location of this plant is directly adjacent to the country's largest scrap tire pile, which was reported to contain about 30 to 40 million tires at its maximum capacity (Clark et al., 1991). Furthermore, the plant was reported to consume about 4.9 million tires annually to generate electricity (U. S. EPA, 1991). The Exeter Energy project, on the other, was reported to consume nearly 11 million tires per year (Borchardt, 1991)

In 1996, 27 cement kilns, 12 pulp and paper mills, and 8 coal-fired utilities were reported to use TDF as a supplemental fuel (Borchardt, 1991). However, the majority of these facilities do not have the capability to burn whole tires. Instead, the tires must be processed into shreds that are 25 to 75 mm in size. Cement kilns utilize about 50 millions tires annually.

Another potential use of scrap tires is pyrolysis, which involves the decomposition of the tire rubber at high temperatures in an oxygen-free atmosphere. Tire rubber pyrolysis results in the recovery of valuable products including hydrocarbon oils and gases, plus a residue of carbonized and nonvolatile materials (San Miguel et al., 1998). The amount and specific characteristics of each product depend on the process conditions, temperature and reaction time (Williams et al., 1995; Dodds et al., 1983). These products are marketable to various degrees. Pyrolytic oils possess high-energy value (approximately 43 MJ/kg) and are hence marketed as fuel or additives in petroleum refinery feedstock. The oils are also a source of chemicals including benzene, toluene, xylene, and limonene (Williams et al., 1995). Pyrolytic gases contain high concentrations of methane, butadiene, and other hydrocarbon gases, which also possess high-energy value (approximately 37 MJ/m^3) sufficient to heat the pyrolysis reactor. The carbonized residue, usually referred to as pyrolytic char, consists of low-grade carbon black and a mixture of products from the degradation of the rubber compound including carbonized rubber polymer, nonvolatile hydrocarbons, plus trace quantities of tire rubber additives such as zinc, sulfur, clays, and silica. The potential reuse of carbon black is restricted to low-quality applications due to the presence of impurities, high ash content, and large particle size. A potential application for the pyrolytic char involves its use as an alternative for activated carbon. Activation involves extra capital, involves higher expensive running costs, and results in a reduction of carbon yield. Studies show that tire rubber pyrolytic chars already possess a well-developed mesopore structure that results in relatively high adsorption capacities for large molecular weight compounds. Therefore, the use of these inactivated chars may be an economically feasible alternative to activated carbon in applications to remove large molecular weight compounds from solution, such as the treatment of textile effluents.

2.3.2 Landfilling and Stockpiling

In 1990, about 80% of the total scrap tires generated in the United States were either landfilled, stockpiles, or illegally dumped (Matthews and Silverman, 1991; U.S. EPA, 1991), but that value has been reduced to about 31% in 1995 as shown in Figure 2.1. Furthermore, it was estimated that over 2 billion scrap tires exist in stockpiles and illegal dumpsites across the United States. According to Manion and Humphrey (1992), most landfills do not accept whole scrap tires because tires are extremely difficult to handle and do not compact as easily as municipal waste. In some instances, whole tires have even worked their way to the top of a closed landfill causing destabilization to the site and costly damages to the landfill cover. Hence, wholes tires that are buried using a thin layer of soil tend to float back to the surface making burial an unacceptable disposal method. Yet, many tires still end up in landfills either as quartered or shredded tires. These methods of disposal are expected to loose significance due to the rapid decrease in landfill space, and high disposal fees charged for tires at most landfills and tire dumps. Furthermore, the environmental and health implications of land filling and stockpiling tires make these disposal methods less acceptable.

2.3.3 Recycling and Reuse

The term *recycling* is often misused. A concise definition of recycling is *the use of material for its originally intended purpose*. In the case of scrap tires, this would mean using recycled tire rubber as a compounding ingredient for new tires. Furthermore, whenever the chemical structure of the rubber is significantly changed or destroyed (as in pyrolysis and incineration) the process should no longer be called recycling at all. In the broader sense, recycling is referred to as the grinding, shredding, and chopping of scrap tires into crumbed rubber and tire shreds for use in applications including lightweight fill in embankments and behind retaining walls, drainage media in leachate collection systems and filters, and as feed stock to manufacture user-end rubber products. The reuse of scrap tires would involve using whole tires for retreading, and other civil engineering applications such as soil reinforcement, breakwaters, and highway crash barriers. In the United States, it was estimated that only about 7% of the annual scrap tire generation was either recycled and/or reused (U.S. EPA, 1991). However, that figure has grown to about 11% in 1995.

2.4 Crumbed Tire Rubber Production

The majority of the published literature focuses on tire shreds. In general, tire shreds are larger than the crumb being considered in this study. Tire shreds (also referred to as tire chips) are scrap tires that have been cut up into 25 to 305 mm (1 to 12 in) pieces. In a survey of four tire shredding operations in the state of Wisconsin, Edil et al. (1990) found tire shred sizes to range from 25 x 50 mm to 100 x 200 mm (1 x 2 in to 4 x 8 in). In addition, tire shreds contain a significant amount of exposed steel belts. However, the amount of exposed steel belts depends on the sharpness of the cutting blades (Humphrey, 1996). In comparison, the crumbs from tires are smaller in size than tire shreds. The terms crumbed tire rubber, crumbed rubber, tire crumbs, granulated tire rubber, and even ground rubber are often used interchangeably. Several authors use the term tire chips to describe either crumbs and/or shreds. In general, tire crumbs are scrap tires that have been ground or shredded into rubber granules with particle sizes ranging from 9.5 mm to 74-µm (3/8 in to No. 200). Recycler's World (2000) categorizes crumbs as materials that are smaller than 6.3 mm (1/4 in). Furthermore, the fiber and steel components of tire crumbs are almost completely removed during the grinding and cleaning processes.

Scrap tires can be processed into tire crumbs in several ways. The most common method is ambient grinding, which involves grinding whole or shredded tires using cracker mills and granulators at ambient temperatures. Another method of producing crumbed tire rubber can be accomplished through cryogenic grinding. In the cryogenic process, rubber is introduced into a bath of liquid nitrogen, which instantly freezes the rubber. Once embrittled, the rubber is struck with an impact device, hence, shattering the rubber. Furthermore, tire crumbs can also be produced from tire buffings, which are by-products from the tire retreading process. The applications for crumbs produced from various processes will depend its specific characteristics including particle shape, size and texture. A detailed description of each production method is presented in the following sections.

2.4.1 Ambient Grinding

The most common method of processing scrap tires into tire crumbs, steel, and reinforcement fiber is with shredders, granulators, cracker mills, and screening equipment operating at ambient temperatures (Ahmed, 1993). The method is usually referred to as ambient grinding. Essentially, the crumb is produced using three basic processes (after Heitzman, 1992). These are: (1) granulator process; (2) crackermill process; and (3) micromill process. The type of processing method used produces crumbs with unique particle sizes and specific characteristics.

2.4.1.1 Granulator Process

Granulators can be categorized as medium to high speed processing systems. The process shears the scrap tire rubber by cutting the rubber with revolving steel knives that pass at close proximity to stationary knives. This process produces cubical, uniformly shaped cut particles with low surface area. The material is produced from 2 in minus tire shreds. Tire crumbs produced from the granulator process are commonly known as granulated crumb rubber additive (Ahmed, 1993). Their particle sizes may range from 9.5 to 2 mm (3/8 in to No. 10).

2.4.1.2 Crackermill Process

The crackermill process is the most common of the three ambient grinding processes (Ahmed, 1993). The process produces irregular shaped torn particles with large surface areas. Tire crumb particles produced from the crackermill process are commonly referred to as ground crumb rubber additive and their particle sizes vary from 4.75 mm to 425 μm (No. 4 to No. 40). A photo of a crackermill is shown in Figure 2.2. A typical sequence through a crackermill process is illustrated below.

1. **Coarse Grinding**. Whole tires are fed into a shredder that reduces them into 50 mm (2 in) shreds. The feedstock of tire shreds includes steel beads, steel belts, fibre cords, rocks and other contaminants.

2. **Primary Crackermill.** The primary crackermill is used to grind the 2 in shreds into 12.5 mm (1/2 in) particles. The machine utilizes two counter rotating corrugated steel drums turning at slow speeds and at close tolerance to rip, tear, and shred the rubber. This also strips away the metal and fibre layers. The 1/2 in particles are then conveyed to a sizing screen to ensure that all particles not fine enough are re-ground. The particles are then sent into the first of several magnetic and air gravity separation systems where the vast majority of the steel wire and fiber components are separated.
3. **Secondary Crackermill.** The secondary crackermill reduces the 1/2 in shreds down to a variety of sizes including No. 4, No. 10, No. 30 and smaller. Product size is controlled by the clearance between the rollers, which is also called the nip (Blumenthal, 1996).
4. **Cleaning and Screening**. Once the 1/2 in shreds are processed to the desired size, the product is sent through a second magnetic separation system. At this stage, all remaining steel is removed. The product is then screened and the over-sized material is returned to the secondary crackermill for further reduction. The desired product size is fed to a second air gravity separation system where the remaining fiber is removed. Before the final rubber particles leave the processing system, the material passes through a finishing mill for final sizing. All products are sent through a system designed to remove any stones, rock, or other types of contaminants. The final product is then screened into its respective product size ranges, bagged and weighed.

2.4.1.3 Micromill Process

The micromill process, also called the wet process, is a patented grinding process for ultra find grinding (Blumenthal, 1996). The process further reduces the crumbed rubber to a very fine particle size by grinding in a liquid medium (usually water). Grinding is performed between two closely spaced grinding wheels. The size of the product is a function of the time spent in the micromill. Tire crumbs produced from the micromill process range in size from 425 to 75 μm (No. 40 to No. 200).

2.4.2 Cryogenic Grinding

The cryogenic process involves cooling tire shreds to a point where they become brittle using liquid nitrogen. A typical tire grinding system using the cryogenic process is shown in Figure 2.3. As illustrated, the process usually involves the ambient grinding of whole tires into 25 to 75 mm (1 to 3 in) tire shreds. The shreds are then chilled with liquid nitrogen and dropped into a hammer mill to be fractured into crumbed rubber, steel and fiber. The process works in conjunction with shaking screens, which separates the steel from the rubber granules, and magnetic separators that remove the steel. The rubber granules are then transported by conveyor to a dryer that removes excess moisture. This allows for easier separation of the remaining fiber and separation of the rubber granules by particle size (Ahmed, 1993). The rubber granules are then passed through a secondary magnetic separator and classified by means of a shaker screen. In this process, 70 to 80% of the crumb is typically smaller than 2 mm (No. 10) (Kohler, 1996).

A variation of the first system involves shredding the tires with one or more shredders, coarse grinding the tire shreds with multiple ambient temperature granulators, separating the metal and fiber, pre-cooling, cryogenically grinding the material, and then sorting the crumb by size. This produces rubber that is substantially smaller than 600 μm (No. 30) (Kohler, 1996). Whenever an application requires crumb rubber that is finer than 600 μm (No. 30), a secondary cryogenic process is used. That is, the process starts with 4.75 to 2.0 mm crumb rubber sizes (No. 4 to No. 10) produced in one of the primary grinding systems. The material is then pre-cooled, cryogenically ground, and then sorted by particle size. This technology is utilized to obtain crumb rubber with 40% of its particle size smaller than 425 μm (No. 40) (Kohler, 1996).

The major difference between particles of rubber generated by ambient and cryogenic processing systems is their shape. Crumbs derived from the cryogenic process have a smooth surface similar to shattered glass. Particles derived from the ambient process, on the other hand, have a rough surface, giving it greater surface area relative to the cryogenically produced particle. Advocates of the cryogenic process claim that low-temperature grinding yields several advantages over ambient grinding systems. These advantages are (after Kohler, 1996):

- Increased productivity. For ambient grinding mills of the same general size and raw material having the same particle size distribution, cryogenic grinding increases throughput by 10 to 30 times.
- Reduced power requirements. Less power is required to produce crumb rubber of the same size than in ambient grinding systems because cryogenically frozen rubber pulverizes much more easily than rubber at ambient temperatures.
- Higher value crumbed rubber. Again, because it is not difficult to pulverize rubber at cryogenic temperatures. Tire crumbs having particle sizes of 30 and smaller are easily attainable. Table 2.2 shows a typical pricing index for crumb rubber. The table shows that the finer the crumbs, the more valuable it is on the open market.
- Reduced maintenance of machinery. Since cryogenically frozen rubber pulverizes much more easily than rubber at ambient temperatures, there is less wear and tear on machinery and maintenance costs are significantly reduced. Furthermore, maintaining sharp cutting edges is much less important in a cryogenic system than in an ambient one.
- Easy liberation of fiber and metal. It is much easier to separate fiber and metal from cryogenically ground rubber. The steel and fiber are almost 100% liberated from the rubber. In addition, the steel is a valuable by-product worth from $80 to $120 US per ton.
- Minimal space requirements. The amount of space required for a cryogenic processing system is considerably less than that needed for an ambient grinding system.
- Greater profitability. The combination of lower production costs and higher value product results in more profits.
- The end product is considerably resistive to degradation; either thermally and/or due to oxidation.

The cryogenic process, however, has several disadvantages. The most obvious is the cost of special equipment. Generally, the choice of equipment depends on existing equipment, starting rubber size, and capital versus operating cost trade-offs. However, most cryogenic processing systems require a pre-cooler, dryer, and liquid nitrogen unit. The liquid nitrogen is usually owned and maintained by the nitrogen supplier. In addition, there is also a trade-off in the cost of the liquid nitrogen. Nitrogen costs are typically $0.02 to $0.06 US per pound of rubber depending on the degree of particle fineness required and the quantity of nitrogen purchased. In absolute terms, a core cryogenic grinding system can be purchased for under $150,000 US for grinding 900 to 1800 kg/hr (2,000 to 4,000 lb/hr) of fiber and metal-free rubber. The addition of dryers, fiber and metal separators, conveyors, etc. can raise that number by a factor of 2 to 5 or even more if a primary shredder is required (Kohler, 1996). To a large extent, the advantages or disadvantages of the product derived from a given processing system are a function of the market application (Blumenthal, 1996).

2.4.3 Retreading Process

Retreading is the application of a new tread to a worn tire that still has a good casing (U.S. EPA, 1991). Crumb rubber produced from the retreading process is called tire buffings and their sizes typically range between 710 µm and 425 µm (No. 25 to No. 40). These are actually rubber from the tread portion of the tire only, and are more costly than rubber produced by ambient processing of tire shreds (Matthews and Silverman, 1991). Hence, the tire buffings are by-products from the tire retreading process and are used primarily in molded or fabricated products. In the United States, about 38 million tires are retreaded annually but the market is almost exclusively for large truck tires (Matthews and Silverman, 1991; Bernal et al., 1996). According to the U.S. EPA (1991), the market for passenger car tire retreads has been shrinking due to the relatively low price of new tires and concerns about the safety of retreads. The market for truck tire retreads, on the other hand, is increasing because truck tries are often retreaded three to five times before being discarded (Bernal et al., 1996).

2.5 Geotechnical Properties of Recycled Tire Rubber

2.5.1 Particle Size and Gradation

As previously mentioned the majority of the published literature refers to the material as tire shreds. To summarize, tire shreds are larger in size than the crumbs considered in this study. Most tire shreds will contain exposed steel belts, steel beads, and fibre reinforcements unless effort is taken to remove them. The focus of this research is the geotechnical properties and geotechnical applications of tire crumbs. To re-emphasize, tire crumbs are scrap tires (in the form of shreds) that have been ground or shredded into rubber granules with particle sizes ranging from 9.5 mm to 75 μm (3/8 in to No. 200). In addition, the fiber and steel components are almost completely removed from the grinding and cleaning processes.

Particle size and gradation is usually determined using the method of sieving. The procedure involves passing the material through an arrangement of sieves of decreasing mesh sizes. The difficulty is choosing a sample weight that is representative of the entire material. Humphrey (1996) indicated that since the specific gravity of recycled tire rubber is less than half the value obtained for common soils, they recommend using a minimum sample weight that is half of the specified standard for soils. Table 2.3 compares the particle size, shape, and the coefficients of uniformity (C_u) and curvature (C_c) of recycled tire rubber as determined by different investigators. The values for certain granular soils are also presented. Their particle size distribution is shown and compared in Figure 2.4.

The particle size and distribution of crumbs is comparable to that of uniform clean sands, and gravelly-sand mixtures. Tire shreds, on the other hand, have particle size and distribution similar to gravels. Newcomb and Drescher (1994) indicated that particle size is a function of the number of passes through the shredding device. Particle shape of tire crumbs varies from angular to irregular. However, tire shreds with sizes in excess of 25 to 50 mm (1 to 2 in) are usually plate-like in shape with the larger dimension typically two to four times the smaller dimension (Tatlisoz et al., 1997; Edil and Bosscher, 1994).

Tire shreds would most closely represent the type of material used in field applications from a size and particle shape standpoint (Benda, 1995). The grinding and shredding of scrap tires generally produce shreds and crumbs with uniform gradations.

2.5.2 Specific Gravity

In geotechnical engineering, specific gravity is defined as the ratio between the density of soil solids and the density of water. The specific gravity of tire crumbs has been determined by several investigators using different test procedures. The results of their findings are presented in Table 2.4 and compared to tire shreds and granular soils. Kershaw and Pamukcu (1997) applied ASTM Test Method D 854. The specific gravity was found to be 1.20 for their crumbs, which ranged in particle size from 0.6 to 1.18 mm. Masad et al. (1997) also applied the same test procedures, but found a lower specific gravity of 1.07 for crumbs with a maximum particle size of 4.75 mm.

In general, tire crumbs do not contain significant metal or fabric contents and have a narrow range of specific gravities between 1.07 to 1.20. On the other hand, the specific gravity of tire shreds can be as high as 1.36 and these values vary depending of the their metal content (Edil and Bosscher, 1994; Humphrey and Sandford, 1993). Tire shreds without metal content have a specific gravity of about 1.15 (Edil and Bosscher, 1994). Natural rubber and styrene butadiene rubber elastomers, which are components of modern tires, have specific gravities of 0.93 and 0.91 respectively (Perry et al., 1997). In comparison, the specific gravities of typical granular soils range from 2.60 to 2.70. Hence, the specific gravity of recycled tire rubber is less than half the value of typical granular soils.

2.5.3 Compaction Characteristics

Since the specific gravity of recycled tire rubber is less than half the value of soils, they can be used as a lightweight fill material in highway embankments over soft or unstable soils, behind retaining walls, or for other similar fill applications (Newcomb and Drescher, 1994; Masad et al., 1996; Edil and Bosscher, 1994). For this reason, their placement characteristics and effect on the mechanical properties by specifying the optimum compaction during placement becomes important.

Masad et al. (1996) determined the minimum and maximum index void ratio, and compacted dry density of their crumbs. The minimum index void ratio (e_{min}) is defined as the reference void ratio at the maximum index density (ASTM, 1997). This was determined by placing the material in 12 layers in a mold. A round steel block with a mass of 12 kg. was placed on top of each layer, and compaction was achieved by tapping the side of the mold sharply 15 to 25 times with a rubber mallet. The minimum void ratio was calculated as follow:

$$e_{min} = \frac{\rho_s}{\rho_d} - 1 \qquad \textbf{[Equation 2.1]}$$

where ρ_s = solids density (kg/m^3) and ρ_d = mass of dry solids/volume (kg/m^3).

The maximum index void ratio (e_{max}) is the reference void ratio at the minimum index density (ASTM, 1997). This was determined using ASTM Standard Test Method D 4253. They found the minimum and maximum void ratio to be 0.60 and 1.36 respectively. The compacted dry unit weight was determined using the same compaction mold, and compaction was achieved with a small metal tamping rod. The compacted dry unit weight of their material was found to be 6.2 kN/m^3 at a relative density of 90%.

Edil and Bosscher (1994) also applied ASTM D 4253 and found that the method was inappropriate for studying the compaction behavior of tire shreds because of the absorbent nature of the rubber to vibration. The expose steel wires also became tangle with each other. Field experience also confirmed that vibration provides no significant compaction of tire shreds (Edil and Bosscher, 1992). Hence, the Standard and Modified compaction tests were used instead (ASTM D 698 and ASTM D 1557 respectively). A 305 mm (12 in) mold was fabricated to test shreds larger than 19 mm (3/4 in) because a 152 mm (6 in) mold is restricted to materials having no more than 30% retained on the 3/4 in sieve (ASTM, 1997). Modifications were also made to the compaction hammer to deliver the same compactive energy per unit volume regardless of the size of the compaction mold. They found the dry density for their shreds ranged from 5.5 to 5.8 kN/m^3.

Table 2.5 summarizes the compaction characteristics of tire crumbs using various compaction procedures. The table also compares dry density values to tire shreds and granular soils. The reported dry unit weight of tire crumbs range from 4.4 to 6.6 kN/m^3. The dry unit weight ranged from 2.3 kN/m^3 for shreds loosely placed into a mold to 6.3 kN/m^3 for compacted samples. For comparison, typical values of compacted dry unit weight for granular soils are in the range of 17 to 20 kN/m^3. Hence, the compacted dry unit weight of recycled tire rubber is about one third that of granular soils. Newcomb and Drescher (1994) found that the uncompacted dry unit weight of tire shreds decreases with increasing shred size. This is also in agreement with the study by Ahmed (1993). They also found that the compacted dry unit weight of shreds is not very sensitive to shred size, however, they observed a trend of increasing dry unit weight with increasing shred size. There is insufficient data in Table 2.5 to ascertain a correlation between particle size and density for tire crumbs.

2.5.4 Compressibility

It is important to understand the compressibility behavior of recycled tire rubber in order to predict settlements in both the short-term and long-term, and settlements due to temporary dynamic loading. In general, the compressibility of recycled tire rubber is quite high compared to soils, which results from a reduction in void ratio and compressible grains. Compressibility, hence, will probably be the controlling design variable in applications associated with embankment fills.

The compressibility behavior of recycled tire rubber has been measured in the laboratory using oedometer (Edil and Bosscher, 1994; Newcomb and Drescher, 1994; Ahmed, 1993; Humphrey et al., 1992; Manion and Humphrey, 1992) and triaxial techniques (Benda, 1995). The oedometer technique involves placing the material dry in molds having diameters ranging from 150 to 737 mm (6 to 29 in) and then conducting one-dimensional, laterally confined loading/unloading compression tests where the axial strains caused by an increase or decrease in vertical stresses are measured. Due to limited availability of very large triaxial apparatus, triaxial compression tests are usually performed on tire rubber with small particle sizes (25 mm or less). Furthermore, the triaxial apparatus is not suitable for shreds with protruding steel belts because the membrane can be easily punctured or torn by these protrusions.

Benda (1995) investigated the compressibility behavior of recycled tire rubber with five different grain sizes. Triaxial specimens measuring 100 mm (4 in) in diameter and 200 mm (8 in) in height were compacted according to AASHTO Test Method T 99 and consolidated under isotropic stress conditions in a 165 mm (6.5 in) diameter triaxial cell. Figure 2.5 shows the consolidation response for their different grain-size material. The consolidation behavior of all their samples tested was essentially the same. At consolidation pressures of up to 55 kPa, the samples showed a 27 to 32% reduction in volume. This translated to densities of 6.6 to 7.5 kN/m^3. In general, they found no apparent correlation between particle size, shape or distribution, density, and compressibility for their materials tested. This is consistent with the study carried out Ahmed (1993) who found very little variation in axial strains at different vertical stress levels for compacted tire shreds varying from 12.5 to 50 mm (0.5 to 2 in) in size. They also investigated the effect of different compaction methods but found little effect in the case for samples prepared at standard and modified Proctor compaction efforts. However, slightly higher compressibility was found for shreds compacted at 50% standard Proctor. Loose samples showed twice the compressibility of compacted samples under similar vertical stresses.

Edil and Bosscher (1994) performed confined compression tests on tire shreds with an average dimension of 50 x 70 mm in a 152 mm (6 in) Proctor mold. Figure 2.6 shows a typical hysterisis stress-strain response for their material. The majority of compression takes place during loading at low stresses and then decreases at higher stress levels. A portion of this compression is irrecoverable and there is significant rebound upon unloading. Subsequent cycles displayed similar stress-strain behavior but with less rebound than the first cycle. A vertical stress of 500 kPa corresponds to about 35% axial strain in Figure 2.6. Similarly, Manion and Humphrey (1992) found that the stress-strain response for their shreds, which is shown in Figure 2.7, produced about 40% axial strain at the same stress level. Overall, confined compression tests on shreds indicate high compressibility at low stresses, however, the compression decreases significantly upon loading to higher stresses. According to Edil and Bosscher (1994), tire shreds compress when a load is applied due to two mechanisms: (1) bending and reorientation of shreds into a more compact arrangement; and (2) compression of individual shreds under stress.

In geotechnical engineering, the compressibility and rebound of a soil are characterized by the compression index (C_c) and the swelling index (C_s). These indexes are defined as the slopes of the void ratio versus the logarithm of vertical stress (e versus $\log\sigma_v$) plots, which are obtained directly from one-dimensional compression tests. Figure 2.8 shows a typical e versus $\log\sigma_v$ plot for tire shreds and wood chips. Table 2.6 summarizes the compressibility indices for tire shreds and select materials. The compression index for compacted tire shreds is comparable to granular fill, with values ranging from 0.11 to 0.22 (Ahmed, 1993). For uncompacted tire shreds, the compression index varies from 0.20 to 0.25 (Ahmed, 1993). Newcomb and Drescher (1994) reported a compression index of 0.50 for their uncompacted tire shreds. However, they conducted their compression tests at a much higher vertical stress (up to 400 kPa) than in the study by Ahmed (1993). Tire shreds also show significant rebound, with a swelling index ranging from 0.10 to 0.27. For comparison, the swelling index of wood chips is 0.034. Hence, the swelling index for shredded tires is about two to eight times that of wood chips.

2.5.4.1 Elastic Parameters

For the structural analysis and design of highways as a multi-layer elastic system, two fundamental mechanical properties are required: the Young's modulus (E) and Poisson's ratio (ν). One method to assess Poisson's ratio is to compute it from the coefficient of lateral earth pressure at rest (K_o) in accordance with the following equation:

$$\nu = \frac{K_o}{1+K_o} \qquad \textbf{[Equation 2.2]}$$

K_o can be determined from one-dimensional compression tests using a cylindrical tube in which strain gauges are instrumented to measure the lateral and vertical strains caused by an applied vertical stress. The thickness of the tube must be carefully selected so that the strains are sufficiently low to approximate the at rest condition and sufficiently high to be measured accurately (Edil and Bosscher, 1994). The method was used successfully by

Manion and Humphrey (1992) and Humphrey et al. (1992), however, Edil and Bosscher (1994) had very little success in measuring the Poison's ratio of either sand or tire shreds. Consequently, they decided to use uniaxial (unconfined) compression tests to measure Poisson's ratio directly.

Benda (1995) determine Poisson's ratio using the volumetric strain and axial strain measurements gathered from triaxial compression loading tests. They calculated the lateral strains using the following relationship for triaxial loading conditions:

$$\varepsilon_3 = \frac{\varepsilon_v - \varepsilon_1}{2} \qquad \textbf{[Equation 2.3]}$$

where ε_3 = lateral strains, ε_v = volumetric strains, and ε_1 = axial strains.

The following expression was then used to calculated Poisson's ratio, and consequently, the coefficient of lateral earth pressure at rest:

$$\nu = \frac{\varepsilon_3}{\varepsilon_1} \qquad \textbf{[Equation 2.4]}$$

Young's modulus (E) was determined from the linear portion of the stress strain curves.

Table 2.17 summarizes the elastic parameters of recycled tire rubber as determined by several authors. Benda (1995) found that the Poisson's ratios were relatively unaffected by changes in confining pressures and axial strains for their tire crumbs and shreds tested in a triaxial apparatus. Poisson's ratios ranged from 0.25 to 0.32, and K_o values varied from 0.33 to 0.42 for crumbs with 2 mm particle sizes. The Poisson's ratio and K_o values for tire shreds (9.5 to 38 mm) ranged from 0.23 to 0.33 and 0.30 to 0.49 respectively. Young's modulus varied from 345 to 820 kPa. Bernal and Salgado (1996) found that for their 25 mm (1 in) shreds, K_o stabilizes to an average value of about 0.50 with increasing vertical stresses of up to 275 kPa. For comparisons, the Young's modulus of granular soils is typically in the range from 100 MPa for loose sands to 700 MPa for dense sands (Chen, 1948). Thus, the Young's modulus of recycled tire rubber is about 3 orders of magnitude less then the modulus of typical clean granular soils. A single elastic constant G, the shear modulus, can describe the elastic behavior of rubber under small strains. The Poisson's ratio is effectively 0.5, and the Young's modulus E is given by 3G, to good approximation. The shear modulus of rubber is typically about 0.2 to 5 MPa (Mark et al., 1994).

2.5.5 Hydraulic Conductivity

One potential application of utilizing scrap tire rubber is to use the material in drainage or filter applications. Hence, the hydraulic conductivity of the tire rubber under various overburden pressures and confinement becomes important. The hydraulic conductivity of tire crumbs and shreds reported by several investigators are summarized in Table 2.8. Their work is also briefly discussed below.

The hydraulic conductivity of recycled tire rubber is comparable to or greater than most granular soils. Cecich et al. (1996) conducted constant head permeability test in accordance with ASTM D 2434. Samples containing both crumbs and shreds were prepared using the Modified Proctor compaction method at dry unit weights ranging from 5.5 to 5.9 kN/m^3. The calculated hydraulic conductivity values for their material varied from 0.033 to 0.034 cm/s. Masad et al. (1996), on the other hand, determined the hydraulic conductivity of their crumbs in a triaxial cell. The specimens were prepared and compacted as discussed previously and saturated prior to testing. The unit weight of their material was 6.2 kN/m^3. The hydraulic conductivity was determined at confining pressures ranging from 150 to 350 kPa. However, they found much lower hydraulic conductivity values under confinement, with values ranging from 0.0020 to 0.00049 cm/s at the respective confining pressures. Furthermore, they observed that the hydraulic conductivity decreases almost linearly with confinement. In comparisons to tire shreds, the hydraulic conductivity of tire crumbs is about one to two orders of magnitude less. This is primarily due to less void spaces in the crumbs resulting from a more tightly packed particle arrangement under stress. The hydraulic conductivity of tire shreds varies from 0.44 to 59.3 cm/s.

Edil and Bosscher (1994) pointed out the difficulties in measuring the hydraulic conductivity of tire shreds due to their large particle size. Hence, a large-scale constant head consolidation permeameter was constructed for this purpose. They tested tire shreds with an average particle dimension of 50 x 75 mm under varying overburden pressures and hydraulic gradients. They indicated that the hydraulic conductivity of tire shreds without overburden is dependent on gradient. Furthermore, flow through the pores of the shreds is turbulent and the hydraulic gradient depends on the driving head. However, under an overburden pressure of 100 kPa, the dependency is reduced. Applied pressure reduces the porosity and tends to make the flow less turbulent. The influence of overburden pressure on the hydraulic conductivity of tire shreds is shown in Figure 2.9 at a constant hydraulic head. They found that the most significant drop in hydraulic conductivity takes place at the first increment of applied pressure; thereafter, it continues to drop at a lower rate. Although overburden pressure causes some reduction in the hydraulic conductivity of tire shreds, Edil and Bosscher (1994) noted that a significantly high hydraulic conductivity is retained even at pressures as high as 100 kPa. Nonetheless, the hydraulic conductivity values for tire shreds can be expected to remain high, at least in the order of 10^{-1} cm/s or more under typical overburden pressures; a value comparable to that of clean, coarse gravel. In contrast, the hydraulic conductivities of tire crumbs were reported in the range of 10^{-3} to 10^{-2} cm/s; values which are more typical of clean sands and sand-gravel mixtures. Hence, the hydraulic conductivity of tire crumbs is about 1 to 4 orders of magnitude less than the typical values reported for shreds with similar grain-size distribution under similar test conditions.

Baykal and Alpatli (1995) studied the permeability of rubber-soil liners under confinement. In their study, kaolinite clay and 10% tire crumbs (by weight) were mixed, compacted and tested using a consolidation permeameter. The rubber-soil mixtures contained crumbs with 5 mm maximum particle sizes and were compacted using the Standard Proctor method (ASTM D698) at water content 3% wet of optimum. Testing was conducted using water and gasoline as permeants. They reported a sharp decrease in the hydraulic conductivity when gasoline was permeated through the kaolinite-tire chip mixture. The decrease in hydraulic conductivity was primarily due to the expansion of rubber upon contact with gasoline, which is a reversible physical process. According to Baykal and Alpath (1995), the addition of rubber into soil has several advantages:

- The expansion of rubber exerts pressure on the soil and pore walls causing a decrease in the hydraulic conductivity;
- Large volume of petroleum is absorbed by rubber chips, hence the contamination of the surrounding ground is retarded;
- The lath-like shape of rubber chips and their high tensile strength compared to that of soil makes them behave as reinforcing elements and reduces cracking of the soil mixture;
- Crack propagation is also decreased by the reinforcing action of rubber chips; and
- The flow of permeant through the cracks will be minimized by the bridging of rubber crumbs, which will absorb and swell upon contact with gasoline, hence, sealing the crack.

2.5.6 Strength

Shear strength is a fundamental property that governs fill stability design. Hence, the determination of the resistance behavior of the material compressed or sheared under a constant rate becomes important. Field observations of tire shreds in stockpiles and fills show that tire shreds appear to have high friction angles based on observed angles of repose. End-dumped tire shreds and open cuts in stockpiles stand vertically for extensive periods without collapsing. Hence, the actual shear strength may be higher than that measured in the laboratory using direct shear and triaxial testing techniques (Benda, 1995). The angle of repose of loose tire shreds is typically in the range of 37 to 43°, while the angle of repose of compacted tire shreds was reported as high as 85° (Edil and Bosscher, 1994).

The shear strength in the laboratory is determined from either direct shear tests or triaxial compression tests. The shear strength of tire crumbs and shreds has been measured using direct shear by Cecich et al. (1996), Bernal et al. (1997a), and Humphrey et al. (1992); and using triaxial compression by Bernal et al. (1996), Masad et al. (1996), Benda (1995), and Ahmed (1993). The studies show that the material does not develop well-defined peak shear resistance. Hence, the shear strength parameters for tire rubber must be defined at pre-established magnitudes of deformations (Bernal et al., 1997a) or strains (Masad et al., 1996). The studies conducted by these investigators are examined in the following sections.

2.5.6.1 Direct Shear

Table 2.9 summarizes the shear strength parameters of tire crumbs as measured in direct shear test and compares them to tire shreds. Cecich et al. (1996) conducted direct shear tests on samples containing both crumbs and shreds in accordance with ASTM D 3080 (ASTM, 1997). A total of three direct shear tests were performed under 4, 14, and 28 kPa normal stresses. The stress and deformation behaviour for their material is illustrated in Figure 2.10. Their material shows increased shear resistance with increasing horizontal deformation. Failure of the material was not obtained since no peak shear resistance was observed. Hence, they determined the shear strength parameters at a horizontal deformation equal to 15% of the sample diameter. The corresponding shear strength envelope for their material is shown in Figure 2.11 and was found to be approximately linear. The cohesion intercept and mobilized friction angle was determined from a linear regression analysis and was found to be approximately 7 kPa and 27° respectively.

Bernal et al. (1997a) also conducted direct shear tests in accordance with ASTM D 3080 (ASTM, 1997). In their experiments, tire shreds (50 x 50 mm in size) were tested in a 300 mm (12 in) shear box. The material was placed and compacted in the lower box with a 4 kg. tamper. The upper box was then positioned and filled with three 50 mm thick lifts. Each layer was compacted as before until the final desired height was obtained. The samples were then sheared under 7, 24 and 54 kPa normal stresses. Their results (Figure 2.12), which is in agreement with Cecich et et al. (1996), showed increased shear resistance with increasing horizontal deformations and no peak resistance. The mobilized friction angle is plotted against horizontal deformation for their material in Figure 2.13. The figure shows that the mobilized friction angles increases almost linearly with increasing horizontal deformations. However, it takes significant deformations (up to 40 mm) to mobilize a friction angle of about 30°. The increase in resistance behavior of tire shreds with horizontal deformation can be attributed to the densification of the samples during shear, which causes the particles to interlock with each other due to their irregular shape and the presence of exposed steel belts. The mobilized friction angles corresponding to horizontal deformations from 13 to 64 mm was found to vary from 17 to 35°.

Humphrey et al. (1992) conducted a more elaborate testing program on tire shreds in accordance with AASHTO T 236 (AASHTO, 1986). The shreds, which contained exposed steel belts, ranged in size from 50 to 70 mm (2 to 3 in). Samples were prepared with a 4.5 kg. rammer and compacted with energy equivalent to 60% of Standard Proctor. A typical shear stress versus horizontal deformation for one of their samples is shown in Figure 2.14. Again, the shear resistance increases with increasing horizontal deformations. Since no peak shear resistance was observed, maximum resistance was chosen at a horizontal displacement corresponding to 10% of the length of the shear box (AASHTO, 1986). The strength envelopes were then produced, and the friction angles and cohesion intercepts were determined using a linear regression analysis through the data points. Friction angles and cohesion intercepts for their shreds ranged from 19 to 26° and from 4 to 11 kPa respectively. Additional strength envelopes were produce at different horizontal deformations to investigate the effect this could have on the calculated shear strength parameters. They showed that the cohesion intercept decreased as the horizontal deformations chosen decreased, while the friction angle was only slightly affected. For this reason, they suggested that the cohesion intercept should be neglected or a small value be used for design since it appears that significant deformation is required to develop this cohesion. The effect of testing apparatus on the measured shear strength was also investigated by conducting the same tests using the 400 mm (16 in) and 200 mm (8 in) shear boxes. However, attempts made with the latter shear box were unsuccessful due to testing difficulties. Consequently, they found that the size of the direct shear box had little influence on the shear strength of tire shreds. Figure 2.15 shows the strength envelopes of tire shreds at each of the three loading increments for the tire shreds tested. The strength envelopes were reported to be non-linear and concave downward. Hence, if data is to be fitted to a linear failure envelope the range of stresses that will occur in the laboratory and field must be considered. They also noted that smaller shreds with more equidimensional shape have more resistance than others.

During shearing, these shreds tend to lock together instead of sliding over one another like the larger, flatter pieces. Furthermore, flat pieces tend to be oriented parallel to the horizontal shear plane. Another comment is that shreds containing large amount of exposed steel belts have higher cohesion, which also causes them to interlock. It was also noted that shreds with large amounts of exposed steel belts do not rely on normal stress to develop their resistance.

2.5.6.2 Triaxial Compression

Stress-Strain Behaviour

Figures 2.16 to Figure 2.18 show typical stress and volumetric strain behaviour of various recycled tire rubbers with different particle sizes tested under conventional triaxial compression by different authors. Under these test conditions, both tire crumbs and shreds show linear strain-strengthening behaviour with increasing axial strains. The material does not reach peak deviator stress in the traditional geotechnical sense, but rather it continues to develop resistance even beyond axial strains as high as 25%. There is also an increase in deviator stress at a given strain with increasing confining pressure. Hence, the shear strength parameters must be established using the criterion of allowable strains (Ahmed, 1993). Figure shows the linear strain-strengthening behaviour of tire shreds as observed by Ahmed (1993). They also investigated the effects of particle size and compaction on shear strength but reported that the two parameters had very little effect on the shear behaviour of their material. However, a trend of increasing deviator stresses with increase in shred size and compactive effort was observed.

Wu et al. (1997) and Benda (1995) took a different approach and tested their material under triaxial compression unloading. Their samples were tested without the presence of steel. Preliminary tests were conducted using conventional triaxial compression tests in which the confining pressure (σ_3) was held constant throughout the test. However, the limit of the vertical travel in the test apparatus was realized before the stress-strain curve deviated from a linear relationship. As a result, a second series of tests involving triaxial compression unloading were later performed in which the axial stress (σ_1) was kept constant. Wu et al. (1997) reported to have selected constant σ_1 stress path tests over the conventional stress path for two reasons: (a) the stress path from initial stress state point to failure is shorter; and (b) a decrease in lateral pressure is the stress path that is likely to lead to failure in problems involving stability of retaining walls. In this test procedure, the confining pressure was reduced from the initial consolidation pressure of 35, 45, and 55 kPa until a shear failure in the specimen was achieved or the capacity of the test apparatus was reached (Benda, 1995). To maintain constant σ_1, burette readings and axial displacement measurements were used to calculate changes in the sample volume and area so that the appropriate decreases in cell pressure could be determined at each load increment. A typical plot of deviator stress and volumetric strain versus axial strain for the constant σ_1 tests is shown in Figure 2.20. The plot shows concave stress-strain curves indicating indefinite plastic flow had occurred. Peak deviator stresses, however, were reached. This is very unusual and deviates from conventional triaxial testing, hence implying the importance of stress path on the shear behavior of tire rubber. There is also an increase in deviator stress at a given strain with increasing confining pressure for both tests. No shear plane was observed in all the samples tested under constant σ_1 stress paths, but a significant amount of lateral bulging and dilation was reported to occur.

Volumetric Strain Behavior

The volumetric strain behavior was found to increase linearly with increasing axial strains under different confining pressures (Masad et al., 1996; Benda, 1995). However, Bernal et al. (1996) reported that the volume change for their shreds under low confining pressure is linear up to 5% and stabilizes under higher axial strains (Figure 2.18). The volume change under intermediate confinement is linear up to 15% strain and shows a declining rate at higher strain levels. The volume change under much higher confining pressure is essentially linear throughout the test.

All the volumetric strain values are negative, indicating that only compression is taking place. Masad et al. (1996) and Benda (1995) both observed higher compression at lower confining pressures. This is the opposite of the behaviour of loose sands where more compression takes place at higher confining pressures. Ahmed (1993) found that at low confining pressures, their samples compressed vertically with symmetrical, lateral bulging. At higher confining pressures, however, their samples compressed vertically but with very little lateral bulging.

Shear Strength Parameters

Table 2.10 summarizes the shear strength parameters of tire rubber with different particle sizes as measured in triaxial compression by different authors. The friction angles of tire crumbs reported by Benda (1995) tested under conventional triaxial compression varied from 26 to 30° at the respective strain levels ranging from 10 to 15%. Under constant σ_1 stress paths, however, friction angles for the same material ranged from 30 to 42°. Cohesion intercepts for their material was not reported since the strength envelopes were set to intercept the origin. Masad et al. (1996) found that the friction angles of their crumb material varied from 6 to 15° at axial strain levels from 10 to 20% respectively. Their cohesion intercepts, which range from 70 to 82 kPa, were unusually higher than those reported for shreds. Tire shreds, on the other hand, have cohesion intercepts ranging from 13 to 30 kPa and frictions angles from 6 to 32°. Tire shreds tested under constant σ_1 stress paths were reported as high as 60° (Benda, 1995). For comparison, the peak friction angle of uniform fine to medium sand varies from 30 to 36° (Hough, 1957). Sandy gravels have friction angles ranging from 35 to 50°.

2.5.7 Dynamic Properties

The dynamic characteristic of soils at small strains is of considerable importance for many soil dynamic problems including vibration of machine foundations, response of soil deposits and earth structures to earthquake loads, and the response of marine sediments and supported structures to ocean wave loads. The two most important parameters in any dynamic analysis involving soils are the shear modulus and the damping ratio. Both the shear modulus (G), and the damping ratio (D) are dependent on the shear strain (γ). The shear modulus is usually defined as the slope of a secant line that connects the extreme points on a hysterisis loop at a given shear strain. The damping ratio is a measure of dissipated energy versus elastic strain energy (Rollins et al., 1998). The shear modulus and damping ratio of soils are usually determined in the laboratory by means of cyclic static tests (i.e. torsional or triaxial cyclic tests) or by means of dynamic tests (i.e.

Resonant Column tests and wave propagation velocity measurements with bender elements). A brief overview of the various test methods is described in Woods (1994).

The literature pertaining to the dynamic properties of recycled tire rubber is very limited. The only relevant work done on the subject, to the author's knowledge, is the study conducted by Romero and Pamukcu (1997). In their research, crumb rubber modifier (CRM) mixed with Ottawa sand was tested under torsional excitation in a resonant column to obtain the material signature pattern. The procedure involves using a low-strain, steady state harmonic excitation at randomly selected frequencies to produce waves that propagated through the crumb rubber-sand system. The system wave response is termed the "signature pattern" which was used to predict the actual shear modulus. Then, the shear modulus was used to train an artificial neural network (ANN) to recognize previously unseen signature patterns and to improve signature characterization. In the study, the maximum shear modulus (G_{max}) of the material was selected as the property predicted. However, they reported that the method could also be used to predict other properties including damping ratio, elastic modulus, or Poisson's ratio under various conditions of confining pressure, and density ranges. CRM is fine tire crumbs with a particle size ranging from 0.6 to 1.2 mm. They were mixed with Ottawa sand (5% by mass CRM) and compacted to three dry density ranges by dry tamping. Samples were prepared and tested in a Drnevich Resonant Column under four different confining pressures ranging from 70 to 350 kPa. Each sample was tested at four strain amplitudes to determine the effect on the response. The strain amplitudes fell within the nondestructive range (less than 0.003%). Resonant frequencies were determined for each strain amplitude and was found to range from 110 to 170 Hz. The dynamic responses were obtained from randomly selected excitation frequencies other than the resonant frequency. They found that the response of the samples tested were unique and independent of strain amplitude and excitation frequency. Since the responses were unique to the samples, they are termed the signature pattern of the material and used for predicting dynamic properties. Table 2.11 presents the shear modulus of Ottawa sand-CRM mixture at various strain amplitudes and confining pressures. The shear modulus of their mixture varied from 60 to 80 MPa. These data were subsequently used as a database to train the ANN. They reported that once the network is trained, the process could be repeated on a material of unknown properties. However, the accuracy of this approach can be increased with a larger database of signature patterns thereby increasing the training set.

2.5.8 Thermal Properties

Scrap tires can be used as a thermal insulation to limit frost penetration beneath roads (Humphrey, 1995). They reported that shredded tires are about eight times better than gravel for reducing frost penetration.

Table 2.12 summarizes the thermal conductivity values of scrap tire rubber and compares them with selected materials. Shao et al. (1996) used a guarded hot plate apparatus to test scrap tire rubber with maximum particle sizes ranging from 1 to 25 mm. Measured thermal conductivity values for their material ranged from 0.097 to 0.170 W/m-°C. Their data suggests that the thermal conductivities of tire rubber increase with increasing particle size, water content, and compaction. Furthermore, the thermal conductivity was higher for their material tested under frozen conditions than when tested under thawed conditions. Humphrey and Eaton (1993a, 1993b, 1994, 1995) back calculated a thermal conductivity of 0.173 to 0.346 W/m-°C from a field trial constructed using tire shreds with a maximum size of 50 mm (2 in). They speculated that their values were higher than those found by Shao et al. (1996) since their shreds were larger and contained more steel wire. Natural and styrene butadiene rubber elastomers have thermal conductivity values of 0.0142 and 0.0247 W/m-°C respectively. (Perry et al., 1997). For comparison, the thermal conductivity of typical soils is about 1.0 W/m-°C (Alter, 1969).

2.6 Civil and Geotechnical Applications of Recycled Tire Rubber

2.6.1 Introduction

The civil and geotechnical engineering markets for tire shreds encompass a wide range of potential applications. In most situations, the material replaces or is supplemented to conventional construction material such as engineering fill, gravel, sand and clay. In order to be considered a beneficial use, the performance of the material should be either superior to the conventional material it replaces or equal with some additional benefit such as lower cost. However, before the application is recognized as acceptable, each potential application requires technical, economic and environmental considerations. The following provides a brief summary of the various civil and geotechnical applications of scrap tire rubber.

2.6.2 Highway Construction

The advantages in using recycled tire rubber in highway applications include the following (after Hughes, 1993):

1. material is lightweight,
2. replacement for more expensive or scarce aggregate,
3. high hydraulic conductivities,
4. resistance to ultraviolet radiation,
5. non-biodegradable,
6. improved thermal characteristics relative to frost penetration,
7. reduced cost,
8. technically superior to land filling.

The uses of tire rubber in highway construction consist of lightweight embankments, and asphalt road pavement.

2.6.2.1 Light Weight Embankment

Studies have shown that scrap tires are an excellent lightweight fill material in highway embankments over weak or compressible soils (Manion and Humphrey, 1992; Humphrey, 1996; Masad et al., 1996). The use of scrap tire rubber as a lightweight fill has been studied by various states including Oregon (Read et al., 1991), Virginia (Hughes, 1993) and Washington (Nightingale, 1997). In Oregon, shredded rubber tires were used as a lightweight fill to repair landslide damage under a highway embankment on Highway U.S. 42 in 1990. Approximately 580,000 tires of shredded tires replaced approximately 12,800 tons of soils. The shredded tires where placed and compacted in 0.9 m. (3 ft) lifts using a D-8 bulldozer. The Oregon project resulted in some interesting information to potential users of scrap tire technology. The loose unit weight of the tires from three different vendors varied from 3.8 to 5.2 kN/m^3 probably because of the shredding and handling processes. If long hauls are necessary to bring the material to the job site, the unit weight of the material is important. It was also mentioned that long hauls could tremendously increase the cost of recycled tire rubber. In 1992, the Virginia Department of Transportation (VDOT) utilized more than 2 million scrap tires in overpass embankments. The overpass project on State Route 199, near Interstate 64, used a mixture of shredded tires and soil to build 6 m. (20 ft) highway embankments.

The use of scrap tire rubber as roadfill has become questionable since two road embankments in Washington State spontaneously self-heated and eventually caught on fire in the Fall and Winter of 1995-96 (Nightingale, 1997). The two embankments are respectively the Falling Springs Road in Garfield County and State Route 100 at Fort Canby State Park in Ilwaco. These two incidents have resulted in an estimated use of only 3 to 5 million scrap tires in 1996 and changed the immediate outlook for scrap rubber tire use in civil engineering applications. In both instances, it was believed that the following common factors appear to separate these two road fills from the others that have been constructed across the US. These unique factors are (after Nightingale, 1997):

- The tire chip fills with a maximum depth exceeded 6.1 m (20 ft)
- Introduction or presence of significant amounts of water. The presence of moisture in the ground may have caused the steel contained in the chips to corrode. Since corrosion is basically an exothermic process, the steady heat buildup may have inadvertently ended up as an uncontrolled pyrolysis process.

Other factors that may have caused the two incidents include microbial decomposition of the tire materials, and chemical oxidation of the fine rubber particles. For whatever reasons that led to the spontaneous combustion of the two roadfills, the source is yet to be confirmed (Nightingale, 1997).

2.6.2.2 Asphalt Road Pavement

Several authors reported that a great potential for recycling vast numbers of scrap tires is to reclaim the recycled tire rubber for asphalt additives (Matthews and Silverman, 1991). This involves using the fine crumb rubber particles as a modifier (also known as crumb rubber modifier or CRM) in asphalt road pavement. The technology has been around since the 1950's in both the United States and Europe. The original developmental work, however, was undertaken in an effort to improve the performance of asphalt paving materials. The two basic methods used to incorporate CRM into asphalt pavements are the wet and dry process (Matthews and Silverman, 1991; Hughes, 1993).

In the wet process, CRM is blended with liquid asphalt cement at various ratios from 16% rubber/84% asphalt to 25% rubber/75% asphalt. The rubber and asphalt mixture reacts for about one to two hours, at temperatures between 180 to 220 °C (350 to 425 °F). The end product is called asphalt rubber or rubber-modified asphalt. The rubber in the mixture acts as a binder to hold the aggregate in place. The process, however, requires specialized and expensive machinery to pre-blend the rubber. Furthermore, asphalt rubber must be prepared properly to achieve a consistency of mix to ensure that the material can be applied smoothly during construction. Matthews and Silverman (1991) claimed that approximately 3600 tires can be utilized in each mile of a 2-lane pavement when asphalt rubber is applied as a wearing surface. The asphalt rubber can also be used as a crack/joint sealant in pavement repair or as a surface treatment.

In the dry process, a portion of the aggregate are replaced with CRM to produce Rubber-Modified Asphalt Concrete (RUMAC). To accommodate the introduction of rubber, a certain gradation of aggregate is removed, and replaced with up to 3% CRM. Unlike the wet process, the asphalt is not pre-mixed with the rubber before adding any aggregate. Instead, the rubber along with other aggregates and the asphalt are combined simultaneously. Furthermore, the rubber in RUMAC does not act as a binder, but as the aggregate, it replaces. The dry process, however, does not require specialized equipment. RUMAC can be used as both base and friction courses.

The supporters of asphalt rubber claim that adding CRM has the following advantages:

- Increased pavement flexibility than that would occur in conventional mixes. Increased flexibility means more durable pavements to better absorb the stresses placed on it.
- Reduction in reflective cracking. These are cracks that start at the base layer of the pavement and work their way to the surface.
- Decreased rutting.

Although the use of rubberized asphalt and RUMAC has been shown technically feasible, there are several disadvantages. These include:

- Very little research as been done to assess the feasibility of recycling asphalt pavements containing CRM (Hughes, 1993). That is, if recycling rubberized asphalt is not feasible, the addition of CRM will severely limit the recyclable use of Reclaimed Asphalt Pavement, which many states and the FHWA consider to be a very valuable resource.
- High production costs. The cost of asphalt pavement will increase from 50% to 100% with the addition of CRM. In addition, part of the cost of adding CRM includes the production cost of crumb rubber.

The incorporation of CRM into asphalt road pavement has been experimented or used by several states. Connecticut and Arizona have been testing and using asphalt rubber as a crack sealant since the 1970's. In California, asphalt rubber has been used on approximately 10% of pavement projects where conventional asphalt procedures cannot be used. In 1983, the state of California laid an application of the asphalt mix and found that the mix performs better on roads that experience freeze-thaw cycles as compared to conventional asphalt pavement. Furthermore, in Texas, asphalt rubber has been routinely used as a crack sealant and is reported to perform significantly better than conventional sealant. Other states such as Georgia, Michigan, Minnesota, New Hampshire, Ohio, and Pennsylvania have found that asphalt rubber pavements perform either slightly better than, or about equal, to control sections.

In 1991, the United States passed the Intermodal Surface Transportation Efficiency Act (ISTEA). Under Section 1038 of the ISTEA, it is required that all states use CRM in asphalt paving in federally funded highway construction. However, the act has not been fully implemented due to pressure from several organizations that are against using rubber-modified asphalt. Furthermore, it is speculated that if the requirements of Section 1038 of the act are fully implemented, it is estimated that 70 million tires would be required on an annual basis (Borchardt, 1991).

2.6.3 Landfill Uses

2.6.4 Leachate Drainage Media

Recent studies have reported that shredded tire rubber is a unique construction material with similar properties to the natural aggregates and granular soils often used for drainage and filtration applications. In the United States, the construction of landfill cells requires the installation of a layer at least 0.6 m (2 ft) of high permeability soil above geotechnical membranes to protect the membranes and enhance leachate drainage to collection/treatment systems (T.A.G. Resource Recovery, 1996). Several states, including Florida, currently allow the use of shredded tires as a replacement for soil in the upper foot of such systems. Shreds have been found to increase hydraulic conductivity, reduce spearing penetration of the geotechnical liner during landfill operations and provide economic savings when the required soil is not locally available (T.A.G. Resource Recovery, 1996). The shredded tires are typically no larger than 51 mm by 51 mm (2 in by 2 in) in size (Duffy, 1995). A typical design incorporating shredded tires involves the placement of a minimum 1 ft thick layer of shreds on a granular soil layer overlying the composite liner system. The shred sizes must be carefully controlled to avoid pieces containing wire protrusions that are capable of penetrating the liner. These issues present obvious design considerations and construction difficulties. Some studies also indicate that recycled tire rubber utilized in drainage applications have the potential of sorbing limited quantities of some organic and inorganic compounds, thereby retarding the transmission of these contaminants to the leachate system and cell liner.

Furthermore, it was reported that the tire shred layer has a satisfactory range of hydraulic conductivity under typical solid-waste landfill conditions (Edil et al., 1992).

2.6.5 Daily Landfill Cover

Tire shreds have been used as daily cover in operating landfills in several states (T.A.G. Resource Recovery, 1996). The shreds can offer economic advantages where local borrow areas are not available. However, this alternative disposal method has a low value use with practical operating restrictions. Shreds that contain protruding steel wires present obvious placement difficulties.

2.6.6 On-Site Sewage Disposal System

On-site sewage disposal systems generally utilize a leaching field constructed of crushed stone to enhance biological treatment and liquid distribution. The Vermont Department of Environmental Conservation commissioned a preliminary evaluation of scrap tire shreds as an alternative to crushed stone in on-site sewage disposal systems (Envirologic, Inc., 1990). The use of tire shreds in sewage disposal systems would conserve the use of stone, which is a limited resource and provide a market for waste tires. The report indicated that an average household would use approximately 23 m^3 (30 yd^3) of tire shreds, representing approximately 1,200 passenger tires. The study examined the physical performance characteristics of nominal 2 in tire shreds with and without wires and compared them to 3/4 in to 1/2 in crushed stone. Results indicate that tire shreds have superior ability to absorb load variations to leach field. Additional tests demonstrated the ability of tire shreds to absorb hydraulic shock forces associated with pressurized water discharge without erosion of surface sand cover. There was no significant difference in susceptibility to cover material intrusion, but both materials can be negatively impacted by the absence of a geotechnical fabric cover. Tests also indicated that tire shreds should be compacted to prevent post-construction settlement. The report recommends that shreds and stone be double washed to prevent wash down of iron, fines and dust that might obscure the infiltrative surface.

The design and construction recommendations for using tire shreds in on-site sewage disposal systems include the following:

1. Use the same design criteria as currently established for use with stone.
2. Tires should be washed free of iron, fines and dust as placed.
3. Prior to lateral installation, compact shredded tires with a single pass of a rubber tired or tracked loader, however, caution should be used to avoid puncturing of rubber tires by wire protrusions.
4. Cover shredded tires with filter fabric before placing cover material.
5. Since shoveling tire shreds for lateral trenches can be more difficult than stone, shred should be placed to the invert lateral elevation, then filled to final height after lateral installation.

The report also addressed the leaching of contaminants from tire shreds and rubber products, and concluded that the leachate would not pose a significant source of groundwater contamination. Furthermore, the physical characteristics of tire shreds are sufficiently alike to serve as a replacement for stone in on-site disposal systems. The leachability of scrap tire rubber is discussed in detail in Chapter 4.

2.6.7 Soil Amendment

Tire crumbs has recently been used on athletic fields in the US. It is installed for total field rehabilitation to improve appearance, turf durability, resiliency and surface drainage. This application generally involves the use of 1/4 to 1/2 in tire crumbs. Proper mixing to a depth of at least 6 in is a critical component of successful installation. Installation cost is typically \$1.00 US/ft^2 including proper design and purchase of material. The field is useable within 4 to 6 weeks once turf roots have become established. Other applications use whole, slices or shredded tires as a subsurface layer to trap water. However, the leachability of recycled tire rubber must be considered. Consequently, most states limit the use of recycled tire rubber to applications that do not trap water for extended periods and in areas above the water table.

2.7 Environmental Considerations

The various disposal methods regarding the utilization of recycled tire rubber have generated many environmental concerns. The use of whole-scrap-tires and TDF as fuel raises the question of air pollution. However, based on Oxford Energy's experience, controlled emissions from their Modesto Energy Project compare extremely favorable to controlled emissions from electric utility plants powered by traditional fuels (Clark et al., 1991). Furthermore, it was reported that the use of TDF in pulp and paper mills can be environmentally positive, as indicted by a series of performance tests which concluded that the use of TDF as a supplement in hog fuel boilers enhances combustion of wood waste without necessitating the use of other fossil fuels such as coal (Clark et al., 1991).

Water quality effects of using scrap tires in civil engineering projects have been investigated by Edil et al. (1990), and Humphrey et al. (1997). Edil et al. (1990) found that tire chips show no likelihood of being a hazardous waste and tire leaching test data indicate that scrap tires have little or no effects on ground water. Overall, it was concluded that shredded tires leach very small amounts of substances compared to other wastes. However, field studies were inconclusive, indicating the need for further work in this area. Further work regarding water quality effects were conducted by Humphrey et al. (1997). They conducted two field trials to monitor the effect on water quality of tire shreds placed above the groundwater table. In their study, control wells were used to distinguish the substances naturally present in groundwater from those that leached from the shreds. They concluded that most of the inorganic substances that can potentially leach from tires are already naturally present at low levels in groundwater.

Table 2.1 Typical composition of rubber tire (after Dods et al., 1983)

Component	% by Weight
Styrene-butadiene rubber (SBR)	62.1
Carbon black	31.0
Extender oil	1.9
Zinc oxide	1.9
Stearic acid	1.2
Sulfur	1.1
Accelerator	0.1

Table 2.2 Typical crumb rubber pricing (after Kohler, 1996)

Tire Crumb Size (US Sieve Designation)	Price range ($ US/lb)
4.75 mm (No. 4)	0.07 to 0.09
2 mm (No. 10)	0.10 to 0.12
600 μm (No. 30)	0.17 to 0.19
425 μm (No. 40)	0.19 to 0.25
180 μm (No. 80)	0.33 to 0.35

Table 2.3 Summary of particle size, shape and distribution of tire crumbs and shreds

Material	Particle Size (US sieve designation)	Particle Shape	Gradation	C_c	C_u	Methods	Supplier	References
tire crumbs and shreds	0.85 to 12.5 mm (No. 20 - 1/4")	-	uniform	1.26	2.14	ASTM D 422	-	Cecich et al., 1996
tire crumbs	< 4.75 mm (No. 4 Minus)	-	uniform	1.63^2	3.20^2	ASTM C 136	-	Masad et al., 1996
	2 mm^1 (No. 10)	angular	uniform	1.05^2	1.45	-	Baker Rubber	Benda, 1995
tire shreds	9.5 mm^1 (3/8")	irregular	uniform	1.02^2	3.28	-	RCI	Benda, 1995
	9.5 mm^1 (3/8 in)	elongated	uniform	1.20^2	2.53	-	Palmer Shredding	Benda, 1995
	19 mm^1 (0.75 in)	angular	uniform	1.20^2	1.53	-	Palmer Shredding	Benda, 1995
	38 mm^1 (1.5 in)	flaky	uniform	1.08^2	1.67	-	Palmer Shredding	Benda, 1995
Ottawa sand	-	round	uniform	-	1.1	-	-	Hough, 1969
clean, uniform sand (fine or medium)	-	-	uniform	-	1.2 to 2.0	-	-	Hough, 1969

[1] Steel components removed.

[2] Calculated from particle size distribution curve in Figure 2.4

Table 2.4 Specific gravities of scrap tires and select materials

Material	Particle Size (US Sieve Designation)	Specific gravity	Methods	Note	References
tire crumbs	0.6 to 1.18 (No. 30 - No. 16)	1.20	ASTM D 854	fabric and steel removed	Kershaw and Pamukcu, 1997
	2.0 (No. 10)	1.12	AASHTO T 85-91 & T 100-93	-	Benda, 1995
	0.1 to 4.8 0.2	1.07	ASTM D 854	-	Masad et al., 1996
	9.5 (3/8 in)	1.18	AASHTO T 85-91 & T 100-93	-	Benda, 1995
tire shreds	19.0 (0/75 in)	1.08	AASHTO T 85-91 & T 100-93	-	Benda, 1995
	30.0	1.08	-	-	Newcomb and Drescher, 1994
	38.0 (1/5 in)	1.11	AASHTO T 85-91 & T 100-93	steel removed	Benda, 1995
	6 to 25	1.22	-	-	Park et al., 1996
	50 x 75	1.13 to 1.36	-	depending on metal content	Edil and Bosscher, 1994
	-	1.15	-	without metal content	Edil and Bosscher, 1994
sands	-	2.63 to 2.67	-	-	Das, 1982
styrene butadiene rubber (SBR)	-	0.91	ASTM D 792	component of modern tires	Perry et al., 1997
natural rubber (NR)	-	0.93	ASTM D 792		Perry et al., 1997
reclaimed SBR	-	1.18	-	-	Borchardt, 1991

Table 2.5 Summary of compaction results for recycled tire rubber and granular soils

Material	Particle Size (US Sieve Designation)	Compaction method	γ_d (kN/m^3)	References
tire crumbs	2 mm (No. 10)	AASHTO Test Method T 99-93	5.2	Benda, 1995
	< 4.75 (No. 4 minus)	Nonstandard A[7]	6.6[a]	Masad et al., 1996
	< 4.75 (No. 4 minus)	Vibration[2]	4.4[b]	Masad et al., 1996
	< 4.75 (No. 4 minus)	Nonstandard B[8]	6.2[c]	Masad et al., 1996
	6.3 mm (1/4 in)	Modified[1]	5.3	Ahmed, 1993
	6.3 mm (1/4 in)	Standard[3]	5.8	Ahmed, 1993
	6.3 mm (1/4 in)	Vibration[2]	5.3	Ahmed, 1993
tire crumbs /shreds	0.85 to 12.5 mm (No. 20 - 0.5 in)	Modified[1]	5.5 to 5.9	Cecich et al., 1996
tire shreds	12.5 mm	Vibration[2]	4.6	Ahmed, 1993
	16 mm	Vibration[2]	4.8	Ahmed, 1993
	25 mm	Vibration[2]	4.6 to 5.1	Ahmed, 1993
	50 x 75 mm	Standard[3] (6 in & 12 in mold)	5.5 to 5.8	Edil and Bosscher, 1994
	25 to 75 mm	Loose[4]	4.9 to 3.3	Humphrey et al., 1992, 1993; Humphrey and Sandford, 1993
	50 mm	Loose[4]	4.0	Manion and Humphrey, 1992; Humphrey and Manion, 1992
	25 to 50 mm	Loose[4]	4.8 to 4.6	Ahmed, 1993; Ahmed and Lovell, 1993
	12.5 to 25 mm	Vibration[2]	4.6 to 4.9	Ahmed, 1993; Ahmed and Lovell, 1993
	12.5 to 25 mm	50% Standard[5]	6.3 to 6.0	Ahmed, 1993; Ahmed and Lovell, 1993
	25 to 75 mm	60% Standard[6]	6.1 to 6.3	Humphrey et al., 1992, 1993; Humphrey and Sandford, 1993
	50 mm	60% Standard[6]	6.1	Humphrey et al., 1992, 1993; Humphrey and Sandford, 1993
	30 mm	Loose[4]	4.9	Newcomb and Drescher, 1994
	50 mm	Loose[4]	2.3 to 3.4	Newcomb and Drescher, 1994
	38 mm	AASHTO Test Method T 99-93	5.9	Benda, 1995
	19 mm	AASHTO Test Method T 99-93	5.6	Benda, 1995
	9.5 mm	AASHTO Test Method T 99-93	5.0 to 5.9	Benda, 1995

Table 2.5 Continued

Material	Material size (mm)	Compaction method	γ_d (kN/m^3)	References
silty sand and gravel	-[9]	-[9]	14.0 to 22.9	Hough, 1969
clean, uniform sand	-[9]	-[9]	13.0 to 18.5	Hough, 1969
	-[9]	-[9]	14.5 to 17.3	Hough, 1969
Ottawa sand	-[9]	Nonstandard A[7]	17.7[a]	Masad et al., 1996
	-[9]	Vibration[2]	15.3[b]	Masad et al., 1996
	-[9]	Nonstandard B[8]	17.4[c]	Masad et al., 1996

[1] Modified: Impact compaction with compaction energy of 2693 kJ/m^3.
[2] Vibration: ASTM Test Method D 4253.
[3] Standard: Impact compaction with compaction energy of 593 kJ/m^3.
[4] Loose: no compaction; tire rubber loosely placed into compaction mold.
[5] 50% Standard: Impact compaction with compaction energy of 296 kJ/m^3.
[6] 60% Standard: Impact compaction with compaction energy of 356 kJ/m3.
[7] Nonstandard A: Compaction in 12 layers in a mold; each layer restrained with 12 kg. load while sides tapped sharply 15 to 25 times.
[8] Nonstandard B: Similar to Nonstandard A, but with no load and side tapping.
[9] Not specified
[a] Calculated from e_{min}.
[b] Calculated from e_{max}.
[c] Prepared at 90% relative density.

Table 2.6 Summary of Compressibility results for tire crumbs, shreds, and select materials

Material	Particle Size (US Sieve Designation)	γ_d (kN/m^3)	Compaction	e_o	C_c ($\Delta\sigma_v$, kPa)	C_s ($\Delta\sigma_v$, kPa)	C_r ($\Delta\sigma_v$, kPa)	References
tire shreds	30 mm	4.9	Loose[1]	1.32	0.50 (10 to 400)	0.27 (400 to 20)	-	Newcomb and Drescher, 1994
	12.5 to 50 mm (0.5 to 2 in)	6.0 to 6.3	50% Standard[2]	-	0.11 to 0.14 (14 to 28) 0.18 to 0.19 (28 to 70) 0.19 to 0.22 (70 to 138)	0.11 to 0.12 (70 to 7)	0.13 to 0.15 (28 to 70) 0.17 to 0.19 (70 to 138)	Ahmed, 1993
	25 to 50 mm (1 to 2 in)	6.2 to 6.4	Standard[3]	-	0.12 (14 to 28) 0.16 (28 to 70) 0.19 to 0.20 (70 to 138)	0.10 to 0.11 (70 to 7)	0.13 to 0.14 (28 to 70) 0.17 (70 to 138)	
	25 to 50 mm (1 to 2 in)	6.6 to 6.7	Modified[4]	-	0.11 to 0.12 (14 to 28) 0.16 (28 to 70) 0.18 to 0.21 (70 to 138)	0.10 (70 to 7)	0.13 to 0.14 (28 to 70) 0.19 to 0.19 (70 to 138)	
	25 to 50 mm (1 to 2 in)	4.6 to 4.8	Loose[1]	-	0.20 to 0.21 (14 to 28) 0.23 (28 to 70) 0.25 (70 to 138)	0.13 to 0.14 (70 to 7)	0.14 (28 to 70) 0.21 (70 to 138)	
wood chips	25 mm	1.6	Loose[1]	2.03	0.35 (20 to 4000)	0.034 (4000 to 20)	-	Newcomb and Drescher, 1994
granular fill	2 mm	18.1 to 22.1	Loose[1]	0.14 to 0.85	0 to 0.19 (-)	-	-	Newcomb and Drescher, 1994

[1] Loose: No compaction
[2] 50% Standard: 50% of standard Proctor Energy = 296 kJ/m^3
[3] Standard: Standard Proctor Energy = 593 kJ/m^3
[4] Modified: Modified Proctor Energy = 2693 kJ/m^3

C_c = compression index
C_s = swelling index
C_r = recompression index

Table 2.7 Elastic parameters of tire crumbs and shreds

Material	Particle Size (mm)	σ_3 or σ_1 (kPa)	ε_1 (%)	ν	K_o	E (kPa)	Methods	Comments	References
tire crumbs	2 (No. 10)	35 to 45	5 to 10	0.26 to 0.30 0.25 to 0.26 0.30 to 0.32	0.36 to 0.42 0.33 to 0.35 0.36 to 0.42	455 to 820	triaxial compression test		Benda, 1995
tire shreds	38 (1.5 in)	35 to 45	5 to 15	0.33 0.32 0.33	0.50 0.47 to 0.48 0.49	579 to 689			
	19 (0.75 in)	35 to 45	5 to 15	0.23 to 0.28 0.31 to -^{1} 0.23 to 0.26	0.30 to 0.39 0.45 to -^{1} 0.31 to 0.37	427 to 586			
	9.5 (0.375 in)	35 to 45	5 to 15	0.26 0.24 to 0.26 0.27	0.36 to 0.33 0.31 to 0.34 0.36 to 0.37	345 to 483			
		35 to 45	5 to 15	0.27 0.29 to 0.31 0.28 to 0.29	0.37 to 0.34 0.41 to 0.45 0.37 to 0.40	455 to 607			
	< 50 mm (2 in minus)	< 160	< 30%	0.49^4	0.98^4	76^2 to 230^3	one-dimensional compression tests	samples compacted at 60% standard Proctor	Manion and Humphrey, 1992
		> 160	> 30%	0.30^4	0.44^4	-			
Ottawa sand, medium, rounded	-	101	-	-	-	207,000 to 669,000	triaxial compression tests	repeated loading	Chen, 1948
well graded sand, coarse, subangular						103,000 to 193,000			

[1] Test terminated before 15% axial strain was reached
[2] Initial tangent
[3] Secant tangent at ε_1 = 20%
[4] Average values

Table 2.8 Summary of hydraulic conductivities of recycled tire rubber

Material	Particle size	γ_d (kN/m^3)	k (cm/s)	Methods	Comments	Reference
tire crumbs and shreds	0.85 to 12.5 mm	5.5 to 5.9	0.033 to 0.034	ASTM D2434	Constant head permeability at 0 kPa overburden pressure	Cecich et al., 1996
tire crumbs	< 4.75 mm	6.2	0.0020 to 0.00049	Triaxial cell apparatus	Confining pressures from 150 to 350 kPa	Masad et al., 1996
tire shreds	62.5 mm	4.6	5.3 to 23.5	Large-scale permeameter	-	Bressett, 1984
	62.5 mm	6.0	2.9 to 10.9			
	50 x 75 mm	4.0	0.65 to 0.44		Overburden pressures from 0 to 100 kPa	Edil and Bosscher, 1994
	50 mm	4.6	4.9 to 59.3		-	Bressett. 1984
	50 mm	6.0	3.8 to 22			
	50 mm	6.3	7.7		samples compacted at 60% standard Proctor; compression up to 25% axial strains	Humphrey et al., 1992, 1993
	50 mm	8.2	2.1			
	75 mm	5.9	15.4			
	75 mm	7.9	4.8			
	37.5 mm	6.1	6.9			
	37.5 mm	7.9	1.5			
	37.5 mm	-[1]	0.58		-	Ahmed, 1993
coarse gravel	-[1]	-[1]	0.11	capillarity tests by capillarimeter and by soil filled tubes	-	Lane and Washburn, 1946
sandy gravel			0.016			
fine gravel			0.0071			

[1] Not specified

Table 2.9 Summary of shear strength parameters for tire crumbs and shreds measured in direct shear

Material	Particle size	c (kPa)	ϕ (°)	ΔH (mm)	γ_d (kN/m^3)	Methods	Supplier	Comments	References
tire crumbs and shreds	0.85 to 12.5 mm (No. 20 to 1/2 in)	7	27	15	6.0	ASTM D 3080	-[2]	conducted under normal stresses 4, 14, and 28 kPa; shear strength parameters obtained at deformation equal to 15% sample diameter	Cecich et al., 1996
	2 to 38 mm (No. 10 to 1.5 in)	4 to 11	19 to 26	30	-[2]	ASTM D 3080	Palmer Shredding, RCI, and Baker Rubber	conducted using a 12 in shear box, normal stresses not reported	Benda, 1995
tire shreds	50 x 50 mm (2 x 2 in)	-[2]	17 to 35[1]	13 to 64[1]	5.9	ASTM D 3080	BFI Tire Recyclers	conducted under normal stresses 7, 24, and 54 kPa	Bernal et al., 1997
	50 to 75 mm (2 x 3 in)	8	21	30	5.8	AASHTO T 236	Pine State	conducted under normal stresses 12, 24, and 48 kPa; 300 mm (12 in) shear box	Humphrey et al., 1992
		11	19	30	5.2	AASHTO T 236	Palmer Shredding		
		9	25	30	5.7	AASHTO T 236	F&B Enterprises		
		4	26	40	5.5	AASHTO T 236	Pine State	conducted under normal stresses 12, 24, and 36 kPa; 400 mm (16 in) shear box	

[1] Obtained from interpolation of Figure 2.13
[2] Not reported

Table 2.10 Summary of shear strength parameters for tire crumbs and shreds measured in triaxial compression

Material	Particle size mm (US sieve designation)	c (kPa)	ϕ (°)	ε_1 (%)	γ_s (kN/m³)	Methods	Supplier	Comments	References
tire crumbs	< 4.75 (No. 10 Minus)	70	6	10	6.2	conventional CD triaxial compression loading	-	confining pressures: 150, 200, 250, 300, and 350 kPa	Masad et al., 1996
		71	11	15					
		82	15	20					
	2 (No. 10)	0	25.8	10	5.2	conventional CD triaxial compression loading	Baker Rubber	confining pressures: 35, 45, and 55 kPa	Benda, 1995
			30.4	15					
			-[1]	20					
	2 (No. 10)	0	30.1	1	5.2	CD triaxial compression unloading	Baker Rubber	conducted under constant σ_1 stress paths; confining pressures 35, 45, and 55 kPa	
			41.8	5					
			-[1]	10					
tire shreds	12.5 (1/2 in)	13	6	5	6.1 to 6.3	conventional CD triaxial compression loading	-	confining pressures 36, 88, and 199 kPa; samples compacted with standard Proctor energy	Ahmed, 1993
		23	11	10					
		29	16	15					
		36	20	20					
	25.4 (1 in)	14	10	5	6.3		-	confining pressures 32, 99, and 199 kPa; samples compacted with 50% standard Proctor energy	
		25	13	10					
		33	18	15					
		37	23	20					
	25.4 (1 in)	15	8	5	6.3 to 6.5		-	confining pressures 32, 114, 198, and 301 kPa; samples compacted with standard Proctor energy	
		22	14	10					
		27	20	15					
		33	25	20					
	25.4 (1 in)	17	7	5	6.6 to 6.9		-	confining pressures 32, 99, and 199 kPa; samples compacted with 50% modified Proctor energy	
		25	14	10					
		33	20	15					
		39	25	20					
	38 (1.5 in)	0	21.1	10	5.9	conventional CD triaxial compression loading	Palmer Shredding	confining pressures: 35, 45, and 55 kPa	Benda, 1995
			29.5	15					
			35.5	20					
	19 (0.75 in)	0	21.4	10	5.6		Palmer Shredding		
			28.4	15					
			34.1	20					
	9.5 (0.375 in)	0	17.2	10	5.0		Palmer Shredding		
			23.2	15					
			31.2	20					

[1] Test terminated before axial strains reached

Table 2.10 Continued

Material	Particle size mm (US sieve designation)	c (kPa)	ϕ (°)	ε_1 (%)	γ_d (kN/m³)	Methods	Supplier	Comments	References
	9.5 (0.375 in)	0	20.6 27.0 32.1	10 15 20	5.9	conventional consolidated-drained triaxial compression loading	RCI	confining pressures: 35, 45, and 55 kPa	Benda, 1995
tire shreds	38 (1.5 in)	0	32.6 48.5 57.0	1 5 10	5.9	consolidated-drained triaxial compression unloading	Palmer Shredding	confining pressures reduced from initial consolidation pressure of 35, 45, and 55 kPa until shear failure or capacity of test apparatus was reached	Benda, 1995
	19 (0.75 in)	0	29.1 44.0 52.3	1 5 10	5.6		Palmer Shredding		
	9.5 (0.375 in)	0	30.1 47.0 -	1 5 10	5.0		Palmer Shredding		
	9.5 (0.375 in)	0	29.8 42.7 -	1 5 10	5.9		RCI		

Table 2.11 Shear modulus for Ottawa sand-CRM mixture determined from resonant column testing (after Romero and Pamukcu, 1997)

ρ_d (kg/m3)	σ_3 (kPa)	Shear Strain, ε (%)	G (MPa)
1628	140	0.00040	82.2
		0.00073	82.2
		0.00140	82.2
		0.00240	82.2
1540	140	0.00019	66.2
		0.00041	64.9
		0.00077	64.9
		0.00140	64.9
1575	140	0.00054	78.6
		0.00097	77.3
		0.00180	77.3
		0.00300	76.0
1543	140	0.00044	70.6
		0.00088	69.3
		0.00160	69.3
		0.00280	68.1
1641	140	0.00044	77.7
		0.00086	77.7
		0.00160	77.7
		0.00280	75.0

Table 2.12 Measured thermal conductivities of tire rubber and selected materials

Material	Particle Size mm (US Sieve Designation)	λ (W/m-°C)	Methods	Comments	References
tire crumbs	1 (No. 18)	0.097	ASTM C 177	low compaction; thawed state; less than 1% moisture content; contained steel belts	Shao et al., 1995
tire shreds	25 (1 in)	0.171	ASTM C 177	high compaction; frozen state; 5% moisture content; contained no steel belts	Shao et al., 1995
	50 (2 in)	0.173 to 0.346	back calculation from field trial	contained steel bead wire and steel belts	Humphrey and Eaton, 1993a, 1993b, 1994, 1995
NR (natural rubber)	-	0.142	ASTM C 177	component of modern automobile tires	Perry et al., 1997
SBR (styrene butadiene rubber)	-	0.247	ASTM C 177		Perry et al., 1997
SBR, unfilled vulcanisate	-	0.192 to 0.247	-		Roff et al., 1971
Polystyrene foam	-	0.036	-	-	Alter, 1969
Air	-	0.024	-	dry, still	Johnston, 1981
Air	-	0.026	-	20°C, 1 atm.	Van Wijk, 1963
Snow	-	0.086	-	loose	Johnston, 1981
Snow	-	0.121	-	compacted	Johnston, 1981
Ice	-	2.66	-	-40°C	Alter, 1969
Ice	-	2.32	-	-20°C	Van Wijk, 1963
Ice	-	2.23	-	0°C	Johnston, 1981
Water	-	0.56	-	0°C	Alter, 1969
Water	-	0.58	-	10°C	Weast et al., 1984
Water	-	0.60	-	20°C	Van Wijk, 1963
Clay	-	0.90	-	dry	Alter, 1969
Sand	-	1.10	-	dry	Alter, 1969
Wood	-	0.12 to 0.17	-	-	Alter, 1969
Wood fibre	-	0.036	-	-	Johnston, 1981

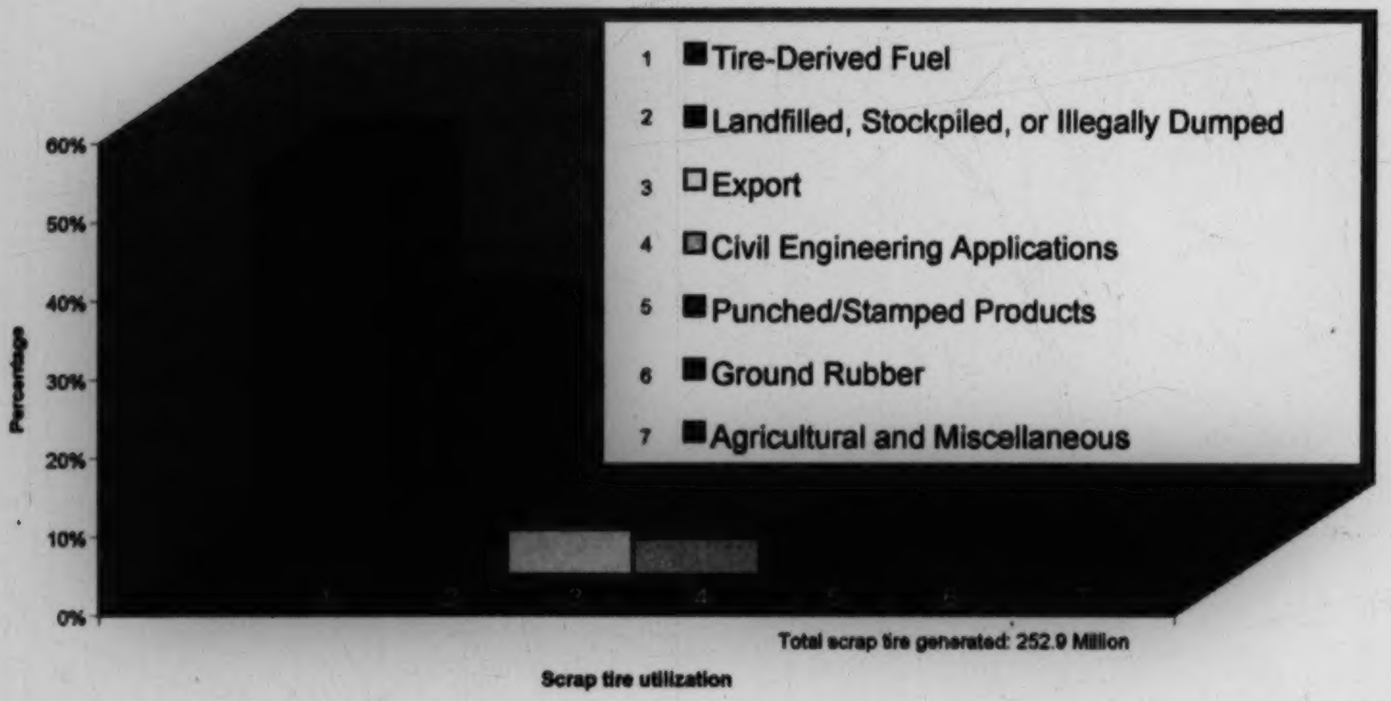

Figure 2.1 Scrap tire utilization in the United States for the year, 1995 (modified from Bernal et al., 1996)

Figure 2.2 Crackermill, Midwest Tire Processors of Vulcan, AB. (photo by Hong, 998)

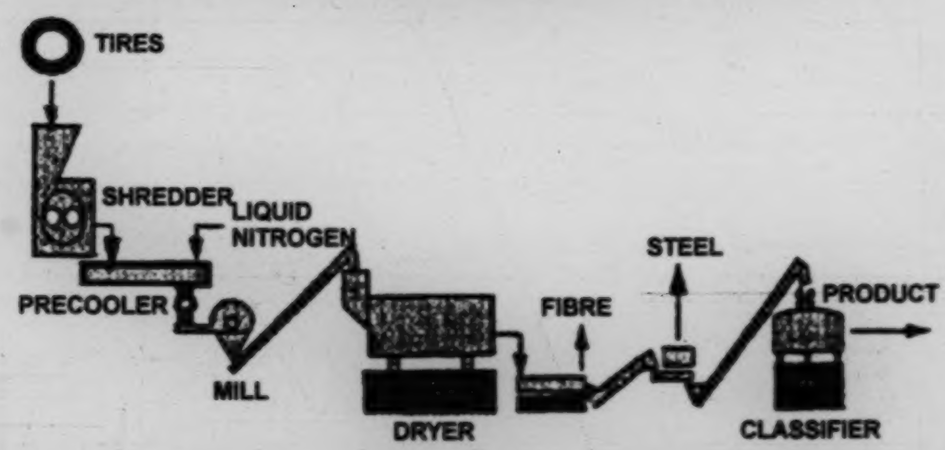
TIRES
SHREDDER
LIQUID NITROGEN
PRECOOLER
MILL
DRYER
FIBRE
STEEL
PRODUCT
CLASSIFIER

Figure 2.3 Schematic of a typical tire grinding system using the cryogenic process for producing tire crumbs (modified from Kohler, 1996)

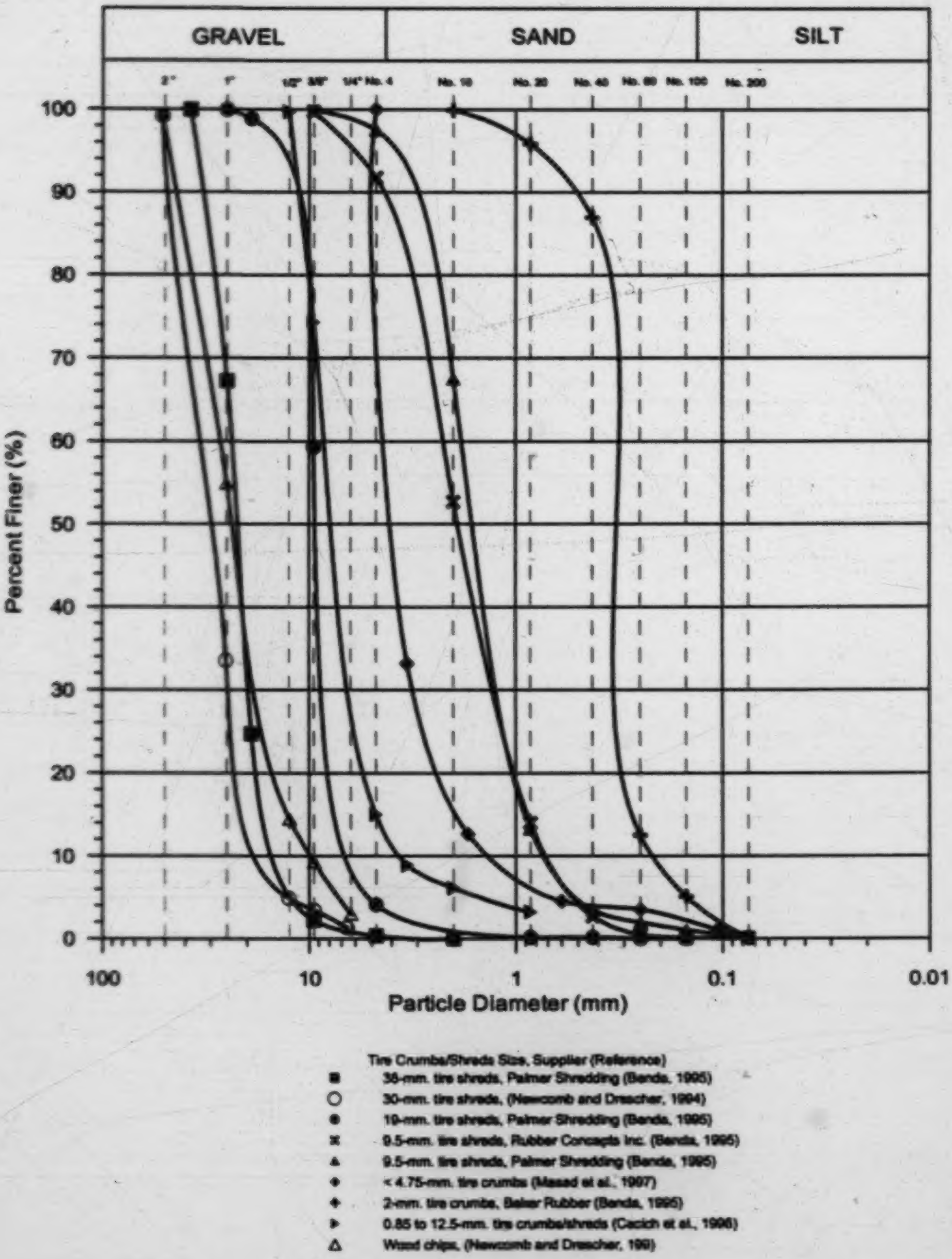

Figure 2.4 Particle-size distribution of tire crumbs and shreds as determined by various authors

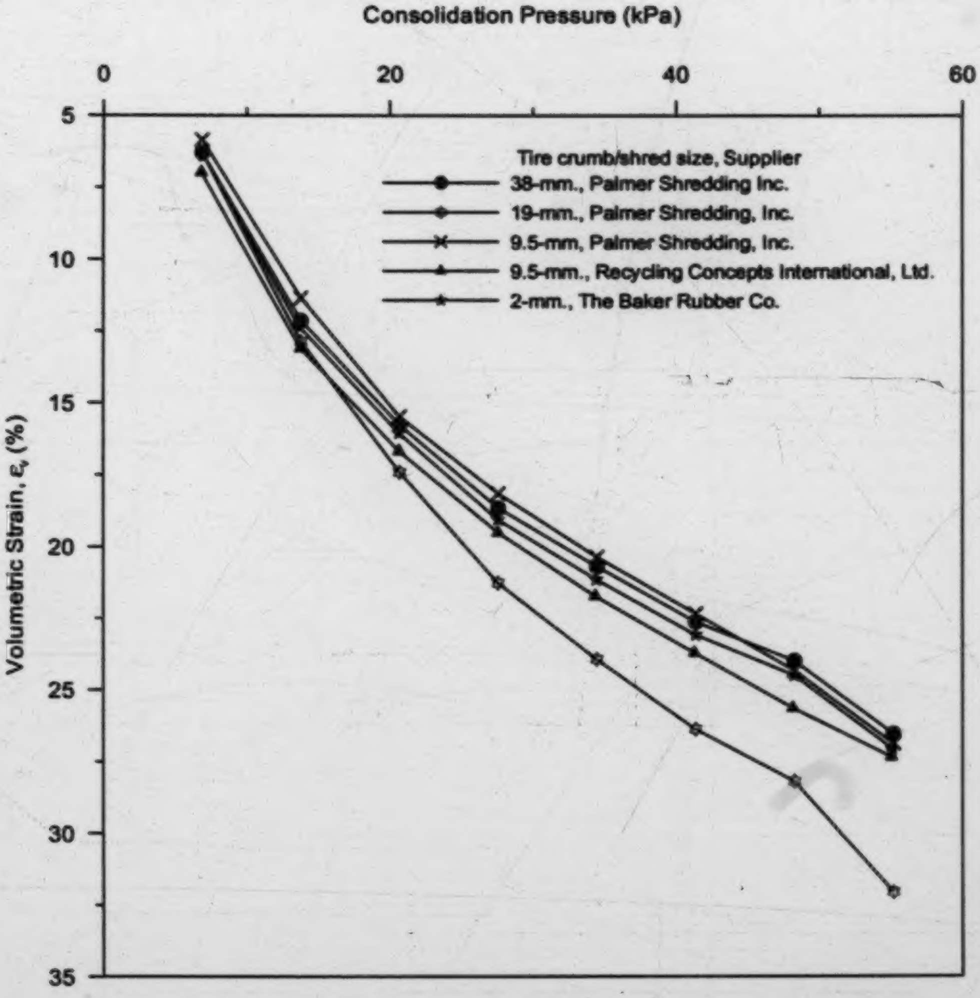

Figure 2.5 Triaxial consolidation response of recycled tire rubber with different grain sizes under isotropic stress conditions (modified from Benda, 1995)

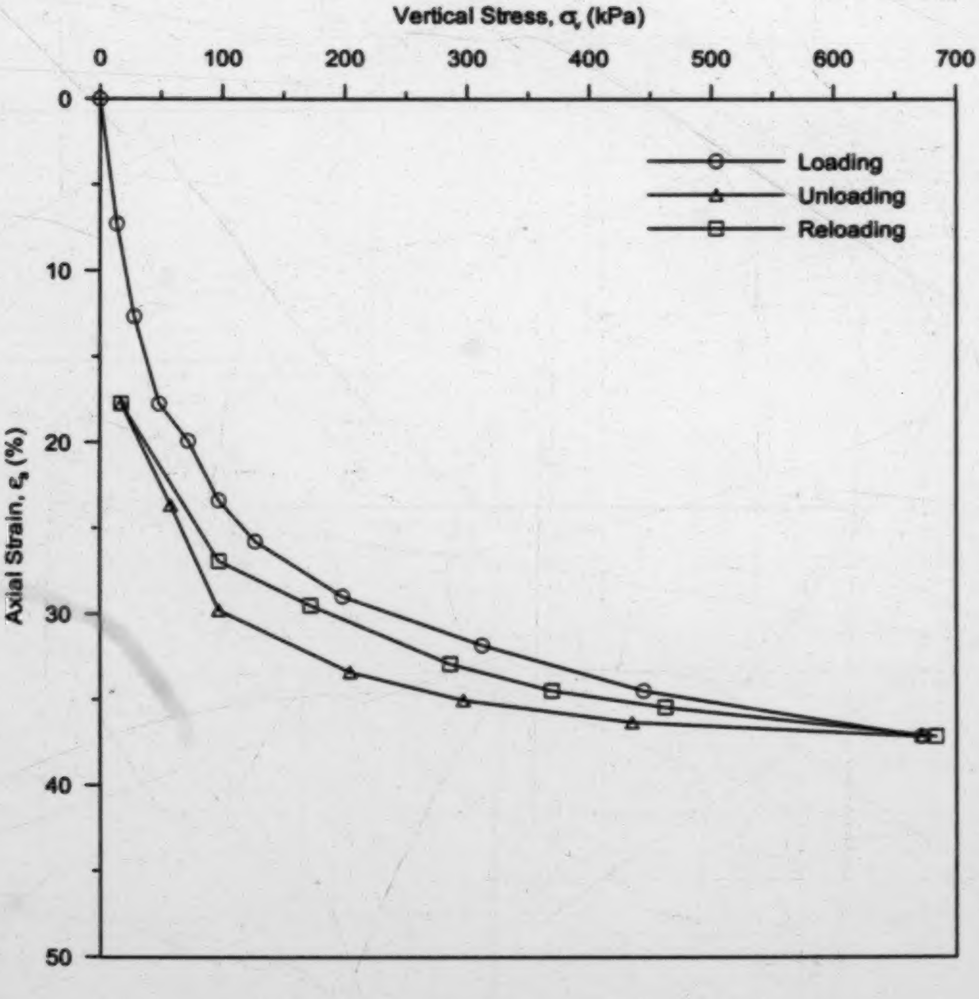

Figure 2.6 Confined stress-strain response of 50 x 70 mm tire shreds (modified from Edil and Bosscher, 1994)

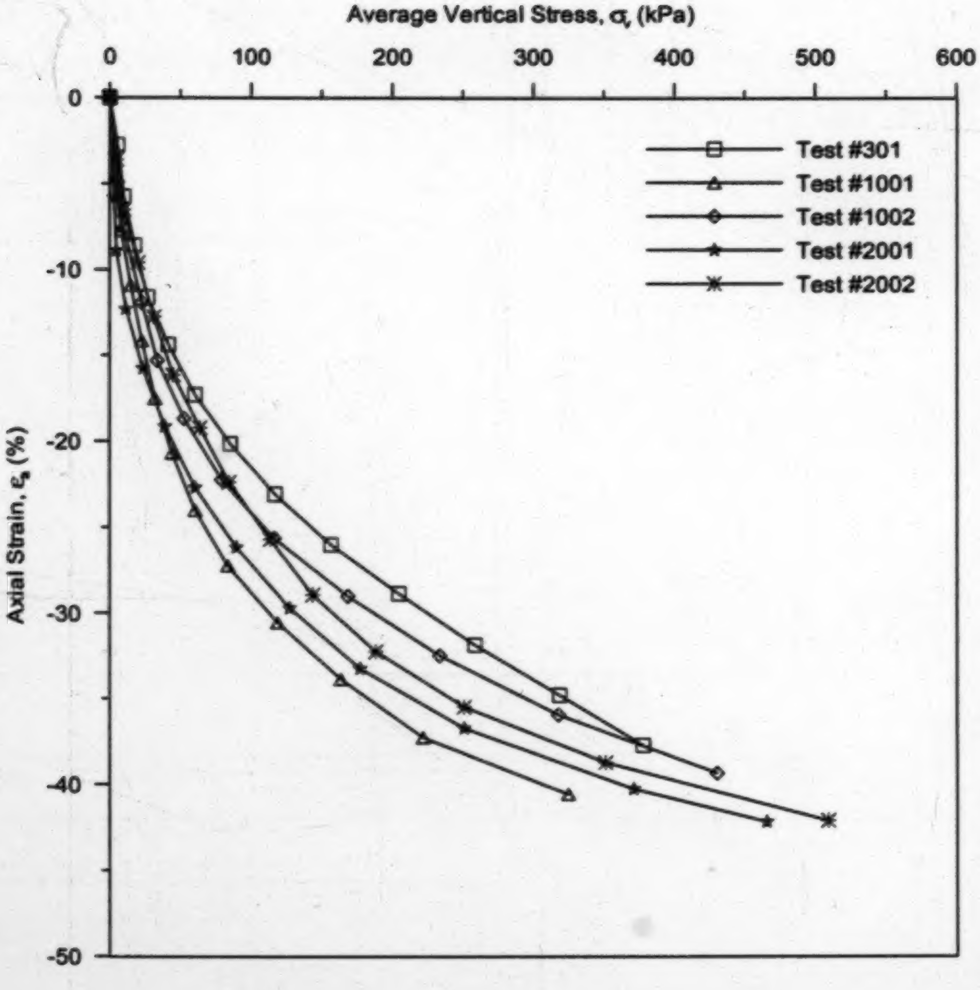

Figure 2.7 Confined initial loading stress-strain curve for 3 in minus tire shreds (modified from Manion and Humphrey, 1992)

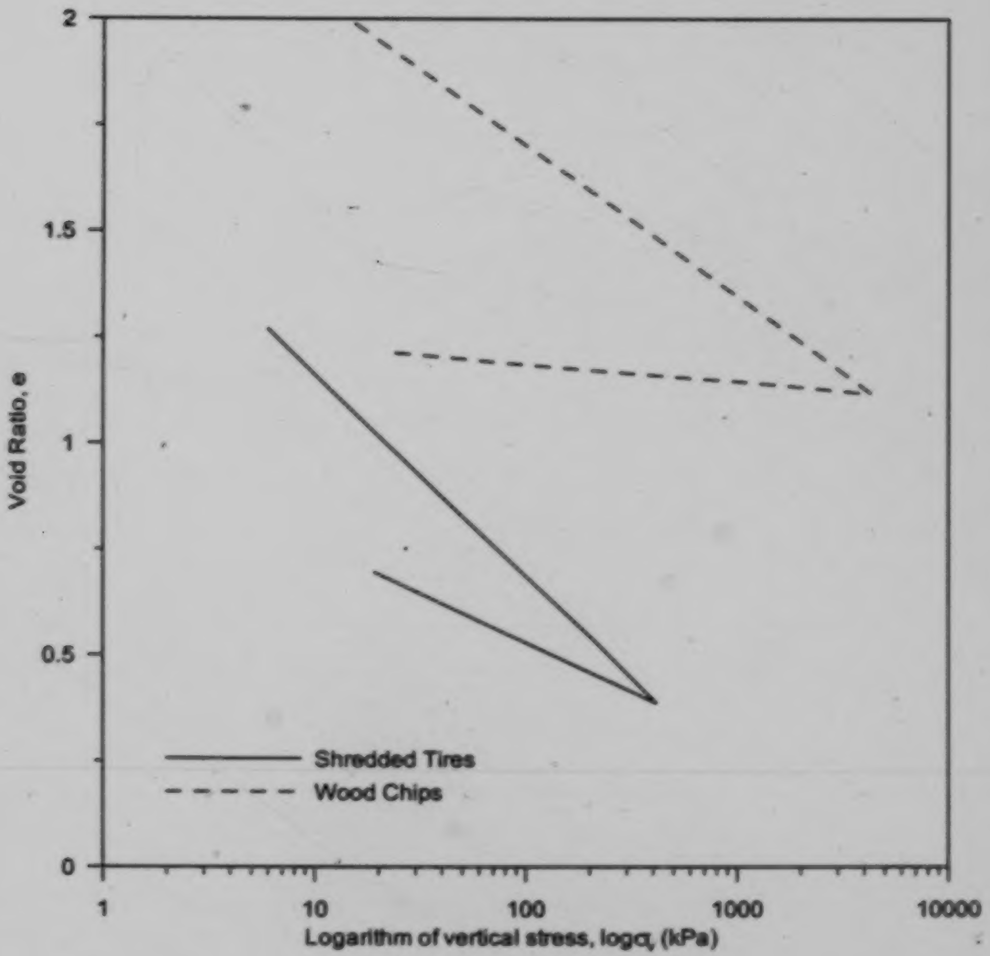

Figure 2.8 Void ratio versus vertical stress for shredded tires and wood chips (modified from Newcomb and Drescher, 1994)

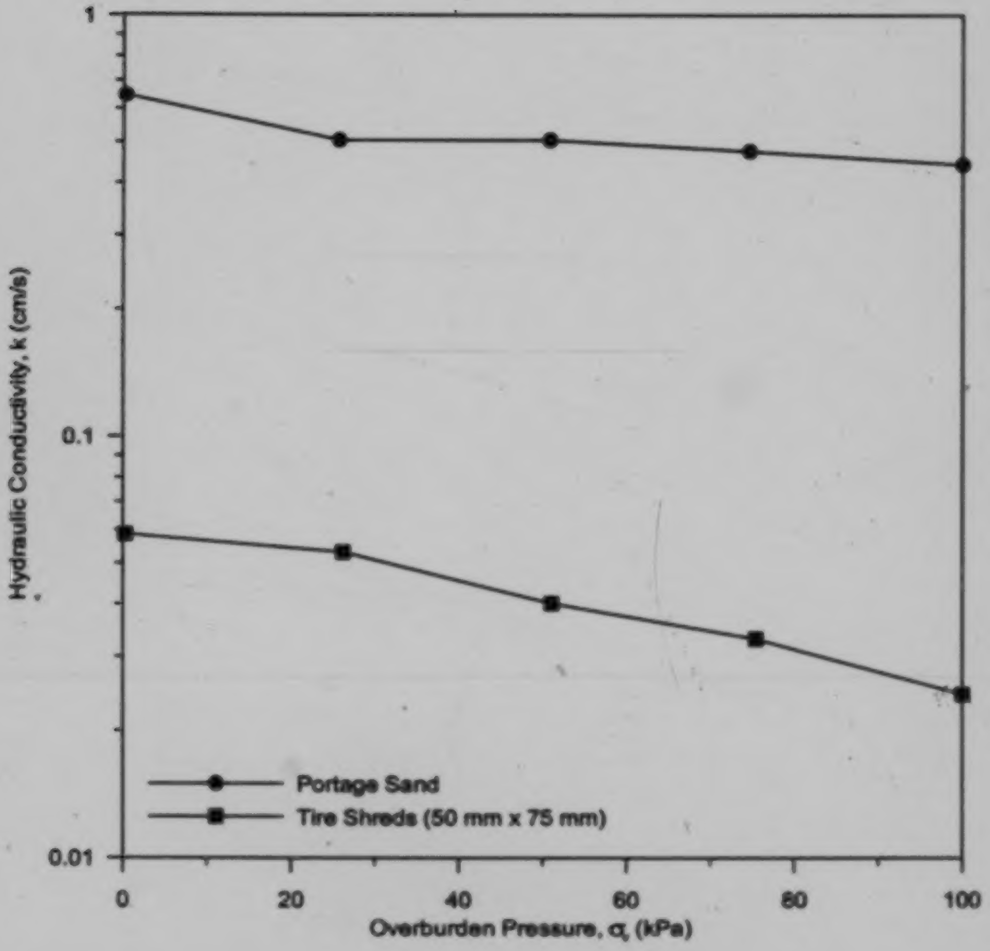

Figure 2.9 Hydraulic conductivity of tire shreds and clean sands at under various overburden pressures (modified from Edil and Bosscher, 1994)

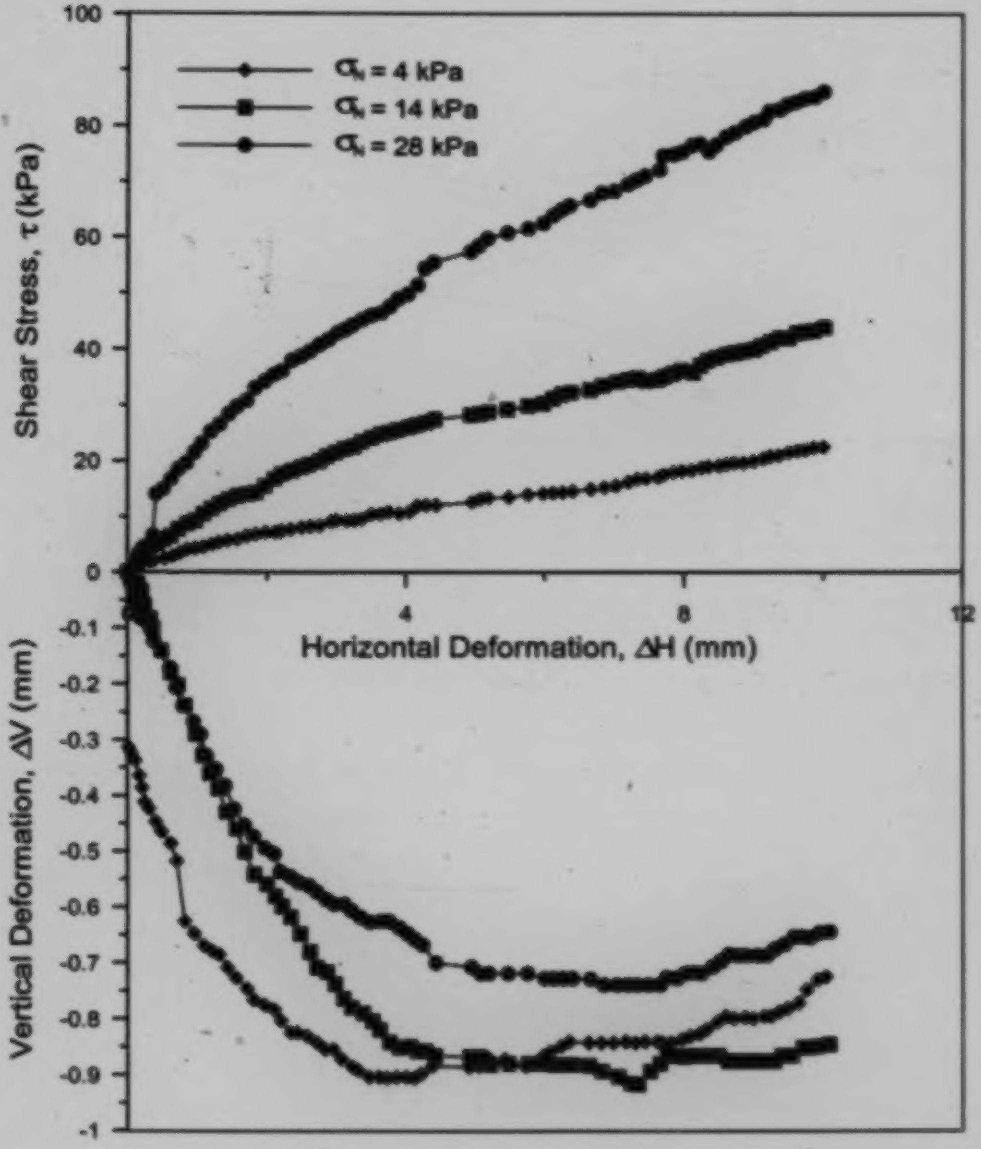

Figure 2.10 Direct shear stress and deformation behavior of samples containing both tire crumbs and shreds (0.85 to 12.5 mm) (modified from Cecich et al., 1996)

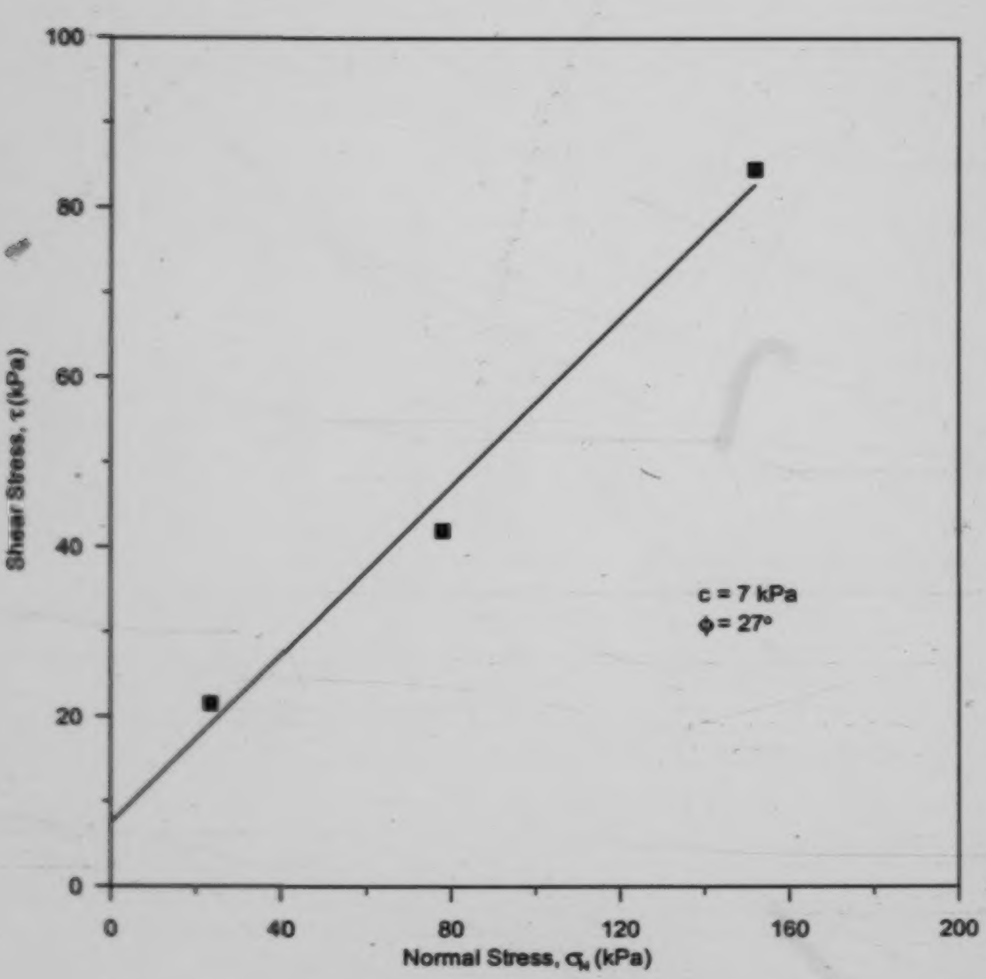

Figure 2.11 Direct shear strength envelope for tire crumbs/shreds with particle size ranging from 0.85 to 12.5 mm (modified from Cecich et al., 1996)

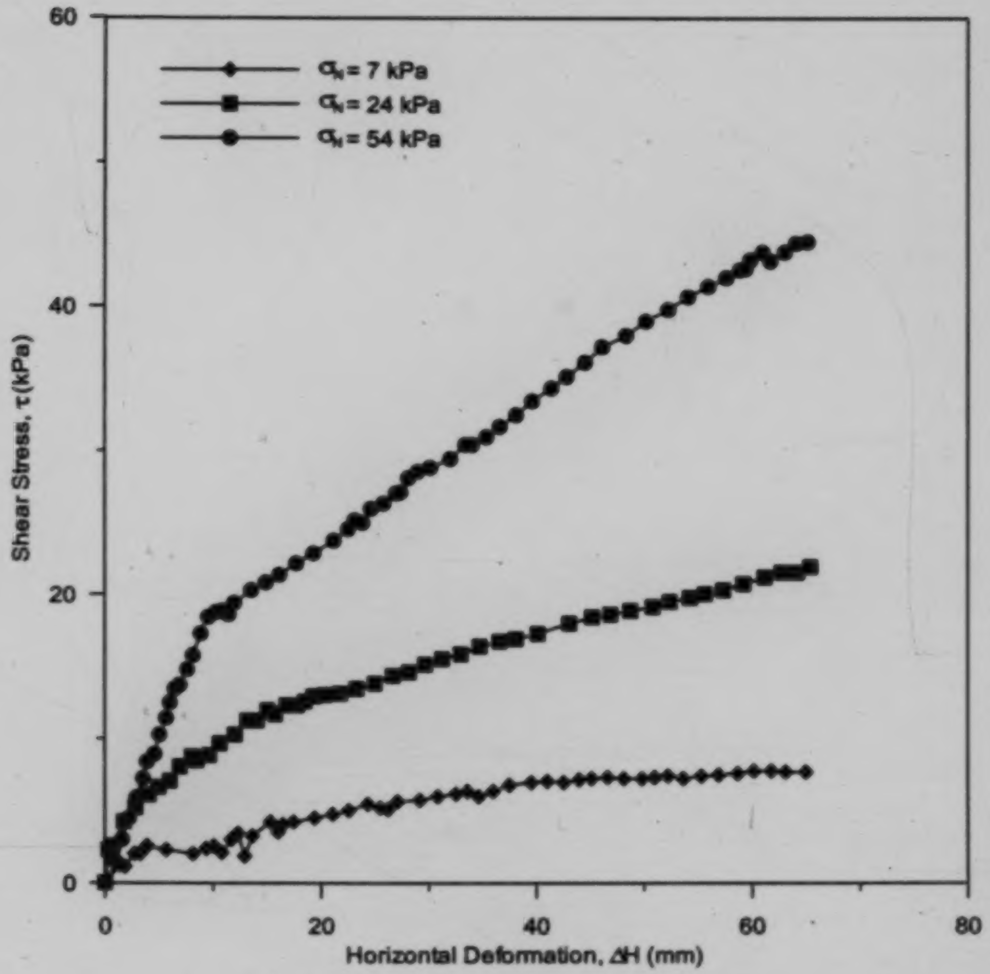

Figure 2.12 Direct stress and deformation behavior of 50 mm x 50 mm tire shreds in direct shear (modified from Bernal et al., 1997)

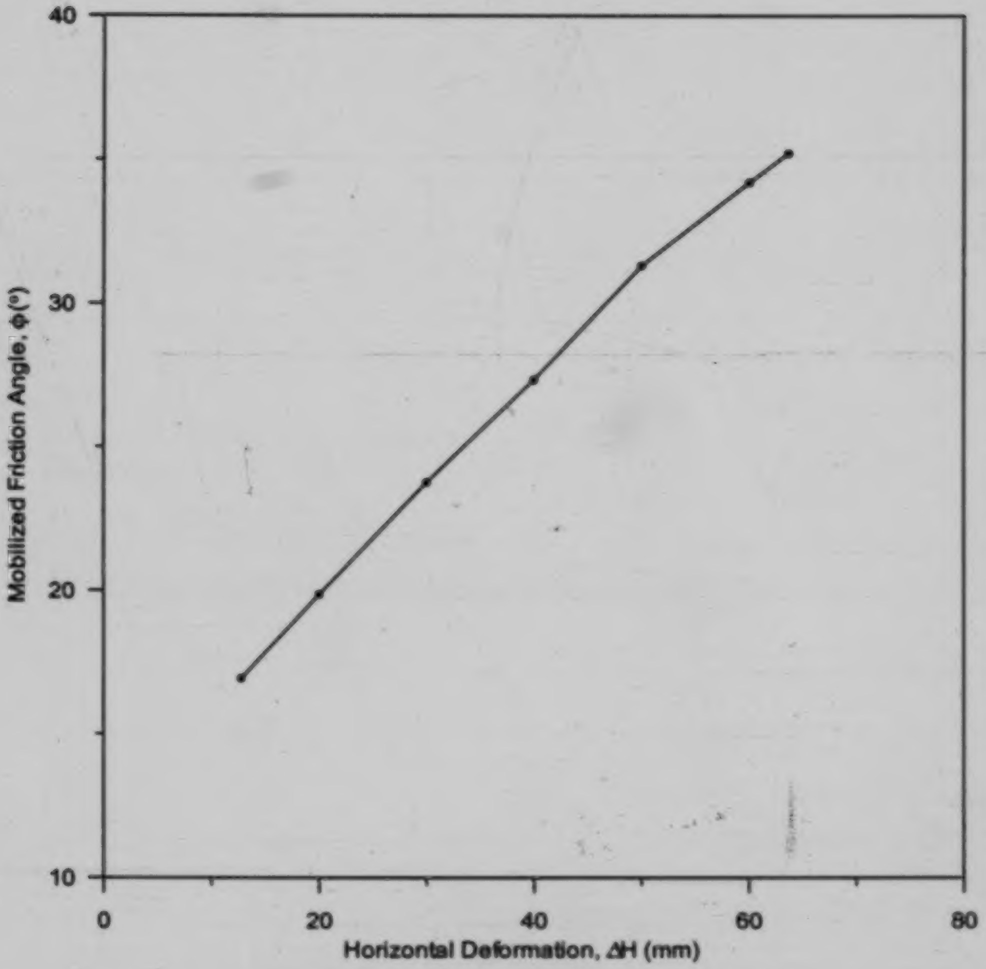

Figure 2.13 Horizontal deformation versus mobilized friction angle for tire shreds with maximum nominal size of 50 x 50 mm from direct shear tests (modified from Bernal et al., 1997)

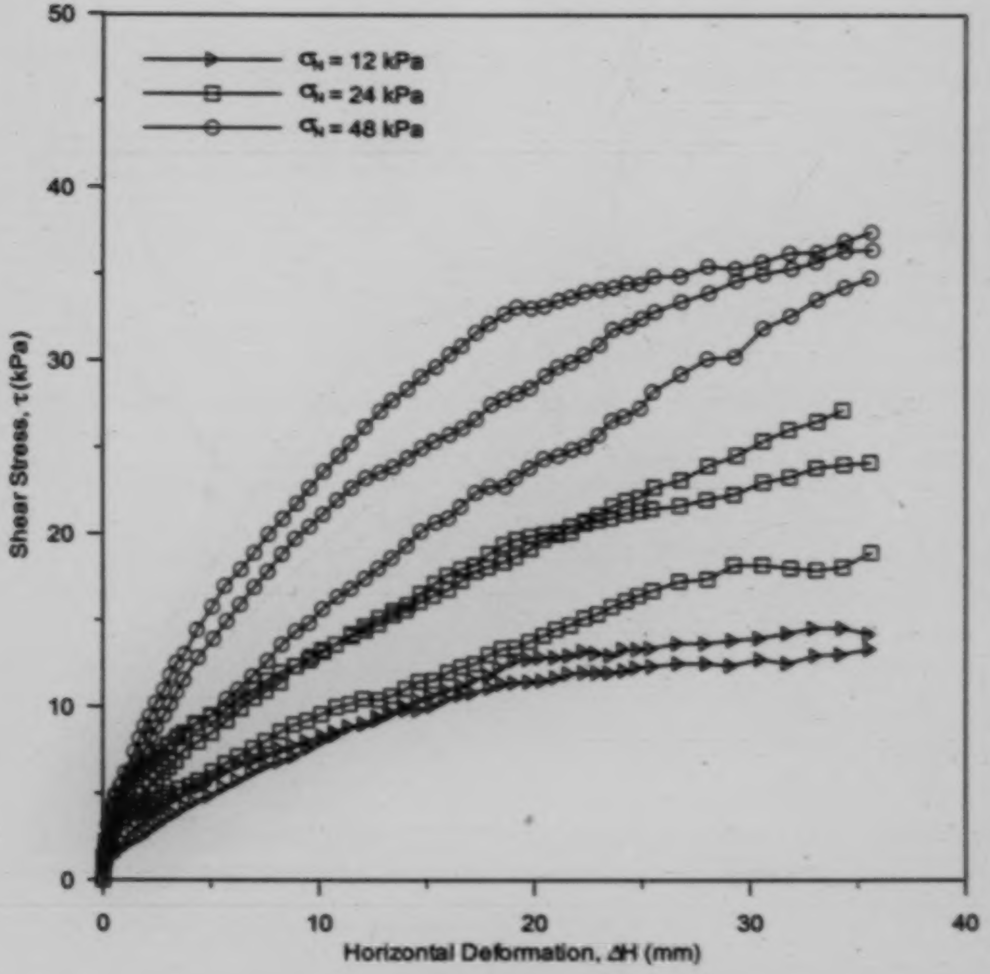

Figure 2.14 Direct stress and deformation behavior of tire shreds (50 to 75 mm, Pine State Recycling) tested in 300 mm (12 in) shear box (modified from Humphrey et al., 1992)

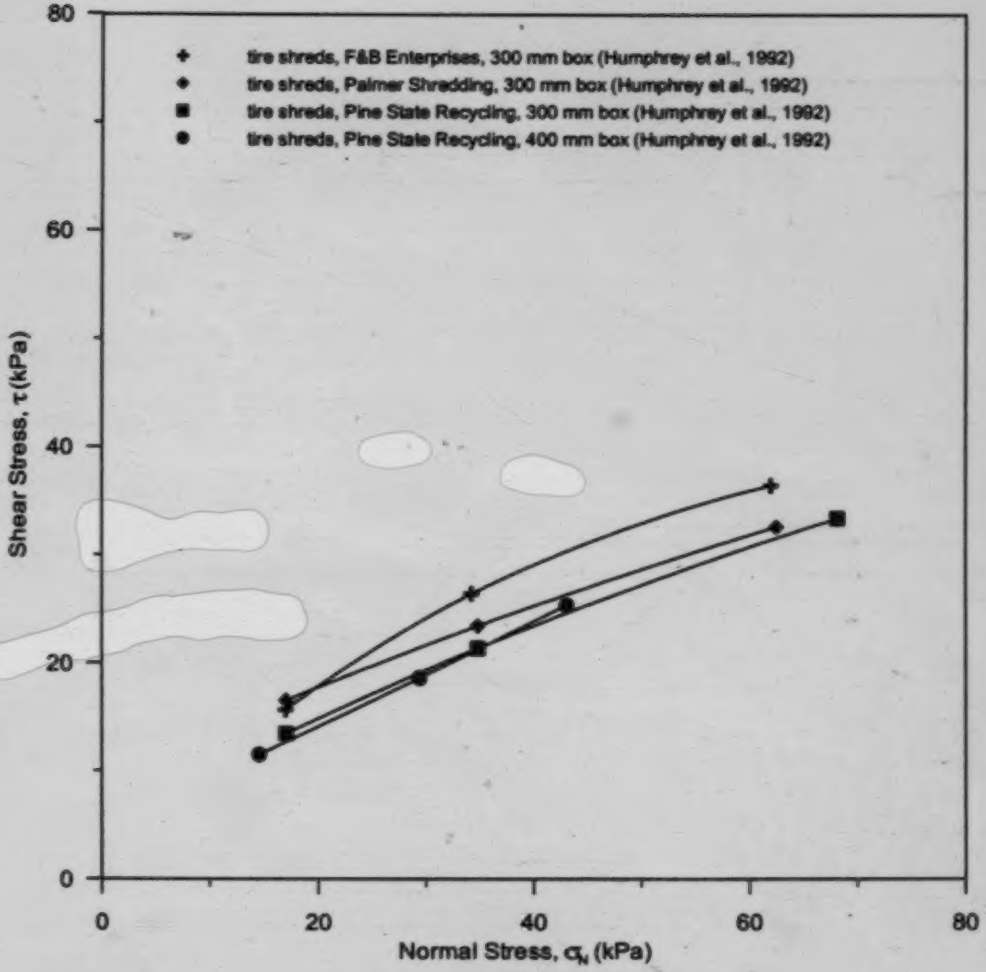

Figure 2.15 Direct shear strength envelopes for tire shreds (50 to 75 mm) (modified from Humphrey et al., 1997)

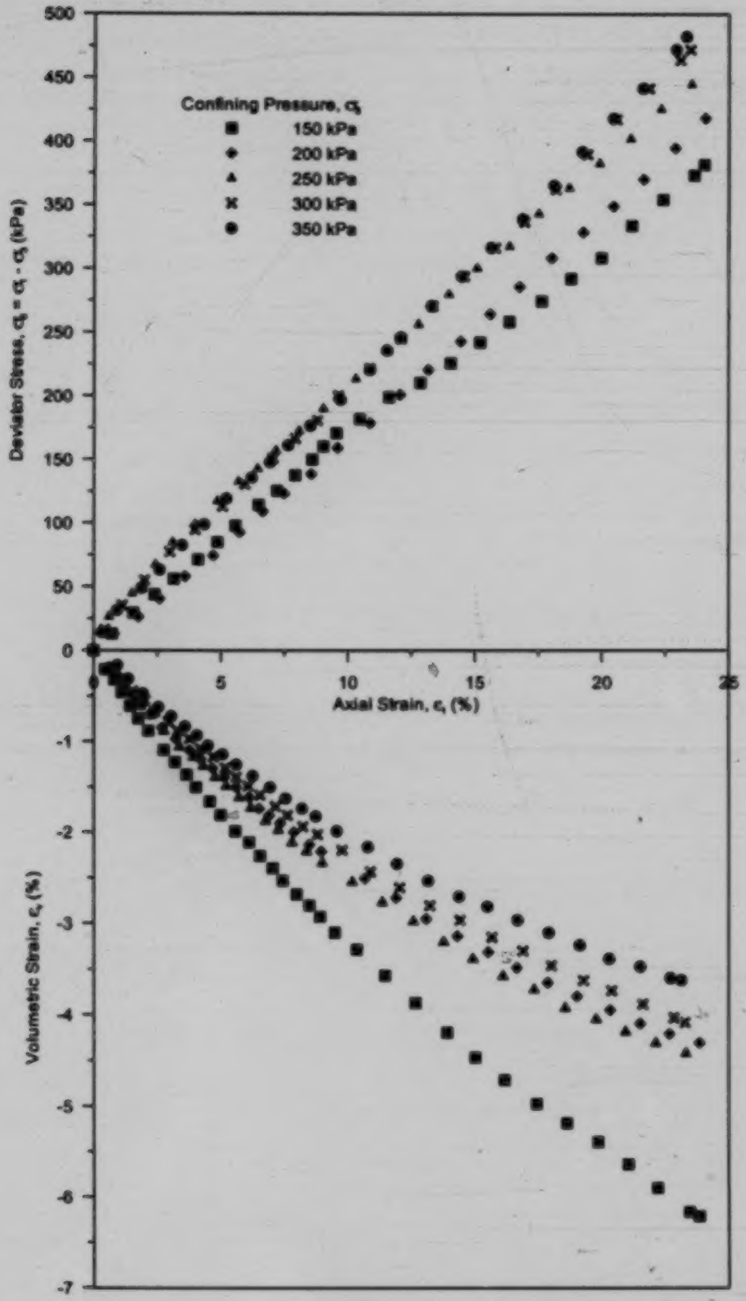

Figure 2.16 CD triaxial stress and volumetric strain behaviour for No. 4 minus tire crumbs (modified from Masad et al., 1996)

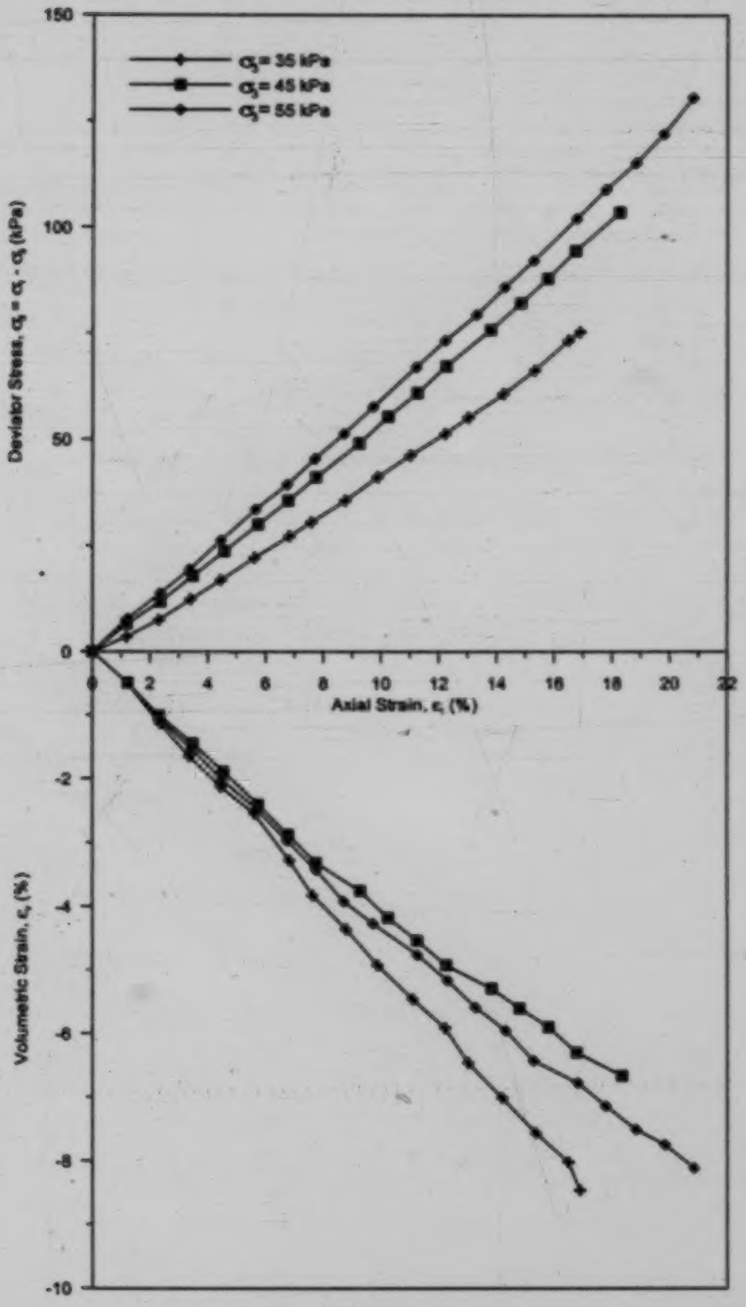

Figure 2.17 Triaxial stress and volumetric strain behavior for 9.5 mm tire shreds (modified from Benda, 1995)

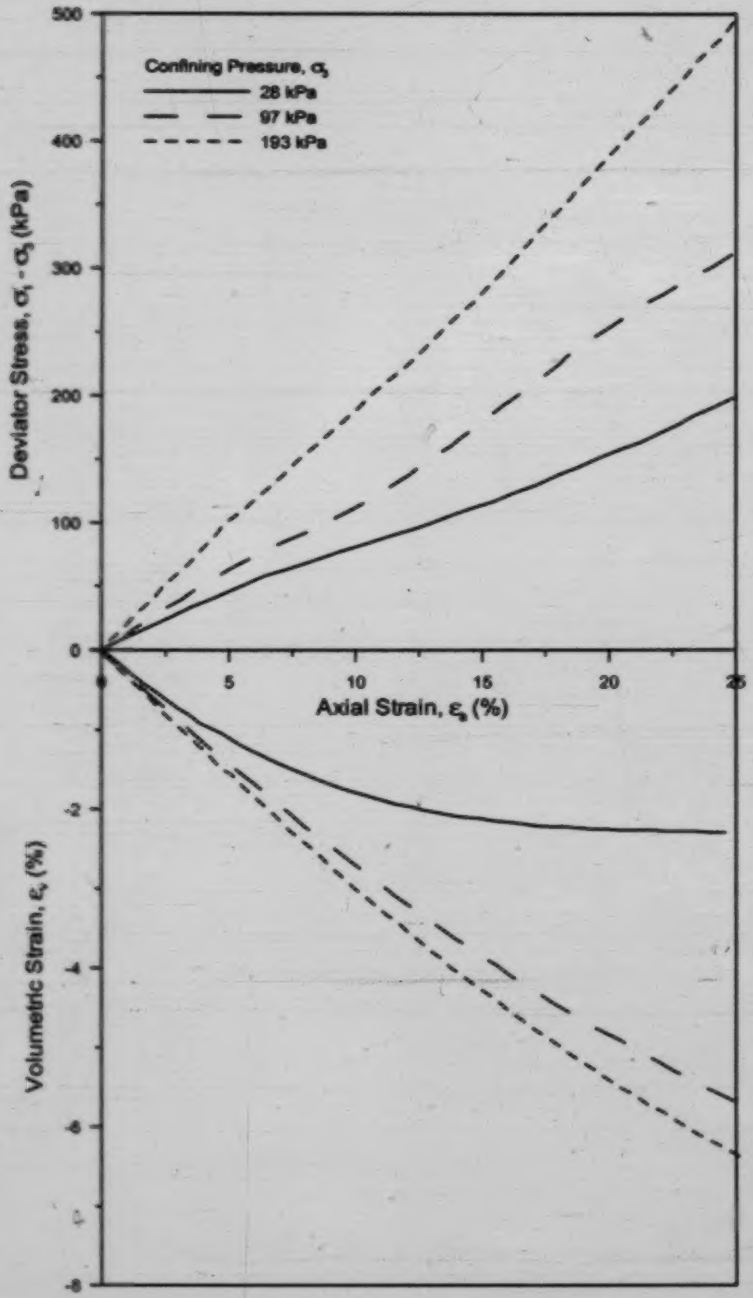

Figure 2.18 Triaxial stress and volumetric strain behavior for 25 mm (1 in) tire shreds (modified and reproduced from Bernal et al., 1996)

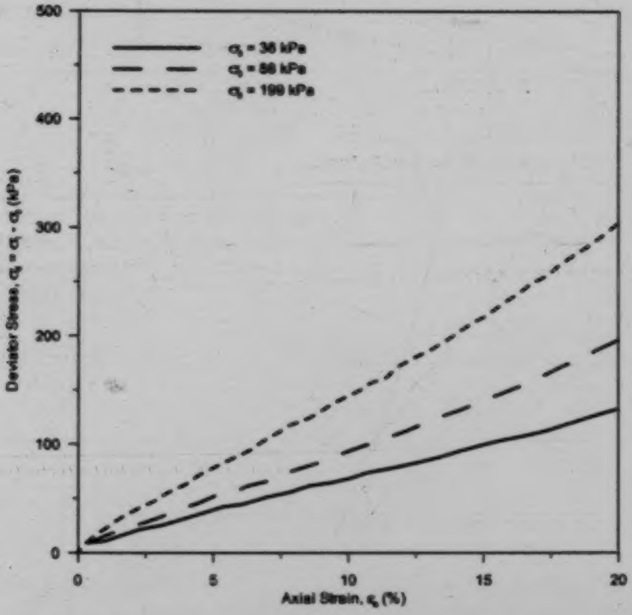

(a) 0.5 in tire shreds - compacted by Standard Proctor method

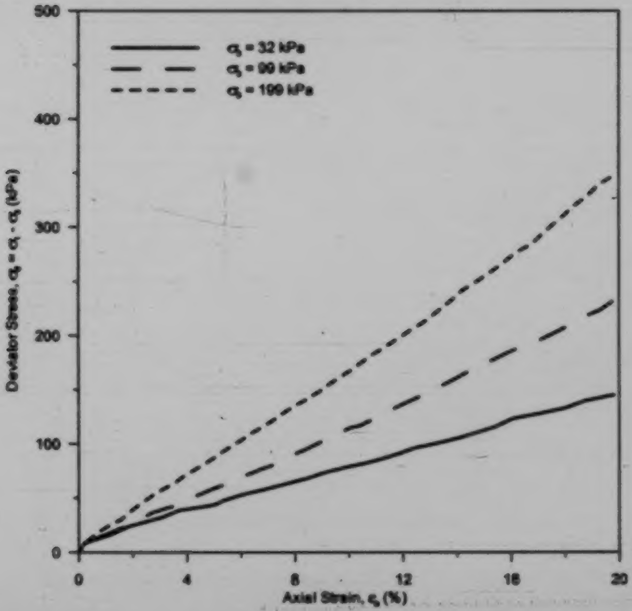

(b) 1 in tire shreds - compacted by 50% standard Proctor method

Figure 2.19 Triaxial stress-strain behaviour to tire shreds prepared at different compaction efforts under various confining pressures (modified from Ahmed, 1996)

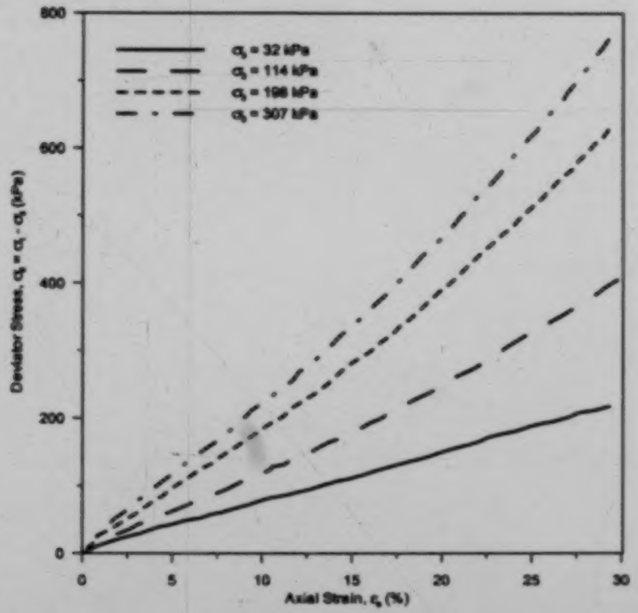

(c) 1 in tire shreds - compacted by standard Proctor method

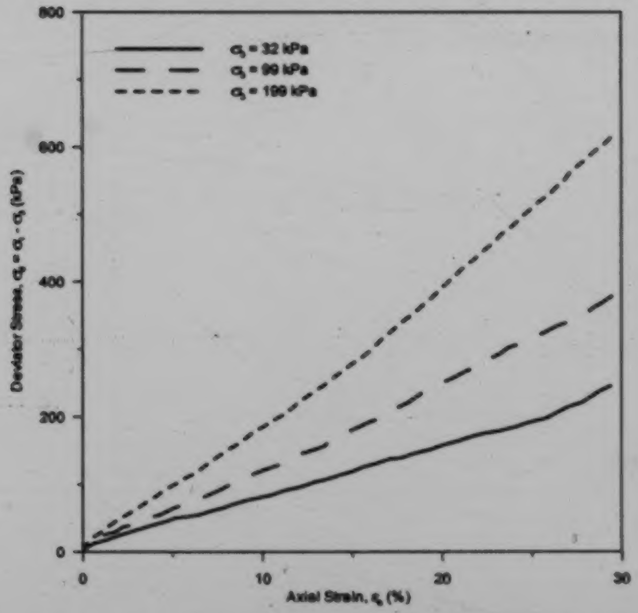

(b) 1 in tire shreds - compacted by modified Proctor method

Figure 2.19 Continued

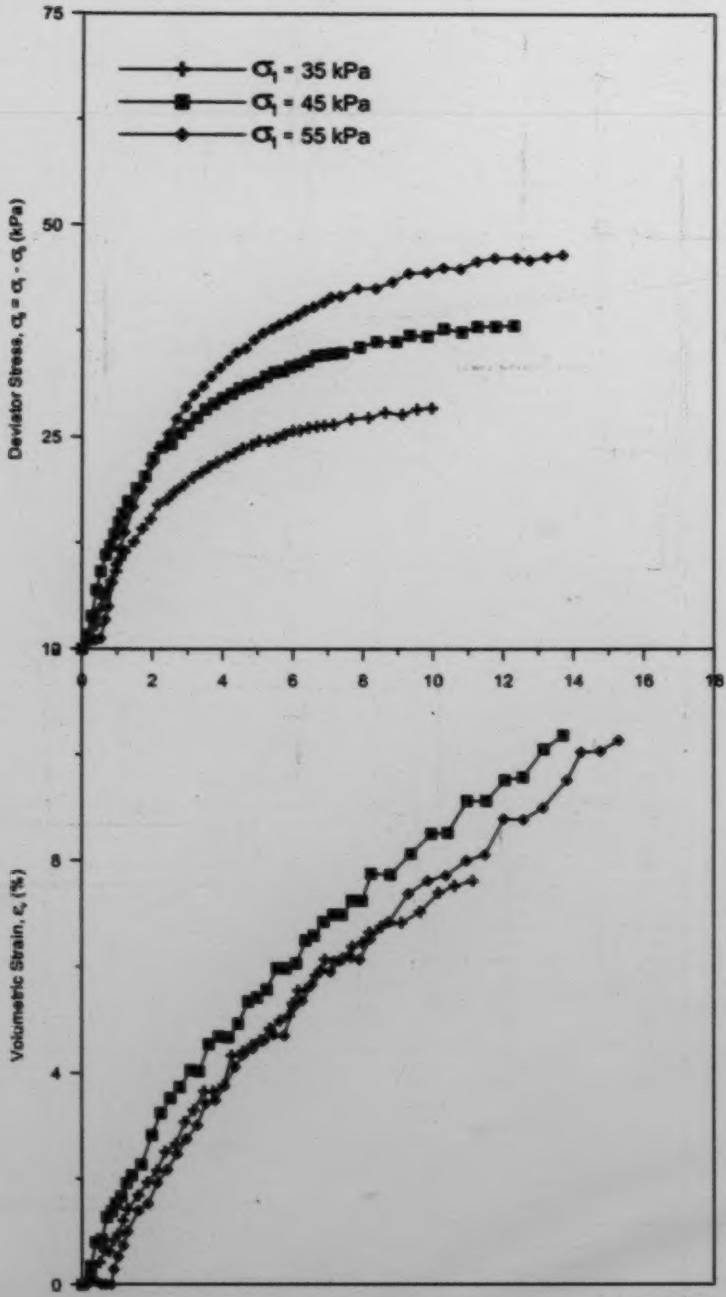

Figure 2.20 Triaxial stress and volumetric strain behaviour for tire shreds (9.5 mm) conducted under constant σ1 stress path (modified from Benda, 1995)

CHAPTER 3 SORPTION PROPERTIES

3.1 Introduction

Extensive research has been carried out by various authors to investigate the ability of recycled tire rubber to sorb various organic and inorganic compounds. The results of past research indicate that recycled tire rubber exhibits significant sorption capacity for various compounds and may be economically and technically feasible for use in various sorption applications. Hence, the focus of this chapter is to present the sorption properties of scrap tire rubber under various testing procedures and conditions, and to compare the results to available sorbents including carbon blacks, granular and powdered activated carbons, clays and other media. The potential applications of using recycled tire rubber as a sorbent agent are also discussed.

3.2 Background Information

The process of sorption includes a combination of adsorption and absorption. Adsorption is defined as the net accumulation of matter at the interface between a solid phase and an aqueous solution phase (Dudas, 1998). Absorption, on the other hand, is the process by which the adsorbate penetrates the adsorbent by at least several nanometers (Weber et al., 1991). The matter that accumulates at the interface is the adsorbate and the solid surface on which it accumulates is the adsorbent. The relationship of the adsorbate concentration in solution to its concentration on the adsorbent is a primary issue in environmental soil chemistry.

To explain the sorption process and permit comparisons between different chemicals and media, equilibrium equations or isotherms have been developed. These equations relate the mass of adsorbate sorbed per unit of adsorbent to the equilibrium concentration in the liquid phase. One of the most widely used isotherms to describe both the adsorption and absorption process is the Freundlich equilibrium equation.

According to the Freundlich isotherm, sorption at equilibrium is expressed by (Dudas, 1998):

$$\frac{X}{m} = K_f C_e^{1/n_f} \qquad \textbf{[Equation 3.1]}$$

where X = mass of adsorbate sorbed (mg); m = mass of adsorbent (kg); K_f = sorption equilibrium constant $(\text{mgkg}^{-1})(\text{mgL}^{-1})^{-1/n_f}$; C_e = solution concentration at equilibrium after sorption (mgL^{-1}); n_f = constant indicative of sorption intensity. The constants defined in Eq. 3.1 are determined by regressing the log of mass of the adsorbate sorbed on the adsorbent (X/m) and the log of the equilibrium concentration (C_e). The intercept is K_f, which gives an indication of sorptive capacity, while $1/n_f$, the slope, indicates sorption intensity. The higher the values for K_f and n_f, the greater the sorption capacity for the medium. Theoretically, Eq. 3.1 predicts that the sorption is infinite. Hence, it should not be extrapolated past the solute concentration for which it was developed (Zytner, 1994).

3.3 Sorption Properties

3.3.1 Sorption of Organic Compounds

Numerous studies have been carried out to investigate the ability of recycled tire rubber to sorb various organic compounds. Park et al. (1996) evaluated the feasibility of using tire shreds for the removal of methylene chloride, trichloroethylene, toluene, and m-xylene from landfill leachates. From their study, a method was proposed to estimate the thickness of a tire shred layer required to remove a targeted amount of organic compound. Kershaw and Pamukcu (1997) examined the use of ground tire rubber in reactive permeable barriers to mitigate BTEX compounds. Kim et al. (1997) investigated the effects of pH, particle size, and temperature on the sorption capacity of organic compounds by ground tire rubber. They derived empirical relationships to predict the partition coefficients of organic compounds sorbed on to tire rubber. Recently, San Miguel et al. (1998) investigated the adsorption properties of pyrolytic chars, which are the carbonized residue left from the pyrolysis of tire rubber. Also, Park et al. (1997)

found that a soil-bentonite slurry cutoff wall amended with ground tire rubber showed significant retardation capacity of organic contaminant movement. They also discovered that the hydraulic conductivity of the ground-tire-amended soil-bentonite backfill increased 1.1 to 1.2 times after sorption of the contaminants. These studies show that recycled tire rubber has significant capacity for sorbing organic compounds. The studies are described in detail below.

Park et al. (1996) performed a series of batch sorption-desorption tests on tire shreds. Their material, which contained exposed metal, varied in sizes from 6 to 25 mm. The batch sorption tests consisted of submerging the tire rubber in a 350 mL glass reactor, mixing the tire rubber with the solution containing the targeted organic compounds for up to 2 weeks, and measuring the concentration periodically. After equilibrium had been reached, the solution containing the targeted organic compounds was replaced with de-ionized water and desorption tests were performed for 7 days. The authors also conducted the same experiments on granular activated carbon (GAC) and compared the results with that of shreds. Methylene chloride (MC), trichloroethylene (TCE), toluene (TOL), and m-xylene (m-XYL) were selected for testing because these organic compounds were the most frequently detected at waste disposal sites (Plumb and Pitchford, 1985). Furthermore, the compounds covered a wide range of aqueous solubility and molecular weight. Another series of batch sorption tests were conducted using a multi-solute mixture. That is, the organic compounds MC, TCE, and TOL were added simultaneously to the reactor to determine whether competitive sorption amongst the compounds would take place. Their results for the single-solute and multi-solute experiments are summarized in Table 3.1 and Table 3.2 respectively. They found that tire rubber has 1 to 4% the sorption capacity of GAC (1.4 to 5.6% by tire volume basis). There also seems to be an insignificant difference between the sorption capacities for the multi-solute and single-solute systems; indicating that competitive sorption between MC, TCE, and TOL does not take place. The half-sorption time ($t_{1/2}$) for TCE and TOL were found to be approximately 3 times less for the 13 mm-size shreds than with the 6 mm shreds. The $t_{1/2}$ for 13 mm size shreds was nearly the same as the 25 mm shreds. Hence, they recommended practical tire shred size for use in landfill leachate systems should range from 13 to 25 mm or greater. Equilibrium was reached within 48 hours for TCE and TOL. Hence, the reaction rate may not be a limiting factor as indicated. Sorption-desorption tests showed that of the organic compounds adsorbed on to tire shreds, only 3.5 to 7.9% were desorbed. This would indicate that the sorption process is irreversible. The study also proposed a model to calculate the thickness of a tire shred layer needed to remove a given amount of organic compound. Hence, the layer thickness to be used in a landfill may be determined from the following relationship (Park et al., 1996):

$$d = 2.47\text{x}10^{-5}\text{x}\frac{M_a}{(1-n)\rho_t} \qquad \textbf{[Equation 3.2]}$$

where d = thickness of tire shred layer (cm); n = porosity of tire shred layer; M_a = required mass of tire chips per unit area (kg/acre); and ρ_t = density of tire rubber (g/cm^3). If a certain percentage of organic compounds require removal from the leachate, then the mass of tire shreds required can be estimated as follows (Park et al., 1996):

$$M_a = \frac{fQ_r t_d \rho_t 10^3}{(1-f)10^{0.824+0.61\log K_{ow}}} \qquad \textbf{[Equation 3.3]}$$

where f = fraction of organic compound to be removed; Q_r = leachate generation rate (m^3/acre/yr); t_d = landfill design life (yr). The models, however, would appear to neglect the contact time requirements, which would be in the order of minutes given the high hydraulic conductivity of tire crumbs and shreds. Figure 3.1 illustrates the thickness of a tire shred layer required for 90% organic compound removal of 1 mg/L concentration of benzene, TCE, m-XYL, and pentachlorophenol in a landfill assuming that the leachate generation rate is 600 m^3/acre/yr and tire shred porosity is 0.5. Hence, for 90% removal of each organic compound for a landfill with a 20 yr design life, the thickness of tire shred layer is estimated to be 39.4, 22.4, 8.7, and 0.7 cm respectively. As a rule of thumb, 10 automobile tires are needed a produce a 10 cm thick layer over 1 m^2 area.

Kershaw and Pamukcu (1997) investigated the ability of ground tire rubber in reactive permeable barriers to remove benzene, toluene, ethylbenzene and xylenes (BTEX) compounds from contaminated groundwater. One of the main concerns with BTEX compounds is the release of the contaminants into groundwater aquifers from leaky underground storage tanks. The contaminants can be removed from groundwater by using reactive permeable barriers that treat the contaminated water as it flows through the barrier. A conceptual schematic is shown in Figure 3.2. The barrier allows for the free flow of water and the sorption medium is design to sorb, react with, or otherwise prevent the contaminant from migrating through it. This study and others (Baykal et al., 1992) found that ground tire rubber may be a possible candidate for the sorption media in reactive permeable barriers. In this study, both single-solute and multi-solute batch equilibrium tests were conducted to determine the sorption capacity of the tire rubber for the BTEX compounds. Packed bed column tests were also conducted to determine the flow through utilization efficiency of the tire rubber. The packed bed column tests consisted of placing a given amount of tire rubber in a column, and then slowly running contaminated water through the packed bed until a breakthrough is achieved. Breakthrough is defined as the point in time where the contaminant concentration in the effluent exceeds the allowable release concentration for that contaminant. The utilization efficiency is a measure of the sorbents ability to reach equilibrium capacity for a given influent concentration at breakthrough. The ground rubber used in the experiments was produced from whole passenger and/or truck tires with the fabric and steel components removed. Particle diameters ranged from 0.6 to 1.18 mm. The results for both the single-solute and multi-solute experiments are shown in Table 3.3. These were obtained by applying the Linear and Freundlich isotherms. A review of the data shows that the sorption capacity of BTEX is best fitted using the Freundlich isotherm. Furthermore, a comparison of the single-solute and multi-solute experiments shows no significant competition between the compounds tested. However, benzene was the only contaminant in which the sorption capacity of the rubber showed a significant decrease when all BTEX compounds were present at roughly the same equilibrium concentrations. The authors compared the sorption capacity of tire rubber for the BTEX compounds with that of activated carbon, and found the tire rubber to exhibit approximately 5%, 4%, 4% and 8% the sorption capacity of activated carbon for benzene, toluene, ethylbenzene and p-Xylene respectively. The results of the packed bed column tests showed that the utilization efficiencies of tire rubber were similar to activated carbon efficiencies when contact times of approximately 36 minutes were employed. Utilization efficiencies of the ground tire rubber varied from 32% to 61% for the sorption of the individual BTEX compounds.

Kim et al. (1997) also conducted batch sorption testing to investigate the effect of pH, ground tire particle size, temperature, and the presence of other organic compounds as well as inorganic compounds on the sorption capacity of ground tire rubber. The rubber used in their experiments varied in size from 1.68 to 2.60 mm. Chloroform (CF), ethylbenzene (EB), methylene chloride (MC), toluene, 1,1,1-trichlorethane (TCA), trichloroethylene (TCE), and m-xylene were the organic compounds selected for testing. These were selected because they were reported to have high detection frequencies in contaminated environments and reasonable ranges of solubility and molecular weight. Sorption tests were also conducted on carbon black for comparison. The adsorption coefficients for the single-solute tests were modeled after the Linear and Freundlich isotherms, which are summarized and compared in Table 3.4. It showed that the ground rubber had the highest sorption capacity for m-XYL, followed by EB, TOL, TCE, TCA, CF, and MC. It should be noted that the first four compounds are hydrophobic, whereas CF and MC are hydrophilic. A comparison of the partition coefficients obtained from the single-solute and multi-solute tests is shown in Table 3.5. The two tests showed similar results, which would indicate that the organic compounds mixed together in solution did not show any significant competition with each other in the concentration ranges tested. The presence of inorganic substances (mainly salts) and pH on the organic sorption of tire rubber was also insignificant (Table 3.6). Batch sorption tests were also conducted to investigate the effect of ground tire rubber size on sorption. They reported that particle sizes within the range tested (1.68, 2.18 and 2.60 mm) was not a factor, however, the same sorption tests on tire shreds (average dimensions of 50 x 100 mm) showed much higher organic compound sorption capacity for ground tire rubber. Tire shreds, which contained significant amounts of steel wires, textile cords, and fabric belts were reported to exhibit approximately 46 to 91% the sorption capacity of ground rubber. Another finding from these tests revealed that the type of polymer used in various parts of tires showed significant differences in sorption capacity. Rubber from the tread portion showed at least two times greater sorption capacity than those of the sidewall. The partition coefficients for carbon black, which were fitted to the Linear isotherm are summarized and compared to GAC and ground tires in Table 3.7. Carbon black, which is a non-activated carbon, showed much less organic compound sorption than GAC. The sorption capacity of carbon black was 20 to 60% that of ground tire rubber. This would indicate that the sorption of organic compounds on to tire rubber is not dominated by carbon black. As mentioned in the preceding sections, tires contain approximately 31% carbon black by weight. Finally, sorption tests conducted at 4° and 55°C revealed that the temperature ranges tested do not affect the sorption of organic compound on to the tire rubber significantly. The authors plotted the log-log relationship between the tire-water partition coefficients (K_p) and the octanol-water partition coefficient (K_{ow}) for the seven organic compounds tested, and derived the following empirical relationships to predict the partition coefficients of untested organic compounds on to ground tire and tire shreds. The linear regression is given as follows (Kim et al., 1997):

Ground tire rubber:

$$\log K_p = -0.124 + 0.978 \log K_{ow} \quad (R^2 = 0.997) \qquad \textbf{[Equation 3.4]}$$

Tire shreds (from data of sidewall and tread portion of tires):

$$\log K_p = -0.026 + 0.859 \log K_{ow} \quad (R^2 = 0.985) \qquad \textbf{[Equation 3.5]}$$

Park et al. (1997) investigated the retardation of volatile organic compound (VOC) movement through a soil-bentonite (SB) slurry cutoff wall amended with ground tire rubber. The objectives of the investigation were to study the effects of adding ground tire rubber to the SB slurry backfill on hydraulic conductivity and retardation of VOC movement, and to determine the parameters that may be used in the design of the SB slurry cutoff walls containing ground tire rubber. The ground tire rubber used in the study contained minimum amounts of fabrics and no steel components. The average diameters of the ground tires were 2.19 mm. In the investigation, batch sorption tests were conducted to determine the partition coefficients of the VOC's with respect to the soil-bentonite mixture. Methylene chloride, trichloroethylene, toluene, and m-xylene were the VOC's selected for testing. Bromide ion was selected as a trace to eliminate any potential effect of cations on the SB mixture. A series of laboratory column permeation tests were also conducted to evaluate VOC transport through a typical soil-bentonite slurry cutoff wall backfill amended with ground tires. They reported that the hydraulic conductivity of the SB backfill was not affected by the addition of the ground tire rubber. The effectiveness of adding ground tires to the SB cutoff backfill was assessed by comparing the breakthrough time for 10% of the influent concentration. These are compared in Table 3.8 for the compounds tested. It is observed that the VOC breakthrough times through the SB backfill were significantly prolonged by the addition of ground tires.

San Miguel et al. (1998) studied the adsorption properties of pyrolytic chars derived from the pyrolysis of tire rubber. In their study, tire crumbs with particle sizes of less than 0.42 mm (No. 40) underwent thermal decomposition in a rotary furnace at various temperatures (from 300 to 1000°C) under a nitrogen atmosphere. The adsorption characteristics and porosity of the untreated tire rubber and rubber chars were measured and compared against three commercially available powdered activated carbons. Untreated tire rubber, pyrolytic chars, and the three activated carbons were analyzed by continuous volumetric nitrogen gas adsorption at liquid nitrogen temperature to determine effective surface areas, mesopore volumes, and micropore volumes. Aqueous adsorption tests were also performed using phenol, methylene blue, and the reactive dyes Procion Turquoise and Procion Red. The aqueous adsorption efficiency of the untreated tire rubber and pyrolytic chars for the four compounds was initially screened using single-point adsorption tests. These tests did not determine the adsorption capacities but provided a basis of comparison of the adsorption efficiencies at different temperatures. To minimize the effect of pH, all stock solutions were buffered with NaHCO3 and their initial pH's were adjusted by the addition of concentrated hydrochloric acid. Aqueous adsorption results were modeled to the Freundlich equation to calculate the adsorption capacities and affinity values. Product yield results (Figure 3.3) from the pyrolysis of tire rubber at different temperatures indicate that pyrolysis occurred at 300°C and was essentially complete at 500°C. The yield of each product produced by weight of original tire rubber was: 53% oil, 42% char, and 5% gas. The nitrogen gas adsorption tests show that tire rubber and pyrolytic char produced at temperatures below 450°C exhibit very low adsorption capacity for nitrogen gas. These temperatures are not sufficient to pyrolyze the tire rubber completely. Chars produced at 450 and 500°C were transition samples exhibiting similar adsorption isotherms to those produced at higher temperatures, but showing lower adsorption capacities. Furthermore, once pyrolysis is complete, the pore structure of the char is essentially unchanged. Figure 3.4 shows the surface area, micropore and mesopore volume from subsequent analysis of the nitrogen gas adsorption tests. Table 3.9 illustrates the same parameters obtained from the three commercial activated carbons. Untreated rubber and chars prepared at temperatures below 450°C do not possess any notable porosity or surface area. However, significant development of the pore structure was observed between 450 and 600°C. In comparison, the commercial activated carbons posses larger surface areas and micropore volume due to their highly developed micropore structure. However, pyrolytic chars exhibit significantly larger mesopore volumes than the Norit W52 and Chemviron GW activated carbons. The relative adsorption efficiencies for phenol, methylene blue, Procion Turquoise and Procion Red exhibited by rubber pyrolytic chars obtained from single-point adsorption tests are shown in Figure 3.5. Tire rubber chars produced at temperatures below 450°C exhibited very low adsorption efficiency for all four compounds. The degree of removal increased significantly in the temperature range between 450°C and 700°C to reach a plateau. Beyond 700°C, the uptake values for the four compounds increased gradually or remained constant. Figures 3.6 (a) to 3.6 (d) represents the adsorption isotherms for phenol, methylene blue, Procion Turquoise and Procion Red exhibited by untreated tire rubber and selected pyrolytic chars. Adsorption parameters, obtained by application of the Freundlich model to the adsorption data, are summarized in Table 3.10. The aqueous adsorption tests show that untreated tire rubber and rubber chars produced at temperatures below 450°C exhibited very low or negligible adsorption capacity for all four adsorbates. Higher preparation temperatures, in the range from 500 to 700°C, resulted in chars with increasing adsorption capacity, predominantly for methylene blue and the reactive dyes. Increasing the pyrolysis temperature from 700 to 1000°C resulted in limited further uptake of the four compounds. The pyrolytic chars showed much lower adsorption capacity for phenol than the commercial activated carbons due to their poorly developed micropore structure. The phenol molecule is relatively small (MW = 94.11 g/mol) and is principally adsorbed in micropores. On the other hand, the pyrolytic chars exhibit relatively higher adsorption capacity for methylene blue, a larger molecule than phenol, but well-below the performance of the more microporous commercial adsorbents. The adsorption of the reactive dyes appears to take place primarily in mesopores. Pyrolytic chars produced at temperatures above 600°C exhibited greater or similar adsorption capacities for the two reactive dyes than the general purpose activated carbons (W52 and GW) but about 50% inferior to Hyd-C, which is specially designed for the adsorption of large molecular weight compounds. Hence, the study shows that tire rubber pyrolytic chars possess relatively high aqueous adsorption capacity for compounds of large molecular weight.

3.3.2 Sorption of Inorganic Compounds

One potential application for using ground tire rubber is for the removal of heavy metals from process waste streams. Various researchers have studied the sorption of heavy metals by tire rubber. Knocke and Hemphil (1981) used tire rubber to remove mercury from solution. They found that the most critical parameter was the solution pH, with efficient sorption obtained for the range of pH 5.0 to 7.0. Other parameters studied were the initial mercury concentration, rubber particle size, solution temperature, and the presence of sulfur. Meng et al. (1998) also studied the sorption of mercury from solution. They also established the dependence of pH on the uptake of mercury (II) but found efficient sorption in the range of pH 2.0 to 7.0. Rowley et al. (1984) investigated the adsorption mechanism of cadmium, mercury and lead on to tire shreds. They discovered that the sorption of mercury and cadmium was caused by an ion-exchange type mechanism involving the displacement of zinc. The sorption of lead, however, did not involve the displacement of zinc. These studies are further discussed below.

Knocke and Hemphill (1981) assessed the capability of waste tire rubber for removing inorganic mercury from solution. Batch isotherm experiments were conducted to investigate the effects of aqueous mercury concentration, tire rubber particle size, solution temperature, pH, and the presence of sulfur on the mercury sorption capacity of the waste tire rubber.

Figure 3.7 shows the relation between mercury concentration and reaction rate constants. The sorption rate constant (k) of mercury was reported to be much faster at lower mercury concentrations, and began to approached a constant value with increased mercury concentrations. Similar equilibrium sorption capacity data for the mercury-tire rubber system reported by Griffith (1975) is compared in Figure 3.8. The slight differences between the two studies are due to tire rubber particle size, which was slightly less in the study by Griffith. Sorption capacities for mercury removal by powdered activated carbon (Humenick and Schoor, 1974) are also shown in Figure 3.8. The comparison shows vulcanized tire rubber is an efficient sorbent similar to powdered activated carbon in removing mercury. The sorption capacity of mercury was also found to be dependent on the tire rubber size. Table 3.11 shows that both the rate and sorption capacity of the rubber increases as the particle diameter decreases, which was directly related to the available surface area. It can be shown that the surface area can be related to $(1/D_p)$ assuming that the tire rubber particles are spherical; where D_p is the diameter of equivalent spheres. Hence, if only surface sorption sites were utilized for mercury removal, the sorption capacity should be proportional to (1/Dp). However, Figure 3.9 shows a linear relationship between sorption capacity and $(1/D_p)^2$. This suggested that additional sorption sites are being utilized other than those directly related to surface area. Weber (1967) upholds that additional sorption sites are due to tiny cracks and channels on the particle surface (i.e. pore diffusion) that provide added surface area. However, pore diffusion can be rate-limiting to the overall sorption process. The sorption of mercury is also influenced by solution temperature. Table 3.12 summarizes the sorption rate and capacity of mercury at various solution temperatures from 5°C to 55°C. Since sorption is an exothermic process, it would be expected that an increased solution temperature would result in decreased sorption capacity. However, since diffusion is an endothermic process, the rate of sorption will increase with increased solution temperature when pore diffusion is the rate-limiting step (Weber, 1967). The results of this study conclude that mercury sorption on to rubber is controlled by pore diffusion. The most critical parameter was the solution pH. Efficient removal of mercury occurred at optimum pH ranging from 5.5 to 6.0. Finally, the presence of sulfur is not essential to mercury uptake, but does not discount the possibility that sulfur may have contributed to the overall sorption process.

Meng et al. (1998) investigated the immobilization of mercury, Hg (II), in contaminated soil with ground tire rubber. In their study, the adsorption mechanism and adsorption capacity for Hg (II) by ground tire rubber were determined using batch equilibrium experiments. The ground tire rubber contained approximately 2 to 4% sulfur and less than 32% carbon black. However, the ground tire particles sizes used in the experiments were not reported. They showed that the adsorption of Hg (II) by ground tire rubber reached equilibrium within 50 hrs and suggested the sorption process may be attributed to the diffusion of Hg (II) into the rubber matrix. The adsorption of Hg (II) was also affected by pH. Figure 3.10 indicate that Hg (II) adsorption by rubber was higher at low pH. The adsorption of Hg (II) also increased when the pH decreased from 10 to 7. They suggested that the reduced Hg adsorption at higher pH values may have been caused by the formation of mercury complexes with hydroxyl ions. Hence, they recommended that the rubber treatment of Hg should be performed in acidic to neutral pH range. The adsorption of Hg (II) was found to be in good agreement with the Langmuir isotherm in Figure 3.11. The adsorption capacity and adsorption equilibrium constant was determined to be 14.6 mg Hg/g and 4.7 l/mg respectively. The authors speculated that the high adsorption capacity of the tire rubber may be attributed to the sulfur groups in the rubber. Hg (II) may have been adsorbed to the sulfur sites through the formation of surface complexes.

Rowley et al. (1984) investigated the adsorption of cadmium (II), mercury (II) and lead (II) on to crumbed tire rubber. Samples of the crumb (2.4 to 3.3 mm in diameter) were packed into a glass chromatography column and nitrate solutions containing the targeted metals were passed through separately. The eluents were collected and analyzed for metal concentrations, as well as concentration of zinc displaced. The amount of zinc was measured because they observed that the uptake of mercury and cadmium were accompanied by zinc displacement, which suggested an ion exchange mechanism. Furthermore, zinc displacement was more prevalent with cadmium adsorption than with mercury. Lead adsorption, on the other had, involved no zinc displacement and was not competitive with cadmium or mercury uptake. Zinc is often present in automobile tires, which is added in the form of zinc oxide as an activator in the vulcanization process. To confirm their observation, they ran tests in which all available zinc in the crumbs was removed by washing the crumbs with a dilute nitric acid. As expected, the results show reduced capacity in the uptake of mercury and cadmium, but the lead capacity was unaffected. They speculated that there were at least two possible mechanisms by which metals were adsorbed by vulcanized rubber. One mechanism involved the displacement of zinc. Further experiments were conducted in which the tire rubber samples were fully saturated with zinc (II) nitrate solution to investigate whether rubber which had already adsorbed zinc (II) would subsequently show increased capacity for adsorption of those metals whose uptake involved zinc displacement. The results show a marked increase in capacity for cadmium, a lesser increase in capacity for mercury, and the capacity for lead was unchanged. This suggested that there were more sites available on the rubber surface for the occupation of zinc ions than are normally utilized in vulcanized rubber that has not been treated with externally applied zinc. A competitive adsorption study found that there was no competition between lead and cadmium or lead and mercury. This confirmed that the sites that bind lead are totally different from those used by cadmium and mercury. The adsorption of metals on to rubber was also pH dependent. They found no evidence of an optimum pH, which had been reported for mercury (Knocke and Hemphill, 1981), and other metals (Netzer and Wilkinson, 1974). Instead, there was an increase in the adsorption capacity of rubber as the pH decreased.

3.4 Summary

This chapter summarizes the extensive research that has been conducted by various authors to investigate the sorption ability of recycled tire rubber. Tire rubber in the form of tire shreds, pyrolytic chars and ground rubber was tested in batch equilibrium sorption and flow through experiments under different test conditions to determine their sorption mechanism and capacity for various organic and inorganic compounds. The sorption isotherm parameters obtained by various authors for different organic and inorganic compounds for recycled tire rubber are summarized in Table 3.13. Note the parameters were obtained for single-solute solutions. Comparisons are also shown for activated carbon, carbon black, clays, and other sorbents.

Past research has indicated that recycled tire rubber exhibits significant sorption capacity. However, in comparison to activated carbons, tire rubber generally exhibits about an order of magnitude less in sorption capacity for various organic compounds. The sorption of organic compounds on to ground rubber was not significantly affected by the presence of other organic or inorganic compounds; indicating competitive sorption between the organic compounds in solution does not occur (Kershaw and Pamukcu, 1997; Kim et al., 1997). The process of sorption to ground tire was also irreversible (Park et al., 1996). The effects of pH and temperature on sorption were insignificant (Kim et al., 1997). Generally, smaller-sized tire particles have higher sorption capacities than larger ones due to higher surface area. However, the sorption study carried out by Kim et al. (1997) and Park et al. (1996) contradicted this generalization. Park et al. (1996) recommended practical shred sizes for use in landfills would range from 13 to 25 mm or greater. Carbon black, which is commonly found in tire rubber, did not appear to play a significant role in the organic sorption onto ground tires (Kim et al., 1997). The organic compound sorption mechanism on to tires is primarily caused by sorption of organic compounds onto the polymeric materials of tire rubber, and diffusion (Kim et al., 1997). San Miguel et al. (1998) found that pyrolytic chars produced from the pyrolysis reaction of tire rubber generated significant sorption capacity. They discovered that untreated tire rubber and pyrolytic chars produced at temperatures before the completion of the pyrolysis reaction (< 450°C) did not exhibit any notable increases in surface areas and showed very limited adsorption capacity. However, at activation temperatures between 450 to 600°C, pyrolytic chars exhibited increased sorption capacity for the large molecular weight compounds (i.e. phenol) due to their significant development of macro pore structure. In comparison to activated carbons, pyrolytic chars produced at high temperatures showed adsorption capacities for two reactive dyes that were significantly greater or similar to general commercial activated carbons, but were inferior to the activated carbon specially designed for the removal of large molecular weight compounds. The study, hence, shows that tire rubber pyrolytic char possesses relatively high adsorption capacity for compounds of large molecular weight. Tire rubber was also investigated to remove heavy metals (Knocke and Hemphill, 1981; Rowley et al., 1984). It was found the sorption of mercury was dependent on tire particle size and surface area, solution temperature, and pH (Knocke and Hemphill, 1981). The sorption mechanism of mercury on tire rubber was due to pore diffusion. Rowley et al. (1984) discovered that the sorption of mercury and cadmium was attributed to the displacement of zinc ions. The adsorption of lead, on the other hand, did not involve the displacement of zinc. There was also competitive sorption between mercury and cadmium; with preference given to the latter metal.

In summary, the use of tire rubber material in various sorption applications has been shown to be technically viable by preliminary research due to its unique sorption capacity for various organic and inorganic compounds.

Table 3.1 Summary of sorption results on tire shreds (6 to 25 mm nominal size) for single-solute experiment (after Park et al., 1996)

Organic Compounds	Tire-liquid ratio, % by volume	C_{eq}/C_o	$t_{1/2}$ (hr)	Tire M_{eq}/M_s (g/kg)	GAC[1] M_{eq}/M_s (g/kg)	K	D (cm^2/s)
MC	1.22	0.476	120	0.9	23	89.0	1.23x10^{-7}
	2.83	0.431	100	0.4	21	45.4	1.37x10^{-7}
	4.65	0.421	95	0.3	20	28.2	1.59x10^{-7}
	5.96	0.418	80	0.2	20	22.0	1.71x10^{-7}
TCE	0.72	0.373	30	3.0	154	230.4	0.74 x10^{-7}
	2.09	0.167	8	1.3	103	234.4	0.65 x10^{-7}
	3.89	0.106	2.7	0.8	77	208.5	1.01 x10^{-7}
	5.26	0.080	1.7	0.6	65	206.3	0.92 x10^{-7}
TOL	1.23	0.202	11	2.6	72	316.1	1.06 x10^{-7}
	2.66	0.096	3	1.3	49	345.0	0.79 x10^{-7}
	3.77	0.083	1.7	0.9	46	280.0	0.92 x10^{-7}
	4.21	0.074	1.9	0.8	44	285.9	0.79 x10^{-7}
m-XYL	0.74	0.135	6.8	5.1	122	856.1	0.24 x10^{-7}
	2.45	0.062	2.1	1.7	105	601.8	0.37 x10^{-7}
	3.52	0.046	1.1	1.2	100	569.1	0.35 x10^{-7}
	4.34	0.038	1.2	1.0	96	555.4	0.33 x10^{-7}

[1] Granular activated carbon; M_{eq}/M_s calculated based on parameters reported by Dobbs and Cohen (1980)

C_{eq} = equilibrium concentration of the organic compound in the solution, (mg/L)
C_o = initial concentration of the organic compound in the solution (mg/L)
$t_{1/2}$ = sorption half-time (hr)
M_{eq} = weight of organic compound sorbed at equilibrium (g)
M_s = initial weight of tire rubber (g)
K = partition coefficient (dimensionless) for linear isotherm
D = diffusion coefficient (cm^2/s)

Table 3.2 Summary of sorption results on tire shreds (6 to 25 mm nominal size) for multi-solute experiment (after Park et al., 1996)

Run no., % tire-liquid ratio, tire chip size	Organic Compound	C_{eq}/C_o	$t_{1/2}$ (hr)	Tire M_{eq}/M_s (g/kg)	Weight gain (%)	K	D (cm^2/s)
Run 1	MC	0.789	NA	1.16	0.12	35.1	NA
0.75%	TCE	0.277	8	3.01	0.30	344.5	NA
25 x 25 mm	TOL	0.254	8	3.50	0.35	233.1	NA
Run 1	MC	0.807	NA	1.03	0.10	28.6	NA
0.82%	TCE	0.267	8	2.54	0.25	332.3	NA
13 x 13 mm	TOL	0.237	8	3.19	0.32	389.3	NA
Run 1	MC	0.866	NA	0.56	0.06	13.7	NA
1.12%	TCE	0.296	27	1.99	0.20	209.9	1.37×10^{-7}
6 x 6 mm	TOL	0.254	24	2.17	0.33	387.6	1.59×10^{-7}

NA = not available

Table 3.3 Summary of sorption results on ground tire rubber (0.6 to 1.18 mm nominal size) for single-solute and multi-solute experiments (after Kershaw and Pamukcu, 1996)

	Contaminants	Linear isotherm		Freundlich isotherm		
		K_L (L/g)	r^2	K_f (mg/g)	$1/n_f$	r^2
Single-solute	Benzene	0.083	0.883	0.157	0.877	0.937
	Toluene	0.261	0.957	0.283	0.970	0.987
	Ethylbenzene	0.767	0.937	0.851	0.935	0.887
	o-Xylene	0.857	0.988	0.625	1.11	0.998
Multi-solute	Benzene	NA	NA	0.069	0.980	0.823
	Toluene	NA	NA	0.308	0.931	0.869
	Ethylbenzene	NA	NA	0.846	0.930	0.876
	o-Xylene	NA	NA	0.887	0.892	0.874

Table 3.4 Adsorption coefficients for ground tire rubber (after Kim et al., 1997)

Organic compounds	Linear isotherm		Freundlich isotherm		
	K_p (L/kg)	r^2	K_f (mg/kg)	n_f	r^2
CF	51.5	0.377	53.1	0.984	0.362
EB	978.8	0.981	1013.5	0.998	0.992
MC	11.1	0.572	3.7	1.304	0.651
TOL	294.2	0.983	303.2	0.991	0.985
TCA	163.0	0.637	278.2	0.839	0.756
TCE	263.3	0.879	163.3	1.155	0.894
m-XYL	1046.3	0.978	1011.4	0.990	0.983

Table 3.5 Comparison of partition coefficients between single-solute and multi-solute sorption tests (after Kim et al., 1997)

Organic compounds	Average observed partition coefficient (L/kg)	
	Single-solute tests	Multi-solute tests
CF	51	54
EB	1012	852
MC	11	12
TOL	297	290
TCA	170	199
TCE	261	237
m-XYL	1000	956

Table 3.6 Effect of inorganic substances and pH on organic sorption (reproduced from Kim et al., 1994)

Organic compounds	Average observed partition coefficient (L/kg)			
	Salts-added solution	pH = 2	pH = 9	pH = 11
CF	57	53	54	NA
EB	936	1036	948	957
MC	14	15	13	10
TOL	318	322	317	274
TCA	218	212	214	185
TCE	265	259	256	240
m-XYL	989	988	975	982

NA = not available because CD degraded under a high-hydroxide condition

Table 3.7 Sorption results on carbon black and comparisons with GAC and ground tire (after Kim et al., 1997)

Organic compounds	K_L of carbon black (L/kg)	K_L of GAC[a] (L/kg)	$K_{L,\text{ ground tire}}/K_{L,\text{ GAC}}$
CF	12	2942	1.9
EB	367	30836	3.0
MC	8	1131	1.1
TOL	178	8274	3.7
TCA	35	7080	2.9
TCE	59	NA	NA
m-XYL	552	22849	4.4

[a] Calculated using data from Dobbs and Cohen (1980); NA = not available

Table 3.8 Breakthrough time to reach 10% of the influent concentration for ground tire rubber in soil-bentonite wall (after Park et al., 1997)

Volatile organic compounds	Column permeation tests containing ground tire rubber, % by weight				
	Col 1-A, 0%[1]	Col 1-B, 0%	Col 2, 7.5%	Col 3, 7.5%	Col, 15%
Methylene chloride	< 10 days	NA	25 days	35 days	40 days
Toluene	< 10 days	150 days	450 days	600 days	1000 days
Trichloroethylene	< 10 days	50 days	410 days	440 days	520 days
m-Xylene	< 10 days	180 days	> 1000 days	1000 days	1000 days

[1] This batch of tests had an order of magnitude greater hydraulic conductivity than the other batches. Therefore, due to the possibility of channelling, another test was repeated successively with a new specimen (Col 1-B)

Table 3.9 Porosity and surface area of three commercial activated carbons (after San Miguel et al., 1998)

	BET[1] surface area (m^2/g)	Micropore volume (mL/g)	Mesopore volume (mL/g)
Norit W52	789	0.33	0.14
Chemviron GW	788	0.32	0.06
Norit Hydrodacro-C	545	0.25	0.25

[1] Surface areas and total micropore volumes were estimated by application of the BET (Brunauer et al., 1938) and the Dubinin-Astakhov (DA) (Stoeckli, 1995) equations.

Table 3.10 Freundlich Adsorption Parameters from Phenol, Methylene Blue, Procion Red, and Procion Turquoise (reproduced from San Miguel et al., 1998)

	methylene blue			phenol			Procion Red			Procion Turquoise		
Adsorbent	K_f (mg/g)	n	r^2	K_f (mg/g)	n	r^2	K_f (mg/g)	n	r^2	K_f (mg/g)	n	r^2
rubber	n/a[a]	n/a[a]	n/a[a]	n/a[a]	n/a[a]	n/a[a]	0.03	1.02	0.97	0.20	1.32	0.92
450[b]	n/a[a]	n/a[a]	n/a[a]	n/a[a]	n/a[a]	n/a[a]	0.06	1.14	0.98	0.05	1.15	0.97
500[b]	1.04	3.33	0.67	n/a[a]	n/a[a]	n/a[a]	0.05	0.96	0.95	0.42	1.82	0.99
600[b]	6.90	2.65	0.92	0.47	2.26	0.98	12.5	4.34	0.99	14.8	3.11	0.92
700[b]	16.7	5.97	0.94	1.18	3.14	0.95	25.6	8.05	0.92	32.1	4.80	0.98
800[b]	16.5	5.68	0.98	1.76	3.65	0.97	22.8	6.19	0.99	31.5	4.85	0.99
1000[b]	22.2	7.94	0.99	2.01	3.73	0.99	29.6	9.05	0.97	35.8	5.66	0.99
W52[c]	161.0	27.8	0.98	49.87	4.87	0.99	26.9	5.62	0.89	40.1	6.94	0.98
GW[c]	187.2	33.0	0.98	48.60	4.69	0.98	4.40	3.16	0.89	5.5	3.25	0.85
Hyd-C[c]	140.1	46.7	0.93	23.82	4.42	0.99	63.0	10.6	0.99	87.4	9.00	0.99

[a] n/a: estimated adsorption capacity below 0.01 mg/g
[b] Tire rubber pyrolytic chars: production temperature
[c] Commerical activated carbon: Norit W52 (W52) and Norit Hydrodarco-C (Hyd-C) (Norit UK Ltd.), Chemviron GW (GW) (Chemviron Carbon Ltd., U.K.). UK Ltd.)

Table 3.11 Sorption rate constant and sorption capacity of Hg (II) on to tire crumbs of varying particle sizes (after Knocke and Hemphill, 1981)

Mean particle size (mm)	Sorption rate constant, k (h^{-1})	Sorption capacity (mg Hg g^{-1} rubber)
0.66	0.23	0.10
0.39	0.36	0.21
0.21	0.42	0.54
0.12	0.76	1.20

Table 3.12 Sorption property of Hg (II) on to tire rubber at various temperatures (after Knocke and Hemphill, 1981)

Solution temperature (°C)	Sorption rate constant, k (h^{-1})	Sorption capacity (mg Hg g^{-1} rubber)
5	0.08	0.27
14	0.14	0.33
20	0.26	-
25	0.28	0.49
35	0.64	0.67
44	0.93	1.67
55	1.33	4.00

Table 3.13 Summary of adsorption isotherm parameters for various organic and inorganic compounds for recycled tire rubber and other sorbents (single-solute solutions)

Compounds Tested	Sorbent	Linear Isotherm		Freundlich Isotherm			Methods	References
		K_L (L/g)	r^2	$1/n_f$	K_f (mg/g)	r^2		
Benzene	Tire crumbs (0.6 to 1.18 mm)	0.083	0.883	0.877	0.157	0.937	Conventional equilibrium batch sorption	Kershaw and Pamukcu, 1997
	Clay [a]			1.55	0.00017	0.89		Zytner, 1994
	GAC, Nuclear 4 x 10 mesh (Westvaco)			0.51	19.6	0.98		
	Organic top soil [b]			0.78	0.00297	0.96		
	Peat moss			1.0	0.013	0.96		
	Sandy loam soil [a]			0.95	0.00058	0.89		
	Regina clay (M.C. = 4.3%)	0.007	0.93				Diffusion batch sorption	Zhang et al., 1998
	Regina clay (M.C. = 75%)	0.0064	0.93					
	Regina clay (M.C. = 120%)	0.0032	0.95					
	Regina clay (M.C. = 37%)	0.0.0072	0.93					
CF	Tire crumbs (1.68 to 2.60 mm)	0.0515	0.377	0.984	0.053	0.362	Conventional equilibrium batch sorption	Kim et al., 1997
	Carbon black	0.012						Kim et al., 1997
	GAC	2.942						Kim et al., 1997
EB	Tire crumbs (0.6 to 1.18 mm)	0.767	0.937	0.935	0.851	0.887		Kershaw and Pamukcu, 1997
	Tire crumbs (1.68 to 2.60 mm)	0.979	0.981	0.998	1.014	0.992		Kim et al., 1997
	Carbon black	0.367						Kim et al., 1997
	GAC	30.836						Kim et al., 1997
MC	Tire crumbs (1.68 to 2.60 mm)	0.0111	0.572	1.304	0.0037	0.651		Kim et al., 1997
	Tire crumbs & shreds (6 to 25 mm)	0.018 to 0.073						Park et al., 1996
	Carbon black	0.008						Kim et al., 1997
	GAC	1.131						Kim et al., 1997
m-XYL	Tire crumbs (1.68 to 2.60 mm)	1.046	0.978	0.990	1.011	0.983		Kim et al., 1997
	Tire shreds (6 to 25 mm)	0.455 to 0.702						Park et al., 1996
	Clay [a]			1.22	0.00080	0.95		Zytner, 1994
	GAC, Nuclear 4 x 10 mesh (Westvaco)							
	Organic top soil [b]			0.60	0.0308	0.99		
	Peat moss			1.49	0.014	0.98		
	Sandy loam soil [a]			1.24	0.00044	0.97		
	Carbon black	0.552						Kim et al., 1997
	GAC	22.849						Kim et al., 1997

Table 3.13 Continued

Compounds Tested	Sorbent	Linear Isotherm		Freundlich Isotherm			Methods	References
		K_L (L/g)	r^2	$1/n_f$	K_f (mg/g)	r^2		
o-XYL	Tire crumbs (0.6 to 1.18 mm)	0.857	0.988	1.11	0.625	0.998	Conventional equilibrium batch sorption	Kershaw and Pamukcu, 1997
	Clay ^{a}			1.22	0.00081	0.87		Zytner, 1994
	GAC, Nuclear 4 x 10 mesh (Westvaco)							
	Organic top soil ^{b}			0.79	0.012	0.99		
	Peat moss			1.56	0.0093	0.97		
	Sandy loam soil ^{a}			1.17	0.00038	0.93		
TCA	Tire crumbs (1.68 to 2.60 mm)	0.163	0.637	0.839	0.278	0.756		Kim et al., 1997
	Carbon black	0.035						Kim et al., 1997
	GAC	7.080						Kim et al., 1997
TCE	Tire crumbs (1.68 to 2.60 mm)	0.263	0.879	1.155	0.163	0.894		Kim et al., 1997
	Tire crumbs & shreds (6 to 25 mm)	0.169 to 0.192						Park et al., 1996
	Carbon black	0.059						Kim et al., 1997
	GAC	-						Kim et al., 1997
TOL	Tire crumbs (0.6 to 1.18 mm)	0.261	0.957	0.970	0.283	0.987		Kershaw and Pamukcu, 1997
	Tire crumbs (1.68 to 2.60 mm)	0.294	0.983	0.991	0.303	0.985		Kim et al., 1997
	Tire crumbs & shreds (6 to 25 mm)	0.230 to 0.283						Park et al., 1996
	Clay ^{a}			0.66	0.00847	0.94		Zytner, 1994
	GAC, Nuclear 4 x 10 mesh (Westvaco)			1.03	115.97	0.91		
	Organic top soil ^{b}			0.83	0.0076	0.98		
	Peat moss			0.83	0.074	0.95		
	Sandy loam soil ^{a}			0.94	0.00082	0.91		
	Carbon black	0.178						Kim et al., 1997
	GAC	8.274						Kim et al., 1997
Methylene Blue	Tire crumbs (<0.42 mm)			NA^{d}	NA^{d}	NA^{d}		Miguel et al., 1998
	Pyrolytic chars (450 – 1000^{e})			NA^{c} - 7.94	NA^{c} - 22.22	NA^{c} - 0.99		Miguel et al., 1998
	PAC (W 52^{f})			27.8	161.0	0.98		
	PAC (GW^{g})			33.0	187.2	0.98		
	PAC (Hyd-C^{h})			46.7	140.1	0.93		

Table 3.13 Continued

Compounds Tested	Sorbent	Linear Isotherm		Freundlich Isotherm			Methods	References
		K$_L$ (L/g)	r^2	1/n$_f$	K$_f$ (mg/g)	r^2		
Methylene Blue	Tire crumbs (<0.42 mm)			NA[d]	NA[d]	NA[d]	Conventional equilibrium batch sorption	Miguel et al., 1998
	Pyrolytic chars (450 – 1000[e])			NA[c] to 7.94	NA[c] to 22.22	NA[c] to 0.99		
	PAC (W 52[f])			27.8	161.0	0.98		
	PAC (GW[g])			33.0	187.2	0.98		
	PAC (Hyd-C[h])			46.7	140.1	0.93		
Phenol	Tire crumbs (<0.42 mm)			NA[c]	NA[c]	NA[c]		
	Pyrolytic chars (450 – 1000[e])			NA[d] to 3.73	NA[d] to 2.01	NA[d] to 0.99		
	PAC (W 52[f])			4.87	49.87	0.99		
	PAC (GW[g])			4.69	48.60	0.98		
	PAC (Hyd-C[h])			4.42	23.82	0.99		
Procion Red H-E3B	Tire crumbs (<0.42 mm)			1.02	0.03	0.97		
	Pyrolytic chars (450 – 1000[e])			1.14 to 9.05	0.06 to 29.6	0.98 to 0.97		
	PAC (W 52[f])			5.62	26.9	0.89		
	PAC (GW[g])			3.16	4.40	0.89		
	PAC (Hyd-C[h])			10.6	63.0	0.99		
Procion Turquoise H-A	Tire crumbs (<0.42 mm)			1.32	0.20	0.92		
	Pyrolytic chars (450 – 1000[e])			1.15 to 5.66	0.05 to 35.8	0.97 to 0.99		
	PAC (W 52[f])			6.94	40.1	0.98		
	PAC (GW[g])			3.25	5.5	0.85		
	PAC (Hyd-C[h])			9.00	87.4	0.99		
Mercury, Hg (II)	Tire crumbs (0.66 mm)			0.79	0.008			Knocke and Hemphill, 1981

[a] Clay: typical soils present in Essex County, Ontario

[b] Organic top soil: purchased from an Essex County nursery selling organic enriched top soil

[c,d] NA: estimated adsorption capacity below 0.01 mg/g.

[e] 450 - 1000: tire rubber pyrolytic char production temperature (°C)

[f] W 52: Norwit W52 (Norit UK Ltd.)

[g] GW: Chemviron GW (Chemviron Carbon Ltd., U.K.)

[h] Hyd-C: Norit Hydrodarco-C (Norit U.K. Ltd.)

PAC - Powdered Activated Carbon

GAC - Granular Activated Carbon

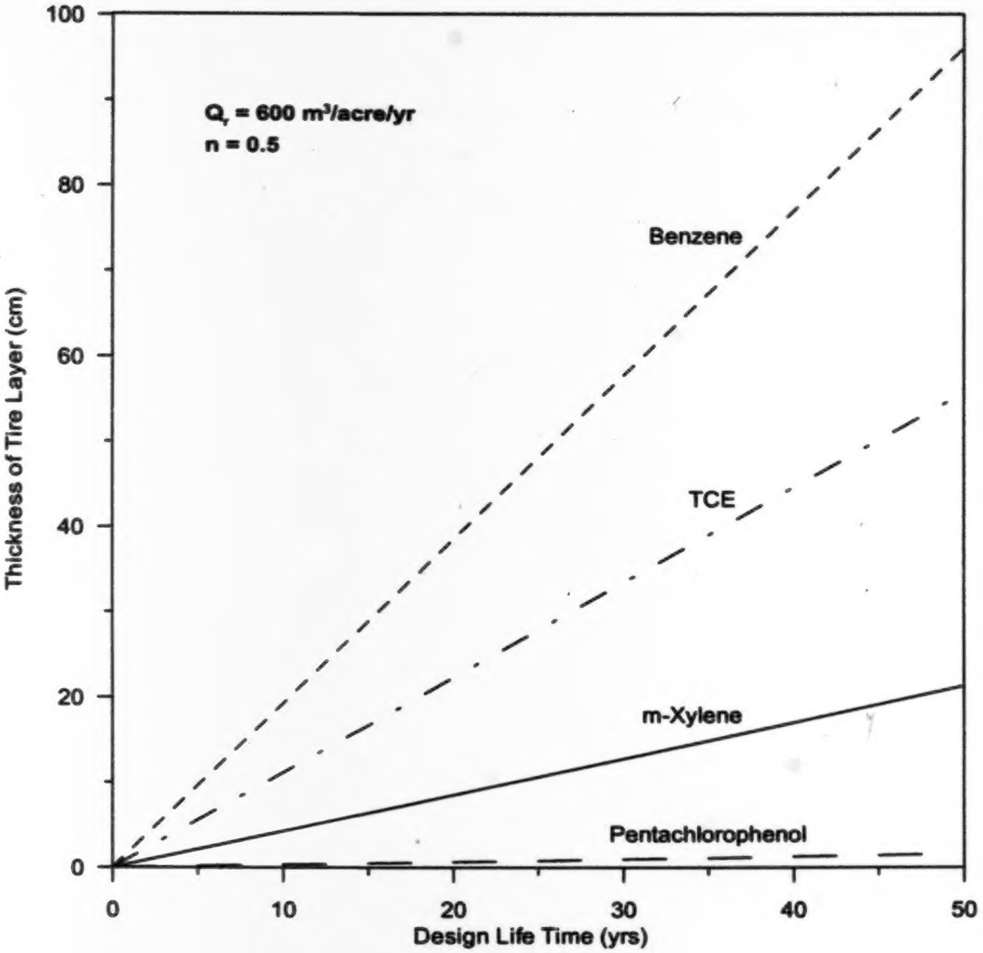

Figure 3.1 Thickness of a layer of tire shreds for 90% organic chemical removal (modified from Park et al., 1996)

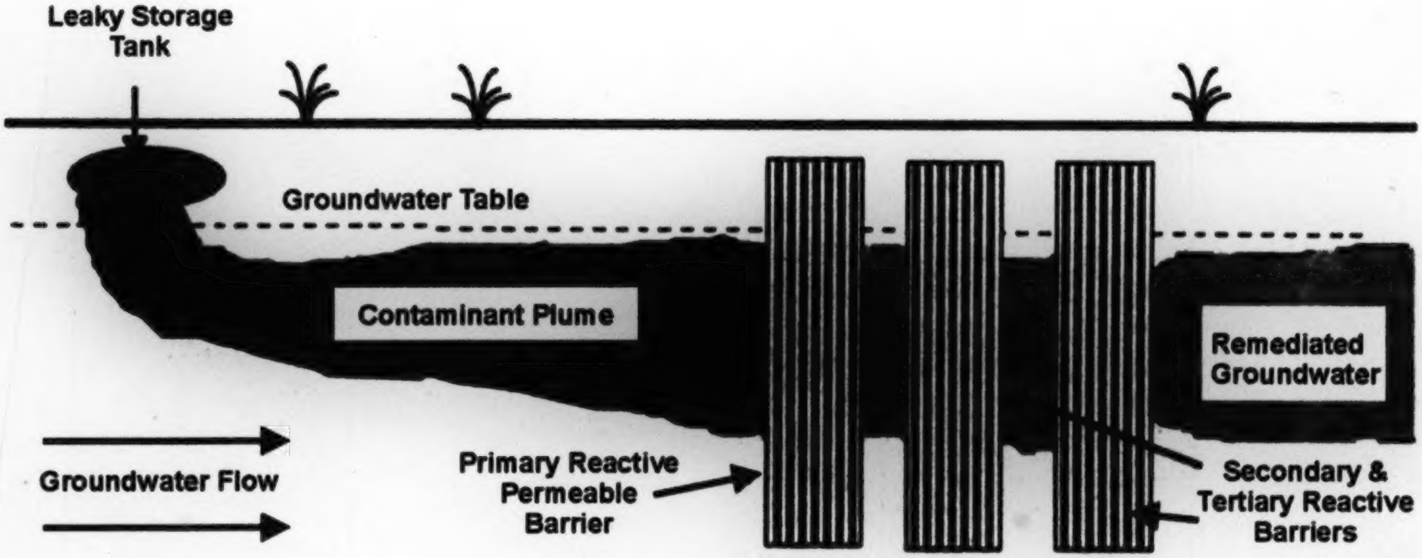
Leaky Storage Tank
Groundwater Table
Contaminant Plume
Remediated Groundwater
Groundwater Flow
Primary Reactive Permeable Barrier
Secondary & Tertiary Reactive Barriers

Figure 3.2 Conceptual schematic of a reactive permeable barrier system (modified from Kershaw and Pamukcu, 1997)

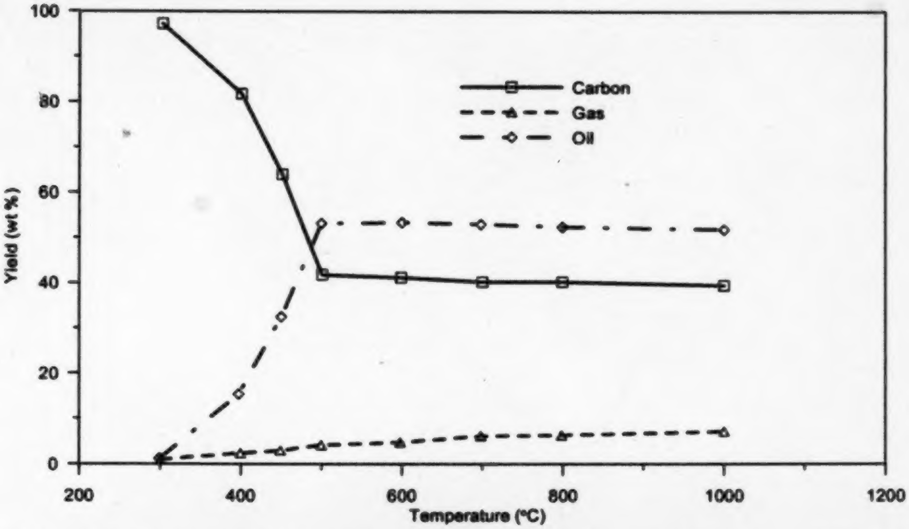

Figure 3.3 Product yields derived from the pyrolysis of tire rubber at different temperatures (modified from San Miguel et al., 1998)

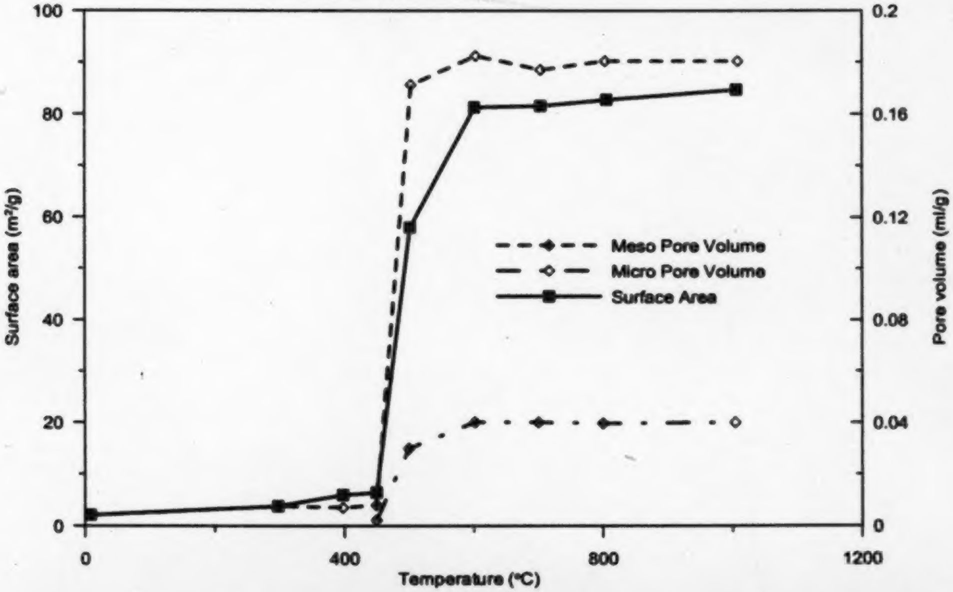

Figure 3.4 Surface area, micropore volume and mesopore volume from pyrolytic chars produced at different temperatures (modified from San Miguel et al., 1998)

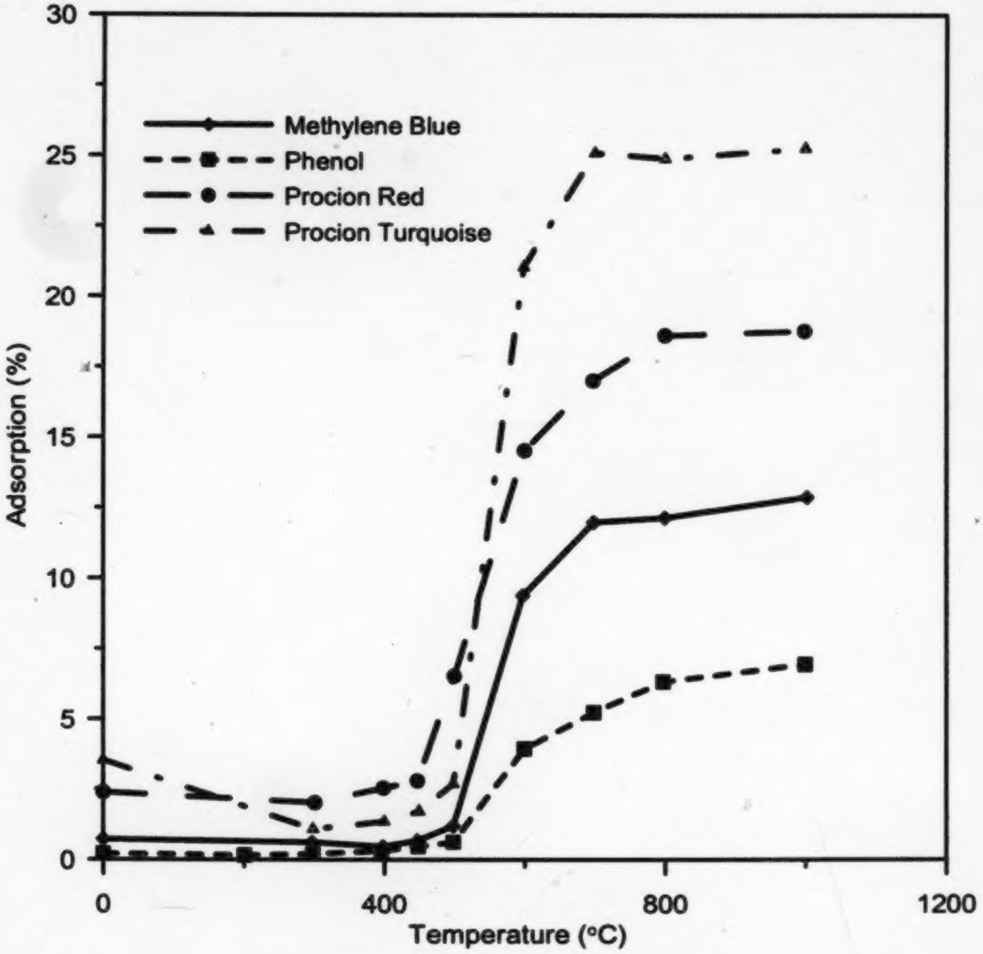

Figure 3.5 Relative aqueous adsorption efficiencies of tire rubber chars at different temperatures (modified from San Miguel et al., 1998)

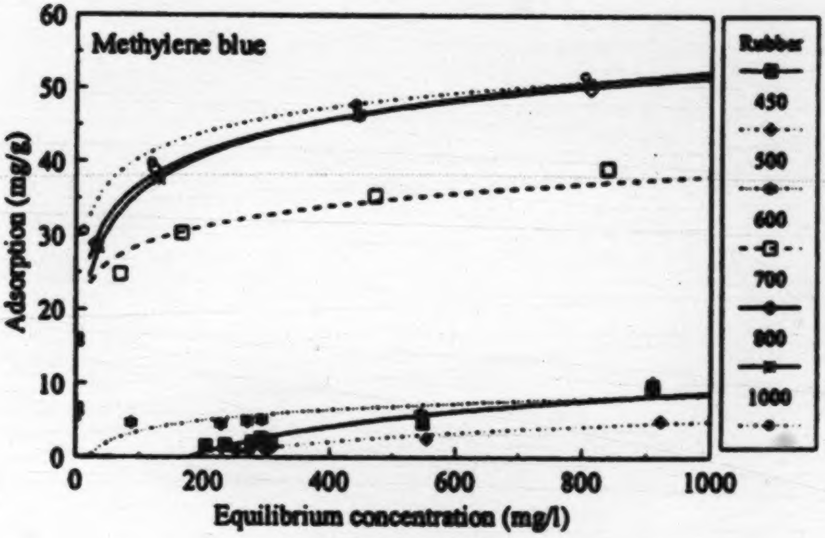

(a) Methylene blue

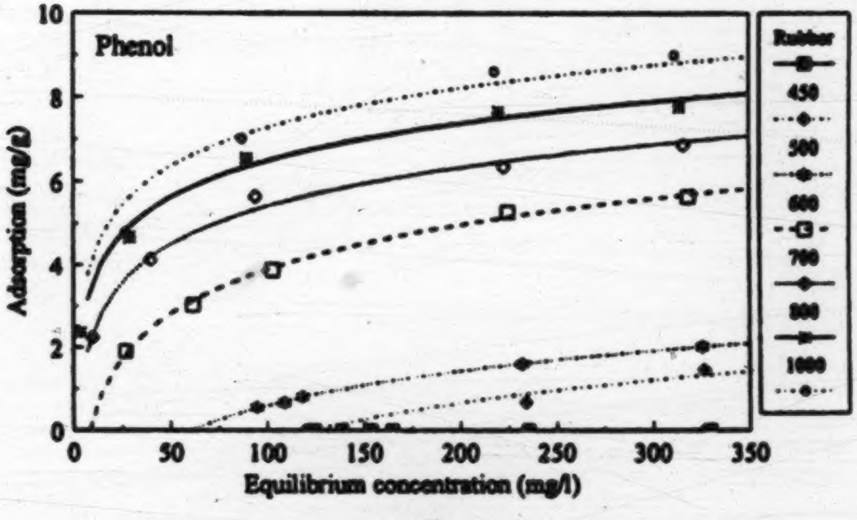

(b) Phenol

Figure 3.6 Adsorption isotherms of methylene blue, phenol, Procion red and Procion Turquoise on to tire rubber chars (modified from San Miguel et al., 1998)

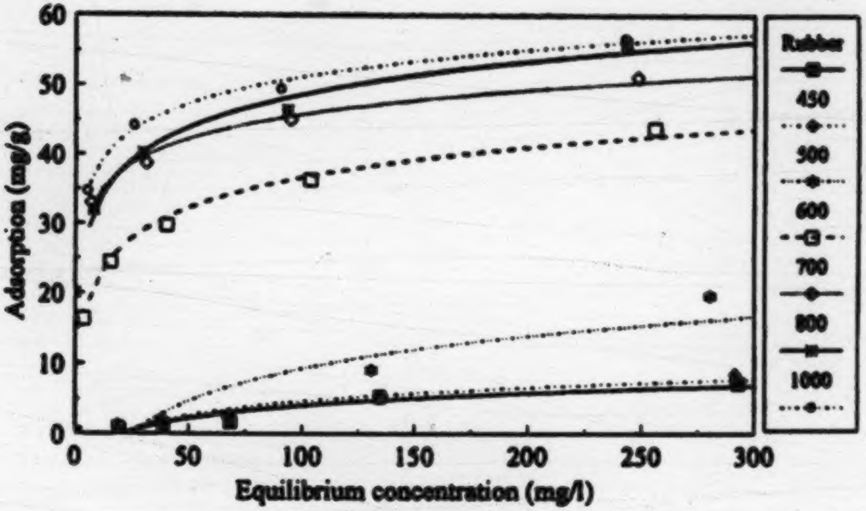

(c) Procion Red

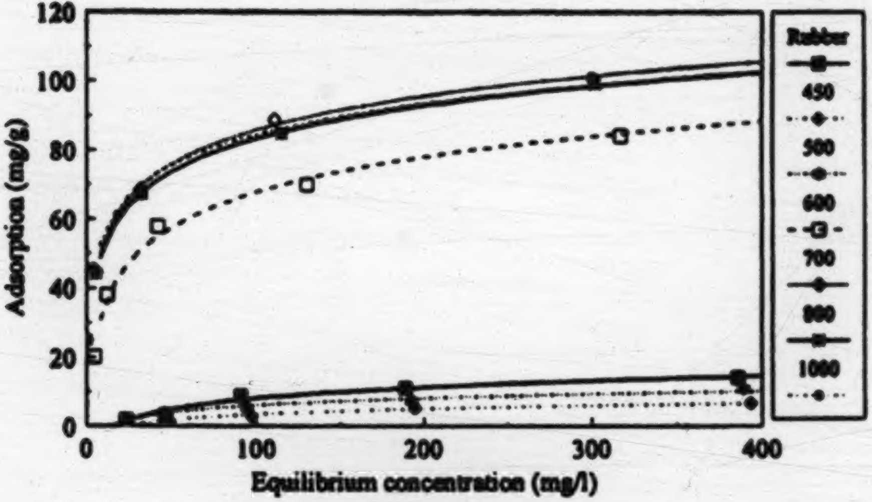

(d) Procion Turquoise

Figure 3.6 Continued (modified from San Miguel et al., 1998)

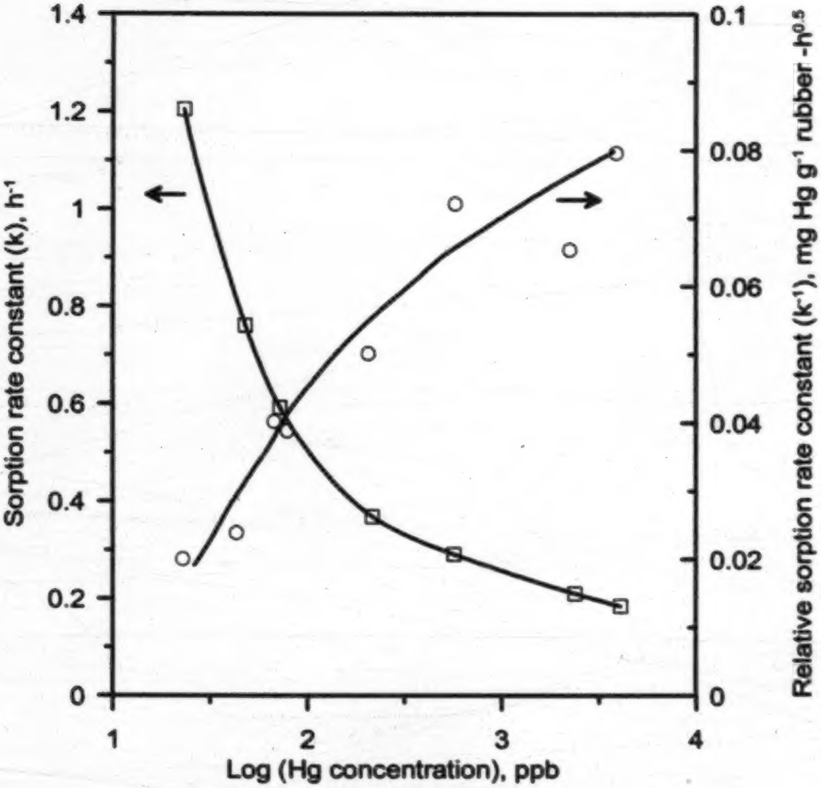

Figure 3.7 Effect of Hg (II) concentration on the observed rate of sorption (modified from Knocke and Hemphill, 1981)

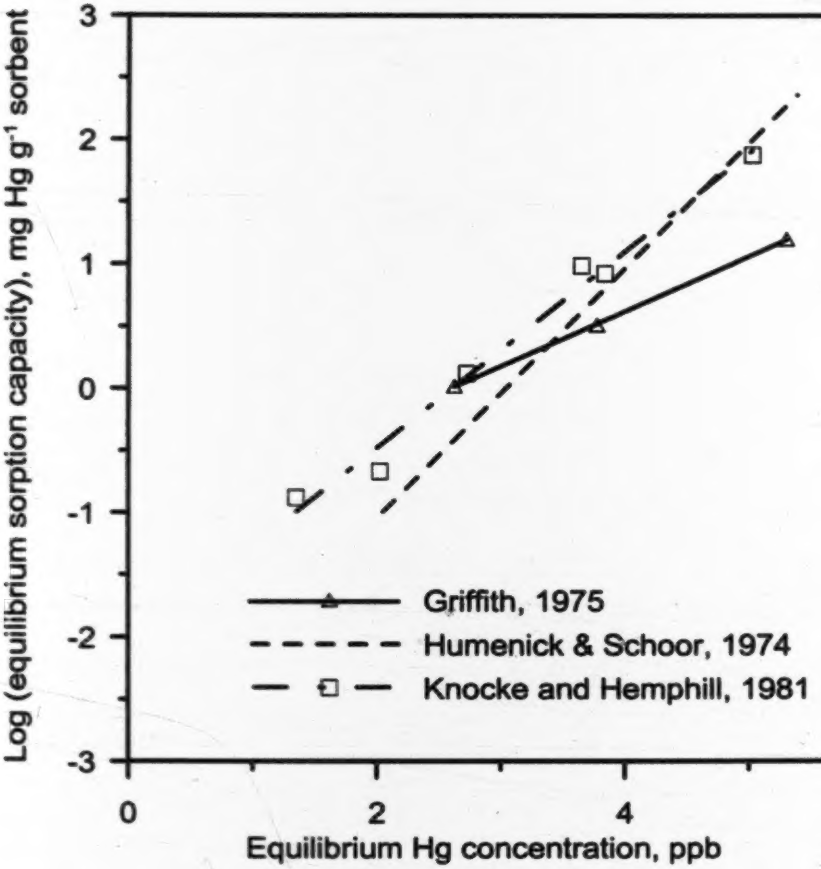

Figure 3.8 Comparative Hg (II) sorption capacity of tire rubber from various authors (modified from Knocke and Hemphill, 1981)

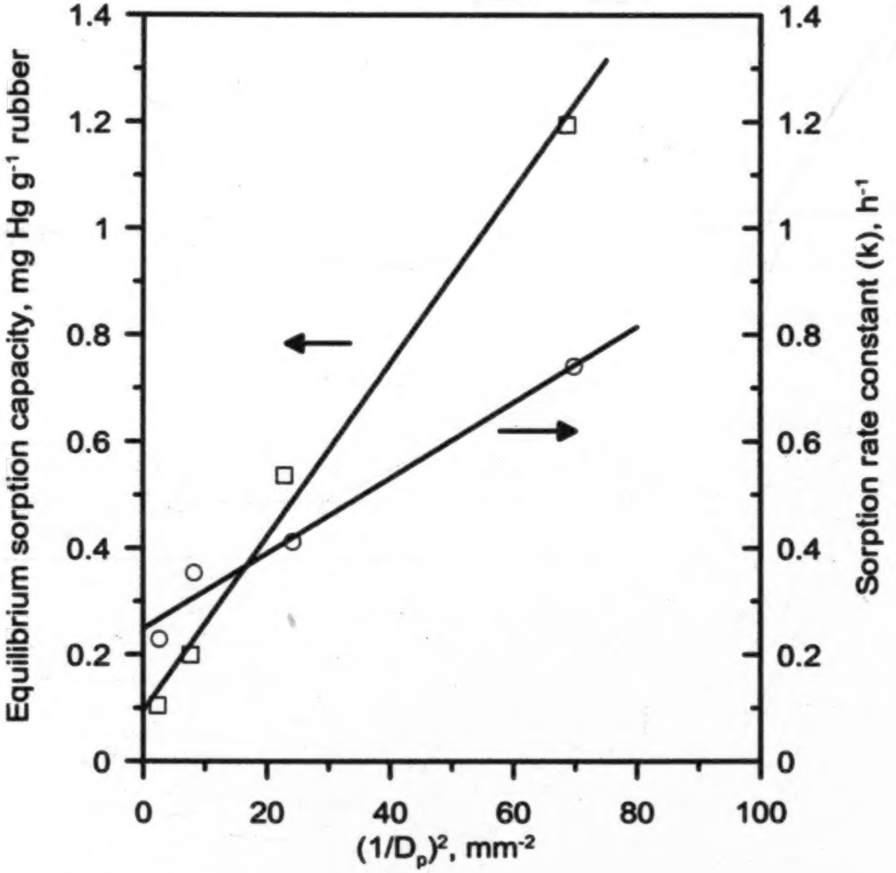

Figure 3.9 Relationship between available sorbent surface area and observed sorption capacity for Hg (II) (modified from Knocke and Hemphill, 1981)

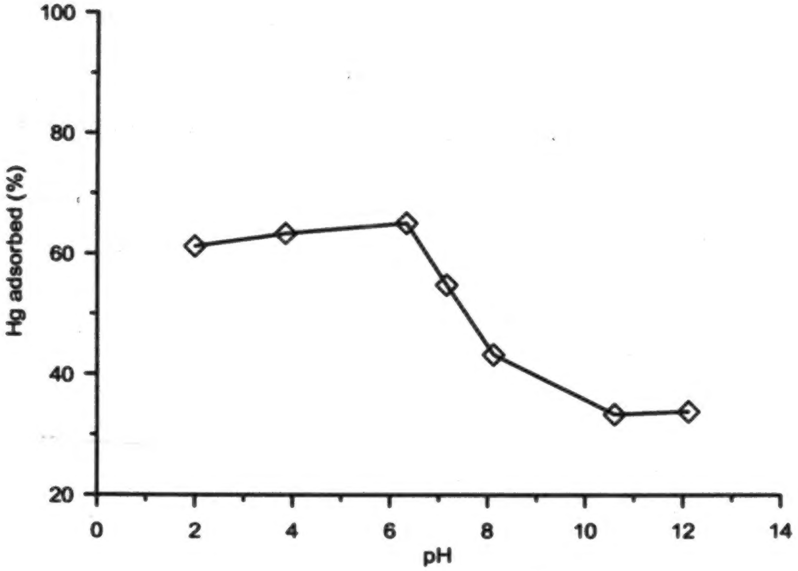

Figure 3.10 Adsorption of Hg (II) by ground tire rubber as a function of pH (modified from Meng et al., 1998)

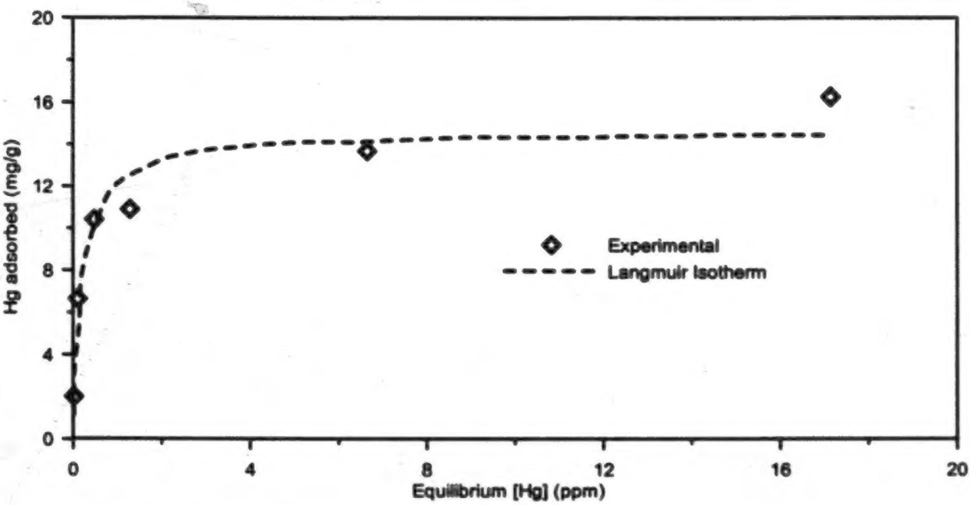

Figure 3.11 Hg (II) adsorption isotherm by ground tire rubber (modified from Meng et al., 1999)

CHAPTER 4 LEACHING PROPERTIES

4.1 Introduction

Tires contain various organic and inorganic compounds. Although tire composition varies by manufacturer and type, iron and zinc/sulfur oxides are the largest inorganic components. Low concentrations of calcium and aluminum are present, along with traces of magnesium, phosphorus, potassium, silica, sodium, titanium and chloride. As a result, waste tire rubber used in various geotechnical applications may have the potential to leach harmful contaminants into the ground water. The main concerns will be the leaching of metals such as zinc, iron, chromium and aluminum. These metals are commonly found in the steel reinforcement that is added throughout the tire to improve strength. The other contaminants of concern include zinc/sulfur oxides, which are used as accelerators in the vulcanization process (Park et al., 1994). Although waste tire rubber may have the potential to leach these contaminants, past research has found that they show no likelihood of being a significant source of ground water contamination (Edil et al., 1990; Envirologic, Inc., 1990; Duffy, 1995; Humphrey et al., 1997). The studies also investigated the type and amount of contaminants leached from scrap tires using various leaching procedures and test scenarios. This chapter will briefly discuss the various test procedures and summarize the results reported by several investigators on the leachability of scrap tire rubber and various rubber products.

4.2 Leaching Properties

An evaluation of the leachability of the scrap tire rubber was based on a review of the available leaching studies. Envirologic, Inc. (1990) summarized the leaching potential of tire shreds and various rubber products from four different leaching studies. They found that the majority of the substances tested were below the regulatory limits and concluded that leachate from tire shreds would not be hazardous to groundwater. Humphrey et al. (1997) investigated the leachability of a tire shred layer placed above the water table. They found, for the majority of the metals tested, the concentrations were below applicable drinking water standards. Yet, another study by Al-Tabbaa et al. (1997) showed significantly high levels of iron and zinc leached from both tire shreds and crumbs that exceeded applicable drinking water standards. Handreck (1996) found that soil-less potting media amended with tire rubber was detrimental to plants grown in the media due to increased zinc toxicity. These studies and others are described in detail below.

The Vermont Department of Environmental Conservation commissioned a preliminary evaluation of scrap tire shreds as an alternative to crushed stone in on-site sewage disposal systems. The report addressed the primary concern of potential contaminants that may be leached from tire shreds and other tire products. The assessment was based on a review of the following leaching studies: (1) an analysis conducted by the Radian Corporation for the Rubber Manufacturers Association (RMA); (2) test results from an experimental septic system in Indiana using tire shreds; (3) a Connecticut whole tire storage pond; and (4) a study conducted by the State of Wisconsin Laboratory of Hygiene for the Wisconsin Department of Natural Resources. The highest level of contaminants reported in each study are presented in Table 4.1 and compared to existing US Environmental Protection Agency (EPA) Drinking Water Standards, Vermont Primary Ground Water Standards and EPA Toxicity Characterization Leaching Procedure (TCLP) regulatory limits (Envirologic, Inc., 1990). The most conclusive tire leachate study was conducted in the RMA Study (Radian Corporation, 1989). They conducted the proposed EPA TCLP test procedures plus the current EP Toxicity procedures on cured, uncured, ground and ungrounded rubber products. These include various RMA rubber products from truck and automobile tires, roofing products, automotive belts and hoses, sealants and printer roller products. The products were leached and tested for various volatile and semi-volatile organics and metals. To leach organics and metals the TCLP employs a containment jar attached to a rotary tumbler turning at a rate of 30 rpm. The volatile organics are leached in a Zero-Head Space apparatus, which is contained in a self-enclosed piston system to force the leach solution through a filter, and effectively separating the leachates from the sample without exposure to air. To simulate field leaching conditions, the leaching solution for both processes used was an acetate buffer at pH of 4.9 and 2.9 for non-alkaline and alkaline constituents respectively. The extraction period for the TCLP is 24 hours and 16 hours for the EP Toxicity procedures. Of the compounds tested, all were reported significantly below the TCLP regulatory limits. The compounds for which Vermont has standards, all were below the limits and only lead and chromium appeared to be close to the limit. Leaching data from the Indiana septic system experiment show no significant differences between samples taken from the tire and stone systems, except for toluene, which was about 70 times higher in the tire system. In fact, the stone system showed higher concentrations for iron and lead but the higher concentrations were reported due to background effluent quality or from the mineral content of the stone. For the compounds tested in the Connecticut tire pond, most of them showed concentrations below the detection limits. Iron was the only compound tested which was occasionally above groundwater standards. In the State of Wisconsin Laboratory of Hygiene study, EP toxicity tests, Base-Neutral Organics tests and the American Foundry Society (AFS) tests were performed on shredded tires (Radian Corporation, 1989). The EP Toxicity tests were performed on regulated metals (barium, cadmium, chromium, lead and mercury) but none of the concentrations were above the detection limits. None of the compounds were also detected in the Base-Neutral Organics tests. The AFS test utilized three sequential pass-throughs for metals, anions, and organic and inorganic indicator parameters. Samples from the AFS test showed detectable but very low release patterns of substances tested and a declining concentration with multiple elutions. In addition, it was reported that the substances released may come from surface coatings rather than the structure of the tire compounds. In general, the report concluded, "leachate from tire shreds would not be a significant source of groundwater pollution".

The work reported by Al-Tabbaa et al. (1997) is summarized in Table 4.2. They also employed the TCLP on scrap tire rubber with particle sizes ranging from 1 to 12 mm. They placed 25 g samples of the various tire rubber sizes in a 500 mL extraction fluid of dilute sodium acetate solution (pH 4.9 ± 0.2). The mixtures were agitated and the contents were then centrifuged and subsequently filtered to separate the leachate from the solids. The leachates were then passed through an atomic absorption spectrometer to quantify the concentrations of iron, zinc and chromium. The results of the TCLP tests show that both iron and zinc exceeded their applicable drinking water standards. It also shows that tire rubber with smaller particle sizes leached higher concentrations of metals. This was directly due to larger surface area associated with the smaller sized rubber. They also conducted the same leaching procedures on various soils and soil-tire mixtures. The results are also shown in Table 4.2. The three soils that were leached on their own showed concentrations of iron exceeding the maximum concentration levels. Bentonite showed the highest iron concentration levels. The kaolin-lime-tire mixtures produced the lowest concentrations of both iron and zinc. This suggests that lime stabilizes all the iron that was leached. Hence, the purpose of including lime is to increase the pH of the leachate solution into the range for which heavy metals have very low solubility. All the leached zinc concentrations for all the soil and soil-tire mixtures were well below the maximum allowable levels. Chromium was also measured, but no detectable concentrations were found.

Duffy (1995) studied the use of tire shreds as leachate drainage layers and examined the potential effects of the shreds on leachate constituents and the related problem of potential degradation of tire shreds in contact with leachates. Constant leach recirculation tests, which involved up to three pass-throughs and utilizing distilled water as the circulation fluid were conducted to measure the potential risk to groundwater by tire shreds. Test results showed detectable but very low release patterns for all substances tested and declining concentration with continued leaching for most substances. However, four metallic elements exhibited increasing concentrations. Of these, only iron and manganese slightly exceeded applicable drinking standards; barium and zinc remained below acceptable drinking water limits. Metals leaching from tire shreds were therefore reported not to represent a major concern. In general, the leaching characteristics of tire chips are far less than most type of wastes. The final concentration levels reported for calcium, chlorine, sulfuric acid, nitrous and nitric acids, lead, and sodium all decreased after multiple pass-throughs. Levels reported for arsenic, cadmium, chromium, copper, selenium, and titanium were not detected. In addition, constant leach recirculation tests were conducted under differing temperature regimes to determine their worst-case potential leachability. The tests were performed on two columns set at temperatures of 23°C and 50°C. Leachate samples were extracted at 0, 30, 60 and 90 day intervals. All the tested parameters exhibited, at most, a slight increase in constituent levels. In the 23°C column, minor increases in barium, cadmium, chromium, selenium, and silver were observed, while minor decreases were reported for arsenic, lead, and sulfide. No significant changes were noted for mercury and cyanide. The 50°C column exhibited slight decreases in cyanide, sulfide, arsenic, barium and lead. No significant changes in cadmium, chromium, mercury, selenium and silver were observed. Furthermore, minor increases in pH were observed in both columns. According to the study, tire shreds themselves do not show signs of degradation or decomposition. The potential for clogging by biological action is equivalent to aggregate material of similar size, and possibly less if the metals inhibit biological growth..

Steer et al. (1995) monitored the concentrations of polychlorinated dibenzo-p-dioxins (PCDD) and polychlorinated dibenzofurans (PCDF) in samples of soil, runoff water, and oily residue collected from a tire fire that occurred on February 12, 1990 in Hagersville, Ontario. The tire fire, which was considered the largest ever in North America, burned for more than 17 days and incinerated between twelve and fourteen million used tires. Surface soil samples (approximately 10 g between 0 to 10 mm depth) were collected from five sites located at 500 m NE, E, SE, S and W from the center of the fire shortly after the fire was extinguished. In addition, samples were collected in May, 1991 from two soil piles present at the fire site. The samples represented (1) clean fill imported for rehabilitation of the site, and (2) soil discarded from the fire site. Large volumes of water were used to extinguish the fire and the resulting runoff was collected in several reservoirs to prevent contamination of groundwater. Water runoff samples were collected 6 days and 12 days after the start of the fire, and 4 weeks after the fire was extinguished. Runoff oil from the burning tires was also collected. The results for the soil samples collected from the site are shown in Table 4.3. Both dioxins and furans were essentially absent for the five samples of surface soil collected at 500 m from the fire (one sample only contained 53 pg/g of 0_8CDD). Table 4.4 shows the concentrations of PCDD/PCDF detected in the runoff water collected from the tire fire site. The concentrations in the water runoff were higher than those observed in a normal Ontario precipitation event. A large water treatment plant was set up on site to process any runoff water before it was allowed to drain into a nearby creek. It was reported that no PCDD/PCDF were detected in either samples (treated and creek water) at concentrations ranging from 2 to 6 parts per quadrillion (ppq) for TCDD/TCDF (tetra-CDD and tetra-CDF) congeners to 20 to 40 ppq for OCDD/OCDF (octa-CDD and octa-CDF) congeners. Theses ranges were well within Ontario's drinking water guideline detection limits. Three samples of the oil runoff produced in the tire fire were analyzed and the results are summarized in Table 4.5. PCDD/PCDF levels in the oil runoff were significant and the oil was treated appropriately.

Handreck (1996) investigated the leaching of zinc from tire rubber used in potting media. In their study, Petunia (Stereo Red) and Impatiens (Impulse Violet) were grown in a potting media produced from bark and sand, which were amended with 0, 5, 10, and 20% by volume of ground tire rubber. The ground rubber varied in particle sizes from less than 0.1 to 6 mm. The concentration of Zn was estimated through extraction of the potting media with diethylenetriamine pentaacetic acid (DTPA) and H_2O, both during potting and at harvest. They found that the growth and health of the plants grown in the tire-amended potting media were harmfully affected within two weeks of planting. Plant leaves showed symptoms ranging from marginal decay to death of whole leaves. This was due to increased zinc toxicity. Plants in the control medium, however, showed none of these symptoms. Figure 4.1 to 4.2 show the concentration of DTPA-extracted and H_20-extracted zinc throughout the experimental period (50 days) respectively. Both figures show an increase in zinc concentrations with increasing rubber content. The authors suggest that the increase in extractable zinc was due to the degradation of the rubber itself, rather than to diffusion from the tire rubber.

Humphrey et al. (1997) investigated the leachability of a tire shred layer placed above the groundwater table. In their study, two field trials were constructed in the state of Maine: (1) Richmond and (2) North Yarmouth. The main purpose of the Richmond Field Trial was to investigate the thermal insulative properties of tire shreds to limit the depth of frost penetration beneath a gravel-surfaced road. The North Yarmouth Field Trial was used to measure the effect of a compressible tire shred layer on the performance of an asphalt-concrete pavement. Both field trails were subsequently used for water quality monitoring purposes. The shreds were made from a mixture of steel and glass-belted tires and had wires protruding from the edges. They were also uniformly graded having nominal maximum size of 51 mm. At the Richmond Field Trial, groundwater monitoring wells were installed at strategic locations to determine the type and amount of inorganic and organic substances that may potentially leach from the shreds. Control wells were also installed to measure background substances naturally present in groundwater. Water quality index tests including pH, alkalinity, chemical oxygen demand, conductivity, and hardness were also performed. Water samples were obtained with a 1 L capacity bailer. Prior to sampling, about three well volumes were bailed from the well. The following sample types were taken from the test wells: (1) leachate filtered and preserved with nitric acid as appropriate for determination of dissolved metals; (2) leachate unfiltered and preserved with nitric acid; and (3) unfiltered leachate with no acid. Table 4.6 summarizes the data on filtered samples for the Richmond Field Trial. They found that most of the metals that can potentially leach from tire shreds were naturally present in the ground water at low levels. This included aluminum, barium, chromium, iron, lead, manganese, and zinc. Chromium levels[1] were consistently reported higher in the control wells than the test wells. Hence, the importance of installing control wells to measure the natural background levels of these substances was emphasized when assessing the effect of tire shreds on water quality. The significant finding was that for the majority of the metals detected the concentrations were below the applicable drinking water standards. The study hence concluded that tire shreds do not increase the concentration of substances that have a primary or secondary drinking water standard. This includes barium, cadmium, chromium, copper, lead and selenium for the former, and aluminum, chloride, sulfate, and zinc for the latter. However, under some solubility conditions, tire shreds may increase the levels of iron and exceed secondary drinking water standards. Furthermore, tire shreds increased the levels of manganese, which also has a secondary drinking water standard. Manganese, however, was reported to be present naturally in groundwater in many areas of the region studied. Although results from the Richmond Field Trial were positive, water quality monitoring continued for only 28 months after construction of the field trial. This may suggest that the elapsed time was insufficient for potential contaminants to migrate from the tire shred layer to the test wells even though the wells were located only a few meters away from the shreds. Furthermore, the sorption capacities of the native soil were not taken into account. The North Yarmouth Project, however, was designed to eliminate the uncertainties imposed by the sorptive capacity of the soil between the tire shreds and the sampling point. The North Yarmouth Field Trial employed a seepage collection basin that projected beyond the edge of the pavement so that runoff from the pavement and from the embankment side slope could infiltrate into the basin without being sorbed onto the native soil prior to sampling. The basin was located directly below the tire shred layer. The detailed results for the North Yarmouth Field Trial are given in Humphrey and Katz (1996). Substances with a primary drinking water standard were also present in trace amounts or were below the detection limit. In general, there were no significant differences between the levels of substances found in both field sections, and the control section. This indicate that for the conditions found at the North Yarmouth Field Trial, tire shreds did not tend to increase the concentrations of the substances tested. Furthermore, the substances were monitored for 2.5 years indicating that the long term leaching potential of the tire shreds was insignificant. Volatile and semi-volatile organics were also measured in two sets of samples taken from the North Yarmouth Field Trial, but the levels were undetectable.

---

[1] Valence species not reported

4.3 Summary

The leaching properties of scrap rubber tire reported by several authors were briefly discussed and summarized. Most of the organics and inorganics tested were either not detected or the concentrations were below applicable drinking water standards (Humphrey et al., 1997, Envirologic, Inc., 1990). However, iron and zinc (Al-Tabbaa et al., 1997; Humphrey et al., 1997; Duffy, 1995) were the metals found that often exceeded the applicable drinking water standards. Furthermore, Humphrey et al. (1997) noted that most of the metals that can potentially leach from tire shreds are naturally present in groundwater at low levels. Hence, the majority of leaching studies indicate that scrap tire rubber do not pose significant hazards to groundwater. The Handreck (1996) study, however, indicated that the levels of zinc in soil may be toxic to certain plants.

Table 4.1 Summary of tire leachate studies from Vermont Department of Environmental Conservation (reproduced from Envirologic, Inc., 1990)

Contaminant	US EPA Drinking Water Standards	VT Primary Ground Water Standards	EPA TCLP Regulations	RMA Assessment			Indiana Onsite Test		CT. Tire Pond	Wisconsin AFS
				TCLP (ground)	TCLP (unground)	EP Toxicity (cured)	Tires	Stone		
Organics										
Acetone				⊗	⊗		54	92		
Acrylonitrile			5000	⊗	⊗					
Benzene		5	70	⊗	⊗		63		⊗	
Bis(2-chloroethyl)ether			50	67	⊗					
Carbon Disulfide			14400	⊗	⊗					
Carbon Tetrachloride		5	70	⊗	⊗				⊗	
Chlorobenzene		100	1400	⊗	⊗					
Chloroform			70	⊗	⊗					
1,2-Dichlorobenzene			4300	⊗	⊗				⊗	
1,4-Dichlorobenzene			10800	⊗	⊗				⊗	
1,2-Dichloroethane		5	400	⊗	⊗				⊗	
1,1-Dichloroethylene		7	100	⊗	⊗				⊗	
2,4-Dinitrotluene			130	⊗	⊗					
Hexachlorobutadiene			720	⊗	⊗					
Isobutanol			36000	⊗	⊗					
Methylene Chloride		5	8600	⊗	⊗				⊗	
Methyl Ethyl Ketone		170	7200	21	⊗					
1,1,1,2-Tetrachloroethane			10000	⊗	⊗				⊗	

⊗ = tested but not detectable

All concentrations in µg/l (ppb)

Table 4.1 Continued

Contaminant	US EPA Drinking Water Standards	VT Primary Ground Water Standards	EPA TCLP Regulations	RMA Assessment			Indiana Onsite Test		CT. Tire Pond	Wisconsin AFS
				TCLP (ground)	TCLP (unground)	EP Toxicity (cured)	Tires	Stone		
Organics Continued										
1,1,2,2-Tetrachloroethane			1300	⊗	⊗				⊗	
Tetrachloroethylene			100	⊗	⊗				⊗	
Toluene		2420	14400	190	⊗		1500	22	⊗	
1,1,1-Trichloroethane		200	30000	⊗	⊗				⊗	
1,1,2-Trichloethane			1200	⊗	⊗				⊗	
Trichloroethylene		5	70	⊗	⊗				⊗	
Vinyl Chloride		2	50	⊗	⊗				⊗	
o,m,p-Cresols (ea)			10000	⊗	⊗					
Hexachlorobenzene		0	130	⊗	⊗					
Hexachloroethane			4300	⊗	⊗					
Nitrobenzene			130	⊗	⊗					
Pentachlorophenol		220	3600	⊗	⊗					
Phenol			14400	46	59					
Pyridine			5000	⊗	⊗					
2,3,4,6-Tetrachlorophenol			1500	⊗	⊗					
2,4,5-Trichlorophenol			5800	⊗	⊗					
2,4,6-Trichlorophenol			300	⊗	⊗					

⊗ = tested but not detectable

All concentrations in μg/l (ppb)

Table 4.1 Continued

Contaminant	US EPA Drinking Water Standards	VT Primary Ground Water Standards	EPA TCLP Regulations	RMA Assessment			Indiana Onsite Test		CT. Tire Pond	Wisconsin AFS
				TCLP (ground)	TCLP (unground)	EP Toxicity (cured)	Tires	Stone		
Inorganics										
Arsenic	50	50	5000	⊗	⊗	⊗	⊗	⊗		⊗
Barium	1000	1000	100000	590	140	73	69	270		110
Cadmium	10	5	1000	⊗	⊗		⊗	⊗	⊗	⊗
Chromium	50	50	5000	48	⊗		3	4		⊗
Copper	1000	1000					15	23	⊗	⊗
Iron	300	300					4810	5780	1950	230
Lead	50	20	5000	16	19	16	18	22		
Manganese	50									300
Mercury	2	2	200	0	⊗	⊗	⊗	⊗		
Nickel		350					6	9	⊗	
Phosphorus							17	211		
Selenium	10		1000	⊗	⊗	2				⊗
Silver	50	50	5000	⊗	⊗	⊗				
Zinc	5000	5000					53	121	30	630

⊗ = tested but not detectable

All concentrations in μg/l (ppb)

Table 4.2 Concentration of iron and zinc in leachate samples (after Al-abbaa et al., 1997)

Material	Particle size (mm)	% tire	pH	Iron (mg/L)	Zinc (mg/L)
Tire crumb	1 to 4	100	4.8	10.29	10.37[1]
Tire crumb	4 to 8	100	4.7	7.52	8.57[1]
Tire shreds	8 to 12	100	4.8	5.91	5.32[1]
Kaolin		0	4.7	0.36	0.51
Kaolin-tire	1 to 4	6	4.7	0.72	1.91
Kaolin-tire	4 to 8	15	4.6	0.88	1.79
Kaolin-tire	8 to 12	15	4.7	1.00	1.29
Kaolin-lime		0	11.1	0.24	0.07
Kaolin-lime-tire	1 to 4	6	10.8	0.28	0.066
Kaolin-lime-tire	4 to 8	15	10.4	0.24	0.049
Kaolin-lime-tire	8 to 12	15	10.6	0.20	0.045
Bentonite		0	4.8	0.80	0.24
Bentonite-tire	1 to 4	6	4.8	1.05	0.55
Bentonite-tire	4 to 8	15	4.7	1.24	0.617
Bentonite-tire	8 to 12	15	4.7	3.24	0.676
Drinking water standards				0.20	5.00

[1] Concentration of zinc greater than drinking water standards

Table 4.3 Concentrations (pg/g) of PCDD and PCDF in soil collected in the vicinity of Hagersville tire fire site (after Steer et al., 1995)

Sample	Clean fill	Discarded soil samples		Site at 500 m
		Minimum	Maximum	
PCDD				
T_4CDD[1]	(2)	(6)	17	(<26)
P_5CDD[2]	(2)	(5)	32	(<26)
H_6CDD[3]	(6)	(5)	36	(<26)
H_7CDD[4]	14	41	50	(<26)
O_8CDD	29	120	140	(<26) & 53
PCDF				
T_4CDF[1]	24	74	150	(<26)
P_5CDF[2]	(3)	50	66	(<26)
H_6CDF[3]	(5)	(10)	51	(<26)
H_7CDF[4]	(2)	(9)	(15)	(<26)
O_8CDF	(5)	(9)	(22)	(<26)

[1] 2,3,7,8-TCDD or 2,3,7,8-TCDF (tetra congener)
[2] 1,2,3,7,8-pentaCDD or 1,2,3,7,8-pentaCDF (penta congener)
[3] 1,2,3,4,7,8-hexaCDD or 1,2,3,4,7,8-hexaCDF (hexa congener)
[4] 1,2,3,4,6,7,8-heptaCDD or 1,2,3,4,6,7,8-heptaCDF (hepta congener)

Numbers in parentheses indicate that no PCDD/PCDF was detected at the concentration shown.

Table 4.4 PCDD/PCDF concentrations (ppt) in water runoff from Hagersville tire fire site (after Steer et al., 1995)

	02/18/90	02/24/90	03/24/90
PCDD			
T_4CDD[1]	0.7	0.03	0.009
P_5CDD[2]	1.2	004	(0.006)
H_6CDD[3]	0.5	0.04	0.03
H_7CDD[4]	1.8	0.04	0.3
O_8CDD	3.1	(0.09)	2.3
Total	7.3	0.5	2.7
PCDF			
T_4CDF[1]	(0.04)	0.009	(0.002)
P_5CDF[2]	0.03	0.003	(0.002)
H_6CDF[3]	(0.01)	(0.003)	0.05
H_7CDF[4]	(0.06)	(0.02)	0.5
O_8CDF	(0.04)	(0.02)	0.5
Total	0.03	0.01	1.0

[1] 2,3,7,8-TCDD or 2,3,7,8-TCDF (tetra congener)
[2] 1,2,3,7,8-pentaCDD or 1,2,3,7,8-pentaCDF (penta congener)
[3] 1,2,3,4,7,8-hexaCDD or 1,2,3,4,7,8-hexaCDF (hexa congener)
[4] 1,2,3,4,6,7,8-heptaCDD or 1,2,3,4,6,7,8-heptaCDF (hepta congener)

Numbers in parentheses indicate that no PCDD/PCDF was detected at the concentration shown.

Table 4.5 PCDD/PCDF concentrations (ppt) in oil runoff from Hagersville tire fire site (after Steer et al., 1995)

	Replicate samples		
	A	**B**	**C**
PCDD			
T$_4$CDD[1]	1400	1300	1100
P$_5$CDD[2]	2100	1800	1500
H$_6$CDD[3]	2200	1900	1500
H$_7$CDD[4]	2000	1900	1200
O$_8$CDD	3700	3200	2700
Total	11400	10100	8000
TEQ[5]	190	160	120
PCDF			
T$_4$CDF[1]	610	520	480
P$_5$CDF[2]	220	180	160
H$_6$CDF[3]	140	120	56
H$_7$CDF[4]	(60)	83	110
O$_8$CDF	(40)	34	47
Total	970	937	853
TEQ[5]	10	13	12

[1] 2,3,7,8-TCDD or 2,3,7,8-TCDF (tetra congener)
[2] 1,2,3,7,8-pentaCDD or 1,2,3,7,8-pentaCDF (penta congener)
[3] 1,2,3,4,7,8-hexaCDD or 1,2,3,4,7,8-hexaCDF (hexa congener)
[4] 1,2,3,4,6,7,8-heptaCDD or 1,2,3,4,6,7,8-heptaCDF (hepta congener)
[5] TEQ: concentrations of PCDD/PCDF converted to 2,3,7,8-TCDD toxicity equivalents (TEZ) by application of the International Toxicity Equivalency Factors (I-TEF)

Numbers in parentheses indicate that no PCDD/PCDF was detected at the concentration shown.

Table 4.6 Water quality results on filtered samples for Richmond Field Trial (after Humphrey et al., 1997)

Well No.	Date	Concentrations with primary limit (mg/L)						Concentrations with secondary limit (mg/L)							Concentration with no limit (Mg/L)			
		Ba	Cd	Cr	Cu	Pb	Se	Al	Fe	Mn	Zn	Cl^-	SO_4	Solids	Ca	Mg	Hard.	Na
R.A.L.		2	0.005	0.1	1.3	0.015	0.05	0.2	0.3	0.05	5	250	250	500	N.A.	N.A.	N.A.	N.A.
0+69	12/23/93	<0.01	<0.005	0.015	<0.01	<0.057	N.D.	<0.1	<0.1	0.145	<0.01	64.7	65.3	N.D.	58.8	10.4	N.D.	30.3
0+69	5/24/94	0.023	<0.005	0.013	0.006	<0.057	N.D.	<0.2	<0.01	0.022	<0.005	122.0	57.3	N.D.	76.2	15.0	N.D.	30.0
0+69	1/18/95	0.030	N.D.	0.011	0.006	<0.005	N.D.	<0.015	<0.1	0.003	0.010	148.0	22.3	430	76.1	15.1	252	32.1
3+00	12/23/93	<0.01	<0.005	<0.01	<0.01	<0.057	N.D.	<0.1	<0.1	0.021	<0.01	135.9	13.2	N.D.	63.4	15.4	N.D.	24.2
3+00	5/24/94	0.045	<0.005	0.009	<0.005	<0.057	N.D.	<0.2	<0.01	0.008	<0.005	123.9	2.7	N.D.	54.6	13.4	N.D.	23.0
3+00	1/18/95	0.028	N.D.	<0.002	<0.004	<0.005	N.D.	<0.015	<0.1	<0.002	<0.003	50.2	12.5	210	27.5	6.5	96	16.0
3+42	12/23/93	<0.01	<0.005	<0.01	<0.01	<0.057	N.D.	0.176	<0.1	0.081	<0.01	5.6	11.8	N.D.	6.4	1.7	N.D.	7.9
3+42	5/24/94	0.005	<0.005	0.005	<0.005	<0.057	N.D.	<0.2	0.010	0.057	<0.005	12.8	4.1	N.D.	9.1	2.3	N.D.	7.8
3+42	1/18/95																	
6+19	12/23/93	<0.01	<0.005	<0.01	<0.01	<0.057	N.D.	<0.1	<0.1	0.294	<0.01	5.8	8.2	N.D.	21.8	2.0	N.D.	7.1
6+19	5/24/94	0.007	<0.005	0.006	0.005	<0.057	N.D.	<0.2	<0.01	0.042	<0.005	5.0	3.1	N.D.	20.6	1.7	N.D.	6.2
6+19	1/18/95	0.008	N.D.	<0.002	<0.004	<0.005	N.D.	<0.015	<0.1	0.006	<0.003	2.2	4.0	80	20.6	1.7	58	5.8
6+77	12/23/93	<0.01	<0.005	<0.01	<0.01	<0.057	N.D.	<0.01	<0.1	0.252	<0.01	3.7	15.8	N.D.	19.9	1.6	N.D.	10.8
6+77	5/24/94	<0.005	<0.005	0.005	<0.005	<0.057	N.D.	<0.2	<0.01	0.080	<0.005	2.8	5.0	N.D.	18.0	1.3	N.D.	7.7
6+77	1/18/95	0.004	N.D.	0.002	<0.004	<0.005	N.D.	<0.015	<0.1	0.009	<0.003	1.6	4.8	40	17.6	1.2	49	8.1
8+32	12/23/93	<0.01	<0.005	<0.01	<0.01	<0.057	N.D.	<0.1	<0.1	<0.01	<0.01	109.4	7.1	N.D.	78.4	12.8	N.D.	14.5
8+32	5/24/94	0.023	<0.005	0.011	<0.005	<0.057	N.D.	<0.2	<0.01	<0.005	<0.005	170.3	4.0	N.D.	105	18.3	N.D.	15.0
8+32	1/18/95	0.024	<0.005	0.005	<0.004	<0.005	N.D.	<0.015	<0.1		0.004	144.0	12.4	490	84.1	16.4	278	19.2
D.L.	12/23/93	0.01	0.005	0.01	0.01	0.057	N.D.	0.1	0.1		0.01	0.64	2.71	N.D.	1	1	N.D.	1
D.L.	5/24/94	0.005	0.005	0.005	0.005	0.057	N.D.	0.2	0.01		0.005	0.64	2.71	N.D.	1	0.2	N.D.	2
D.L.	1/18/95	0.001	0.005	0.002	0.004	0.005	0.001	0.015	0.1		0.003	0.05	0.05	1	0.1	0.1	0.662	0.5

R.A.L - regulatory allowable limit
D.L. = detection limit
N.D. = not determined
N.A. = not applicable
Hard. = hjardness expressed in mg/L as $CaCO_3$
Well no. 3+42 destroyed prior to 1/18/95 sampling data

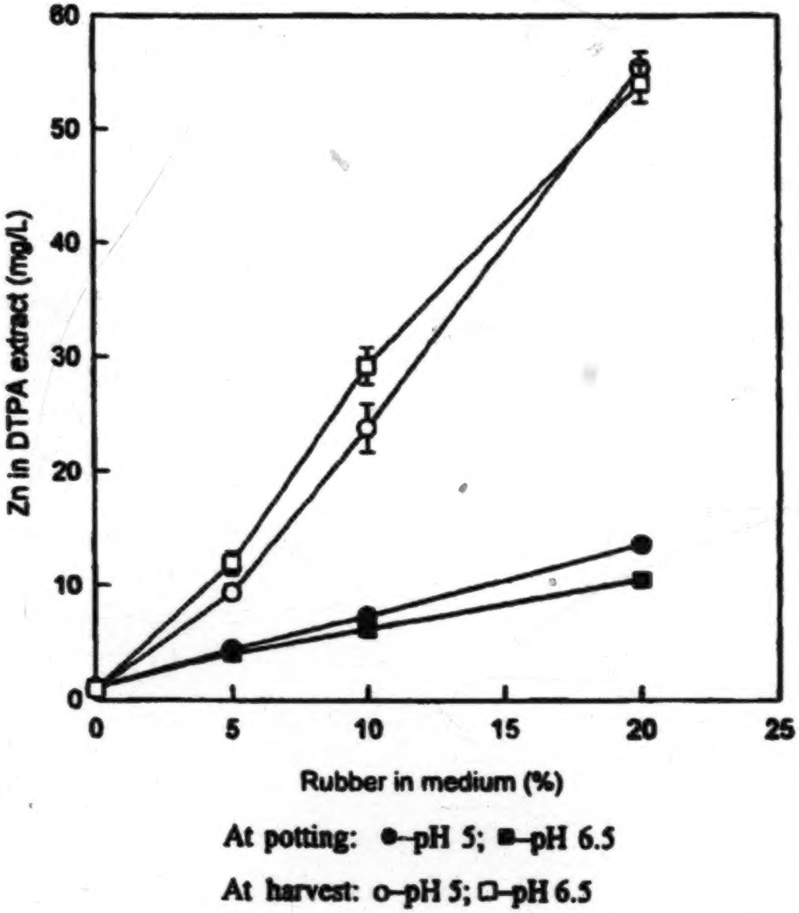

Figure 4.1 Zinc concentrations in DTPA extracts of the potting media as affected by pH and rubber content (modified from Handreck, 1996)

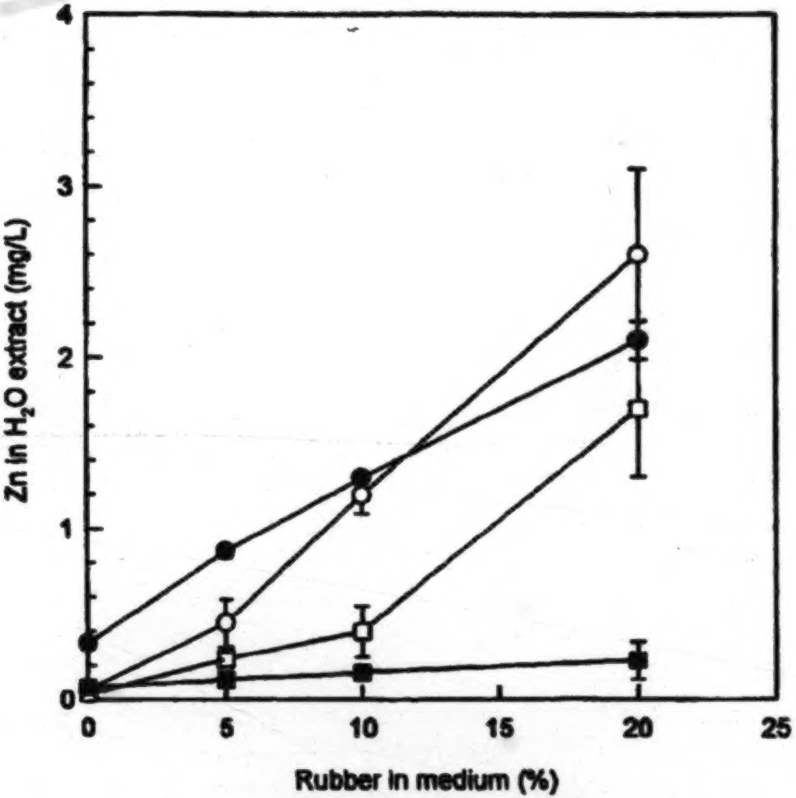

At potting: ●–pH 5; ■–pH 6.5
At harvest: ○–pH 5; □–pH 6.5

Figure 4.2 Zinc concentrations in H_2O extracts of the media as affected by pH and rubber content (modified from Handreck, 1996)

CHAPTER 5 LABORATORY TESTING PROCEDURES

5.1 Introduction

The second phase of this research consisted of laboratory experiments to evaluate the geotechnical properties of crumbed tire rubber including particle size and gradation, compaction characteristics, hydraulic conductivity, strength, thermal properties, and dynamic properties. The subsequent subsections describe the test material, and laboratory experimental apparatus and procedures that were followed throughout this research. A more detailed discussion on the general theory, laboratory testing equipment, and test procedures are also presented for the thermal and dynamic properties of tire crumbs.

5.2 Testing Material

Tire crumbs with various particle sizes and gradations were obtained from different crumb manufacturers in Alberta. Table 5.1 summarizes the different grain-size distribution of crumbs that were obtained from the different suppliers. The crumbs varied in size from less than 0.85 mm (No. 20 minus) to 6.3 mm (1/4 in). The grain-size distributions were specified by the manufacturers, which were based on the ASTM US sieve designations. For example, the No. 10 grain-size distribution represents tire crumbs where 95% or more of the material passes the No. 10 mesh, with up to 5% retained on the No. 10 mesh and no material retained on the No. 8 mesh. A detailed description of the particle size, shape, and particle gradation is given in Section 6.1.

5.3 Particle Size and Gradation

The grain-size distribution of the tire crumbs was determined using a mechanical sieve analysis according to ASTM D 422 (Standard Test Method for Particle-Size Analysis of Soils) (ASTM, 1997). For the smaller tire crumb sizes, in particular the No. 20 minus, No. 10 - 20, and No. 10, the particles tended to adhere to one another due to electrostatic attraction. Hence, a small quantity of talc (1% by mass of tire crumb) was added and mixed thoroughly with the rubber to eliminate particle attraction and retention on larger sized sieves. This method was adapted from Tire Recyclers of Calgary (TROC). The grain-size distribution analysis was then presented on standard particle size distribution plots.

The indication of the spread (or range) of particle size and the shape of the distribution curve was described by the coefficient of uniformity (C_U) and the coefficient of curvature (C_C) respectively:

$$C_U = \frac{D_{60}}{D_{10}}$$ **[Equation 5.1]**

$$C_C = \frac{D_{30}^2}{D_{60}D_{10}}$$ **[Equation 5.2]**

The letter D refers to the size, or apparent diameter of the solid particles and the subscript (10, 30, 60) denotes the percent that is smaller. For example, D_{10} denotes the size such that 10% of the particles are smaller than that size.

5.4 Specific Gravity

The specific gravity of crumbed tire rubber was determined in accordance with ASTM D854 (Standard Test Method for Specific Gravity of Soils). The test method describes the determination of the specific gravity of soils that pass the No. 4 sieve using a 500 mL volumetric flask (or pycnometer). Prior to testing, the tire crumbs were de-aired by boiling in distilled water in the flask for about 10 to 15 minutes. Then the samples were left to cool to room temperature and a vacuum was applied for about 10 minutes using an aspirator. The specific gravity tests were conducted three times for each grain-size distribution for repeatability and verification of results.

The specific gravity was determined using the following relationship:

$$G_s = \frac{W_s}{Ws + W_{b+w} - W_{b+w+s}} \quad \text{[Equation 5.3]}$$

Where:

G_s = specific gravity of dry tire crumbs

W_s = weight of dry tire crumbs (g)

W_{b+w+s} = weight of flask + water + tire crumbs at T°C (g)

W_{b+w} = weight of flask + water at T°C (obtained from flask calibration curves) (g)

5.5 Compaction Characteristics

The minimum dry unit weights of tire crumbs were determined according to ASTM D 4254 (Standard Test Method for Minimum Index Density and Unit Weight of Soils and Calculation of Relative Density) (ASTM, 1997). The crumbs were placed loosely into a 0.1 ft^3 mold using a funnel to minimize particle segregation. The funnel was filled with tire crumbs, which were placed loosely into the mold by pouring from the spout in a steady stream, and holding the funnel upright and vertical. The funnel was retracted slowing while continuously adjusting the height of the spout to maintain continuous flow.

The compacted dry unit weight was determined according to ASTM D 4253 (Maximum Index Density and Unit Weight of Soils Using a Vibratory Table), which specifies a 11 kg mass of specimen for soils with a maximum particle size of 9.5 mm. However, this specification would require a tremendous volume of tire crumbs. Therefore, enough crumbs (about 1 kg) were used to completely fill the compaction mold in a loose state. Since the tire crumbs were comparable in particle size to sands and gravels, moisture effects were considered negligible. For tire shreds, Humphrey et al. (1992) found that water had little effect on the dry unit weights.

5.6 Compressibility

One-dimensional confined compressibility tests were conducted using a large-strain consolidation apparatus to accommodate the larger crumb sizes as well as to anticipate large material compression. The large-strain consolidation apparatus was developed by the University of Alberta to originally test the mechanical properties of mine tailings (Qiu and Sego, 1998). The compressibility tests were conducted at various overburden pressures under both dry and saturated conditions at room temperature. The test apparatus set-up under dry and saturated conditions are shown in Figures 5.1 and 5.2 respectively. A schematic of the large-strain consolidation apparatus is shown in Figure 5.3. The apparatus is 100 mm in diameter and can accommodate sample heights of only up to 130 mm. The vertical pressure is applied to the sample via air pressure and rolling diaphragm/PVC loading piston. The vertical displacement was measured using a linear potentiometer transducer that is attached to the displacement rod. The test data was collected using a data acquisition system (Fluke Helios Plus 2287A) and a desktop computer.

Dry specimens were prepared by loosely placing the tire crumb into the consolidation apparatus using a funnel. The procedures are described in ASTM D 4253. Saturated specimens were prepared by first boiling the tire crumbs in distilled water for approximately 30 minutes. The purpose of boiling the tire crumbs rubber was to saturate the sample by eliminating entrained air. The saturated samples were then left to cool to room temperature, and then placed into the consolidation apparatus using a scoop.

The one-dimensional compressibility tests were conducted under 10, 20, 50, and 100 kPa pressures under the condition of no lateral yield. The pressures were applied incrementally, and the vertical deformation with time was monitored for up to 12 hrs. Subsequent unloading tests were also conducted at the same pressures to evaluate the rebound properties of crumbed tire rubber. After unloading, the samples were then reloaded incrementally to evaluate their recompression properties.

The compressibility of tire crumbs was then represented graphically on a semi-log plot of void ratio versus the logarithm of vertical stress (e versus $\log\sigma_v$). The void ratio for the dry specimens was calculated using the following expression:

$$e = \frac{G_s \gamma_w}{\gamma_d} - 1 \qquad \textbf{[Equation 5.4]}$$

where:

e = void ratio
G_s = apparent specific of tire crumbs
γ_w = unit weight of water (9.81 kN/m^3)
γ_d = dry unit weight of tire crumbs (kN/m^3)

The void ratio for the saturated specimens at the end of each stress increment was calculated from the dry weight of the specimen using the following expression (after Craig, 1992):

$$e_1 = \frac{H_1 - H_s}{H_s} = \frac{H_1 - Ms / AG_s \rho_w}{Ms / AG_s \rho_w} \qquad \textbf{[Equation 5.5]}$$

where:

e_l = void ratio at the end of each stress increment
H_l = sample height at the end of each stress increment (cm)
H_s = equivalent sample height (cm)
M_s = dry weight of tire crumbs measured at the end of test (g)
G_s = apparent specific gravity of tire crumbs
ρ_w = density of water (1g/cm^3)

The e versus logσ_v plots were subsequently used to determine the compression index (C_c), swelling index (C_s), and recompression index (C_r).

5.7 Hydraulic Conductivity

Constant head permeability tests were conducted to evaluate the hydraulic conductivity under various hydraulic gradients and overburden pressures. The permeability tests were conducted in conjunction with the compressibility tests under saturated conditions using distilled, de-aired water as the liquid permeant.

The hydraulic conductivity was determined from Darcy's law:

$$v = ki \qquad \textbf{[Equation 5.6]}$$

where:

v = discharge velocity (cm/s)
k = hydraulic conductivity (cm/s)
i = hydraulic gradient

5.8 Strength

To determine the shear strength of crumbed tire rubber, direct shear and consolidated drained (CD) triaxial compression tests were conducted.

5.8.1 Direct Shear Test

The direct shear tests were conducted according to similar procedures outlined in ASTM D 3080 (Standard Test Method for Direct Shear Tests of Soils Under Consolidated Drained Conditions) (ASTM, 1997). The tire crumbs were tested under dry and saturated conditions. Direct shear tests were conducted using a 100 x 100 mm (4 in) direct shear box to accommodate the larger grain-size. The samples were prepared by compaction in 5 to 7 layers using a vibratory scriber. A total of three direct shear tests were performed on each grain-size distribution under normal stresses of 25, 50, and 100 kPa. During each test, the shear force was measured using a load cell, and the horizontal and vertical deformations were measured using two linear variable differential transformer (LVDT) transducers. The normal stresses were applied using a hanger/lever loading system.

Since the area of contact at the interface between the upper and lower halves of the box decreases as the sample is sheared, a correction was made. For a box with interior dimensions of l by w, where l is the dimension parallel to the direction of movement, the area of contact, or corrected area A_c is given by:

$$A_c = w(l - 2\Delta H)$$ **[Equation 5.7]**

where ΔH is the horizontal displacement of the top half of the shear box in millimetres.

5.8.2 Triaxial Compression

Triaxial compression specimens were prepared using a split mold having an inside diameter of 64 mm and height of 150 mm. First, a latex membrane (64 mm in diameter) was placed on the base pedestal and sealed with two "O" rings. The split mold was then assembled around the membrane and it was folded out and over the top of the mold. A vacuum was applied to the side of the split mold to remove any wrinkles by pulling the membrane out to the walls of the mold. Tire crumbs were then placed into the mold and compacted in 5 to 10 layers using a small tamping rod with a 30 mm diameter tamping foot as shown in Figure 5.4. The top cap was then placed on top of the specimen, and the latex member was pulled over the cap and sealed with two other "O" rings. A vacuum was also applied to the top cap as shown in Figure 5.5. The split mold was then removed and the sample dimensions were recorded (Figure 5.6). The specimens were saturated by applying equal increments of back and cell pressures up to a maximum of 400 kPa. The samples were assumed saturated when this pressure was maintained for about 20 to 30 minutes. The cell pressure was then increased to represent the applied confining pressure and the specimens were consolidated under isotropic conditions. Volume changes were measured using a volumetric transducer. After 30 minutes of consolidation, a vertical load was applied at a constant displacement rate of 0.3 mm/min until the sample was deformed to 20% axial strain. The test procedures were conducted at confining pressures of 25, 50, and 100 kPa. One test was conducted for each confining pressure per grain-size distribution.

5.9 Thermal Properties

5.9.1 General Theory

Geotechnical applications that require knowledge of the thermal conductivity of soils may include the analysis of heat dissipation from buried electrical cables, prediction of frost penetration, and sampling using ground freezing techniques. The thermal conductivity of soils is highly variable and is governed by temperature, soil type, pore fluid, degree of saturation, soil density, and processes associated with freeze-thaw. To measure the thermal conductivity of soils, it is necessary to set up a temperature gradient across the soil sample being tested. The two primary test methods to measure the thermal conductivity of soils are the steady state and transient methods. In the former method, the soil being tested should be in a thermal steady state when the measurements are made. The most important steady state method is the guarded hot plate (GHP) test, which has been standardized by ASTM (Farouki, 1981). With transient methods, the temperature of the soil varies with time during the measurement. Such methods are more versatile than the steady state methods and can be more easily performed.

In this study, transient state thermal conductivity tests using the thermal needle method (also referred to as thermal probe method or line source method) were carried out on tire crumbs. The method is based on the measurement of the rate of temperature rise along a line heat source within a semi infinite, homogeneous and isotropic medium (Farouki, 1981, Mitchell and Kao, 1978). The thermal needle method incorporates relatively simple apparatus and instrumentation. The needle or probe consists of a heater element producing thermal energy at a constant rate and a temperature-sensing device (usually a thermocouple or thermistor). The thermal needle is inserted into the material to be tested, and being relatively thin, the needle should cause little sample disturbance. The rate of rise in the temperature of the needle depends on the thermal conductivity of the surrounding material (Farouki, 1981). The main advantage of using the thermal needle over other methods is that the thermal conductivity can be computed directly from the test data without knowledge of the heat capacity of the material being tested (Mitchell and Kao, 1978). The method is also much more versatile than the steady state methods and can be easily performed. Unlike the GHP test, the probe method requires less time. Attainment of the steady state in the GHP test may sometimes take considerable amount of time after the initial temperature difference has been applied (Farouki, 1981).

5.9.2 Thermal Testing Apparatus

To investigate the influence of pore fluid, compaction, overburden pressure, and temperature on the thermal properties of tire crumbs, the following testing apparatus were used.

Thermal Needle and Aluminum Cells

The thermal needle and an aluminum cell (or thermal cell) were used to investigate the influence of pore fluid, temperature, and compaction. A photo of the thermal needle and aluminum cell is depicted in Figure 5.7 and a schematic of the thermal needle and top cap is shown in Figure 5.8. The thermal needle is a 1/4 in diameter cartridge heater with a stainless steel sheath (Model CSH-103260/120V) (OMEGA Engineering, Inc., 1995). A resistance temperature detector (RTD) was epoxied to the exterior of the thermal needle to measure the change in electrical resistance with time as a result of changes in temperature.

Combined Thermal Needle and Large-Strain Apparatus

To investigate the influence of dry unit weight and pore fluid, the thermal needle was mounted inside on the bottom of a large-strain consolidation apparatus. These tests were conducted under various vertical stresses of up to 100 kPa under both dry and water-saturated conditions at room temperature.

5.9.3 RTD Calibration

Prior to testing, the RTD's were calibrated to obtain the resistance reading at 0°C. The thermal needle was submerged in a jug containing ice water, and shaken. The changes in resistance and temperature were monitored simultaneously with a digital multi-meter and thermometer respectively. When the resistance reached a constant value, it was recorded as R_O, which represented the RTD resistance at 0°C. For an ideal RTD, the measured resistance is 100 ohms at 0°C. The RTD calibrations are included in Appendix F.

5.9.4 Sample Preparation

Samples for the thermal needle and aluminum cells were prepared in the loose and dense state under dry and saturated conditions. Dry, loose samples were prepared according to the procedures outlined in ASTM D 4254. Saturated samples were prepared according to the same procedures followed for the compressibility tests under saturated conditions.

Compacted dry and saturated samples were prepared by compaction using a vibratory table with a 30 kPa surcharge in increments of 5 layers. After the samples were prepared, the caps containing the thermal needle were installed into each cell by pushing them into the cell from the top. The samples were then transferred to a portable cooler as shown in Figure 5.9. The first set of tests was carried out at room temperature.

For the combined thermal needle and large-strain apparatus, dry and saturated samples were prepared loosely using the procedures followed for the compressibility tests.

5.9.5 Thermal Conductivity Measurement

The thermal conductivity measurements were made by connecting the heating cartridge element and RTD to the constant current source and multimeter respectively. The constant current to the heating element was supplied by a DC power supply (6 V) (Hewlett Packard 6434B). A schematic of the connection is shown in Figure 5.10. A current controlling resistor was placed in series between the power source and the heating element. The resistance and voltage drop across the resistor were measured with digital multimeters (Fluke 8050A). The data for the thermal conductivity tests were recorded manually. At time = 0, the current was directed to the heater, and the RTD readings were recorded at 5 to 15 second intervals for up to a maximum duration of 15 to 20 minutes, or until a constant reading in resistance was observed with time. The test procedures for the thermal needle and aluminum cells apparatus were repeated at different temperatures after sufficient time had passed between tests for the samples to establish thermal equilibrium (usually between 12 to 24 hours). Table 5.2 summarizes the sequence of tests in which the thermal conductivity measurements were made. For the combined method, thermal conductivity measurements were made subsequent to applying the incremental vertical stresses. Time was allocated (usually about 12 hours) between stress increments so that the samples could reach full consolidation of the material and to established thermal equilibrium before the next set of measurements were carried out.

5.9.6 Analysis of Results

The thermal conductivity measurements were analyzed by converting the measured resistance to temperature using the following expression:

$$T = \frac{R_T - R_O}{\alpha}$$ **[Equation 5.8]**

where:

T = temperature at any time (°C)

R_T = resistance at temperature T (ohms)

R_O = resistance at temperature T = 0°C (ohms; obtained from RTD calibration)

α = 0.385 ohms/°C (resistance temperature coefficient for RTD's used; Model DIN43760) (OMEGA Engineering, Inc., 1995)

A plot of temperature rise at the heat source against the natural logarithm of time conforms to an S-curve, from which the slope of the linear portion of the experimental curve can be used to calculate the thermal conductivity, λ, according to the equation (Mitchell and Kao, 1978; Farouki, 1981):

$$\lambda = \frac{Q}{4\pi(T_2 - T_1)} \ln\left(\frac{t_2}{t_1}\right)$$ **[Equation 5.9]**

and

$$Q = \frac{EI}{L} = \frac{(V_p - V_r)(V_r / 2)}{L}$$ **[Equation 5.10]**

where:

λ = thermal conductivity (Watts/m-°C)

Q = power consumption of heater wire that is assumed to be the equivalent of heat output per unit length of heating probe (Watts/m)

T_1 = temperature at time t_1 (°C)

T_2 = temperature at time t_2 (°C)

t_1 = initial time (sec)

t_2 = final time (sec)

E = voltage across heating probe, V_p - V_r (volts)

V_p = applied voltage to heating probe (volts)
V_r = potential drop across heating probe (volts)
I = current to heating probe, $V_r/R = V_r/2$ (amps)
R = resistance in the system (ohms)
L = length of heating probe (m)

The derivation of Equation 5.10 is presented in Mitchell and Kao (1978), and Farouki (1981).

5.10 Dynamic Properties

5.10.1 General Theory

In many practical systems, the mechanism by which the vibrational energy is gradually converted into heat is known as damping (Rao, 1995). Although the amount of energy converted into heat is relatively small, the consideration of damping becomes extremely important to accurately predict the vibrational response of a system. In many practical problems involving vibrational analysis, viscous damping is the most commonly used damping mechanism. When a mechanical system vibrates, for example in a fluid, the amount of dissipated energy due to the resistance offered by the fluid depends on many factors including the shape and size of the vibrating body, the frequency of vibration, the viscosity of the fluid, and the velocity of the vibrating body. In viscous damping, the damping force is proportional to the velocity of the vibrating body (Rao, 1995). Another damping mechanism used in vibrational analysis is material damping (or hysteretic damping). When a material is subjected to vibrations, the material deforms and energy is absorbed and dissipated. The effect is due to frictional resistance between internal planes, which slip and slide as the deformations take place. Hence, for a body exhibiting material damping, the stress-strain diagram shows a hysterisis loop. The area of this loop corresponds to the energy lost per unit volume of the body per cycle due to damping.

5.10.2 Free Vibration with Viscous Damping

A single degree of freedom system with a viscous damper is shown in Figure 5.11. As stated earlier, the viscous damping force, F, is proportional to the velocity, $\dot{x}$, and can be expressed as (after Rao, 1995):

$$F = -c\dot{x} \qquad \textbf{[Equation 5.11]}$$

where c is the damping constant or coefficient of viscous damping. The negative sign indicates that the damping force is opposite to the direction of velocity. If x is measured from the equilibrium position, O, of the mass m, then the application of Newton's law yields the following equation of motion:

$$m\ddot{x} = -c\dot{x} - kx$$

or

$$m\ddot{x} + c\dot{x} + kx = 0 \qquad \textbf{[Equation 5.12]}$$

where $\ddot{x}$ represents the acceleration of the mass.

To solve Equation 5.12, the function of the form

$$x(t) = Ce^{st} \qquad \textbf{[Equation 5.13]}$$

is assumed where C and s are constants which need to be determined. The first and second differential of the function is then substituted into Equation 5.12, which leads to the characteristic equation

$$ms^2 + cs + k = 0 \qquad \textbf{[Equation 5.14]}$$

The roots of Equation 5.14 are

$$s_{1,2} = \frac{-c \pm \sqrt{c^2 - 4mk}}{2m} = -\frac{c}{2m} \pm \sqrt{\left(\frac{c}{2m}\right)^2 - \frac{k}{m}} \qquad \textbf{[Equation 5.15]}$$

These roots give two solutions to Equation 5.12:

$$x_1(t)=C_1e^{s_1t} \text{ and } x_2(t)=C_2e^{s_2t}$$ **[Equation 5.16]**

Therefore, the general solution to Equation 5.12 is given by a combination of the two solutions $x_1(t)$ and $x_2(t)$ (after Rao, 1995):

$$x(t)=C_1e^{\left\{-\frac{c}{2m}+\sqrt{\left(\frac{c}{2m}\right)^2-\frac{k}{m}}\right\}t}+C_2e^{\left\{-\frac{c}{2m}-\sqrt{\left(\frac{c}{2m}\right)^2-\frac{k}{m}}\right\}t}$$ **[Equation 5.17]**

where C_1 and C_2 are arbitrary constants to be determined from the initial conditions of the system.

5.10.3 Critical Damping Constant and the Damping Ratio

The critical damping constant, c_{cr}, is defined as the value of the damping constant c for which the radical in Equation 5.15 becomes zero (Rao, 1995). That is when

$$\left(\frac{c_{cr}}{2m}\right)^2-\frac{k}{m}=0$$

or $$c_{cr}=2m\sqrt{\frac{k}{m}}=2\sqrt{km}=2m\omega_n$$ **[Equation 5.18]**

where ω_n is the undamped natural frequency of the system.

For any damped system, the damping ratio, D, is defined as the ratio of the damping constant to the critical damping constant:

$$D=\frac{c}{c_{cr}}$$ **[Equation 5.19]**

Using Equations 5.18 and 5.19,

$$\frac{c}{2m}=\frac{c}{c_{cr}}\frac{c_{cr}}{2m}=D\omega_n$$ **[Equation 5.20]**

and hence substitution into Equation 5.15 gives

$$s_{1,2} = \left(-D \pm \sqrt{D^2 \,\text{[illegible]}\, 1}\right)\omega_n \qquad \textbf{[Equation 5.21]}$$

Equation 5.17 can then be written as

$$x(t) = C_1 e^{\left(-D+\sqrt{D^2-1}\right)\omega_n t} + C_2 e^{\left(-D-\sqrt{D^2-1}\right)\omega_n t} \qquad \textbf{[Equation 5.22]}$$

The solutions to Equation 5.22 are governed by the roots s_1 and s_2, which depend on the magnitude of damping. It can be seen that for the case where $D = 0$ leads to an undamped system. That is, there is no element that causes the dissipation of energy during vibration, and the amplitude of motion remains constant with time. However, when D is assumed ≠ 0, there are three cases to be considered.

Case 1. Underdamped System ($D < 1$ or $c < c_{cr}$ or $c/2m < \sqrt{k/m}$)

The solution that corresponds to the free vibrations of an underdamped system is given as (after Rao, 1995):

$$x(t) = e^{-D\omega_n t}[x_o \cos\sqrt{1-D^2}\,\omega_n t] +$$

$$e^{-D\omega_n t}\left[\frac{\dot{x}_o + D\omega_n x_o}{\sqrt{1-D^2}\,\omega_n}\sin\sqrt{1-D^2}\,\omega_n t\right] \qquad \textbf{[Equation 5.23]}$$

where x_o refers to an initial displacement at time $t = 0$, $\dot{x}_o$ is the initial velocity at time $t = 0$, and e is the base of the natural logarithms. The motion described by Equation 5.23 is for a damped harmonic motion with a damped angular frequency, $\omega_d = \sqrt{1-D^2}\,\omega_n$. However, the factor $e^{-D\omega_n t}$ causes the amplitude to decrease exponentially with time, which is shown in Figure 5.12. The underdamped case is very important in the study of mechanical vibrations, since it is the only case that leads to an oscillatory motion (Rao, 1995).

Case 2. Critically Damped System ($D = 1$ or $c = c_{cr}$ or $c/2m = \sqrt{k/m}$)

The solution that corresponds to the free vibrations of a critically damped system is given as (after Rao, 1995):

$$x(t) = \left[x_o + \left(\dot{x}_o + \omega_n x_o\right)t\right]e^{-\omega_n t} \qquad \textbf{[Equation 5.24]}$$

It can be seen that the motion represented by Equation 5.24 is non-periodic. Since $e^{-\omega_n t} \rightarrow 0$ as $t \rightarrow \infty$, the motion will eventually diminish to zero, as shown in Figure 5.13.

Case 3. Overdamped System ($D > 1$ or $c > c_{cr}$ or $c/2m > \sqrt{k/m}$)

Since $\sqrt{D^2 - 1} > 0$ shows that the roots s_1 and s_2 in Equation 5.21 are real and distinct, they are given by

$$s_1 = \left(-D + \sqrt{D^2 - 1}\right)\omega_n < 0$$

$$s_2 = \left(-D - \sqrt{D^2 - 1}\right)\omega_n < 0$$

with $s_2 \ll s_1$. In this case, the solution is given by Equation 5.22. Figure 5.13 shows that the motion for an overdamped system is non-periodic regardless of the initial conditions imposed on the system (Rao, 1995).

5.10.4 Experimental Determination of Material Damping

It was stated that when $D < 1$, damping leads to the case for an underdamped system. This concept is very important in the study of mechanical vibrations because it is the only case that leads to an oscillatory motion. Therefore, damping can be obtained from the plot of amplitude versus time in which Equation 5.23 defines a sinusoidal type curve with decreasing amplitude, which was shown in Figure 5.12. In other words, the vibration will decay as a result of internal damping within the mass, and the vibration will eventually disappear. If taken into account that the maximum point on the sine curve is close to the point of tangency with the curve $x(t)=e^{-D\omega_n t}$, then the ratio of the successive peaks can be approximated with x_1 and x_2 at the corresponding times t_1 and t_2 respectively (Hall and Richart, 1963). Hence, the decay of the free vibration with viscous damping can be described by the logarithmic decrement, δ, which is defined as the natural logarithm of two successive peaks or amplitudes of motion (Richart et al., 1970). Generally, the logarithmic decrement, δ, for soils can be obtained experimentally, for example, by setting a soil sample into steady-state forced vibration, and then shutting off the driving power and recording the amplitude decay with time. The logarithmic decrement is determined directly from the decay curve by plotting the logarithm of each amplitude against the cycle number. If damping measured in the material corresponds to that predicted by the theory for viscously damped free vibrations, a straight line will develop on the semi-log plot. An example is shown in Figure 5.14 for a test conducted on Ottawa sand. Hence, δ is determined from Figure 5.14 as the slope of the line using the following expression:

$$\delta = \frac{1}{n} ln\left(\frac{x_1}{x_{n+1}}\right) \qquad \textbf{[Equation 5.25]}$$

where x_1 and x_{n+1} denote the amplitudes corresponding to times t_1 and t_{n+1} and n is an integer, which represents the number of cycles.

Hall and Richart (1963) showed that δ can be related to D by the following expression:

$$\delta = \frac{2\pi D}{\sqrt{1-D^2}} \qquad \textbf{[Equation 5.26]}$$

From Equation 5.26, it is clear that for very small values of damping (i.e. $D \ll 1$), $\delta \cong 2\pi D$.

The logarithmic decrement can also be taken directly from an experimental amplitude-frequency curve, which is shown in Figure 5.15. However, this procedure depends primarily on the frequency range bounded by the curve at a specified amplitude (Hall and

Richart, 1963). The general expression for the logarithmic decrement is given by (after Richard et al., 1970):

$$\delta = \frac{2\pi D}{\sqrt{1-D^2}} = \frac{\pi}{2}\frac{\left(f_2^2 - f_1^2\right)}{f_o^2}\sqrt{\frac{A^2}{A_m^2 - A^2}}\frac{\sqrt{1-2D^2}}{1-D^2} \qquad \textbf{[Equation 5.27]}$$

where f_1 and f_2 are the frequencies bounded to the left and right of the resonant frequency, f_o, respectively. A is the amplitude that intersects the amplitude-frequency curve, f_o is the resonant frequency, and A_m is the maximum amplitude (or the resonant amplitude). For convenience, A in Equation 5.27 is usually taken at $\frac{1}{2}A_m$ or $\frac{1}{\sqrt{2}}A_m$.

The disadvantages of this method are that a large number of data points are required to define the amplitude-frequency curve, and the resonant amplitude must be accurately determined (Brocanelli and Rinaldi, 1998). Furthermore, the procedure is very subjective in that the amplitude-frequency curve must be symmetrical with respect to f_o. These conditions make the accurate measurement of damping experimentally difficult with the standard oscilloscopes and signal generators, especially at higher frequencies.

An alternative approach to determining the material damping is given by Ewins (1988). He showed that the dynamic mobility (Y) of a single-degree-of-freedom system

$$Y(\omega) = \frac{c\omega^2 + j\omega\left(k - \omega^2 m\right)}{\left(k - \omega^2 m\right)^2 + (\omega c)^2} \qquad \textbf{[Equation 5.28]}$$

can be rewritten in terms of its complex conjugates as

$$\left[Re(Y) - \frac{1}{2c}\right] + \left[Im(Y)\right]^2 = \left(\frac{1}{2c}\right)^2 \qquad \textbf{[Equation 5.29]}$$

where $Re(Y)=\dfrac{\omega^2 c}{(k-\omega^2 m)^2+(\omega c)^2}$ and $Im(Y)=\dfrac{\omega^2(k-\omega^2 m)}{(k-\omega^2 m)^2+(\omega c)^2}$ are the real and imaginary components respectively, m is the mass, c is the damping coefficient, k is the spring constant, and $j = (-1)^2$.

Accordingly, Equation 5.31 plots in the complex plane (also known as the Nyquist plane) as a circle with a radius of $\dfrac{1}{2c}$ as illustrated in Figure 5.16. The damping ratio, D, can then be calculated for points close to that corresponding to the maximum amplitude by means of the following equation (Ewins, 1988):

$$D=\frac{\omega_2^2-\omega_1^2}{2\omega_o\left[\omega_2\, tan\left(\frac{\alpha_2}{2}\right)+\omega_1\, tan\left(\frac{\alpha_1}{2}\right)\right]} \qquad \textbf{[Equation 5.30]}$$

where ω_o is the angular frequency corresponding to the maximum sweep angular velocity, ω_1 and ω_2 are the angular frequencies, and α_1 and α_2 are the angles at both sides of ω_o. The main advantage with this method as opposed to the method using Equations 5.27 is that the circle can be defined with a few data points, which may not necessarily include that of the maximum amplitude (Brocanelli and Rinaldi, 1998). However, the method permits the analysis of the influence of close peaks near the resonant mode of interest, as they may distort the shape of the circle.

5.10.5 Dynamic Testing Apparatus

Traditionally, the dynamic properties of soils are determined in the laboratory using a resonant column, which is an apparatus that can determine the natural frequency of oscillation of a soil specimen. ASTM standard (D 5015) (Standard Test Methods for Modulus and Damping of Soils by the Resonant Column) defines the test procedure. However, due to the unavailability and high costs associated with the resonant column apparatus, it was not used in this study. Instead, the damping properties of tire crumbs were measured using the direct wave propagation method according to the test procedures that were modified from Brocanelli and Rinaldi (1998). In order to set up a sample under steady state vibration, bender elements discussed later were used as both transmitter and receiver elements. Two different apparatus incorporating bender elements were used: (1) triaxial cell; and (2) large-strain consolidation apparatus. Figure 5.17 shows the schematic of the triaxial cell with bender elements mounted onto the loading head and base pedestal. Figure 5.18 and Figure 5.19 shows a photo and schematic of the peripheral devices associated with the large-strain consolidation apparatus

Initially, the input signals were generated using a signal generator similar to that used by Brocanelli and Rinaldi (1998) in their experiments. However, attempts made to receive the transmitted signals through the crumb samples were discouraging, and consequently, the signal generator was abandoned. A DC power supply (Model Hewlett Packard 6438 B) with a maximum voltage capability of 100 V was used instead to generate the input signals. Due to the limitations of the DC power supply, only square-wave signals could be transmitted. Furthermore, the frequencies of the transmitted signal could be adjusted with the DC power supply.

The receiver bender element was connected to an amplifier and the signal was digitized using an oscilloscope (Model Phillips PM 3350 A). The signals were also recorded and visualized on a computer using the commercially available data acquisition and analysis software, LabVIEW ® (National Instruments Corporation, 2000). A low input to high-output DC relay switch (Potter and Brumfield, Model 0 DC - 5 A) was also connected in series between the DC power supply and the oscilloscope to increase the power entering the system. A high capacity resistor was connected at the entry of the transmitter bender element as a precaution to prevent the bender element from overheating.

The bender element is an electro-mechanical transducer that consists of two piezoceramic plates bonded together as shown in Figure 5.20. The bender element has the ability to convert electrical energy to mechanical deformation and vice versa depending on its direction of polarization. If the elements are arranged in series (Figure 5.20 A), a mechanical deformation produces optimum electrical output voltage. Note that the polarization of the ceramic material is oriented in opposite directions for each plate. Thus, a bender element connected in series is most effective as a receiver bender element. If the elements are arranged in parallel (Figure 5.20 B), an applied voltage causes optimum deformation making this arrangement best as a transmitter bender element. In geotechnical dynamic testing, the strains associated with bender elements are less than 10^{-3} %, which falls in the elastic range of soils (Brignoli et al., 1996). For a more thorough description of using bender elements in geotechnical dynamic testing, the reader is referred to Woods (1994), and Dyvik and Madshus (1985)

5.10.6 Dynamic Test Procedures

The damping ratio and shear wave velocity measurements were carried out under dry conditions. Only a few samples consisting of crumbs with the smallest and largest grain-size distribution were tested to give the extreme ranges of dynamic properties resulting from different particle sizes. To investigate the influence of dry unit weight, the tests were conducted under different vertical stresses of up to 100 kPa. The sample heights were also limited to about 50 mm in order to obtain a clear signal through the material due to the anticipated high material damping.

5.10.6.1 Comparison of Bender Elements

Dry samples of Ottawa sand were first tested using the triaxial cell set-up. The samples were prepared following the procedures outlined in Section 5.8.2. The tests were conducted under isotropic confining pressures of up to 100 kPa. The pressures were applied using air instead of water. The damping ratios obtained under the corresponding confining pressures where then compared to those reported by other investigators to assess the reliability and accuracy of the bender elements used in this study. The material damping was also determined for the Ottawa sand using the large-strain consolidation apparatus under zero vertical stresses to give a comparison of the damping properties using the different test procedures (i.e. triaxial cell versus large-strain apparatus).

5.10.6.2 Shear Wave Velocity and Shear Modulus

Shear wave measurements were carried out in the time domain by introducing a single square-wave excitation with a maximum peak-to-peak amplitude of 50 V at the transmitter bender element and recording the signal when it arrived at the receiver bender element. Note that the shear wave velocity was measured for tire crumbs only. Figure 5.21 illustrates a typical square wave excitation and received signal in tire crumbs. The measurements were repeated at the following vertical stresses: 10, 20, 50, and 100 kPa. The time of arrival for the shear wave was determined following the criteria presented by Dyvik and Madshus (1985), Brignoli et al. (1996), and Jovicic et al. (1996). The shear wave velocity was calculated from the following relationship:

$$V_s = \frac{L_t}{T_t} \qquad \textbf{[Equation 5.31]}$$

where:

V_s = shear wave velocity (m/s)
L_t = travel length (m)
T_t = travel time (s)

From previous experimental work by Viggiani and Atkinson (1996), and Dyvik and Madshus (1985), L_t was taken as the distance between the tips of the transmitter and receiver bender elements.

At very low strains (less than 10^{-4}%), which are typical of foundation vibration problems, the shear modulus and damping remain essentially constant (Rollins et al., 1998). Therefore, at low strains, the shear modulus is at its maximum value, G_{max}, which is simply related to the shear wave velocity by (Rollins et al., 1998; Dyvik and Madshus, 1985):

$$G_{max} = \rho V_s^2 \qquad \textbf{[Equation 5.32]}$$

where:

G_{max} = maximum small strain shear modulus (MPa)
ρ = density of the soil or tire crumb (kg/m^3)

The measurement of shear wave velocity, therefore, provides a convenient method for measuring material stiffness.

5.10.6.3 Material Damping

Ottawa Sand

The material damping of Ottawa sand was determined in this study from the decay curve of amplitude with time (i.e. logarithmic decrement method), and from the amplitude-frequency curves as previously discussed in Section 5.10.4. Brocanelli and Rinaldi (1998), on the other hand, used a sweep test in the frequency domain to obtain their material damping. For their tests, the bottom bender element was excited with a steady sine signal of constant voltage and the amplitude and phase difference between the transmitted and reflected waves were measured at the receiver bender element. They repeated this process at different frequencies until the whole spectrum of the sample response was perfectly defined to obtain the resonant frequency and amplitude of the first mode of vibration. Then the peak amplitude corresponding to the shear mode and the measured phase angle were isolated and plotted in Figure 5.22 (a). The damping ratio was then obtained from the complex plane diagram (Figure 5.22 (b)), which was discussed in Section 5.10.4.

Tire Crumbs

Due to the expected high material damping, the logarithmic decrement and damping ratio cannot be determined directly from the decay curve of amplitude with time. Therefore, the material damping was obtained from the experimental amplitude-frequency curves. A Fast Fourier Transform (FFT) algorithm that was incorporated into LabVIEW® was used to convert the time domain response to the frequency domain response. This procedure was also used for Ottawa sand. The logarithmic decrement was then determined from Equations 5.28 or 5.29, and the damping ratio was subsequently determined from Equation 5.26.

Table 5.1 Crumbed tire rubber used in laboratory experiments

Tire Crumb Manufacturer	Grain-Size Distribution (US Sieve Designation)	Sieve Opening (mm)	Truck or passenger tires
Alberta Environmental Rubber Products, Edmonton	No. 20 Minus	< 0.85	truck
	No. 10 - No. 20	2 to 0.85	
	1/4 in	6.3	
Midwest Tire Processors of Vulcan	No. 10	2	passenger
	1/4 in	6.3	
Tire Recyclers of Calgary	No. 20 Minus	< 0.85	
	No. 10 - No. 20	2 to 0.85	
	No. 8 - No. 14	2.4 to 1.4	
	No. 4 - No. 8	4.8 to 2.4	
	1/4 in	6.3	

Table 5.2 Sequence of tests for thermal conductivity measurements

Test No.	Test Temperature	Location[1]
No. 1	+24°C (room temperature, unfrozen)	Laboratory Room B-31
No. 2	-10°C (frozen)	Back Freezer in Laboratory Room B-10
No. 3	-5°C (frozen)	Back Freezer in Laboratory Room B-31
No. 4	+3°C (unfrozen, thawed)	Front Freezer in Laboratory Room B-31
No. 5	+24°C (unfrozen, thawed)	Laboratory Room B-31

[1] All tests were conducted in the basement of the Civil & Environmental Engineering Building, University of Alberta

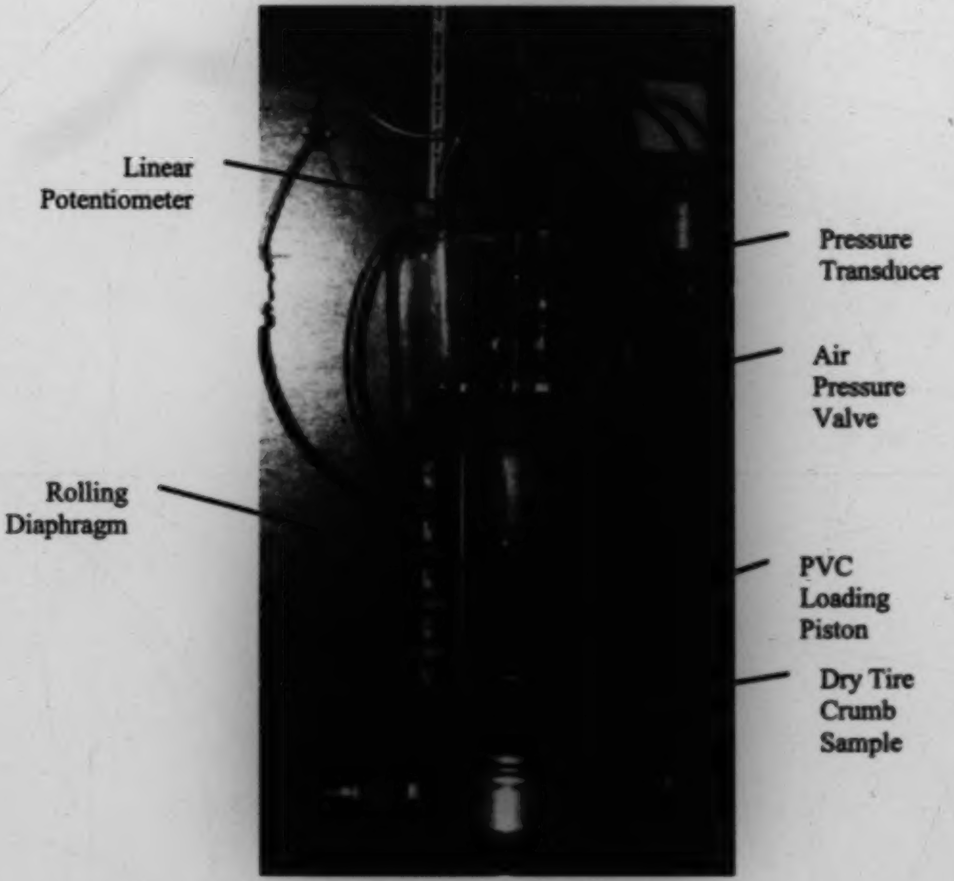
Linear Potentiometer
Pressure Transducer
Air Pressure Valve
Rolling Diaphragm
PVC Loading Piston
Dry Tire Crumb Sample

Figure 5.1 Large-strain consolidation apparatus set-up under dry conditions (photo by H. Hong, 1998)

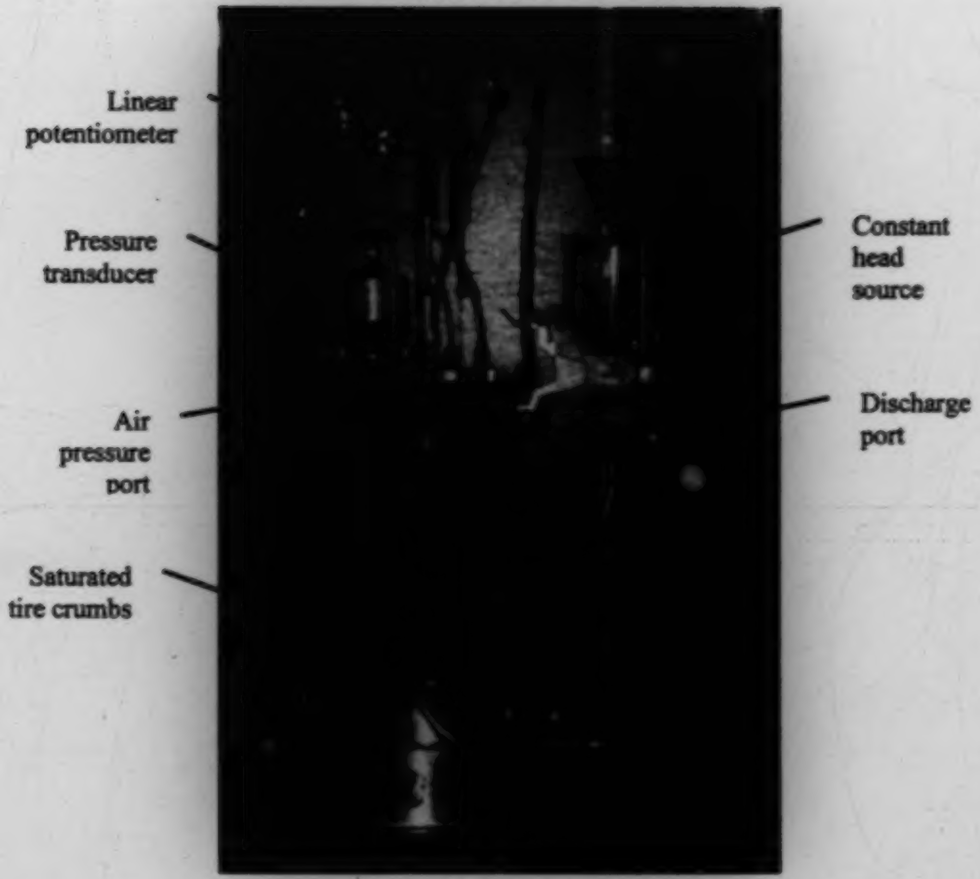
Linear potentiometer
Pressure transducer
Air pressure port
Saturated tire crumbs
Constant head source
Discharge port

Figure 5.2 Large-strain consolidation apparatus set-up under saturated conditions (photo by H. Hong, 1998)

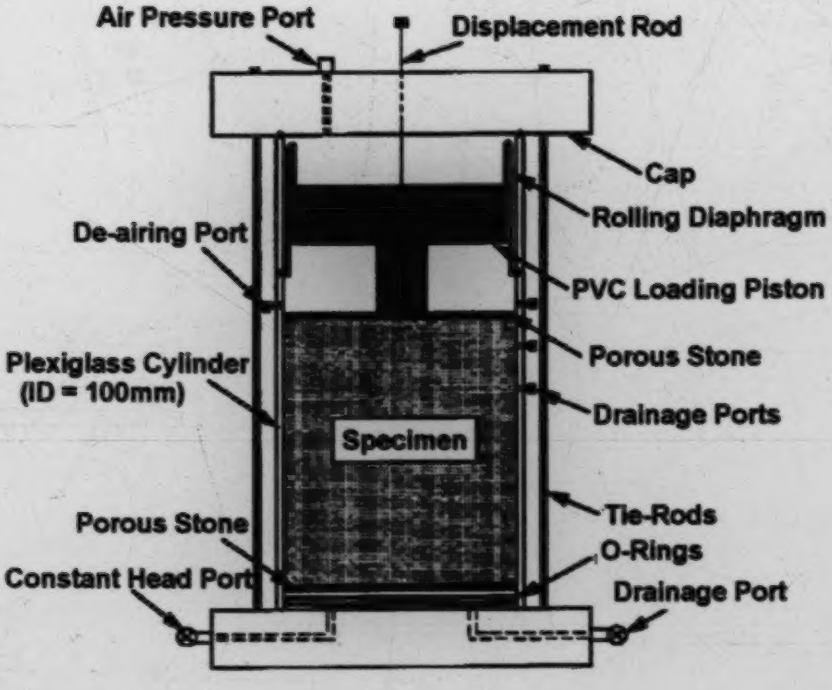
Air Pressure Port
Displacement Rod
Cap
Rolling Diaphragm
De-airing Port
PVC Loading Piston
Porous Stone
Plexiglass Cylinder
(ID = 100mm)
Drainage Ports
Specimen
Tie-Rods
Porous Stone
O-Rings
Constant Head Port
Drainage Port

Figure 5.3 Schematic of large-strain consolidation apparatus (modified from Qiu and Sego, 1998)

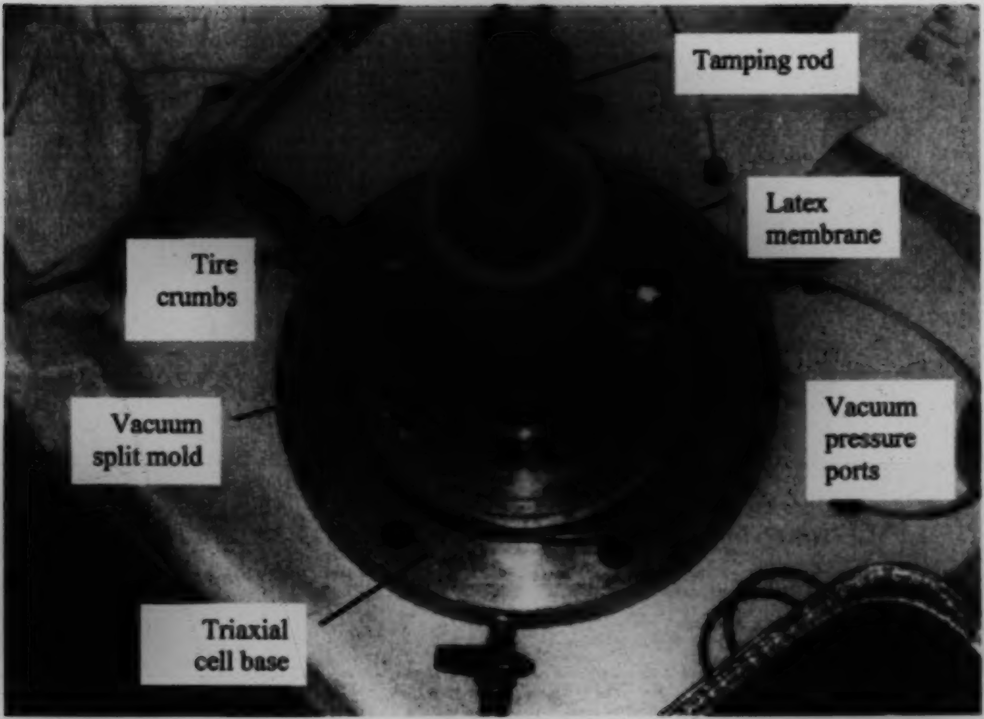
Tamping rod
Latex membrane
Tire crumbs
Vacuum split mold
Vacuum pressure ports
Triaxial cell base

Figure 5.4 Compaction of tire crumbs in vacuum split mold (photo by H. Hong, 1998)

Figure 5.5 Applying vacuum to top cap of vacuum split mold (photo by H. Hong, 1998)

Figure 5.6 Triaxial specimens after removing vacuum split mold (photo by H. Hong, 1998)

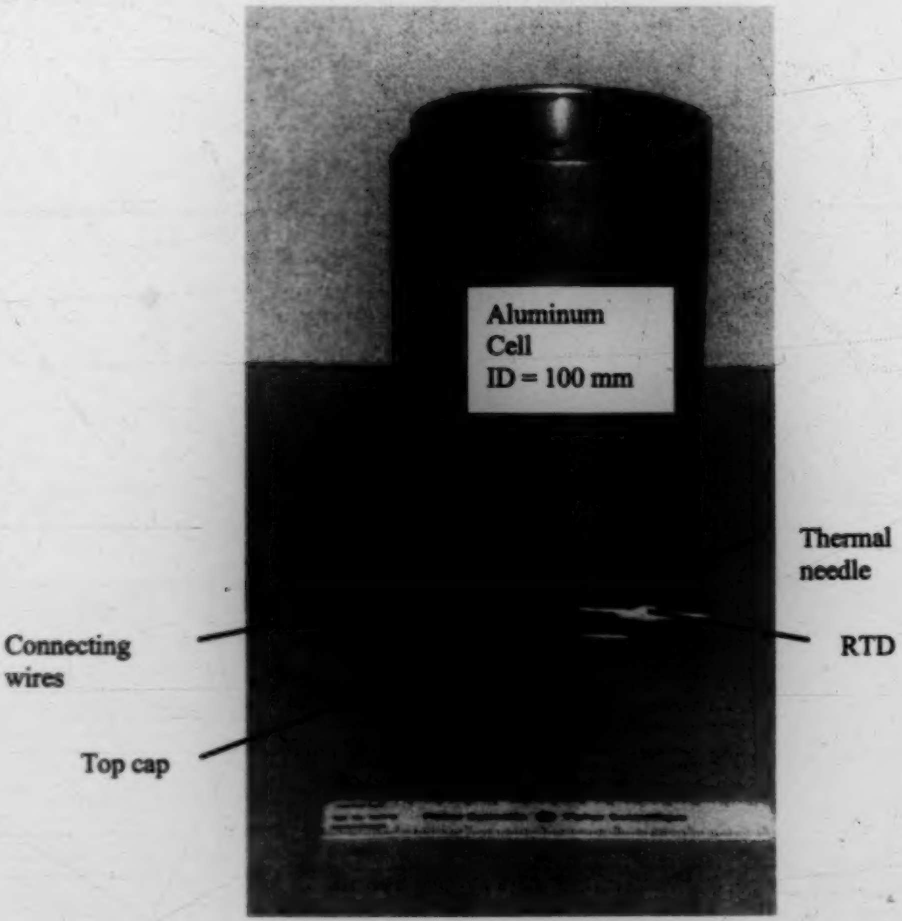
Aluminum
Cell
ID = 100 mm
Thermal needle
Connecting wires
RTD
Top cap

Figure 5.7 Thermal needle, top cap, and aluminum cell (photo by H. Hong, 1998)

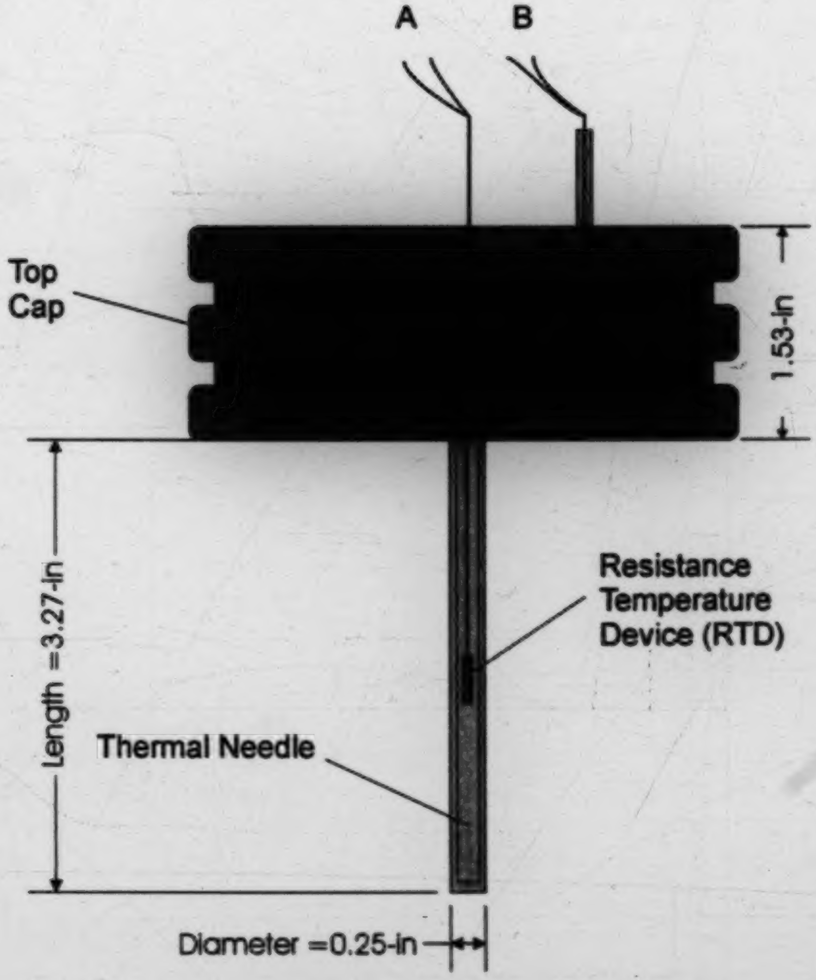
A
B
Top Cap
1.53-in
Resistance Temperature Device (RTD)
Length =3.27-in
Thermal Needle
Diameter =0.25-in

A = wires connecting heater cartridge to
DC power source
B = wires connecting RTD to multi-meter

Figure 5.8 Schematic of thermal needle

Figure 5.9 Thermoconductivity cells in portable cooler (photo by H. Hong, 1998)

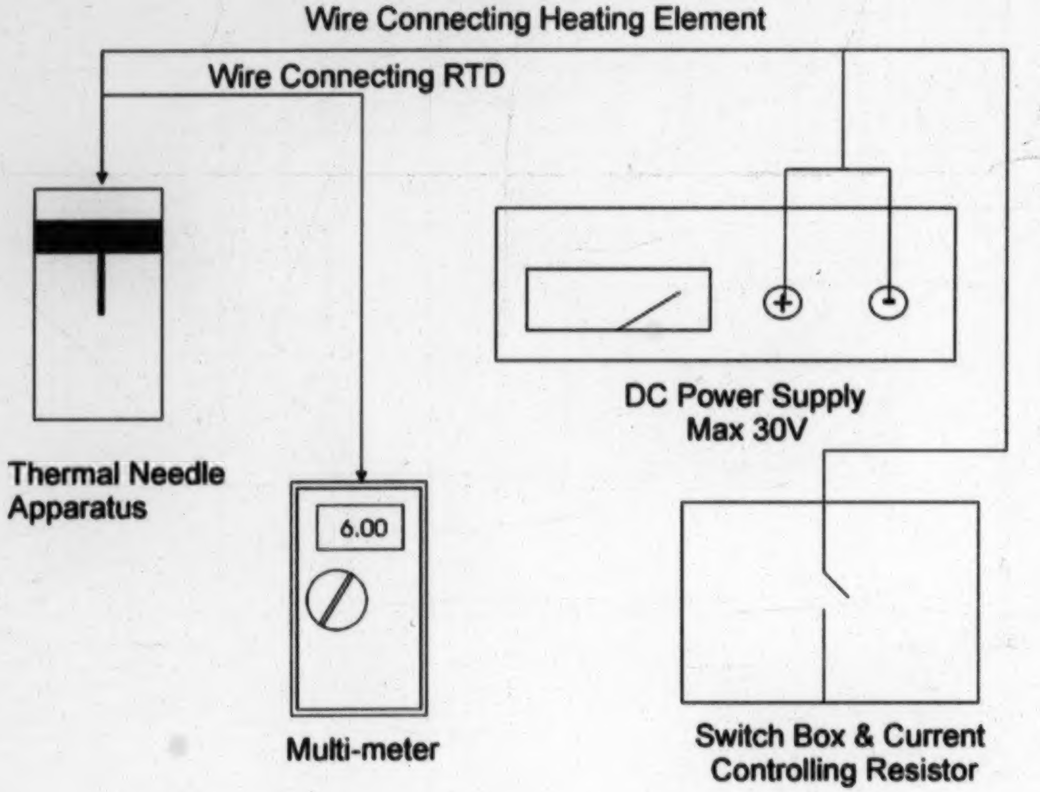
Wire Connecting Heating Element
Wire Connecting RTD
+
-
DC Power Supply
Max 30V
Thermal Needle
Apparatus
6.00
Multi-meter
Switch Box & Current
Controlling Resistor

Figure 5.10 Apparatus set-up for thermal testing (Not to scale)

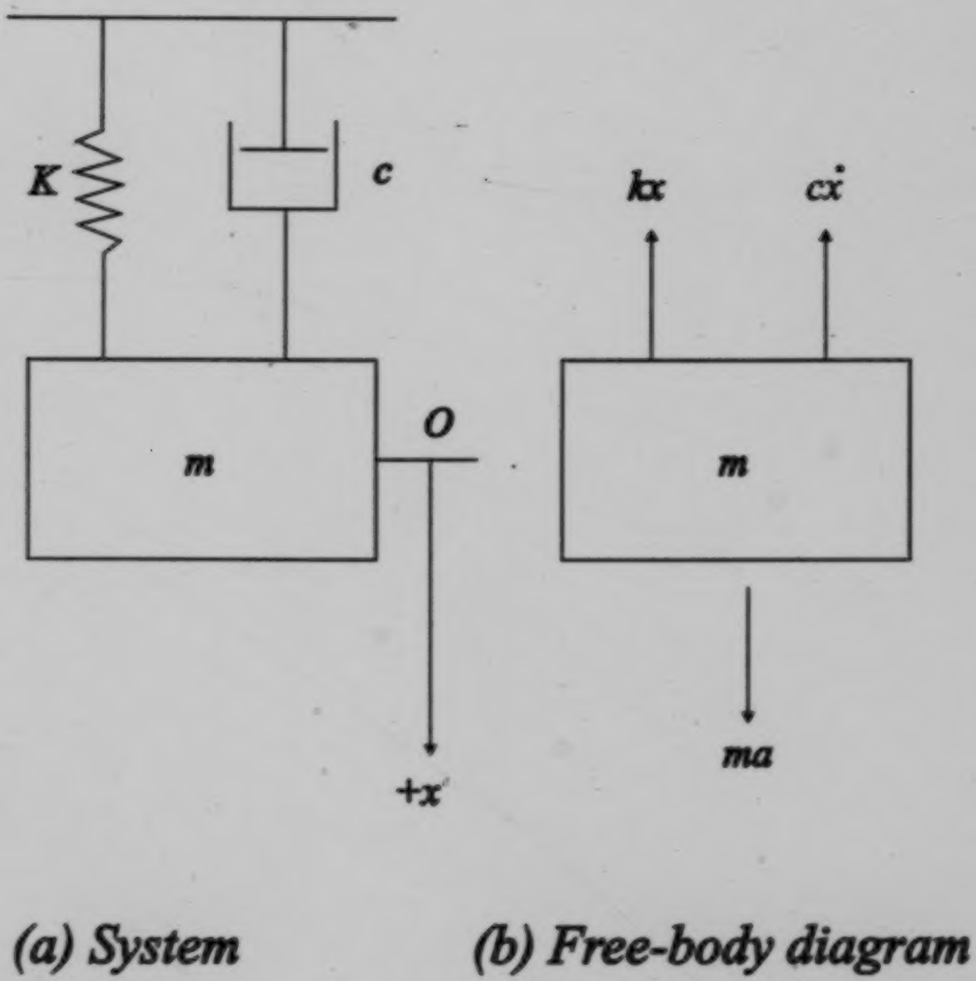
K
c
m
O
+x
kx
$c\dot{x}$
m
ma
(a) System
(b) Free-body diagram

Figure 5.11 Single degree of freedom system with viscous damping (modified from Rao, 1995)

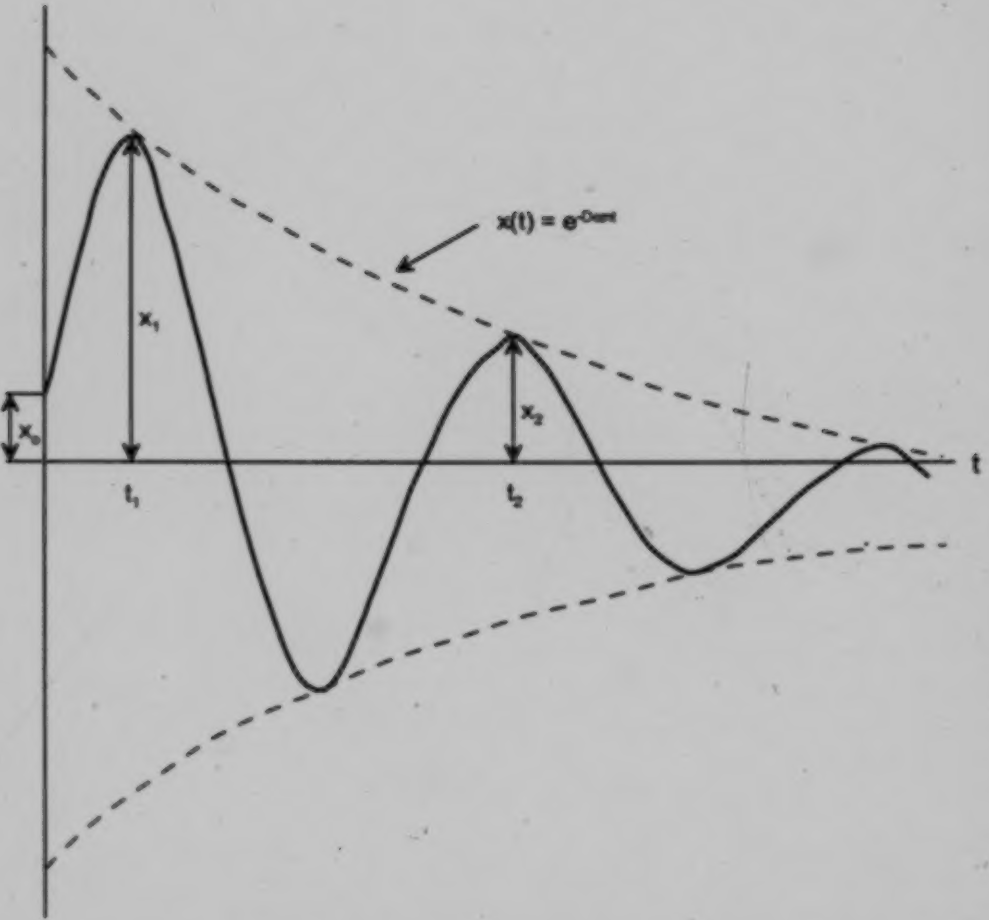

Figure 5.12 Vibration decay with time for an underdamped system with one-degree-of-freedom (modified from Hall and Richart, 1963)

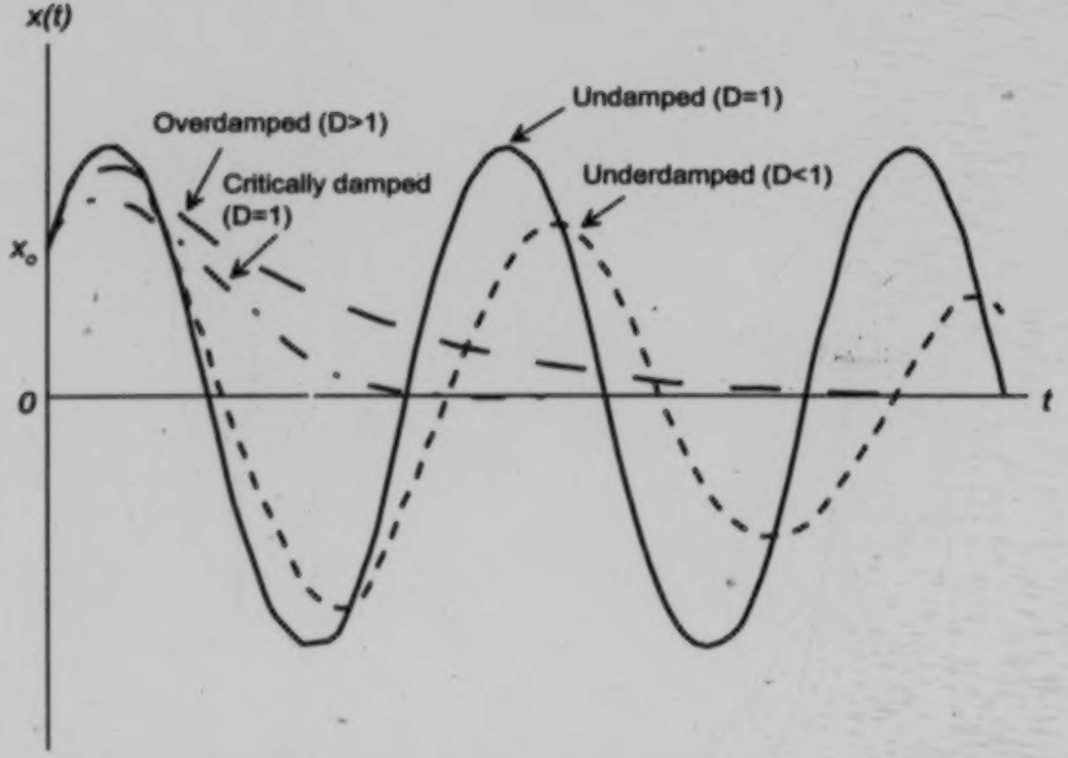

Figure 5.13 Comparison of motion with different types of damping (modified from Rao, 1995)

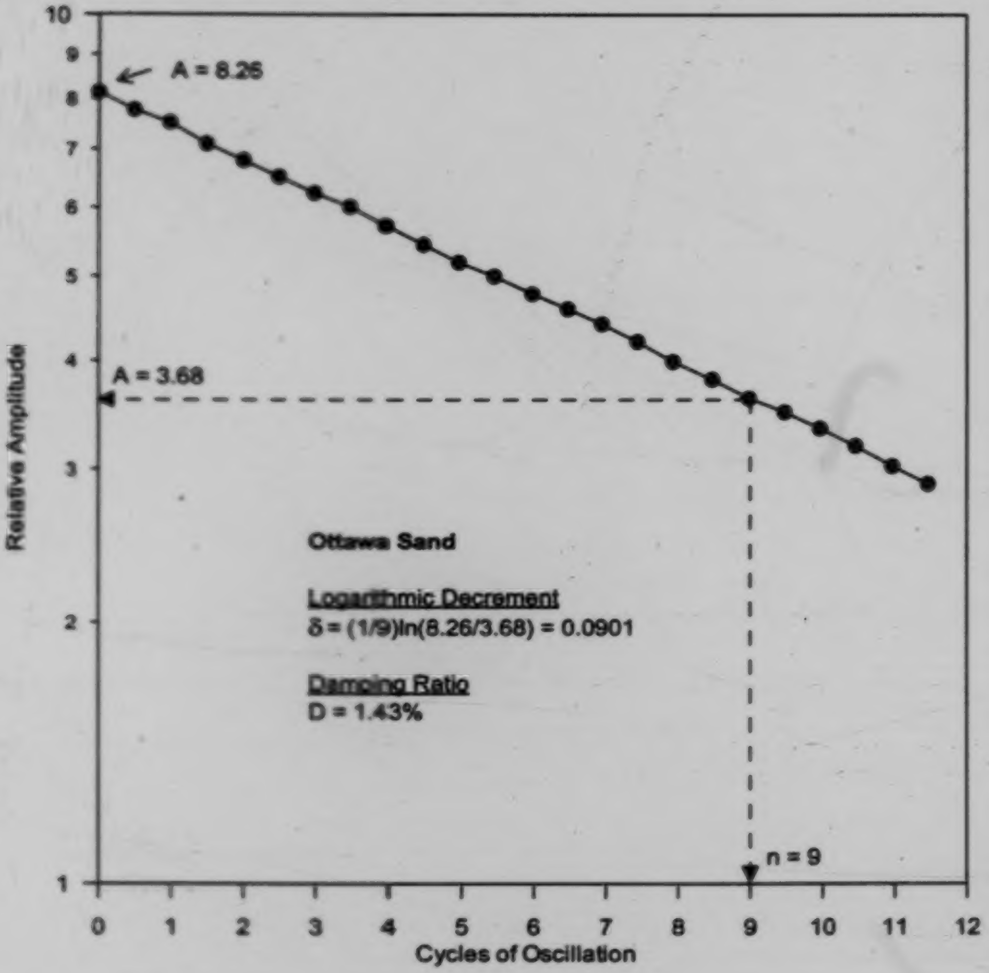

Figure 5.14 Amplitude versus cycle number plot for Ottawa sand (modified from Hall, 1963)

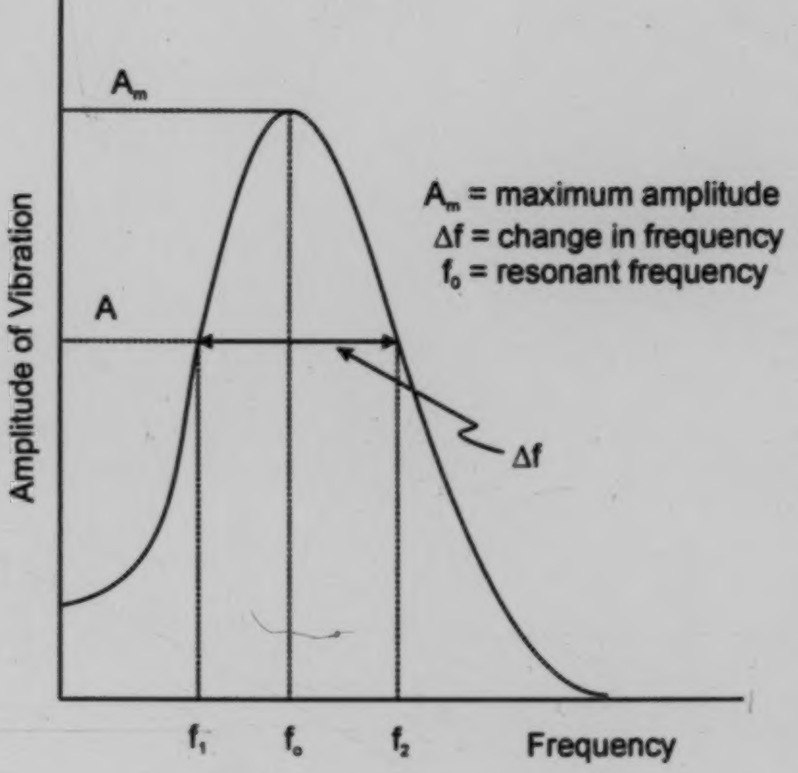

Figure 5.15 Amplitude-frequency curve for a constant force type of excitation (modified from Brocanelli and Rinaldi, 1998)

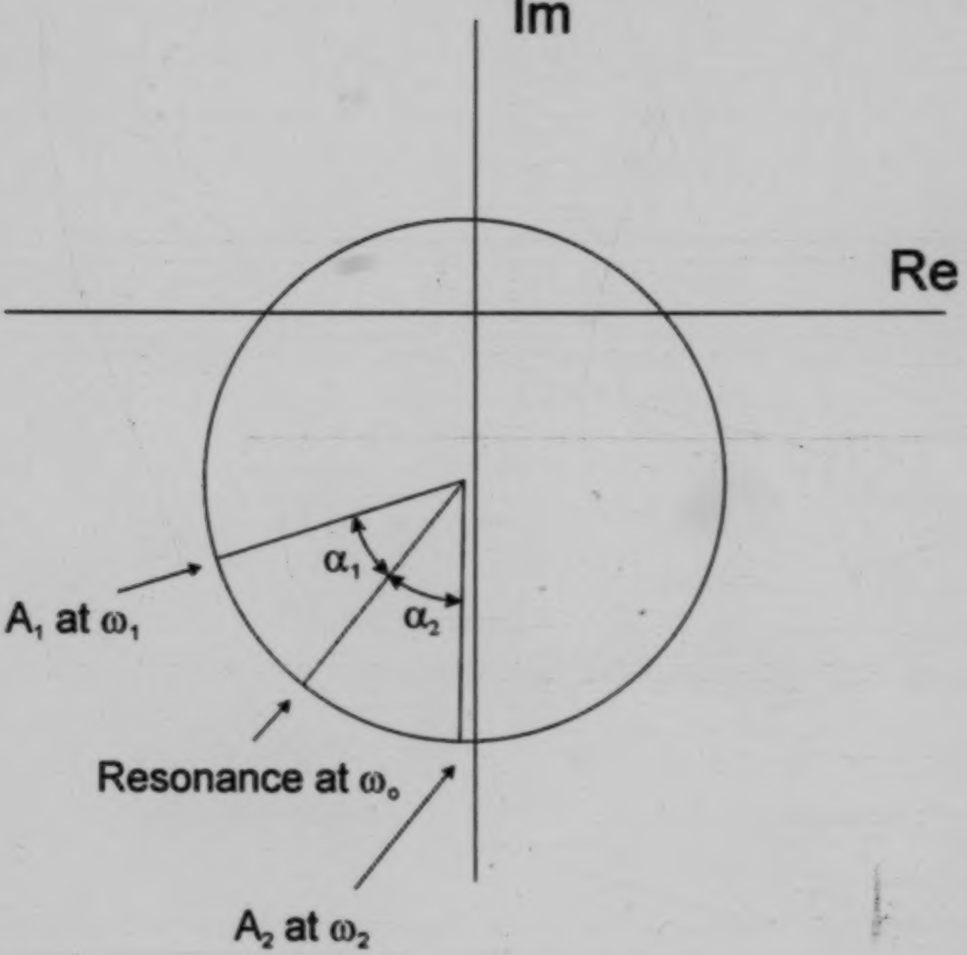
Im
Re
α_1
α_2
A_1 at ω_1
Resonance at ω_o
A_2 at ω_2

Figure 5.16 The Nyquist diagram (modified from Brocanelli and Rinaldi, 1998)

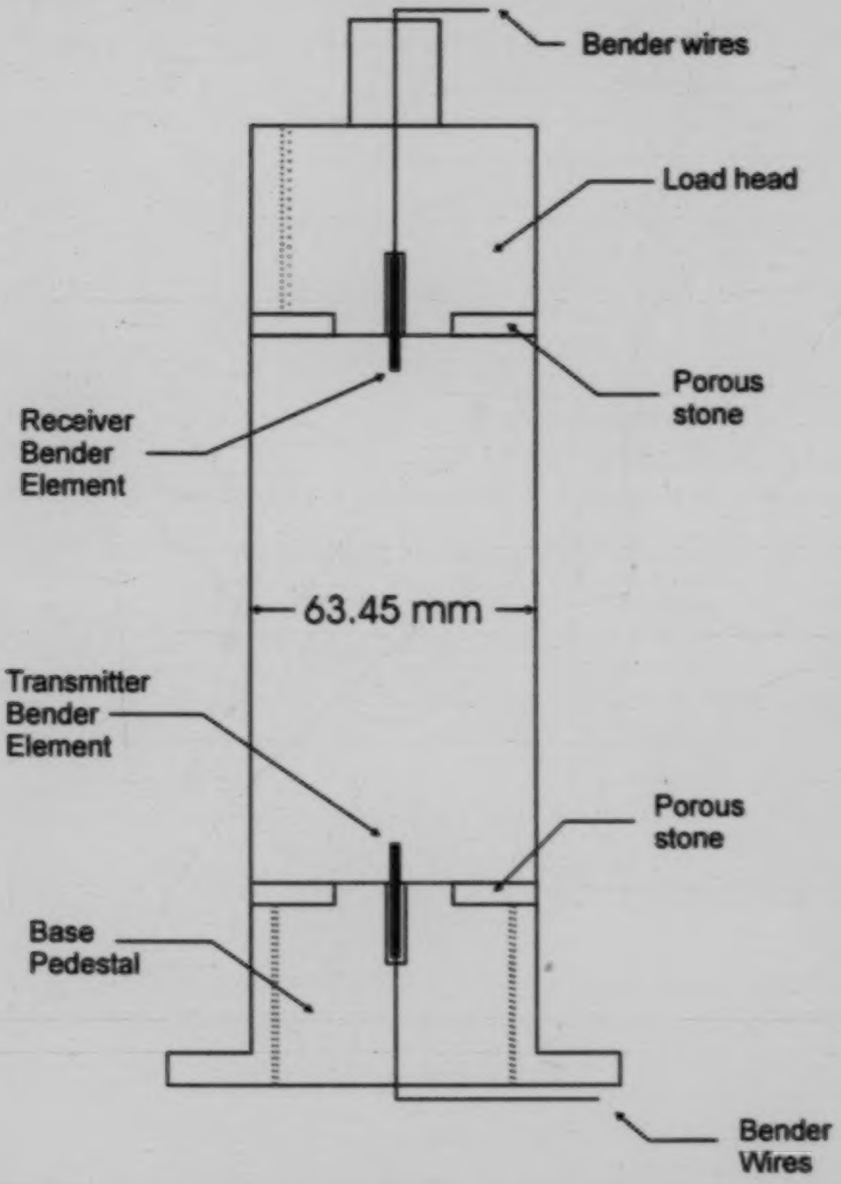
Bender wires
Load head
Porous stone
Receiver Bender Element
63.45 mm
Transmitter Bender Element
Porous stone
Base Pedestal
Bender Wires

Figure 5.17 Protuding bender element system in triaxial cell head and base (modified from Cunning, 1994)

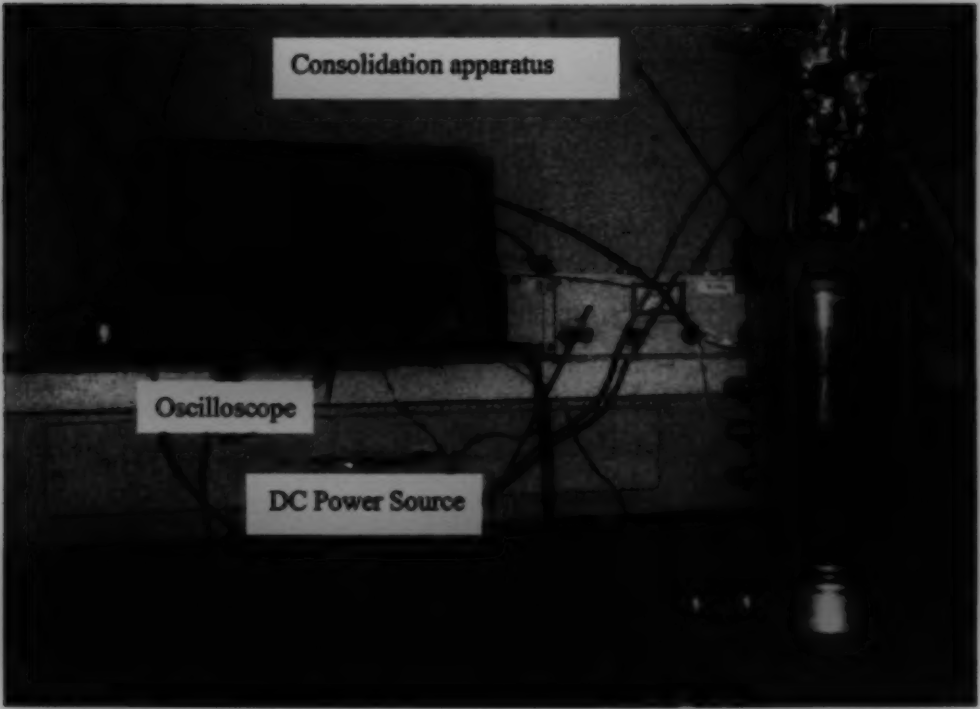
Consolidation apparatus
Oscilloscope
DC Power Source

Figure 5.18 Photo of dynamic testing apparatus set-up (photo by H. Hong, 1999)

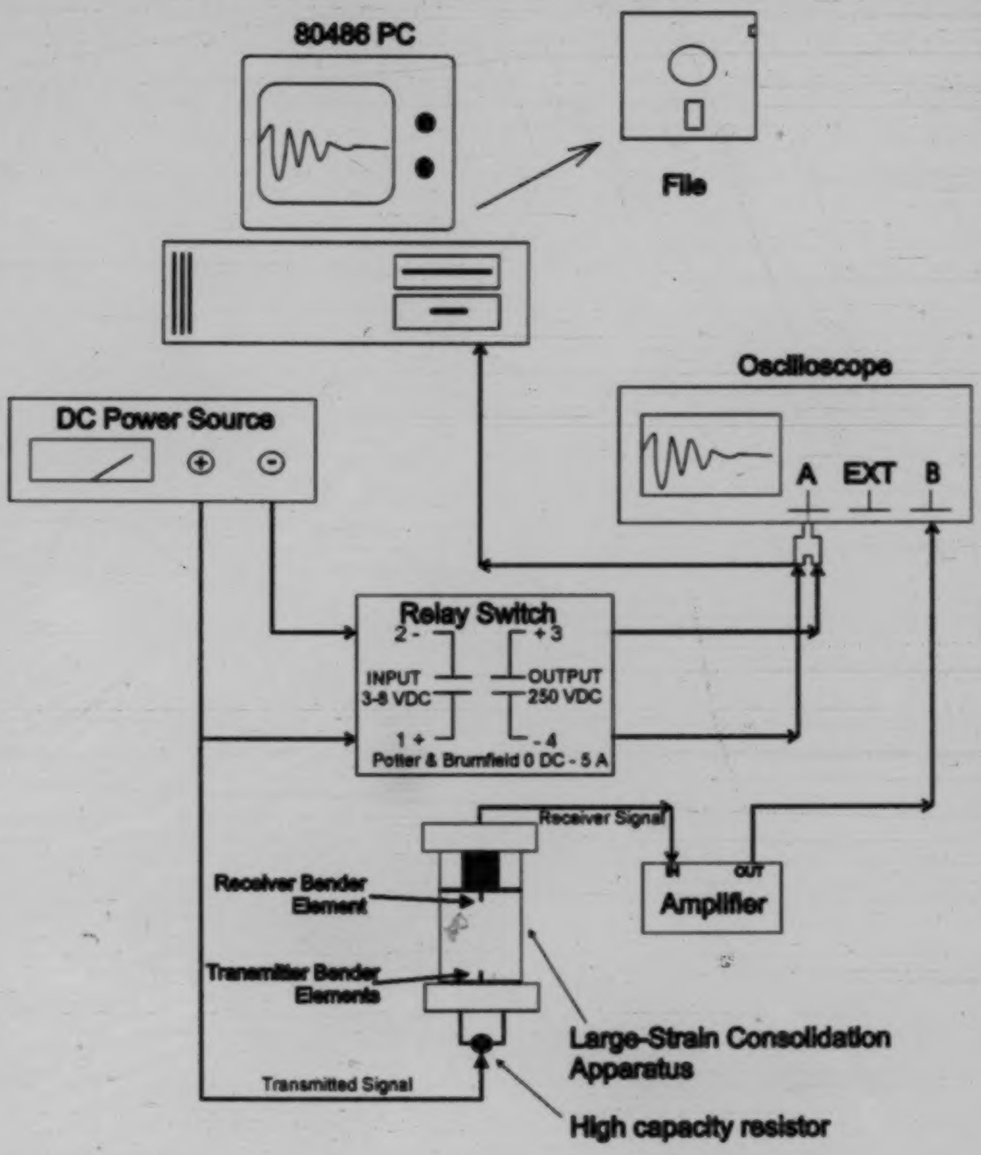
80486 PC
File
Oscilloscope
A
EXT
B
DC Power Source
Relay Switch
2 -
+ 3
INPUT
3-8 VDC
OUTPUT
250 VDC
1 +
- 4
Potter & Brumfield 0 DC - 5 A
Receiver Signal
IN
OUT
Amplifier
Receiver Bender Element
Transmitter Bender Elements
Large-Strain Consolidation Apparatus
High capacity resistor
Transmitted Signal

Figure 5.19 Apparatus set-up for dynamic testing

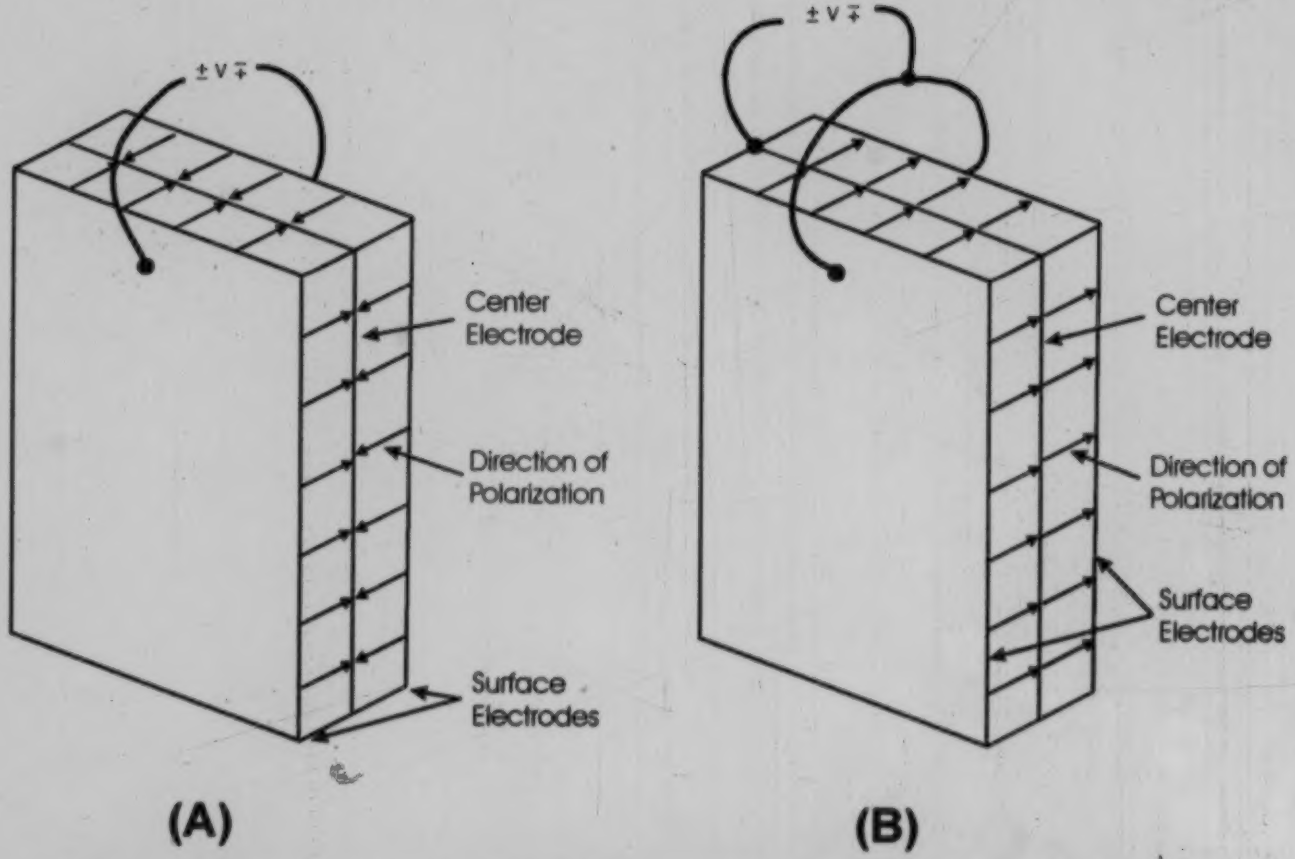
± V ∓
Center Electrode
Direction of Polarization
Surface Electrodes
(A)
± V ∓
Center Electrode
Direction of Polarization
Surface Electrodes
(B)

Figure 5.20 Schematic of piezoceramic bender elements: (A) series connected, (B) parallel connected (modified from Dyvik and Madshus, 1985)

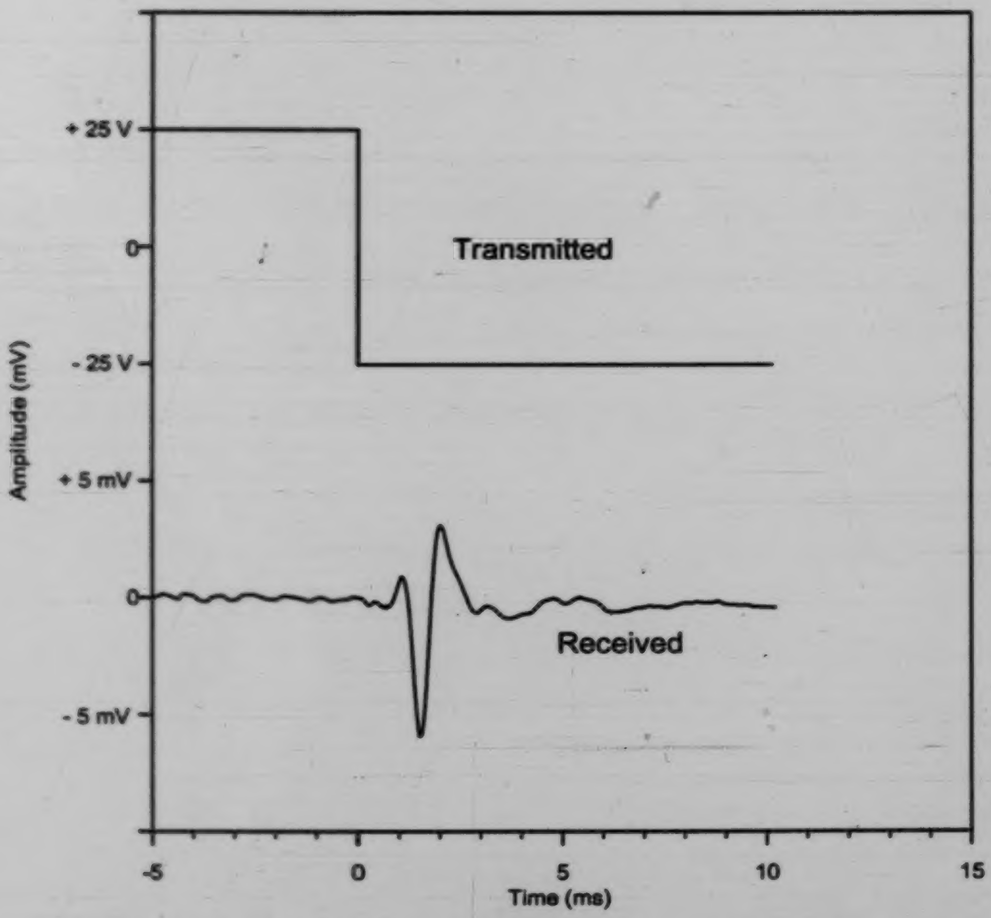

Figure 5.21 Typical bender element output trace for a square input wave in tire crumbs

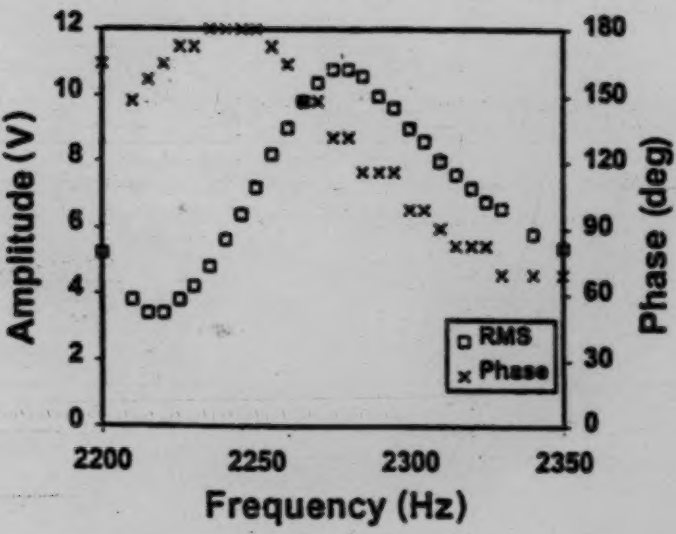

(a)

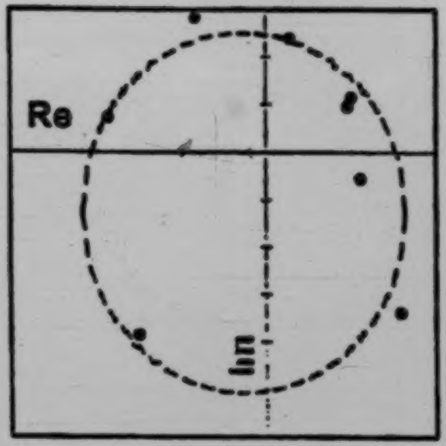

(b)

Figure 5.22 (a) Amplitude and phase angle in the resonant mode; (b) Corresponding Nyquist diagram and plot of the circle that best fits the results (modified from Brocanelli and Rinaldi, 1998)

CHAPTER 6 EXPERIMENTAL RESULTS AND DISCUSSION

6.1 Particle Size and Gradation

A mechanical sieve analysis was conducted to determine the particle size and gradation of tire crumbs. A visual inspection was also undertaken of the material to assess its particle shape, and for the presence of impurities such as rocks, fibre reinforcements, metals, and glass that may be present in the samples. Table 6.1 summarizes the particle size, gradation, C_u and C_c values, and the type of impurities present in the samples obtained from the different suppliers. The grain-size distribution curves of all the samples tested are shown in Figure 6.1. The detailed results are included in Appendix A.

The crumbs collected from the three different suppliers varied in particle size, shape, and gradation. However, there was very little variation in the particle shapes and sizes between similar grain-size distribution produced from the Vulcan and Calgary suppliers. Both suppliers use the crackermill process to produce their crumbs with irregular, angular shaped particles with rough, torn edges. As previously discussed, the crackermill process tears apart scrap tire rubber by passing the material between two counter-rotating corrugated steel drums. Therefore, the physical characteristics obtained from the two respective suppliers were consistent with this type of process.

Tire crumbs collected from the Edmonton plant, on the other hand, were uniformly shaped, angular cut particles with fairly smooth edges. These crumbs were produced using the granulator process, which is consistent with their physical characteristics. The granulator process produces tire crumbs by cutting with revolving knives that pass at close tolerance. One important remark is that the crumbs obtained from the Edmonton supplier were produced entirely from truck tires (McCullough, 1998), while the crumbs obtained from Vulcan and Calgary suppliers were produced mainly from the tires of passenger vehicles.

Tire crumbs obtained from both the Calgary and Vulcan suppliers also contained varying amounts of metal, fibre reinforcements, and rocks. The visual inspection indicated that the amount of contaminants increased with increasing grain-size distribution. The No. 20 minus crumbs contained minute quantities of metal dust and fine fibres, whereas, the 1/4 in crumbs contained a great deal of fibre cords, threads, as well as some rocks. Intermediate particle sizes contained fewer fibre cords and threads. Crumbs from the Edmonton supplier, however, did not contain any impurities. This may indicate that the type of tires (truck versus passenger) greatly influences the levels of purities associated with crumb production. However, this is unlikely since larger tires such as those for heavy trucks, farm and agricultural vehicles, earthmoving equipment, and large aircraft tend to comprise both steel wire and fabric reinforcements (Mark et al., 1994). Therefore, the level of QA/QC is likely the main factor contributing to amount of impurities found in these crumbs.

The grain-size distribution curves presented in Figure 6.1 represent an average of the two mechanical sieve tests conducted for each grain-size distribution. The spread (or range) of particle size and the shape of the distribution curves were described by the coefficient of uniformity (C_U) and the coefficient of curvature (C_C) respectively. For the majority of the samples tested, C_U values varied from 1.3 to 2.1, with the exception of No. 20 minus crumbs from the Calgary supplier (C_U = 3.1), and the 1/4 in crumb from the Vulcan supplier (C_U = 2.7). These values indicate that the D_{10} and D_{60} sizes do not differ appreciably. C_C values were close to unity, which ranged from 0.8 to 1.2. Therefore, the grain-size distribution curves, C_u and C_c values of the various crumbs collected generally indicated a uniform gradation. This is also consistent with the gradation of crumbs determined by other investigators (Cecich et al., 1996; Masad et al., 1996; Benda, 1995). In comparison to soils, the particle size and gradation of tire crumbs are similar to that of uniform clean sands, and gravely-sand mixtures.

6.2 Specific Gravity

The specific gravities of tire crumbs are presented and correlations are made regarding specific gravity, particle size, and supplier. Comparisons are also made with tire shreds, and soils. The detailed results are included in Appendix B.

Table 6.2 summarizes the apparent specific gravity of tire crumbs, which is the specific gravity of the solids making up the material. Each value is the average of at least two specific gravity tests conducted. The specific gravity of tire crumbs is slightly greater than water, with values falling within a narrow range of 1.14 to 1.18. There is no apparent correlation between specific gravity and particle size, however, there is a slight variation between the different suppliers. Crumbs obtained from the Edmonton supplier, have specific gravities ranging between 1.14 to 1.15. Crumbs obtained from both the Vulcan and Calgary suppliers, on the other hand, have slightly higher specific gravities in the range of 1.16 to 1.18. The slight difference is due to the amount of impurities present. Tire crumbs collected from Vulcan and Calgary contained varying amounts metal dust, fine fibres, fibre cords, treads, and rocks, and thus expected to have higher specific gravities and those collected from the Edmonton plant. Table 6.3 presents the specific gravity of tire crumbs and compares them with tire shreds, and selected materials from different authors. The experimental specific gravity values from this study fall within the range reported. Benda (1995) and Wu et al. (1997) reported specific gravities of 1.12 to 1.18 for their crumbs, while Masad et al. (1996) reported a value of 1.07. In general, the specific gravity of tire crumbs vary from 1.07 to 1.20. The specific gravity of tire shreds, on the other had, may range from 1.08 to as high as 1.36 depending on their metal content (Edil and Bosscher, 1994). Tire shreds without metal content have a specific gravity of about 1.15. In comparison, the specific gravities of soils are typically 2.60 to 2.80. Hence, the specific gravity of tire crumbs is generally less than half the typical value for soils.

6.3 Compaction Characteristics

The loose and compacted dry unit weights of tire crumbs are presented in Table 6.4.

6.3.1 Loose Dry Unit Weight

The loose dry unit weight was determined using ASTM Test Method D 4254 (ASTM, 1997). Tire crumbs placed loosely into the compaction mold have dry unit weights ranging from 3.4 kN/m^3 for the No. 20 minus crumbs to about 4.0 kN/m^3 for the 1/4 in from the Vulcan supplier. The 1/4 in crumbs from Edmonton, however, had the highest loose unit weight of 5.0 kN/m^3. The void ratio varied from 2.4 to 1.8 for crumbs with increasing grain-size distribution; with the exception of the 1/4 in crumb from the Edmonton supplier, which had the lowest void ratio of 1.3. The results indicate that the loose unit weight increases with increasing grain-size distribution. The larger-sized crumbs can achieve a more compact state due to fewer voids as a result of larger particle size.

This observation is inconsistent with those reported by Newcomb and Drescher (1994), and Ahmed (1993), who found that the dry uncompacted unit weight of tire shreds decreased with increasing shred size. The most likely explanation is that the larger the shed size, the more exposed steel wires they contain. The steel wires may tend to become tangled with each other during their placement, hence, giving a false reduction in the mass of shreds for the same volume occupied, which ultimately reduces its unit weight. For shreds with particle sizes ranging from 25 to 50 mm, Ahmed (1993) reported loose dry unit weights varying from 4.8 to 4.6 kN/m^3 respectively. Newcomb and Drescher (1994) reported unit weights between 2.3 to 3.4 kN/m^3 for their 50 mm shreds, which is rather at the low end.

6.3.2 Compacted Dry Unit Weight

The compacted dry unit weight was determined using a vibratory table (ASTM Test Method D 4253). The compacted dry unit weights varied within a narrow range between 5.3 to 5.7 kN/m^3, with the exception of the 1/4 in crumb from Edmonton, which had the lowest compacted dry unit weight of 4.8 kN/m^3. There is no apparent correlation between the compacted dry unit weight and the different grain-size distribution tested resulting from vibratory compaction methods, since the method gave relatively consistent results between the different grain-sizes. Furthermore, it appears that vibration has little influence on the compaction of the 1/4 in crumb from the Edmonton supplier. The void ratio for the compacted samples was fairly consistent, with values varying from 1.0 to 1.3.

The compaction characteristics of crumbs found in this study are in agreement with the results reported by other investigators. Ahmed (1993), who also used the same vibratory compaction procedures, found little variation between particle size and the compacted dry unit weight for tire rubber. The dry unit weight of was reported to be 5.3 kN/m^3 for their 1/4 in crumb, and for tires shreds ranging from 12.5 to 25 mm (1/2 to 1 in) in size, the dry compacted unit weight varied from 4.6 to 5.1 kN/m^3. However, they found that the dry unit weight achieved with vibration compaction tend to decreased with increasing chip size. This was expected since the smaller size rubber particles rearrange more easily under vibration and can achieve better packing. However, vibration compaction was found to be relatively ineffective for shred sizes larger than 1/4 in. In addition, they found that the particle size had little influence on the compacted dry unit weights obtained from dynamic compaction methods. Masad et al. (1996), on the other hand, used a non standard method of compaction and found dry unit weights in the range of 6.2 to 6.6 kN/m^3 for their No. 4 minus crumbs; which is slightly higher than the those found in this study or reported by Ahmed (1993).

Comparing the compacted and loose unit weights, it is observed that compaction by vibratory methods increased the dry unit weight of tire crumbs by 38 to 62%. In general, the dry unit weights of tire crumbs ranged from 3.4 to 5.0 kN/m^3 for crumbs loosely placed into a mold, to values between 4.8 to 5.7 kN/m^3 for crumbs compacted using a vibratory table. In comparison to tire shreds, the dry unit weight varied from 2.3 to 4.9 kN/m^3 for tire shreds loosely placed into a mold and from 4.6 to 5.1 kN/m^3 for shreds compacted using a vibratory table. Hence it appears under similar compaction procedures, both shreds and crumbs have similar dry unit weights. Tire shreds, however, compacted with various impact methods have unit weights ranging from 5.6 to 6.3 kN/m^3. The compacted dry unit weight of soils is typically 19 to 21 kN/m^3. Hence, the dry unit weight of tire crumbs is about 1/4 to 1/3 the typical values for soils.

6.4 Compressibility

The compressibility behaviour was measured in the laboratory using a large-strain consolidation apparatus to accommodate the larger particle sizes, as well as to anticipate expected large deformations. One-dimensional confined compressibility tests were conducted on loose, uncompacted samples under the condition of no lateral yield. Both dry and saturated samples were subjected to various loading, unloading, and reloading increments. The stress-strain response of the different-grain sized tire crumbs under different loading and tests conditions are summarized in Table 6.5, along with the corresponding values of dry unit weight and void ratio. Table 6.6 summarizes the compressibility indices and coefficients of volume compressibility. A summary of the results is also included in Appendix D.

6.4.1 Stress-Strain Response

It is evident in Table 6.5 that loading causes about up to 50% compression strains for tire crumbs placed loosely into the consolidation apparatus; with the smaller grain-size generally undergoing more compression strains than the larger grain-sizes. Reloading causes only about 5 to 10% strains. Figure 6.2 shows a typical hysterisis stress-strain response for the smallest and largest grain-size distribution tested under dry conditions. The stress-strain response for the initial loading increments is very steep and then flattens out under higher stress levels. This behaviour is expected since the steep portion of the stress-strain curve indicates high compressibility primarily due to the reduction in voids and the flatter portion indicates a decrease in compressibility as a result of tire particle rearrangement and compression under stress. Hence, tire crumbs are highly compressible under the application of load possibly due to two mechanisms: (1) reduction in void ratio under low stresses; and (2) bending and reorientation of highly compressible tire particles under higher stresses. The compression strains are also irrecoverable but there is some rebound upon unloading.

Figure 6.3 shows a typical stress-strain response for 25 mm (1 in) uncompacted tire shreds resulting from a one-dimensional confined compressibility test. A comparison of Figure 6.3 and Figure 6.2 show that shreds and crumbs display similar stress-strain responses in that high compressibility is observed during initial loading, which decreases upon loading to higher stresses. Under a vertical stress of 100 kPa, the 1 in shreds undergo only about 30 to 35% compression strain while tire crumbs undergo strains ranging from 35% to 55% for the largest and smallest grain-sizes respectively. Hence, tire crumbs are generally about two times more compressible than shreds under similar testing conditions and vertical stresses.

6.4.2 Effect of Grain-Size Distribution

To illustrate the influence of grain-size distribution on compressibility, Figure 6.4 shows only the loading stress-strain curves for the different grain-size distribution tested, including the results reported by Edil and Bosscher (1994) and Ahmed (1993). Under a vertical stress of 100 kPa, the No. 20 minus crumbs underwent the most compression with a strain magnitude of up to 55%. The No. 4 - No. 8 and 1/4 in crumb underwent the least compression with strain magnitudes of up to 36 and 42% respectively. Intermediate crumb sizes underwent compression strains ranging from 43 to 49%. The difference in compressibility between the different grain-sizes is probably due to the initial void ratio. As previously discussed, smaller crumb sizes produce higher void ratios when loosely placed. No. 20 minus crumbs was prepared at an initial void ratio of 2.4, which was slightly higher than the rest, and therefore underwent the most compression strain. No. 4 - No. 8 and 1/4 in crumbs were prepared at a void ratio of 1.8 and 2.0 respectively, and thus less compressibility was observed for those sizes.

Figure 6.4 also shows and compares the initial loading stress-strain curves resulting from confined compressibility tests carried out by other investigators on uncompacted tire shreds. Under 100 kPa vertical stress, Ahmed (1993) showed compression strains of about 35% for both 1 in and 2 in tire shreds, while Edil and Bosscher (1994) observed a compression strain of about 20% for their 3 in minus shreds. In comparison, the No. 20 minus crumb is about 2.5 to 3 times more compressible than the largest shred shown under vertical stresses beyond 20 kPa. Although there are some inconsistencies with the results for tire crumbs, it appears that the compressibility of loose, uncompacted recycled tire rubber increases with grain-size distribution. Nonetheless, there is a great difference in the compressibility behaviour between the largest and smallest grain-size.

Ahmed (1993) also investigated the influence of compaction on the compressibility of tire shreds. They showed that particle size and the compactive effort (standard and modified Proctor) had very little effect on the compressibility behaviour of shreds with particle sizes ranging from 12.5 to 50 mm (0.5 to 2 in). However, samples compacted using 50% of standard Proctor effort yielded vertical strains 2 to 4% higher during the first loading cycle than those compacted with standard or modified effort. Furthermore, he found that loose shreds are about 1.5 to 2.5 times more compressible than compacted shreds tested under similar stress levels. Therefore, his results indicate that compaction significantly reduces the compressibility of tire shreds. Benda (1995) also investigated the influence of grain-size distribution on compressibility. Their crumbs and shreds ranging in size from 2 to 38 mm were compacted according to AASHTO Test Method T 99 and consolidated under isotropic stress conditions in a triaxial apparatus. They, however, reported no apparent correlation between particle size, shape or distribution, density, and compressibility. The results reported by Ahmed (1993) and Benda (1995) indicate that the grain-size distribution has no apparent effect on the compressibility behaviour of compacted tire shreds. However, for loose crumbs and shreds, this study found that the grain-size distribution evidently has a major influence on their compressibility behaviour.

6.4.3 Effect of Pore Fluid

To investigate the influence of pore fluid on compressibility, both dry and water-saturated samples were tested. Figure 6.5 and Figure 6.6 shows the typical plot of void ratio versus the logarithm of vertical stress (e versus logσ_v) under both dry and water-saturated conditions for the smallest and largest grain-size distribution tested respectively. In general, the stress-strain responses under both dry and saturated conditions are similar for the different grain-sizes, which indicates that water has very little influence on their compressibility. Figure 6.7 shows only the initial loading portion of the stress-strain curves to illustrate the compressibility of the different grain-sizes under water-saturated conditions. Despite some inconsistencies, a trend of increasing compressibility with decreasing grain-size is also observed, as was the case under dry conditions. As previously explained, the inconsistencies are primarily due to the initial void ratio.

6.4.4 Compressibility Parameters

The compressibility of tire crumbs was characterized by the following indices: (1) compression index, C_c; (2) swelling index, C_s; and recompression index, C_r. Figures 6.5 and 6.6 show that when the e is plotted versus $\log\sigma_v$, the slope of the initial loading curve was approximately linear. Hence, the compression index was calculated from the slope of the e versus $\log\sigma_v$ plot through a linear-regression analysis under the entire stress range from 10 to 100 kPa. The swelling and recompression indices were approximated to a straight line under the rebound and reloading portions of the e versus $\log\sigma_v$ plots. The coefficient of volume compressibility, m_v, was also characterized, which represents the change in unit volume per unit increase in vertical stress. Since m_v is not constant for a particular loading path, it was calculated over a specified stress range. The compressibility parameters for the different grain-sized distributions are summarized in Table 6.6.

The C_c values for the loosely placed crumbs were in the range from 0.5 to 0.7, which is expected for a highly compressible material. The C_c values reported by Ahmed (1993) for loose tire shreds were found to vary from 0.2 to 0.25 for shreds ranging in size from 25 to 50 mm (1 to 2 in). Hence, under similar vertical stress ranges, tire crumbs are up to 3 times more compressible than shreds. Tire crumbs also show some rebound upon unloading, with C_s values similar to that of shreds in the range from 0.1 to 0.25. Newcomb and Drescher (1995) found a C_s value of 0.27 for their 30 mm tire shreds. The coefficient of volume of compressibility (m_v) under the specified stress ranges indicates decreasing compressibility with increasing vertical stresses. Under the stress range from 0 to 10 kPa, m_v varies from $2\text{x}10^{-2}$ to $3\text{x}10^{-2}$ m^2/kN. The m_v values decreases to about $0.1\text{x}10^{-2}$ to $0.3\text{x}10^{-2}$ m^2/kN under higher stress ranges. Furthermore, there is only a slight variation in the m_v values under dry and saturated conditions. In comparison to soils, the typical values of C_c for normally consolidated clays are about 0.2 to 0.5 (Holtz and Kovacs, 1981). Therefore, loosely placed tire crumbs are about 1 to 4 times as compressible as clays. For peats, the C_c values can be as high as 10 to 15 (Holtz and Kovacs, 1981).

6.5 Hydraulic Conductivity

Constant head permeability tests were conducted using the large-strain consolidation apparatus to investigate the influence of grain-size, hydraulic gradient and overburden pressure on the hydraulic conductivity of tire crumbs. The average measured hydraulic conductivity values are summarized in Table 6.7 along with the corresponding values of void ratio, porosity and dry unit weight. Figure 6.8 and Figure 6.9 illustrate, respectively, the typical plots of discharge velocity versus hydraulic gradient for the smallest and largest grain-size distribution tested under different overburden pressures. Figure 6.10 shows the influence of overburden pressure on hydraulic conductivity for all the grain-sizes tested. The detailed investigation is included in Appendix E.

The plots of discharge velocity versus hydraulic gradient were used to obtain the hydraulic conductivity under different overburden pressures by taking the slope of the best-fit curve through each corresponding set of data points. Since temperature affects the viscosity of water, which in turns affects its ability to flow, the discharge velocity was corrected to a temperature of 20°C. Hence, Table 6.7 reports the k_{20} values, which are the hydraulic conductivities that take into account the effect of temperature.

6.5.1 Influence of Overburden Pressure

Figure 6.10 shows a decrease in hydraulic conductivity with increasing overburden pressure. This is expected since increasing overburden pressure primarily results in the reduction of voids and compressibility of tire particles, hence reducing the hydraulic conductivity. For all crumbs except for the No. 20 minus, the most significant drop in hydraulic conductivity occurred under the vertical stress range between 0 and 20 kPa, which was consistent with the increase in compressibility. The hydraulic conductivity thereafter continued to decrease somewhat linearly with increasing vertical pressure.

Under 10 and 100 kPa, the hydraulic conductivity measured for the No. 20 minus crumbs was about 20 x 10^{-3} cm/s and 2 x10^{-3} cm/s respectively. For the remaining grain sizes, the hydraulic conductivity varied from 40 to 12 x10^{-3} cm/s respectively. Hence, the application of overburden pressure resulted in a 90% reduction in hydraulic conductivity for the No. 20 minus crumb, and a 30 to 60% reduction for the remaining grain-sizes.

The measured hydraulic conductivities are in good agreement with the results reported by other investigators. Cecich et al. (1996) conducted constant head permeability tests in accordance with ASTM D 2434. Samples containing a uniform distribution of both crumbs and shreds (0.85 to 12.5 mm in size) were compacted using the Modified Proctor method to dry unit weights varying from 5.5 to 5.9 kN/m^3. They found that the hydraulic conductivity for their material varied from 33 to 34 x10^{-3} cm/s. These values are consistent with those measured in the laboratory (27 to 20 x10^{-3} cm/s) for the No. 10 - No. 20 to 1/4 in grain-size distributions tested under 20 to 50 kPa respectively. Masad et al. (1996), on the other hand, conducted permeability tests on No. 4 minus crumbs in a triaxial cell. They found an inverse linear relationship between hydraulic conductivity and confining pressures of up to 350 kPa. The hydraulic conductivity for their crumbs varied from 2 to 0.5 x10^{-3} cm/s, which is more consistent with the values obtained for the No. 20 minus crumbs under 100 kPa vertical stress.

6.5.2 Effect of Grain-Size Distribution

The hydraulic conductivity is generally influenced by porosity, which is in turn related to the grain-size distribution, particle shape and macro structure. In Figure 6.10, the majority of the samples tested showed slight discrepancies in the hydraulic conductivity measured for the different grain-size distributions; with the exception of the No. 20 minus crumbs. This was expected since the No. 20 minus crumb underwent the most compression, which resulted in fewer voids and hence lower hydraulic conductivities. Overall, the grain-size distribution showed a minor influence on the hydraulic conductivity of tire crumbs for the samples tested.

In general, the hydraulic conductivity of tire crumbs determined in the laboratory is in the range of 10^{-3} to 10^{-2} cm/s, which are values typical of clean sands and clean sand-gravel mixtures with similar grain-size distribution. In contrast, the hydraulic conductivity of tire shreds is in the order of 10^{-1} to 10 cm/s; values which are more typical of clean gravels. Hence, the hydraulic conductivity of tire crumbs is about 1 to 4 orders of magnitude less than the typical values reported for shreds under similar test conditions.

6.6 Thermal Properties

Transient state thermal conductivity tests were conducted to determine the influence of grain-size distribution, compaction, vertical stress, pore fluid and temperature on the thermal properties of tire crumbs. The results and discussions are presented in the following sections according to the test apparatus used and procedures followed. Section 6.6.1 presents the results using the thermal needle and aluminum cells apparatus, which was used to investigate the effect of compaction, pore fluid and temperature. To examine the effect of dry unit weight and pore fluid, the thermal needle method was combined with the large-strain consolidation apparatus, and the thermal conductivity tests were conducted under different vertical stresses at room temperature. The results of the combined method are presented in Section 6.6.2.

6.6.1 Thermal Needle and Aluminum Cells

Table 6.8 summarizes the average measured thermal conductivity for all the grain-size distribution tested under different combinations of pore fluid, compaction and temperature. The corresponding values of average dry unit weight and void ratio are also presented. The data are presented graphically in Figure 6.11 to Figure 6.13.

6.6.1.1 Influence of Pore Fluid on Thermal Conductivity

The pore fluid has a tremendous influence on the measured thermal conductivity of tire crumbs. To investigate this influence, the thermal conductivity tests were conducted for both dry and saturated samples. Since the conductivity of water is about 22 times that of air, saturated tire crumbs are expected to give significantly higher thermal conductivities than similar crumbs tested dry. Farouki (1981) indicated that the presence of a small amount of moisture in soils causes water bridges that improve the thermal contacts between soil particles and therefore increases its thermal conductivity.

Figure 6.11 shows the ratio of the thermal conductivity of saturated tire crumbs to that of dry crumbs ($\lambda_{sat}/\lambda_{dry}$) as a function of temperature above 0°C for compacted and loose samples. That is, the figure illustrates the effect of water on the measured thermal conductivity as opposed to dry samples. As expected, water increased the thermal conductivity of dry tire crumbs by about 4 times for compacted samples, and by as much as 9 times for loose samples. For compacted tire crumbs, water may simply provide a bridge that improves the thermal contacts between tire particles as Farouki (1981) indicated for soils. The increase for loose crumbs, however, is much greater due to higher porosities (i.e. more water filled voids). Farouki (1981) also indicated that as the porosity approaches 100% (i.e. zero solids volume) the thermal conductivity of unfrozen saturated soils may be expected to approach the value of water. In this case, the average measured thermal conductivity of loose, unfrozen saturated tire crumbs was found to be about 0.6 W/m-°C; a value that is similar to the thermal conductivity of water at 20°C.

6.6.1.2 Influence of Temperature on Thermal Conductivity

The thermal properties of soils may vary considerably with temperature. This is particularly important when water is present. The influence of temperature was investigated by conducting the thermal conductivity tests on both dry and saturated samples at the following temperatures: (1) +24°C (unfrozen); (2) -10 and -5°C (frozen); and (3) +3 and +24°C (unfrozen, but thawed).

Figure 6.12 shows the measured thermal conductivity as a function of temperature for all the grain-sizes tested under different degrees of saturation and compaction. The solid lines drawn through each set of data points represent the average thermal conductivities determined at the corresponding temperature for each combined condition of saturation and compaction. The lines of average values, however, do not distinguish between the various grain-sizes. As expected, the thermal conductivity of frozen saturated tire crumbs is much greater than that of the unfrozen crumbs because ice has a conductivity of about four times that of water. For loose, saturated crumbs the average measured thermal conductivity when frozen is about 1.4 W/m-°C; a value that is approaching the thermal conductivity of ice. For saturated frozen soils, Farouki (1981) also indicated that as the porosity approaches 100% the thermal conductivity may be expected to increase towards that of ice. The thermal conductivity for saturated unfrozen crumbs was found to be 0.6 W/m-°C. Compacted samples have thermal conductivities of 0.9 W/m-°C and 0.4 W/m-°C when tested frozen and unfrozen respectively. Hence, the thermal conductivity of saturated crumbs measured in the frozen state is about twice that measured in the unfrozen state. Furthermore, it appears that temperature has little effect on the thermal conductivity of dry tire crumbs; either compacted or loose.

6.6.1.3 Influence of Compaction on Thermal Conductivity

The compaction of dry or saturated soils generally results in the reduction of air or water filled voids, which increases the interfacial surface contacts between the soil particles. The importance of heat transfer at these contacts between the soil particles was emphasized by Farouki (1981) since heat transfer is a major factor that determines the overall measurement of thermal conductivity.

Figure 6.13 shows the logarithm of thermal conductivity as a function of dry unit weight to illustrate the influence of compaction. The solid lines represent the best-fit curve, assuming a linear correlation, for each of four sets of data points under the different conditions of compaction and saturation. The assumption, however, does not take into consideration the influence of grain-size distribution. Although there is some scatter with the data, a trend of increasing thermal conductivity with compaction is observed for both frozen and unfrozen dry tire crumbs. Compaction reduces air voids and increases heat transfer at the surface contacts between tire particles, thereby increasing its thermal conductivity. Compaction, however, had the opposite effect on saturated tire crumbs. Farouki (1981) indicated that for fully saturated soils, compaction would generally increase the thermal conductivity only if the soil solid has a higher thermal conductivity than the water it replaces. For example, sandy soils are often composed of quartz, which has a thermal conductivity about 15 times that of water. Therefore, sands are expected to show an increase in thermal conductivity with increasing dry unit weight (or density).

Since the thermal conductivity of the tire rubber solid[2] is about 3 and 10 times less than water and ice respectively, compaction therefore decreases the thermal conductivity of both the frozen and unfrozen saturated tire crumbs. For frozen saturated crumbs, the behaviour deviates from frozen saturated soils. As in the case of unfrozen soils, saturated frozen soils show an increase in the thermal conductivity with dry density. However, Farouki (1981) indicated that for over-saturated ice-rich soils (i.e. undisturbed permafrost), the thermal conductivity is shown to decrease significantly with increasing ice content. The decrease was attributed to the presence of many small air bubbles and discontinuities in the ice-rich permafrost.

6.6.2 Combined Thermal Needle and Large-Strain Apparatus

Table 6.9 summarizes the measure thermal conductivity of tire crumbs tested under different conditions of saturation and vertical stresses using the combined thermal needle and large-strain apparatus. The data are also presented graphically in Figure 6.14 and Figure 6.15.

6.6.2.1 Influence of Dry Unit Weight on Dry Samples

Figure 6.14 plots the logarithm of thermal conductivity as a function of dry unit weight for all the grain-size distribution tested under dry conditions. It is observed that the thermal conductivity increases with dry unit weight. This behaviour can be explained with respect to soils. Farouki (1981) indicated that an increase in the dry density of a soil resulted with an increase in the thermal conductivity mainly due to three factors: (1) more solid matter per unit soil volume; (2) less pore air per unit soil volume; and (3) better heat transfer across the contacts between soil particles.

The logarithm of thermal conductivity is also shown to increase linearly with increasing dry unit weight in Figure 6.14, which justifies the assumption of linearity made in Section 6.6.1.3. A trend of linearity between the logarithm of thermal conductivity and dry density has also been observed for soils. Smith and Byers (1938) established that the logarithm of thermal conductivity of dry natural heavy soils increased linearly with their dry density, while data from the U.S.S.R. Building Code (1960) showed that the logarithm of thermal conductivity of unfrozen sandy soils versus dry density at constant moisture content is also linear.

---

[2] Thermal conductivity of tire rubber solid is about 0.25 W/m-°C for styrene butadiene rubber (see Table 2.12)

6.6.2.2 Influence of Dry Unit Weight on Saturated Samples

For unfrozen, fully saturated soils, an increase in dry unit weight (or density) means that the solids fraction replaces some of the water in the pores. An increase in the thermal conductivity will therefore result only if the solid has a higher thermal conductivity than the water it replaces. The solid in this case is tire rubber, which has a thermal conductivity of about 3 times less than water. Therefore, a trend of decreasing thermal conductivity with increasing unit weight was observed as shown in Figure 6.15.

6.6.3 Comparisons Between Methods

Figure 6.16 plots and compares the measured thermal conductivities as a function of dry unit weight using the different thermal testing apparatus and procedures followed in this study under unfrozen, dry and saturated conditions. The combined thermal needle and large-strain consolidation apparatus generally gave higher thermal conductivity than the thermal need and aluminum (thermal cell) apparatus. The factors causing this difference are:

1. **Method of compaction.** The crumbs in the thermal cells were compacted using a vibratory table. Under saturated conditions, compaction may have caused the build up of pore pressure and introduced air bubbles within the crumb rubber matrix and ultimately lowering the thermal conductivity values. For dry compacted samples, the crumbs may have experienced rebound upon removing the 30 kPa surcharge, which may have resulted in the increase of air voids and reduced particle contact. Thermal measurements with the large-strain apparatus, on the other hand, were carried out under a constant vertical stress. Tire particles were kept intact during the measurement, which increases the heat transfer across the surface contacts, thus, increasing the thermal conductivity.
2. **Probe contact with medium.** When the thermal needle was inserted into the tire crumbs, there was no direct way of ensuring complete probe contact with the

surrounding material. Hence, an air gap between the bottom of the cap and the top surface of the sample would seriously hinder the thermal measurements. Farouki (1981) pointed out the difficulties in using the thermal needle method when the probe lies partly in a void space. With the large-strain consolidation apparatus, the application of vertical stress causes the probe to make complete contact with the surrounding tire crumbs, and hence, increasing the thermal conductivity measurements.

3. **Inconsistent probe lengths.** Probe length may also be a factor in measuring the thermal conductivity. The probe length used for the large-strain consolidation apparatus was 40 mm. Those used for the thermal cells varied in length from 50 to 80 mm. Hence, shorter probe lengths means more power per heated unit length of probe, which resulted in more efficient heat transfer and increased thermal conductivities.
4. **Freeze-thaw processes.** The values shown in Figure 6.16 include those for crumbs that have undergone a cycle of freeze-thaw using the thermal cell apparatus. The effects of the freeze-thaw process have considerable consequences on the thermal conductivity of soils. For example, when soil freezes, water is drawn to the freezing front, thereby altering the soil's thermal properties in both the frozen and unfrozen zones (Farouki, 1981). Although the effects of freeze-thaw of tire crumbs is unknown, it is observed that crumbs that have under gone a cycle of freeze-thaw have lower thermal conductivities than those that did not experience a freeze-thaw cycle.

6.6.4 Comparisons of Measured Thermal Conductivities

The measured thermal conductivity for tire crumbs are in relatively good agreement with those reported by other investigators. Table 6.10 compares the measured thermal conductivity of tire crumbs to the values reported by Shao et al. (1995). The particle size, testing apparatus and testing conditions are moderately close to one another to make a decent comparison. Using a guarded hot plate apparatus, Shao et al. (1995) found that the thermal conductivity of their 1 mm crumbs tested thawed with a water content of less than 1% was about 0.097 W/m-°C. This value is comparable to the thermal conductivity of 0.082 to 0.091 W/m-°C measured for the No. 20 minus crumbs tested dry in a loose state when thawed at temperatures of +2 and +25°C respectively. They also determined that the thermal conductivity for their 25 mm compacted shreds tested in a frozen state with a water content of 5% was about 0.17 W/m-°C. This is also comparable to the thermal conductivity of 0.12 to 0.14 W/m-°C for frozen 1/4 in crumbs tested dry in a compacted state. Overall, their results showed slightly higher thermal conductivities than those found in this study. The slight variation is likely due to the fact that moisture was present in their samples, and that their tire rubber were larger in size than the crumbs used in this study for comparison. Another factor that may have caused the variability in the comparison is different testing apparatus. However, tests on insulating materials showed good agreement between the thermal conductivity values obtained by the probe method and those obtained by the GHP test (D'Eustachio and Schreiner, 1952). Data comparisons on the thermal conductivities using both methods carried out on unsaturated sands showed that the probe method generally resulted in somewhat higher thermal conductivity values.

6.7 Shear Strength

6.7.1 Direct Shear

Direct shear tests were performed using a 4 in direct shear box to accommodate the larger crumb sizes. The tests were conducted for each grain-size distribution under normal stresses of 25, 50 and 100 kPa. Both dry and saturated samples were tested to investigate the effect of water on the shear strength parameters. Under saturated conditions, however, only the smallest and largest grain-sizes were tested.

6.7.1.1 Shear and Deformation Behaviour

Dry Conditions

Figures 6.17 to Figure 6.19 show the typical plots of shear stress versus horizontal deformation and vertical deformation versus horizontal deformation for tire crumbs tested dry under normal stresses of 25, 50 and 100 kPa respectively. As expected, tire crumbs show an increase in shear resistance with increasing shear deformation even beyond relatively high shear displacements of up to 12 mm; especially under high normal stress. Dense sands, in comparison, show a peak or maximum shear resistance at relatively low displacements between 2 to 5 mm (Head, 1982) that decreases to an ultimate or critical value with further shearing. The increase in resistance behaviour of tire crumbs can be attributed to the densification of the samples during shear, which results in the reduction of air voids, compressibility of tire grains, and the interlocking of particles. Under low normal stress (i.e. 25 kPa) the shear behaviour of tire crumbs is similar to that of loose sands in which the shear resistance approaches an asymptotic value.

The volume change relationship of tire crumbs is also similar to that of dense sands, except that tire crumbs show dilation at higher shear displacements (roughly around 4 to 6 mm) for the majority of the grain-size distribution tested under different normal stresses with the exception of the No. 20 minus, No. 10 - No. 20 and No. 10 crumbs. These grain-sizes showed contraction throughout shearing under a normal stress of 25 kPa. This is very unusual and deviates from the results reported by Cecich et al (1996) as shown in Figure 2.10. They observed dilation for their material (mixture of crumbs and shreds with particle sizes ranging from 0.85 to 12.5 mm) even under a low vertical stress of 4 kPa. The deviation, however, may be insignificant because the shear behaviour for the three grain-sizes of interest does not differ appreciably with the rest of the results. The influence of dilation, on the other hand, may have an important effect on the frictional resistance of tire crumbs as will be discussed later. It is believed that the dilation of tire crumbs occur when the shear displacement causes the tire particles to roll and perhaps slide over one another, probably after overcoming particle interlocking. The effects of dilation are especially important for dense sands in which dilation causes a decrease from peak resistance to a residual value.

Saturated Conditions

Figures 6.20 to Figure 6.22 compares the stress and deformation of tire crumbs conducted under dry and saturated conditions. The stress-deformation behaviour under both conditions are similar, however, saturated crumbs show slightly reduced shear resistance than dry crumbs under similar shear displacements. The comparison is further discussed in Section 6.7.1.5. Similar experience has shown that the shear strength results obtained on saturated sands are very similar to those for dry sand, provided that the sand remains saturated and that drainage takes place freely during shear (Head, 1982).

6.7.1.2 Analysis of Data

Crumbs tested under direct shear do not exhibit well-defined peak shear resistance as shown by their stress-deformation curves. Hence, the shear strength parameters must be determined using the criterion of allowable deformation. In the direct shear test, failure is considered to be the peak shear resistance or, if no peak is reached, ASTM D 3080 specifies that failure is the shear resistance at 15 to 20% relative lateral displacement (ASTM, 1997). However, it would be interesting to analyze the strength parameters at various established levels of deformation. Hence, horizontal displacements of 2, 4, 8 and 12 mm were chosen for analysis. The 4 mm displacement was chosen because the value is in the deformation range at which contraction stops and dilation begins. The shear resistances were then determined for the corresponding established levels of deformations and normal stresses. Shear strength parameters, namely the apparent cohesion, *c*, and mobilized friction angle, ϕ_{mob}, were determined using the following regression methods.

Method A - Linear Regression with c ≠ 0

The failure envelope was assumed linear according to the following Mohr-Coulomb failure criterion.

$$\tau = c + \sigma_N \tan(\phi) \qquad \textbf{[Equation 6.1]}$$

where τ = shear stress (kPa), *c* = apparent cohesion intercept (kPa), σ_N = normal stress (kPa), and ϕ = angle of shearing resistance (°).

Method B - Linear Regression with c = 0

The failure envelope was also assumed liner, however, the apparent cohesion intercept was forced through the origin. Equation 6.1 then becomes:

$$\tau = \sigma_N \tan(\phi) \qquad \textbf{[Equation 6.2]}$$

Method C - Power Regression

In this method, a non-linear failure envelope was assumed using the power function of the following general form:

$$\tau = b\sigma_N^m \qquad \textbf{[Equation 6.3]}$$

were b and m are constants.

The angle of shearing resistance in Equations 6.2 and 6.3 was determined from the slope of the best-fit curve, while ϕ for the non-linear failure envelope was approximated with the secant tangent taken over the stress range of interest.

6.7.1.3 Shear Strength Parameters

Figure 6.23 to Figure 6.25 shows the typical failure envelopes for the 1/4 in crumb from the Edmonton supplier obtained from the three regression methods. Similar strength envelopes developed for other grain-sizes are included in Appendix G. The shear strength parameters are summarized in Table 6.11. In general, all three regression methods fitted the data reasonably well in that the coefficients of determination (R^2) were all near unity.

Results from Method A

Figure 6.23 indicates that tire crumbs tested under a constant rate of shear tend to exhibit some degree of apparent cohesion, which is most likely caused by the compressibility of tire particles, and by their unique angular shape that results in the interlocking of individual grains. The angle of shear resistance and cohesion intercept was found to vary from 5 to 20° and from 0 to 6 kPa respectively at a shear displacement of 2 mm. At a shear displacement of 12 mm, the ϕ values vary from 30 to 33° and c varies from 1 to 7 kPa. The c values seem reasonable since tire crumbs do appear to exhibit some apparent cohesion. The strength parameters are also in good agreement with those reported by other investigators. Cecich et al. (1996) reported ϕ and c values of 27° and 7 kPa, respectively, at a shear displacement of 15 mm for their samples containing a mixture of both crumbs and shreds with particle sizes ranging from 0.85 to 1/2 in. For tire shreds, typical values range from 17 to 35° and from 4 to 11 kPa (see Table 2.9) at shear displacements between 10 to 60 mm. In comparison to granular soils, typical ranges of ϕ for fine to medium grained, angular, dry sands with a uniform gradation are from 35 to 43° tested under loose and dense states respectively. Furthermore, angles of shearing resistance range from 40° for loose to 50° for dense angular gravels. Hence, the shearing resistance of tire crumbs at high shear displacements are very similar to that of loose sands.

It is observed that with increasing levels of shear displacement, the cohesion intercept tends to increase slightly while the friction angles increased significantly. Humphrey et al. (1992) also observed the same increase in cohesion intercept for tire shreds at higher shear displacements and suggested to neglect or use a small value for design since it appears that significant deformation is required to develop this cohesion in tire shreds. They also found that the friction angles were only slightly affected by changes in shear displacement. For tire crumbs, Figure 6.27 shows that the angle of shearing resistance increased by as much as 5 times for the 1/4 in crumbs with a 10 mm increase in shear displacement. There is also quite a difference in resistance between the smallest and largest grain-size under similar shear displacements. The influence of particle size on shear strength is discussed in Section 6.7.1.4.

Results from Method B

The angle of shear resistance corresponding to shear displacements of 2 and 12 mm varies from 7 to 19° and 32 to 37° respectively. In general, Method B is expected to give slightly higher friction angles (1 to 2 times greater) than Method A. Furthermore, there is not much variation in the coefficient of determination between the two methods, but overall, Method A gave a better fit of the data.

Results from Method C

The secant tangents were taken over a stress range between 0 and 100 kPa. This gave intermediate angles of shearing resistance with values ranging from 7 to 18° and 32 to 36° at 2 and 12 mm shear displacements respectively.

Figure 6.26 shows that over the stress range of interest (from 0 to 100 kPa), Method B gave the highest angle of shearing resistance, followed by Method C, then Method A. One interesting point is that the mobilized friction angle increases rapidly from 0 to

4 mm. However, beyond 4 mm, the crumbs begin to show a reduction in resistance, which is consistent with the onset of dilation. Further shear displacement beyond 8 mm shows even more reduction in resistance. In Figure 2.13, Bernal et al. (1997) showed an almost linear increase in shear resistance with increasing shear displacements of up to 70 mm in tire shreds. For tire crumbs, it takes only about 8 mm to mobilize a friction angle of roughly 30°. However, for shreds, it may take significant shear displacements of up to 40 mm to mobilize the same resistance.

6.7.1.4 Influence of Grain-Size Distribution

The effect of particle size on the shear strength of tire crumbs is illustrated in Figure 6.27. Although there is some scatter, it appears that under similar conditions, crumbs with the smaller grain-size distribution will generally show higher shear resistance. This is primarily because the smaller crumbs undergo higher vertical compression than the larger sizes under similar normal stresses, which appears to have an influence on its shearing resistance. Furthermore, it is believed that during shear, the smaller crumbs tend to lock together instead of rolling and sliding over one another like the larger particles. It was also established that crumbs show higher shear resistance than shreds under similar shear displacements. Humphrey et al. (1992) indicated that tire shreds also contain flat pieces that tend to orient themselves parallel to the horizontal shear plane, causing them to slide over one another during shear and resulting in reduced resistance.

6.7.1.5 Influence of Water

Figure 6.28 plots the ratio of the friction angle of saturated crumbs to that of dry crumbs, ϕ_{sat}/ϕ_{dry}, under similar shear displacements. Only the smallest and largest grain-sizes were tested under saturated conditions. It is expected that water should have very little influence on the direct shear strength of tire crumbs because water had little effect on the compressibility as was discussed in Section 6.4.3. However, saturated crumbs gave slightly lower shearing resistance than that of dry crumbs as shown in Figure 6.28. This is perhaps due to poor drainage because the depth of the shear box did not allow for the use of two porous plates, let alone a retaining plate and two solid grid plates. It was important to obtain a sample of adequate height for the anticipated high compression and to prevent the shear box from shearing the upper solid grid plate. As a consequence, pore pressure may have build up and hence resulting in reduced shear resistance. Another factor may be due to size effects from the testing apparatus. This may be important for tire crumbs in that it relates to the minimum number of grains in a sample in order to obtain representative results. Humphrey et al. (1992), however, found that the size of the direct shear box had little influence on the direct shear strength of 50 to 70 mm (2 to 3 in) tire shreds tested in a 8 in, 12 in and 16 in direct shear box.

6.7.2 Triaxial Compression

Consolidated-drained triaxial compression tests were conducted to evaluate the shear strength and deformation behaviour of tire crumbs under various confining pressures. The tests were conducted once per confinement stress for each grain-size distribution under the confining pressures of 25, 50 and 100 kPa. Table 6.13 summarizes the calculated shear strength parameters obtained using the criterion of allowable strains from the different regression analysis. The plots of deviatoric stress versus axial strain and volumetric strain versus axial strain under the different confining pressures for all the grain-size distribution tested are shown in Figure 6.29 to Figure 6.31.

6.7.2.1 Shear Behaviour of Tire Crumbs

Tire crumbs exhibit strain-strengthening behaviour as shown in their stress-strain curves. This behaviour was typically observed by past researchers for both tire crumbs (Wu et al., 1997; Masad et al., 1996; and Benda, 1995) and shreds (Wu et al., 1997; Bernal et al., 1997b; Ahmed, 1993; and Benda, 1995) tested under confinement. The majority of the samples tested showed linear stress-strain behaviour beyond 5% axial strains, with increasing resistance up to 20% strains. The increase in resistance is perhaps due to considerable interlocking between individual tire particles during compression. The same inter-particle locking may have contributed to the increased resistance of crumbs under direct shear testing as discussed in Section 6.7.1.4. For the 1/4 in crumb from the Edmonton supplier, the stress-strain curves under 25 and 50 kPa confinement (Figures 6.29 and 6.30 respectively) deviated from the strain-strengthening behaviour and appeared to be asymptotic. This is unusual and deviates from the typical stress-strain behaviour of tire crumbs but agrees well with the stress-strain response observed by Benda (1995) and Wu et al. (1997) for crumbs and shreds tested under constant σ_1 stress paths (Figure 2.20). At 100 kPa, however, the stress-strain behaviour for the 1/4 in crumb was again linear as was observed with the other crumbs from the other suppliers.

The deviatoric stresses at the same strain level also increased significantly with increasing confining pressure for all samples tested. Furthermore, all samples tested did not reach peak deviatoric stresses under different confinement. This would suggest that allowable strain should be the criterion in selecting the strength parameters of tire crumbs as was suggest by Ahmed (1993) and Masad et al. (1997).

The stress-strain curves in Figure 6.29 to Figure 6.31 also show the variation in grain-size distribution with deviatoric stresses under the different confining pressures. Although there was some discrepancy, a trend of increasing deviatoric stresses with increasing grain-size was observed. The exception was with the 1/4 in crumb from the Vulcan supplier, which showed the lowest resistance under all confinement. The 1/4 in crumb from the Edmonton supplier, and the No. 4 - No. 8 crumb showed the highest resistance at higher confining pressures. In general, there was some difference in the shear resistance between the largest and smallest grain-sizes.

6.7.2.2 Deformation Behaviour of Tire Crumbs

The deformation of tire crumbs was characterized by high compressibility and lateral bulging of the samples during shearing. Again, there was some variation in the data but the following trend was observed. At low confining pressures of 25 and 50 kPa, decreasing volumetric strains (or contraction) were observed at up to about 5% axial strain, and thereafter stabilized with increasing strains. Likewise, Bernal et al. (1996) observed similar volumetric strain behaviour for their 1 in shreds conducted under 28 kPa confinement as shown in Figure 2.18. Volume compressibility of tire crumbs at low confining pressures was also characterized by significant lateral bulging; an example of which is pictured in Figure 6.32. In a few samples, volumetric dilation was also observed. At 100 kPa confining stress, the volume did not stabilize with increasing strain but continued to decrease linearly, which also agrees with Figure 2.18. The volumetric behaviour at 100 kPa was also characterized by high material compressibility, but lateral bulging was not observed until 10 to 15% axial strain had occurred.

Masad et al. (1997) found greater compressibility for their No. 4 minus tire crumbs under lower confinement at similar axial strain levels. Bernal et al. (1996), on the other hand, found that the compressibility of 1 in tire shreds increased with increasing confining pressure. In this study, there was a great deal of inconsistency in the volumetric strain behaviour at different confining stresses, therefore, no apparent correlation can be made between compressibility and confining pressure because a few of the samples showed greater compressibility at higher confinement, whereas in other instances, the opposite held true.

6.7.2.3 Analysis of Data

Triaxial compression tests also showed that tire crumbs do not exhibit well-defined peak shear resistance as illustrated by their stress-strain curves. Hence, the shear strength parameters were computed using the criterion of allowable strains suggested by Ahmed (1993) and Masad et al. (1996). To determine the effect of allowable strains on the strength parameters, four levels of axial strains were selected: 5%, 10%, 15%, and 20%. To avoid constructing Mohr circles and determining the strength parameters graphically, p-q plots were employed. By plotting $q = \frac{1}{2}(\sigma_1 - \sigma_3)$ against $p = \frac{1}{2}(\sigma_1 + \sigma_3)$, any state of stress can be represented by a stress point rather than by a Mohr circle. The failure envelopes could then be obtained from a regression analysis through the stress points using similar procedures followed for the analysis of the direct shear tests.

Method A' - Linear Regression with $c \neq 0$

Method A' assumes a linear failure envelope represented by the following modified Mohr-Coulomb failure criterion.

$$\frac{1}{2}(\sigma_1-\sigma_3)=a+\frac{1}{2}(\sigma_1+\sigma_3)tan\alpha$$

[Equation 6.4]

where a and α are the modified shear strength parameters.

Method B' - Linear Regression with c = 0

Method B' also assumes a linear failure envelope as in Equation 6.4 but with the intercept, a, forced through the origin. The failure envelope in this method is represented by:

$$\frac{1}{2}(\sigma_1-\sigma_3)=\frac{1}{2}(\sigma_1+\sigma_3)tan\alpha$$

[Equation 6.5]

Method C' - Power Regression

Method C' assumes a non-linear modified failure envelope using a power regression. The following represents the modified failure envelope:

$$\frac{1}{2}(\sigma_1-\sigma_3)=b\frac{1}{2}(\sigma_1+\sigma_3)^m$$

[Equation 6.6]

The modified shear strength parameters, α and a, in Equations 6.4 and 6.5 were determined from the slope and intercept of the best-fit line though the stress points. The shear strength parameters, ϕ' and c', were then determined from the following relationships:

$$\phi'=\sin^{-1}(\tan\alpha)$$

[Equation 6.7]

$$c'=\frac{a}{\cos\phi}$$

[Equation 6.8]

In Method C', ϕ' was approximated with the secant tangent taken over the stress range of interest.

6.7.2.4 Shear Strength Parameters

Figure 6.33 to Figure 6.35 depict the typical modified failure envelopes for the 1/4 in crumb from the Edmonton supplier. Table 6.13 summarizes the shear strength parameters calculated from the three different regression methods. The corresponding strain levels and coefficients of determination are also presented.

Results from Method A'

Figure 6.36 shows the mobilized friction angle, ϕ'_{mob}, as a function of axial strain for all the different grain-size distributions when the apparent cohesion intercept was not equated to zero. The calculated friction angles were inconsistent and found to vary considerably between the different grain-sizes at their respective strain levels. The No. 4 - No. 8 crumb showed the highest values of ϕ', while the 1/4 in crumb from the Vulcan supplier showed the least. The apparent cohesion intercepts were also found to vary considerably. The majority of grain-sizes, with exception of the No. 20 minus, showed c' values ranging from 10 to 20 kPa at 5 to 20% strains respectively. These values are unreasonably high considering tire crumbs are inherently a cohesionless material. However, the cohesion intercepts are in the range reported by Ahmed (1993) for tire shreds ranging from 12.5 to 25 mm (1/2 to 1 in) in size and containing a small percentage of exposed steel wires. They reported c' values between 10 and 40 kPa at strain values of 5 and 20% respectively. Masad et al. (1996), on the other hand, found extremely high cohesion intercepts in the range of 70 to 80 kPa for their No. 4 minus crumbs. Therefore, when the cohesion intercept was account for, there does not appear to be a definite correlation between grain-size distribution and frictional resistance, as shown in Figure 6.36. Nonetheless, the figure shows a linear increase in frictional resistance with increasing compression strains. At 5% vertical strain, the average ϕ' value was about 10°, which doubled to a value of about 22° at 20% strain. The latter value is consistent with the results obtained by others for both crumbs and shreds.

Figure 6.37 shows and compares the average ϕ'_{mob} values of tire crumbs found in this study with those reported by Ahmed (1993) and Masad et al. (1996) using the modified Mohr-Coulomb failure criterion and similar regression techniques. Ahmed (1993) conducted large-scale (152 mm diameter) triaxial compression tests on their tire shreds ranging from 12.5 to 25 mm (1/2 to 1 in) in size. However, their samples were prepared using impact compaction techniques with compactive efforts equivalent to the modified, standard, and 50% of standard Proctor. They reported ϕ' values for their shreds to vary between 20 and 25° at 20% strain. They also indicated that the size of shreds and compactive efforts did not significantly affect the shear behaviour, even though a trend of increasing shear resistance with increasing shred size and compactive effort was observed. Masad et al. (1996), however, reported a lower frictional resistance of only 15° at 20% strain for their No. 4 minus crumbs.

Results from Method B'

Figure 6.38 shows the mobilized friction angle, ϕ'_{mob}, as a function of axial strain for all the different grain-size distribution tested when the apparent cohesion intercept was equated to zero. This procedure gave fairly consistent ϕ' values that could be directly correlated by grain-size at their respective strain levels. Furthermore, there was less variability in ϕ'. With the exception of the 1/4 in crumb from the Vulcan supplier, there appears to be a trend of increasing frictional resistance with increasing grain-size. At 5% axial strain the ϕ' values showed some variability between 15 to 22°. At 20% strain there was less variability with the ϕ' values, which ranged from 27 to 30°. Overall, the calculated frictional resistance is slightly higher when the cohesion intercepted was neglected, which was generally expected.

Figure 6.39 shows the average ϕ'_{mob} of tire crumbs determined in this study and compares them with the results reported by Benda (1995). They conducted large-scale (100 mm diameter) triaxial compression tests on tire crumbs and shreds ranging from 2 to 38 mm (No. 10 to 1.5 in) in size and containing no steel components. Prior to testing, the samples were compacted according to AASHTO Test Method T 99. The failure envelopes were also determined using the modified Mohr-Coulomb failure criterion with the cohesion intercepts set to zero. They reported ϕ' values for their material between 10 and 18° at 10% strain, which were considerably lower than those determined in this study. However, at 20% strain, they reported much higher ϕ' values between 27 to 36°, which was consistent with the larger shred size. They also indicated that the values at higher strain levels were consistent with field observations.

Results from Method C'

For the non-linear failure envelopes, the secant tangents were taken over the stress increments between 25 to 50 kPa, and 50 to 100 kPa normal stresses. As expected, the shear strength parameters were slightly lower when the secant tangents were taken over the stress increments between 50 to 100 kPa. Furthermore, there was no noticeable correlation in Figure 6.42 between ϕ'_{mob} with the different grain-sizes. However, the ϕ'_{mob} values taken over the 25 to 50 kPa stress increments showed increased shear resistance with increasing grain-size; a definite correlation as shown in Figure 6.41 that is similar to Figure 6.38.

Overall, the assumption of Method B' (linear failure envelope with the apparent cohesion intercept set to zero) gave the best fit of data from the triaxial compression tests, as indicated by their coefficients of determination. Also, the assumption is consistent with a cohesionless material.

6.8 Dynamic Properties

The dynamic properties were measured using direct wave propagation methods with bender elements. The following subsections present the results from the dynamic testing of both Ottawa sand and tire crumbs.

6.8.1 Damping Measurements for Ottawa Sand

Prior to conducting the dynamic tests on tire crumbs, the tests were carried out on Ottawa sand using both the large-strain apparatus and triaxial cell set-ups. The material damping determined under the different test conditions were then compared to those reported by others in order to ascertain the reliability and accuracy of the bender elements used in this study.

6.8.1.1 Large-Strain Apparatus and Bender Elements

Table 6.15 summarizes the dynamic results obtained from the large-strain apparatus tests of Ottawa sand under zero vertical stress. The material damping was calculated from both the amplitude-frequency and amplitude-decay curves as shown in Figure 6.42 and Figure 6.43 respectively.

Figure 6.43 illustrates the subjectivity in determining the material damping from the amplitude-frequency curve, which depends primarily on the frequency range bounded by the curve at a specified amplitude (Hall and Richart, 1963). The material damping was calculated for several amplitudes, A, which intersected the curve at various locations. At a location where the curve does not plot symmetrical with respect to f_o, point 4 for example, D was found to be about 17%. However, when A intersected the curve at a location that plotted symmetrical about f_o (i.e. at points 1, 2, or 3), there was very little difference between the damping ratios, which were found to vary from about 5 to 6%. The later values are more consistent with the damping obtained from the vibration-decay curve (Figure 6.44) in which D was found to be about 5%.

6.8.1.2 Triaxial Cell and Bender Elements

Table 6.16 summarizes the dynamic results obtained from the triaxial cell and bender element tests of Ottawa sand under various confining pressures. Figures 6.45 and 6.46 are the typical amplitude-frequency curves, and Figures 6.47 and 6.48 are typical amplitude-decay curves and plots of amplitude versus cycle number under 0 kPa and 100 kPa confining stresses respectively.

Under zero confining stress, the damping ratio obtained from the amplitude-frequency and amplitude-decay curves was respectively 6% and 4%. These values are similar to those obtained using the large-strain apparatus and bender elements under zero vertical stresses (D = 5 to 6%), indicating that both apparatus produced similar results. The damping ratio of Ottawa sand found in this study under different confining pressures is also shown and compared to the results reported by other investigators in Figure 6.49. Under a confining pressure of 20 kPa, both Brocanelli and Rinaldi (1998) and Hardin (1965) reported a damping ratio of about 2%, while in this study, the damping ratio was about 6%; a value which is about 3 times higher. Under a confining stress of 100 kPa, the damping ratio found in this study was about 2%, which is slightly higher than the 1.5% damping found by Hall and Richart (1963).

Overall, the material damping of Ottawa sand found in this study was generally higher than those reported by the investigators. The discrepancies are likely due primarily to the different methods of analysis, testing procedures and equipment. Hall and Richart (1963) carried out their testing using a fixed-end free-end resonant column apparatus. Measurements for damping were made by driving the specimen at the resonant frequency in both the longitudinal and torsional modes, then cutting off the driving power and recording the decay of amplitude with time. Brocanelli and Rinaldi (1998), on the other had, carried out their tests using bender elements, but determined their material damping by analyzing the peak amplitude in the complex plane as discussed in Section 5.10.4. Despite these differences, however, the shear strains associated with typical foundation vibration problems are less than 10^{-4}%, and hence, damping should remain essentially constant (Rollins et al., 1998). Therefore, the results from Ottawa sand would indicate that tests conducted on tire crumbs with the bender elements used in this study would likely overestimate its material damping.

6.8.2 Damping Measurements for Tire Crumbs

6.8.2.1 Shear Wave Velocity and Shear Modulus

The principal problem with the method using piezoceramic bender elements has always been the subjectivity in the determination of the arrival time used to calculate V_s. Generally, a square wave input is used, but the complexity arises from the fact that a square wave is composed of a spectrum of different frequencies (Jovicic et al., 1996). Figure 6.49 shows the typical oscilloscope signals for a bender element test on a sample of reconstituted boulder clay. The instant of transmission of the shear wave is clearly defined at point 0', but its arrival at the receiving bender element is not. The first deflection of the received signal corresponds to point 0. The signal intensity gradually increases up to point 1, where there is a sharp inversion. After a number of peaks and troughs the signal fades. It is common practice to locate the first arrival of the shear wave at the point of first deflection or significant jump (i.e. point 0) in the received signal (Dyvik and Madshus,1985; Viggiani and Atkinson, 1995). However, theoretical studies have shown that the first deflection of the signal may not correspond to the arrival of the shear wave but to the arrival of the so-called near-field component that travels with the velocity of the compression wave (Salinero et al., 1986). The arrival of the shear wave, hence, could correspond to one of the points 0, 1, or 2. Numerical analysis conducted by Viggiani and Atkinson (1995) on the signals from bender elements tests carried out on reconstituted boulder clay demonstrated that the travel time should not be taken as the time corresponding to the point of first deflection (point 0) in Figure 6.49. For simple analysis, they indicated that the first arrival of the shear wave could be taken as the point of the first inversion of the received signal, at point 1. However, this may lead to an overestimation of the shear modulus by up to about 14% as demonstrated for the reconstituted boulder clay sample. Furthermore, numerical analysis of the waveforms has shown that the most accurate time of arrival of the shear wave corresponds to an intermediary location between points 1 and 2 in Figure 6.49. Hence, for this study, the time of arrival corresponding to the average times located between points 1 and 2 was used as an approximation for the arrival of the shear wave, to determine the shear wave velocity, V_s, and shear modulus, G_{max}. A typical received signal from the bender element tests on tire crumbs using a square-wave excitation is shown in Figure 6.50. The average arrival times, t, are given in Table 6.17, along with the corresponding V_s and G_{max} values. Figure 6.51 to Figure 6.53 show the variation in arrival time, shear wave velocity and shear modulus respectively as a function of dry unit weight for the different grain-sizes tested.

In Figure 6.51, both the 1/4 in and the No. 10 - No. 20 crumb showed a significant decrease in arrival time with increasing dry unit weight, which reflected a significant increase in V_s and G_{max} in Figures 6.53 and 6.54 respectively. The other crumb sizes, however, showed a weak correlation of decreasing arrival time, increasing V_s and G_{max} with decreasing grain-size. Furthermore, the increase in V_s and G_{max} was almost linear with increasing dry unit weight for the grain-sizes tested. The values of V_s and G_{max} for tire crumbs were found to range from 10 to 20 m/s and from 0.1 to 0.5 MPa respectively under vertical stresses of up to 100 kPa. The shear modulus, G, of rubber is typically about 0.2 to 5 MPa (Mark et al., 1994). In comparisons to soils, the typical G_{max} values for sands may range from 150 to 400 MPa. The shear wave velocity through tire crumbs is plotted as a function of void ratio in Figure 6.54. A similar plot is shown in Figure

6.55 for quartz sands with different grain-sizes tested under different confining stresses. Typical V_s values for the sands are in the range of 200 to 400 m/s, compared to the 10 to 20 m/s for tire crumbs found in this study. Furthermore, V_s increases with increasing confining pressure for quartz sands.

6.8.2.2 Material Damping

To acquire the calculated damping ratio, D, the time domain data obtained at different vertical stresses were decomposed into a group of harmonic waves of known frequency and amplitude. A convenient algorithm for this purpose was the fast Fourier transform (FFT). Figure 6.56 to Figure 6.57 show the typical FFT algorithm of the time-domain record for the No. 20 minus crumbs using LabVIEW. To obtain D, it is convenient to take the amplitude, A, at $\frac{1}{2}A_{max}$ or $\frac{1}{\sqrt{2}}A_{max}$, as suggested by Hall and Richart (1963). The procedure works well for a good FFT of the time-domain data, for example in Figure 6.56, in which the amplitude-frequency curve plots more or less symmetrical about the resonant frequency, f_o. The material damping was found to vary only slightly from 46 to 47%. However, for the FFT algorithm shown in Figure 6.57, the subjectivity of the procedure arises depending on the location of A. When A was taken at a value of 0.422 mV, the amplitude-frequency curve plotted symmetrical about f_o, and the damping ratio was found to be about 30%. However, when A was taken at $\frac{1}{2}A_{max}$ or $\frac{1}{\sqrt{2}}A_{max}$, the damping ratio varied from 55 to 60%, which is about 2 times greater than that taken at the previous intersection. Therefore, subsequent analysis of the material damping for the rest of the crumb sizes was carried out by choosing a frequency range, (f_1 - f_2), in which the amplitude-frequency curve plotted symmetrical with respect to f_o.

The values of δ and D for the tire crumbs under the corresponding vertical stresses tested are summarized in Table 6.17, along with values of dry unit weight, γ_d, and void ratio, e. Figure 6.58 to Figure 6.60 illustrate the variation in damping with dry unit weight, void ratio, and vertical stress on a semi-log scale. The results were fitted with a liner relationship. Although there was a high degree of scatter in the experimental data, the following were observed:

- At low vertical stress, there was high material damping with D values ranging from about 35% to 45%, with the exception of the No. 10 - No. 20 crumbs.
- At higher vertical stress, damping decreased to values ranging from 25% to 35%.
- Under higher vertical stresses, there was a trend of decreasing damping with decreasing particle size, with the exception of the No. 10 - No. 20 crumb. This cannot be stated conclusively, although the trends are supported by the dynamic testing of granular material carried out by Hall and Richart (1963).

In their experiments, dense and loose sample of Ottawa sand and glass beads were set into steady-state, forced vibration in a resonant column at relatively large amplitudes in the longitudinal and torsional modes. The decay in amplitude with time was monitored after shutting off the power to the driving system. The dense samples of Ottawa sand and glass beads were prepared by pouring the material, in layers, into the column and vibrating each layer with a brass rod attached to a small vibrator. This resulted in a condition close to 100% relative density. The loose condition for the Ottawa sand was obtained by pouring the sand through a funnel. They also examined the logarithmic decrement with different pore fluid (air and water), grain-size, confining pressure, and amplitude. Their results are shown in Figure 6.61 and Figure 6.62 for Ottawa sand in the dense and loose state, respectively, with different pore fluid, amplitude of vibration, and confining stresses. The figures were modified from the original to show the variation of damping ratio with amplitude instead of logarithmic decrement. The findings from their experiments on Ottawa sand and glass beads are summarized below:

- Damping for dry Ottawa sand decreased with decreasing amplitude of vibration.
- Damping generally decreased as the confining pressure increased.
- The values of damping ratio for the dense Ottawa sand varied from about 0.5% to 2% for dry samples, and from 2% to 3% for saturated samples

- The values of damping ratio for the loose Ottawa sand varied from 0.5% to 1.5% for dry samples, and from 2% to 4% for saturated samples
- Water, therefore, was reported to increase the damping by a factor of 1.5 to 4 times under similar testing conditions. Furthermore, saturated Ottawa sands were reported to show little variation in damping with the amplitude of vibration.
- There was a small difference in damping between the loose and dense samples under longitudinal type vibration.
- For glass beads, they indicated that it was difficult to determine whether the difference in damping between the large and small sizes was due to the size effect or the difference in density, although they reported that a smaller amount of damping was associated with the higher density beads.

In general, tire crumbs show a significant potential in damping applications since the crumbs are about 6 to 9 times more effective in damping vibrations than typical granular materials.

Table 6.1 Visual examination and sieve analysis of tire crumbs

Supplier	Particle Size, US Sieve Designation	Truck or passenger tires	Gradation	Particle shape	Impurities	$C_U = D_{60}/D_{10}$	$C_C = D_{30}^2/(D_{60}D_{10})$
Tire Recyclers of Calgary	No. 20 minus	passenger	uniform	angular, irregular	Minute amounts of metal dust, fine fibres	2.0	1.1
	No. 10 - No. 20	passenger	uniform	angular, irregular	fine fibres	1.4	0.9
	No. 8 - No. 14	passenger	uniform	angular, irregular	few fibre cords	2.1	0.7
	No. 4 - No. 8	passenger	uniform	angular, irregular	Lots of fibre threads/cords, and few rocks	1.3	1.1
	1/4 in	passenger	uniform	angular, irregular	Lots of fibre threads/cords and few rocks	1.4	0.8
Midwest Tire Processors of Vulcan	No. 10	passenger	uniform	angular, irregular	few fibre threads	2.0	1.2
	1/4 in	passenger	uniform	angular, irregular	Lots of fibre threads/cords and few rocks	2.7	0.8
Alberta Environmental Rubber Products	No. 20 Minus	truck	uniform	angular, uniform	none	3.1	1.0
	No. 10 - No. 20	truck	uniform	angular, irregular	none	1.4	0.9
	1/4 in	truck	uniform	angular, uniform	none	1.5	0.9

Table 6.2 Apparent specific gravity, G_s, of tire crumbs

Tire Crumb Size (US Sieve Designation)	Supplier	G_s
No. 20 Minus	Tire Recyclers of Calgary	1.17
	Alberta Environmental Rubber Products	1.15
No. 10 - No. 20	Tire Recyclers of Calgary	1.16
	Alberta Environmental Rubber Products	1.14
No. 10	Midwest Tire Processors of Vulcan	1.18
No. 8 – No. 14	Tire Recyclers of Calgary	1.16
No. 4 - No. 8	Tire Recyclers of Calgary	1.16
1/4 in	Alberta Environmental Rubber Products	1.14
	Tire Recyclers of Calgary	1.18
	Midwest Tire Processors of Vulcan	1.18

Table 6.3 Apparent specific gravities, G_s, of scrap tires and select materials from other investigators

Material	Particle Size (mm)	Specific Gravity	Reference
Tire crumbs	0.1 to 4.8	1.07	Masad et al., 1996
	0.6 to 1.18	1.20	Kershaw and Pamukcu, 1997
	2.0	1.12	Benda, 1995; Wu et al., 1997
	9.5	1.18	Benda, 1995; Wu et al., 1997
Tire shreds	19.0	1.08	Benda, 1995; Wu et al., 1997
	38.0	1.11	
	50 x 75	1.13 to 1.36	Edil and Bosscher, 1994
	< 38.1	1.14 to 1.27	Humphrey et al., 1992
Reclaimed styrene butadiene rubber	-	1.18	Borchardt, 1991
Sand	-	2.63 to 2.67	Das, 1982
Silts	-	2.65 to 2.70	
Clay and silt clays	-	2.67 to 2.80	
Organic soil	-	<2.00	

Table 6.4 Laboratory dry unit weights of tire crumbs

Compaction Method	Tire Crumb Size (US Sieve Designation)	Tire Crumb Manufacturer	γ_d (kN/m^3)	e
Loose	No. 20 Minus	Tire Recyclers of Calgary	3.4	2.4
	No. 10 - No. 20	Tire Recyclers of Calgary	3.8	2.1
	No. 10	Midwest Tire Processors of Vulcan	3.6	2.2
	No. 8 - No. 14	Tire Recyclers of Calgary	3.8	2.1
	No. 4 - No. 8	Tire Recyclers of Calgary	4.0	1.9
	1/4 in	Midwest Tire Processors of Vulcan	4.1	1.8
	1/4 in	Alberta Environmental Rubber Products	5.0	1.3
Vibration	No. 20 Minus	Tire Recyclers of Calgary	5.5	1.1
	No. 10 - No. 20	Tire Recyclers of Calgary	5.3	1.1
	No. 10	Midwest Tire Processors of Vulcan	5.4	1.1
	No. 8 - No. 14	Tire Recyclers of Calgary	5.3	1.2
	No. 4 - No. 8	Tire Recyclers of Calgary	5.5	1.1
	1/4 in	Midwest Tire Processors of Vulcan	5.7	1.0
	1/4 in	Alberta Environmental Rubber Products	4.8	1.3

Loose = no compaction; tire crumbs loosely placed into compaction mold; method ASTM D 4254
Vibration = compaction using a vibratory table; method ASTM 4253

Table 6.5 Compressibility tests on tire crumbs

Tire Crumb Size (US Sieve Designation)	Supplier	Test Condition	e at specified vertical stress		γ_d at specified vertical stress (kN/m^3)		$\Delta\varepsilon_v$ at specified stress range (%)		
			0 kPa	100 kPa	0 kPa	100 kPa	(Loading) 0 to 100 kPa	(Rebound) 100 to 10 kPa	(Reloading) 10 to 100 kPa
No. 20 Minus	Tire Recyclers of Calgary	dry	2.4	0.5	3.4	7.7	-55.1	3.2	-4.7
		saturated	2.9	0.8	2.9	6.4	-53.5	3.7	-4.8
No. 10 - No. 20	Tire Recyclers of Calgary	dry	2.0	0.6	3.9	7.0	-44.1	8.0	-8.1
		saturated	2.3	0.7	3.4	6.9	-46.7	4.0	-5.0
No. 10	Midwest Tire Processors of Vulcan	dry	2.1	0.6	3.7	7.3	-48.6	5.6	-6.3
		saturated	2.3	0.9	3.5	6.2	-41.2	4.0	-4.1
No. 8 - No. 14	Tire Recyclers of Calgary	dry	2.0	0.7	3.9	6.8	-42.8	8.3	-8.6
		saturated	2.1	0.7	3.7	6.5	-40.3	3.3	-3.7
No. 4 - No. 8	Tire Recyclers of Calgary	dry	1.8	0.8	4.1	6.3	-36.3	7.2	-5.9
		saturated	1.9	0.6	3.9	6.9	-41.3	5.7	-7.5
1/4 in	Midwest Tire Processors of Vulcan	dry	2.0	0.7	3.9	6.7	-41.8	7.8	-8.4
		saturated	2.3	0.9	3.5	6.2	-45.0	6.3	-4.8

Table 6.6 Compressibility indices and coefficient of volume compressibility of tire crumbs

Tire Crumb Size (US Sieve Designation)	Supplier	Test Condition	Compressibility Indices			m_v at specified stress range ($x10^{-3}$ m^2/kN) Stress Range (kPa)			
			C_c	C_s	C_r	0 - 10	10 - 20	20 - 50	50 - 100
No. 20 Minus	Tire Recyclers of Calgary	dry	0.74	0.11	0.16	3.3	1.3	0.41	0.25
		saturated	0.77	0.14	0.19	3.4	1.0	0.42	0.22
No. 10 - No. 20	Tire Recyclers of Calgary	dry	0.67	0.24	0.24	2.1	0.89	0.41	0.23
		saturated	0.72	0.14	0.18	2.7	1.1	0.38	0.23
No. 10	Midwest Tire Processors of Vulcan	dry	0.67	0.17	0.20	2.7	1.10	0.39	0.21
		saturated	0.68	0.14	0.14	2.3	1.1	0.39	0.14
No. 8 - No. 14	Tire Recyclers of Calgary	dry	0.65	0.24	0.25	2.1	0.78	0.39	0.23
		saturated	0.67	0.11	0.12	2.2	0.98	0.41	0.16
No. 4 - No. 8	Tire Recyclers of Calgary	dry	0.53	0.20	0.16	1.7	0.67	0.36	0.14
		saturated	0.68	0.16	0.22	1.8	1.0	0.41	0.19
1/4 in	Midwest Tire Processors of Vulcan	dry	0.72	0.23	0.25	1.7	1.0	0.37	0.24
		saturated	0.61	0.21	0.16	2.7	0.82	0.41	0.13

Table 6.7 Hydraulic conductivity, k_{20}, for tire crumbs

Tire Crumb Size (US Sieve Designation)	Tire Crumb Manufacturer	σ_v (kPa)	e	n	γ_d (kN/m^3)	k_{20} (x10^{-3}cm/s)
No. 20 Minus	Tire Recyclers of Calgary	10	1.6	0.62	4.4	19.9
		20	1.3	0.57	4.9	20.3
		50	1.1	0.51	5.6	5.1
		100	0.8	0.45	6.3	1.7
No. 10 – No. 20	Tire Recyclers of Calgary	10	1.4	0.59	4.7	40.4
		20	1.2	0.54	5.3	26.7
		50	0.9	0.48	4.9	23.0
		100	0.7	0.41	6.7	15.4
No. 10	Midwest Tire Processors of Vulcan	10	1.6	0.61	4.5	32.5
		20	1.3	0.56	5.1	26.0
		50	1.0	0.50	5.7	20.0
		100	0.9	0.47	6.2	11.6
No. 8 – No. 14	Tire Recyclers of Calgary	10	1.4	0.59	4.7	32.4
		20	1.2	0.54	5.2	25.9
		50	0.9	0.48	5.9	22.1
		100	0.8	0.43	6.5	17.3
No. 4 – No. 8	Tire Recyclers of Calgary	10	1.4	0.58	4.8	28.7
		20	1.1	0.53	5.3	27.0
		50	0.9	0.47	6.1	21.2
		100	0.7	0.41	6.7	11.8
1/4 in	Midwest Tire Processors of Vulcan	10	1.4	0.58	4.8	29.0
		20	1.2	0.55	5.2	25.5
		50	0.9	0.48	6.0	23.5
		100	0.8	0.45	6.4	20.1

Table 6.8 Average measured thermal conductivity, λ_{avg}, from thermal needle method

Test Condition	Temperature	λ_{avg} (W/m-°C)	γ_d (kN/m^3)	e
loose, unfrozen-dry	+2 to +24°C	0.11 to 0.12	4.1	1.8
loose, frozen-dry	-5 to -10°C	0.09 to 0.12	4.1	1.8
loose, unfrozen-saturated	+3 to +23°C	0.45 to 0.66	3.7	2.1
loose, frozen-saturated	-5 to -10°C	1.36 to 1.38	3.7	2.1
compacted, unfrozen-dry	+3 to +22°C	0.12 to 0.13	5.6	1.1
compacted, frozen-dry	-5 to -12°C	0.12 to 0.13	5.6	1.0
compacted, unfrozen-saturated	+3 to +22°C	0.33 to 0.38	5.4	0.8
compacted, frozen-saturated	-5 to -10°C	0.91 to 0.92	5.4	0.8

Table 6.9 Measured thermal conductivity, λ, from combined thermal needle and consolidation apparatus

Particle Size	Supplier	Stress range from 0 to 100 kPa			Test Condition
		λ (W/m-°C)	γ_d (kN/m^3)	e	
No. 20 minus	Tire Recyclers of Calgary	0.14 to 0.22	3.8 to 6.8	2.0 to 0.7	dry
		0.79 to 0.61	3.8 to 7.4	2.1 to 0.6	saturated
No. 10 - No. 20	Tire Recyclers of Calgary	0.13 to 0.21	4.0 to 6.8	1.8 to 0.7	dry
No. 10	Midwest Tire Processors of Vulcan	0.13 to 0.22	3.8 to 7.0	2.0 to 0.6	
No. 8 - No. 14	Tire Recyclers of Calgary	0.14 to 0.22	3.9 to 7.3	1.9 to 0.6	
No. 4 - No. 8	Tire Recyclers of Calgary	0.14 to 0.21	4.0 to 6.9	1.9 to 0.7	
1/4 in	Midwest Tire Processors of Vulcan	0.13 to 0.20	4.0 to 6.7	1.9 to 0.7	dry
		0.55 to 0.53	3.8 to 7.0	2.0 to 0.7	saturated
1/4 in	Alberta Environmental Rubber Products	0.16 to 0.19	5.3 to 6.7	1.1 to 0.7	dry
		0.60 to 0.54	3.8 to 5.0	2.0 to 1.3	saturated

Table 6.10 Comparisons of measured thermal conductivity, λ

	Laboratory Experiment		Shao et al. (1995)		% difference	
Particle Size	> 20 mm (No. 20 minus)	1/4 in	1 mm (No. 18)	25 mm (1 in)		
Test Condition	loose, thawed state, dry	compacted, frozen, dry	low compaction, thawed state, less than 1% moisture content	high compaction, frozen state, 5% moisture content		
Test Method	thermal needle method		guarded hot plate apparatus			
λ (W/m-°C)	0.082 to 0.091[3]	0.12 to 0.14[4]	0.097	0.17	-7 to -18%	-20 to -40%

---

[3] See Table F.2

[4] See Table F.3

Table 6.11 Shear strength parameters from direct shear tests under dry conditions

			Shear Strength Parameters							
Tire Crumb Size	Supplier	ΔH (mm)	Method A			Method B, c=0		Method C, c=0		
			ϕ (°)	c (kPa)	R^2	ϕ (°)	R^2	Secant Tangent, ϕ (°) 0 to 50 kPa	0 to 100 kPa	R^2
No. 20 minus	Tire Recyclers of Calgary	2	20	0	0.973	19	0.994	20	18	0.947
		4	26	0	0.994	26	0.999	26	25	0.990
		8	32	2	0.998	33	0.999	33	33	0.998
		12	33	5	1.000	35	0.998	37	35	1.000
No. 10 - No. 20	Tire Recyclers of Calgary	2	6	2	0.988	7	0.983	8	7	0.996
		4	14	2	0.990	15	0.995	16	15	0.993
		8	27	1	0.991	28	0.998	28	28	0.989
		12	31	1	0.998	32	0.999	32	32	0.998
No. 10	Midwest Tire Processors of Vulcan	2	15	3	0.987	17	0.993	19	17	0.991
		4	21	4	0.989	24	0.993	25	23	0.993
		8	30	4	0.994	32	0.997	34	32	0.996
		12	35	4	0.999	37	0.998	38	36	1.000
No. 8 - No. 14	Midwest Tire Processors of Vulcan	2	10	6	0.997	15	0.970	18	13	0.977
		4	18	5	1.000	21	0.992	23	20	0.999
		8	27	7	1.000	31	0.993	34	30	0.997
		12	30	5	1.000	33	0.997	35	32	1.000
No. 4 - No. 8	Tire Recyclers of Calgary	2	17	1	0.968	18	0.993	18	16	0.933
		4	23	1	0.976	24	0.995	25	23	0.949
		8	33	1	0.993	34	0.998	34	33	0.986
		12	34	3	0.998	36	0.999	37	35	0.994
1/4 in	Midwest Tire Processors of Vulcan	2	7	3	0.982	9	0.979	11	8	0.944
		4	16	2	0.987	18	0.995	19	17	0.967
		8	31	0	0.989	31	0.997	32	30	0.979
		12	36	1	1.000	36	1.000	37	36	0.999
1/4 in	Alberta Environmental Rubber Products	2	5	6	0.979	10	0.945	12	8	0.924
		4	12	8	0.996	18	0.970	21	16	0.976
		8	24	9	1.000	30	0.988	33	28	0.994
		12	30	7	0.999	33	0.994	36	32	0.995

Table 6.12 Shear strength parameters from direct shear testing under saturated conditions

Tire Crumb Size	Supplier	ΔH (mm)	Shear Strength Parameters							
			Method A, c ≠ 0			Method B, c=0		Method C, c=0		
								Secant Tangent, ϕ (°)		
			ϕ (°)	c (kPa)	R^2	ϕ (°)	R^2	0 to 50 kPa	0 to 100 kPa	R^2
No. 20 minus	Tire Recyclers of Calgary	2	12	1	0.981	13	0.995	14	12	0.947
		4	19	1	0.997	14	0.999	21	19	0.990
		8	29	2	1.000	15	0.999	31	30	0.998
		12	33	4	1.000	20	0.998	37	35	1.000
1/4 in	Midwest Tire Processors of Vulcan	4	8	2	0.990	10	0.989	11	9	0.944
		8	15	3	1.000	17	0.994	19	16	0.967
		12	26	3	1.000	28	0.998	30	28	0.979
		2	29	1	1.000	30	1.000	30	30	0.999
1/4 in	Alberta Environmental Rubber Products	4	6	6	0.893	11	0.940	13	9	0.924
		8	12	9	0.960	18	0.961	22	16	0.976
		12	22	11	0.998	28	0.980	32	26	0.994
		2	34	9	0.999	38	0.993	40	36	0.995

Table 6.13 Shear strength parameters from consolidated-drained triaxial compression tests

Tire Crumb Size	Supplier	ε (%)	Shear Strength Parameters									
			Method A', c ≠ 0			Method B', c = 0		Method C'				
								Secant Tangent over stress ranges				
								25 to 100 kPa		50 to 100 kPa		
			ϕ (°)	c (kPa)	R^2	ϕ (°)	R^2	ϕ (°)	c (kPa)	ϕ (°)	c (kPa)	R^2
No. 20 minus	Tire Recyclers of Calgary	5	15	0	0.996	15	0.999	15	0	14	0	0.993
		10	19	1	0.998	20	0.999	19	0	18	0	0.994
		15	22	3	0.998	23	0.999	22	0	21	0	0.995
		20	25	4	0.999	27	0.999	25	0	23	0	0.996
No. 10 - No. 20	Tire Recyclers of Calgary	5	9	17	0.911	19	0.956	15	0	11	0	0.955
		10	14	17	0.961	22	0.973	20	0	16	0	0.983
		15	18	17	0.980	25	0.983	24	0	19	0	0.991
		20	21	15	0.987	28	0.990	26	0	23	0	0.994
No. 10	Midwest Tire Processors of Vulcan	5	11	15	0.968	19	0.965	16	0	12	0	0.988
		10	14	16	0.976	23	0.977	21	0	16	0	0.991
		15	19	15	0.985	26	0.986	24	0	20	0	0.994
		20	22	13	0.987	28	0.991	26	0	23	0	0.994
No. 8 - No. 14	Midwest Tire Processors of Vulcan	5	8	20	0.871	19	0.949	15	0	10	0	0.930
		10	13	20	0.957	23	0.970	21	0	15	0	0.980
		15	17	19	0.982	26	0.982	24	0	20	0	0.993
		20	22	16	0.997	28	0.990	27	0	23	0	1.000

Table 6.13 Continued

Tire Crumb Size	Supplier	ε (%)	Shear Strength Parameters Method A', c ≠ 0 ϕ (°)	c (kPa)	R²	Method B', c = 0 ϕ (°)	R²	Method C' Secant Tangent over stress ranges 25 to 100 kPa ϕ (°)	c (kPa)	50 to 100 kPa ϕ (°)	c (kPa)	R²
No. 4 - No. 8	Tire Recyclers of Calgary	5	17	11	0.937	22	0.982	21	0	18	0	0.965
		10	20	11	0.957	25	0.988	24	0	22	0	0.976
		15	24	10	0.973	28	0.992	26	0	24	0	0.985
		20	26	8	0.986	30	0.996	27	0	26	0	0.992
1/4 in	Midwest Tire Processors of Vulcan	5	4	9	0.644	10	0.911	6	0	4	0	0.789
		10	8	11	0.889	15	0.957	13	0	9	0	0.942
		15	14	10	0.946	19	0.979	18	0	15	0	0.971
		20	19	8	0.967	23	0.990	22	0	20	0	0.981
1/4 in	Alberta Environmental Rubber Products	5	11	17	0.817	20	0.958	18	0	13	0	0.898
		10	16	18	0.917	25	0.975	23	0	18	0	0.956
		15	20	16	0.978	27	0.987	26	0	22	0	0.990
		20	24	11	0.999	29	0.996	27	0	24	0	1.000

Table 6.14 Comparison of triaxial strength parameters for tire crumbs and shreds

Material	γ_d (kN/m³)	c (kPa)	ϕ (°)	σ_3 (kPa)	Reference	Comments
Tire crumbs (max. size 4.75 mm) ε_a = 10% to 20%	6.2	70.0 to 82.0	6.0 to 15.0	150, 200, 250, 300, and 350	Masad et al. (1996)	
Tire shreds (0.5 in) compacted with standard Proctor energy ε_a = 5% to 20%	6.1 – 6.3	13.4 to 35.8	6.4 to 20.5	36, 88, and 199	Modified from Ahmed (1993)	
Tire shreds (1 in) compacted with 50% standard Proctor energy ε_a = 5% to 20%	6.3	14.5 to 37.3	9.8 to 22.7	32, 99, and 199		
Tire shreds (1 in) compacted with standard Proctor energy ε_a = 5% to 20%	6.3 – 6.5	14.8 to 33.2	8.3 to 25.3	32, 114, 198, and 301		
Tire shreds (1 in) compacted with modified Proctor energy ε_a = 5% to 20%	6.6 – 6.9	17.1 to 39.2	7.5 to 24.7	32, 99, and 199		
Tire shred (38 mm)	5.9	0	57.0	40 to 55	Wu et al. (1997)	Triaxial tests were conducted under constant σ_1 stress paths
Tire shreds (19 mm)	5.6	0	54.0			
Tire shreds (9.5 mm)	5.0	0	60.0			
Tire shreds (9.5 mm)	5.9	0	47.0			
Tire crumbs (2 mm)	5.2	0	45.0			
Tire crumb (No. 20 Minus) ε_a = 5% to 20%	6.0 to 6.9	(0 to 4.8) 0	(15.3 to 25.6) 15.3 to 26.9	25, 50 and 100		Analysed using 2 Mohr-Coulomb relationships ($\tau = C + \sigma\tan\phi$) $\tau = \sigma\tan\phi$
Tire crumb (No. 10 - No. 20) ε_a = 5% to 20%	6.0 to 7.7	(17.1 to 15.5) 0	(9.5 to 22.8) 18.2 to 27.6			
Tire crumb (No. 10) ε_a = 5% to 20%	7.8 to 7.9	(15.6 to 14.2) 0	(10.8 to 23.3) 18.5 to 27.7			
Tire crumb (No. 8 - No. 14) ε_a = 5% to 20%	7.6 to 7.7	(20.6 to 17.2) 0	(8.6 to 22.6) 19.0 to 27.9			
Tire crumb (No. 4 - No. 8) ε_a = 5% to 20%	7.4 to 7.6	(10.9 to 8.4) 0	(16.5 to 26.4) 21.3 to 28.7			
Tire crumb (1/4 in, AERP) ε_a = 5% to 20%	6.5 to 6.7	(17.6 to 11.2) 0	(11.2 to 25.0) 19.7 to 28.2			
Tire crumb (1/4 in, Vulcan) ε_a = 5% to 20%	6.2 to 6.5	(9.8 to 8.5) 0	(3.7 – 20.4) 10.0 – 23.6			

Table 6.15 Logarithmic decrement and damping ratio from large-strain apparatus and bender element tests of Ottawa, $\sigma_v = 0$ kPa

	Amplitude-Frequency Curve				Amplitude-Decay Curve	
Amax (mV)	A (mV)		δ	D (%)	δ	D (%)
1.53	$0.5A_{max}$	0.76	1.07	16.8	0.25 to 0.29	4.0 to 6.2
	-	0.90	0.37	5.9		
	$0.707A_{max}$	1.08	0.37	5.9		
	-	1.34	0.29	4.7		

Table 6.16 Logarithmic decrement and damping ratio from triaxial cell and bender element tests of Ottawa sand

		Amplitude-Frequency Curve				Amplitude-Decay Curve	
σ_3 (kPa)	Amax (mV)	A (mV)		δ	D (%)	δ	D (%)
0	1.019	$0.707A_{max}$	0.721	0.36	5.7	0.23	3.6
20	0.903	$0.707A_{max}$	0.639	0.35	5.6	0.09	1.4
40	0.986	$0.707A_{max}$	0.697	0.27	4.2	0.37	5.8
60	1.407	$0.707A_{max}$	0.995	0.20	3.2	0.17	2.7
80	1.339	-	1.222	0.30	4.7	0.12	1.9
100	1.616	-	1.160	0.13	2.0	0.11	1.8

Table 6.17 Dynamic results from bender element tests of tire crumbs

Grain-Size Distribution	Supplier	σ_v (kPa)	D (%)	δ	γ_d (kN/m^3)	e	t (ms)	V_s (m/s)	G_{max} (MPa)
No. 20 Minus	Tire Recyclers of Calgary	10	46.6	3.3	7.1	0.61	1.5	16.9	0.2
		20	33.5	2.2	7.5	0.54	1.3	17.7	0.2
		50	31.2	2.1	8.5	0.35	1.0	19.6	0.3
		100	26.1	1.7	9.5	0.21	0.7	20.2	0.4
No. 10 - No. 20	Tire Recyclers of Calgary	10	16.5	1.0	5.0	1.26	5.6	11.0	0.1
		20	21.1	1.3	5.3	1.13	5.0	11.4	0.1
		50	15.6	1.0	6.3	0.82	3.3	14.1	0.1
		100	14.1	0.9	6.9	0.66	1.6	24.9	0.4
No. 10	Midwst Tire Processors of Vulcan	10	38.0	2.4	7.2	0.61	1.5	16.4	0.2
		20	39.0	2.5	7.8	0.48	1.1	18.2	0.3
		50	25.2	1.6	8.7	0.33	0.9	19.7	0.3
		100	30.3	1.9	9.4	0.23	0.6	23.6	0.5
1/4-in	Midwst Tire Processors of Vulcan	10	47.4	3.0	6.6	0.75	2.5	12.1	0.1
		20	25.0	1.6	7.0	0.65	2.1	13.4	0.1
		50	47.7	3.0	8.1	0.44	1.4	15.3	0.2
		100	23.3	1.5	8.8	0.31	1.0	18.9	0.3
1/4-in	Alberta Environmental Rubber Products	0	35.1	2.2	5.9	0.90	3.8	9.0	0.0
		10	35.1	2.2	6.3	0.79	2.4	13.2	0.1
		50	30.7	1.9	6.9	0.62	1.6	16.8	0.2
		100	26.8	1.7	7.5	0.48	1.0	23.2	0.4

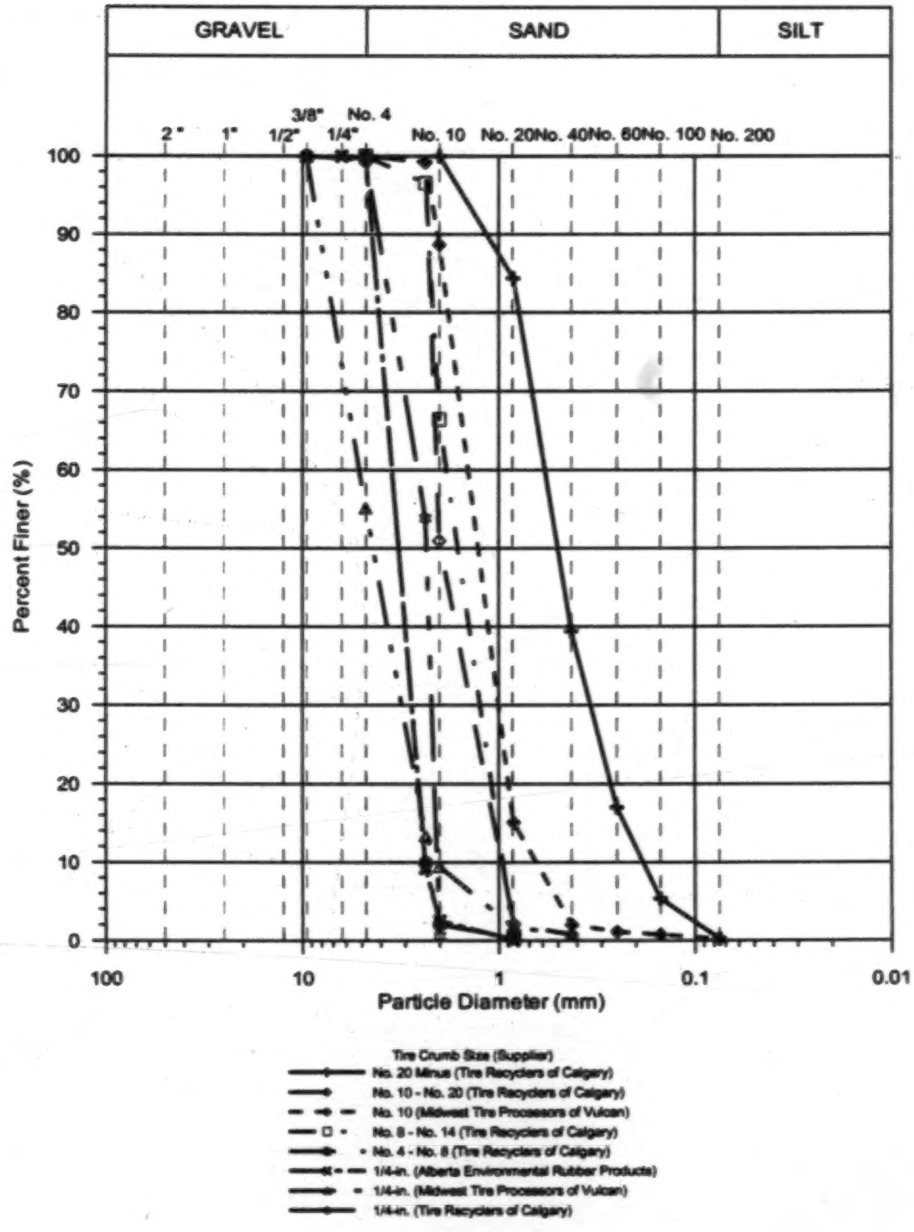

Figure 6.1 Grain-size distribution of tire crumbs

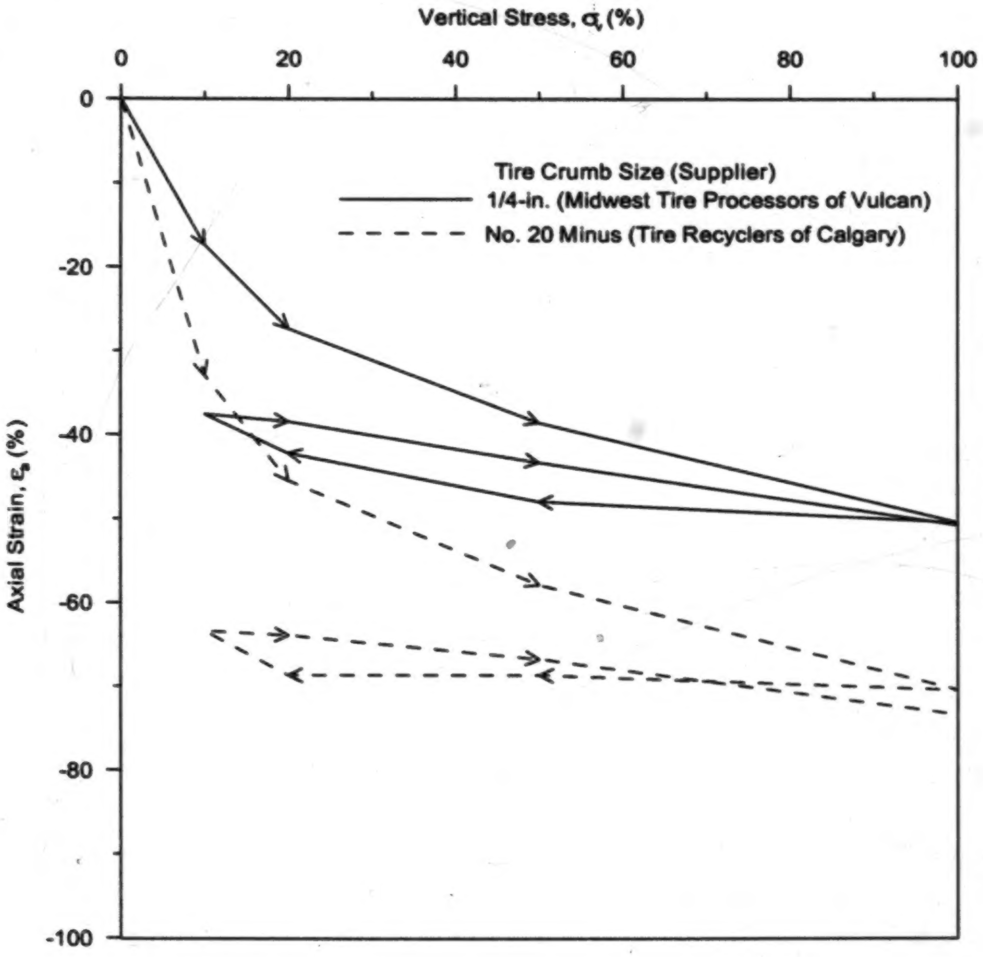

Figure 6.2 Typical stress-strain response of tire crumbs tested under dry conditions

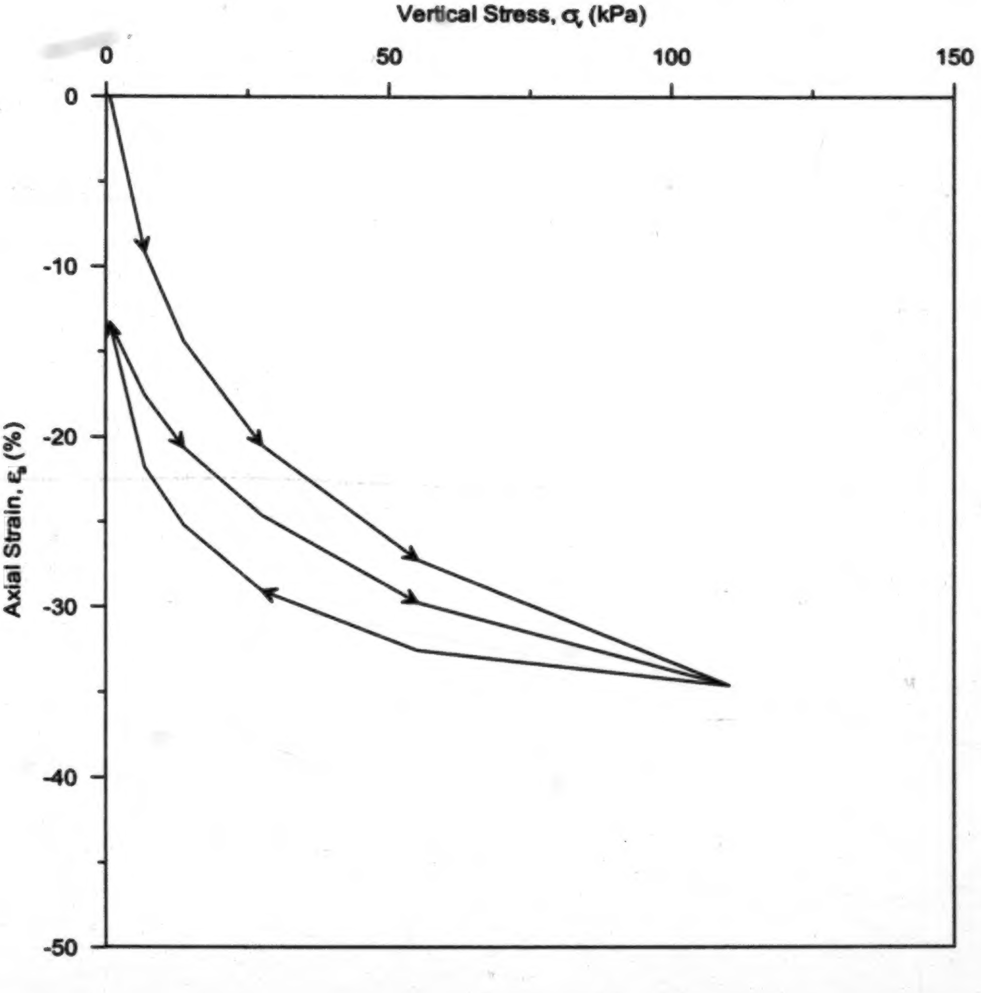

Figure 6.3 Hysterisis stress-strain response of 1 in uncompacted tire shreds under dry conditions from one-dimensional confined compressibility tests (modified from Ahmed, 1993)

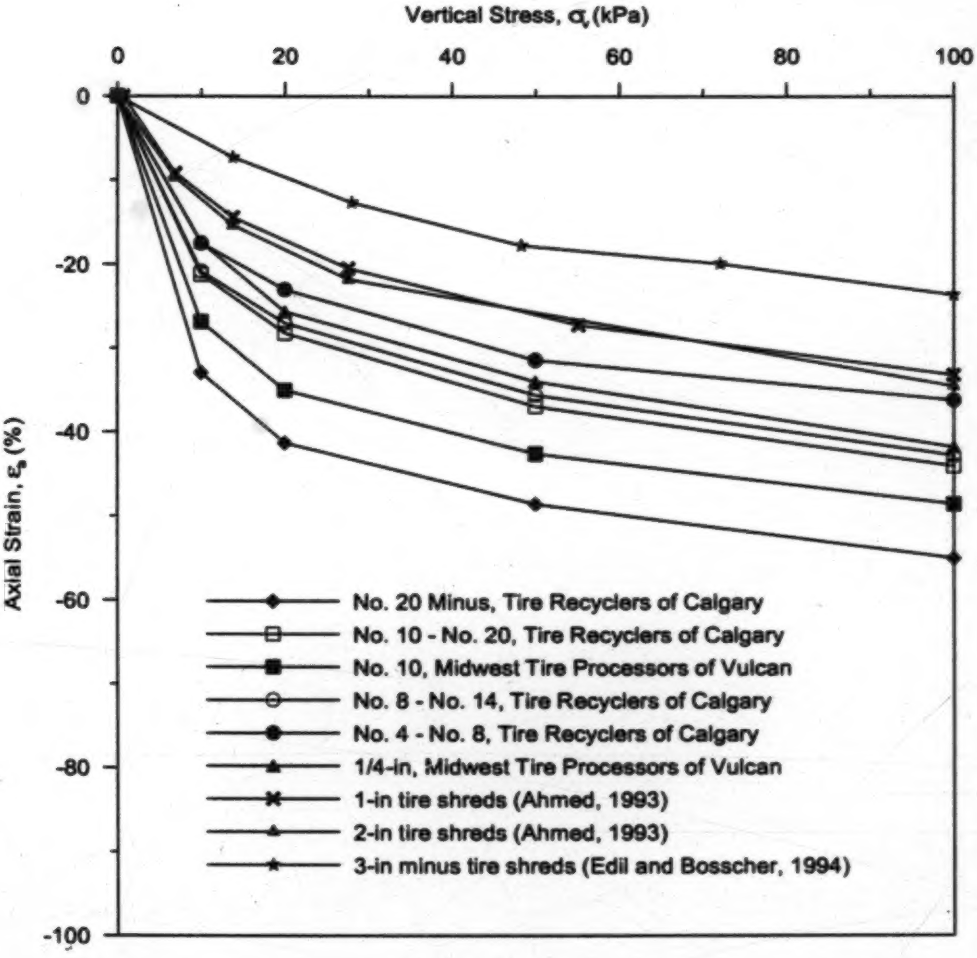

Figure 6.4 Initial loading stress-strain response of tire crumbs with different grain-size distribution under dry conditions

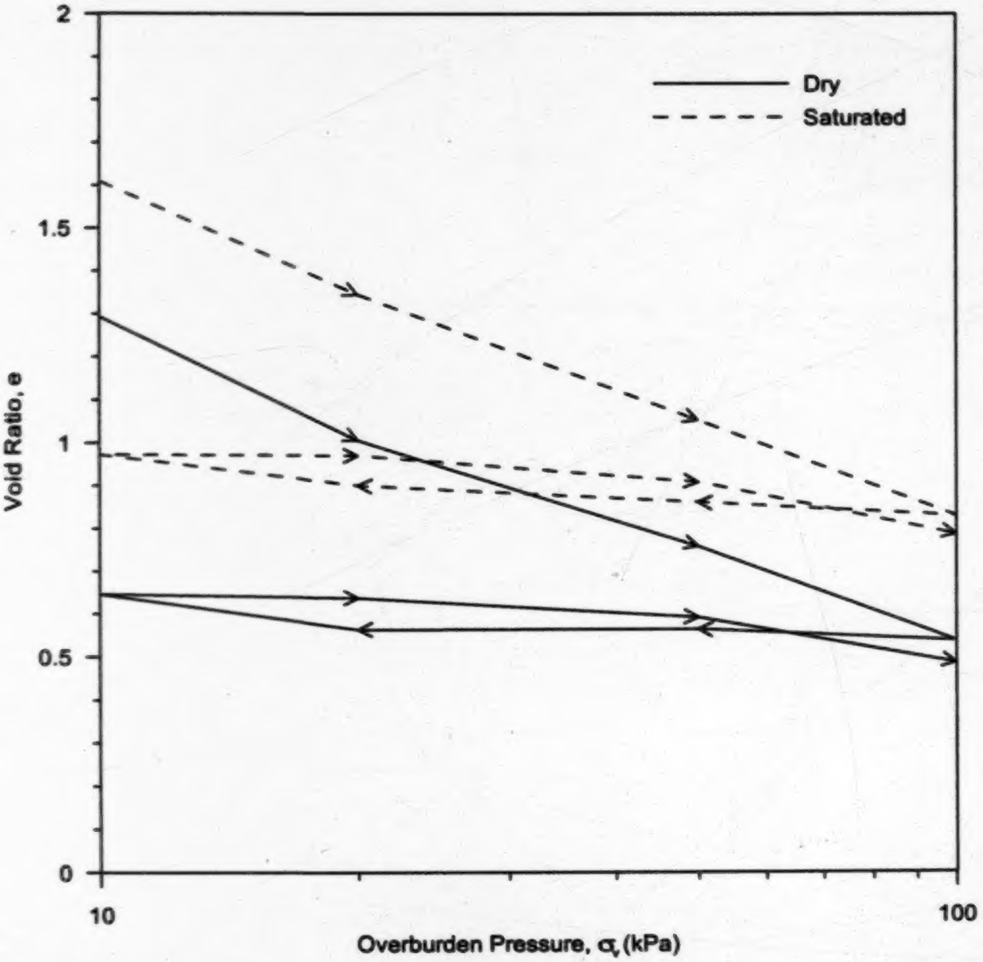

Figure 6.5 e versus logσ_v plot for No. 20 Minus tire crumbs (Tire Recyclers of Calgary)

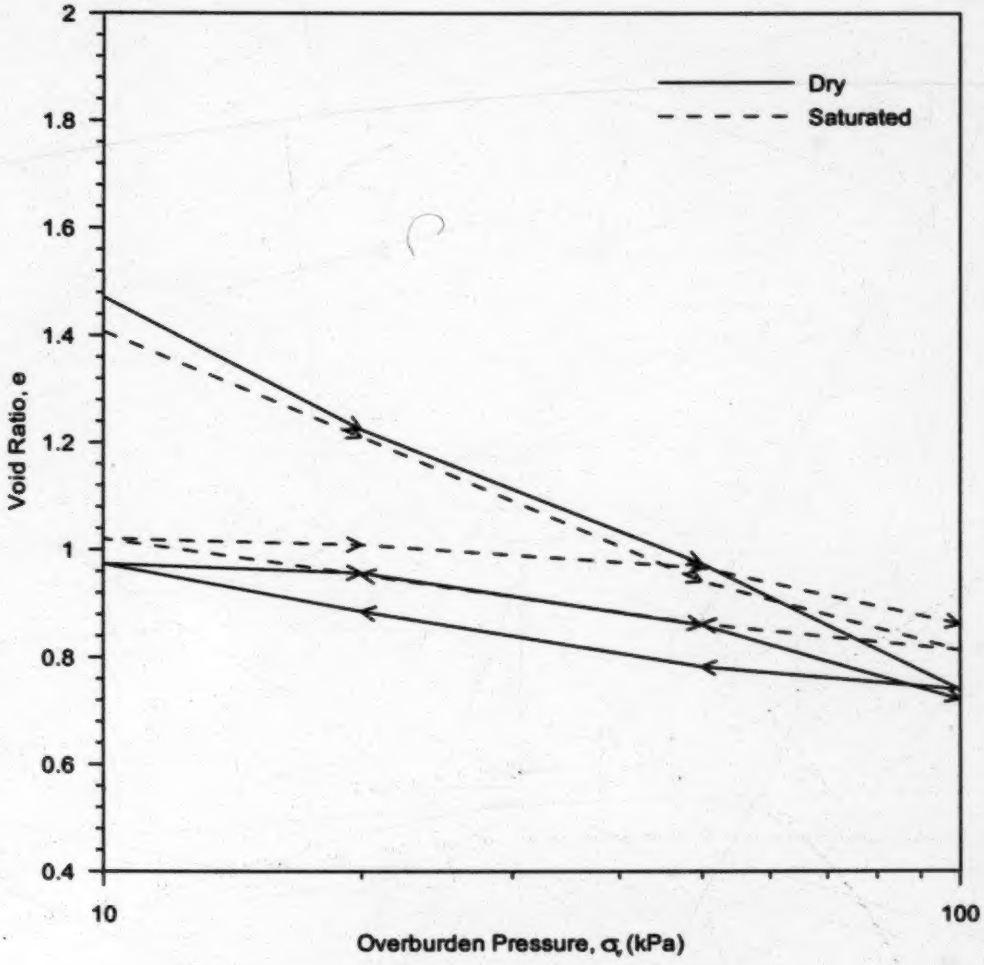

Figure 6.6 e versus logσ_v plot for 1/4 in tire crumbs (Midwest Tire Processors of Vulcan)

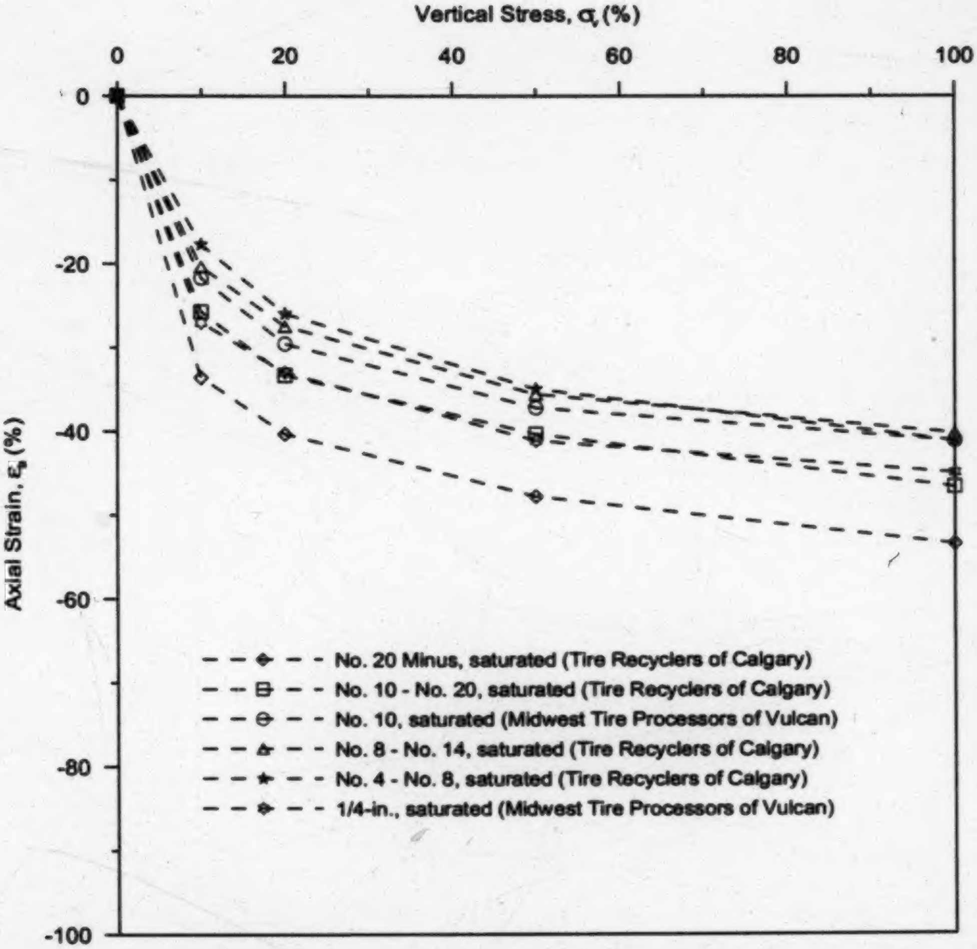

Figure 6.7 Initial loading stress-strain response of tire crumbs with different grain-size distribution under water-saturated conditions

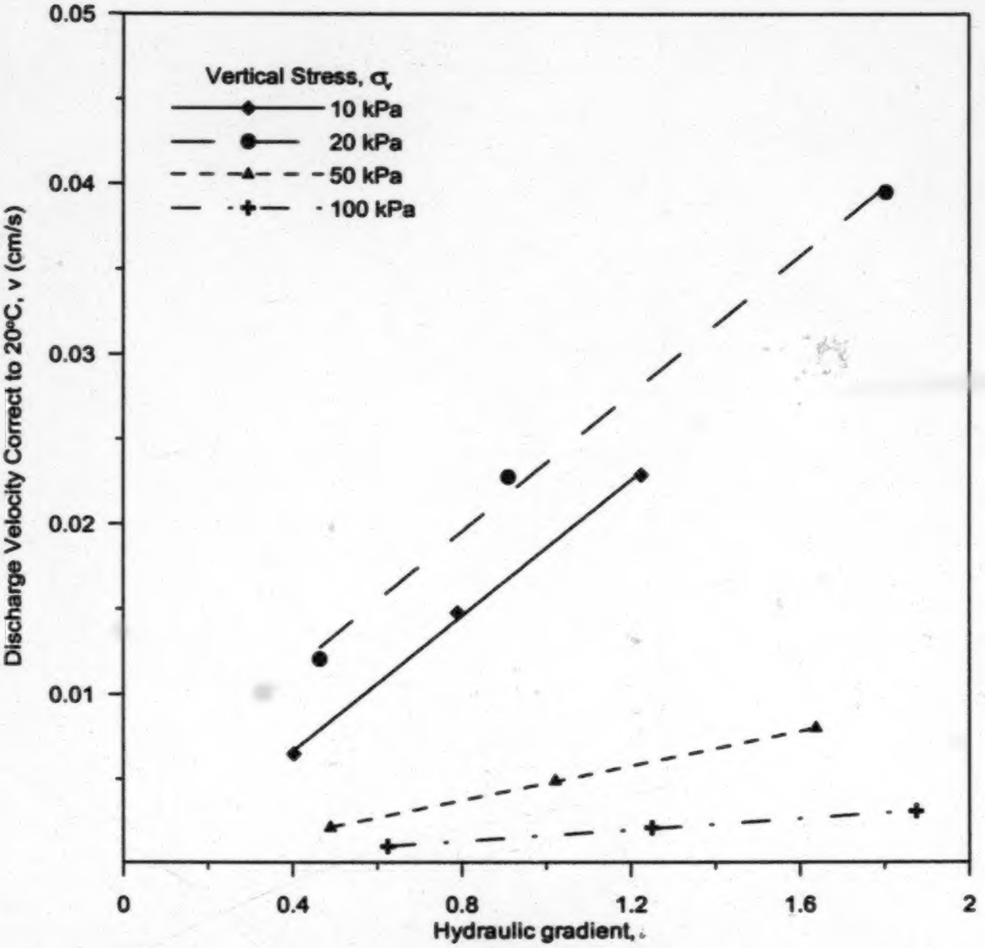

Figure 6.8 Discharge velocity versus hydraulic gradient for No. 20 Minus tire crumbs

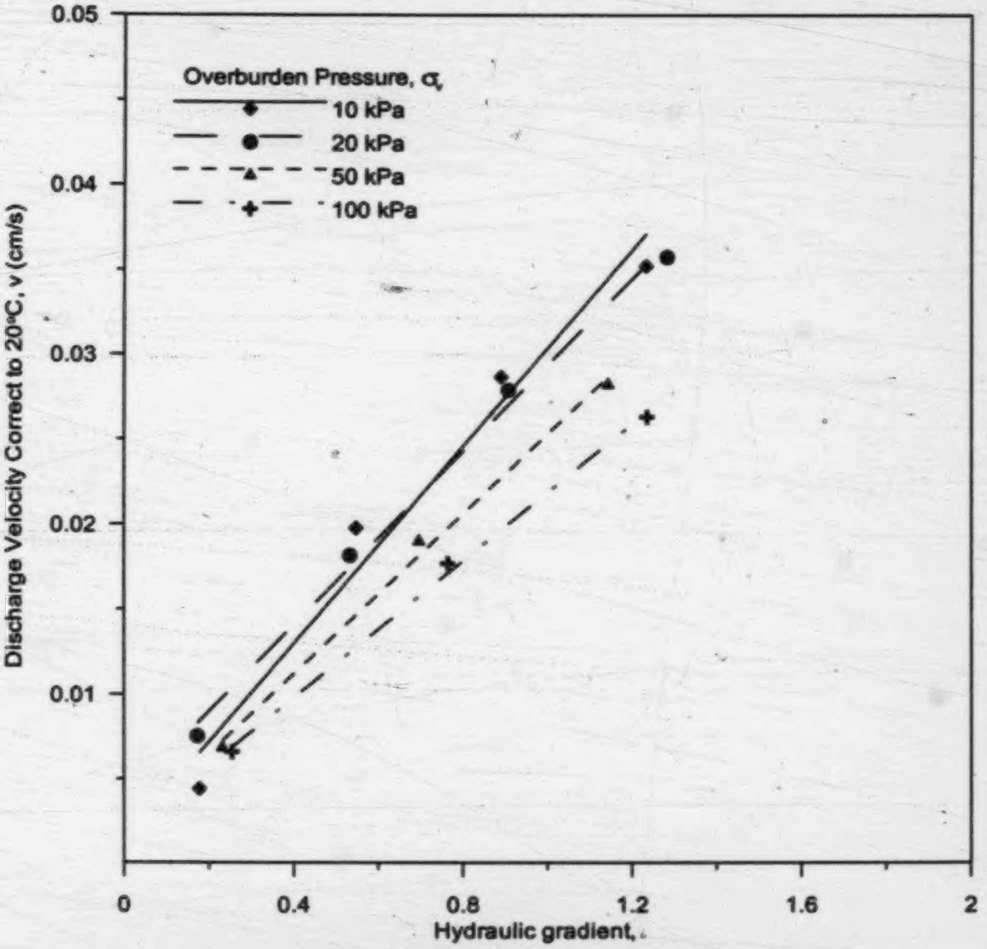

Figure 6.9 Discharge velocity versus hydraulic gradient for 1/4 in tire crumbs (Midwest Tire Processors of Vulcan)

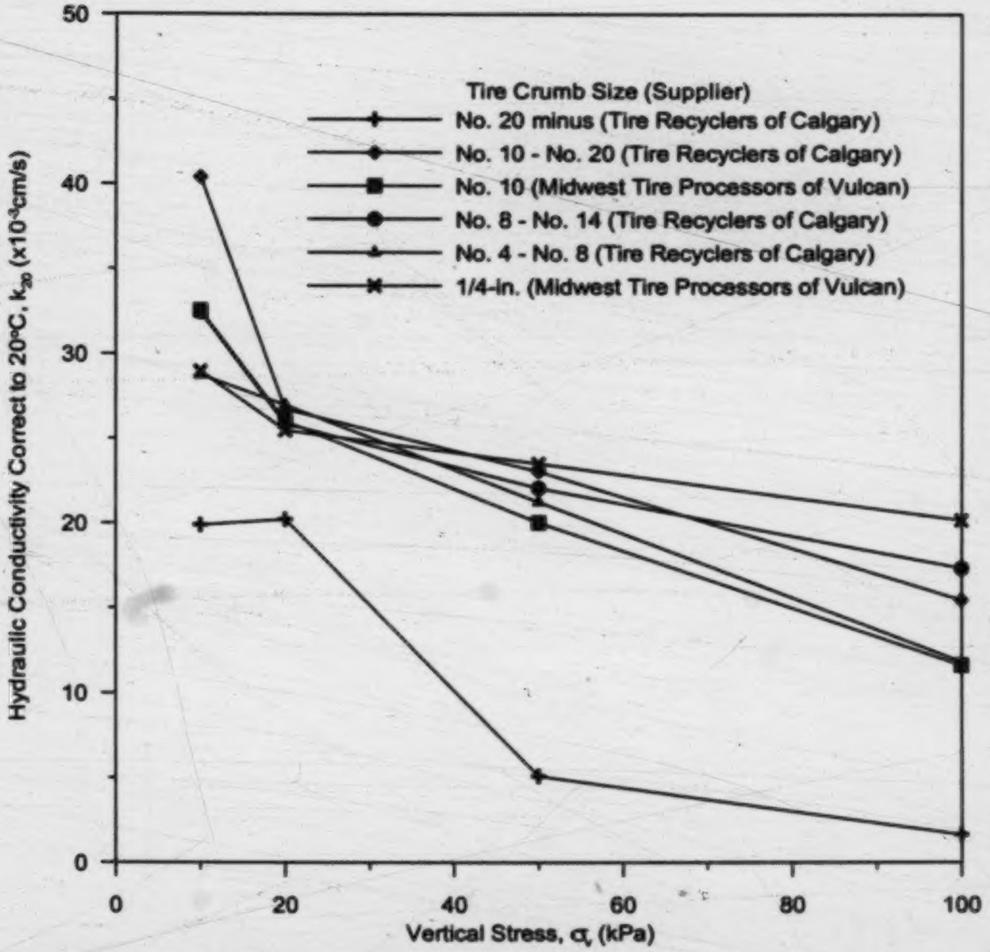

Figure 6.10 Hydraulic conductivity versus overburden pressure for all tire crumbs tested

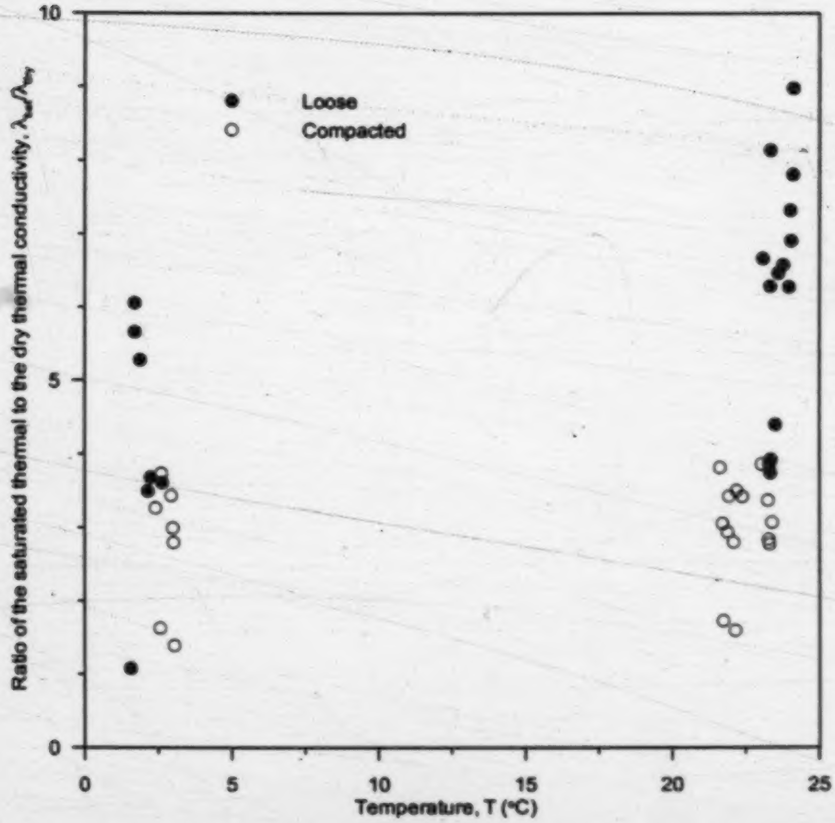

Figure 6.11 $\lambda_{sat}/\lambda_{dry}$ **for unfrozen, compacted and loose tire crumbs using thermal needle method**

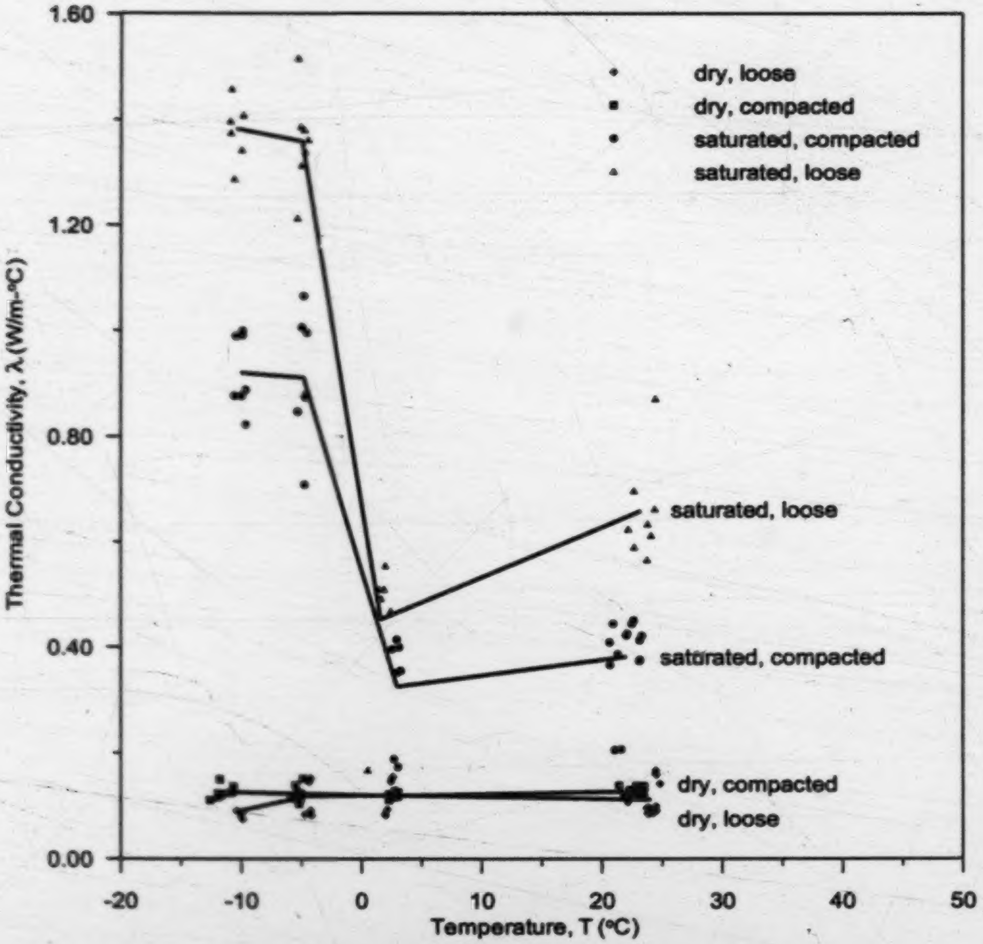

Figure 6.12 Measured thermal conductivity as a function of temperature under different degrees of saturation and compaction

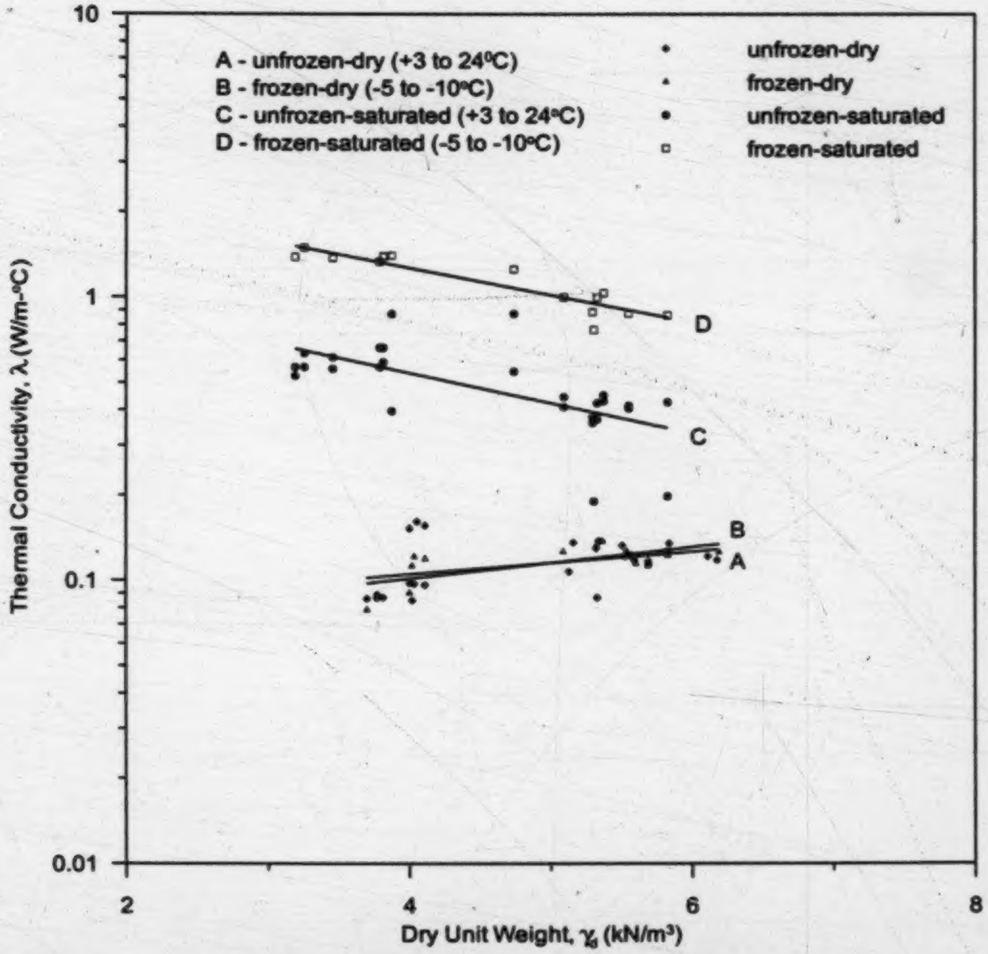

Figure 6.13 Measured thermal conductivity, λ, as a function of unit weight for tire crumbs, frozen or unfrozen, and dry or saturated

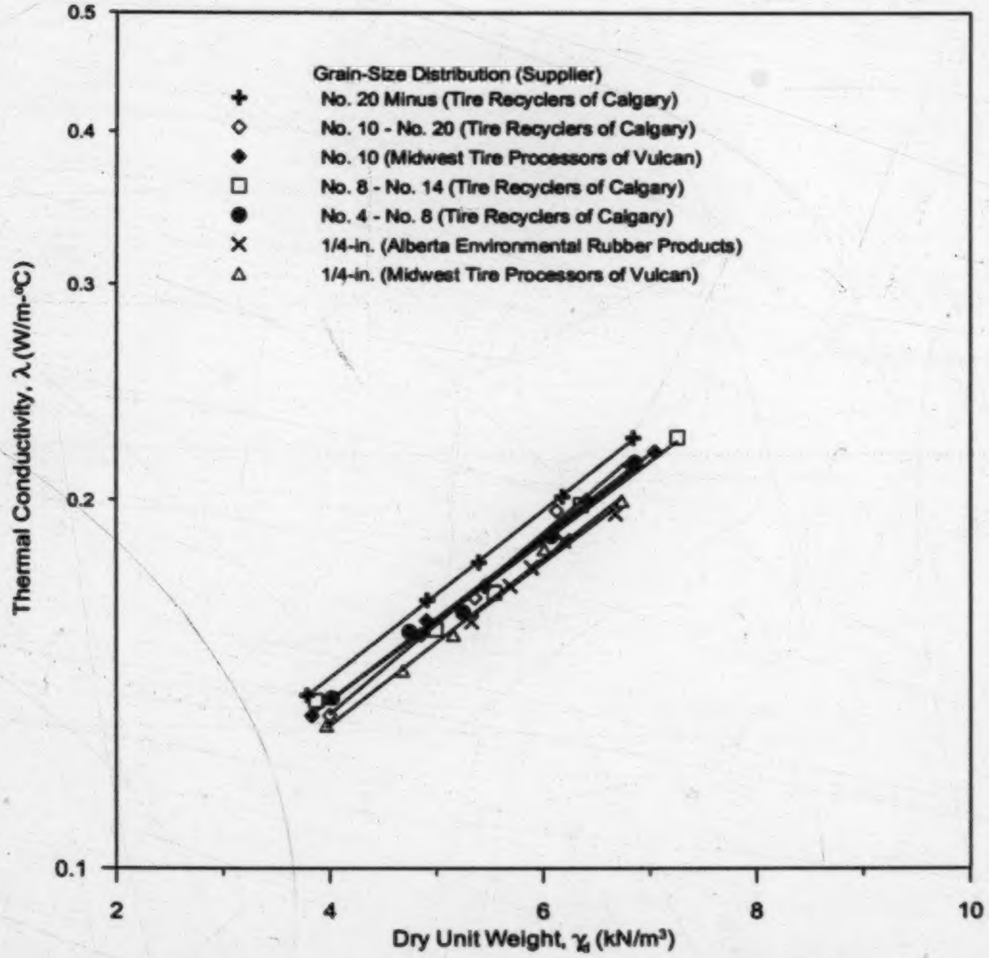

Figure 6.14 Measured thermal conductivity, λ, versus dry unit weight for dry tire crumbs using combined thermal needle and consolidation apparatus

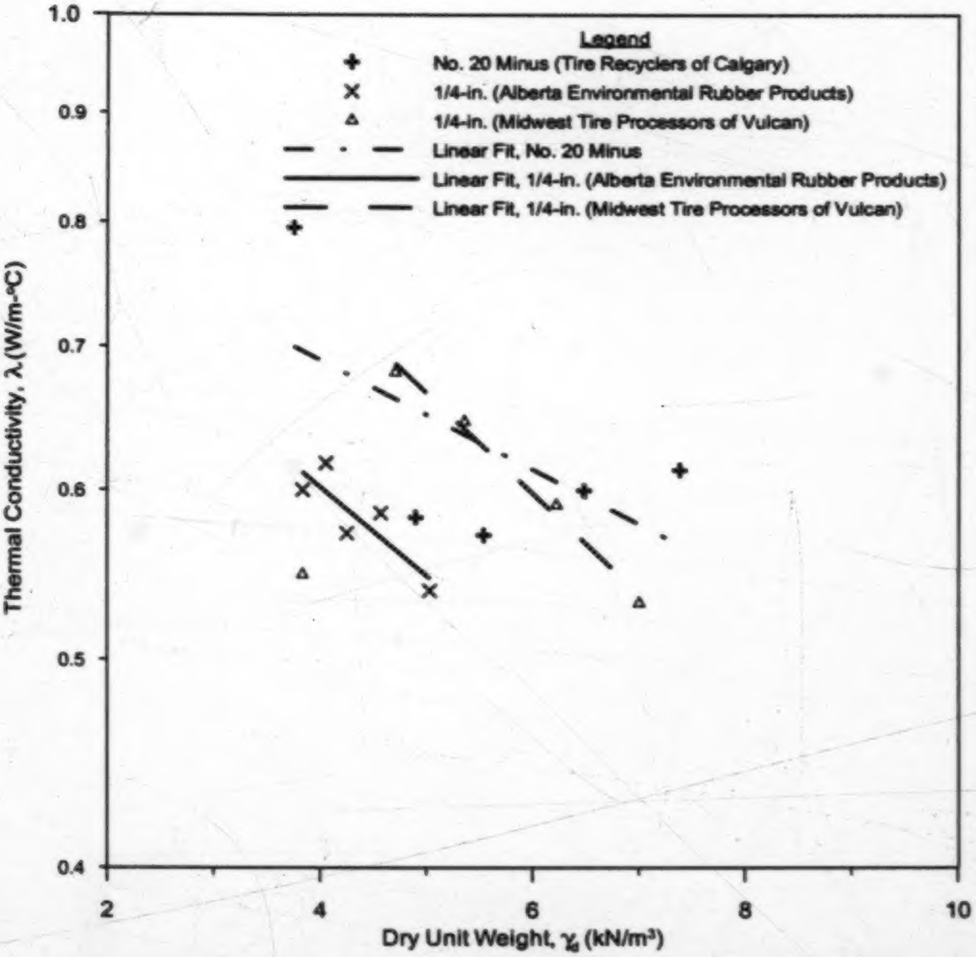

Figure 6.15 Measured thermal conductivity, λ, versus dry unit weight for saturated tire crumbs, combined thermal needle and consolidation apparatus

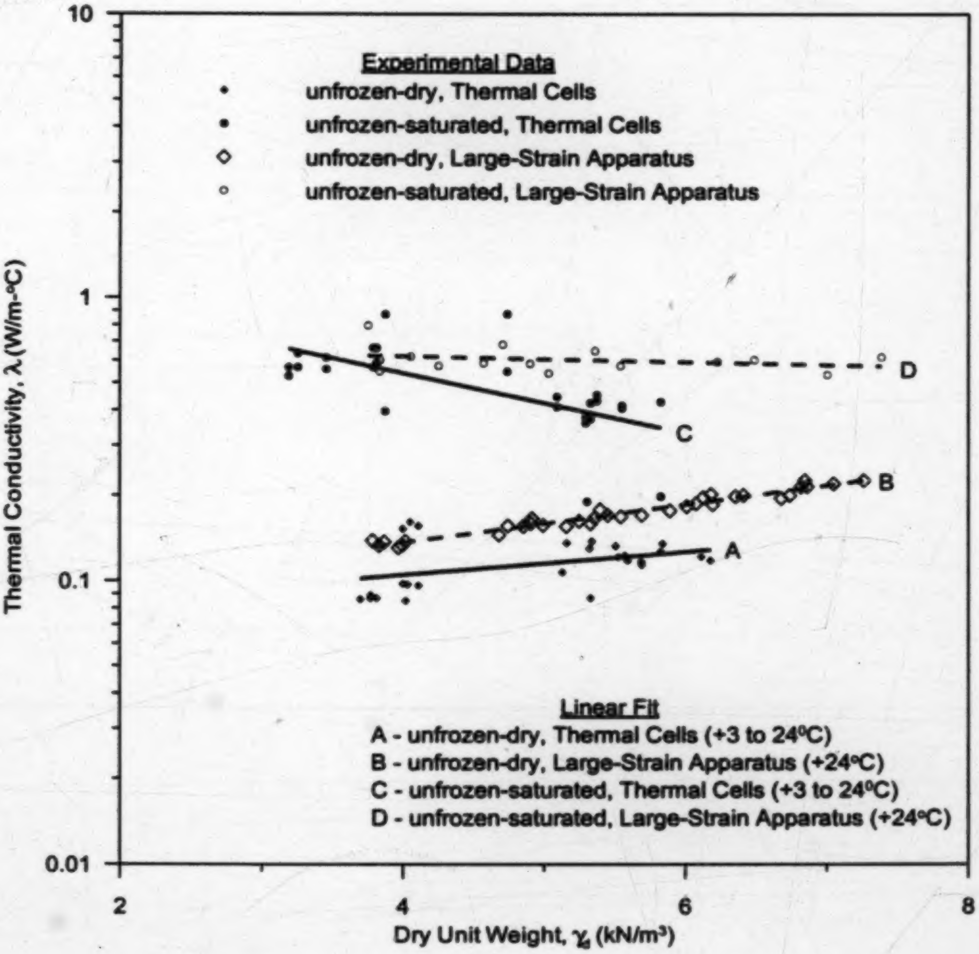

Figure 6.16 Comparison of measured thermal conductivities versus dry unit weight between thermal cells and large-strain apparatus

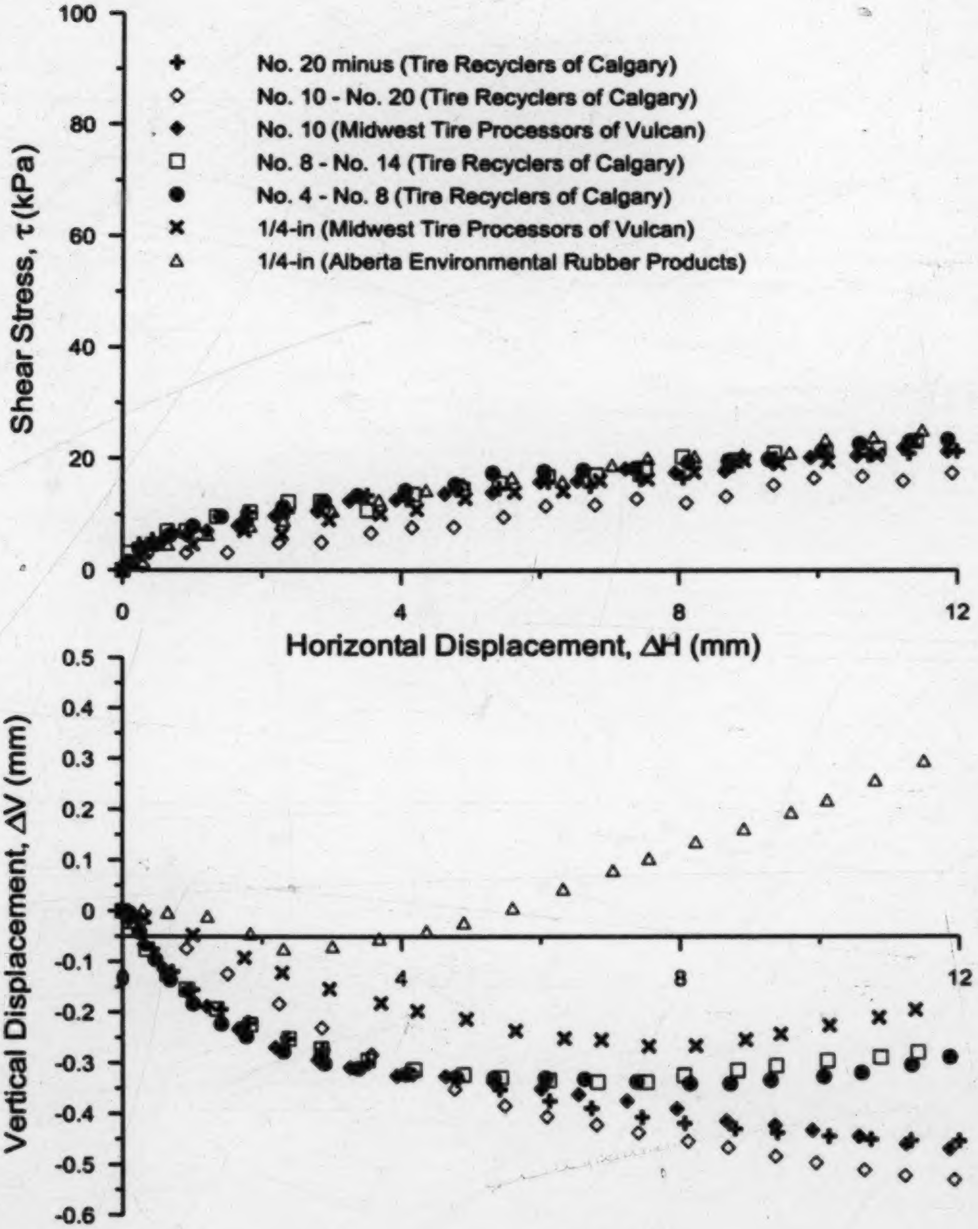

Figure 6.17 Stress and deformation response under direct shear, dry, $\sigma_N = 25$ kPa

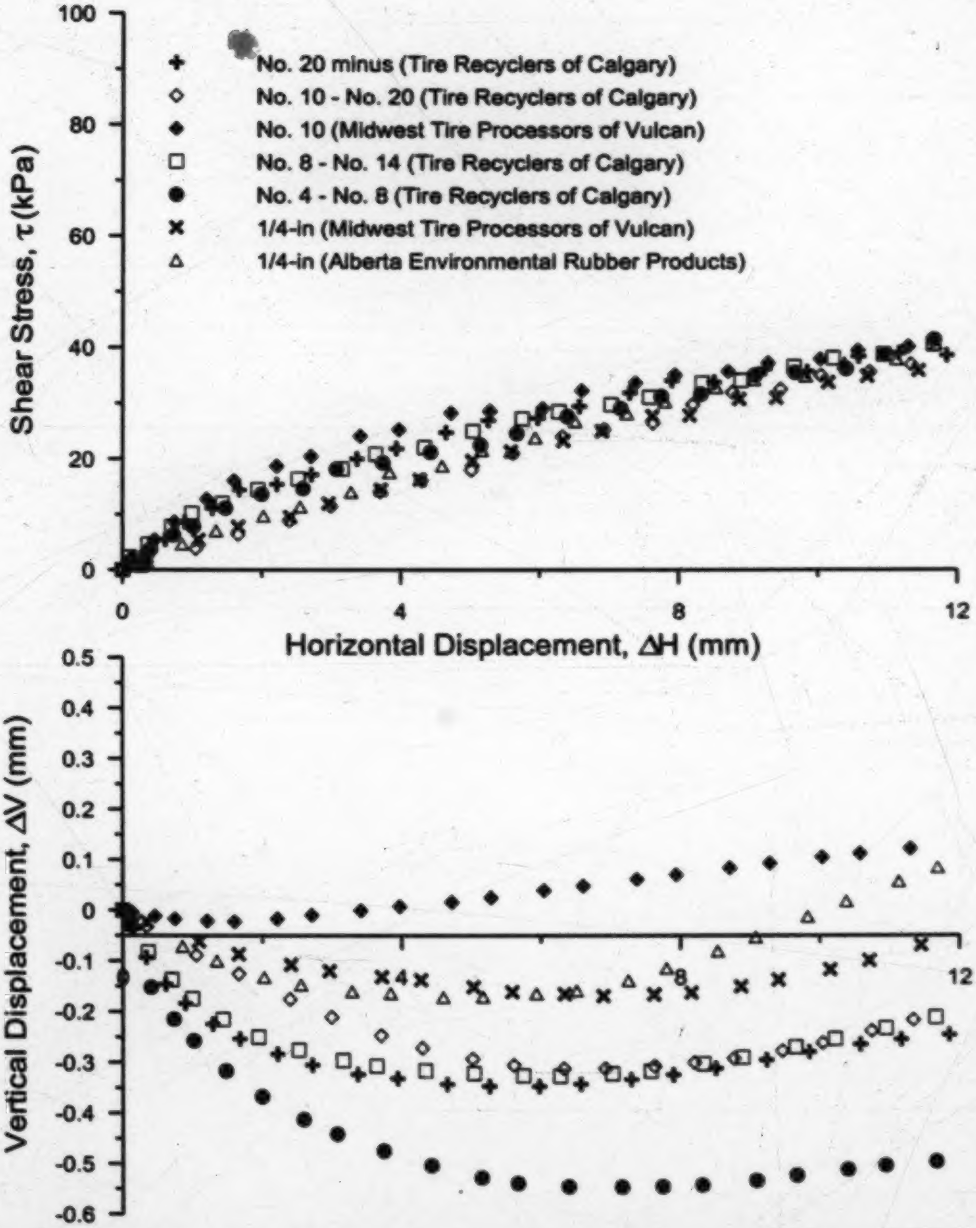

Figure 6.18 Stress and deformation response under direct shear, dry, $\sigma_N = 50$ kPa

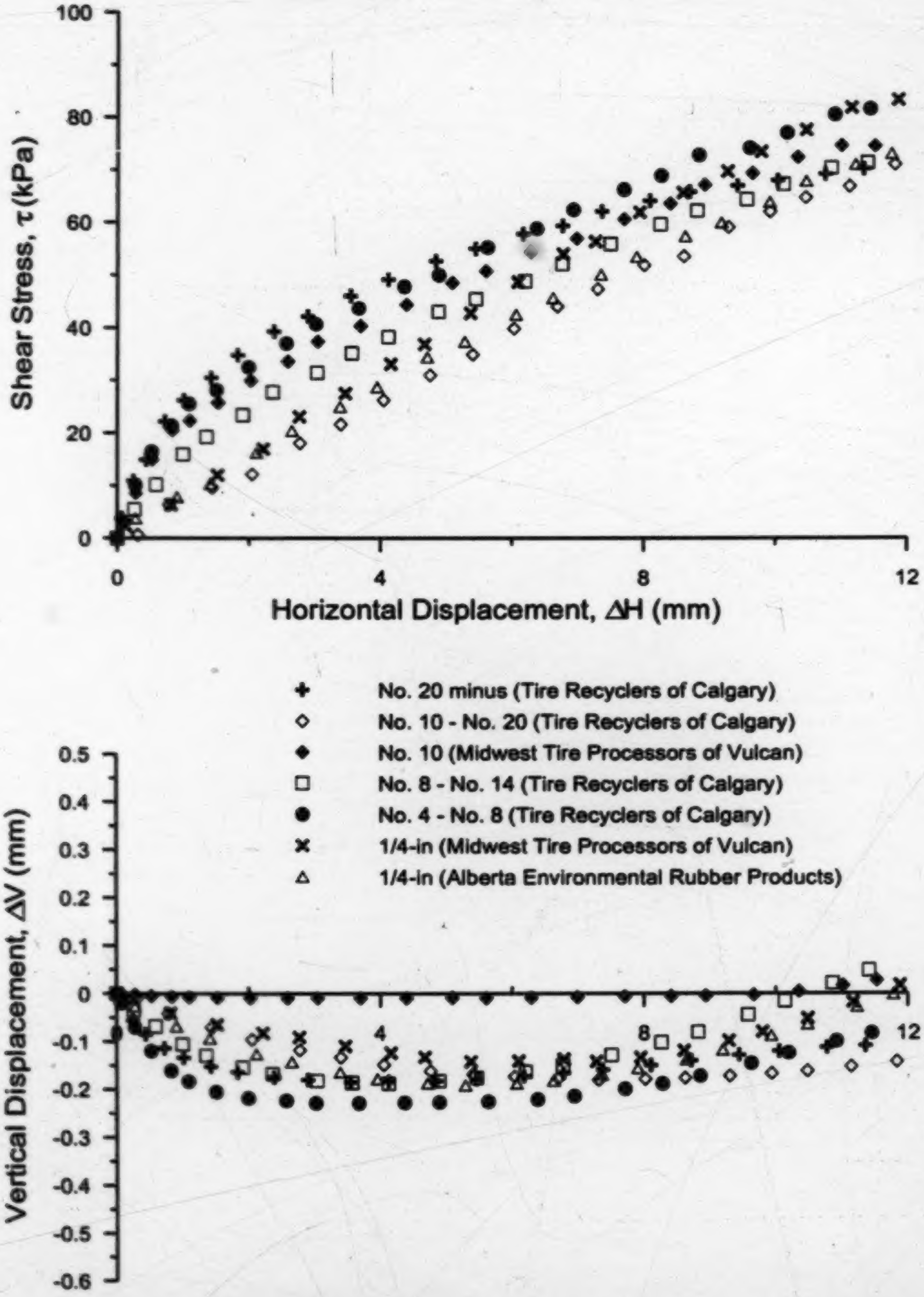

Figure 6.19 Stress and deformation response under direct shear, dry, $\sigma_N = 100$ kPa

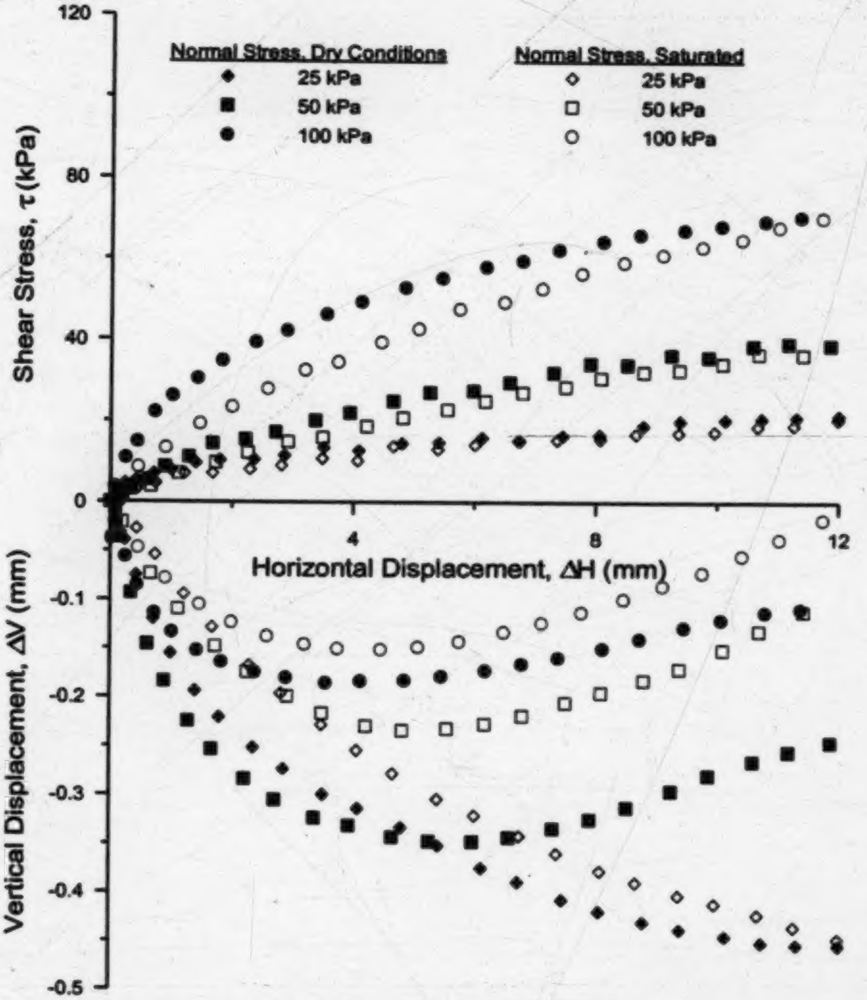

Figure 6.20 Comparison of direct shear stress and deformation behaviour, saturated and dry, No. 20 minus (Tire Recyclers of Calgary)

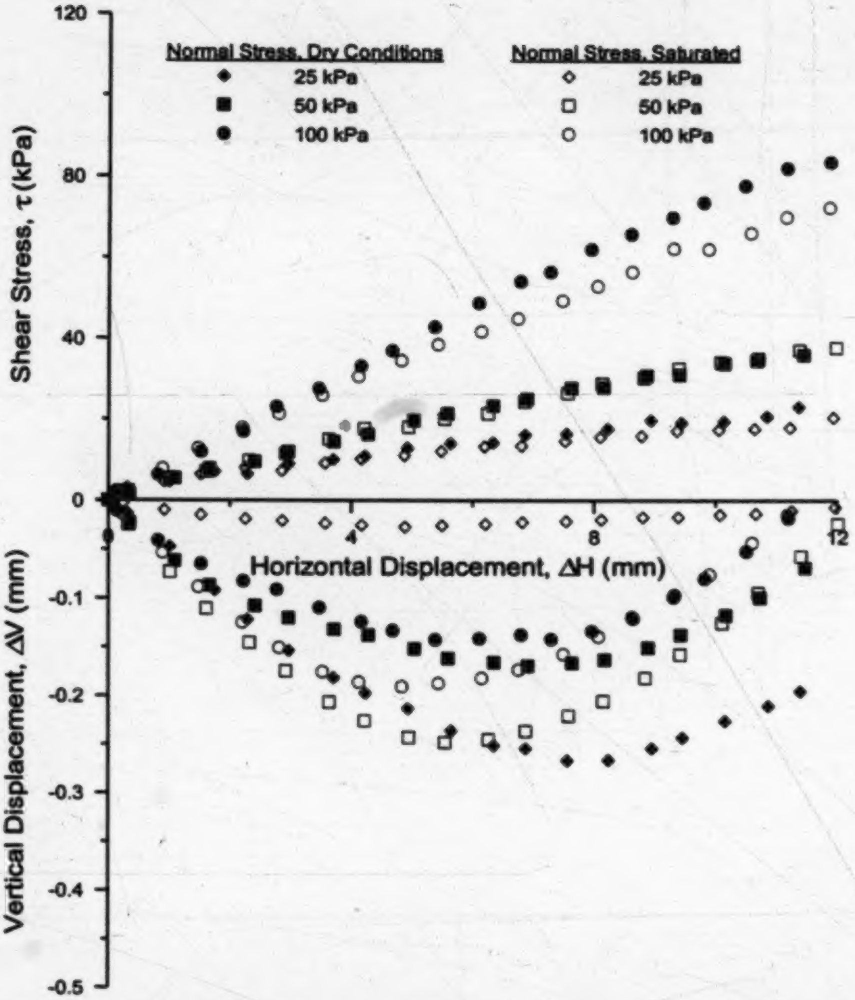

Figure 6.21 Comparison of direct shear stress and deformation behaviour, saturated and dry, 1/4 in (Midwest Tire Processors of Vulcan)

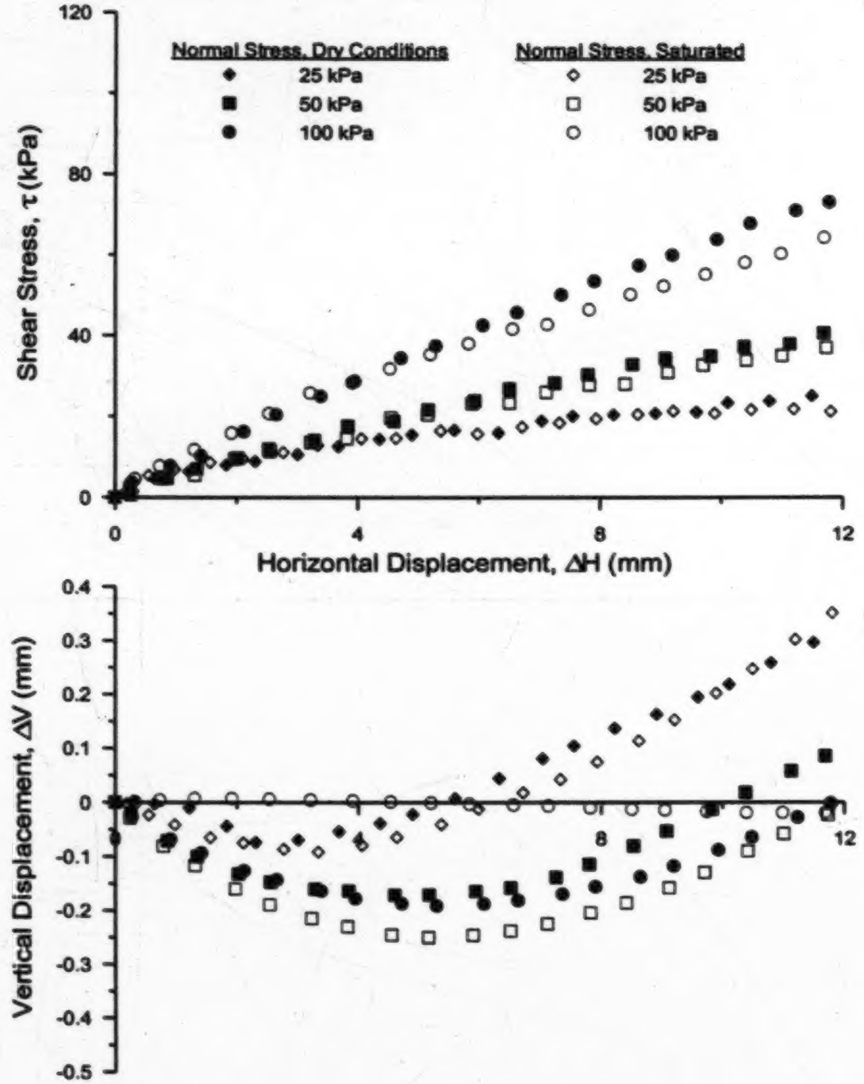

Figure 6.22 Comparison of direct shear stress and deformation behaviour, saturated and dry, 1/4 in (Alberta Environmental Rubber Products)

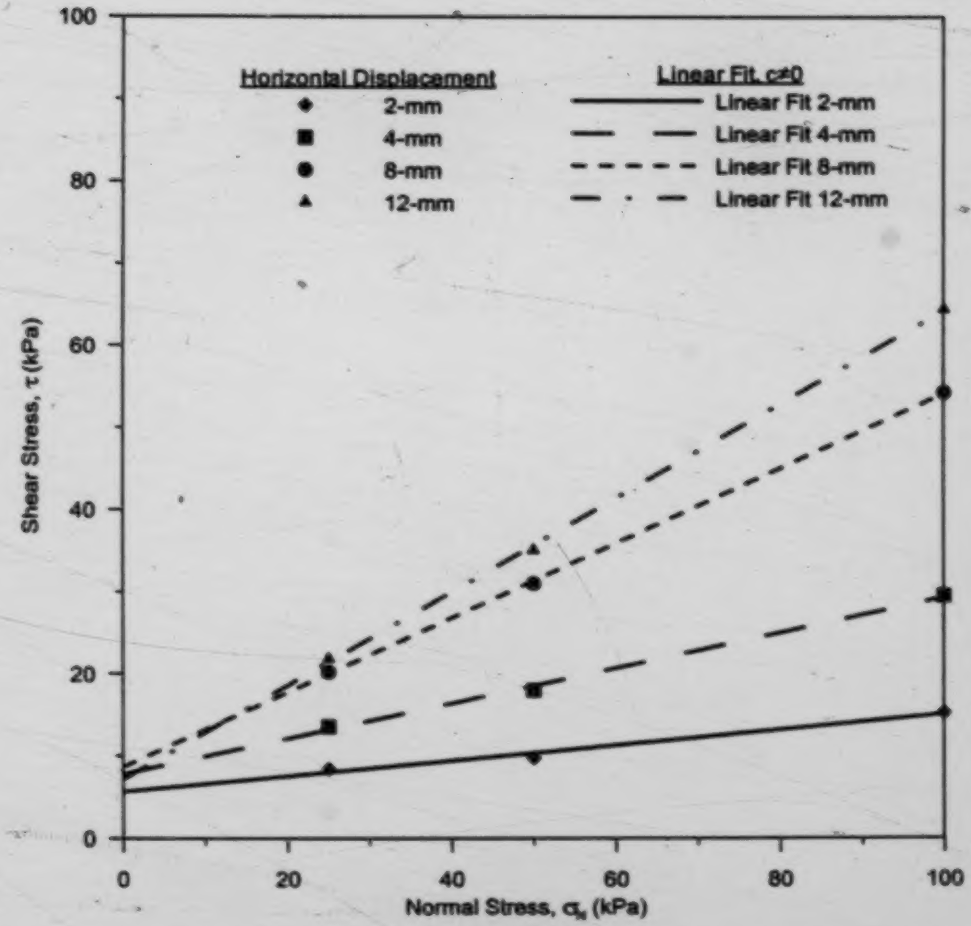

Figure 6.23 Direct shear strength envelopes, dry, 1/4 in (Alberta Environmental Rubber Products), Method A

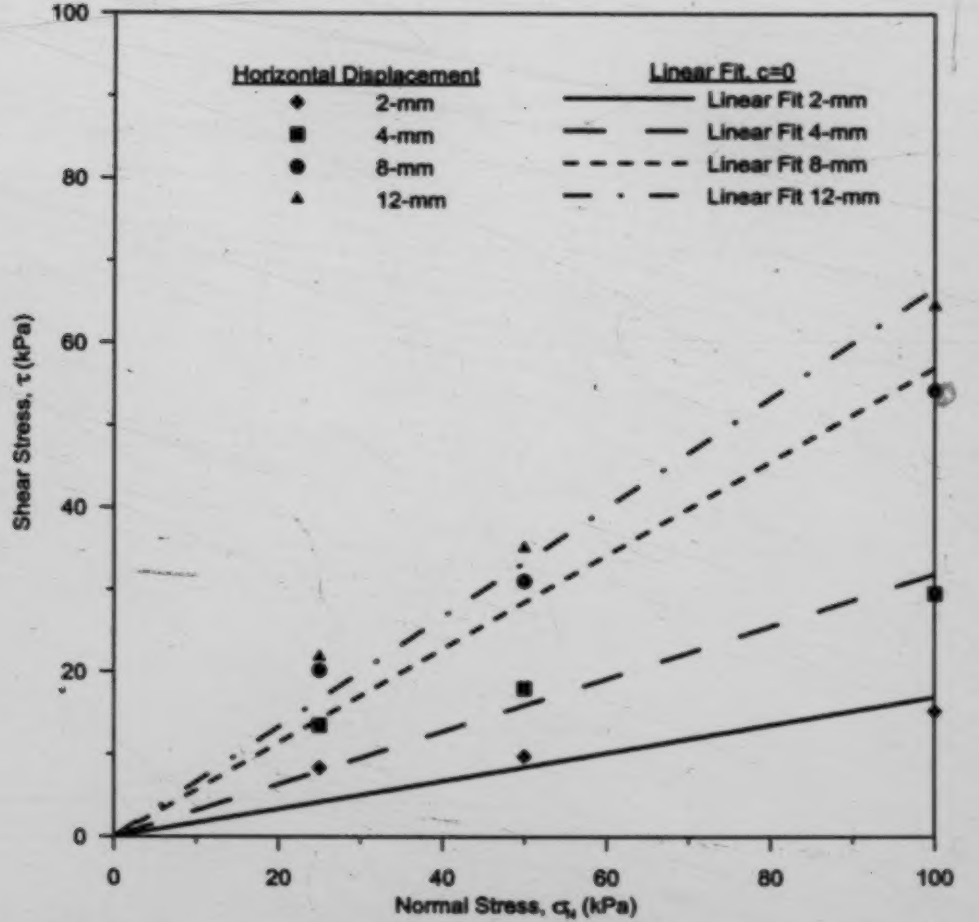

Figure 6.24 Direct shear strength envelopes, dry, 1/4 in (Alberta Environmental Rubber Products), Method B

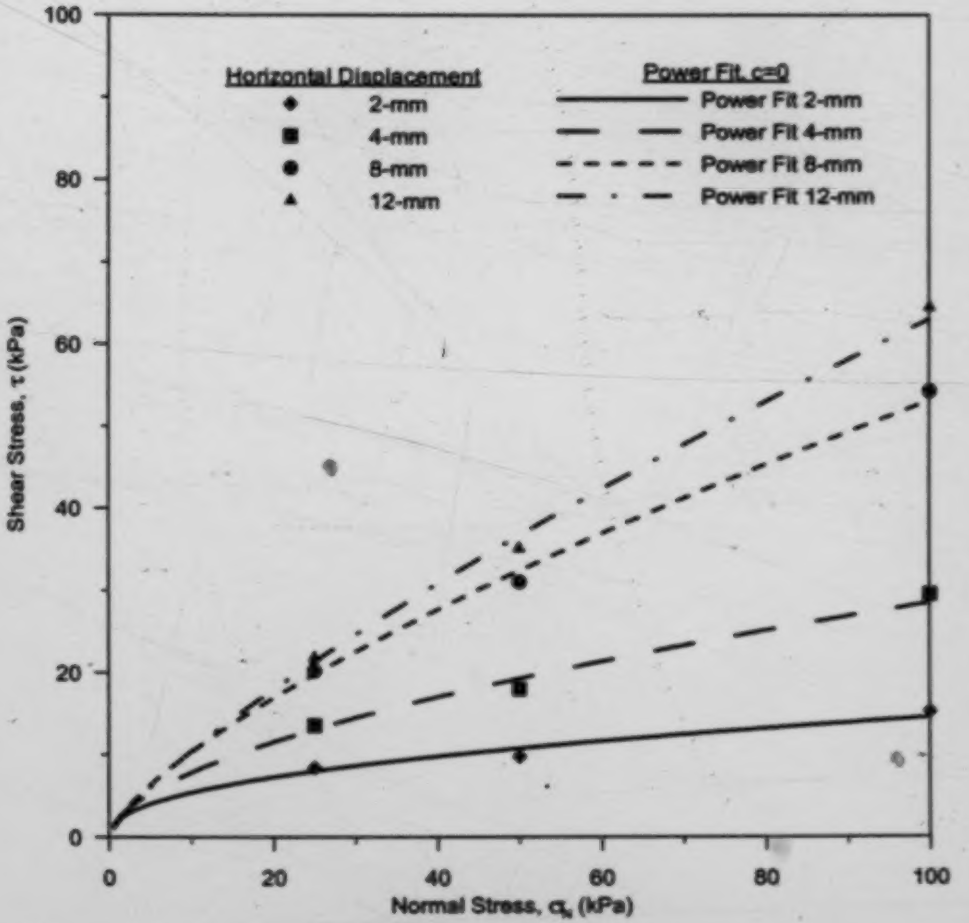

Figure 6.25 Direct shear strength envelopes, dry, 1/4 in (Alberta Environmental Rubber Products), Method C

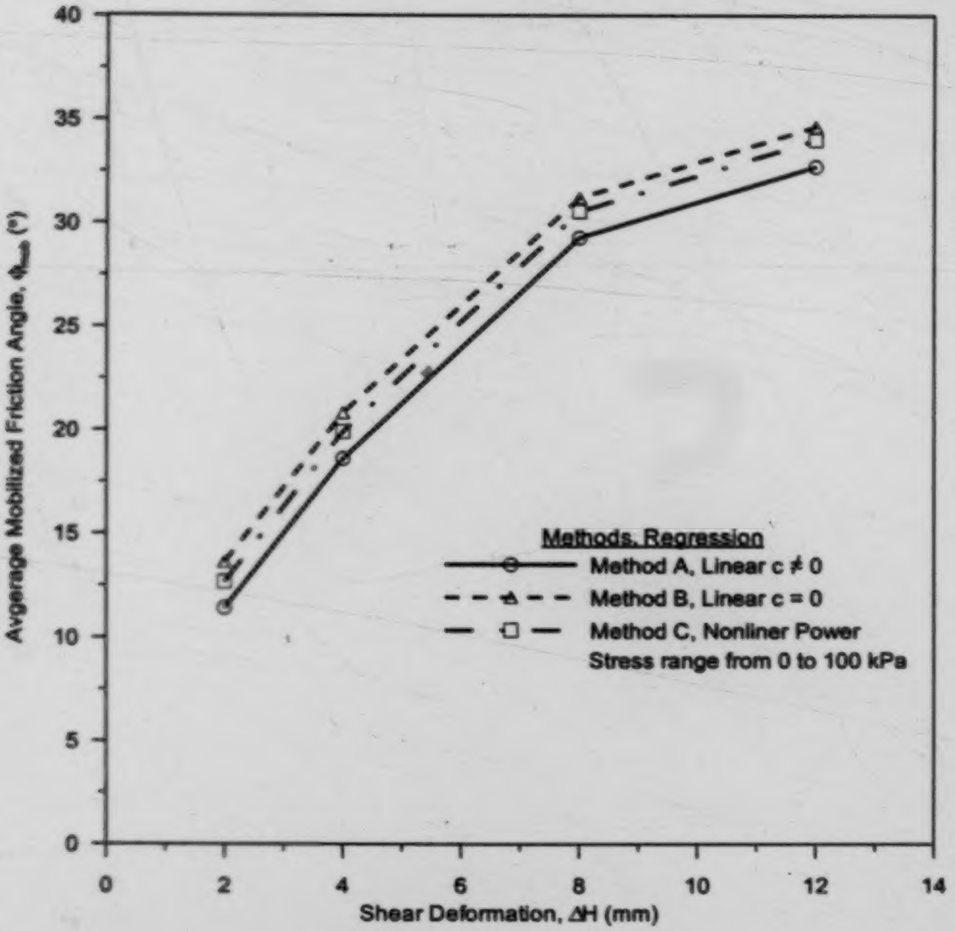

Figure 6.26 Direct shear mobilized friction angle, ϕ_{mob}, versus shear deformation, average values for all crumb sizes tested under dry conditions

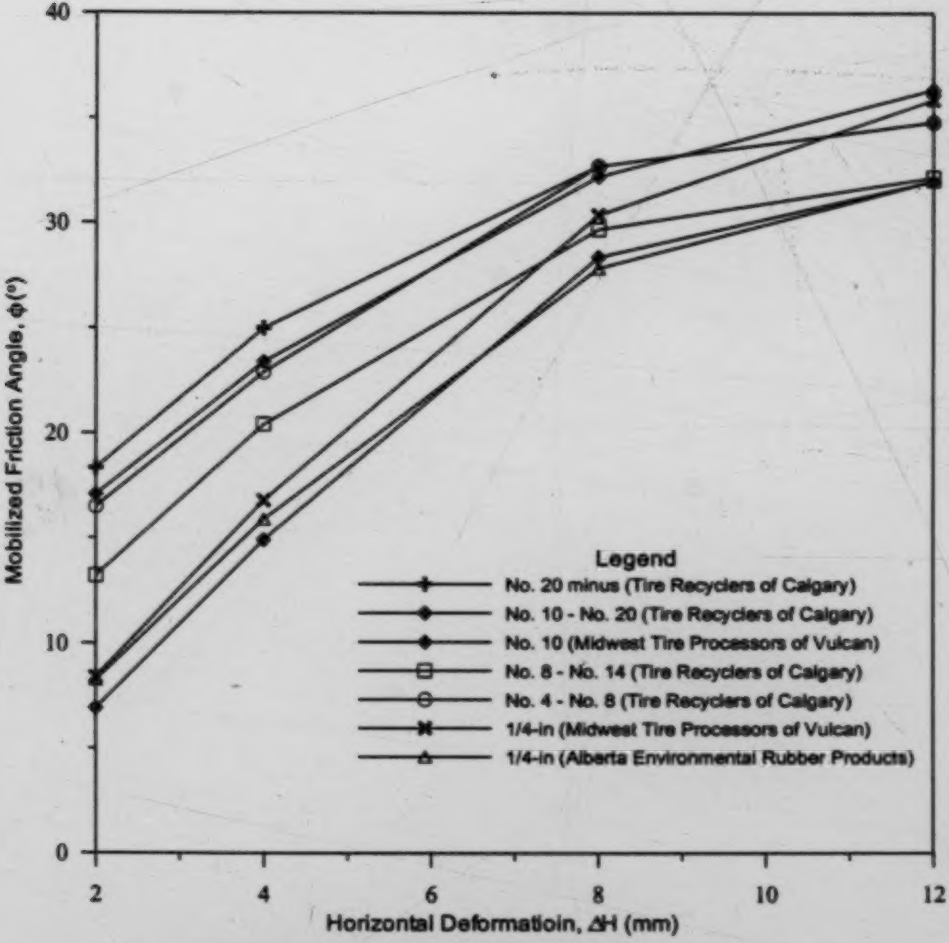

Figure 6.27 Direct shear mobilized friction angle, ϕ_{mob}, versus horizontal displacement for all grain-sizes tested dry, Method C

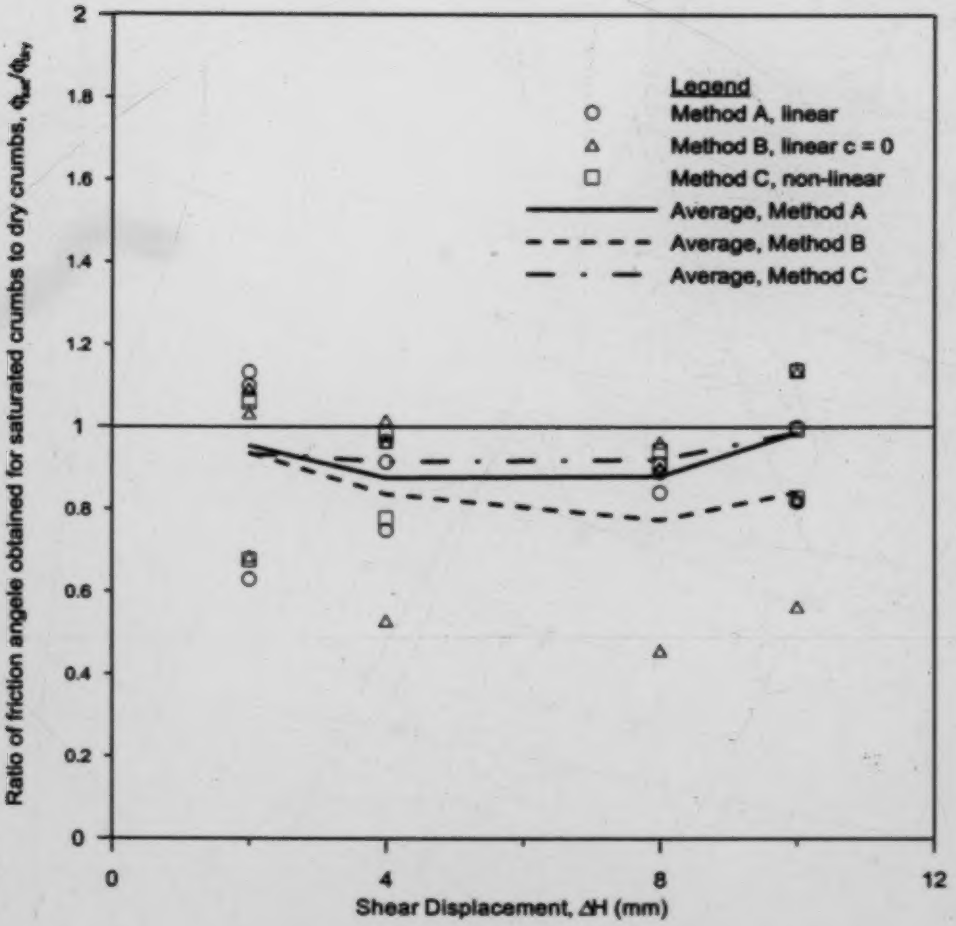

Figure 6.28 ϕ_{sat}/ϕ_{dry} for tire crumbs under direct shear, No. 20 minus and 1/4-in crumbs only

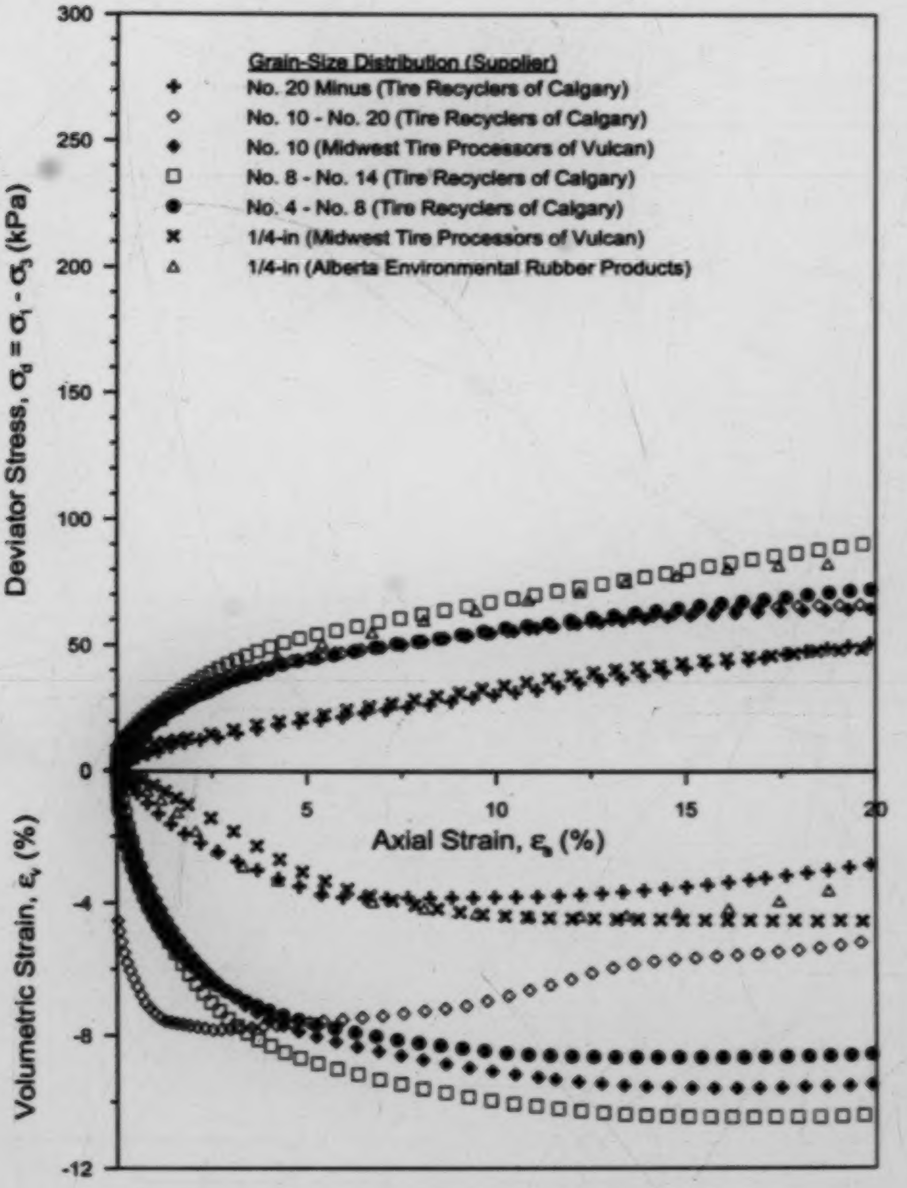

Figure 6.29 Triaxial stress and volumetric strain behaviour of tire crumbs, all grain-size distribution, σ_3 = 25 kPa

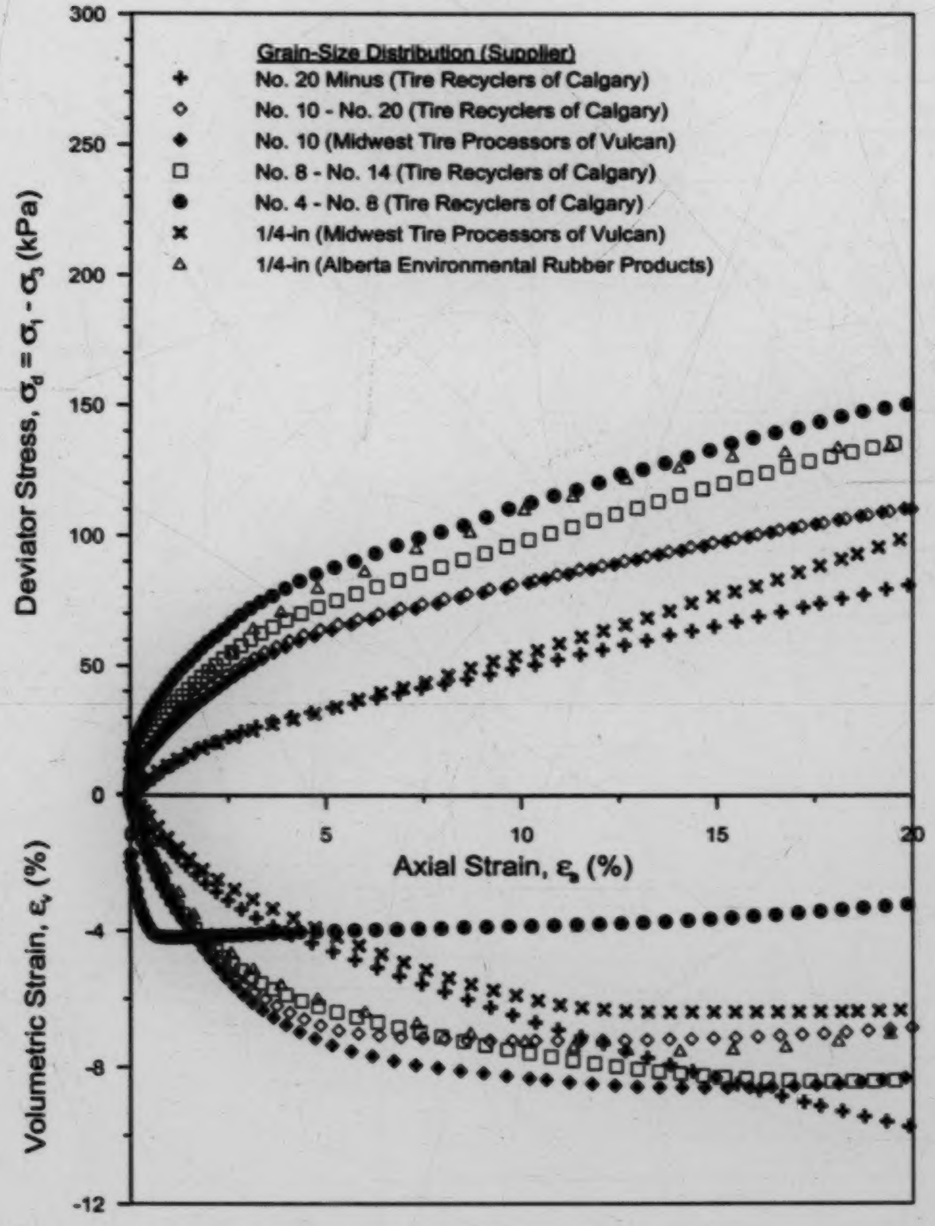

Figure 6.30 Triaxial stress and volumetric strain behaviour of tire crumbs, all grain-size distribution, $\sigma_3 = 50$ kPa

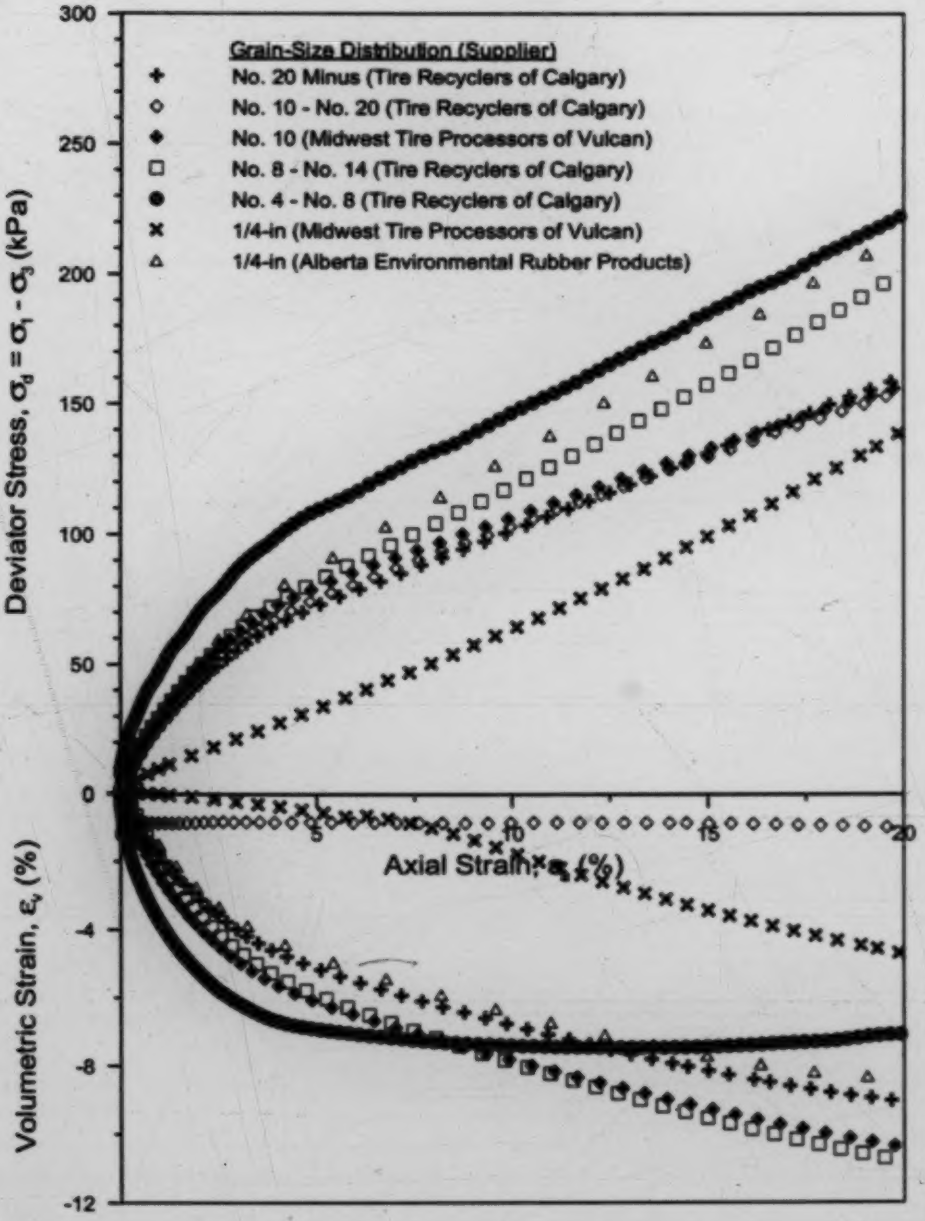

Figure 6.31 Triaxial stress and volumetric strain behaviour of tire crumbs, all grain-size distribution, σ_3 = 100 kPa

Figure 6.32 Lateral bulging at low confining pressure for 1/4 in tire crumbs (Midwest Tire Processors of Vulcan)

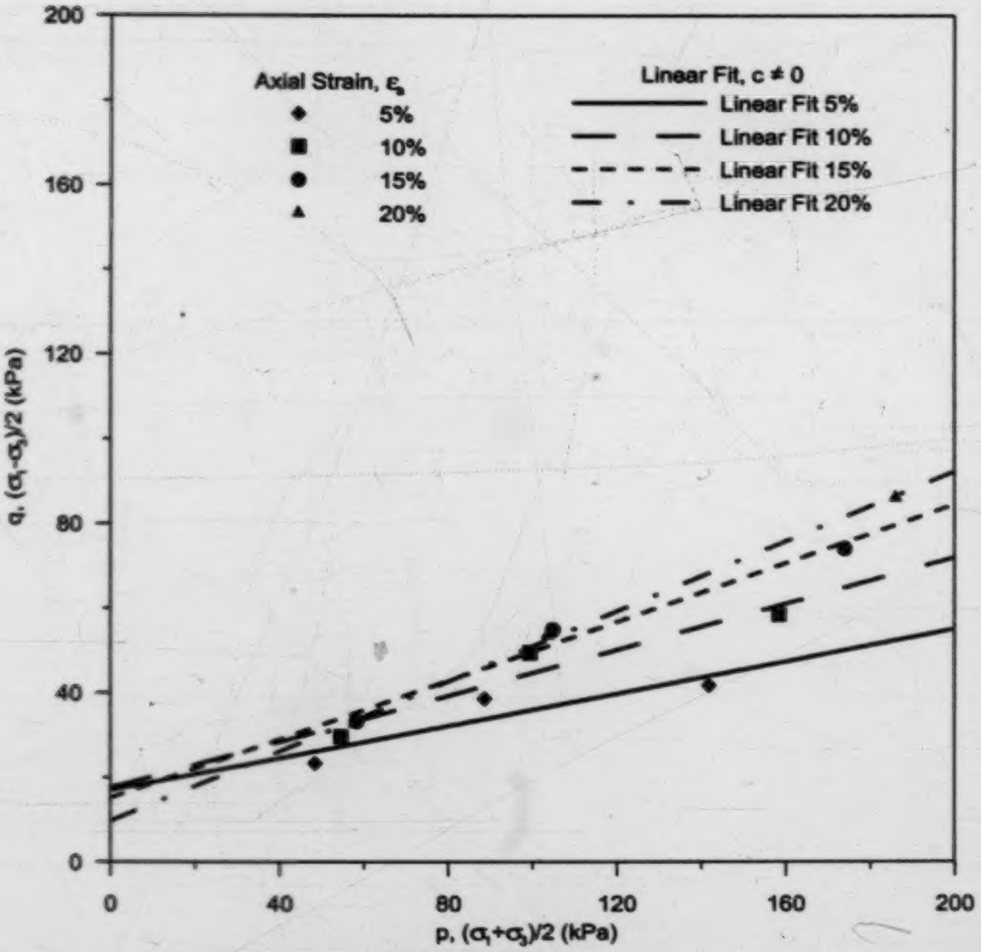

Figure 6.33 Modified shear strength envelopes from CD triaxial tests, 1/4 in (Alberta Environmental Rubber Products), Method A' (c ≠ 0)

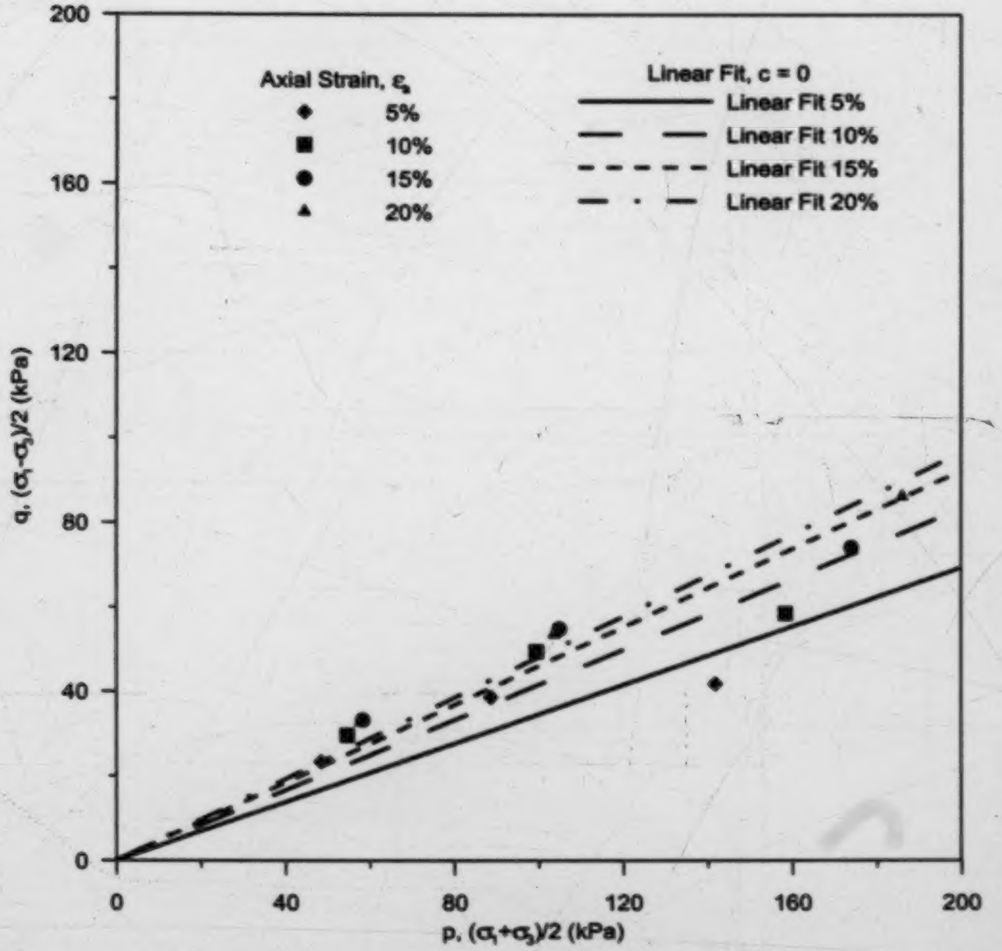

Figure 6.34 Modified CD triaxial shear strength envelopes from CD triaxial tests, 1/4 in (Alberta Environmental Rubber Products), Method B' (c = 0)

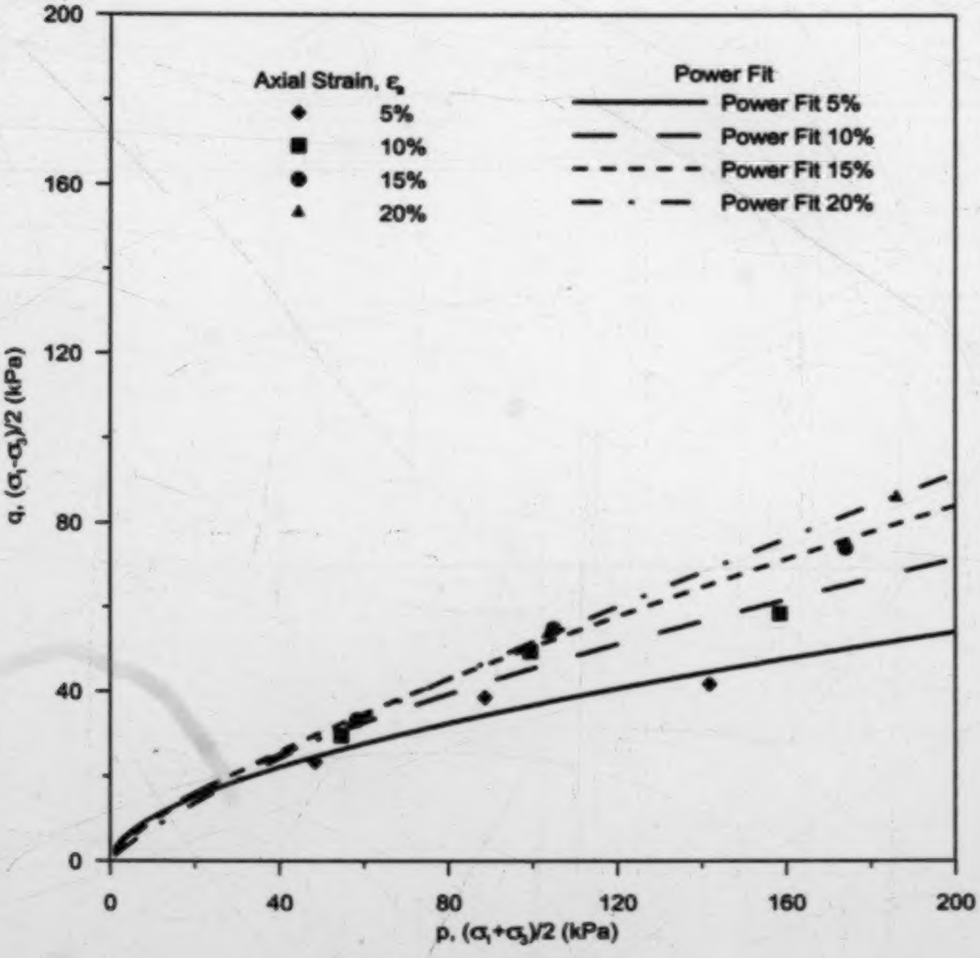

Figure 6.35 Modified non-linear shear strength envelopes from CD triaxial tests, 1/4 in (Environmental Rubber Products), Method C'

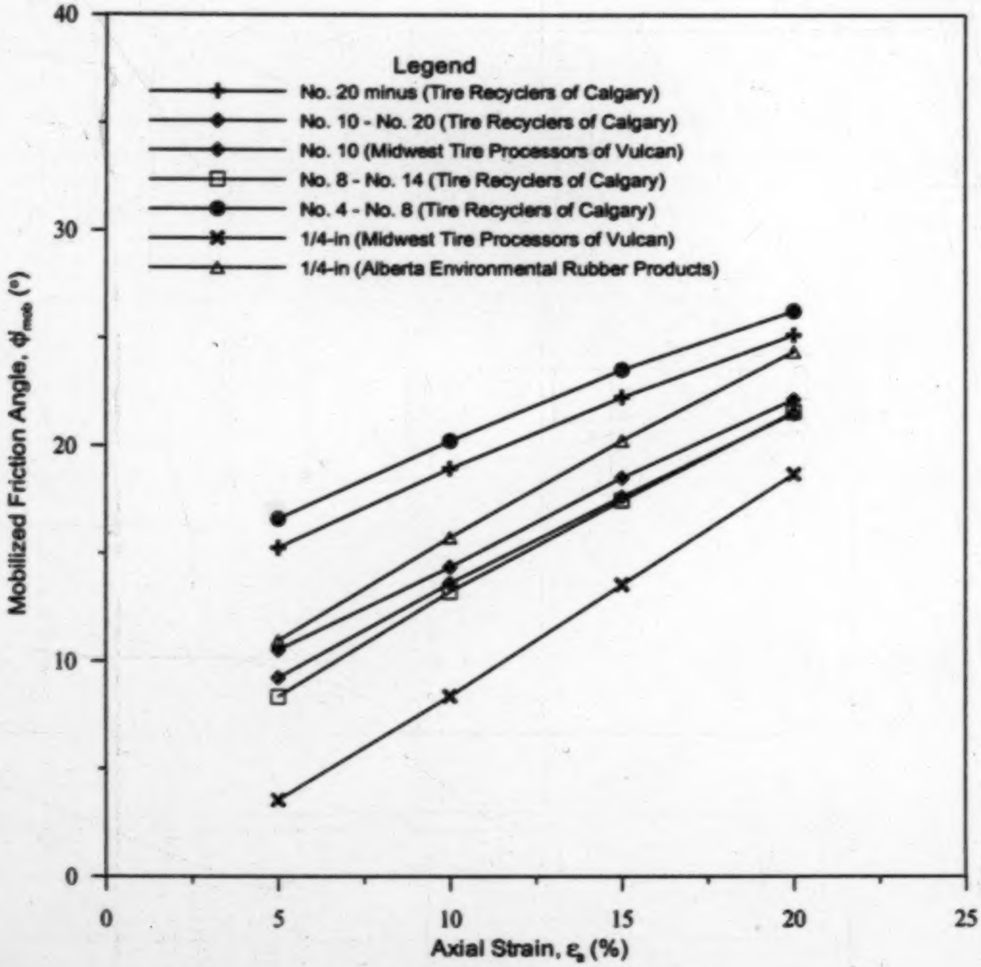

Figure 6.36 Triaxial mobilized friction angle, ϕ'_{mob}, versus axial strain, all grain-size distribution, Method A' ($c \neq 0$)

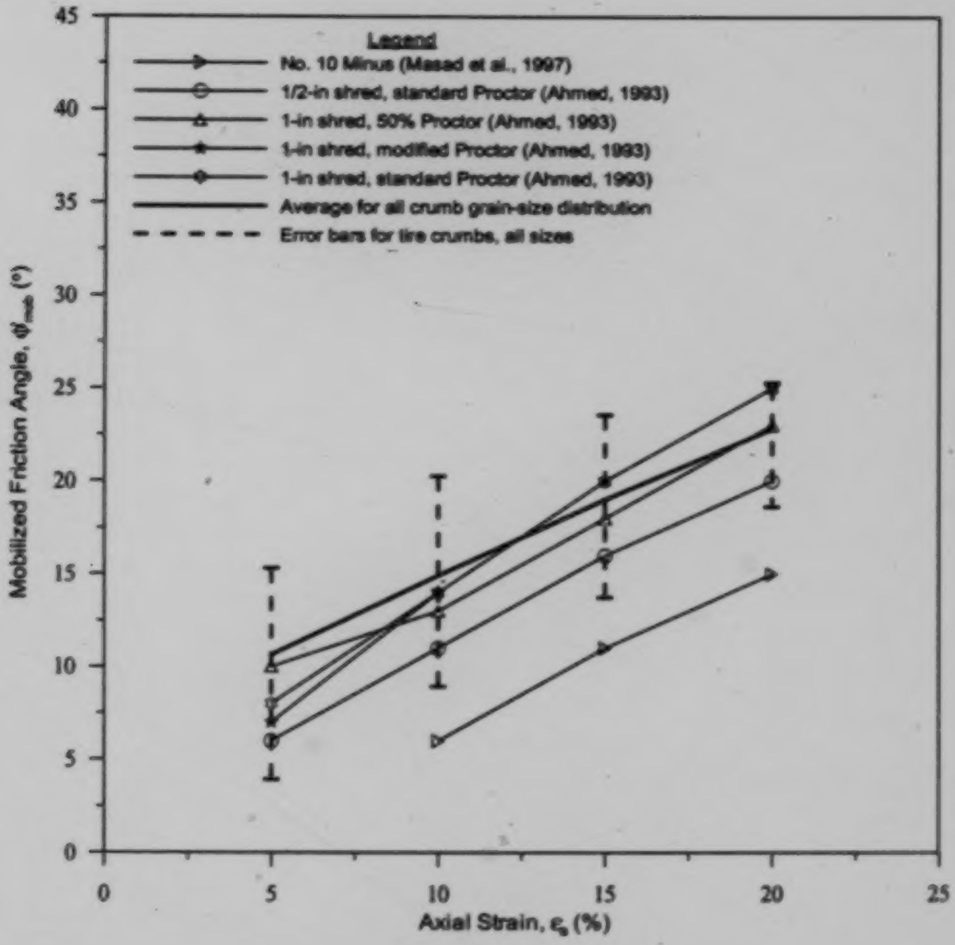

Figure 6.37 Comparison of triaxial mobilized friction angle, ϕ'_{mob}, of tire crumb at respective strain levels with others, Method A' ($c \neq 0$)

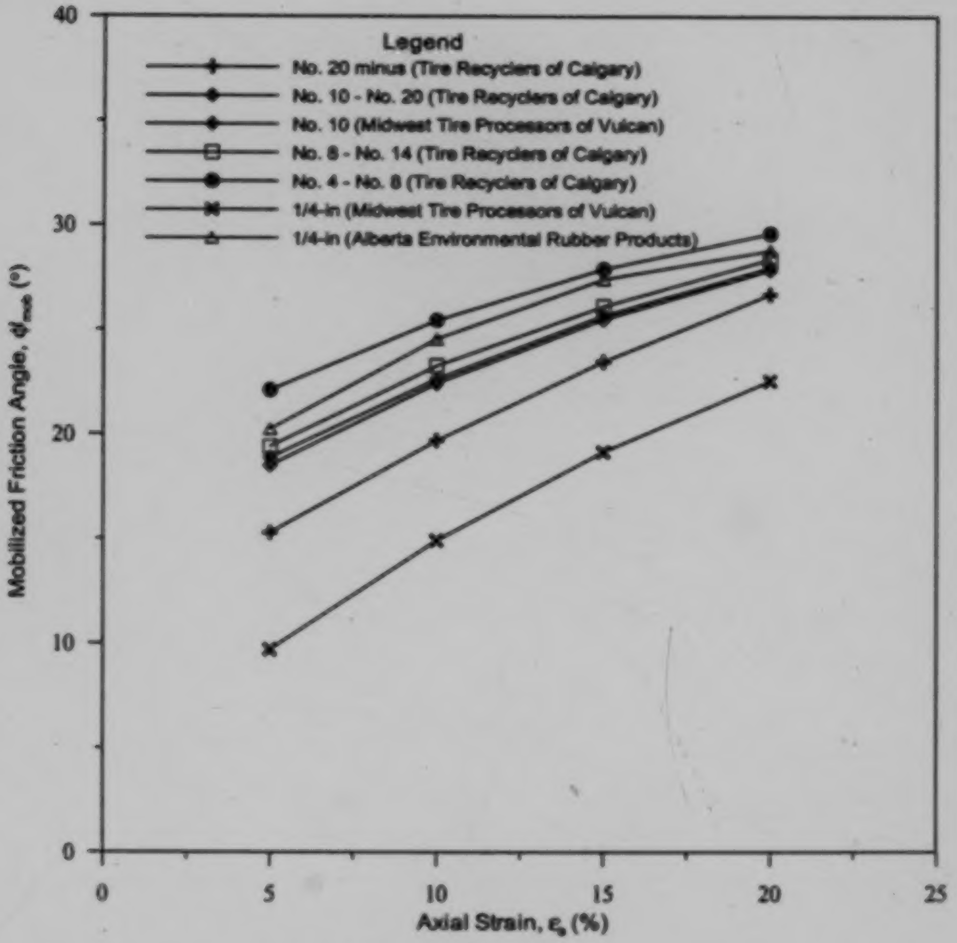

Figure 6.38 Triaxial mobilized friction angle, ϕ'_{mob}, versus axial strain, all grain-size distribution, Method B' ($c = 0$)

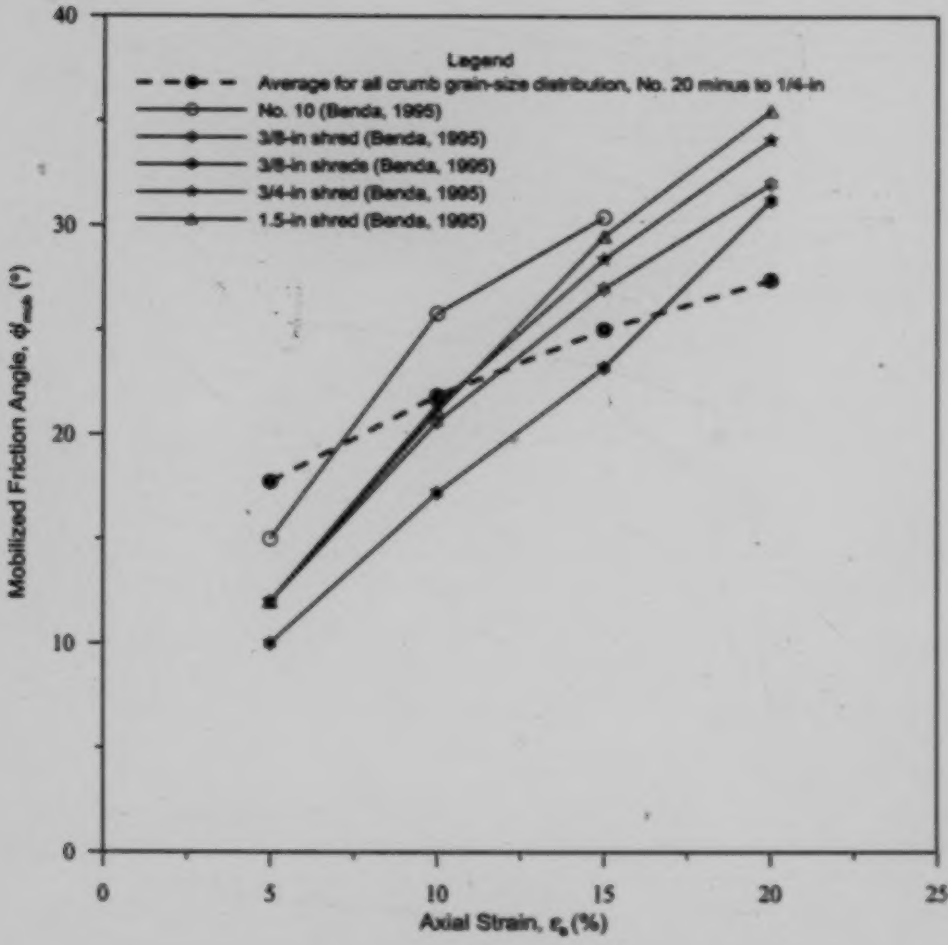

Figure 6.39 Comparison of the triaxial mobilized friction angle, ϕ'_{mob}, of tire crumbs with others, Method B' ($c = 0$)

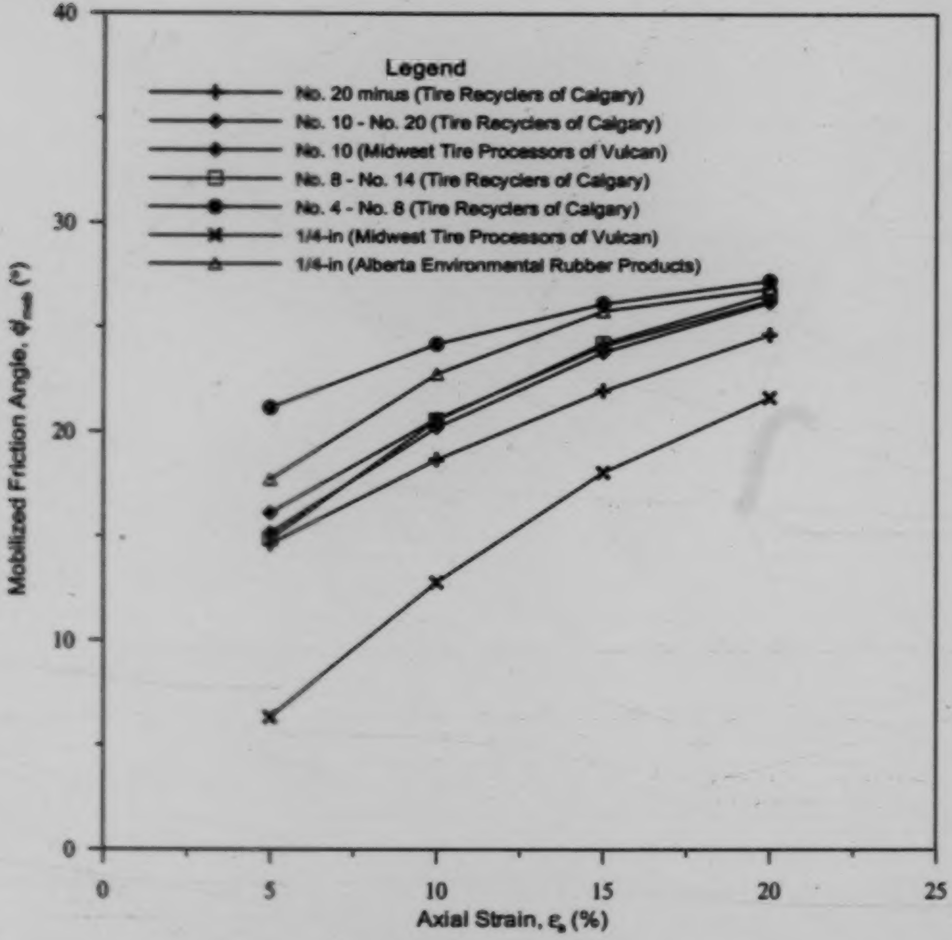

Figure 6.40 Triaxial mobilized friction angle, ϕ'_{mob}, versus axial strain from secant tangents taken over 25 to 50 kPa stress range, Method C' (non-linear)

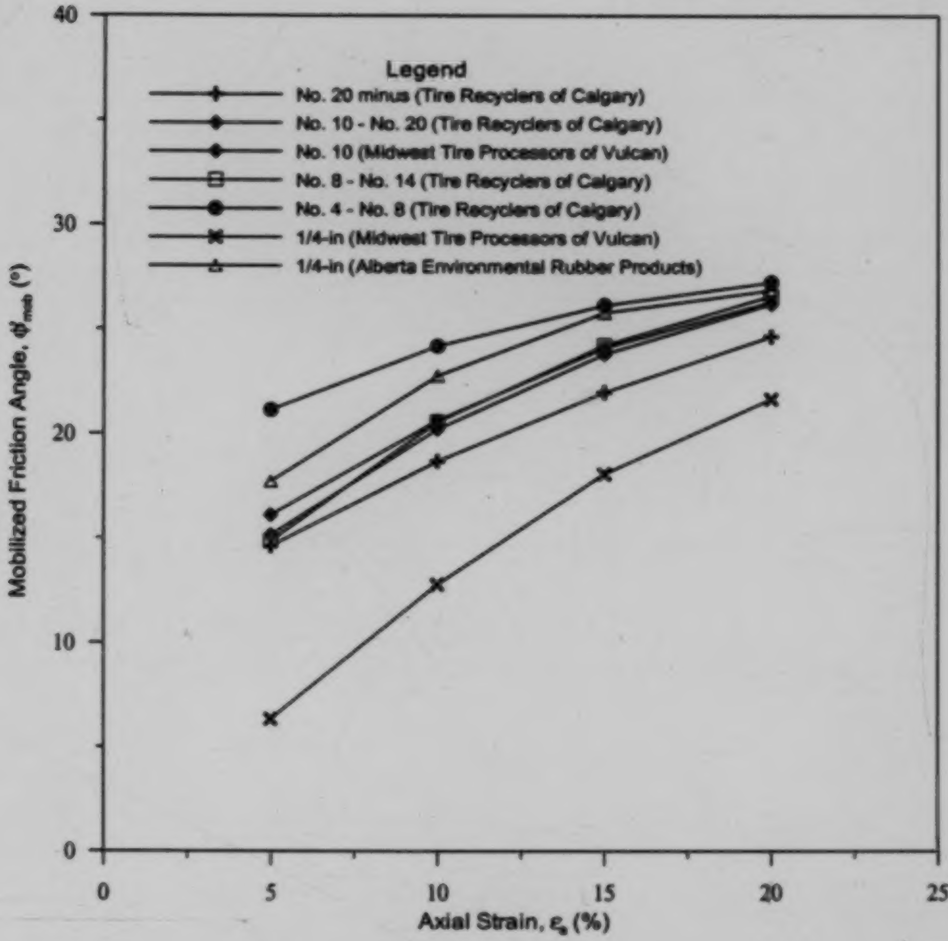

Figure 6.41 Triaxial mobilized friction angle, ϕ'_{mob}, versus axial strain from secant tangents taken over 50 to 100 kPa stress range, Method C' (non-linear)

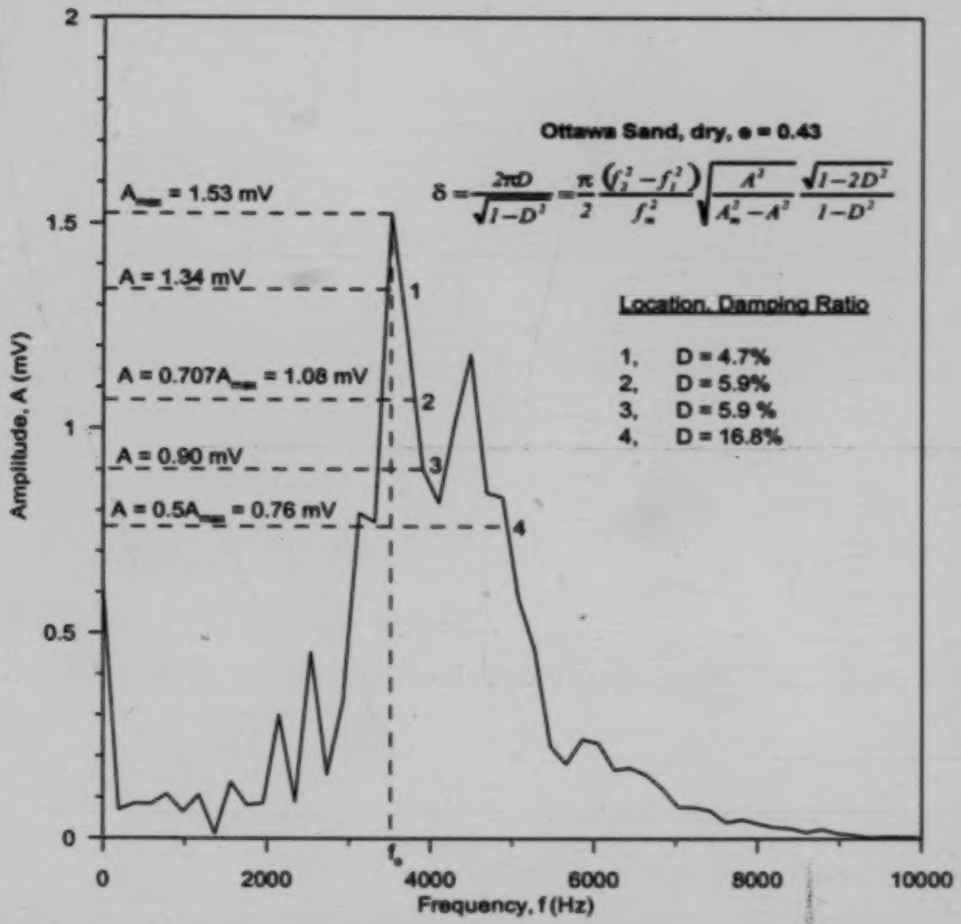

Figure 6.42 Amplitude-frequency curve obtained from large-strain apparatus and bender element tests of Ottawa sand

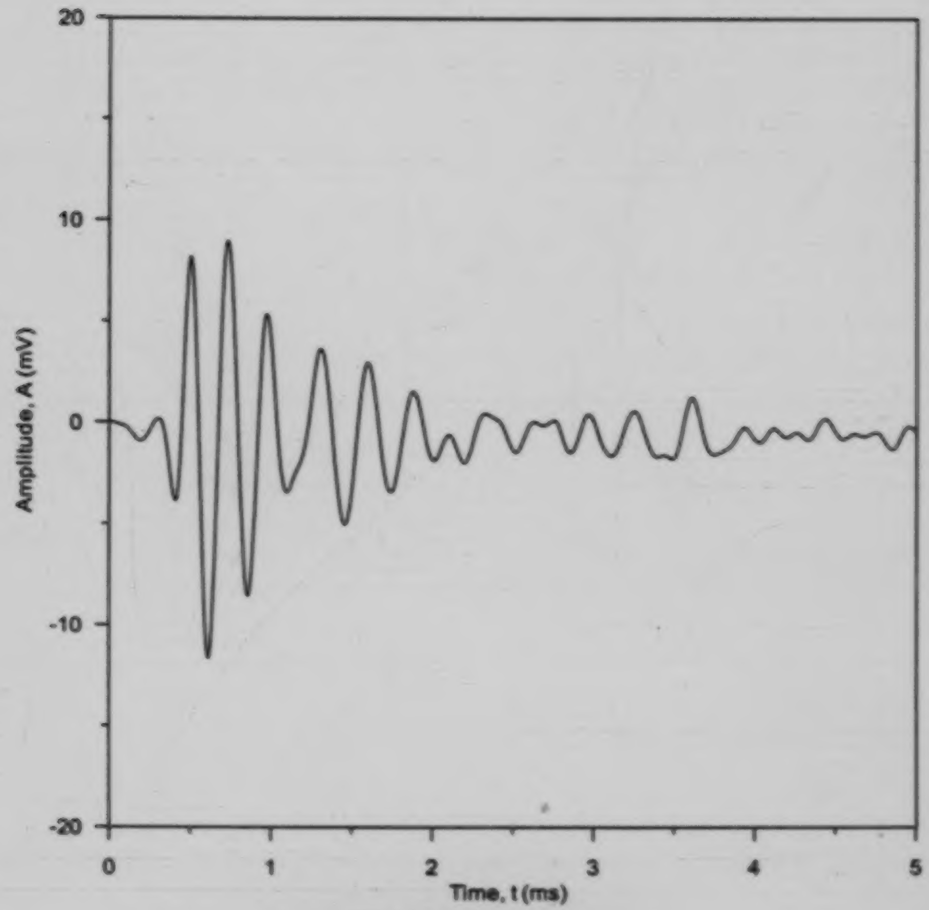

(a) Amplitude-time decay curves.

Figure 6.43 Dynamic properties obtained from large-strain apparatus and bender element tests of Ottawa sand.

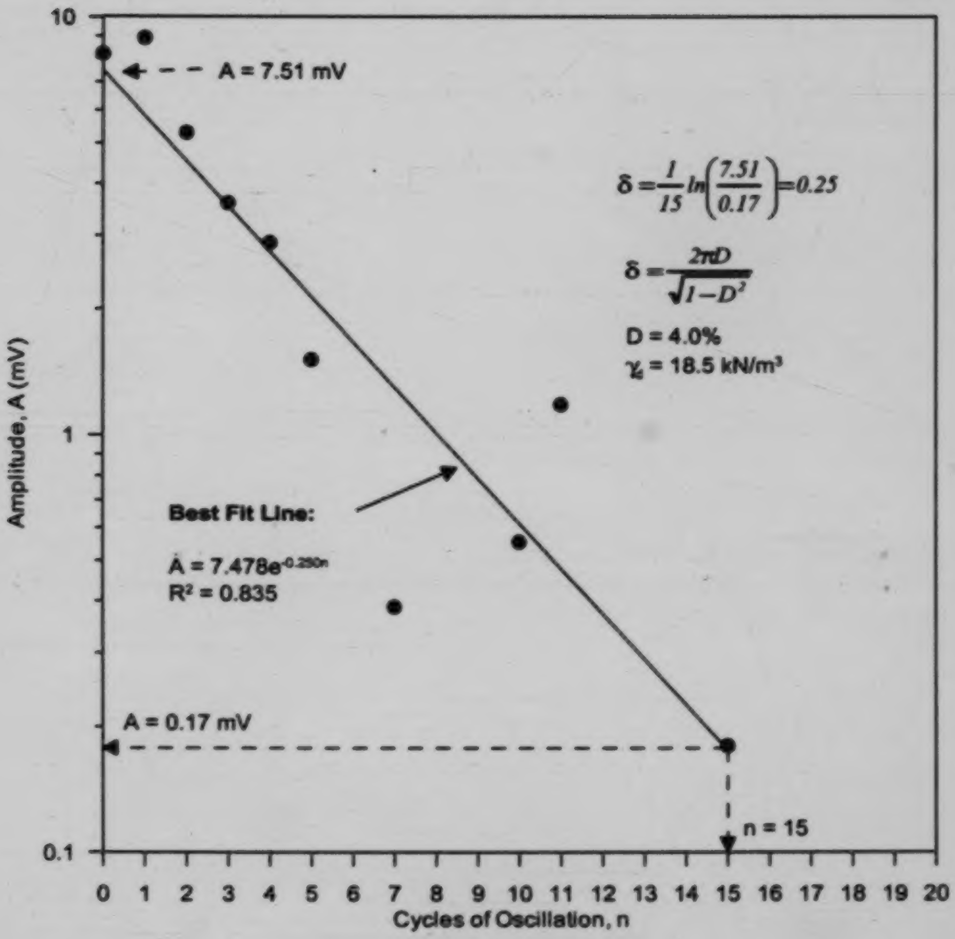

(b) Amplitude versus cycle number plot.

Figure 6.43 Continued

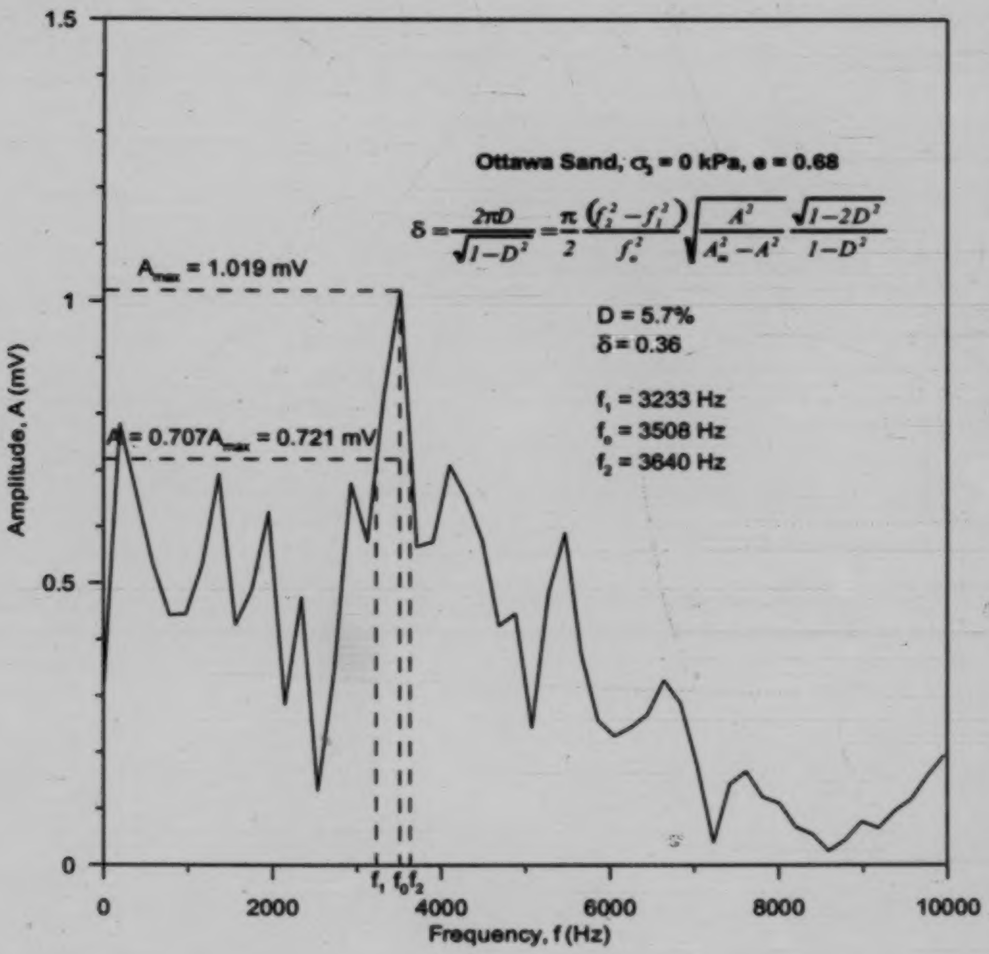

Figure 6.44 Typical amplitude-frequency curve obtained from triaxial cell apparatus and bender element tests of Ottawa sand, $\sigma_3 = 0$ kPa

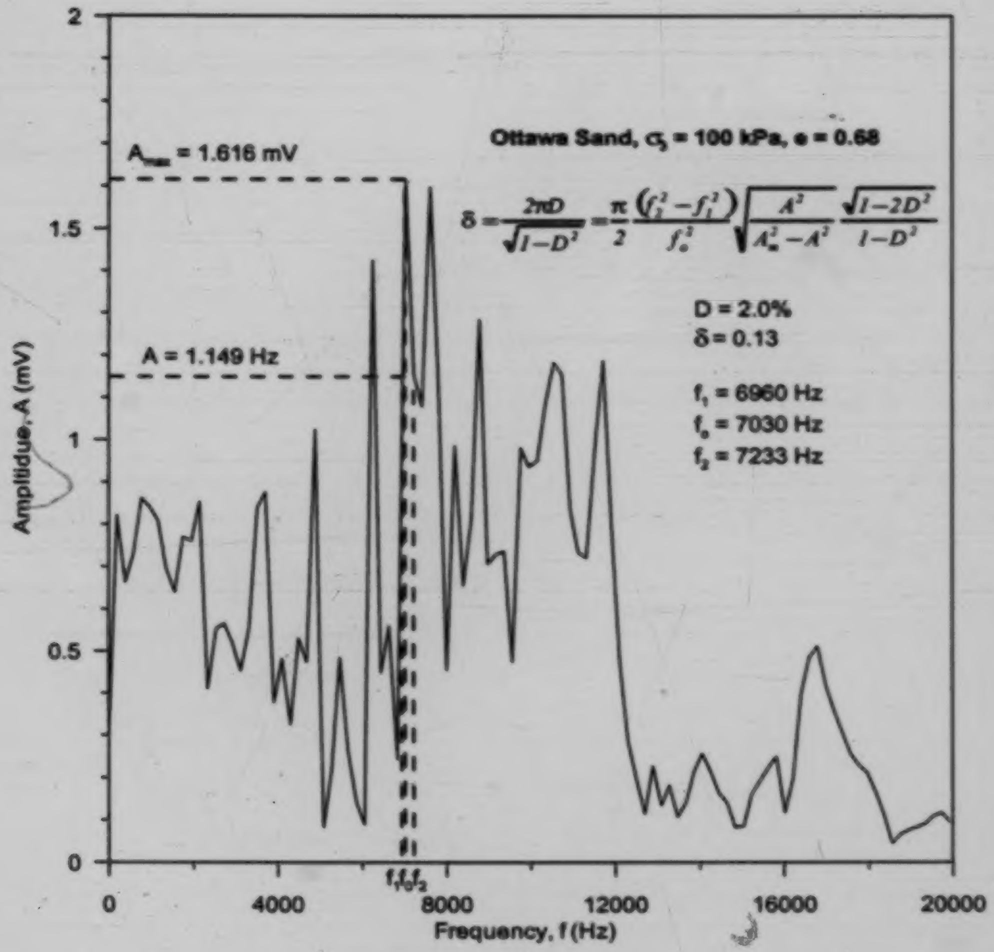

Figure 6.45 Typical amplitude-frequency curve obtained from triaxial cell apparatus and bender element tests of Ottawa sand, σ_3 = 100 kPa

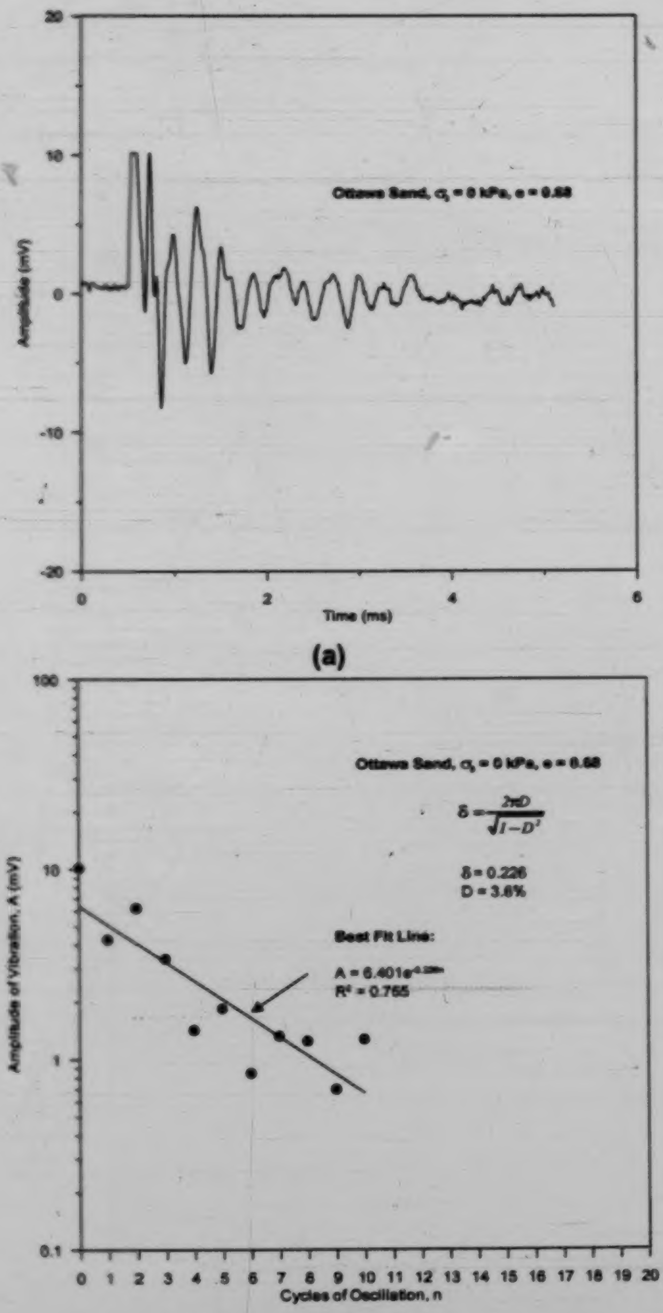

(a)

(b)

Figure 6.46 Dynamic properties obtained from triaxial cell apparatus and bender element tests of Ottawa sand, $\sigma_3 = 0$ kPa. (a) Amplitude-time decay curves. (b) Amplitude versus cycle number plot.

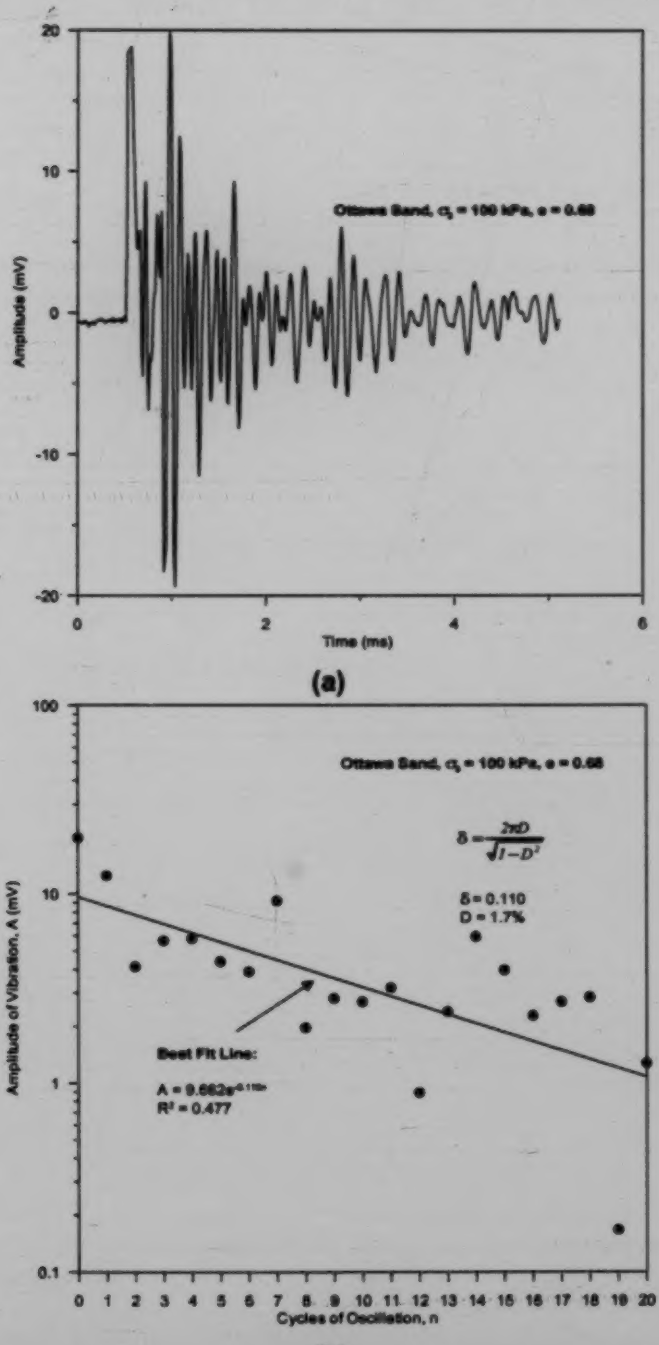

Figure 6.47 Dynamic properties obtained from triaxial cell apparatus and bender element tests of Ottawa sand, $\sigma_3 = 100$ kPa. (a) Amplitude-time decay curves. (b) Amplitude versus cycle number plot.

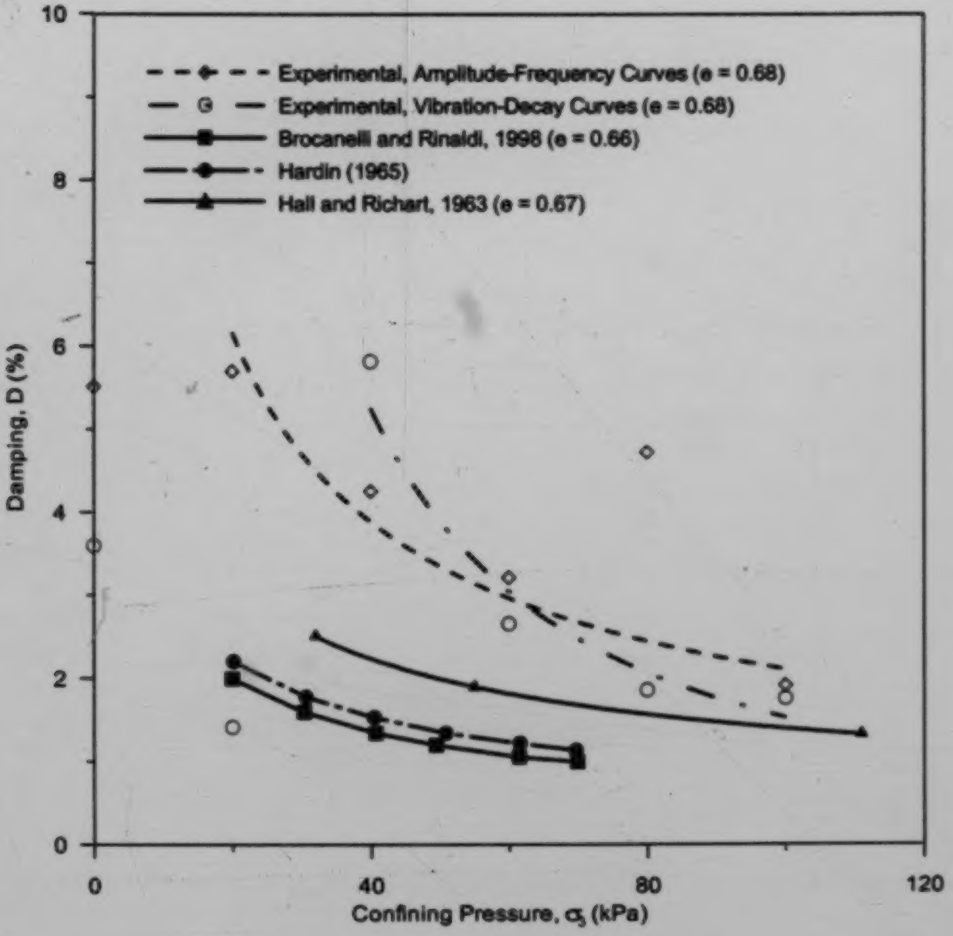

Figure 6.48 Comparisons of damping ratios of Ottawa sand under different confining pressures

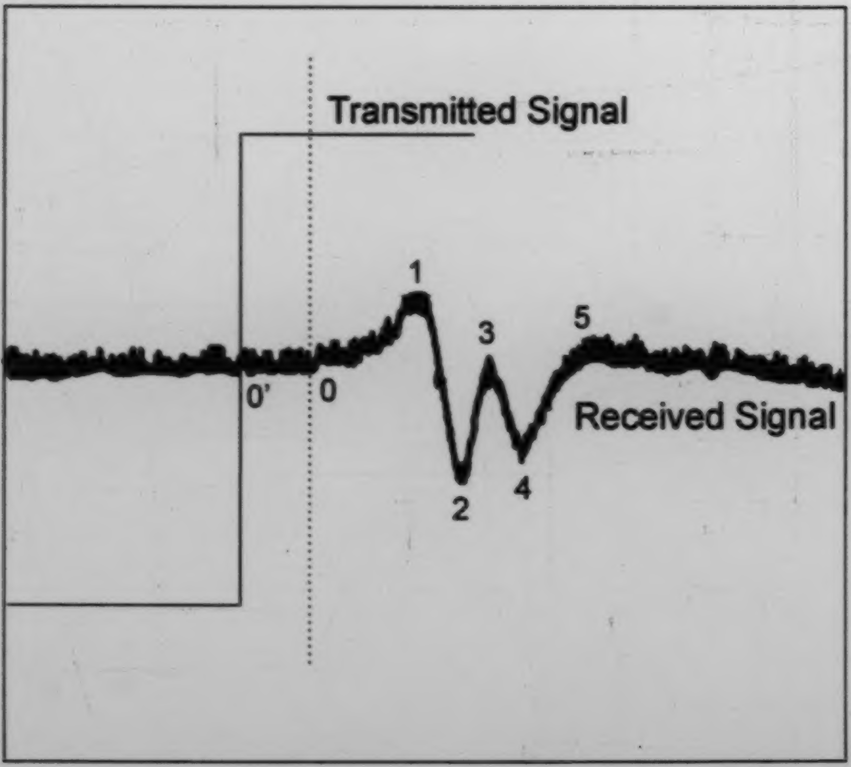

Figure 6.49 Typical oscilloscope signals from a bender element test with a square wave pulse excitation on boulder clay (modified from Viggiani and Atkinson, 1995)

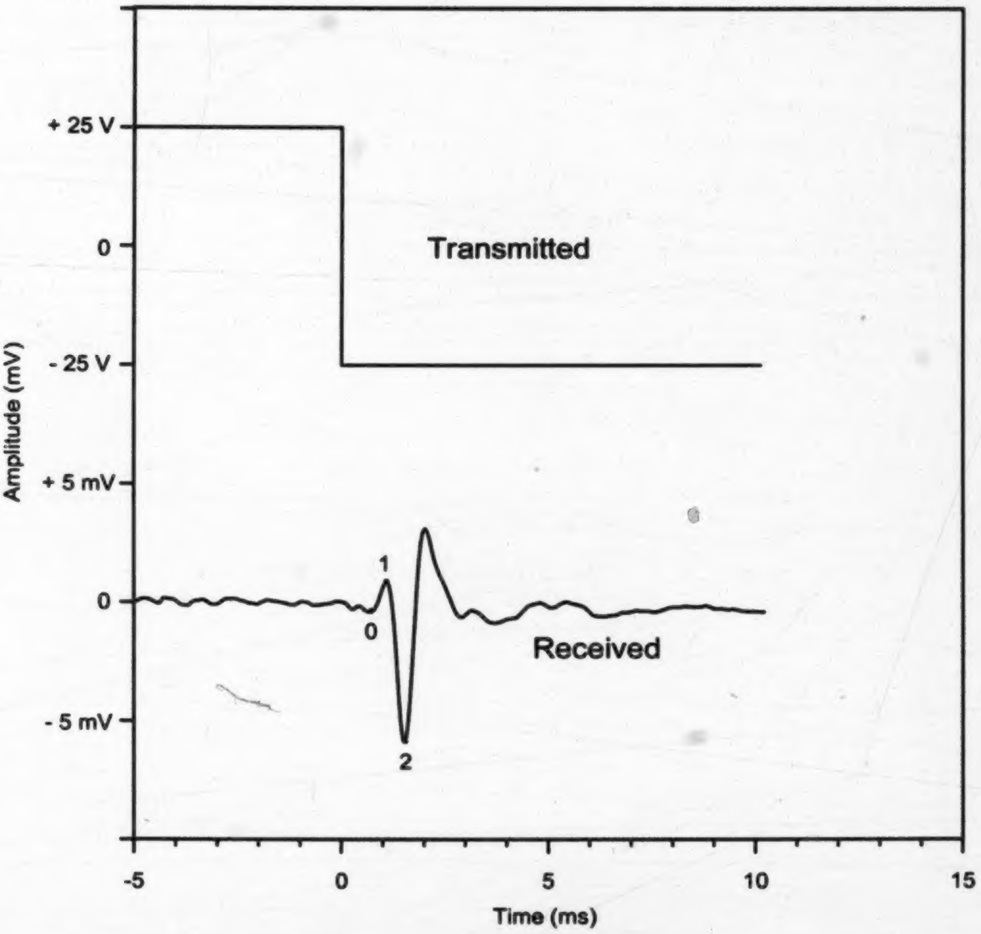

Figure 6.50 Typical oscilloscope signals from a bender element test on tire crumbs with a square wave excitation

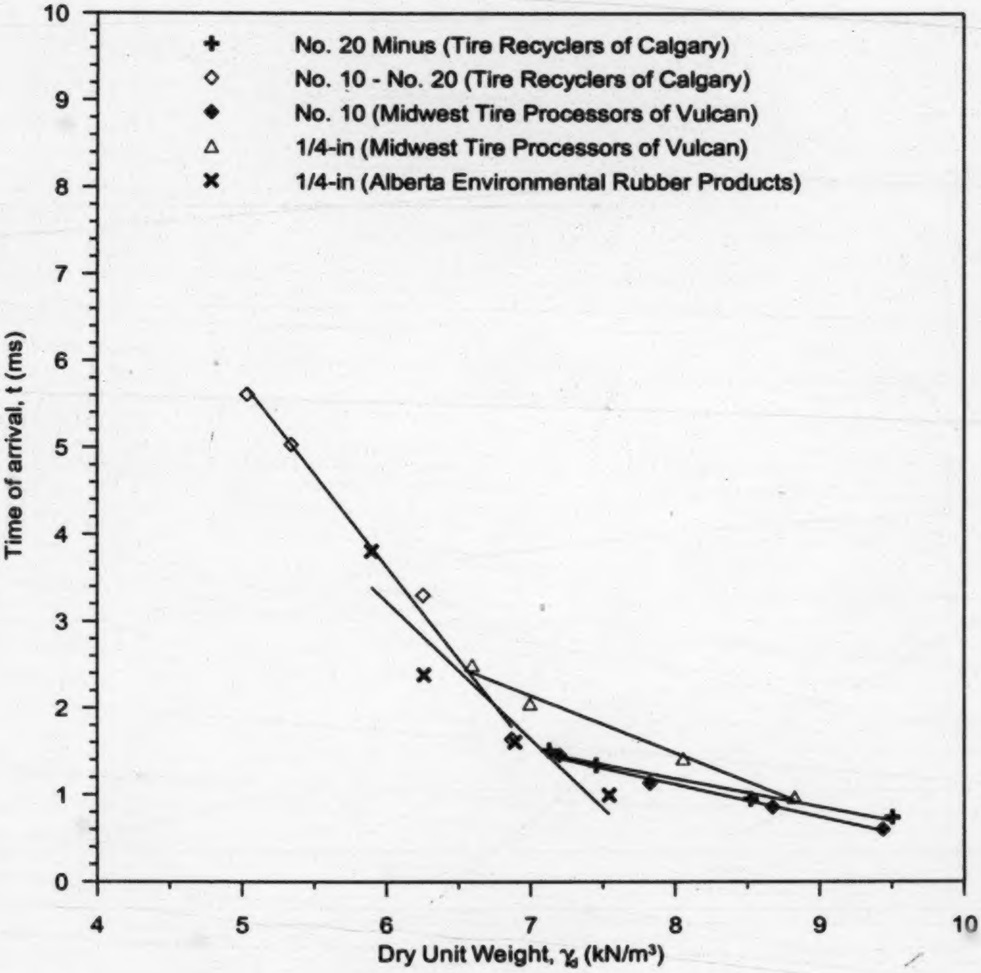

Figure 6.51 Times of arrival, t, versus dry unit weight

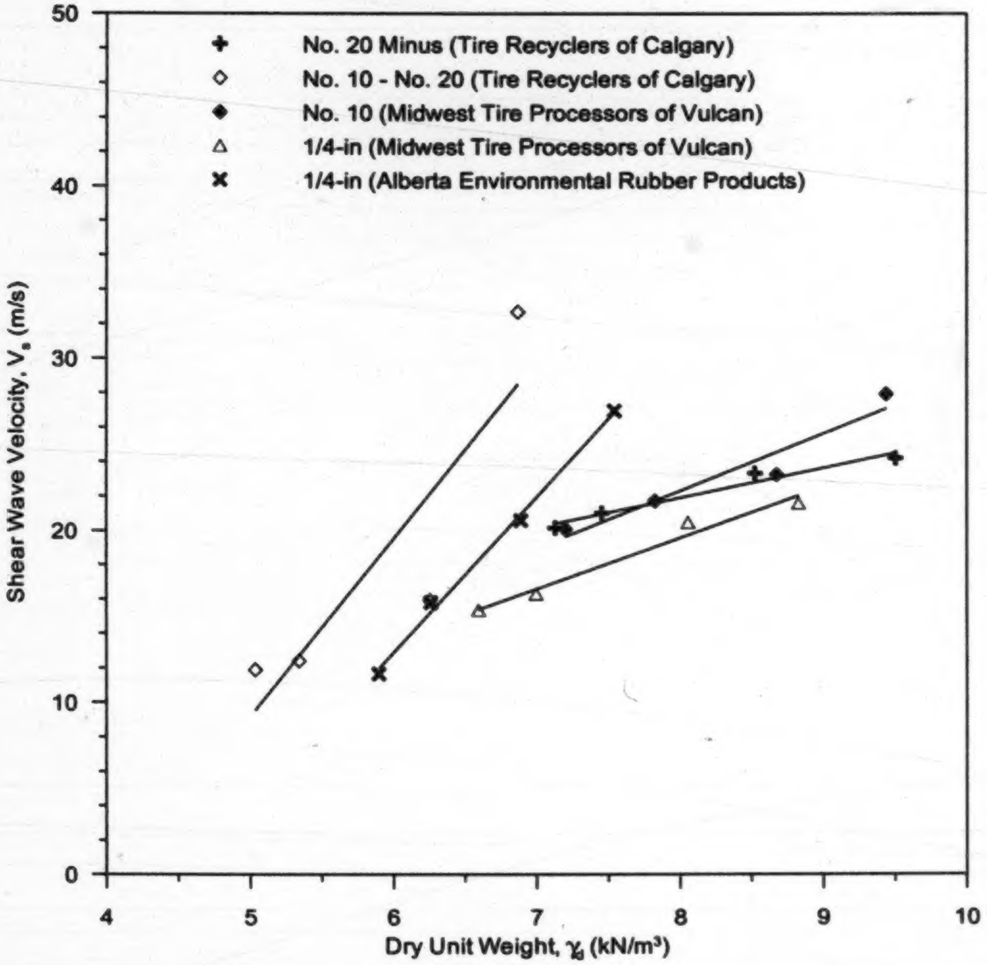

Figure 6.52 Shear wave velocity, V_s, as a function of dry unit weight

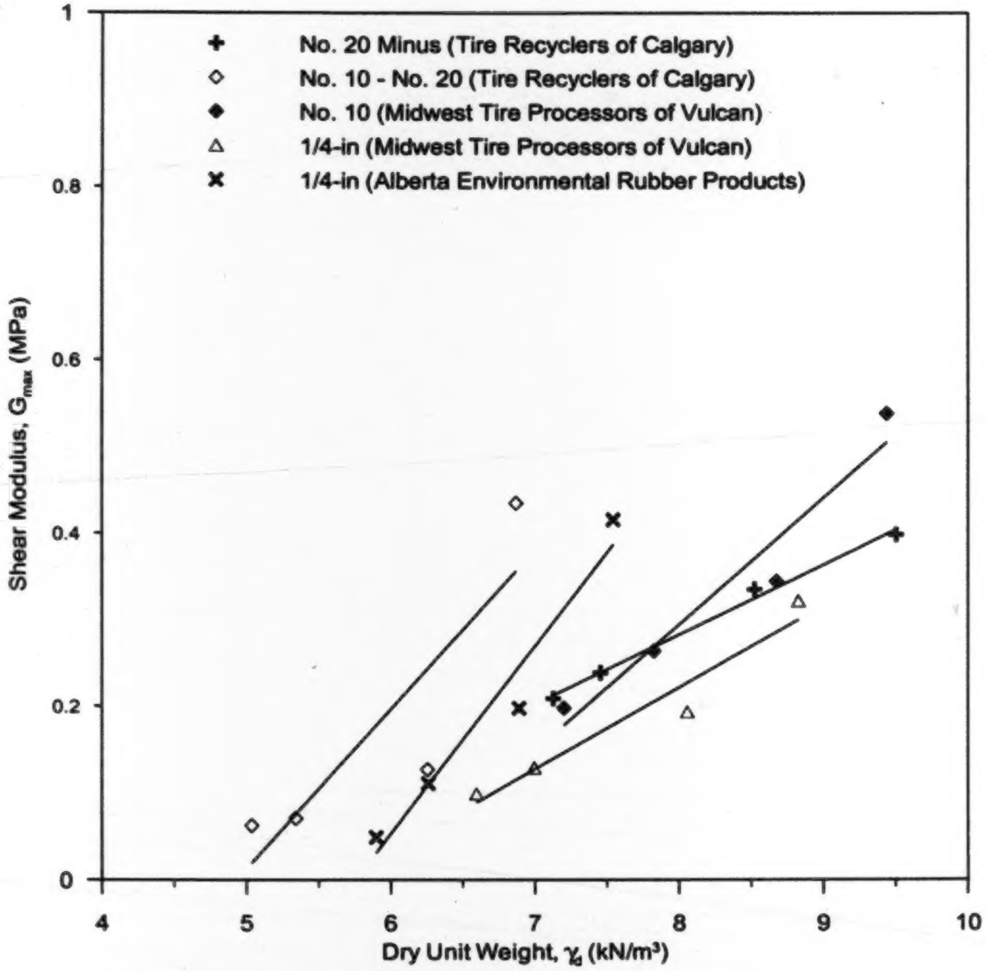

Figure 6.53 Shear modulus, G_{max}, as a function of dry unit weight

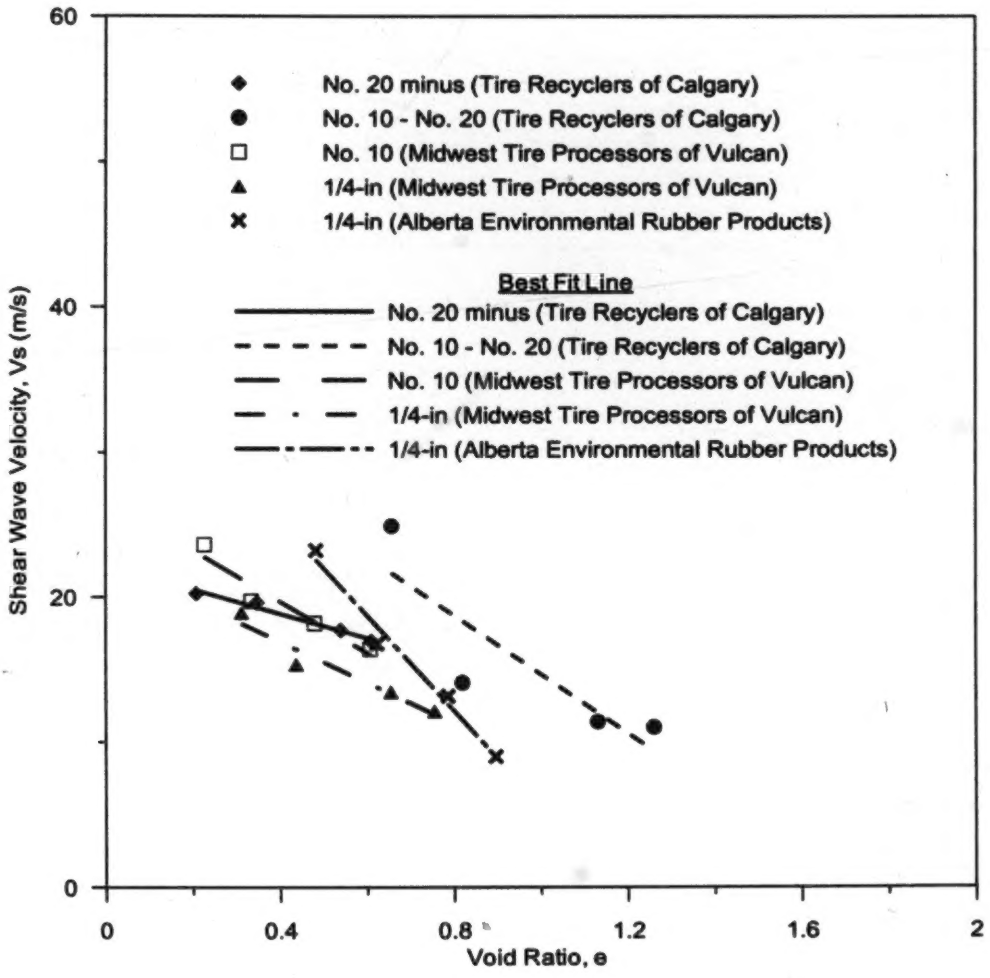

Figure 6.54 Shear wave velocity, V_s, as a function of void ratio, e

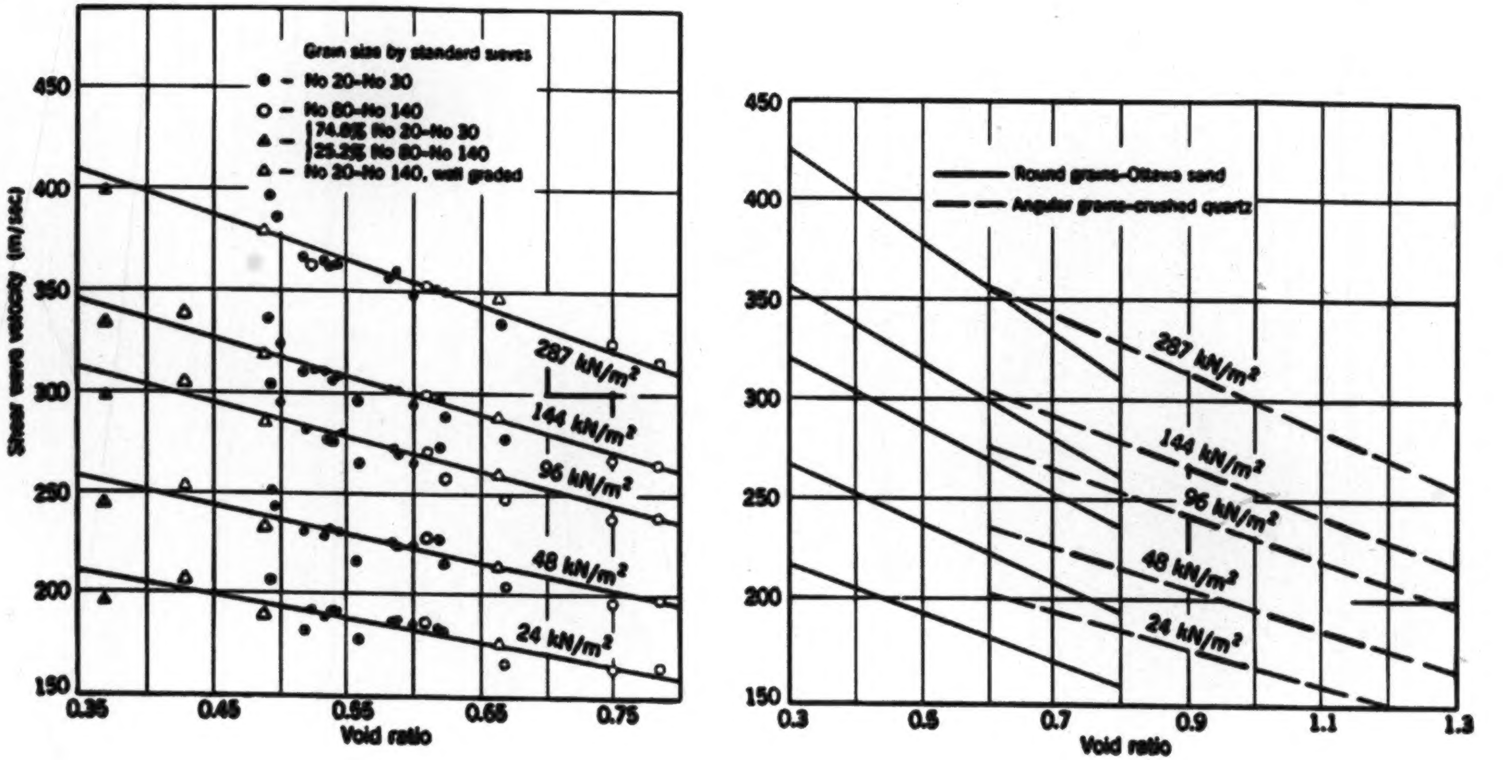

Figure 6.55 Shear wave velocities through quartz sands (after Hardin and Richart, 1963)

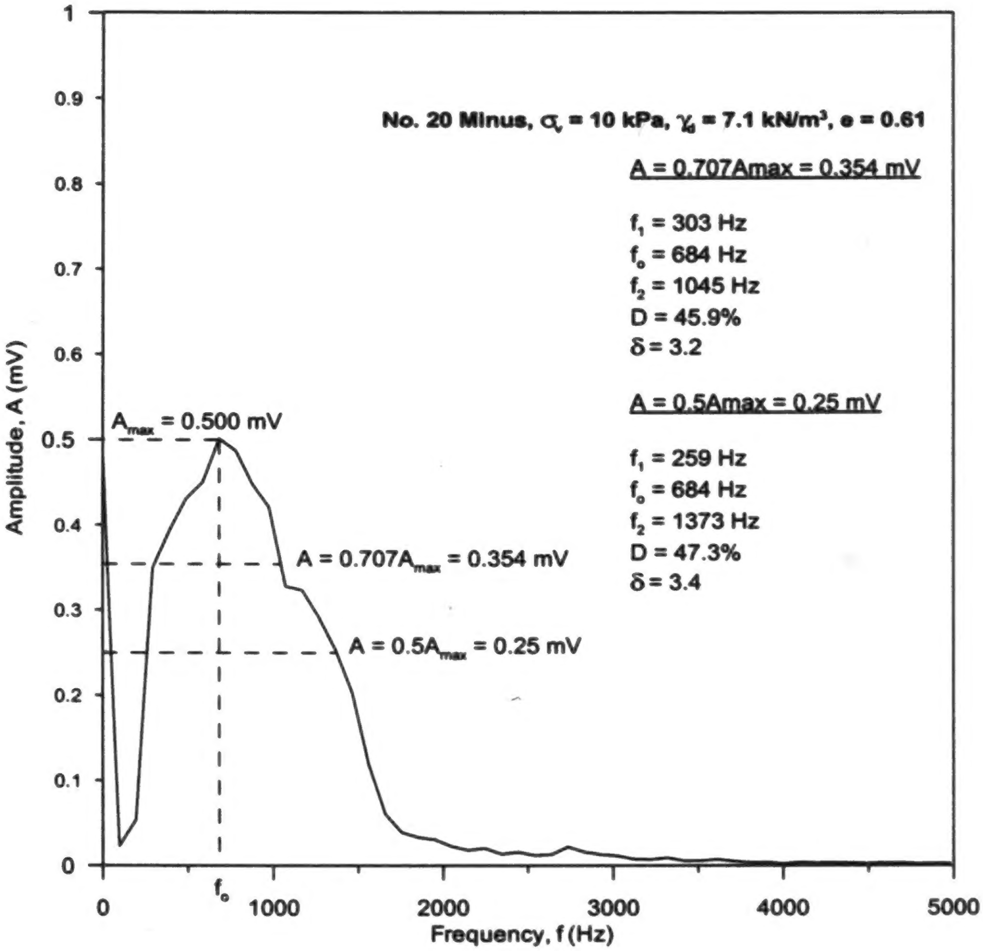

Figure 6.56 Amplitude-frequency curve for No. 20 minus tire crumbs, σ_v = 10 kPa

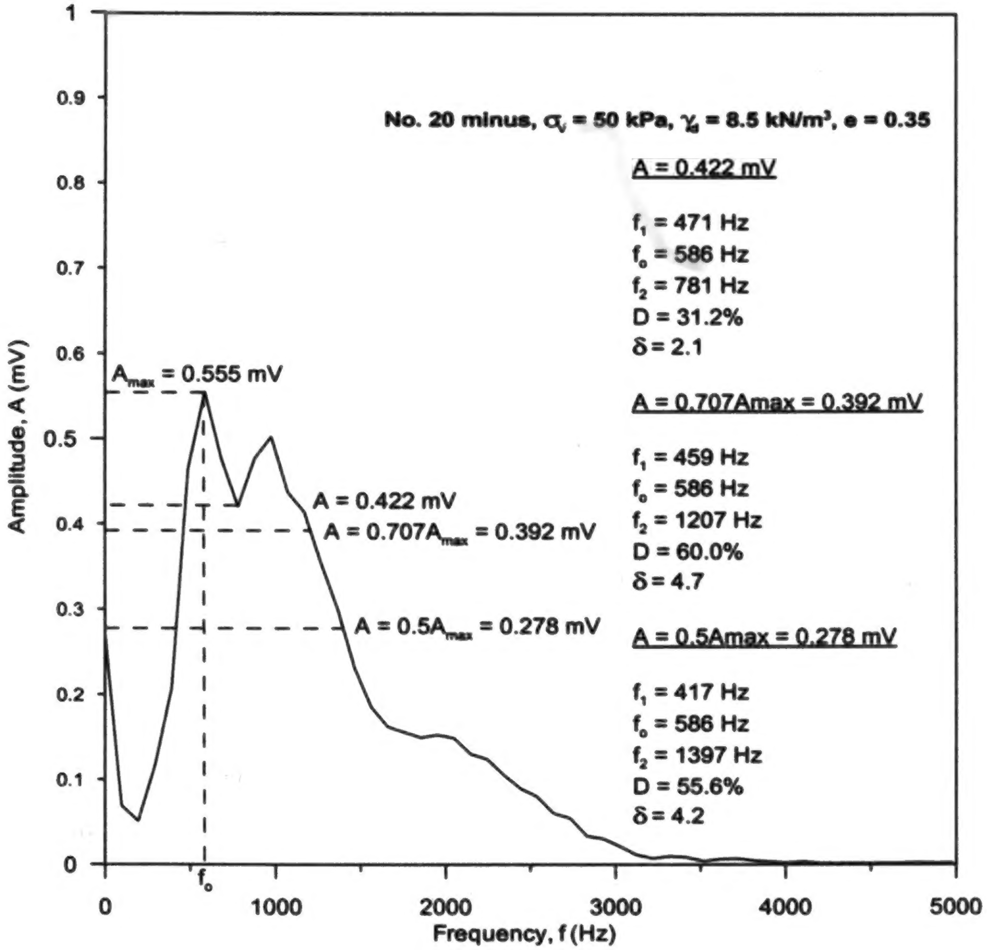

Figure 6.57 Amplitude-frequency curve for No. 20 minus tire crumbs, σ_v = 50 kPa

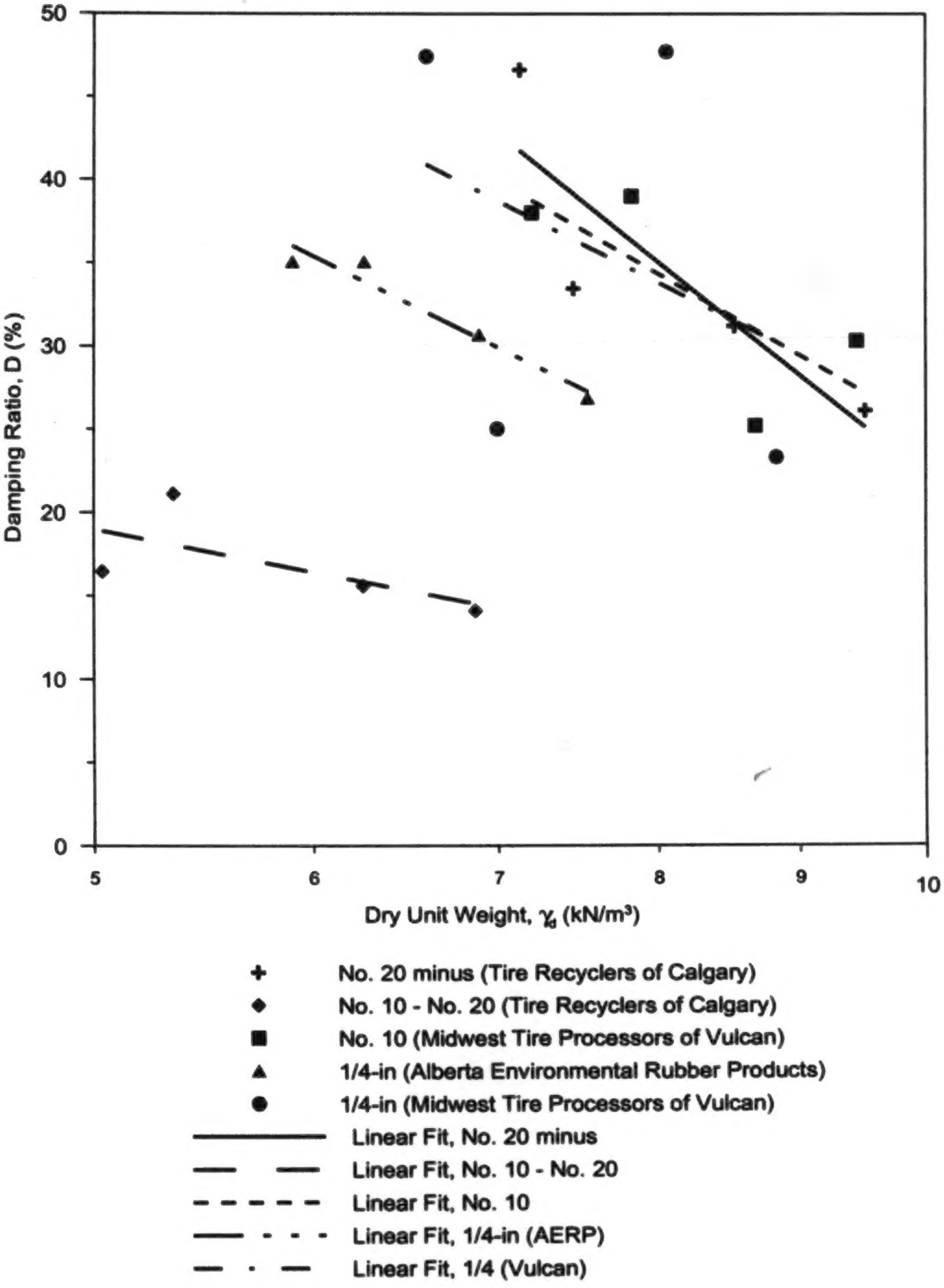

Figure 6.58 Variation of damping ratio, D, with dry unit weight, γ_d, for all tire crumb sizes tested

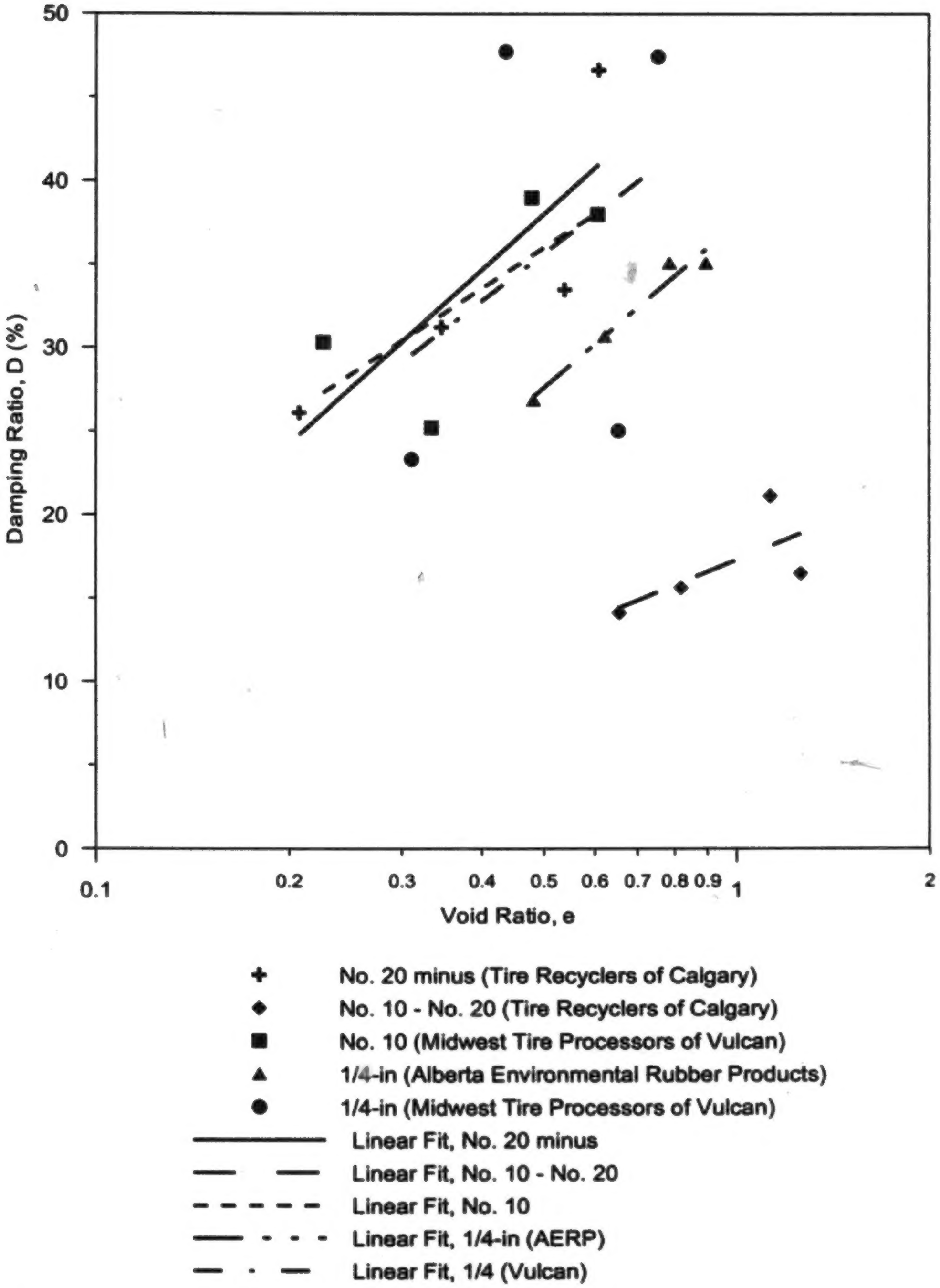

Figure 6.59 Variation of damping ratio, D, with void ratio, e, for all tire crumb sizes tested

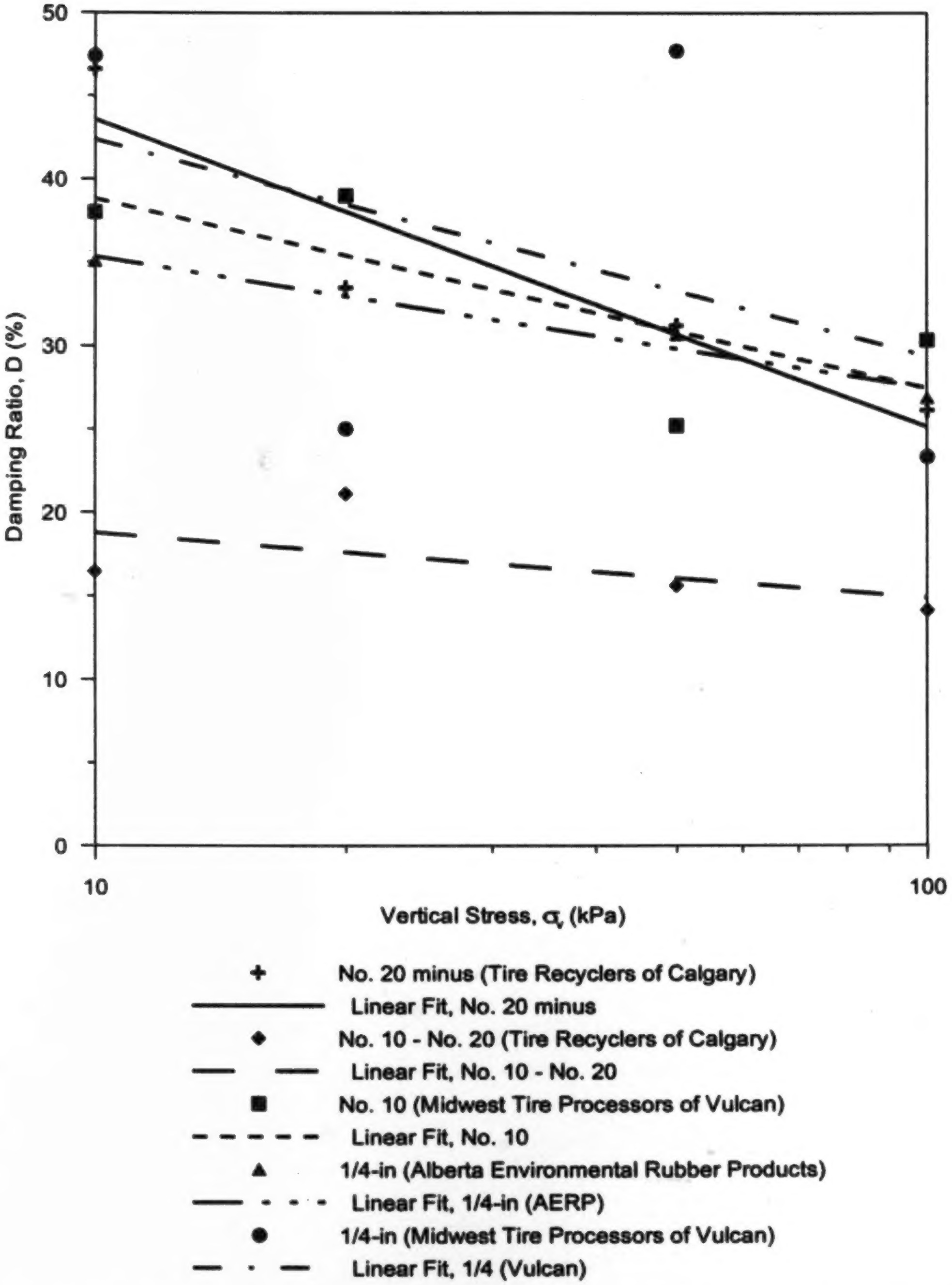

Figure 6.60 Variation of damping ratio, D, with vertical stress, σ_v, for all tire crumb sizes tested

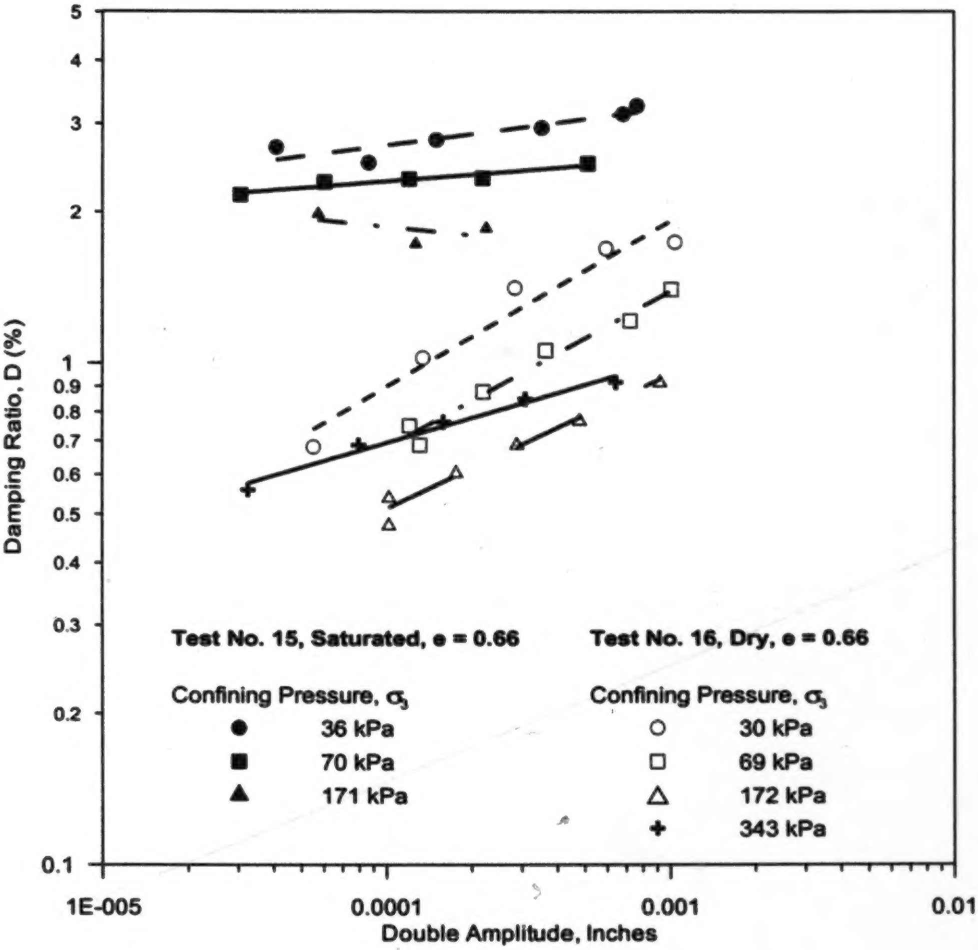

Figure 6.61 Comparison of the damping ratio with ampltidue for dry and saturated Ottawa sand in longitudinal oscillation, dense samples (modified from Hall and Richart, 1963)

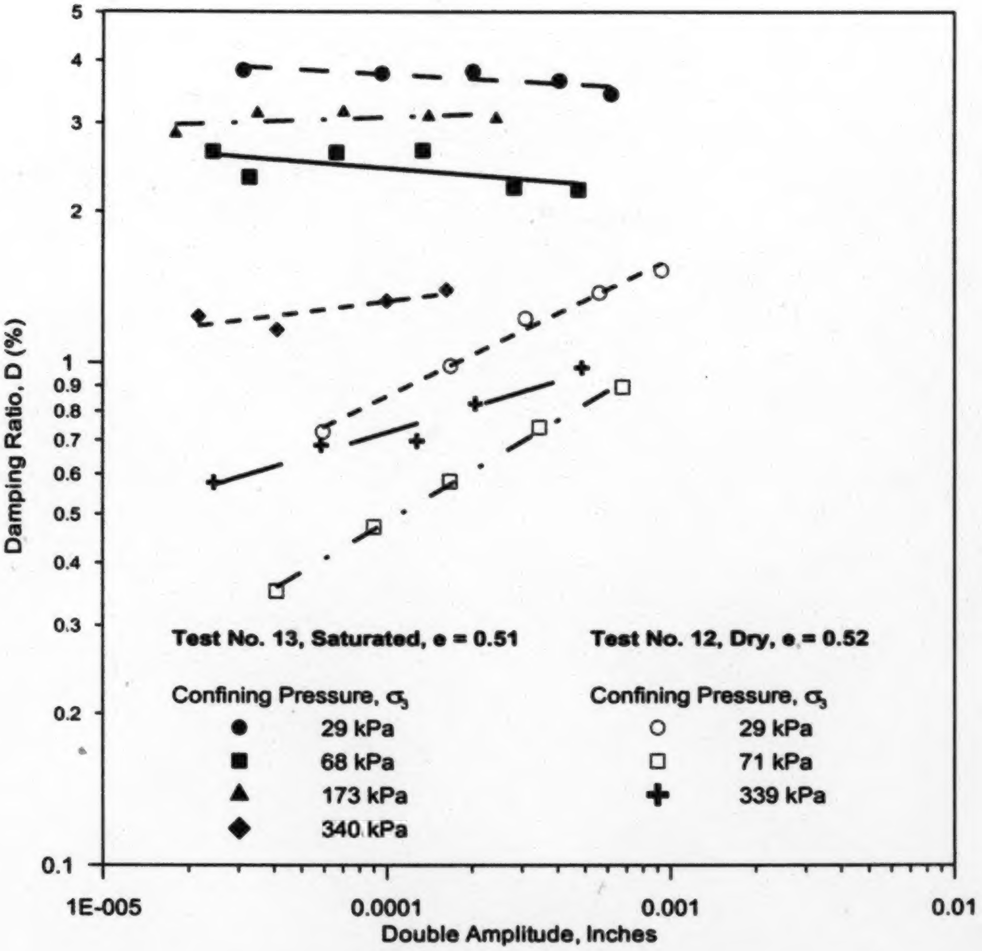

Figure 6.62 Comparison of the damping ratio with amplitude for dry and saturated Ottawa sand in longitudinal oscillation, loose samples (modified from Hall and Richart, 1963)

CHAPTER 7 CONCLUSIONS, AND RECOMENDATIONS

7.1 General

The scrap tire disposal problem presents an enormous and challenging task. In North America, over 300 million used automobile and truck tires are discarded annually. Until recently, scrap tires have generally been disposed of in landfills and stockpiles. Those buried in landfills tend to float back to the surface, and stockpiled tires present great environmental and heath concerns. An enormous potential exists in recycling these scrap tires into crumbed tire rubber and potentially using them in geotechnical engineering applications.

The first goal of this research was to conduct a detailed literature review to examine and compare the general behaviour and engineering properties of tire crumbs with tire shreds, and traditional geo-materials. Special focus was given to material property testing and evaluations. The literature review also examined, in detail, the sorption properties and leachability of recycled tire rubber. The findings from the literature review later provided a basis to proceed with laboratory testing. The second objective was primarily to focus on characterizing the geotechnical properties including particle size and distribution, specific gravity, compaction characteristics, compressibility, shear strength behaviour, thermal properties and dynamic properties. The geotechnical properties of crumbed tire rubber can be summarized as uniformly graded, lightweight, highly compressible, high strength, free draining, a good thermal insulator, and an excellent vibration dampener.

7.2 Summary and Conclusions

Tire crumb samples, which varied in particle shape, size, and gradation, were collected from three different suppliers in Alberta. The crumbs ranged in particle size from the No. 20 minus to 1/4 in. The physical characteristics were similar between crumbs with similar grain-size distribution produced from the Vulcan and Calgary suppliers. These generally had irregular, angular shaped torn particles with rough edges that were consistent with the crackermill process. Furthermore, the crumbs from the Vulcan and Calgary suppliers were produced mainly from the tires of passenger vehicles. Crumbs from the Edmonton supplier, on the other hand, were produced primarily from truck tires, which were uniformly shaped, angular cut particles with relatively clean edges. Tire crumbs produced from the Edmonton supplier were consistent with the granulator process. The crumbs produced from the Vulcan and Calgary suppliers also contained varying amounts of impurities (i.e. metal dust, fibre reinforcements, fine fibres, and rocks). The amount of impurities generally increased with increasing grain-size distribution. Crumbs from the Edmonton supplier, however, did not contain any impurities. It is likely that the level of QA/QC is the main factor contributing to the amount of impurities. A mechanical sieve analysis was also conducted, and the grain-size distribution curves generally indicated a uniform gradation. In comparisons to soils, the particle size and gradation are similar to that of uniform clean sands, and gravely-sand mixtures.

The specific gravity of tire crumbs is slightly greater than water, with values falling within a narrow range from 1.07 to 1.20. The values are comparable to that of tire shreds, however, the specific gravity of the shreds may be as high as 1.36 depending on the amount of steel wires. There was also little variation in the specific gravity between the different crumb sizes. However, tire crumbs obtained from the Edmonton supplier have slightly lower specific gravities than the crumbs obtained from both the Vulcan and Calgary suppliers. In general, the specific gravity of tire crumbs is generally less than half the typical values for soils.

The compaction characteristics were determined using ASTM standard test methods. Crumbs placed loosely into a compaction mold generally have dry unit weights ranging from 3.4 to 5.0 kN/m^3. The dry loose unit weight was found to increase with increasing grain-size because the larger-sized crumbs can achieve a more compact state due to fewer voids as a result of larger particle size. Newcomb and Drescher (1994) and Ahmed (1993), on the other hand, found that the dry uncompacted unit weight of tire shreds decreased with increasing shred size due to presence of exposed steel wires. Tire crumbs compacted in a vibratory table was found to have relatively consistent dry unit weights ranging between 5.3 to 5.7 kN/m^3. Compaction by vibratory methods, therefore, increased the dry unit weight of tire crumbs by 36 to 62%. Furthermore, tire crumbs compacted using vibratory methods show no apparent correlation between the compacted dry unit weight and grain-size distribution. This observation was also in agreement with Ahmed (1993) who used the same vibratory compaction procedures. He also found that for shreds larger than the 1/4 in, compaction by vibration was relatively ineffective. Further studies showed that the compaction characteristics of crumbs and shreds were relatively unaffected by compactive effort and particle size (Ahmed, 1993; Manion and Humphrey, 1992). In comparison to soils, the compacted dry unit weight is typically in the range from 19 to 21 kN/m^3. Hence, the dry unit weight of compacted tire crumbs is about one-fourth to one-third the typical values for soils.

One-dimensional confined compressibility tests were conducted under the condition of no lateral yield to determine the load-deformation and rebound behaviour of tire crumbs. Samples were placed loosely into a large-strain consolidation apparatus and vertical stresses of 10 kPa, 20 kPa, 50 kPa and 100 kPa were applied incrementally under dry and saturated conditions. Subsequent unloading and reloading tests were also conducted to evaluate the rebound and recompression behaviour. The load-deformation response of loose tire crumbs indicated the following: (a) high compressibility under low stresses primarily due to a reduction in voids; and (b) decreasing compressibility due to the bending and reorientation of highly compressible tire particles under loading to higher stresses. Loading under 100 kPa vertical stress caused about up to 50% compression strains, depending on the grain-size. There were also some irrecoverable strains upon unloading. The compressibility behaviour under saturated conditions was also similar, indicating that water has very little influence. The compressibility of tire crumbs was found to increase with decreasing grain-size. This contradicted the observations reported by Benda (1995) who found little variation between particle size, shape or distribution, density and compressibility for their crumb and shred samples that were consolidated under isotropic stress conditions. In comparison to shreds, loose tire crumbs are about 2 times more compressible under similar test conditions and vertical stresses. Compressibility tests carried out by Ahmed (1993) also showed that the particle size and compactive effort (standard and modified Proctor) had very little influence on the compressibility of both shreds and crumbs. However, they found that samples compacted using 50% standard Proctor underwent slightly greater compression strains (2 to 4% higher) during the first loading cycle than those compacted with the standard or modified effort. Furthermore, they found that loose shreds are about 1.5 to 2.5 times more compressible than compacted shreds under similar vertical stresses. The results obtained from this study and others indicated that the compressibility of tire crumbs can be significantly reduced by: (1) compaction; (2) increasing the overburden pressure; (3) using crumbs with larger particle size (i.e. 1/4 in); (3) using crumbs with a well-graded particle-size distribution; and (4) filling the air voids with a material that is less compressible than the crumb.

Constant head permeability tests were conducted using a large-strain consolidation apparatus. The influence of grain-size distribution, hydraulic gradients and overburden pressure on the hydraulic conductivity of tire crumbs was investigated. The most significant drop in hydraulic conductivity occurred under a vertical stress range between 0 to 20 kPa. Thereafter, the hydraulic conductivity was found to decrease almost linearly with increasing vertical stresses. There was also little variation in the hydraulic conductivity values between the different grain-sizes. In general, the hydraulic conductivities of tire crumbs were found to be in the range from 10^{-3} to 10^{-2} cm/s, which are typical values for clean sands and clean sand-gravel mixtures with similar grain-size distributions. Even under vertical stresses of up to 100 kPa, the hydraulic conductivity of tire crumbs still remained high. In comparison, the hydraulic conductivities of tire shreds are in the order of 10^{-1} to 10 cm/s; values that are more typical of clean gravels. Hence, the hydraulic conductivities of tire crumbs are about 1 to 4 orders of magnitude less than those reported for shreds under similar test conditions.

Transient state thermal conductivity tests were carried out using the thermal needle method to investigate to thermal properties of tire crumbs. Two different thermal tests apparatus were used. The thermal cells tested samples with different compaction, pore fluid, and temperature. To investigate the influence of vertical stress, and pore fluid, the combined thermal needle and large-strain consolidation apparatus was used. Based on comprehensive evaluations, several conclusions can be drawn from the thermal conductivity testing of tire crumbs:

- Water increased the thermal conductivity of dry tire crumbs by about 4 times for compacted samples, and by as much as 9 times for loose samples.
- For loose, unfrozen-saturated tire crumbs, the thermal conductivity approaches that of unfrozen water.
- For loose, frozen-saturated tire crumbs, the thermal conductivity approaches the value of ice.
- The thermal conductivity of saturated crumbs measured in the frozen state is about twice that measured in the unfrozen state.
- Compaction increased the thermal conductivity of both the frozen and unfrozen tire crumbs tested dry due to increased interfacial surface contacts between tire particles, which in turn resulted in better heat transfer across the contacts.
- For saturated frozen and unfrozen tire crumbs, compaction decreased the thermal conductivity since the tire rubber solid has a conductivity that is about 3 times less than water, and 10 times less than ice.
- The logarithm of thermal conductivity of dry tire crumbs increased linearly with increasing dry unit weight.
- For saturated tire crumbs, the logarithm of thermal conductivity decreased linearly with increasing dry unit weight.
- The combined thermal probe and consolidation apparatus generally gave slightly higher thermal conductivities than those measured using the thermal cells. The main reason was attributed to better particle contact under vertical stresses. Other factors include probe length, probe contact with the tire crumbs, and freeze-thaw processes.
- Dry tire crumbs, either loose or compacted, have the lowest thermal conductivities making them an excellent thermal insulator. Furthermore, the thermal conductivity of dry tire crumbs is relatively unaffected by temperature changes.

- The thermal conductivity of dry, tire crumbs is about 0.1 W/m-°C.

Direct shear tests were conducted on tire crumbs using a 100 mm shear box to measure the stress-deformation response. The tests were conducted dry and saturated under normal stresses of 25 kPa, 50 kPa , and 100 kPa. The following important conclusions were drawn concerning the shear strength behaviour of tire crumbs when sheared under a constant rate:

- Tire crumbs show an increase in shear resistance with increasing shear deformations.
- The increase in resistance behaviour is likely caused by the densification of the samples during shear, which resulted in compression and interlocking tire particles.
- Tire crumbs showed dilation at shear displacements between 4 to 6 mm, which was likely caused by the rolling and sliding of tire particles over one another after overcoming particle interlocking.
- Since tire crumbs do not exhibit well-defined peak shear resistance, the shear strength parameters must be established using the criterion of allowable deformations.
- Tire crumbs tend to exhibit some degree of apparent cohesion, which is most likely caused by the compressibility of tire particles, and by their unique angular shape that resulted in the interlocking of individual grains.
- It was found that moderate shear displacements of about 12 mm are required to develop an apparent cohesion of about 1 to 7 kPa, and to mobilize a friction angle of about 30 to 33°. In contrast, tire shreds may require significant shear displacements of up to 40 mm to mobilize the same strength and shearing resistance. The shear strength parameters found in this study showed are also in good agreement with those reported by Cecich et al. (1996).
- In comparison to granular soils, the shearing resistance of tire crumbs at high shear displacements are very similar to that of loose sands with a uniform gradation.

- The shearing resistance of tire crumbs also increased rapidly from 0 to 4 mm shear displacements. Thereafter, the resistance is reduced due to dilation. Further shear displacements beyond 8 mm showed even more reduction in resistance.
- It was found that crumbs with the smaller grain-size distribution generally showed higher shear resistance because smaller crumbs undergo higher vertical compression than the larger sizes under similar normal stresses. In addition, the smaller sized crumbs tend to lock together instead of rolling and sliding over one another unlike the larger grain-sizes.
- Saturated crumbs gave slightly lower shearing resistance than crumbs tested dry.

The shear strength of tire crumbs was measured by carrying out consolidated-drained triaxial compression tests on 60 mm diameter samples. The crumbs were first consolidated under isotropic stress conditions, and then sheared under confining stresses of 25 kPa, 50 kPa, and 100 kPa. The following conclusions are drawn regarding the shear strength of tire crumbs under triaxial compression:

- Unlike soils, tire crumbs do not fail by yielding or have a single shear plane. Instead the crumbs exhibited a strain-strengthening behaviour. The strain-strengthening behaviour is also consistent with those observed by other investigators for both tire crumbs and shreds (Masad et al., 1996; Benda, 1995; Ahmed, 1993)
- The majority of the samples tested showed linear stress-strain behaviour beyond 5% axial strains, with increasing shear resistance even up to 20% strains.
- The increase in resistance is likely due to inter-particle locking between tire particles during compression.
- Under low confining pressures of 25 and 50 kPa, decreasing volumetric strains were observed at up to about 5% axial strains, and thereafter stabilized with increased straining. Samples under low confining pressure also showed lateral bulging. However, under 100 kPa confining pressure,

volumetric strains did not stabilize but continued to decrease almost linearly with increasing axial strains. The volumetric behaviour under high confining pressure was also characterized by high material compression, but lateral bulging was not observed until 10 to 15% axial strains had occurred. The volumetric strain behaviour is consistent with those observed by Bernal et al. (1996)

- There does not appear to be a correlation between grain-size distribution and frictional resistance when the failure envelopes accounted for apparent cohesion. The ϕ' and c' values varied considerably between the different grain-sizes. The average ϕ' values ranged from 10 to 22° at 5 to 20% axial strains respectively for the crumb sizes tested. The c' values were in the range from 10 to 20 kPa, which were unreasonably high considering tire crumbs are inherently a cohesionless material. The shear strength parameters, however, were in the range reported by Ahmed (1993) for both shreds and crumbs.
- For the failure envelopes that were set through the origin, there was less variability in the shear resistance between the different grain-sizes, and hence, gave the best fit of data. With the exception of the 1/4 in crumb from the Vulcan supplier, there appeared to be a trend of increasing shear resistance with increasing grain-size. At 20% axial strains, the ϕ' values ranged between 27 to 30° for all the crumb sizes tested. These values are also consistent with those reported by Benda (1995) at higher strain levels.

Piezoceramic bender elements were incorporated into the triaxial cell and large-strain apparatus to measure the damping properties of tire crumbs. These tests were carried out dry for a number of different tire crumb sizes. Prior to conducting the tests on crumbs, the adequacy and reliability of the bender elements were assessed using Ottawa sand. The damping ratios for Ottawa sand obtain in this study were about 3 times higher (under low confining stresses) than the values reported by others (Brocanelli and Rinaldi, 1998; Hardin, 1965; Hall and Richart, 1963). The variations in damping are primarily due to different testing procedures, analysis, and equipment. The results on Ottawa sands, therefore, would indicate that tests carried out on tire crumbs with the bender elements used in this study would over-estimate its material damping. Some conclusions concerning the dynamic properties of tire crumbs are:

- The material damping taken directly from an experimental amplitude-frequency curve is highly subjective, and the procedure depends primarily on the frequency range, f_2 and f_1, bounded by the curve at a specified amplitude. In addition, the amplitude-frequency curve must be symmetrical with respect to the resonant frequency, f_o. The material damping taken where the curve does not plot symmetrical about f_o may over-estimated the damping ratio by a factor of 2.
- Damping of tire crumbs decreased with increasing vertical stress (or dry unit weight). Under low vertical stress, the damping ratio, D, varied from about 35 to 45%, while under higher vertical stress of up to 100 kPa, D decreased to about 25 to 35%.
- There was an observed trend of decreasing damping ratio with decreasing grain-size under higher vertical stresses. This observation is consistent with that reported by Hall and Richart (1963) who reported that the damping of glass beads decreased as the average grain-sizes decreased.
- Hall and Richart (1963) also showed that damping decreased with decreasing amplitude, increasing confining pressure, and increasing dry density. Water, however, increased damping by a factor of 1.5 to 4 times. The damping ratio of Ottawa sands are in the range of 0.5 to 2% for dry samples, and 2 to 4% for saturated samples.
- Tire crumbs are about 6 to 9 times more effective in damping vibrations than sands.

Recent studies have indicated that recycled tire rubber exhibits significant sorption capacity for both organic and inorganic compounds. The studies concluded the following:

- The sorption capacity of tire rubber is about 1 to 4% that of granular activated carbon (1.4 to 5.6% by tire volume basis)

- Competitive sorption between organic compounds does not occur.
- The sorption process is irreversible.
- The effects of pH and temperature were insignificant.
- Smaller-sized tire particles generally have greater sorption capacities than the larger particles due to higher surface area.
- Carbon black did not appear to play a significant role in the sorption of organic compounds.
- The primary sorption mechanisms of organic compounds are (a) diffusion; and (b) sorption of organic compounds onto the polymeric materials of tire rubber.
- Tire rubber pyrolytic chars have significant sorption capacity for large molecular weight compounds due to their development of macro pore structure as a result of the pyrolysis reaction.
- Pyrolytic chars showed sorption capacities that were significantly greater, or similar to general commercial activated carbons, but inferior to activated carbons specially designed for the removal of large molecular weight compounds.
- The sorption capacity of inorganic compounds (i.e. mercury) was dependent on tire particle size and surface area, solution temperature, and pH.
- Competitive sorption occurred for various inorganic compounds.
- Tire crumbs may therefore be useful to remove large organic molecules from pulp or other industrial wastes.

Leaching studies showed that tire rubber placed below the ground water table do not pose significant hazards to groundwater. The majority of the organics and inorganics tested were either not detected or the concentrations were below applicable drinking water standards. However, iron and zinc were the metals found that often exceeded to applicable drinking water standards.

7.3 Recommendations for Future Research

The results of this study indicate that crumbed tire rubber holds potential for a number of novel geotechnical applications. These may include incorporating tire crumbs in lightweight embankment fill, asphalt road pavement, drainage media in road subgrades and leachate collection systems, and for various soil amendment uses. However, using tire crumbs as a lightweight fill for example, may be regarded as a low-value application considering that extra costs are required to reduce the larger sized shreds into crumbs. Furthermore, tire shreds may prove to be a more suitable material than crumbs for certain applications from a material property and practicality standpoint.

The results of this study indicate that tire crumbs holds the greatest potential in thermal insulation, and vibration damping applications. However, a more detailed analytical and laboratory-testing program may be required to substantiate the findings from the preliminary thermal conductivity and dynamic investigations before proceeding on to field applications. The recommendations are discussed in the following subsections.

7.3.1 Thermal Insulation Applications

The recommendations for using tire crumbs in thermal insulation applications should include:

1. **Insulative concrete.** Tire crumb should be incorporated into Portland cement and tested as lightweight/insulative concrete.
2. **Modelling tire crumbs as an insulative barrier.** Tire crumbs should be modeled as an insulative barrier behind retaining structures or as an insulative cover over/around water pipes.

7.3.2 Vibration Damping Applications

The recommendations for using tire crumbs in vibration applications should include:

1. **Re-evaluation of material damping using bender elements.** The damping properties of tire crumbs were determined in this study from the amplitude-

frequency diagram. However, due to the subjectivity and difficulty associated with this procedure, it is recommended that the dynamic tests be carried out to include phase angle measurements. The damping ratio would then be obtained from the complex plane diagram as suggested by Ewins (1988) and demonstrated for Ottawa sand by Brocanelli and Rinaldi (1998).

2. **Alternative dynamic testing methods.** It is possible that the bender elements may not be an appropriate tool for measuring the damping properties of tire crumbs. Alternative dynamic test methods, including the resonant column, cyclic triaxial and cyclic simple shear tests may be more appropriate in this situation. It is strongly recommended that such tests be carried out initially on Ottawa sand to replicate or confirm the results reported by and Brocanelli and Rinaldi (1998), Hardin (1965) and Hall and Richart (1963). After doing so, the tests can then be carried out on tire crumbs under similar test conditions.
3. **Field scale tests.** Field-scale tests are also recommended to investigate using tire crumbs or rubber mats to mitigate vibration through soils.

7.3.3 Re-evaluation of Shear Strength Behaviour

It was unfortunate that the shear strength tests were not carried out to yield. Therefore, the shear strength data should be re-evaluated under the framework for spray ice (Instanes, 1993).

REFERENCES

AASHTO. 1986. Standard Specifications for Transportation Materials and Methods of Sampling and Testing, Part II: Methods of Sampling and Testing, 14th Edition, American Association of State Highway and Transportation Officials, Washington, DC., 1275 pp.

Ahmed, I. 1993. Laboratory Study on Properties of Rubber Soils. Report No. FHWA/IN/JHRP-93/94, Purdue University, West Lafayette, IN.

Al-Tabbaa, A., Blackwell, O. and Porter, S. A. 1997. An Investigation Into the Geotechnical Properties of Soil-Tyre Mixtures. Environmental Technology, 18: 855 – 860.

Alter, A. J. 1969. Water Supply in Cold Regions. U.S. Army Cold Regions Research Engineering Laboratory Monogram, 111-C5a.

Baykal, G. and Alpatli, H. M. 1994. Permeability of Rubber-Soil Liners Under Confinement. In. ASCE Geotechnical Special Publication No. 46, Geoenvironment 2000. Edited by Yalcin B. Acar and David E. Daniel, ASCE, 718 - 731.

Benda, C. C. 1995. Engineering Properties of Scrap Tires Used in Geotechnical Applications. Report 95-1, Materials and Research Division, Vermont Agency of Transportation, Montpelier, Vt.

Bernal, A., Lovell, C. W. and Salgado, R. 1996. Final Report, Laboratory Study on the use of Tire Shreds and Rubber-Sand in Backfills and Reinforced Soil Applications, FHWA/IN/JHRP-96/12, Purdue University, West Lafayette, Indiana.

Bernal, A., Salgado, R., Swan Jr., R. H. and Lovell, C. W. 1997. Interaction Between Tire Shreds, Rubber-Sands and Geosynthetics. Geosynthetics International, 4 (6): 623 - 643.

Blumenthal, M. H. 1996. Producing Ground Scrap Tire Rubber: A Comparison Between Ambient and Cryogenic Technologies. Proceedings. 17th Biennial Waste Processing Conference, Atlantic City, NJ, USA. pp. 367 - 374.

Borchardt, J. K. 1991. Recycling, Plastics. *In* Kirk-Othmer Encyclopedia of Chemical Technology, Vol. 21, Fourth Edition. John Wiley & Sons, New York, NY, pp. 41.

Brignoli, E. G. M., Gotti, M. and Stokoe, K. H. 1996. Measurement of Shear Waves in Laboratory Specimens, by Means of Piezoelectric transducers. Geotechnical Testing Journal, 19: 384 - 397.

Brocanelli, D. and Rinaldi, V. 1998. Measurement of Low-Strain Material Damping and Wave Velocity With Bender Elements in the Frequency Domain. Canadian Geotechnical Journal, 35 (6): 1032 - 1040.

Cecich, V., Gonzales, L. Hoisaeter, A. Williams, J. and Reddy, K. 1996. Use of Shredded Tires as Lightweight Backfill Material for Retaining Structures. Waste Management & Reasearch, 14: 433 - 451.

Chen, L. S. 1948. An Investigation of Stress-Strain and Strength Characteristics of Cohesionless Soils by Triaxial Compression Tests. Proceedings. 2nd International Conference in Soil Mechanics and Foundation Engineering, Vol. 5., p. 35.

Clark, C., Meardon, K. and Russel, D. 1991. Burning Tires for Fuel and Tire Pyrolysis: Air Implications, EPA-450/3-91-024, December.

Cunning, J. 1994. Shear Wave Velocity Measurement of Cohesionless Soils for the Evaluation of In-situ State. M.Sc. thesis, University of Alberta, Edmonton, AB.

Das, B. 1982. Soil Mechanics Laboratory Manual, 1st Edition, Engineering Press Inc., San Jose, CA.

D'Eustachio, D. and Schreiner, R. E. 1952. A Study of a Transient Method for Measuring Thermal Conductivity. Transactions of the American Society of Heating and Ventilating Engineers, Vol. 58, June, pp. 113 - 117.

Dodds, J., Domenico, W. F., Evans, D. R., Fish, L. W., Lassahn, P. L. and Toth, W. J. 1983. Scrap Tires: A Resource and Technology Evaluation of Tire Pyrolysis and Other Selected Alternative Technologies, Rep. EGG-2241, U. S. Dept. of Energy, Washington, D. C.

Dudas, M. J. 1998. Soils 450: Soil Environmental Chemistry Lecture Notes, Winter 1998. University of Alberta, AB.

Duffy, D. P. 1995. Using Tire Chips as a Leachate Drainage Layer, Waste Age, September, pp. 113 - 122.

Dyvik, R. and Madshus, C. 1985. Lab Measurements of G_{max} Using Bender Elements. Advances in the Art of Testing Soils Under Cyclic Conditions, Proceedings of a session sponsored by the Geotechnical Engineering Division, ASCE Detroit Convention.

Edil, T. B. and Bosscher, P. J. 1994. Engineering Properties of Tire Chips and Soil Mixtures. Geotechnical Testing Journal, 17 (4): 453 - 464.

Edil, T. B. and Bosscher, P.J. 1992. Development of Engineering Criteria for Shredded Waste Tires in Highway Applications, Final Report to Wisconsin Departments of Transportation and Natural Resources. Research Report GT-92-9, Madison, WI.

Edil, T. B., Bosscher, P. J. and Eldin, N. N. 1990. Development of Engineering Criteria for Shredded or Whole Tires in Highway Applications, Interim Report to Wisconsin Department of Transportation, Madison, WI.

Edil, T. B., Fox, P. J. and Ahl, S. W. 1992. Hydraulic Conductivity and Compressibility of Waste Tire Chips. Proceedings. 15th Annual Madison Waste Conference, Department of Engineering Professional Development, University of Wisconsin, Madison, pp. 49 - 61.

Envirologic, Inc. 1990. A Report on the use of Shredded Scrap Tires in On-Site Sewage Disposal Systems/prepared for: The Department of Environmental Conservation, State of Vermont, Recycling Market Development Grant. Envirologic, Inc., Brattleboro, VT.

Ewins, D. J. 1988. Model Testing: Theory and Practise. Research Studies Press ltd., Letchworth, Hertfordshire, England.

Farouki, O. T. Thermal Properties of Soils, CRREL Monograph 81-1. U.S. Army Cold Regions Research and Engineering Laboratory, Hanover, New Hampshire.

Griffith, G. P. 1975. Removal of ionic mercury from waste water using modified scrap rubber. Removal of Soluble Mercury from Waste Water Complexing Techniques, Bulletin 74, Virgina Water Resources Research Center.

Hall, J. R. and Richart, F. E. 1963. Dissipation of Elastic Wave Energy In Granular Soils. Journal of Soil Mechanics and Foundation Division, Proceedings of the American Society of Civil Engineers, Vol. 89, No. SM6, pp. 27 - 56.

Handreck, K. A. 1996. Zinc Toxicity From Tire Rubber in Soilless Potting Media. Communications in Soil Science and Plant Analysis, 27 (13 - 14): 2615 - 2623.

Hardin, B. O. 1965. The Nature of Damping in Sands. Journal of the Soil Mechanics and Foundations Division, ASCE, 91 (SM1): 63 - 97.

Hough, B. K. 1969. Basic Soils Engineering, 2nd Edition, The Ronald Press Company, New York.

Hughes, C. S. 1993. Scrap Tire Utilization Technologies. National Asphalt Pavement Association and State Asphalt Pavement Association Executives, Lanham, MD.

Humenick, M. J. Jr. and Schoor, J. L. 1974. Emproving Hg (II) Removal by Activated Carbon. Journal of Environmental Engineering Division, American Society of Civil Engineers 100, No. EE6.

Humphrey, D. N. and Eaton, R. A. 1993a. Tire Chips as Insulation Beneath Gravel Surfaced Roads, Proceedings of the Second International Symposium on Frost in Geotechnical Engineering, A. A. Balkema, Rotterdam, Netherlands, pp. 137 - 149.

Humphrey, D. N. and Eaton, R. A. 1993b. Tire Chips as Subgrade Insulation - Field Trail, Proceedings of the Symposium on Recovery and Effective Reuse of Discarded Materials and By-Products for Construction of Highway Facilities, Federal Higway Administration, Washington, D.C., pp. 5 - 68.

Humphrey, D. N. and Eaton, R. A. 1994. Performance of Tire Chips as an Insulating Layer Beneath Gravel Surface Roads, Proceedings of the Fourth International Symposium on Cold Region Development, Espoo, Finland, pp. 125 - 126.

Humphrey, D. N. and Eaton, R. A. 1995. Filed Performance of Tire Chips as Subgrade Insulation for Rural Roads, Proceedings of the Sixth International Conference on Low-Volume Roads, Transportation Research Board, Vol. 2.

Humphrey, D. N. and Katz, L. E. 1996. Water Quality Testing for Dingley Road Tire Chip Test Project, Report for Town of Richmond, Maine. Department of Civil and Environmental Engineering, University of Maine, Orono, Maine.

Humphrey, D. N. and Manion, W. P. 1992. Tire Chips as Lightweight and Conventional Embankment Fill: Phase I – Laboratory. University of Maine, Department of Civil and Environmental Engineering, Orono, Maine.

Humphrey, D. N. and Sandford, T. 1993. Tire Chips as Lighweight Subgrade fill and Retaining Wall Backfill. Proceedings. Symposium on Recovery and Effective Reuse of Discarded Materials and By-Products for Construction of Highway Facilities, Federal Highway Administration, Denver, pp. 5-55 – 5-68.

Humphrey, D. N., Katz, L. E. and Blumenthal, M. 1997. Water Quality Effects of Tire Chip Fills Placed Above the Groundwater Table. Proceedings. *In* Testing Soil Mixed with Waste or Recycled Materials, ASTM STP 1275. *Edited by* Mark A. Wasemiller and Keith B. Hoddinott.

Humphrey, D. N., Sandford, T. C., Cribbs, M. M., Gharegrat, H. G. and Manion, W. P. 1992. Tire Chips as Lightweight Backfill for Retaining Walls – Phase I: A Study for the New England Transportation Consortium. University of Maine, Department of Civil Engineering, Orono, Maine.

Humphrey, D. N., Sandford, T. C., Cribbs, M. M., Gharegrat, H., and Manion, W. P. 1993. Shear Strength and Compressibility of Tire Chips for use as Retaining Wall Backfill. Transportation Research Board No. 1422, Transportation Research Board, pp. 29 - 35.

Instanes, A. 1993. An Experimental Study of the Mechanical Behaviour of Spray Ice. Ph.D. thesis, Norwegian Institute of Technology, Oslo, Norway.

Johnston, G. H. 1981. Permafrost, engineering design and construction. Wiley & Sons, Toronto, ON.

Jovičić, V., Coop, M. R. and Simić, M. 1996. Objective Criteria for Determining G_{max} From Bender Element Tests. Géotechnique, 46 (2): 357 - 362

Kershaw, D. S. and Pamukcu, S. 1997. Use of Ground Tire Rubber in Reactive Permeable Barriers to Mitigate BTEX Compounds. *In* Testing Soil Mixed with Waste or Recycled Materials, ASTM STP 1275. *Edited by* Mark A. Wasemiller and Keith B. Hoddinott.

Kim, J. Y., Park, J. K. and Edil, T. B. 1997. Sorption of Organic Compounds in the Aqueous Phase Onto Tire Rubber. Journal of Environmental Engineering, 123 (9): 827 - 835.

Knocke, W. R. and Hemphill, L. H. 1981. Mercury (II) sorption by waste rubber. Water Research, 15 (2): 275 - 282.

Kohler, R. 1996. Cryogenic Processing of Scrap Tires. Polymer Recycling, 2 (2): 83 - 88.

Manion, W. P. and Humphrey, D. N. 1992. Tire Chips as Lightweight and Conventional Embankment Fill, Phase I - Laboratory: A Study for the main Department of Transportation. Department of Civil and Environmental Engineering, University of Maine, Orono, Maine.

Mark, J. E., Erman, B. and Eirich, F. R. 1994. Science and Technology of Rubber, 2nd Edition, Academic Press.

Masad, E., Taha, R., Ho, C. and Papagiannakis, T. 1996. Engineering Properties of Tire/Soil Mixtures as a Lightweight Fill Material. ASTM Geotechnical Testing Journal, 19 (3): 297 - 304.

Matthews, J. and Silverman, P. 1991. The Road to Less Waste: Recycling New York State's Scrap Tires into Asphalt Paving Material. A Staff Report to the Chairman Assemblymember Maurice D. Hinchey NYS Legislative Commission on Solid Waste Management, Albany, New York.

McCullough, B. 1998. Personal communications. Alberta Environmental Rubber Products, 13500 156 Street NW, Edmonton, AB., Canada.

Meng, X., Hua, Z., Dermatas, D., Wang, W. and Kuo, H. Y. 1998. Immobilization of Mercury (II) in Contaminated Soil With Used Tire Rubber. Journal of Harzardous Materials, 57 (1 - 3): 231 - 241.

Mitchell, J. K. and Kao, T. C. 1978. Measurement of Soil Thermal Resistivity. A.S.C.E. Proceedings GT, Journal of Geotechnical Engineering Division, ASCE, New York, Vol. 104, No. GT19, pp. 1307 - 1320.

National Instruments Corporation. 2000. 11500 N Mopac Expwy, Austin, TX.

Newcomb, D. E. and Drescher, A. 1995. Engineering Properties of Shredded Tires in Lightweight Fill Applications. Transportation Research Record 1437, pp. 1 - 7.

Nightingale, D. 1997. Tire Chips, Roadbeds, and Spontaneous Reactions: The Autocombustion Theory. Proceedings of the 1997 SWANA Northwest Regional Solid Waste Symposium, Seattle Washington, Solid Waste Association of North America.

Nightingale, D. E. B. and Green, W. P. 1997. An Unresolved Riddle: Tire Chips, Two roadbeds and Spontaneous Reactions. *In* Testing Soil Mixed with Waste or Recycled Materials, ASTM STP 1275. *Edited by* Mark A. Wasemiller and Keith B. Hoddinott.

OMEGA Engineering, Inc. 1995. The Temperature Handbook ™, Vol. 29. OMEGA Engineering, Inc., Stanford, CT.

Park, J. K., Kim, J. Y. and Edil, T. B. 1996. Mitigation of Organic Compound Movement in Landfills by a Layer of Shredded Tires. Water Environment Research, 68 (1): 4 - 10.

Park, J. K., Kim, J. Y., Madsen, C. D. and Edil, T. B. 1997. Retardation of Volatile Organic Compound Movement by a Soil-Bentonite Slurry Cutoff Wall Amended With Ground Tires. Water Environment Research, 69 (5): 1022 - 1031.

Perry, R. H., Green, D. W. and Maloney, J. O. 1997. Perry's Chemical Engineer's Handbook, 7th Edition. McGraw-Hill, New York, NY.

Qiu, Y. and Sego, D. C. 1998. Laboratory test method for mine tailings. Proceedings. 51st Canadian Geotechnical Conference, Edmonton, AB. pp. 155.

Radian Corporation. 1989. A Report on the RMA TCLP Assessment Project: Prepared for the Rubber Manufacturers Association. Washington, D.C.

Rao, S. S. 1995. Mechanical Vibrations, 3rd Edition. Addison-Wesley Publishing Company.

Read, J., Dotson, T. and Thomas, J. 1991. Experimental Project use of Shredded Tires for Lightweight Fill, Post Construction Report. Oregon State Division of Highways, DTFH-71-90-601-OR-11, February.

Recycler's World. Granulated Rubber (Tire Crumb) Category. < http://www.recycle.net/recycle/Rubber/granule/index.html>. March 2000.

Richart, Jr., F. E., Hall, Jr. and Woods, R. D. 1970. Vibrations of Soils and Foundations, Prentice-Hall, Englewood Cliffs, N.J.

Rollins, K. M., Evans, M. D., and Diehl, N. B. 1998. Shear Modulus and Damping Relationships for gravels. Journal of Geotechnical and Geoenvironmental Engineering, 124 (7): 585 - 594.

Rollins, K. M., Evans, M. D., Diehl, N. B. and Daily, W. D. 1998. Shear Modulus and Damping Relationships for Gravels. Journal of Geotechnical and Geoenvironmental Engineering, 124 (7): 396 - 405.

Romero, S. and Pamukcu, S. 1997. Prediction of Dynamic Properties by Low Strain Excitation of Residual Materials. *In* Testing Soil Mixed with Waste or Recycled Materials, ASTM STP 1275. *Edited by* Mark A. Wasemiller and Keith B. Hoddinott.

Rowley, A. G., Husband, F. M. and Cunningham, A. B. 1984. Mechanisms of metal adsorption from aqueous solutions by waste tyre rubber. Water Research, 18 (8): 981 - 984.

Ruff, W. J. and Scott, J. R. 1971. Fibres, Films, Plastics and Rubbers. Butterowrths Scientific Publications, London, England.

Salinero, I. S., Ropesset, J. M. and Stokoe, K. H. 1986. Analytical studies of body wave propagation and attenuation. Report GR 86-15. University of Texas at Austion.

San Miguel, G., Fowler, G. D. and Sollars, C. J. 1998. Pyrolysis of tire rubber: Porosity and adsorption characteristics of the pyrolytic chars. Industrial Engineering Chemistry Resource, 37: 2430 - 2435.

Shao, J., Sarling, J. P. and Esch, D. 1996. Thermal Conductivity of Recycled Tire Rubber for Insulation Beneath Roadways. Transportation Research Record. (In Press)

Smith, W. O. and Byers, M. G. 1938. The Thermal Conductivity of dry Soils of certain of the great soil groups. Soil Science Society of America Proceedings, Vol. 3, pp. 13 - 19.

Steer, P. J., Tashiro, C. H. M., Mcillveen, W. D. and Clement, R. E. 1995. PCDD and PCDF in air, soil, vegetation, and oil run-off from a tire fire. Water, Air, & Soil Pollution, 82 (3 - 4): 659 - 674.

T.A.G. Resource Recovery, 1996. Introduction to Civil Engineering Applications for Waste Tires. Prepared for Province of Alberta, Tire Recycling Management Board, February 1996.

Tatlisoz, N., Benson, C. H. and Edit, T. B. 1997. Effect of Fines on Mechanical Properties of Soil-Tire Chip Mixtures. *In* Testing Soil Mixed with Waste or Recycled Materials, ASTM STP 1275. *Edited by* Mark A. Wasemiller and Keith B. Hoddinott.

U.S.S.R Building Code. 1960. Technical Considerations in Designing Foundations in Permafrost. State Construction Publishing House, Moscow, S.N. 91-60.

Van Wijk, W. R. 1964. Thermal Properties of Soils. In International Study Group on Soils. Lectures at Meeting in Cambridge, England, July 12 - 26.

Viggiani, G. and Atkinson, J. H. 1995. The Interpretation of the Bender Element Tests. Géotechnique, 45 (1): 149 - 155.

Waste Age. 1990. Tire Fire Burns for 17 Days. Waste Age, May, pp. 20, 148.

Weast, R. C., Astle, M. J. and Beyer, W. H. 1984. CRC Handbook of Chemistry and Physics, CRC Press, Boca Raton, FL.

Weber, W. J., McGinley, P. M. and Katz, L. E. 1991. Sorption Phenomena in Subsurface Systems: Concepts, Models and Effects on Contaminant Fate and Transport, Water Resources, 25 (5): 499 - 528.

Williams, P. T., Bestler, S., Taylor, D. T., Botrill, R. P. 1995. The pyrolysis of automotive tire waste. Journal of the Institute of Energy, 68 (11).

Woods, R. D. 1994. Laboratory measurement of Dynamic Soil Properties. *In* Dynamic Geotechnical Testing II, ASTM STP 1213. Edited by Ronald J. Ebelhar, Vincent P. Drnevich, and Bruce L. Kutter. American Society for Testing and Materials, Philadelphia.

Wu, W. Y., Benda, C. C. and Cauley, R. F. 1997. Triaxial Determination of Shear Strength of Tire Chips. Journal of Geotechnical and Geoenvironmental Engineering, 123 (5): 479 – 482.

Zhang, X., Barbour, S. L. and Headly, J.V. 1998. A diffusion batch method for determined of the adsorption coefficient of benzene on clay soils. Canadian Geotechnical Journal, 35: 622 - 629.

Zytner, R. G. 1994. Sorption of Benzene, Toluene, Ethylbenzene and Xylenes to Various Media, Journal of Hazardous Materials, No. 38, pp. 127 - 144.

APPENDIX A - PARTICLE SIZE AND GRADATION

Table A. 1 Particle size and distribution, No. 20 Minus (Tire Recyclers of Calgary)

Grain-Size Distribution: No. 20 minus Date: 06-July-98
Supplier: Tire Recyclers of Calgary
Description of material: black, angular grain, very fine
Impurities: fine metal dust, fine fibre dust

Mass of crumb used: 116.3
Mass of talk used: 1.14 g
Test No.: 1

Sieve No.	Sieve Opening (mm)	Mass Retained (g)	% Retained	% Passing
10	2.00	0	0.0	100.0
20	0.85	17.5	15.0	85.0
40	0.425	52.3	45.0	40.0
60	0.250	26.2	22.5	17.5
100	0.150	13.2	11.3	6.1
200	0.075	6.9	5.9	0.2
Pan	-	0	-	-
		Σ = 116.1 g		

Mass of crumb used: 100.1 g
Mass of talk used: 1.14 g
Test No.: 2

Sieve No.	Sieve Opening (mm)	Mass Retained (g)	% Retained	% Passing
10	2.00	0	0.0	100.0
20	0.85	16.3	16.3	83.7
40	0.425	45.0	44.9	38.8
60	0.250	22.3	22.3	16.6
100	0.150	12.0	12.0	4.6
200	0.075	4.4	4.4	0.2
Pan	-	0	-	-
		Σ = 100 g		

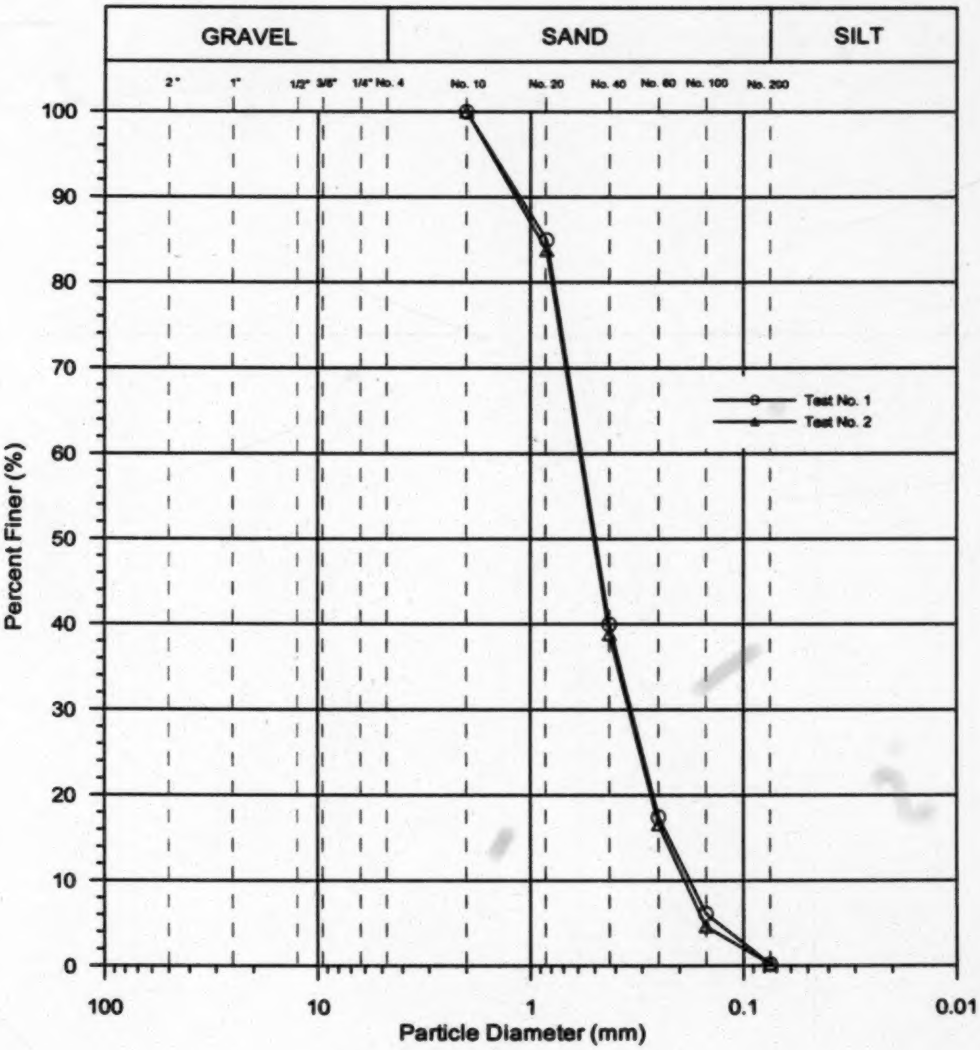

Figure A. 1 Grain-size distribution curve, No. 20 minus (Tire Recyclers of Calgary)

Table A. 2 Particle size and distribution, No. 20 minus (Alberta Environmental Rubber Products)

Grain-Size Distribution: No. 20 minus
Date: 28-March-98
Supplier: Alberta Environmental Rubber Products
Description of material: black, angular grain, very fine
Impurities: none

Mass of crumb used: 100 g
Mass of talk used: 1 g
Test No.: 1

Sieve No.	Sieve Opening (mm)	Mass Retained (g)	% Retained	% Passing
10	2.00	0	0	100.0
20	0.85	0.8	0.8	99.2
40	0.425	72.5	71.8	27.4
60	0.250	21.8	21.6	5.8
100	0.150	4.8	4.8	1.1
200	0.075	1.0	1.0	0.1
Pan	-	0.1	0.1	0.0
		Σ = 101 g		

Mass of crumb used: 200 g
Mass of talk used: 1 g
Test No.: 2

Sieve No.	Sieve Opening (mm)	Mass Retained (g)	% Retained	% Passing
10	2	0	0.0	100.0
20	0.85	16.3	16.3	83.7
40	0.425	45.0	44.9	38.8
60	0.250	22.3	22.3	16.6
100	0.150	12.0	12.0	4.6
200	0.075	4.4	4.4	0.2
Pan	-	0	-	-
		Σ = 1201 g		

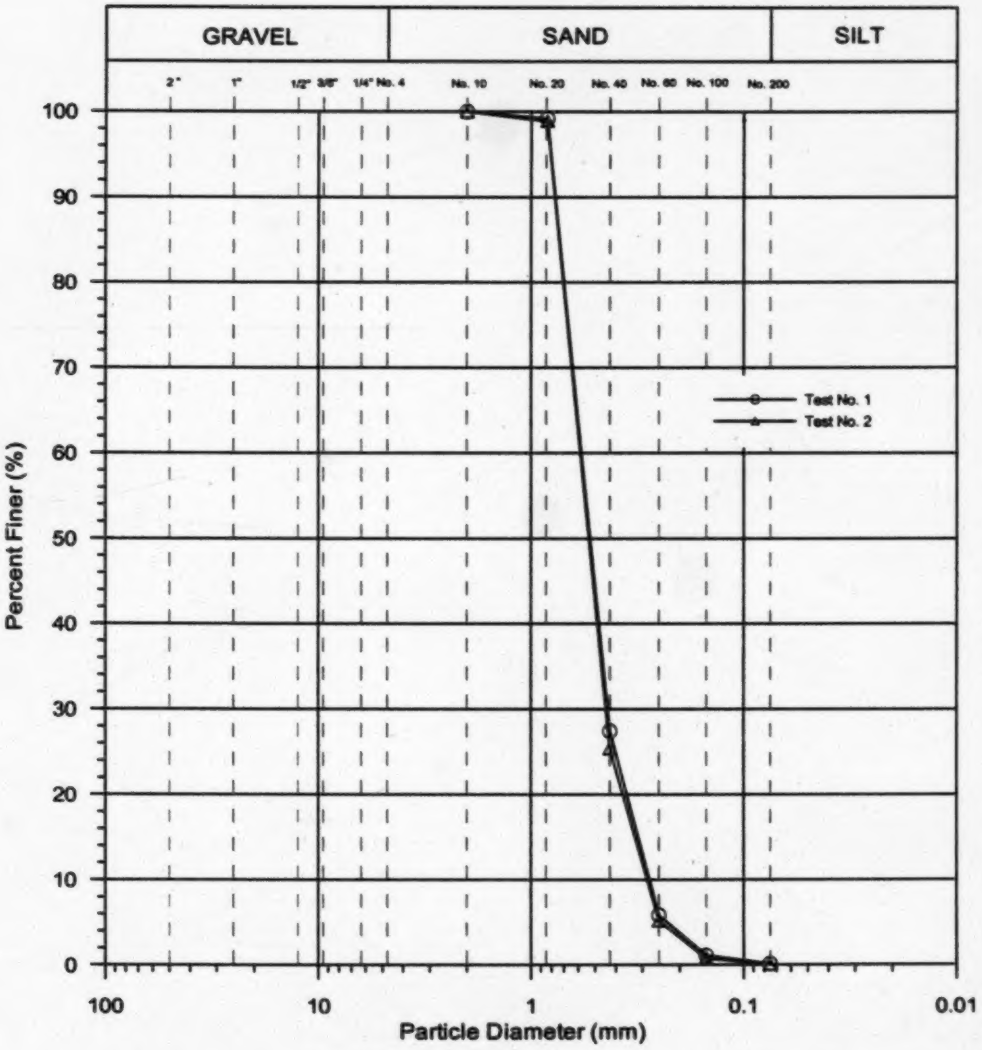

Figure A. 2 Grain-size distribution curve, No. 20 minus (AERP)

Table A. 3 Particle size and distribution, No. 10 - No. 20 (Tire Recyclers of Calgary)

Grain-Size Distribution: No. 10 - No. 20 Date: 07-July-98
Supplier: Tire Recyclers of Calgary
Description of material: black, angular grain, very fine
Impurities: fine metal dust, fine fibre dust

Mass of crumb used: 99 g
Mass of talk used: 1.01 g
Test No.: 1

Sieve No.	Sieve Opening (mm)	Mass Retained (g)	% Retained	% Passing
8	2.36	0	0	100.0
10	2.00	1.2	1.2	98.8
20	0.85	96.2	95.4	3.4
40	0.425	2.4	2.4	1.0
60	0.250	0	0	1.0
100	0.150	0.4	0.4	0.6
200	0.075	0	0	0.6
Pan	-	0	-	-
		Σ = 100.2 g		

Mass of crumb used: 99 g
Mass of talk used: 1 g
Test No.: 2

Sieve No.	Sieve Opening (mm)	Mass Retained (g)	% Retained	% Passing
4	4.75	0	0	100
8	2.36	0.2	0.2	99.8
10	2.00	1.3	1.3	98.5
20	0.85	95.9	95.3	3.2
40	0.425	2.8	2.8	0.4
60	0.250	0.06	0.1	0.3
100	0.150	0.12	0.1	0.2
200	0.075	0.19	0.2	0.0
Pan	-	0.04	-	-
		Σ = 100.61 g		

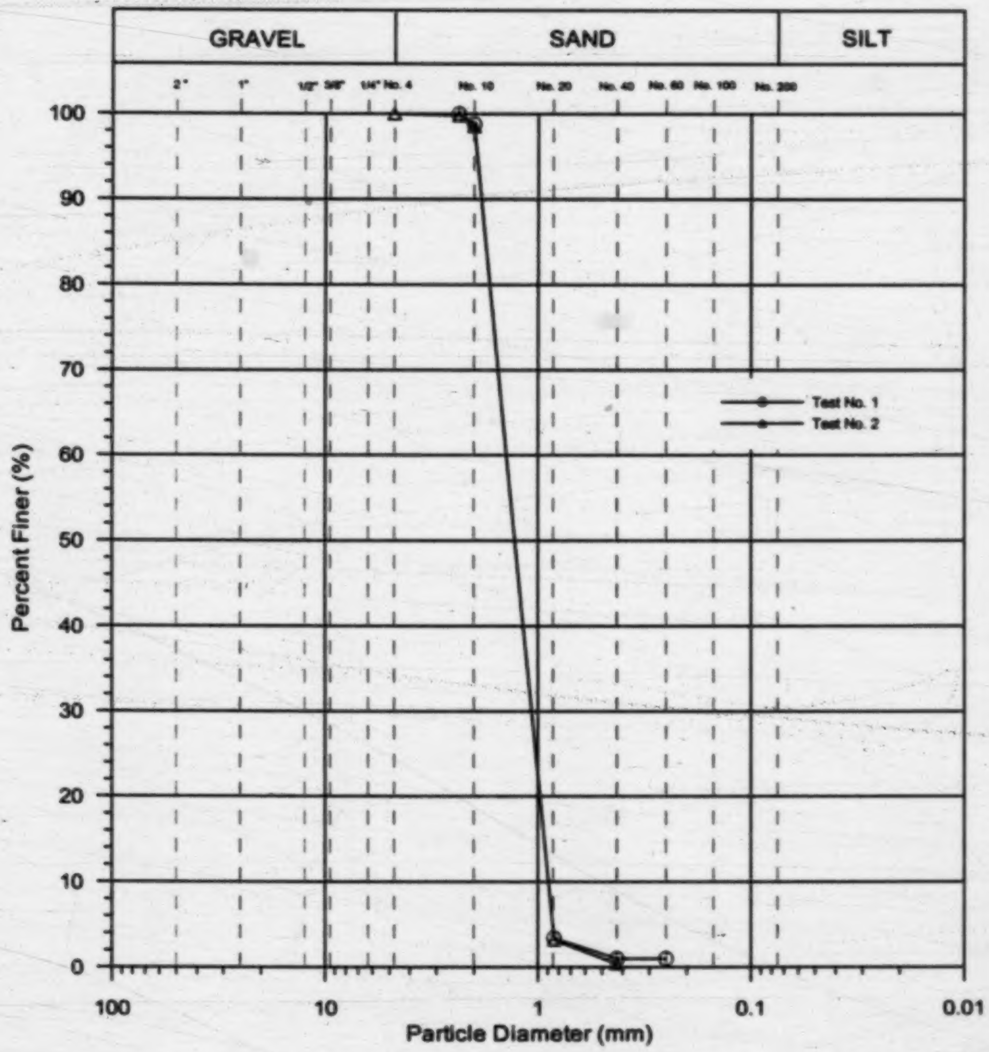

Figure A. 3 Grain-size distribution curve, No. 10 - No. 20 (Tire Recyclers of Calgary)

Table A. 4 Particle size and distribution, No. 10 - No. 20 (Alberta Environmental Rubber Products)

Grain-Size Distribution: No. 10 - No. 20 Date: 27-October-98
Supplier: Alberta Environmental Rubber Products
Description of material: black, angular grain, irregular
Impurities: none

Mass of crumb used: 200 g
Mass of talk used: 0.7 g
Test No.: 1

Sieve No.	Sieve Opening (mm)	Mass Retained (g)	% Retained	% Passing
4	4.75	0	0	100.0
8	2.36	0.2	0.1	99.9
10	2.00	1.8	0.9	99.0
20	0.85	186.4	92.9	6.1
40	0.425	11.2	5.6	0.5
60	0.250	0.6	0.3	0.2
100	0.150	0.3	0.1	0.1
200	0.075	0.2	0.1	0
Pan	-	0	-	-
		Σ = 200.7 g		

Mass of crumb used: 300.09 g
Mass of talk used: 1 g
Test No.: 2

Sieve No.	Sieve Opening (mm)	Mass Retained (g)	% Retained	% Passing
4	4.75	0	0	100.0
8	2.36	0.5	0.2	99.8
10	2.00	3.3	1.1	98.7
20	0.85	279.8	92.6	6.2
40	0.425	16.8	5.6	0.6
60	0.250	1.0	0.3	0.3
100	0.150	0.6	0.2	0.1
200	0.075	0.3	0.1	0
Pan	-	0.0	-	-
		Σ = 302.3 g		

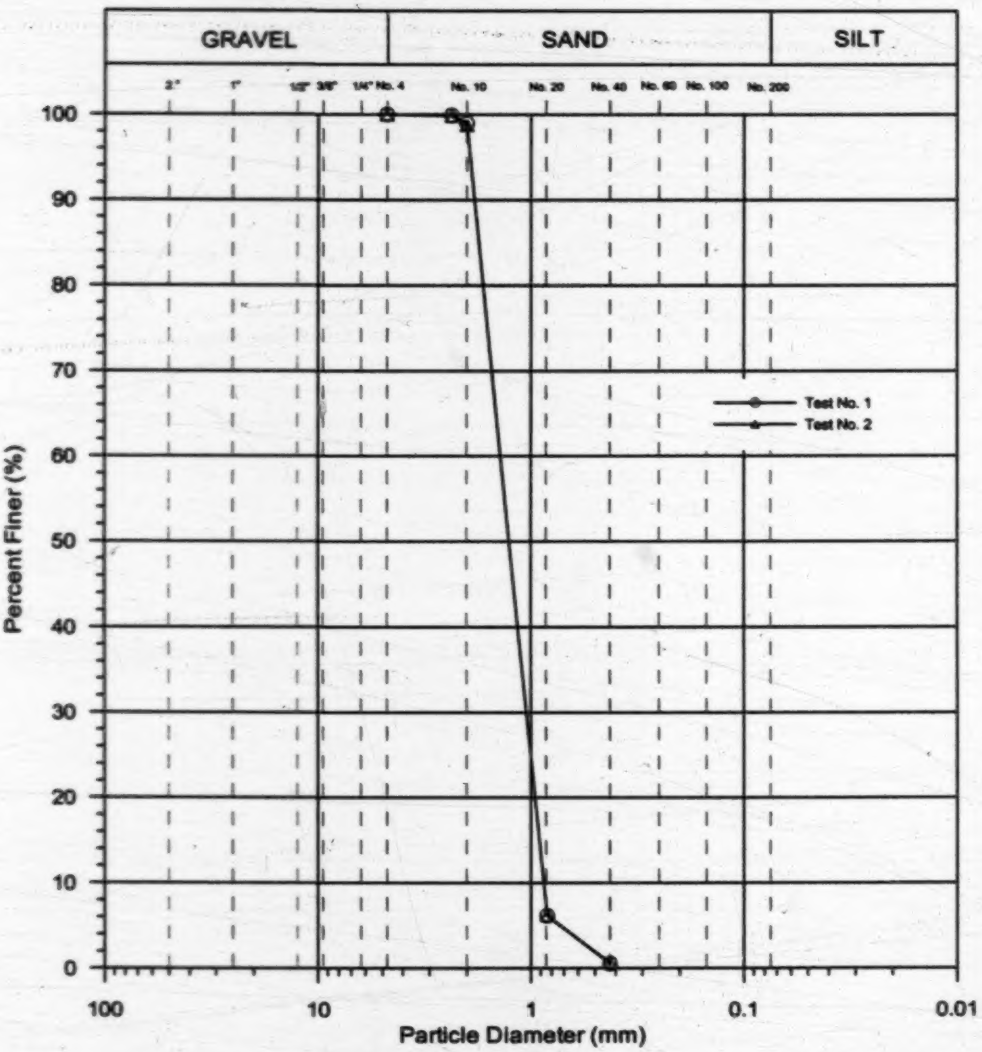

Figure A. 4 Grain-size distribution curve, No. 10 - No. 20 (Alberta Environmental Rubber Products)

Table A. 5 Particle size and distribution, No. 10 (Midwest Tire Processors of Vulcan)

Grain-Size Distribution:	No. 10	Date: 07-July-98
Supplier:	Midwest Tire Processors of Vulcan	
Description of material:	black, angular grain	
Impurities:	few fibre threads	

Mass of crumb used: 99 g
Mass of talk used: 1.01 g
Test No.: 1

Sieve No.	Sieve Opening (mm)	Mass Retained (g)	% Retained	% Passing
8	2.36	0	0	100.0
10	2.00	1.2	1.2	98.8
20	0.85	96.2	95.4	3.4
40	0.425	2.4	2.4	1.0
60	0.250	0	0	1.0
100	0.150	0.4	0.4	0.6
200	0.075	0	0	0.6
Pan	-	0	-	-
		Σ = 100.2 g		

Mass of crumb used: 99 g
Mass of talk used: 1 g
Test No.: 2

Sieve No.	Sieve Opening (mm)	Mass Retained (g)	% Retained	% Passing
4	4.75	0	0	100
8	2.36	0.2	0.2	99.8
10	2.00	1.3	1.3	98.5
20	0.85	95.9	95.3	3.2
40	0.425	2.8	2.8	0.4
60	0.250	0.06	0.1	0.3
100	0.150	0.12	0.1	0.2
200	0.075	0.19	0.2	0.0
Pan	-	0.04	-	-
		Σ = 100.61 g		

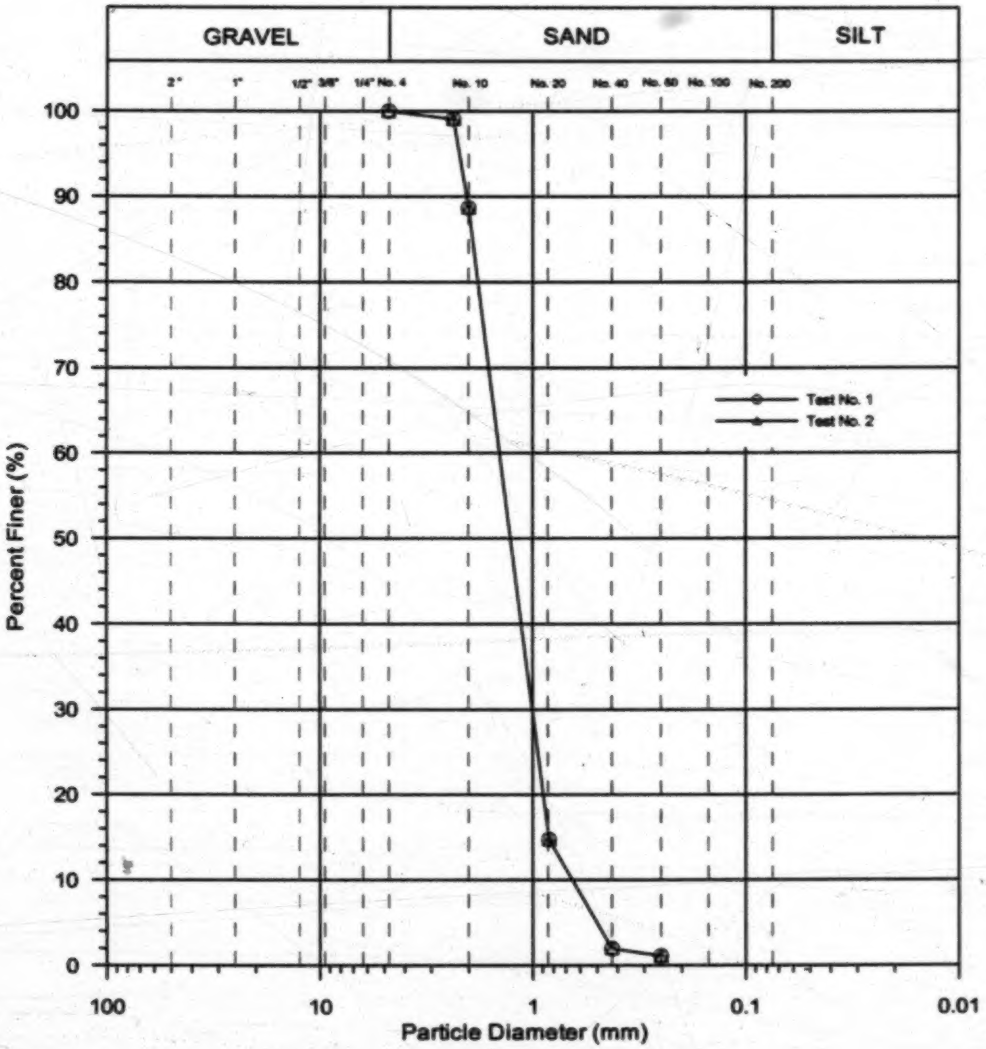

Figure A. 5 Grain-size distribution curve, No. 10
(Midwest Tire Processors of Vulcan)

Table A. 6 Particle size and distribution, No. 8 - No. 14 (Tire Recyclers of Calgary)

Grain-Size Distribution:	No. 8 - No. 14	Date: 07-July-98
Supplier:	Tire Recyclers of Calgary	
Description of material:	black, angular grain	
Impurities:	lots of fibre reinforcements	

Mass of crumb used: 149 g
Mass of talk used: 1.1 g
Test No.: 1

Sieve No.	Sieve Opening (mm)	Mass Retained (g)	% Retained	% Passing
4	4.75	0	0.0	100.0
8	2.36	5.6	3.7	96.3
10	2.00	45.2	30.1	66.2
20	0.85	98.6	65.6	0.6
40	0.425	0.2	0.1	0.5
60	0.250	0	0.0	0.5
100	0.150	0	0.0	0.5
200	0.075	0	0.0	0.5
Pan	-	0.2	-	-
		Σ = 149.8 g		

Mass of crumb used: 149 g
Mass of talk used: 1.05 g
Test No.: 2

Sieve No.	Sieve Opening (mm)	Mass Retained (g)	% Retained	% Passing
4	4.75	0	0.0	100.0
8	2.36	6.1	4.1	95.9
10	2.00	44.6	29.7	66.2
20	0.85	98.6	65.7	0.5
40	0.425	0.2	0.1	0.4
60	0.250	0.3	0.2	0.2
100	0.150	0	0.0	0.2
200	0.075	0	0.0	0.2
Pan	-	0	-	-
		Σ = 150 g		

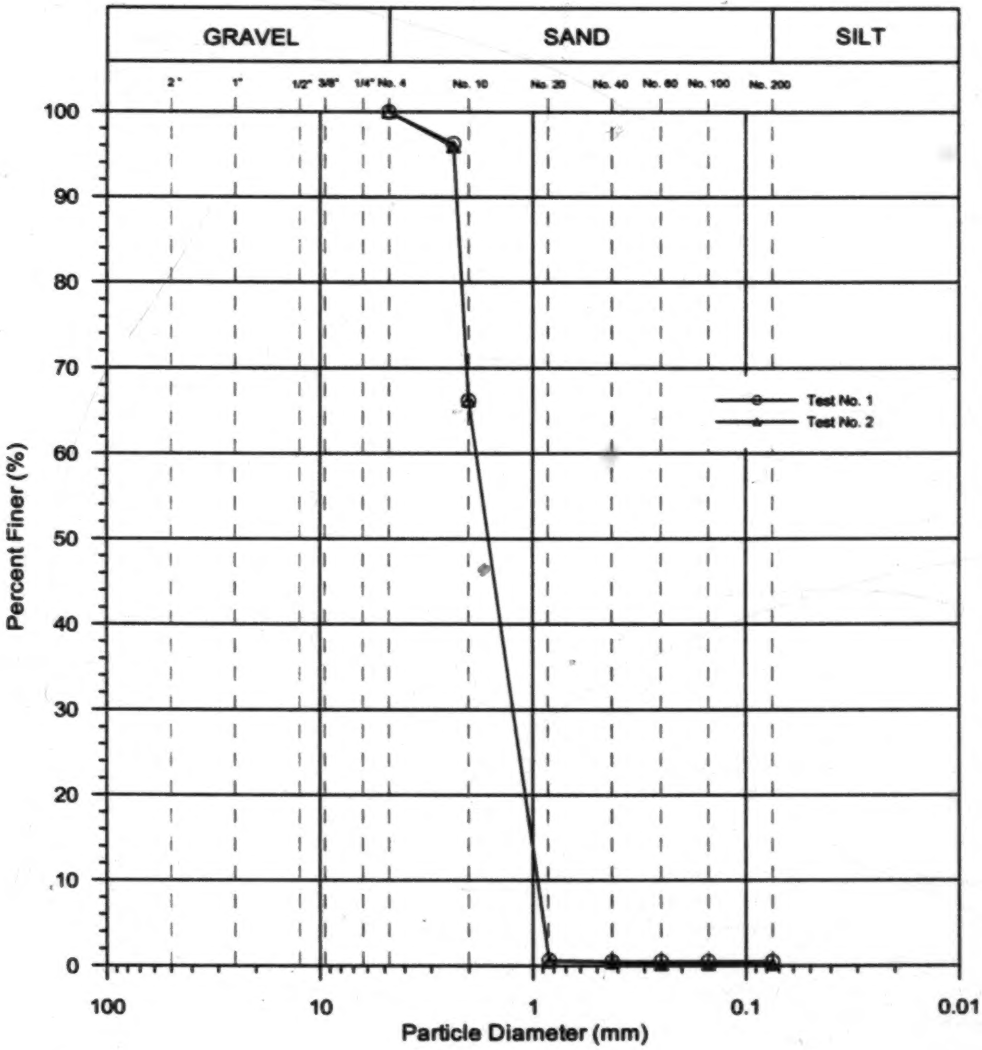

Figure A. 6 Grain-size distribution curve, No. 8 - No. 14 (Tire Recyclers of Calgary)

Table A. 7 Particle size and distribution, No. 4 - No. 8 (Tire Recyclers of Calgary)

Grain-Size Distribution:	No. 4 - No. 8	Date:	07-July-98
Supplier:	Tire Recyclers of Calgary		
Description of material:	waster fibres retained on No. 10 sieve, angular		
Impurities:	lots of fibre reinforcements		

Mass of crumb used: 149 g
Mass of talk used: 0 g
Test No.: 1

Sieve No.	Sieve Opening (mm)	Mass Retained (g)	% Retained	% Passing
3/8 in	9.50	0	0	100
4	4.75	0.5	0.3	99.7
8	2.36	135.8	89.5	10.2
10	2.00	12.2	8.0	2.1
20	0.85	2.6	1.7	0.4
40	0.425	0	0	
60	0.250	0	0	
100	0.150	0	0	
200	0.075	0	0	
Pan	-	0	-	-
		Σ = 151.1 g		

Mass of crumb used: 149 g
Mass of talk used: 0 g
Test No.: 2

Sieve No.	Sieve Opening (mm)	Mass Retained (g)	% Retained	% Passing
3/8 in	9.50	0	0	100
4	4.75	0.9	0.6	99.4
8	2.36	135.5	89.8	9.6
10	2.00	11.5	7.6	2.0
20	0.85	2.7	1.8	0.2
40	0.425	0	0	
60	0.250	0	0	
100	0.150	0	0	
200	0.075	0	0	
Pan	-	0	-	-
		Σ = 150.6 g		

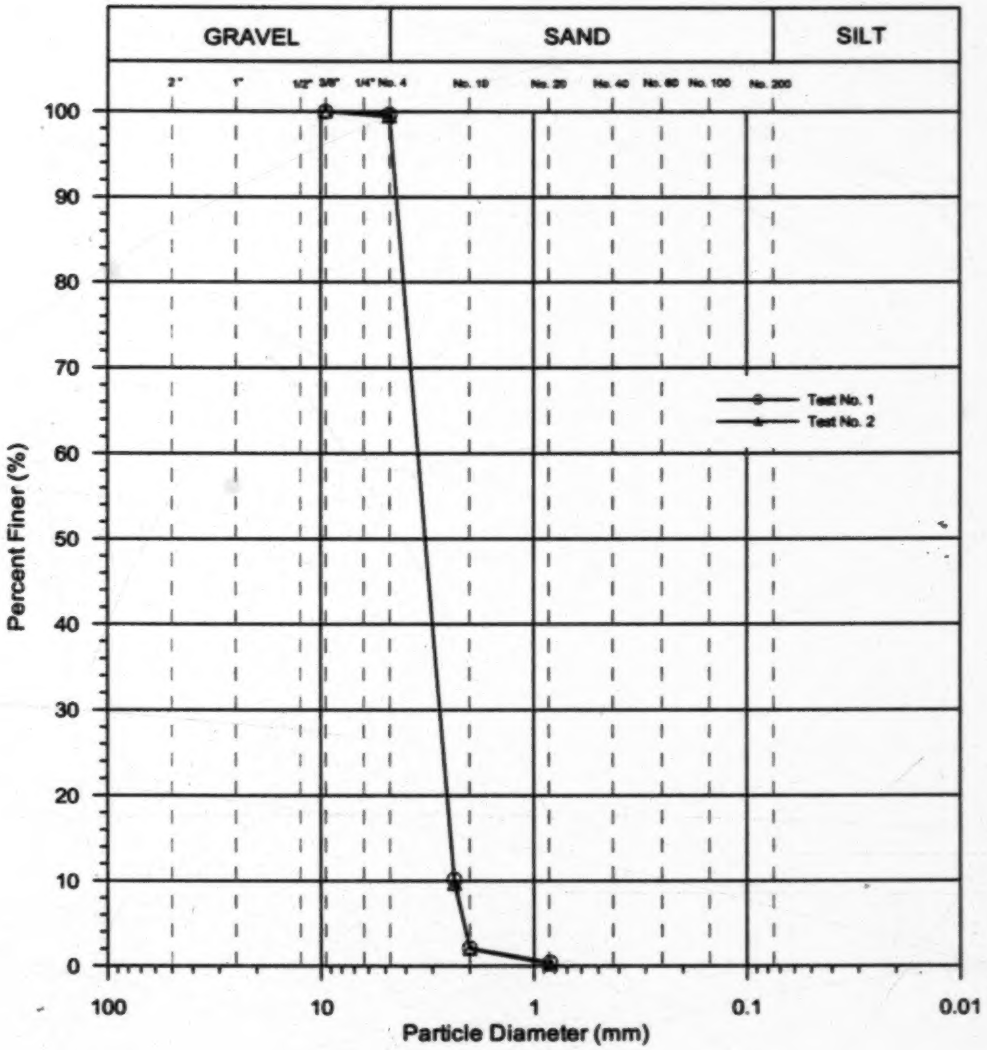

Figure A. 7 Grain- size distribution curve, No. 4 - No. 8 (Tire Recyclers of Calgary)

Table A. 8 Particle size and distribution, 1/4 in (Midwest Tire Processors of Vulcan)

Grain-Size Distribution:	1/4 in	Date:	07-July-98
Supplier:	Midwest Tire Processors of Vulcan		
Description of material:	angular, irregular, elongated		
Impurities:	lots of threads, cords, few rocks		

Mass of crumb used: 301 g
Mass of talk used: 0 g
Test No.: 1

Sieve No.	Sieve Opening (mm)	Mass Retained (g)	% Retained	% Passing
3/8 in	9.50	0.0	0.0	100.0
4	4.75	156.7	52.0	48.0
8	2.36	123.1	40.9	7.1
10	2.00	8.7	2.9	4.2
20	0.85	12.2	4.1	0.2
40	0.425	0.2	0.1	0.1
60	0.250	0.1	0.0	0.1
100	0.150	0.1	0.0	0.1
200	0.075	0.1	0.0	0.0
Pan	-	0.1	-	-
		Σ = 301.2 g		

Mass of crumb used: 300 g
Mass of talk used: 0 g
Test No.: 2

Sieve No.	Sieve Opening (mm)	Mass Retained (g)	% Retained	% Passing
3/8 in	9.50	0.0	0.0	100.0
4	4.75	119.5	39.7	60.3
8	2.36	135.2	44.9	15.5
10	2.00	15.3	5.1	10.4
20	0.85	28.8	9.6	0.8
40	0.425	0.6	0.2	0.6
60	0.250	0.2	0.1	0.6
100	0.150	0.2	0.1	0.5
200	0.075	0.5	0.2	0.4
Pan	-	0.5	-	-
		Σ = 300.7 g		

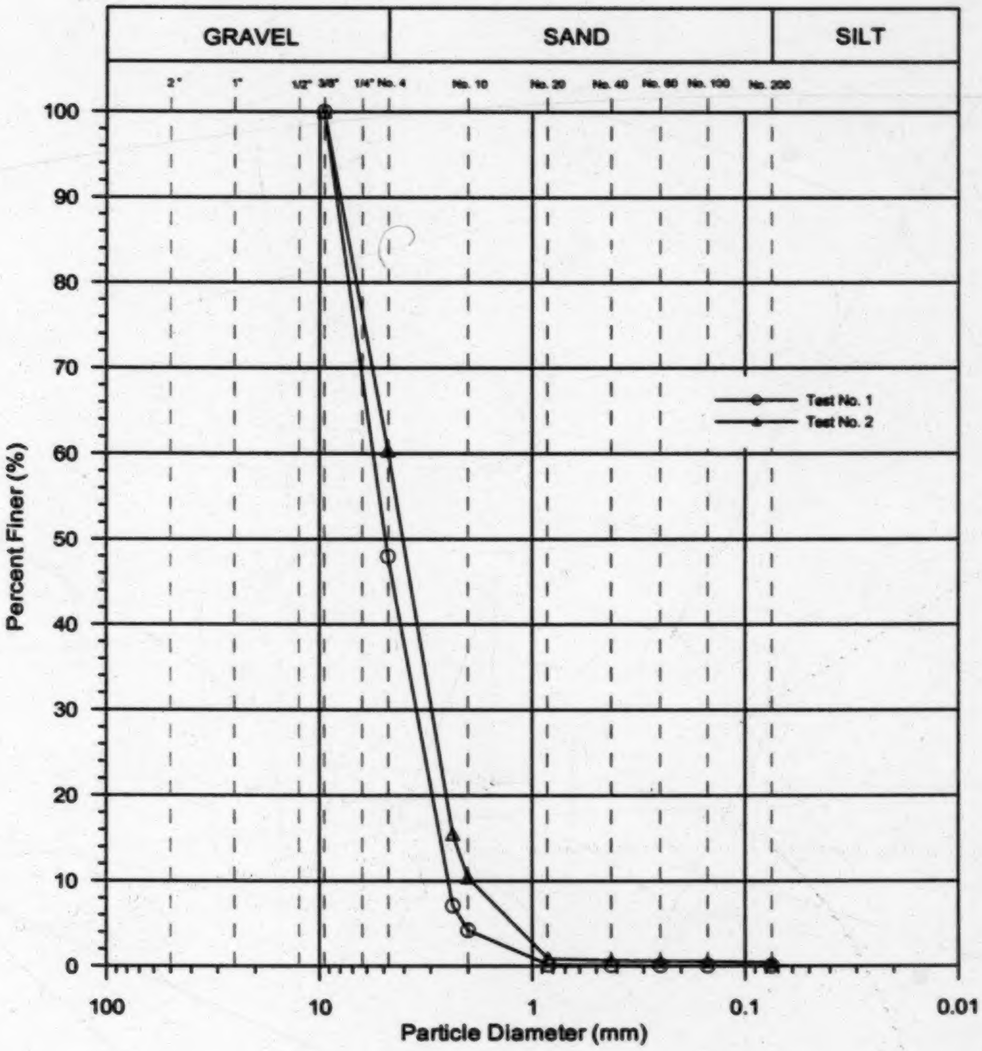

Figure A. 8 Grain-size distribution curve, 1/4 in (Midwest Tire Processors of Vulcan)

Table A. 9 Particle size and distribution, 1/4 in (Alberta Environmental Rubber Products)

Grain-Size Distribution:	1/4 in	Date:	27-October-98
Supplier:	Alberta Environmental Rubber Products		
Description of material:	angular, uniform, clean edges		
Impurities:	none		

Mass of crumb used: 200 g
Mass of talk used: 0 g
Test No.: 1

Sieve No.	Sieve Opening (mm)	Mass Retained (g)	% Retained	% Passing
1/4 in	6.30	0	0	100.0
3/8 in	9.50	0.80	0.4	99.6
4	4.75	181.80	90.3	9.3
8	2.36	13.60	6.8	2.6
10	2.00	5.00	2.5	0.1
20	0.85	0.20	0.1	0.0
40	0.425	0	0	100.0
60	0.250	-	-	-
100	0.150	-	-	-
200	0.075	-	-	-
Pan	-	-	-	-
		Σ = 201.4 g		

Mass of crumb used: 300.5 g
Mass of talk used: 0 g
Test No.: 2

Sieve No.	Sieve Opening (mm)	Mass Retained (g)	% Retained	% Passing
1/4 in	6.30	0	0	100.0
3/8 in	9.50	0.3	0.1	99.9
4	4.75	272.6	90.7	9.2
8	2.36	20.4	6.8	2.4
10	2.00	7.1	2.4	0
20	0.85	0.1	0.0	0
40	0.425	0	0	100.0
60	0.250	-	-	-
100	0.150	-	-	-
200	0.075	-	-	-
Pan	-	-	-	-
		Σ = 300.5 g		

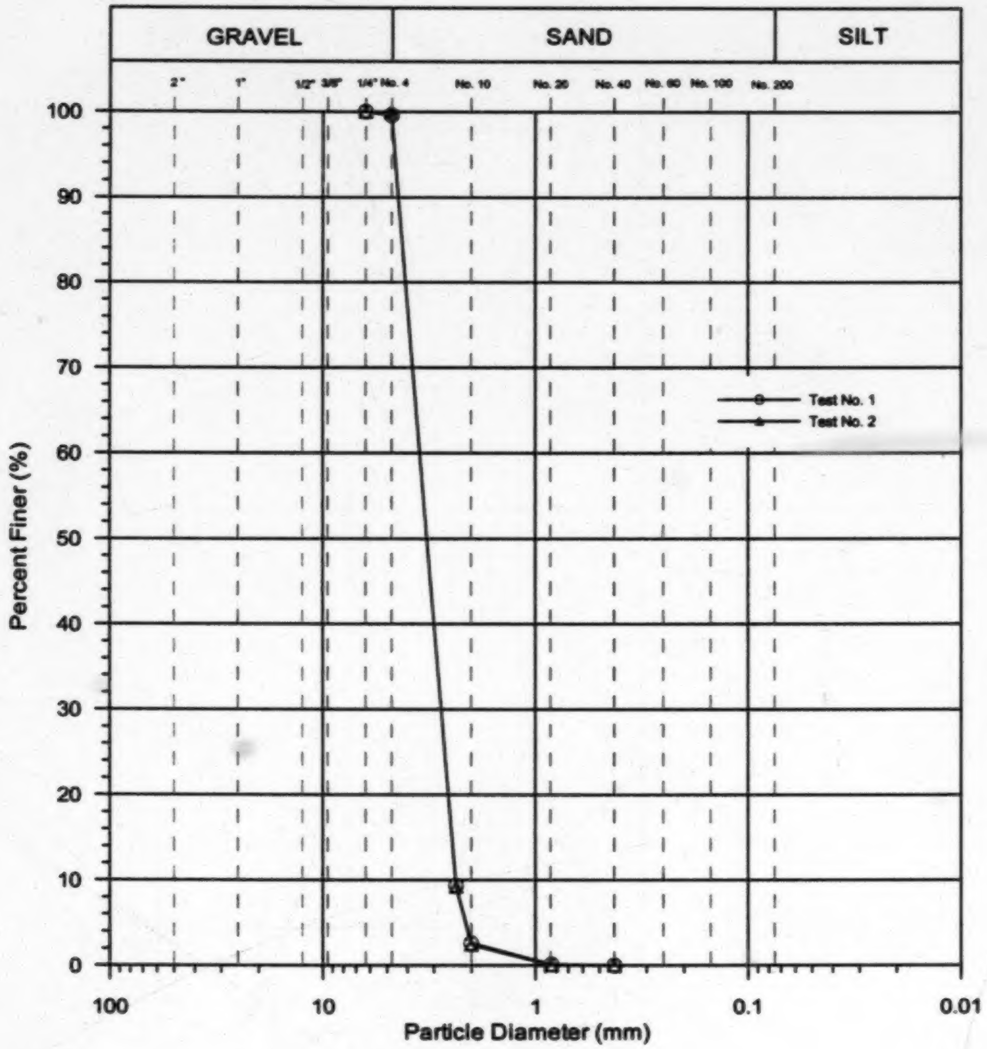

Figure A. 9 Grain-size and distribution curve, 1/4 in (Alberta Environmental Rubber Products)

APPENDIX B - SPECIFIC GRAVITY

Table B. 1 Specific gravity, G_s, No. 20 Minus (Tire Recyclers of Calgary)

Date Obtained	11-Jun-98	11-Jun-98	11-Jun-98	09-Sep-98
Sample No.	1	2	3	4
Flask No.	GC-2	TC-1	RJR	RJR
Method of Air Removal	vacuum	boil, vacuum	boil, vacuum	boil, vacuum
W_{b+w+s} (g)	678.45	675.56	673.58	674.40
Temperature (°C)	25.85	26.30	28.85	23.50
W_{b+w} (g)	675.07	671.98	670.01	670.70
Evaporating Dish No.	#1	TC1	RJR#1	SG-1
Wt. Sample Dry + Dish (g)	61.43	743.17	892.33	75.74
Tare Dish (g)	37.37	718.29	867.52	51.26
W_s (g)	24.06	24.88	24.81	24.48
$G_s = W_s/(W_s+W_{b+w} - W_{b+w+s})$	1.16	1.17	1.17	1.18

Table B. 2 Specific gravity, G_s, No. 20 Minus (Alberta Environmental Rubber Products)

Date Obtained	05-Oct-98
Sample No.	1
Flask No.	RJR
Method of Air Removal	boil, vacuum
W_{b+w+s} (g)	674.05
Temperature (°C)	22.60
W_{b+w} (g)	670.80
Evaporating Dish No.	TC12
Wt. Sample Dry + Dish (g)	1073.91
Tare Dish (g)	1049.12
W_s (g)	24.79
$G_s = W_s/(W_s+W_{b+w} - W_{b+w+s})$	1.15

Table B. 3 Specific gravity, G_s, No. 10 - No. 20 (Tire Recyclers of Calgary)

Date Obtained	11-Jun-98	11-Jun-98	09-Sep-98
Sample No.	1	2	3
Flask No.	GC-2	TC-1	GC-2
Method of Air Removal	boil, vacuum	boil, vacuum	boil, vacuum
W_{b+w+s} (g)	678.67	675.46	678.02
Temperature (°C)	23.20	26.10	23.60
W_{b+w} (g)	675.40	672.00	675.35
Evaporating Dish No.	GC2	TC1	SG-2
Wt. Sample Dry + Dish (g)	885.47	743.07	70.84
Tare Dish (g)	860.73	718.28	50.82
W_s (g)	24.74	24.79	20.02
$G_s = W_s/(W_s+W_{b+w} - W_{b+w+s})$	1.15	1.16	1.15

Table B. 4 Specific gravity, G_s, No. 10 - No. 20 (Alberta Environmental Rubber Products)

Date Obtained	05-Oct-98
Sample No.	1
Flask No.	B31
Method of Air Removal	boil, vacuum
W_{b+w+s} (g)	674.32
Temperature (°C)	22.70
W_{b+w} (g)	671.32
Evaporating Dish No.	RJR#1
Wt. Sample Dry + Dish (g)	892.46
Tare Dish (g)	867.52
W_s (g)	24.94
$G_s = W_s/(W_s+W_{b+w} - W_{b+w+s})$	1.14

Table B. 5 Specific gravity, G_s, No. 10 (Midwest Tire Processors of Vulcan)

Date Obtained	11-Jun-98	11-Jun-98	11-Jun-98	09-Jun-98
Sample No.	1	2	3	4
Flask No.	B-31	RJR	TC-1	GC-4
Method of Air Removal	boil, vacuum	boil, vacuum	boil, vacuum	boil, vacuum
W_{b+w+s} (g)	674.44	674.11	675.85	680.04
Temperature (°C)	26.50	26.35	25.80	29.25
W_{b+w} (g)	670.84	670.36	672.04	676.40
Evaporating Dish No.	B-31	RJR#1	GC-2	GC-2
Wt. Sample Dry + Dish (g)	798.43	892.31	885.10	884.83
Tare Dish (g)	773.63	867.53	860.76	860.76
W_s (g)	24.80	24.78	24.34	24.07
$G_s = W_s/(W_s+W_{b+w} - W_{b+w+s})$	1.17	1.18	1.19	1.18

Table B. 6 Specific gravity, G_s, No. 8 - No. 14 (Tire Recyclers of Calgary)

Date Obtained	11-Jun-98	11-Jun-98	11-Jun-98
Sample No.	1	2	3
Flask No.	B-31	RJR	TC-1
Method of Air Removal	boil, vacuum	boil, vacuum	boil, vacuum
W_{b+w+s} (g)	674.44	674.11	675.85
Temperature (°C)	26.50	26.35	25.80
W_{b+w} (g)	670.84	670.36	672.04
Evaporating Dish No.	B-31	RJR#1	GC-2
Wt. Sample Dry + Dish (g)	798.43	892.31	885.10
Tare Dish (g)	773.63	867.53	860.76
W_s (g)	24.80	24.78	24.34
$G_s = W_s/(W_s+W_{b+w} - W_{b+w+s})$	1.17	1.18	1.19

Table B. 7 Specific gravity, G_s, No. 4 - No. 8 (Tire Recyclers of Calgary)

Date Obtained	11-Jun-98	11-Jun-98	11-Jun-98
Sample No.	1	2	3
Flask No.	B-31	GC-4	GC-4
Method of Air Removal	boil, vacuum	boil, vacuum	boil, vacuum
W_{b+w+s} (g)	674.20	680.44	681.19
Temperature (°C)	26.80	26.30	22.40
W_{b+w} (g)	670.81	676.83	677.30
Evaporating Dish No.	B31	GC4	A2
Wt. Sample Dry + Dish (g)	798.49	904.37	868.12
Tare Dish (g)	773.65	879.49	840.71
W_s (g)	24.84	24.88	27.41
$G_s = W_s/(W_s+W_{b+w} - W_{b+w+s})$	1.16	1.17	1.17

Table B. 8 Specific gravity, G_s, 1/4 in (Midwest Tire Processors of Vulcan)

Date Obtained	11-Jun-98	11-Jun-98	11-Jun-98
Sample No.	1	2	3
Flask No.	GC-4	B-31	GC-2
Method of Air Removal	boil, vacuum	boil, vacuum	boil, vacuum
W_{b+w+s} (g)	681.33	674.98	678.54
Temperature (°C)	21.60	22.65	27.50
W_{b+w} (g)	677.40	671.30	674.85
Evaporating Dish No.	A1	A2	TC-12
Wt. Sample Dry + Dish (g)	870.80	865.96	1072.20
Tare Dish (g)	845.26	840.65	1049.17
W_s (g)	25.54	25.31	23.03
$G_s = W_s/(W_s+W_{b+w} - W_{b+w+s})$	1.18	1.17	1.19

Table B. 9 Specific gravity, G_s, 1/4 in (Alberta Environmental Rubber Products)

Date Obtained	05-Oct-98	05-Oct-98
Sample No.	1	2
Flask No.	GC-2	GC-4
Method of Air Removal	boil, vacuum	boil, vacuum
W_{b+w+s} (g)	678.48	680.50
Temperature (°C)	22.80	22.70
W_{b+w} (g)	675.45	677.27
Evaporating Dish No.	B-31	GC-4
Wt. Sample Dry + Dish (g)	798.62	904.35
Tare Dish (g)	773.64	879.44
W_s (g)	24.98	24.91
$G_s = W_s/(W_s+W_{b+w} - W_{b+w+s})$	1.14	1.15

APPENDIX C - COMPACTION

Table C. 1 Determination of the minimum dry index density

Mass of Mold (g) = 3728.3
Diam. of Mold (mm) = 151.7
Ht. of Mold (mm) = 155.2
Volume of Mold (m^3) = 2.8×10^{-03}

GSD (US Sieve Designation)	Supplier	$M_{mold+rubber}$ (g)	M_{rubber} (kg)	γ_d (kN/m^3)	e_{max}	Avg. e_{max}
No. 20 Minus	Tire Recyclers of Calgary	4701.8	0.974	3.4	2.4	2.4
		4710.2	0.982	3.4	2.4	
		4707.3	0.979	3.4	2.4	
No. 10 - No. 20	Tire Recyclers of Calgary	4807.7	1.079	3.8	2.1	2.1
		4807.2	1.079	3.8	2.1	
		4809.1	1.081	3.8	2.1	
No. 10	Midwest Tire Processors of Vulcan	4754.1	1.026	3.6	2.2	2.2
		4745.1	1.017	3.6	2.3	
		4743.9	1.016	3.6	2.3	
No. 8 - No. 14	Tire Recyclers of Calgary	4806.5	1.078	3.8	2.1	2.1
		4803.6	1.075	3.8	2.1	
		4805.0	1.077	3.8	2.1	
No. 4 - No. 8	Tire Recyclers of Calgary	4873.1	1.145	4.0	1.9	1.9
		4886.0	1.158	4.0	1.9	
		4884.6	1.156	4.0	1.9	
1/4 in	Alberta Environmental Rubber Products	5170.5	1.442	5.0	1.3	1.3
		5163.6	1.435	5.0	1.3	
		5186.2	1.458	5.1	1.3	
1/4 in	Midwest Tire Processors of Vulcan	4926.8	1.199	4.2	1.8	1.8
		4901.4	1.173	4.1	1.8	
		4911.2	1.183	4.1	1.8	

Table C. 2 Determination of the maximum dry index density

Mass of Mold (g) = 3728.3
Diam. of Mold (mm) = 151.7
Ht. of Mold (mm) = 155.2
Volume of Mold (m^3) = $2.8\text{x}10^{-03}$

Tire Crumb Size (US Sieve Designation)	Tire Crumb Manufacturer	Avg. Sample Ht. (mm)	$M_{mold+rubber}$ (g)	M_{rubber} (kg)	Volume of Rubber ($\text{x}10^{-3}$ m^3)	γ_d (kN/m^3)	e_{min}
No. 20 Minus	Tire Recyclers of Calgary	108.2	4828.8	1.1	2.0	5.4	1.1
No. 10 - No. 20	Tire Recyclers of Calgary	108.2	4783.8	1.1	1.9	5.3	1.1
No. 10	Midwest Tire Processors of Vulcan	108.2	4735.5	1.0	1.8	5.4	1.1
No. 8 - No. 14	Tire Recyclers of Calgary	108.2	4785.9	1.1	2.0	5.3	1.2
No. 4 - No. 8	Tire Recyclers of Calgary	108.2	4928.9	1.2	2.1	5.5	1.1
1/4 in	Midwest Tire Processors of Vulcan	108.2	4931.9	1.2	2.1	5.7	1.0
1.4 in	Alberta Environmental Rubber Products	108.2	4937.9	1.2	2.5	4.8	1.3

APPENDIX D - COMPRESSIBILITY

Table D.0-1 Compressibility results, sample and apparatus dimensions

Apparatus Dimensions:
Diam. = 101.16 mm
Area = 0.00804 m^3

Dry Conditions

Particle Size	Supplier	$M_{(i)}$ (kg)	$M_{(f)}$ (kg)	M_{crumbs} (kg)	Vol. crumbs ($x10^{-3}$ m^3)	Initial Sample Ht. (mm)	e_o
No. 20 minus	TROC	0.395	0.120	0.275	0.804	100	2.4
No. 10 - No. 20	TROC	0.510	0.192	0.318	0.804	100	2.0
No. 10	Vulcan	0.448	0.143	0.305	0.804	100	2.1
No. 8 - No. 14	TROC	0.504	0.187	0.317	0.804	100	1.9
No. 4 - No. 8	TROC	0.501	0.167	0.334	0.804	100	1.8
1/4 in	Vulcan	0.434	0.116	0.317	0.804	100	2.0

$M_{(i)}$ = initial mass of dry crumbs + tare
$M_{(f)}$ = final mass of dry crumbs + tare

Saturated Conditions

Particle Size	Supplier	$M_{rubber\ dry}$ (kg)	H_s (mm)	e_o
No. 20 minus	TROC	0.094	25.4	2.9
No. 10 - No. 20	TROC	0.160	2.85	2.3
No. 10	Vulcan	0.162	28.7	2.3
No. 8 - No. 14	TROC	0.120	2.99	2.1
No. 4 - No. 8	TROC	0.190	3.47	1.9
1/4 in	Vulcan	0.163	3.03	2.3

Table D.0-2 Pressure transducers and linear potentiometer calibrations

Dry Conditions

GSD	Supplier	Press. Trans. No. 1 Channel	Press. Trans. No.2 Channel	Press. Trans. No. 1 Calibration (kPa/mV)	Press. Trans. No. 2 Calibration (kPa/mV)	LP Channel	LP Serial No.	LP Calibration (mm/V)
No. 20 minus	TROC	12	13	1.559	1.556	14	1947	8.264
No. 10 - No. 20	TROC	16	17	1.564	1.579	18	1949	8.292
No. 10	Vulcan	12	-	1.564	-	14	1947	8.264
No. 8 - No. 14	TROC	12	13	1.37	1.556	14	1947	8.264
No. 4 - No. 8	TROC	22	23	1.37	1.564	14	1951	8.286
1/4 in	Vulcan	27	28	1.369	1.37	29	1941	8.295

Saturated Conditions

GSD	Supplier	Press. Trans. No. 1 Channel	Press. Trans. Line	Press. Trans. No. 1 Calibration (kPa/mV)	LP Channel	LP Serial No.	LP Calibration (mm/V)
No. 20 minus	TROC	22	26	1.37	29	1941	8.295
No. 10 - No. 20	TROC	17	39	1.579	18	1949	8.292
No. 10	Vulcan	12	31	1.559	14	1947	8.264
No. 8 - No. 14	TROC	16	36	1.564	15	1955	8.381
No. 4 - No. 8	TROC	23	29	1.564	24	1951	8.286
1/4 in	Vulcan	27	24	1.369	28	1946	8.263

LP = Linear Potentiometer
Press. Trans. = Pressure Transducer

Table D. 1 Compressibility results, No. 20 minus (TROC)

Dry Conditions

Loading	σ_v (kPa)	ΔH_s (mm)	H_1 (mm)	γ_d (kN/m^3)	e	ε_a (%)
—	0	0.0	100.0	3.4	2.4	0.0
Load	10	32.9	67.1	5.0	1.3	-32.9
Load	20	8.4	58.7	5.7	1.0	-41.3
Load	50	7.3	51.4	6.5	0.8	-48.6
Load	100	6.5	44.9	7.5	0.5	-55.1
Unload	50	-0.8	45.8	7.3	0.6	-54.2
Unload	20	0.0	45.7	7.3	0.6	-54.3
Unload	10	-2.4	48.1	7.0	0.6	-51.9
Reload	20	0.3	47.9	7.0	0.6	-52.1
Reload	50	1.4	46.5	7.2	0.6	-53.5
Reload	100	3.1	43.5	7.7	0.5	-56.5

Saturated Conditions

Loading	σ_v (kPa)	ΔH_s (mm)	H_1 (mm)	γ_d (kN/m^3)	e	ε_a (%)
—	0	0.0	100.0	2.9	2.9	0.0
Load	10	33.6	66.4	4.4	1.6	-33.6
Load	20	6.7	59.7	4.9	1.3	-40.3
Load	50	7.5	52.2	5.6	1.1	-47.8
Load	100	5.7	46.5	6.3	0.8	-53.5
Unload	50	-0.8	47.4	6.2	0.9	-52.6
Unload	20	-1.0	48.4	6.0	0.9	-51.6
Unload	10	-1.8	50.2	5.8	1.0	-49.8
Reload	20	0.1	50.1	5.8	1.0	-49.9
Reload	50	1.6	48.6	6.0	0.9	-51.4
Reload	100	3.1	45.4	6.4	0.8	-54.6

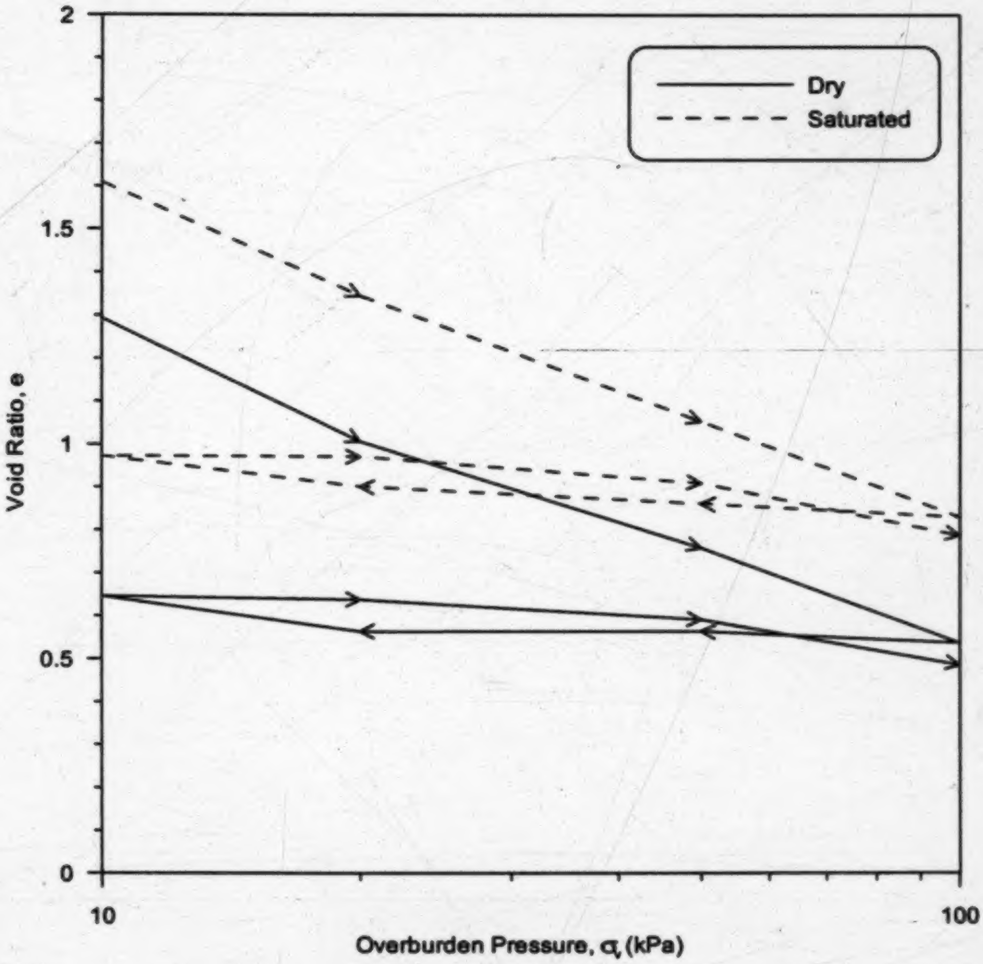

Figure D. 1 e versus logσv plot, No. 20 minus (TROC)

Table D. 2 Compressibility results, No. 10 - 20 (TROC)

Dry Conditions

Loading	σ_v (kPa)	ΔH_s (mm)	H_1 (mm)	γ_d (kN/m^3)	e	ε_a (%)
—	0	0.0	100.0	3.9	1.9	0.0
Load	10	21.2	78.8	4.9	1.3	-21.2
Load	20	7.0	71.8	5.4	1.1	-28.2
Load	50	8.8	63.0	6.2	0.8	-37.0
Load	100	7.2	55.9	6.9	0.6	-44.1
Unload	50	-1.9	57.8	6.7	0.7	-42.2
Unload	20	-3.4	61.2	6.3	0.8	-38.8
Unload	10	-2.7	63.9	6.1	0.9	-36.1
Reload	20	1.0	62.9	6.2	0.8	-37.1
Reload	50	2.8	60.1	6.5	0.8	-39.9
Reload	100	4.2	55.8	7.0	0.6	-44.2

Saturated Conditions

Loading	σ_v (kPa)	ΔH_s (mm)	H_1 (mm)	γ_d (kN/m^3)	e	ε_a (%)
—	0	0.0	95.0	3.4	2.3	0.0
Load	10	25.8	69.2	4.7	1.4	-25.8
Load	20	7.6	61.7	5.3	1.2	-33.3
Load	50	7.0	54.6	5.9	0.9	-40.4
Load	100	6.3	48.3	6.7	0.7	-46.7
Unload	50	-0.7	49.0	6.6	0.7	-46.0
Unload	20	-1.8	50.8	6.4	0.8	-44.2
Unload	10	-1.5	52.3	6.2	0.8	-42.7
Reload	20	0.4	51.9	6.2	0.8	-43.1
Reload	50	1.6	50.2	6.5	0.8	-44.8
Reload	100	3.0	47.3	6.9	0.7	-47.7

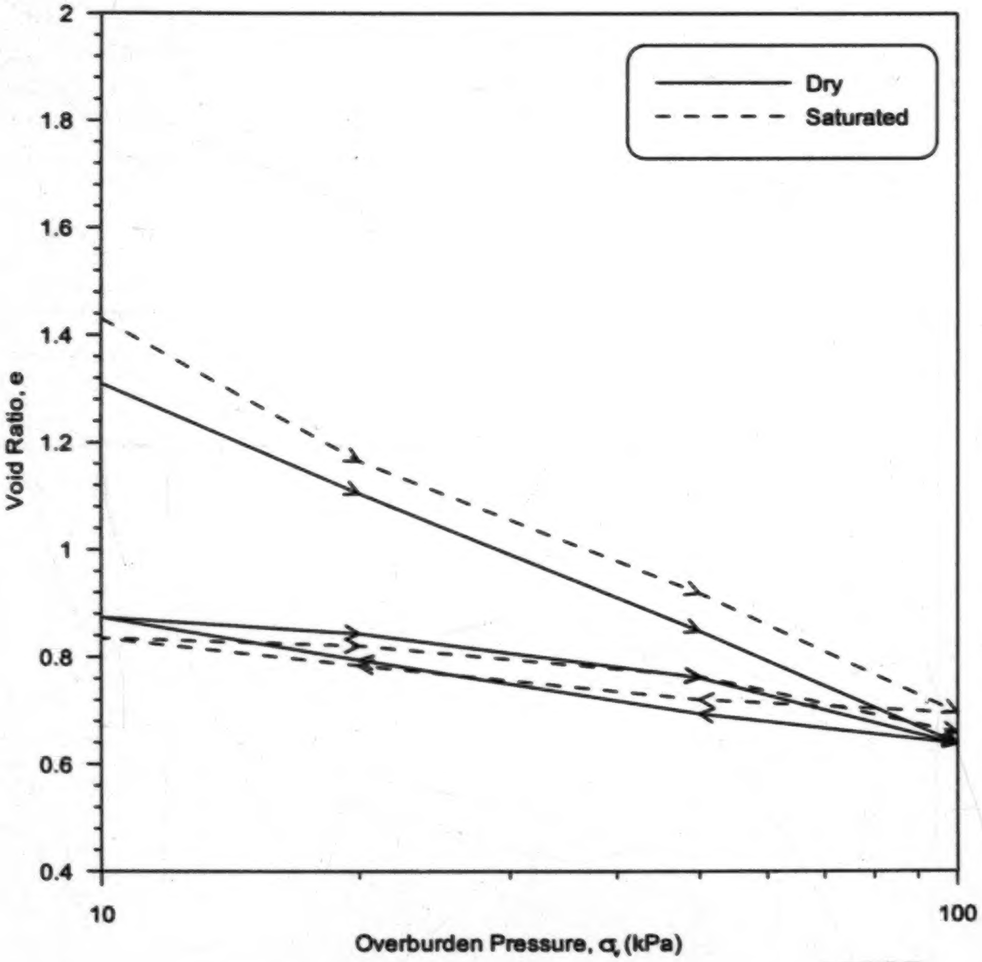

Figure D. 2 e versus logσ$_v$ plot, No. 10 - 20 (TROC)

Table D. 3 Compressibility results, No. 10 minus (Vulcan)

Dry Conditions

Loading	σ_v (kPa)	ΔH_a (mm)	H_1 (mm)	γ_d (kN/m^3)	e	ε_a (%)
—	0	0.0	100.0	3.7	2.1	0.0
Load	10	26.9	73.1	5.1	1.3	-26.9
Load	20	8.2	65.0	5.7	1.0	-35.0
Load	50	7.6	57.4	6.5	0.8	-42.6
Load	100	6.0	51.4	7.2	0.6	-48.6
Unload	50	-1.1	52.5	7.1	0.6	-47.5
Unload	20	-2.5	55.0	6.8	0.7	-45.0
Unload	10	-2.0	57.0	6.5	0.8	-43.0
Reload	20	0.4	56.5	6.6	0.8	-43.5
Reload	50	2.4	54.2	6.9	0.7	-45.8
Reload	100	3.5	50.7	7.3	0.6	-49.3

Saturated Conditions

Loading	σ_v (kPa)	ΔH_a (mm)	H_1 (mm)	γ_d (kN/m^3)	e	ε_a (%)
—	0	0.0	95.0	3.5	2.3	0.0
Load	10	21.7	73.3	4.5	1.6	-21.7
Load	20	7.9	65.4	5.1	1.3	-29.6
Load	50	7.7	57.7	5.7	1.0	-37.3
Load	100	4.0	53.8	6.2	0.9	-41.2
Unload	50	-0.6	54.4	6.1	0.9	-40.6
Unload	20	-1.8	56.2	5.9	1.0	-38.8
Unload	10	-1.6	57.8	5.7	1.0	-37.2
Reload	20	0.2	57.6	5.8	1.0	-37.4
Reload	50	1.3	56.2	5.9	1.0	-38.8
Reload	100	2.6	53.7	6.2	0.9	-41.3

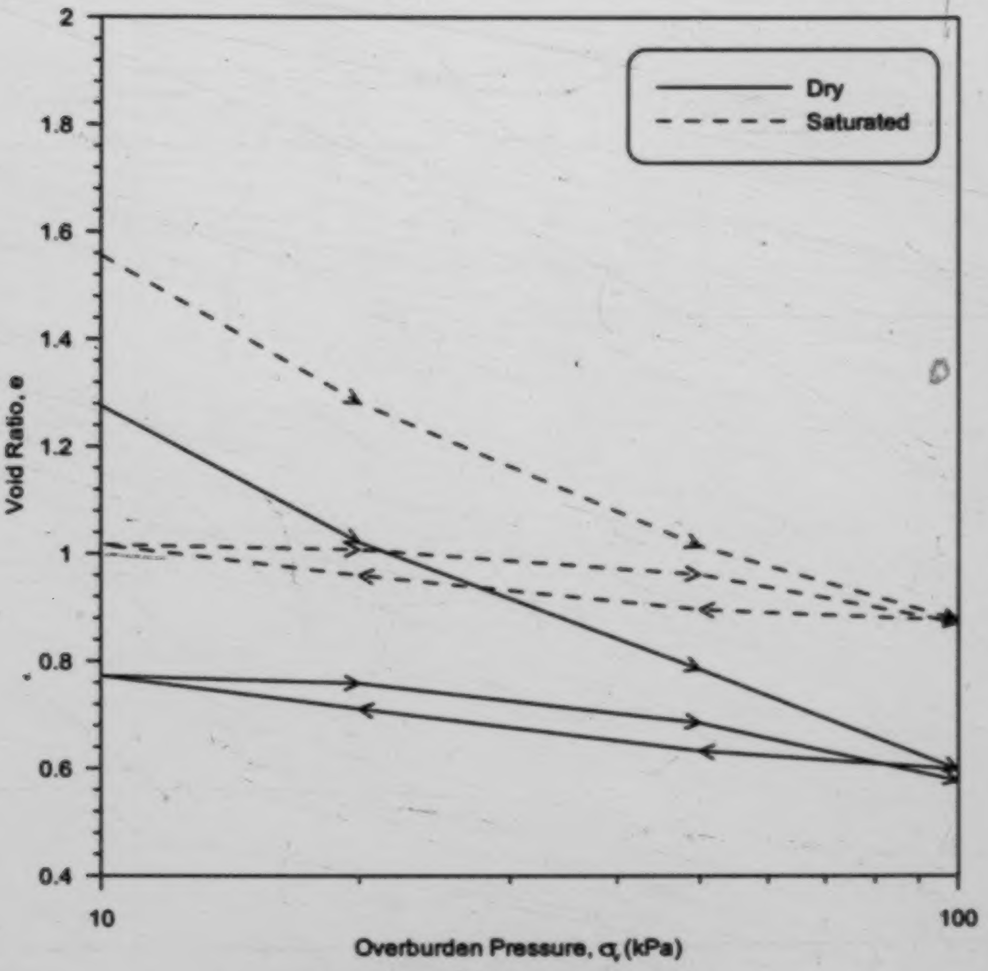

Figure D. 3 e versus logσ_v plot, No. 10 (Vulcan)

Table D. 4 Compressibility results, No. 8 - No. 14 (TROC), dry

Dry Conditions

Loading	σ_v (kPa)	ΔH_s (mm)	H_1 (mm)	γ_d (kN/m^3)	e	ε_v (%)
—	0	0.0	100.0	3.9	1.9	0.0
Load	10	20.8	79.2	4.9	1.3	-20.8
Load	20	6.2	73.0	5.3	1.1	-27.0
Load	50	8.6	64.4	6.0	0.9	-35.6
Load	100	7.2	57.2	6.8	0.7	-42.8
Unload	50	-1.9	59.1	6.5	0.7	-40.9
Unload	20	-3.7	62.8	6.2	0.8	-37.2
Unload	10	-2.7	65.5	5.9	0.9	-34.5
Reload	20	0.9	64.6	6.0	0.9	-35.4
Reload	50	3.1	61.5	6.3	0.8	-38.5
Reload	100	4.6	56.8	6.8	0.7	-43.2

Saturated Conditions

Loading	σ_v (kPa)	ΔH_s (mm)	H_1 (mm)	γ_d (kN/m^3)	e	ε_v (%)
—	0	0.0	93.0	3.7	2.1	0.0
Load	10	20.4	72.6	4.7	1.4	-20.4
Load	20	7.1	65.5	5.2	1.2	-27.5
Load	50	8.2	57.4	5.9	0.9	-35.6
Load	100	4.7	52.7	6.5	0.8	-40.3
Unload	50	-0.5	53.2	6.4	0.8	-39.8
Unload	20	-1.5	54.7	6.2	0.8	-38.3
Unload	10	-1.3	56.0	6.1	0.9	-37.0
Reload	20	0.3	55.6	6.1	0.9	-37.4
Reload	50	1.3	54.4	6.3	0.8	-38.6
Reload	100	2.1	52.2	6.5	0.7	-40.8

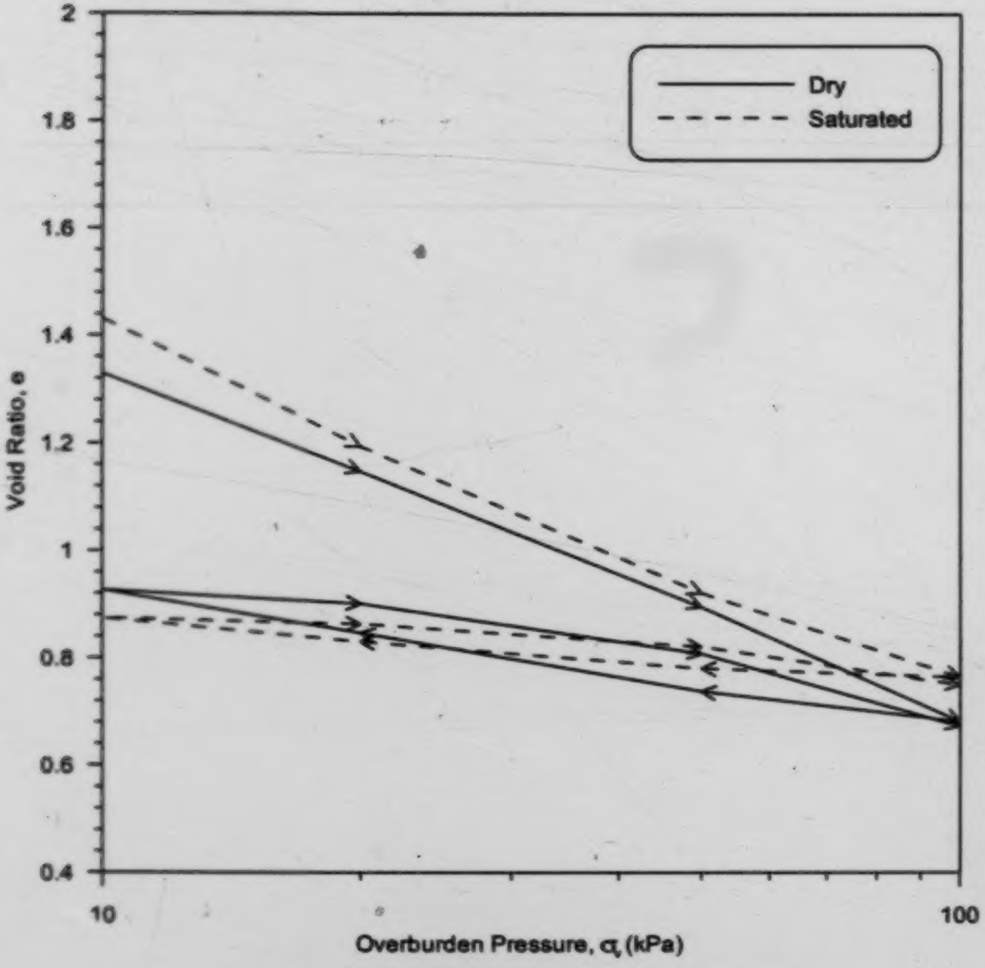

Figure D. 4 e versus logσv plot, No. 8 - No. 14 (TROC)

Table D. 5 Compressibility results, No. 4 - No. 8 (TROC)

Dry Conditions

Loading	σ_v (kPa)	ΔH_s (mm)	H_1 (mm)	γ_d (kN/m^3)	e	ε_a (%)
—	0	0.0	100.0	4.1	1.8	0.0
Load	10	17.5	82.5	4.9	1.3	-17.5
Load	20	5.5	77.0	5.3	1.1	-23.0
Load	50	8.4	68.5	5.9	0.9	-31.5
Load	100	4.8	63.7	6.4	0.8	-36.3
Unload	50	-1.5	65.2	6.3	0.8	-34.8
Unload	20	-2.9	68.1	6.0	0.9	-31.9
Unload	10	-2.8	70.9	5.7	1.0	-29.1
Reload	20	0.6	70.3	5.8	1.0	-29.7
Reload	50	2.0	68.3	6.0	0.9	-31.7
Reload	100	3.3	65.0	6.3	0.8	-35.0

Saturated Conditions

Loading	σ_v (kPa)	ΔH_s (mm)	H_1 (mm)	γ_d (kN/m^3)	e	ε_a (%)
—	0	0.0	100.0	3.9	1.9	0.0
Load	10	17.7	82.3	4.8	1.4	-17.7
Load	20	8.3	74.0	5.3	1.1	-26.0
Load	50	9.0	65.0	6.1	0.9	-35.0
Load	100	6.2	58.7	6.7	0.7	-41.3
Unload	50	-0.5	59.2	6.7	0.7	-40.8
Unload	20	-3.2	62.4	6.3	0.8	-37.6
Unload	10	-2.0	64.4	6.1	0.9	-35.6
Reload	20	0.7	63.7	6.2	0.8	-36.3
Reload	50	2.6	61.2	6.5	0.8	-38.8
Reload	100	4.3	56.9	6.9	0.6	-43.1

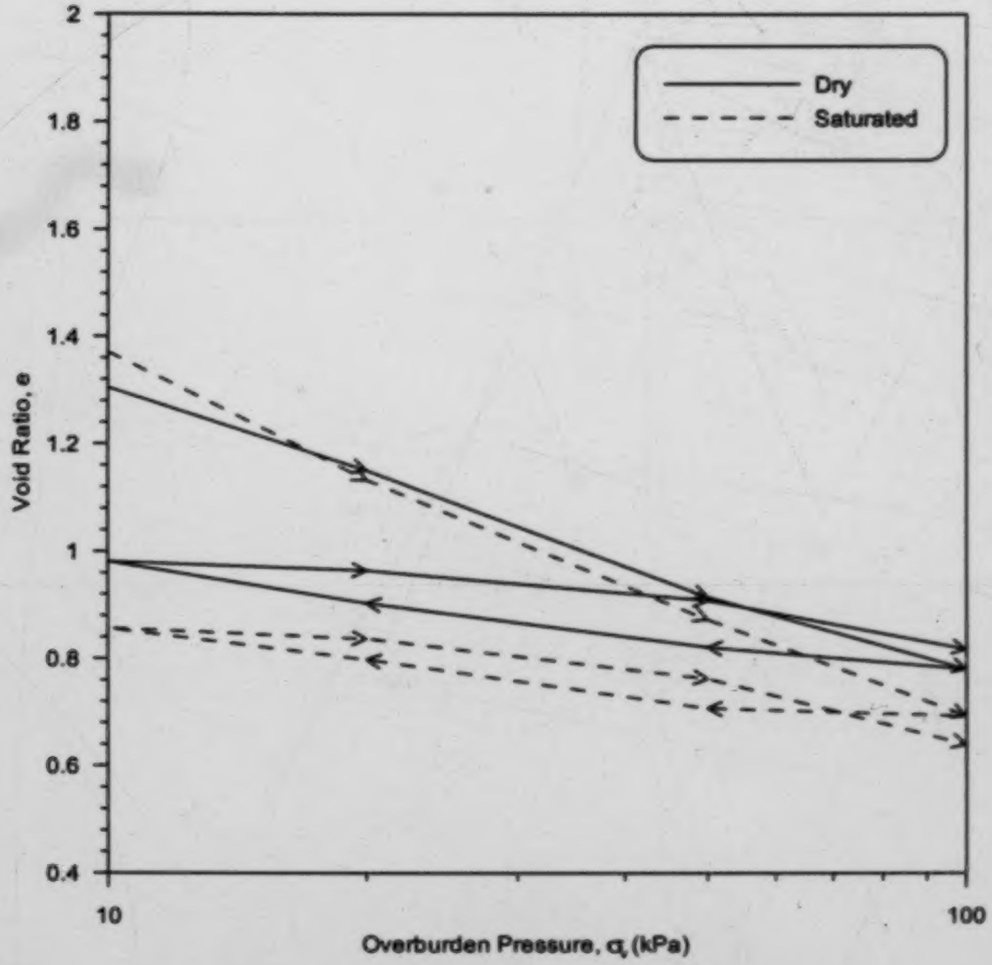

Figure D. 5 **e versus logσ_v plot, No. 4 - No. 8 (TROC)**

Table D. 6 Compressibility results, 1/4 in (Vulcan)

Dry Conditions

Loading	σ_v (kPa)	ΔH_v (mm)	H_1 (mm)	γ_d (kN/m^3)	e	ε_a (%)
—	0	0.0	100.0	3.9	2.0	0.0
Load	10	17.4	82.6	4.7	1.5	-17.4
Load	20	8.3	74.4	5.2	1.2	-25.6
Load	50	8.4	66.0	5.9	1.0	-34.0
Load	100	7.9	58.2	6.7	0.7	-41.8
Unload	50	-1.5	59.6	6.5	0.8	-40.4
Unload	20	-3.4	63.0	6.1	0.9	-37.0
Unload	10	-2.9	66.0	5.9	1.0	-34.0
Reload	20	0.6	65.4	5.9	1.0	-34.6
Reload	50	3.2	62.2	6.2	0.9	-37.8
Reload	100	4.7	57.6	6.7	0.7	-42.4

Saturated Conditions

Loading	σ_v (kPa)	ΔH_v (mm)	H_1 (mm)	γ_d (kN/m^3)	e	ε_a (%)
—	0	0.0	100.0	3.5	2.3	0.0
Load	10	27.0	73.0	4.8	1.4	-27.0
Load	20	6.0	67.0	5.2	1.2	-33.0
Load	50	8.2	58.8	6.0	0.9	-41.2
Load	100	3.9	55.0	6.4	0.8	-45.0
Unload	50	-1.5	56.4	6.2	0.9	-43.6
Unload	20	-2.8	59.2	5.9	1.0	-40.8
Unload	10	-2.0	61.2	5.7	1.0	-38.8
Reload	20	0.3	60.9	5.8	1.0	-39.1
Reload	50	1.3	59.6	5.9	1.0	-40.4
Reload	100	3.2	56.4	6.2	0.9	-43.6

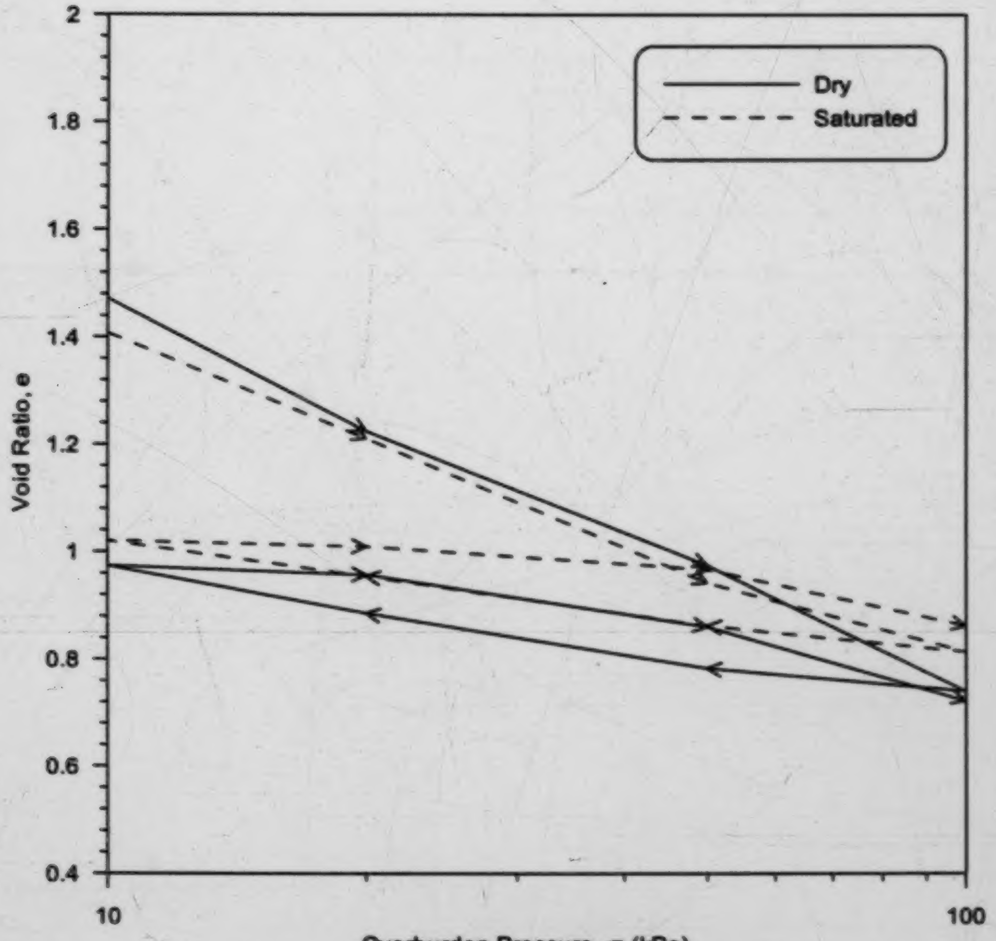

Figure D. 6 e versus logσ_v plot, 1/4 in (Vulcan)

APPENDIX E - HYDRAULIC CONDUCTIVITY

Table E. 1 Hydraulic conductivity results

Grain-Size Distribution	Supplier	σ_v (kPa)	e	n	γ_d (kN/m^3)	i	V @ 20°C (x10^{-2} cm/s)	k_{20} (x10^{-3} cm/s)
No. 20 minus	Tire Recyclers of Calgary	10	1.6	0.62	4.4	0.40 0.79 1.23	0.65 1.48 2.29	19.9
		20	1.3	0.57	4.9	0.46 0.91 1.80	1.21 2.28 3.95	20.2
		50	1.1	0.51	5.6	0.49 1.02 1.64	0.21 0.49 0.80	5.1
		100	0.8	0.45	6.3	0.63 1.25 1.88	0.10 0.21 0.31	1.7
No. 10 - No. 20	Tire Recyclers of Calgary	10	1.4	0.59	4.7	0.34 0.73 1.10	0.85 1.84 3.93	40.4
		20	1.2	0.54	5.3	0.55 0.95 1.40	1.95 3.18 4.23	26.7
		50	0.9	0.48	5.9	0.64 1.13 1.57	1.67 2.86 3.80	23.0
		100	0.7	0.41	6.7	0.71 1.23 1.73	1.17 1.96 2.75	15.4
No. 10	Midwest Tire Processors of Vulcan	10	1.6	0.61	4.5	0.30 0.65 1.03	1.14 2.43 3.52	32.5
		20	1.3	0.56	5.1	0.35 0.77 1.22	1.43 2.71 3.68	26.0
		50	1.0	0.50	5.7	0.40 0.87 1.38	1.09 2.17 3.06	20.0
		100	0.9	0.47	6.2	0.46 1.01 1.64	0.27 1.16 1.66	11.6

Table E. 1 Continued

Grain-Size Distribution	Supplier	σ_v (kPa)	e	n	γ_d (kN/m^3)	i	V @ 20°C ($x10^{-1}$ cm/s)	k_{20} ($x10^{-1}$ cm/s)
No. 8 - No. 14	Tire Recyclers of Calgary	10	1.4	0.59	4.7	0.28 0.64 0.97	0.78 1.98 3.03	32.4
		20	1.2	0.54	5.2	0.46 0.83 1.23	1.53 2.57 3.53	25.9
		50	0.9	0.48	5.9	0.55 0.98 1.45	1.37 2.44 3.38	22.1
		100	0.8	0.43	6.5	0.60 1.08 1.60	1.27 2.22 3.00	17.3
No. 4 - No. 8	Tire Recyclers of Calgary	10	1.4	0.58	4.8	0.32 0.62 1.26	1.40 2.51 4.17	28.7
		20	1.1	0.53	5.3	0.35 0.68 1.35	1.21 2.28 3.95	27.0
		50	0.9	0.47	6.1	0.47 0.90 1.31 1.76	0.70 1.78 2.73 3.43	21.2
		100	0.7	0.41	6.7	0.40 0.83 1.22	0.80 1.43 1.78	11.8
1/4 in	Midwest Tire Processors of Vulcan	10	1.4	0.58	4.8	0.18 0.55 0.89 1.23	0.44 1.98 2.87 3.52	29.0
		20	1.2	0.55	5.2	0.17 0.53 0.91 1.28	0.75 1.82 2.79 3.57	25.5
		50	0.9	0.48	6.0	0.23 0.70 1.14	0.68 1.90 2.82	23.5
		100	0.8	0.45	6.4	0.25 0.76 1.24	0.66 1.77 2.63	20.1

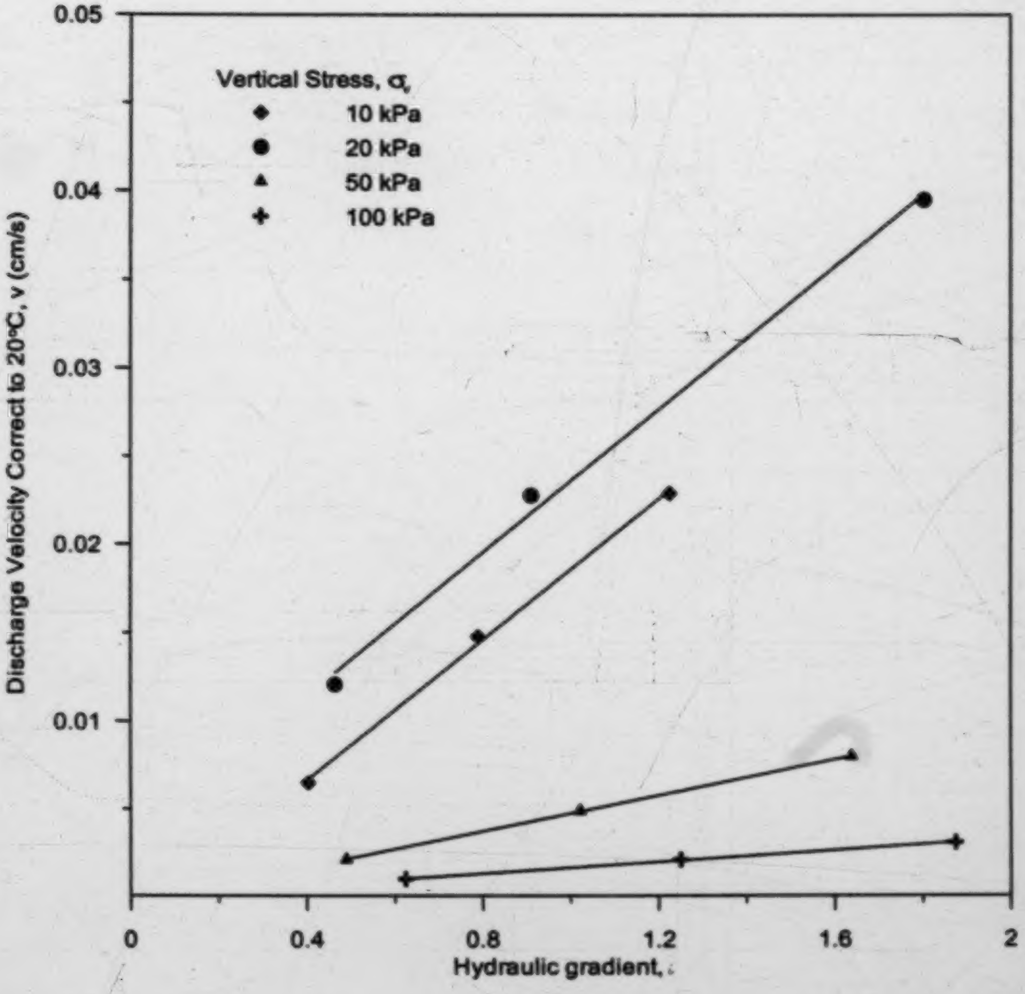

Figure E. 1 Discharge velocity versus hydraulic gradient, No. 20 minus (TROC)

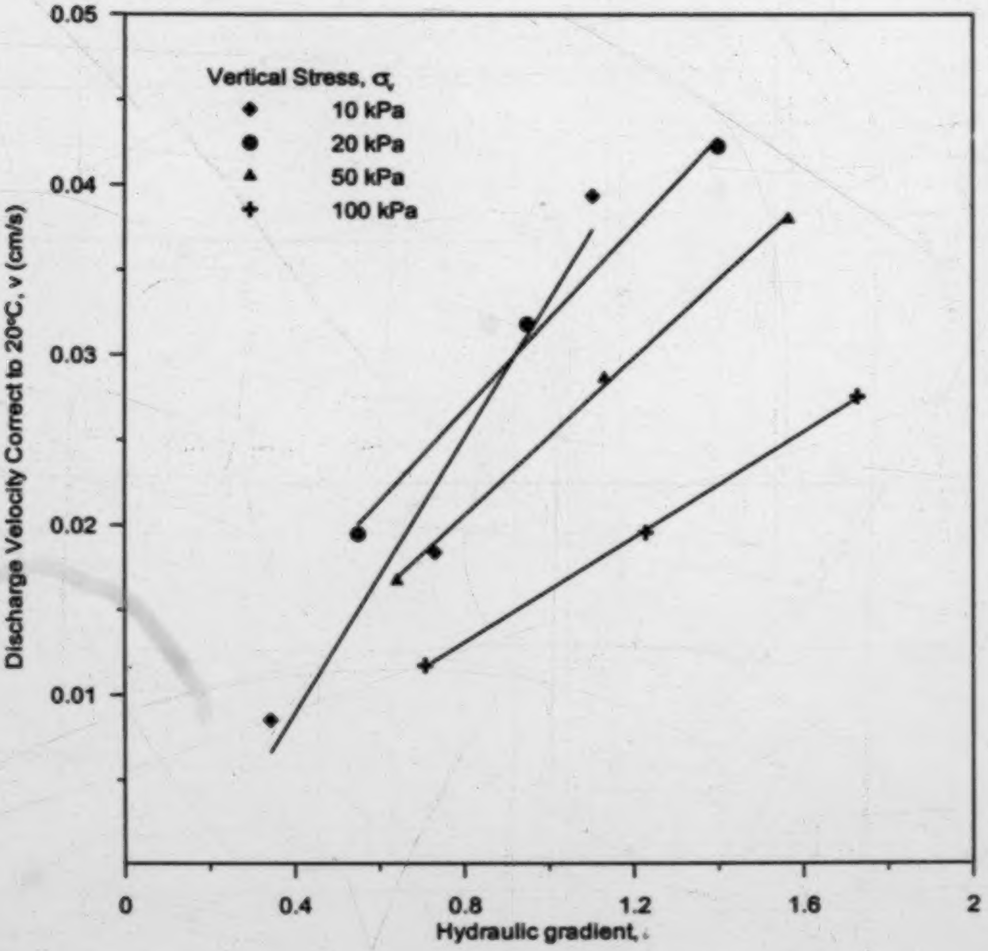

Figure E. 2 Discharge velocity versus hydraulic gradient, No. 10 - 20 (TROC)

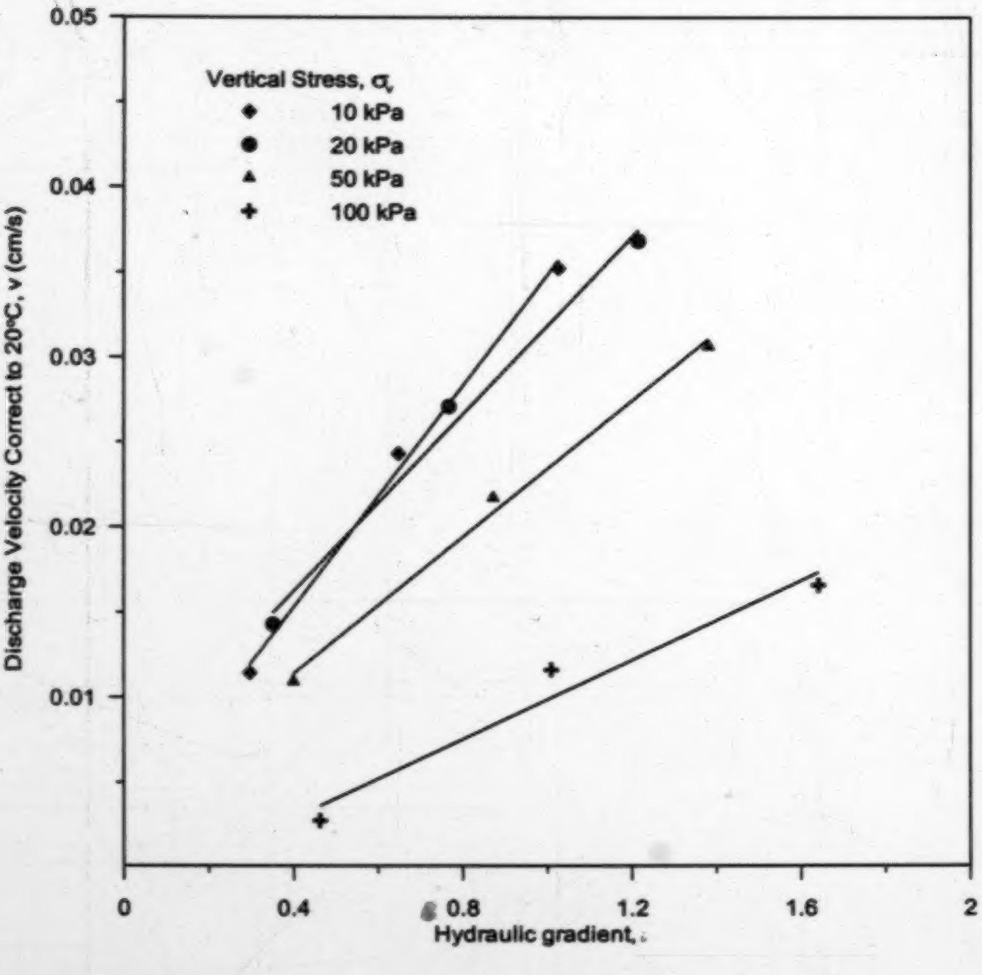

Figure E. 3 Discharge velocity versus hydraulic gradient, No. 10 (Vulcan)

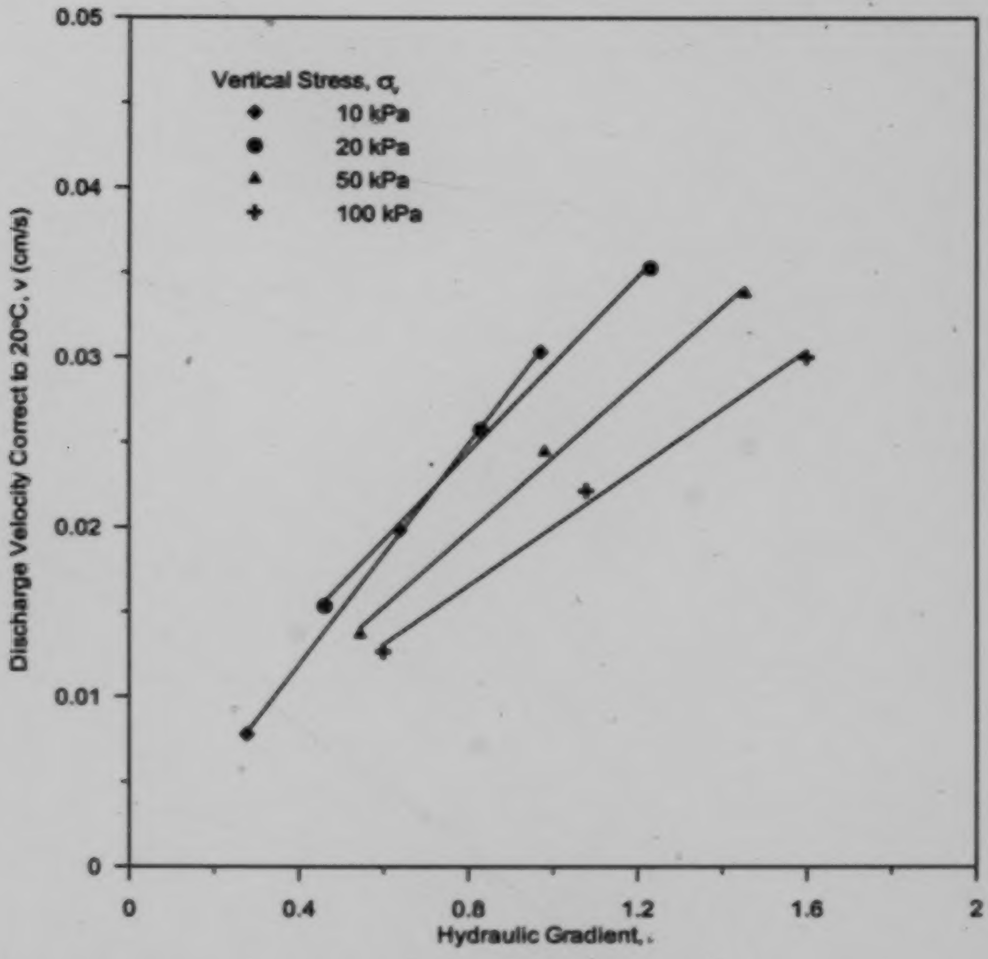

Figure E. 4 Discharge velocity versus hydraulic gradient, No. 8 - No. 14 (TROC)

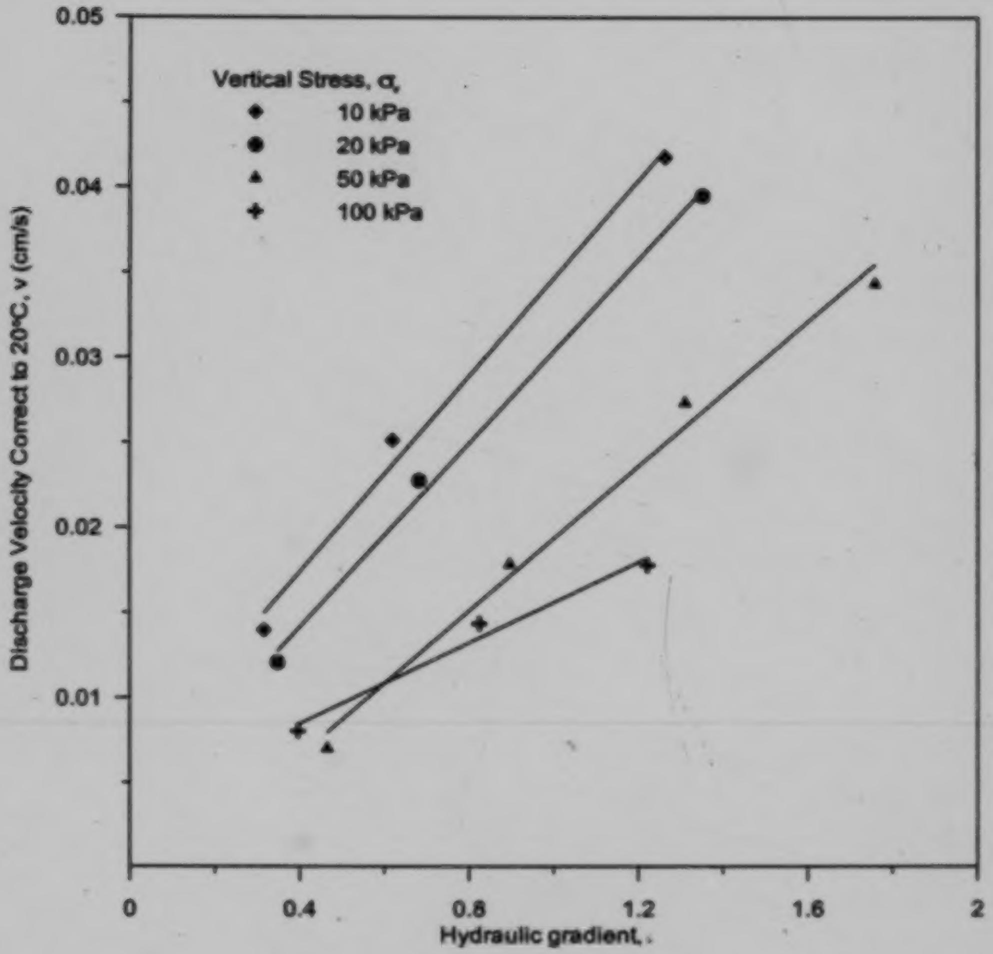

Figure E. 5 Discharge velocity versus hydraulic gradient, No. 4 - No. 8 (TROC)

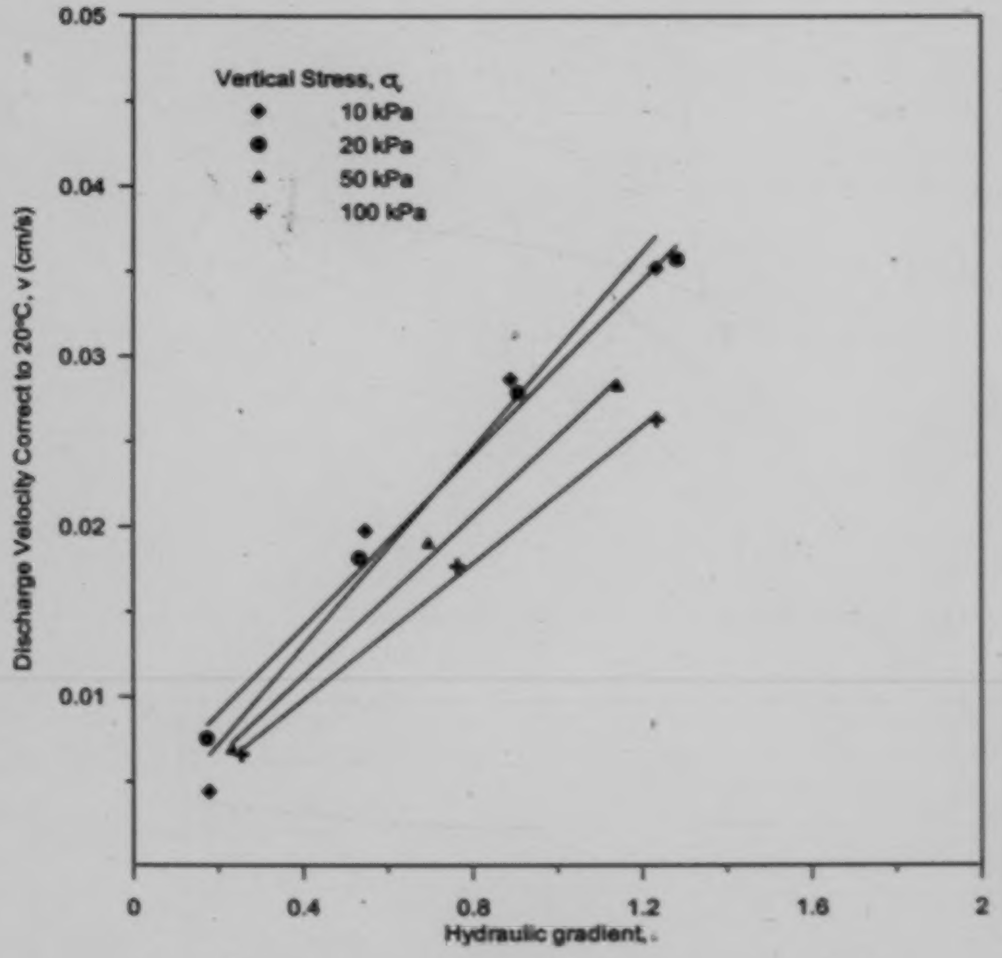

Figure E. 6 Discharge velocity versus hydraulic gradient, 1/4 in (Vulcan)

APPENDIX F - THERMAL CONDUCTIVITY

Table F. 1 RTD Calibrations

Cell No.	RTD No.	Temperature. (°C)	Calibrated RTD Reading, R_o (ohms)
1	1	0	100.37
2	2	0	100.22
3	3	0	100.54
4	4 (TC 1)	0	100.84
5	5 (TC 2)	0	100.68
6	6 (TC 3)	0	100.68

Example Calculations

GSD: No. 10
Supplier: Midwest Tire Processors of Vulcan
Cell No.: 3

State of Compaction: Loose
Degree of Saturation: 0% (dry)
Test Temp: +24°C (unfrozen)

Time (mm.ss.ss)	Time Elapsed (sec)	ln time (sec)	R_T (ohms)	Temperature (°C)	Time (mm.ss.ss)	Time Elapsed (sec)	ln time (sec)	RTD Reading (ohms)	Temp. (°C)
00:00.0	0.00		109.88	24.3	06:20.0	380.00	5.94	111.92	29.6
00:05.0	5.00	1.61	109.91	24.3	06:30.0	390.00	5.97	111.95	29.6
00:10.0	10.00	2.30	109.98	24.5	06:40.0	400.00	5.99	111.97	29.7
00:20.0	20.00	3.00	110.09	24.8	06:50.0	410.00	6.02	111.99	29.7
00:30.0	30.00	3.40	110.20	25.1	07:00.0	420.00	6.04	112.01	29.8
00:40.0	40.00	3.69	110.31	25.4	07:10.0	430.00	6.06	112.03	29.8
00:50.0	50.00	3.91	110.42	25.7	07:20.0	440.00	6.09	112.05	29.9
01:00.0	60.00	4.09	110.50	25.9	07:30.0	450.00	6.11	112.07	29.9
01:10.0	70.00	4.25	110.59	26.1	07:40.0	460.00	6.13	112.09	30.0
01:20.0	80.00	4.38	110.66	26.3	07:50.0	470.00	6.15	112.11	30.1
01:30.0	90.00	4.50	110.74	26.5	08:00.0	480.00	6.17	112.13	30.1
01:40.0	100.00	4.61	110.81	26.7	08:10.0	490.00	6.19	112.15	30.2
01:50.0	110.00	4.70	110.88	26.9	08:20.0	500.00	6.21	112.17	30.2
02:00.0	120.00	4.79	110.94	27.0	08:30.0	510.00	6.23	112.19	30.3
02:10.0	130.00	4.87	111.00	27.2	08:40.0	520.00	6.25	112.2	30.3
02:20.0	140.00	4.94	111.06	27.3	08:50.0	530.00	6.27	112.22	30.3
02:30.0	150.00	5.01	111.11	27.5	09:00.0	540.00	6.29	112.24	30.4
02:40.0	160.00	5.08	111.17	27.6	09:10.0	550.00	6.31	112.25	30.4
02:50.0	170.00	5.14	111.21	27.7	09:20.0	560.00	6.33	112.26	30.4
03:00.0	180.00	5.19	111.24	27.8	09:30.0	570.00	6.35	112.28	30.5
03:10.0	190.00	5.25	111.28	27.9	09:40.0	580.00	6.36	112.30	30.5
03:20.0	200.00	5.30	111.35	28.1	09:50.0	590.00	6.38	112.31	30.6
03:30.0	210.00	5.35	111.39	28.2	10:00.0	600.00	6.40	112.32	30.6
03:40.0	220.00	5.39	111.44	28.3	11:00.0	660.00	6.49	112.40	30.8
03:50.0	230.00	5.44	111.47	28.4	12:00.0	720.00	6.58	112.48	31.0
04:00.0	240.00	5.48	111.51	28.5	13:00.0	780.00	6.66	112.54	31.2
04:10.0	250.00	5.52	111.55	28.6	14:00.0	840.00	6.73	112.60	31.3
04:20.0	260.00	5.56	111.58	28.7	15:00.0	900.00	6.80	112.65	31.5
04:30.0	270.00	5.60	111.61	28.8	16:00.0	960.00	6.87	112.70	31.6
04:40.0	280.00	5.63	111.65	28.9	17:00.0	1020.00	6.93	112.74	31.7
04:50.0	290.00	5.67	111.68	28.9	18:00.0	1080.00	6.98	112.79	31.8
05:00.0	300.00	5.70	111.71	29.0	19:00.0	1140.00	7.04	112.82	31.9
05:10.0	310.00	5.74	111.74	29.1	20:00.0	1200.00	7.09	112.86	32.0
05:20.0	320.00	5.77	111.77	29.2					
05:30.0	330.00	5.80	111.79	29.2					
05:40.0	340.00	5.83	111.82	29.3					
05:50.0	350.00	5.86	111.85	29.4					
06:00.0	360.00	5.89	111.88	29.5					
06:10.0	370.00	5.91	111.90	29.5					

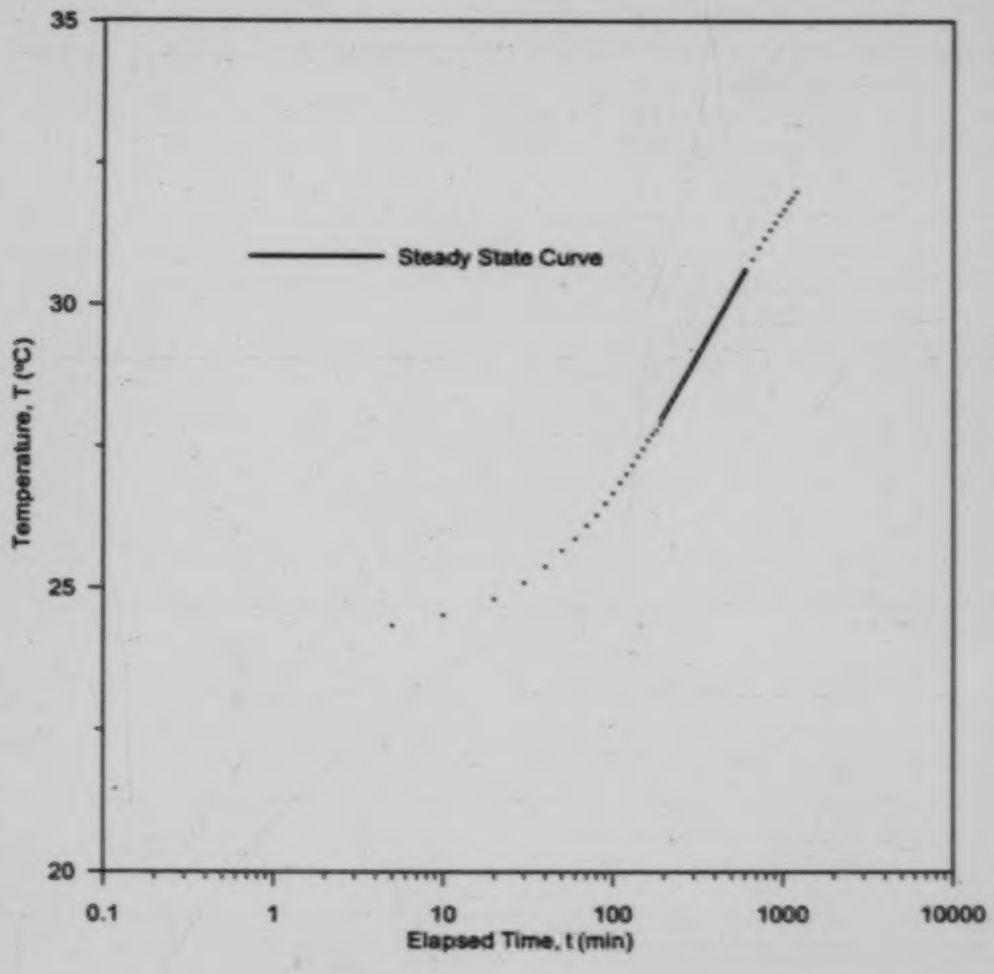

Date: 28-September-1998
Cell No. 3
H_c: 18.87 mm
Potential Drop, Vr: 0.041 V
Voltage to Heater Probe, Vp: 6.0 V
R_c: 100.54 ohms
Current, I: 0.02 amps
Voltage Across Heater, $V_p - V_r$: 5.96 V

Power at Probe: 0.12 W
Probe Length: 0.0483 m
Power/Unit Length Probe, Q: 2.53 W/m
Slope of Steady State Curve: 2.324
Thermal Conductivity, λ: 0.0483 W/m-°C

$$Q = \frac{EI}{L} = \frac{(V_p - V_r)(V_r/2)}{L}$$

$$\lambda = \frac{Q}{4\pi(T_2 - T_1)} \ln\left(\frac{t_2}{t_1}\right)$$

Table F. 2 Thermal conductivity, λ, from thermal needle method, dry-loose

Tire Crumb Size	Supplier	γ_d (kN/m³)	e	T (°C)	λ (W/m-°C)
No. 20 Minus	Tire Recyclers of Calgary	3.7	2.1	24	0.086
				-10	0.075
				-4	0.083
				2	0.082
				25	0.091
No. 10 - No. 20	Tire Recyclers of Calgary	4.0	1.8	24	0.098
				-10	0.089
				-4	0.091
				2	0.093
				24	0.099
No. 10	Midwest Tire Processors of Vulcan	3.8	2.1	24	0.087
				-10	0.091
				-5	0.084
				2	0.084
				24	0.094
No. 8 - No. 14	Tire Recyclers of Calgary	4.0	1.8	24	0.085
				-10	0.080
				-4	0.145
				2	0.146
				25	0.159
No. 4 - No. 8	Tire Recyclers of Calgary	4.1	1.8	24	0.096
				-10	0.088
				-4	0.150
				2	0.151
				24	0.161
1/4 in	Midwest Tire Processors of Vulcan	4.0	1.9	24	0.097
				-10	0.089
				-4	0.152
				3	0.155
				24	0.167
1/4 in	Alberta Environmental Rubber Products	5.1	1.2	22	0.107
				-11	0.125
				-5	0.127
				3	0.130
				25	0.142

Table F. 3 Thermal conductivity, λ, from thermal needle method, dry-compacted

Tire Crumb Size	Supplier	γ_d (kN/m³)	e	T (°C)	λ (W/m-°C)
No. 20 Minus	Tire Recyclers of Calgary	5.3	1.2	22	0.130
				-11	0.125
				-6	0.139
				2	0.121
				21	0.138
No. 10 - No. 20	Tire Recyclers of Calgary	5.4	1.1	24	0.137
				-12	0.123
				-5	0.151
				3	0.127
				23	0.138
No. 10	Midwest Tire Processors of Vulcan	5.7	1.0	23	0.117
				-13	0.110
				-6	0.115
				2	0.111
				22	0.117
No. 8 - No. 14	Tire Recyclers of Calgary	5.6	1.0	23	0.123
				-12	0.116
				-5	0.113
				3	0.116
				23	0.119
No. 4 - No. 8	Tire Recyclers of Calgary	5.5	1.1	23	0.133
				-12	0.150
				-5	0.104
				3	0.118
				23	0.125
1/4 in	Midwest Tire Processors of Vulcan	5.8	1.0	24	0.135
				-12	0.121
				-5	0.124
				3	0.125
				23	0.129
1/4 in	Alberta Environmental Rubber Products	6.2	0.8	22	0.122
				-11	0.136
				-5	0.115
				2	0.116
				22	0.120

Table F. 4 Thermal conductivity, λ, from thermal needle method, saturated-loose

Tire Crumb Size	Supplier	γ_d (kN/m^3)	e	T (°C)	λ (W/m-°C)
No. 20 Minus	Tire Recyclers of Calgary	3.2	2.8	24	0.566
				-11	1.376
				-5	1.388
				1	0.466
				23	0.590
No. 10 - No. 20	Tire Recyclers of Calgary	3.5	2.2	24	0.612
				-11	1.398
				-5	1.340
				2	0.493
				22	0.624
No. 10	Midwest Tire Processors of Vulcan	3.3	2.5	24	0.634
				-11	1.459
				-5	1.517
				1	0.510
				22	0.624
No. 8 - No. 14	Tire Recyclers of Calgary	3.8	2.0	24	0.663
				-10	1.343
				-5	1.314
				2	0.510
				22	0.624
No. 4 - No. 8	Tire Recyclers of Calgary	3.8	1.9	24	0.663
				-10	1.410
				-4	1.363
				2	0.555
				22	0.624
1/4 in	Midwest Tire Processors of Vulcan	3.9	1.9	24	0.871
				-10	1.409
				-5	1.381
				1	0.168
				22	0.624
1/4 in	Alberta Environmental Rubber Products	4.7	1.3	25	0.872
				-11	1.288
				-5	1.214
				2	0.468
				22	0.624

Table F. 5 Thermal conductivity, λ, from thermal needle method, saturated-compacted

Tire Crumb Size	Supplier	γ_d (kN/m³)	e	T (°C)	λ (W/m-°C)
No. 20 Minus	Tire Recyclers of Calgary	5.1	0.9	22	0.444
				-10	0.989
				-5	1.006
				3	0.396
				22	0.423
No. 10 - No. 20	Tire Recyclers of Calgary	5.3	0.9	23	0.422
				-10	0.991
				-5	0.995
				3	0.356
				21	0.387
No. 10	Midwest Tire Processors of Vulcan	5.4	0.9	23	0.451
				-10	0.999
				-5	1.065
				3	0.415
				21	0.444
No. 8 - No. 14	Tire Recyclers of Calgary	5.6	0.8	23	0.413
				-10	0.876
				-5	0.874
				3	0.400
				21	0.409
No. 4 - No. 8	Tire Recyclers of Calgary	5.3	0.8	23	0.376
				-10	0.888
				-5	0.879
				3	0.352
				21	0.367
1/4 in	Midwest Tire Processors of Vulcan	5.3	0.9	23	0.374
				-10	0.822
				-5	0.709
				3	0.174
				21	0.206
1/4 in	Alberta Environmental Rubber Products	5.8	0.4	22	0.426
				-11	0.877
				-5	0.847
				3	0.189
				22	0.207

Table F. 6 Measured thermal conductivity, λ, for dry tire crumbs under different vertical stresses

Tire Crumb Size, US Sieve Designation	Supplier	σ_v (kPa)	λ (W/m-°C)	γ_d (kN/m³)	e
No. 20 Minus	Tire Recyclers of Calgary	0	0.14	3.8	2.0
		10	0.17	4.9	1.3
		20	0.18	5.4	1.1
		50	0.20	6.2	0.9
		100	0.22	6.8	0.7
No. 10 - No. 20	Tire Recyclers of Calgary	0	0.13	4.0	1.8
		10	0.16	4.9	1.3
		20	0.17	5.4	1.1
		50	0.20	6.1	0.9
		100	0.21	6.8	0.7
No. 10	Midwest Tire Processors of Vulcan	0	0.13	3.8	2.0
		10	0.16	4.9	1.4
		20	0.17	5.5	1.1
		50	0.20	6.4	0.8
		100	0.22	7.0	0.6
No. 8 - No. 14	Tire Recyclers of Calgary	0	0.14	3.9	1.9
		10	0.16	5.0	1.3
		20	0.17	5.5	1.1
		50	0.20	6.4	0.8
		100	0.22	7.3	0.6
No. 4 - No. 8	Tire Recyclers of Calgary	0	0.14	4.0	1.9
		10	0.16	4.7	1.4
		20	0.16	5.2	1.2
		50	0.19	6.1	0.9
		100	0.21	6.9	0.7
1/4 in	Midwest Tire Processors of Vulcan	0	0.13	4.0	1.9
		10	0.15	4.7	1.5
		20	0.16	5.2	1.2
		50	0.18	6.0	0.9
		100	0.20	6.7	0.7
1/4 in	Alberta Environmental Rubber Products	0	0.16	5.3	1.1
		10	0.17	5.7	1.0
		20	0.18	5.9	0.9
		50	0.19	6.2	0.8
		100	0.19	6.7	0.7

Table F. 7 Measured thermal conductivity, λ, for saturated tire crumbs under different vertical stresses

Tire Crumb Size, US Sieve Designation	Supplier	σ_v (kPa)	λ (W/m-°C)	γ_d (kN/m^3)	e
No. 20 Minus	Tire Recyclers of Calgary	0	0.79	3.8	2.1
		10	0.58	4.9	1.3
		20	0.57	5.5	1.1
		50	0.60	6.5	0.8
		100	0.61	7.4	0.6
1/4 in	Midwest Tire Processors of Vulcan	0	0.55	3.8	2.0
		10	0.68	4.7	1.5
		20	0.65	5.4	1.2
		50	0.59	6.2	0.9
		100	0.53	7.0	0.7
1/4 in	Alberta Environmental Rubber Products	0	0.60	3.8	2.0
		10	0.62	4.1	1.9
		20	0.57	4.3	1.7
		50	0.59	4.6	1.5
		100	0.54	5.0	1.3

APPENDIX G - SHEAR STRENGTH

DIRECT SHEAR

Table G. 1 Direct shear results

Grain-Size Distribution	Supplier	Test Conditions	σ_N (kPa)	ΔH (mm)	τ (kPa)
No. 20 minus	Tire Recyclers of Calgary	Dry	25	2	10.3
				4	13.0
				8	16.7
				12	21.1
			50	2	15.0
				4	22.3
				8	34.2
				12	38.4
			100	2	36.1
				4	48.6
				8	63.8
				12	70.5
		Saturated	25	2	7.6
				4	10.4
				8	15.6
				12	20.5
			50	2	10.9
				4	17.8
				8	30.1
				12	37.7
			100	2	23.6
				4	36.4
				8	57.3
				12	69.8
No. 10 - No. 20	Tire Recyclers of Calgary	Dry	25	2	4.4
				4	7.5
				8	12.3
				12	15.7
			50	2	7.6
				4	15.2
				8	28.8
				12	32.9
			100	2	11.9
				4	25.8
				8	52.0
				12	61.9
No. 10	Midwest Tire Processors of Vulcan	Dry	25	2	4.4
				4	7.5
				8	12.3
				12	15.7
			50	2	7.6
				4	15.2
				8	28.8
				12	32.9
			100	2	11.9
				4	25.8
				8	52.0
				12	61.9

Table G. 1 Continued

Grain-Size Distribution	Supplier	Test Conditions	σ_N (kPa)	ΔH (mm)	τ (kPa)
No. 8 - No. 14	Tire Recyclers of Calgary	Dry	25	2	11.2
				4	12.8
				8	20.2
				12	19.4
			50	2	14.9
				4	21.5
				8	32.6
				12	34.5
			100	2	24.3
				4	37.5
				8	58.4
				12	63.9
No. 4 - No. 8	Tire Recyclers of Calgary	Dry	25	2	9.9
				4	14.2
				8	19.2
				12	21.3
			50	2	13.7
				4	20.2
				8	31.7
				12	36.0
			100	2	23.4
				4	45.8
				8	67.7
				12	72.5
1/4 in	Midwest Tire Processors of Vulcan	Dry	25	2	6.8
				4	10.6
				8	17.3
				12	19.7
			50	2	8.6
				4	15.5
				8	27.9
				12	37.2
			100	2	15.7
				4	32.0
				8	62.3
				12	74.2
		Saturated	25	2	6.3
				4	10.0
				8	15.5
				12	14.8
			50	2	8.7
				4	16.8
				8	28.3
				12	29.6
			100	2	16.4
				4	29.9
				8	52.7
				12	57.0

Table G. 1 Continued

Grain-Size Distribution	Supplier	Test Conditions	σ_N (kPa)	ΔH (mm)	τ (kPa)
1/4 in	Alberta Environmental Rubber Products	Dry	25	2	8.4
				4	13.5
				8	20.2
				12	21.8
			50	2	9.8
				4	18.0
				8	31.0
				12	35.1
			100	2	15.3
				4	29.5
				8	54.2
				12	64.4
		Saturated	25	2	9.8
				4	15.2
				8	21.3
				12	26.5
			50	2	9.8
				4	17.3
				8	30.1
				12	41.9
			100	2	17.0
				4	30.1
				8	50.9
				12	76.8

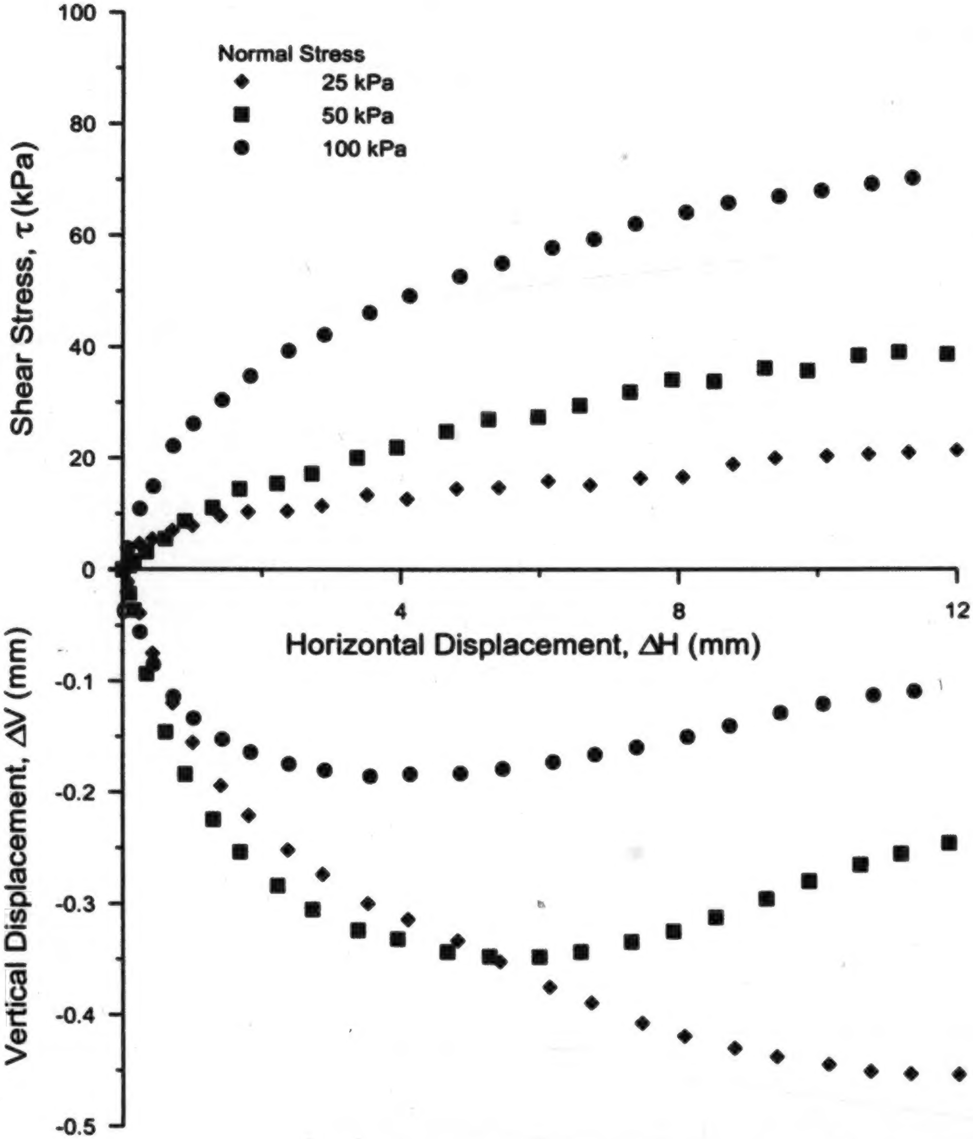

Figure G. 1 Shear stress and vertical displacement versus horizontal displacement, dry, No. 20 minus (Tire Recyclers of Calgary)

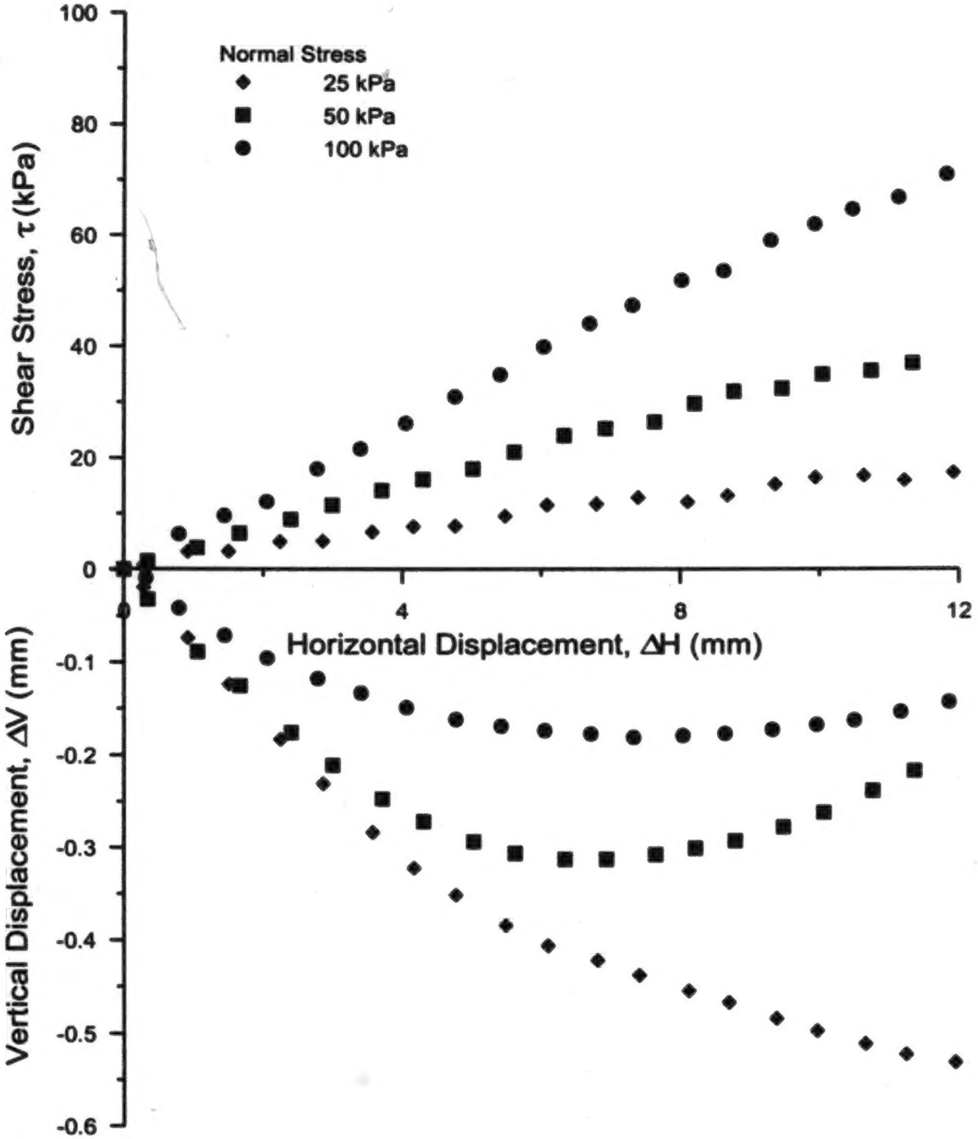

Figure G. 2 Shear stress and vertical displacement versus horizontal displacement, dry, No. 10 - No. 20 (Tire Recyclers of Calgary)

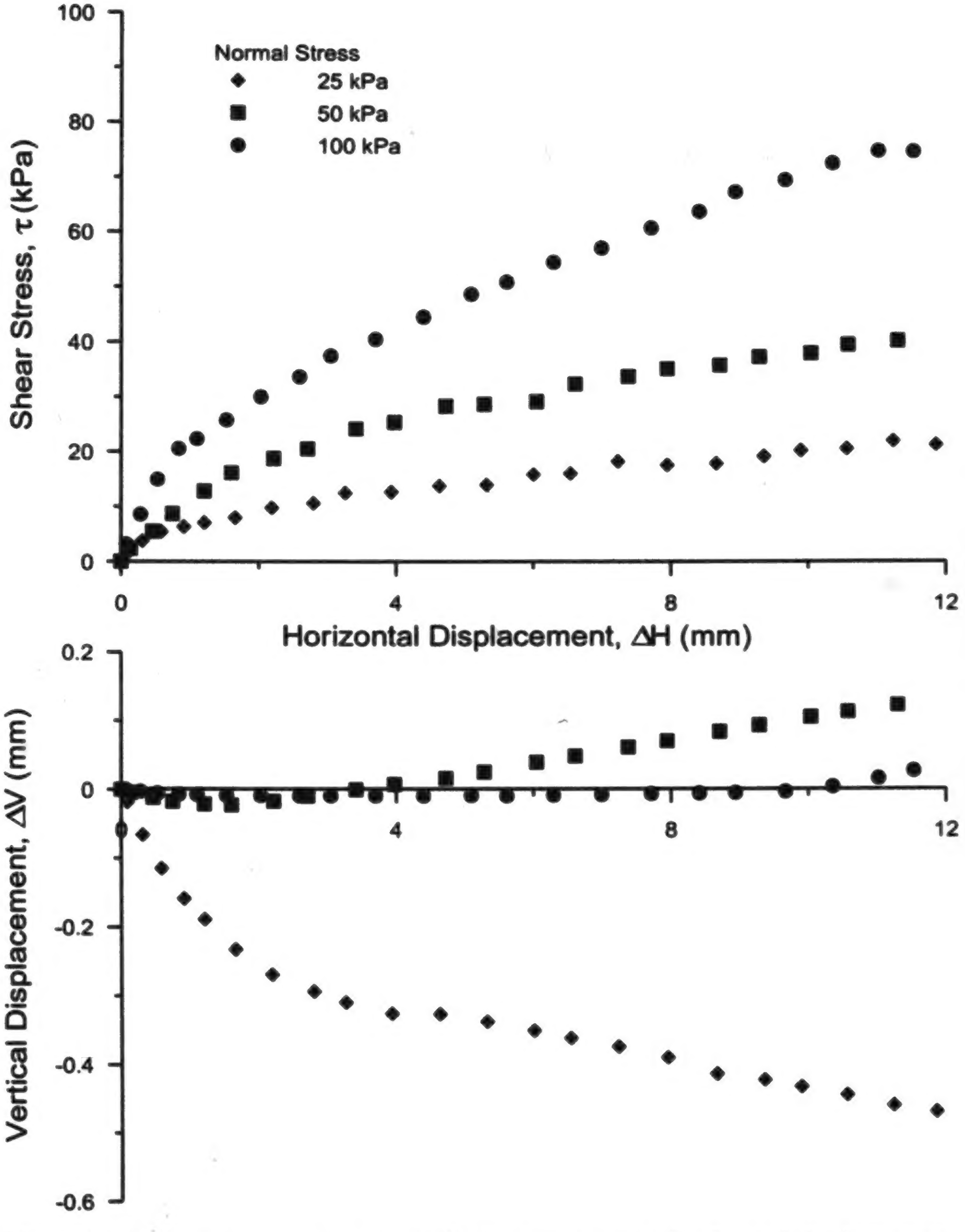

Figure G. 3 Shear stress and vertical displacement versus horizontal displacement, dry, No. 10 (Midwest Tire Processors of Vulcan)

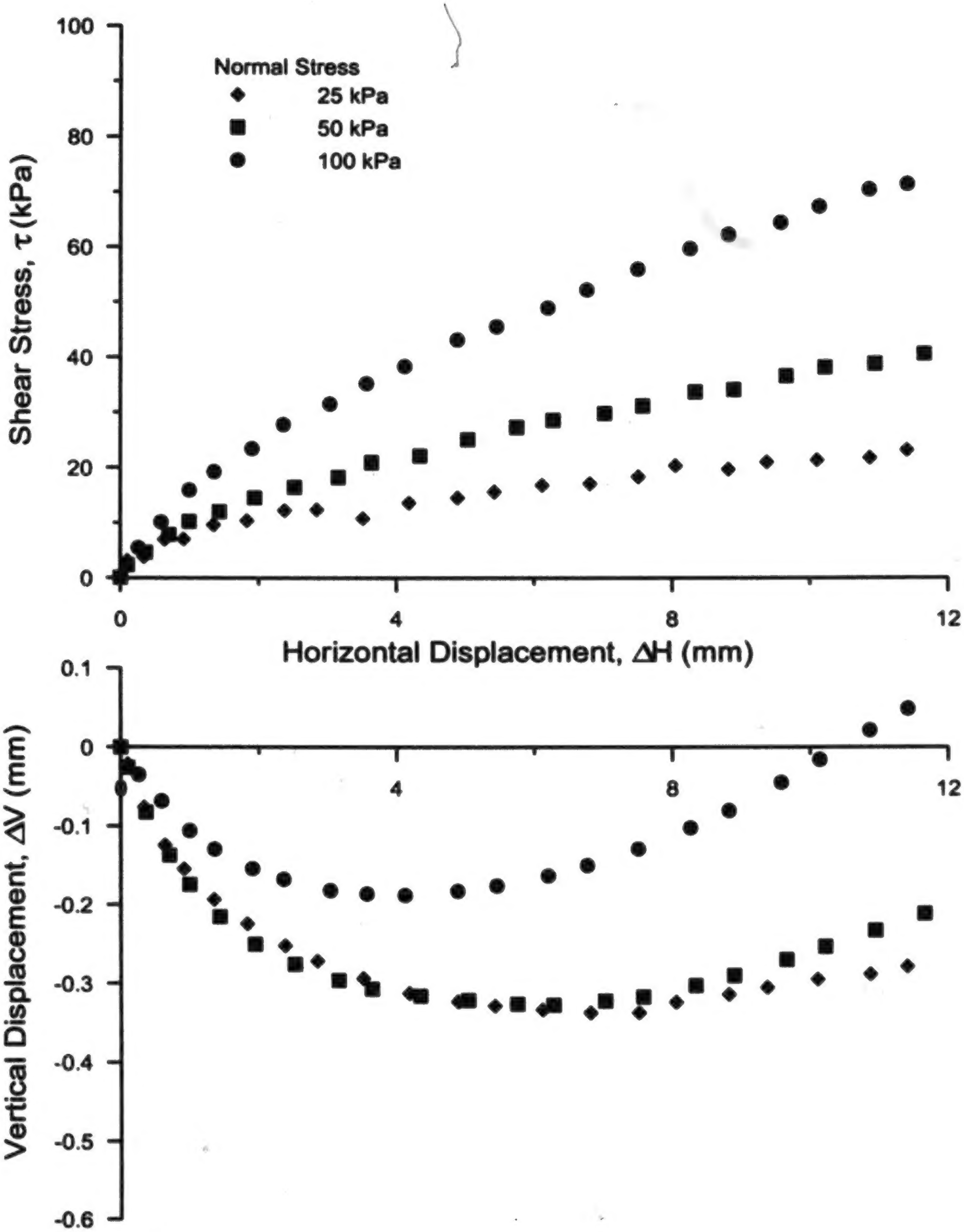

Figure G. 4 Shear stress and vertical displacement versus horizontal displacement, No. 8 - No. 14 (Tire Recyclers of Calgary)

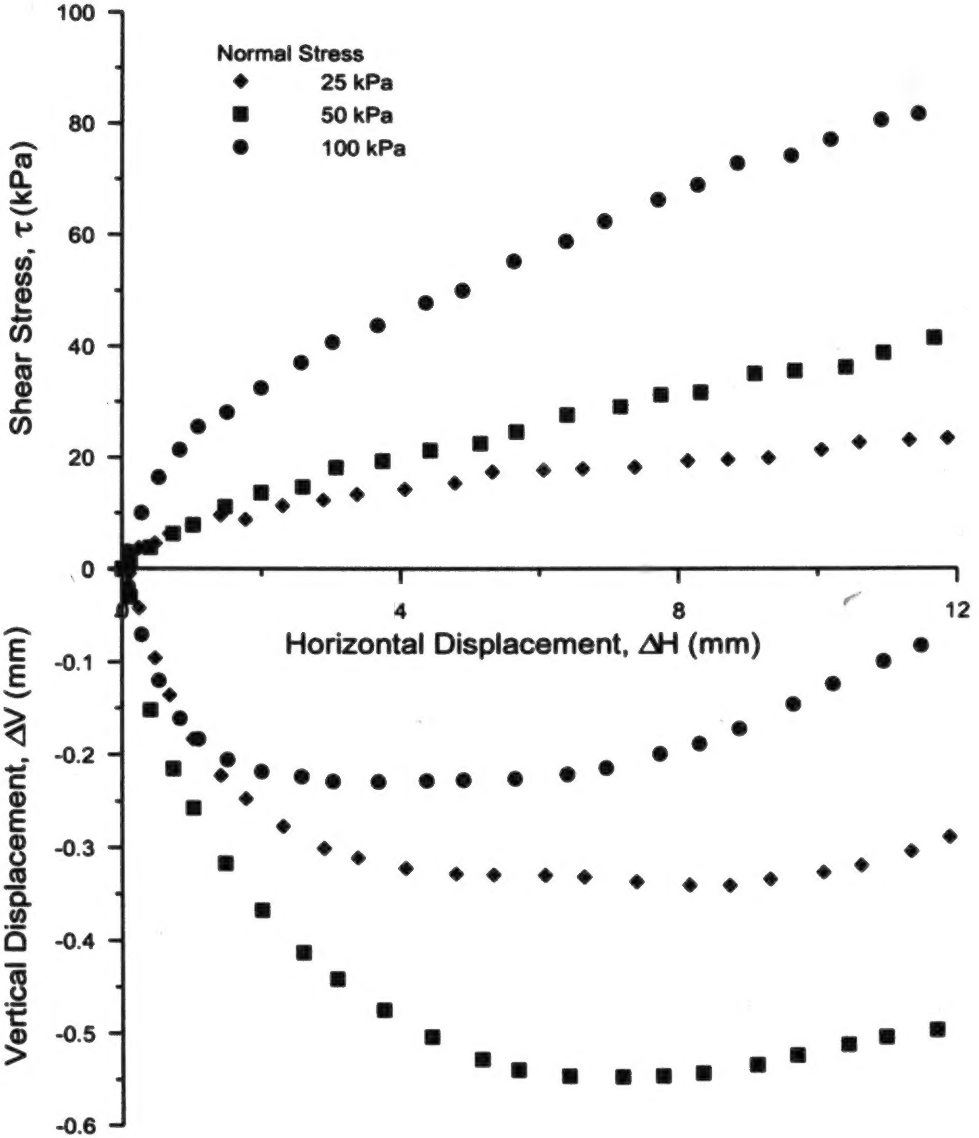

Figure G. 5 Shear stress and vertical displacement versus horizontal displacement, dry, No. 4 - No. 8 (Tire Recyclers of Calgary)

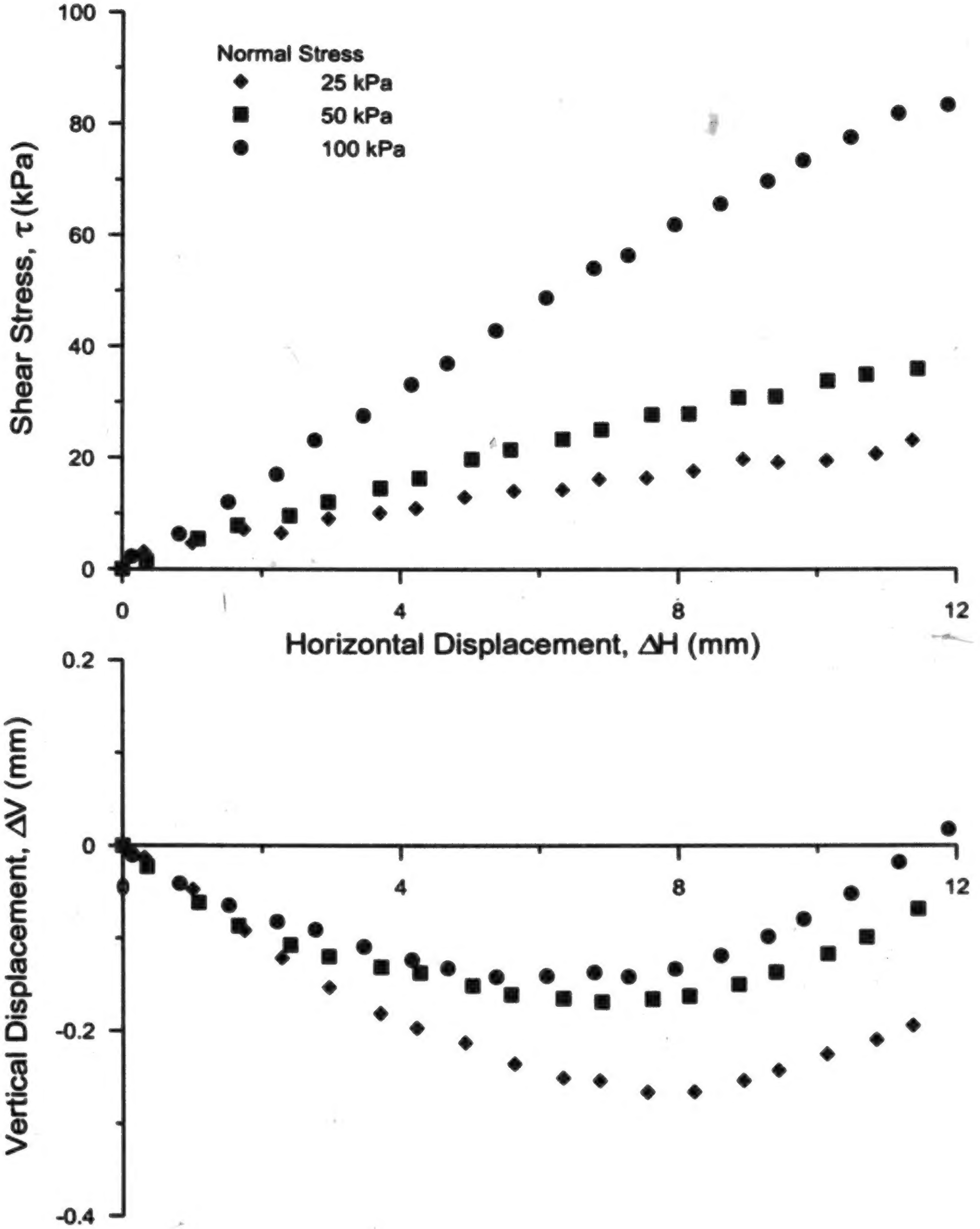

Figure G. 6 Shear stress and vertical displacement versus horizontal displacement, dry, 1/4 in (Midwest Tire Processors of Vulcan)

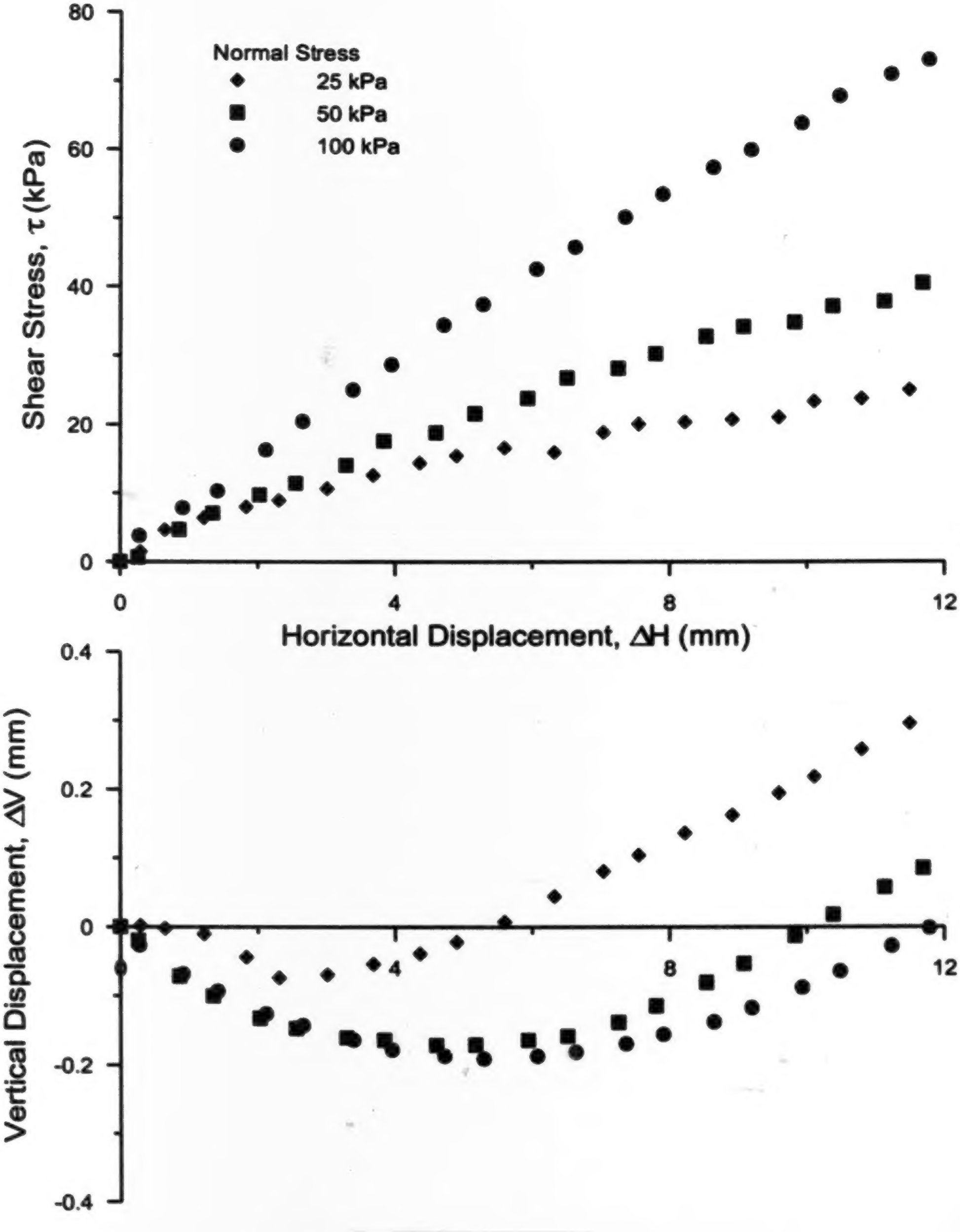

Figure G. 7 Shear stress and vertical displacement versus horizontal displacement, dry, 1/4 in (Alberta Environmental Rubber Products)

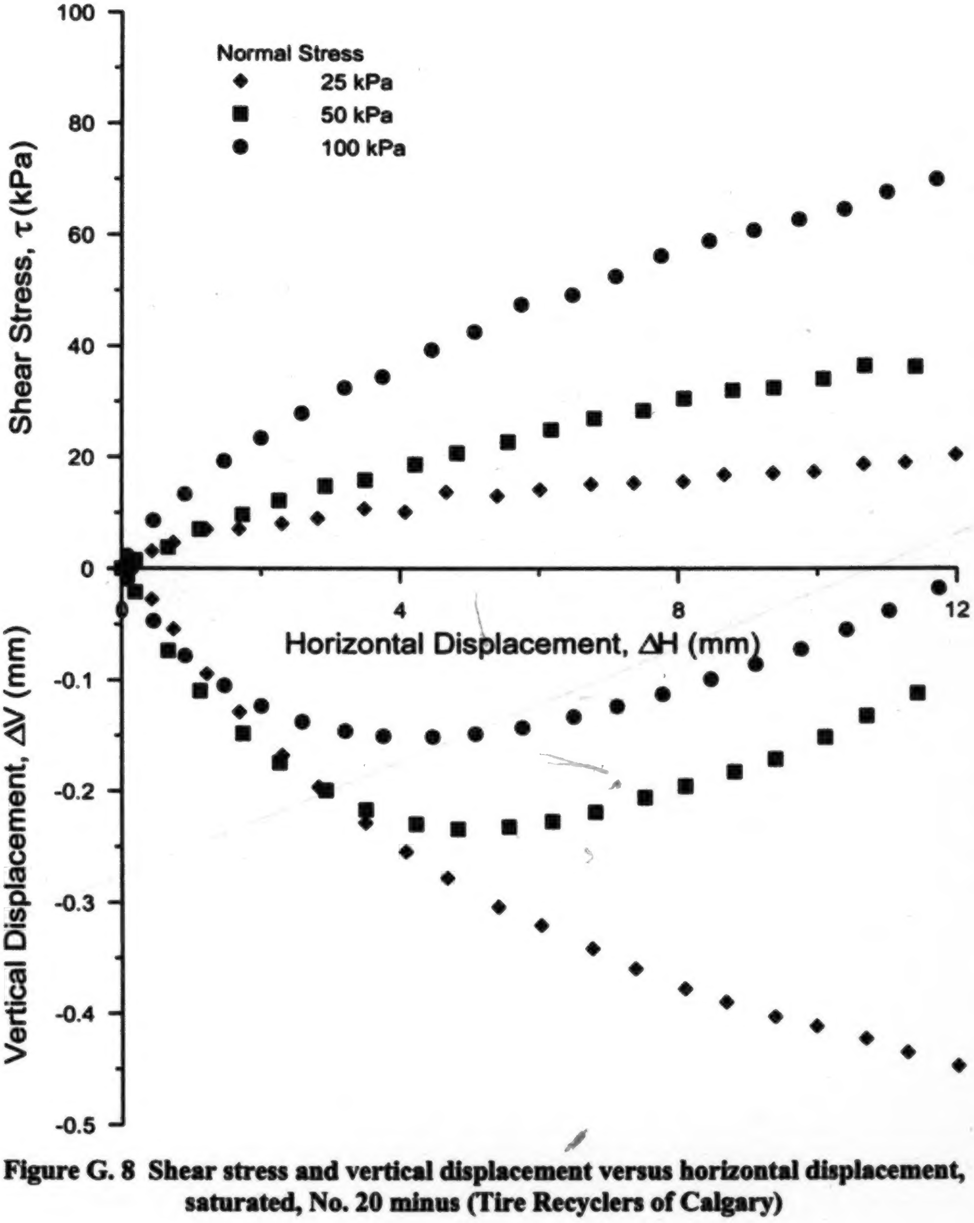

Figure G. 8 Shear stress and vertical displacement versus horizontal displacement, saturated, No. 20 minus (Tire Recyclers of Calgary)

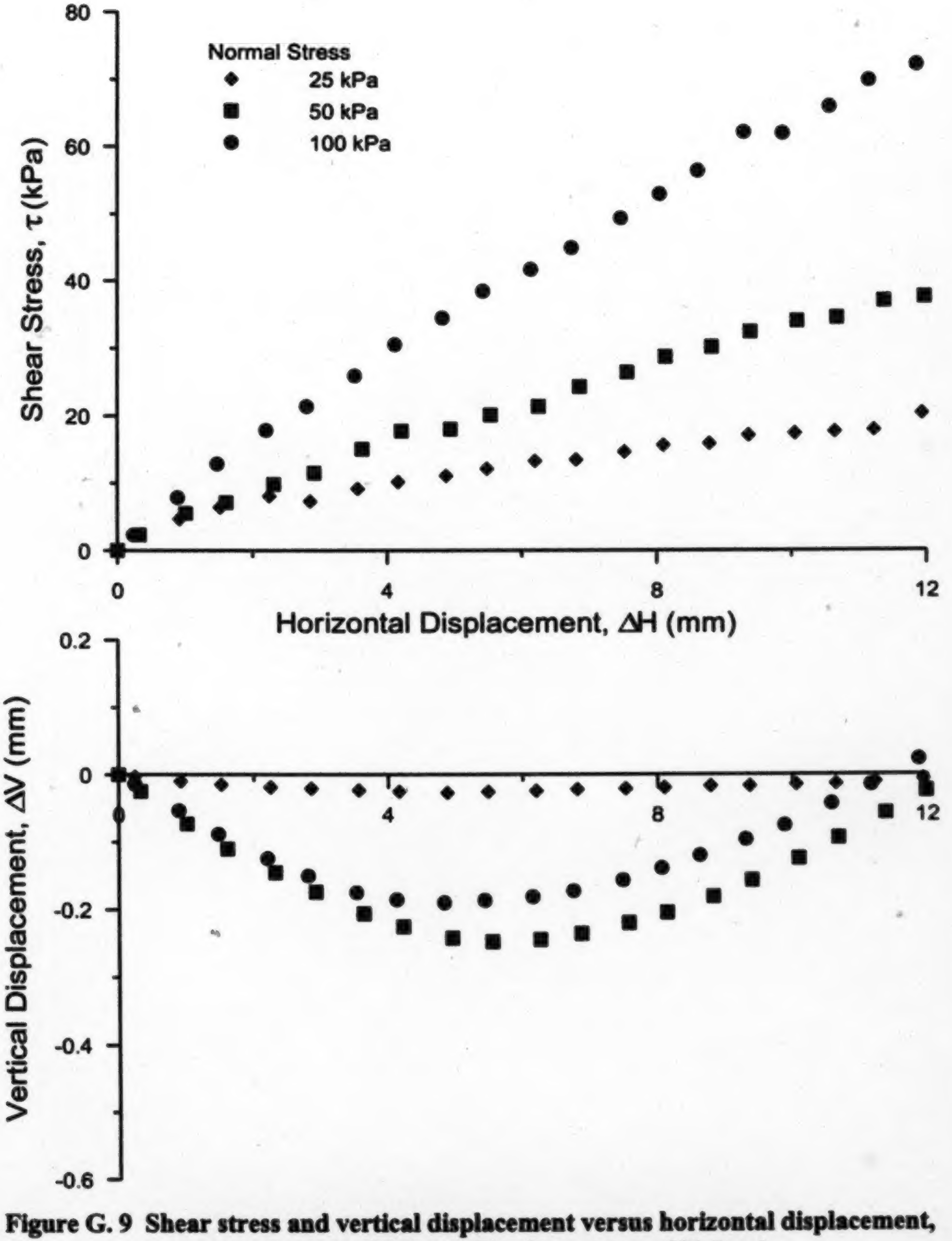

Figure G. 9 Shear stress and vertical displacement versus horizontal displacement, saturated, 1/4 in (Midwest Tire Processors of Vulcan)

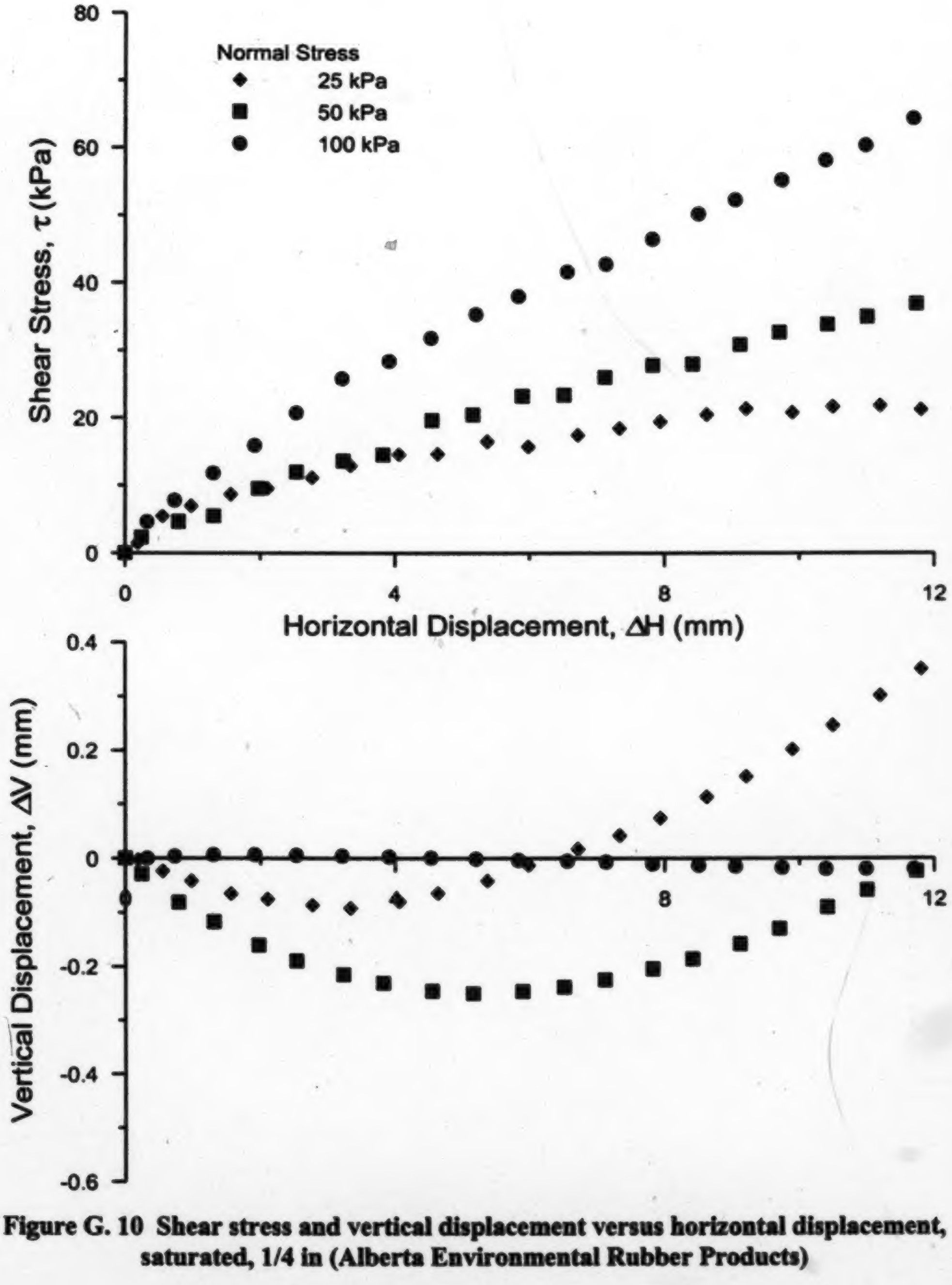

Figure G. 10 Shear stress and vertical displacement versus horizontal displacement, saturated, 1/4 in (Alberta Environmental Rubber Products)

Table G. 2 Shear strength parameters, direct shear, Method A ($c \neq 0$)

Size	Supplier	Condition	ΔH (mm)	tan(ϕ)	c (kPa)	ϕ (°)	R^2
No. 20 minus	Tire Recyclers of Calgary	dry	2	0.36	0	20	0.973
			4	0.48	0	26	0.994
			8	0.62	2	32	0.998
			12	0.66	5	33	1.000
		saturated	2	0.22	1	12	0.981
			4	0.35	1	19	0.997
			8	0.55	2	29	1.000
			12	0.66	4	33	1.000
No. 10 - No. 20	Tire Recyclers of Calgary	dry	2	0.10	2	6	0.988
			4	0.24	2	14	0.990
			8	0.52	1	27	0.991
			12	0.61	1	31	0.998
No. 10	Midwest Tire Processors of Vulcan	dry	2	0.27	3	15	0.987
			4	0.38	4	21	0.989
			8	0.59	4	30	0.994
			12	0.70	4	35	0.999
No. 8 - No. 14	Tire Recyclers of Calgary	dry	2	0.18	6	10	0.997
			4	0.33	5	18	1.000
			8	0.51	7	27	1.000
			12	0.59	5	30	1.000
No. 4 - No. 8	Tire Recyclers of Calgary	dry	2	0.31	1	17	0.968
			4	0.43	1	23	0.976
			8	0.66	1	33	0.993
			12	0.69	3	34	0.998
1/4 in	Midwest Tire Processors of Vulcan	dry	2	0.14	2	8	0.990
			4	0.27	3	15	1.000
			8	0.49	3	26	1.000
			12	0.56	1	29	1.000
		saturated	2	0.12	3	7	0.982
			4	0.29	2	16	0.987
			8	0.61	0	31	0.989
			12	0.73	1	36	1.000
1/4 in	Alberta Environmental Rubber Products	dry	2	0.10	6	6	0.893
			4	0.21	9	12	0.960
			8	0.40	11	22	0.998
			12	0.67	9	34	0.999
		saturated	2	0.09	6	5	0.979
			4	0.22	8	12	0.996
			8	0.45	9	24	1.000
			12	0.57	7	30	0.999

Table G. 3 Shear strength parameters, direct shear, Method B (c = 0)

Size	Supplier	Condition	ΔH (mm)	tan(φ)	φ (°)	R^2
No. 20 minus	Tire Recyclers of Calgary	dry	2	0.35	19	0.994
			4	0.48	26	0.999
			8	0.65	33	0.999
			12	0.72	35	0.998
		saturated	2	0.24	13	0.995
			4	0.24	14	0.999
			8	0.27	15	0.999
			12	0.36	20	0.998
No. 10 - No. 20	Tire Recyclers of Calgary	dry	2	0.13	7	0.983
			4	0.27	15	0.995
			8	0.53	28	0.998
			12	0.63	32	0.999
No. 10	Midwest Tire Processors of Vulcan	dry	2	0.31	17	0.993
			4	0.44	24	0.993
			8	0.64	32	0.997
			12	0.76	37	0.998
No. 8 - No. 14	Tire Recyclers of Calgary	dry	2	0.26	15	0.970
			4	0.39	21	0.992
			8	0.61	31	0.993
			12	0.66	33	0.997
No. 4 - No. 8	Tire Recyclers of Calgary	dry	2	0.32	18	0.993
			4	0.45	24	0.995
			8	0.67	34	0.998
			12	0.73	36	0.999
1/4 in	Midwest Tire Processors of Vulcan	dry	2	0.16	9	0.979
			4	0.32	18	0.995
			8	0.61	31	0.997
			12	0.74	36	1.000
		saturated	2	0.17	10	0.989
			4	0.31	17	0.994
			8	0.54	28	0.998
			12	0.58	30	1.000
1/4 in	Alberta Environmental Rubber Products	dry	2	0.17	10	0.945
			4	0.32	18	0.970
			8	0.57	30	0.988
			12	0.67	33	0.994
		saturated	2	0.19	11	0.940
			4	0.32	18	0.961
			8	0.54	28	0.980
			12	0.79	38	0.993

Table G. 4 Shear strength parameters, direct shear, Method C

Size	Supplier	Test Conditions	ΔH (mm)	m	b	R^2	Secant Tangent			
							0 to 50 kPa		0 to 100 kPa	
							tan (ϕ)	ϕ (°)	tan (ϕ)	ϕ (°)
No. 20 Minus	Tire Recyclers of Calgary	dry	2	0.9	1	0.947	0.35	20	0.33	18
			4	1.0	1	0.990	0.48	26	0.47	25
			8	1.0	1	0.998	0.66	33	0.65	33
			12	0.9	1	1.000	0.77	37	0.70	35
		saturated	2	0.8	1	0.958	0.25	14	0.22	12
			4	0.9	1	0.994	0.38	21	0.35	19
			8	0.9	1	1.000	0.60	31	0.57	30
			12	0.9	1	1.000	0.76	37	0.70	35
No. 10 - No. 20	Tire Recyclers of Calgary	dry	2	0.7	0	0.996	0.15	8	0.12	7
			4	0.9	0	0.993	0.29	16	0.27	15
			8	1.0	0	0.989	0.53	28	0.54	28
			12	1.0	1	0.998	0.63	32	0.63	32
No. 10	Midwest Tire Processors of Vulcan	dry	2	0.9	1	0.991	0.34	19	0.31	17
			4	0.9	1	0.993	0.48	25	0.43	23
			8	0.9	1	0.996	0.67	34	0.64	32
			12	0.9	1	1.000	0.80	38	0.75	36
No. 8 - No. 14	Tire Recyclers of Calgary	dry	2	0.6	2	0.977	0.32	18	0.23	13
			4	0.8	1	0.999	0.44	23	0.37	20
			8	0.8	2	0.997	0.67	34	0.57	30
			12	0.9	1	1.000	0.70	35	0.63	32
No. 4 - No. 8	Tire Recyclers of Calgary	dry	2	0.9	1	0.933	0.33	18	0.30	16
			4	0.8	1	0.949	0.47	25	0.42	23
			8	0.9	1	0.986	0.69	34	0.65	33
			12	0.9	1	0.994	0.76	37	0.70	35

Table G. 4 Continued

Size	Supplier	Test Conditions	ΔH (mm)	m	b	R^2	Secant Tangent 0 to 50 kPa		0 to 100 kPa	
							tan(ϕ)	ϕ (°)	tan(ϕ)	ϕ (°)
1/4 in	Midwest Tire Processors of Vulcan	dry	2	0.6	1	0.944	0.19	11	0.15	8
			4	0.8	1	0.967	0.35	19	0.30	17
			8	0.9	1	0.979	0.62	32	0.59	30
			12	1.0	1	0.999	0.76	37	0.74	36
		saturated	2	0.7	1	0.969	0.19	11	0.16	9
			4	0.8	1	0.999	0.34	19	0.30	16
			8	0.9	1	1.000	0.57	30	0.53	28
			12	1.0	1	1.000	0.58	30	0.57	30
1/4 in	Alberta Environmental Rubber Products	dry	2	0.4	2	0.924	0.22	12	0.15	8
			4	0.6	2	0.976	0.39	21	0.28	16
			8	0.7	2	0.994	0.65	33	0.53	28
			12	0.8	2	0.995	0.73	36	0.63	32
		saturated	2	0.4	2	0.750	0.23	13	0.16	9
			4	0.5	3	0.888	0.40	22	0.28	16
			8	0.6	3	0.986	0.64	32	0.49	26
			12	0.8	2	0.994	0.88	40	0.75	36

Table G. 5 Triaxial compression results

Grain-Size Distribution	Supplier	ε_a (%)	$\sigma_d = \sigma_1 - \sigma_3$ (kPa)	σ_3 (kPa)	σ_1 (kPa)	$(\sigma_1 + \sigma_3)/2$ (kPa)	$(\sigma_1 - \sigma_3)/2$ (kPa)
No. 20 minus	Tire Recyclers of Calgary	5	19.8	25	44.8	34.9	9.9
			33.2	50	83.2	66.6	16.6
			72.4	100	172.4	136.2	36.2
		10	30.2	25	55.2	40.1	15.1
			49.3	50	99.3	74.6	24.6
			101.2	100	201.2	150.6	50.6
		15	40.8	25	65.8	45.4	20.4
			65.1	50	115.1	82.6	32.6
			130.8	100	230.8	165.4	65.4
		20	51.1	25	76.1	50.6	25.6
			81.0	50	131.0	90.5	40.5
			160.3	100	260.3	180.1	80.1
No. 10 - No. 20	Tire Recyclers of Calgary	5	44.8	25	69.8	47.4	22.4
			64.4	50	114.4	82.2	32.2
			74.9	100	174.9	137.4	37.4
		10	55.2	25	80.2	52.6	27.6
			81.9	50	131.9	91.0	41.0
			102.9	100	202.9	151.5	51.5
		15	62.9	25	87.9	56.4	31.4
			97.1	50	147.1	98.6	48.6
			129.7	100	229.7	164.8	64.8
		20	66.1	25	91.1	58.1	33.1
			109.9	50	159.9	104.9	54.9
			154.8	100	254.8	177.4	77.4
No. 10	Midwest Tire Processors of Vulcan	5	45.0	25	70.0	47.5	22.5
			63.2	50	113.2	81.6	31.6
			79.6	100	179.6	139.8	39.8
		10	55.1	25	80.1	52.5	27.5
			81.2	50	131.2	90.6	40.6
			106.0	100	206.0	153.0	53.0
		15	61.7	25	86.7	55.9	30.9
			96.7	50	146.7	98.3	48.3
			133.1	100	233.1	166.6	66.6
		20	64.4	25	89.4	57.2	32.2
			110.3	50	160.3	105.1	55.1
			157.1	100	257.1	178.6	78.6

Table G. 5 Continued

Grain-Size Distribution	Supplier	ε_a (%)	$\sigma_d = \sigma_1 - \sigma_3$ (kPa)	σ_3 (kPa)	σ_1 (kPa)	$(\sigma_1 + \sigma_3)/2$ (kPa)	$(\sigma_1 - \sigma_3)/2$ (kPa)
No. 8 - No. 14	Tire Recyclers of Calgary	5	42.2	25	67.2	46.1	21.1
			82.2	50	132.2	91.1	41.1
			104.1	100	204.1	152.1	52.1
		10	50.5	25	75.5	50.3	25.3
			100.3	50	150.3	100.1	50.1
			131.8	100	231.8	165.9	65.9
		15	55.3	25	80.3	52.6	27.6
			113.6	50	163.6	106.8	56.8
			157.1	100	257.1	178.6	78.6
		20	57.8	25	82.8	53.9	28.9
			120.5	50	170.5	110.2	60.2
			179.2	100	279.2	189.6	89.6
No. 4 - No. 8	Tire Recyclers of Calgary	5	50.8	25	75.8	50.4	25.4
			70.0	50	120.0	85.0	35.0
			77.7	100	177.7	138.9	38.9
		10	61.0	25	86.0	55.5	30.5
			87.3	50	137.3	93.7	43.7
			107.0	100	207.0	153.5	53.5
		15	67.8	25	92.8	58.9	33.9
			101.0	50	151.0	100.5	50.5
			133.8	100	233.8	166.9	66.9
		20	72.5	25	97.5	61.3	36.3
			109.2	50	159.2	104.6	54.6
			160.9	100	260.9	180.4	80.4
1/4 in	Midwest Tire Processors of Vulcan	5	20.3	25	45.3	35.2	10.2
			31.0	50	81.0	65.5	15.5
			31.3	100	131.3	115.7	15.7
		10	30.2	25	55.2	40.1	15.1
			48.6	50	98.6	74.3	24.3
			57.2	100	157.2	128.6	28.6
		15	36.7	25	61.7	43.3	18.3
			65.3	50	115.3	82.7	32.7
			84.3	100	184.3	142.1	42.1
		20	39.1	25	64.1	44.5	19.5
			80.3	50	130.3	90.2	40.2
			111.7	100	211.7	155.9	55.9

Table G. 5 Continuted

Grain-Size Distribution	Supplier	ε_a (%)	$\sigma_d = \sigma_1 - \sigma_3$ (kPa)	σ_3 (kPa)	σ_1 (kPa)	$(\sigma_1 + \sigma_3)/2$ (kPa)	$(\sigma_1 - \sigma_3)/2$ (kPa)
1/4 in	Alberta Environmental Rubber Products	5	46.8	25	71.8	48.4	23.4
			77.3	50	127.3	88.6	38.6
			83.6	100	183.6	141.8	41.8
		10	59.2	25	84.2	54.6	29.6
			98.8	50	148.8	99.4	49.4
			116.8	100	216.8	158.4	58.4
		15	66.5	25	91.5	58.3	33.3
			109.7	50	159.7	104.9	54.9
			147.9	100	247.9	173.9	73.9
		20	65.4	25	90.4	57.7	32.7
			107.2	50	157.2	103.6	53.6
			171.9	100	271.9	186.0	86.0

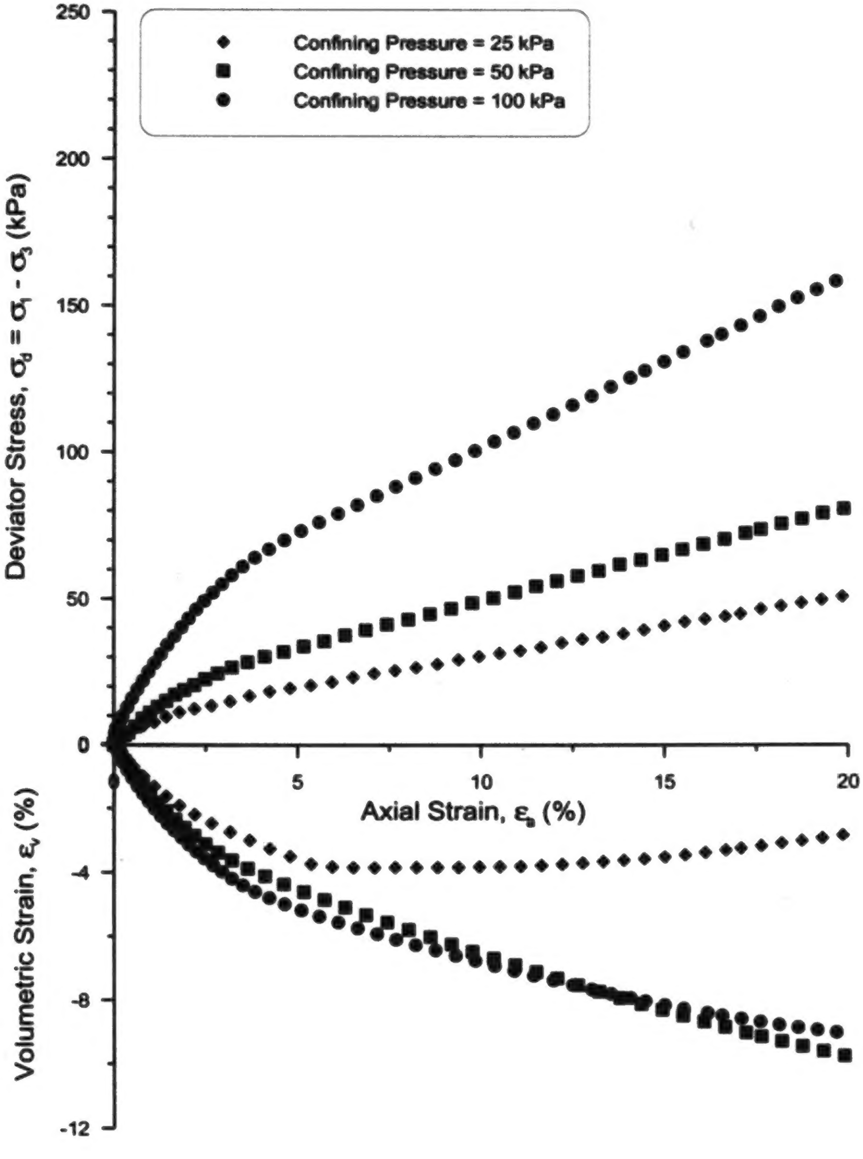

Figure G. 11 Deviatoric stress and volumetric strain versus axial strain, No. 20 minus (Tire Recyclers of Calgary)

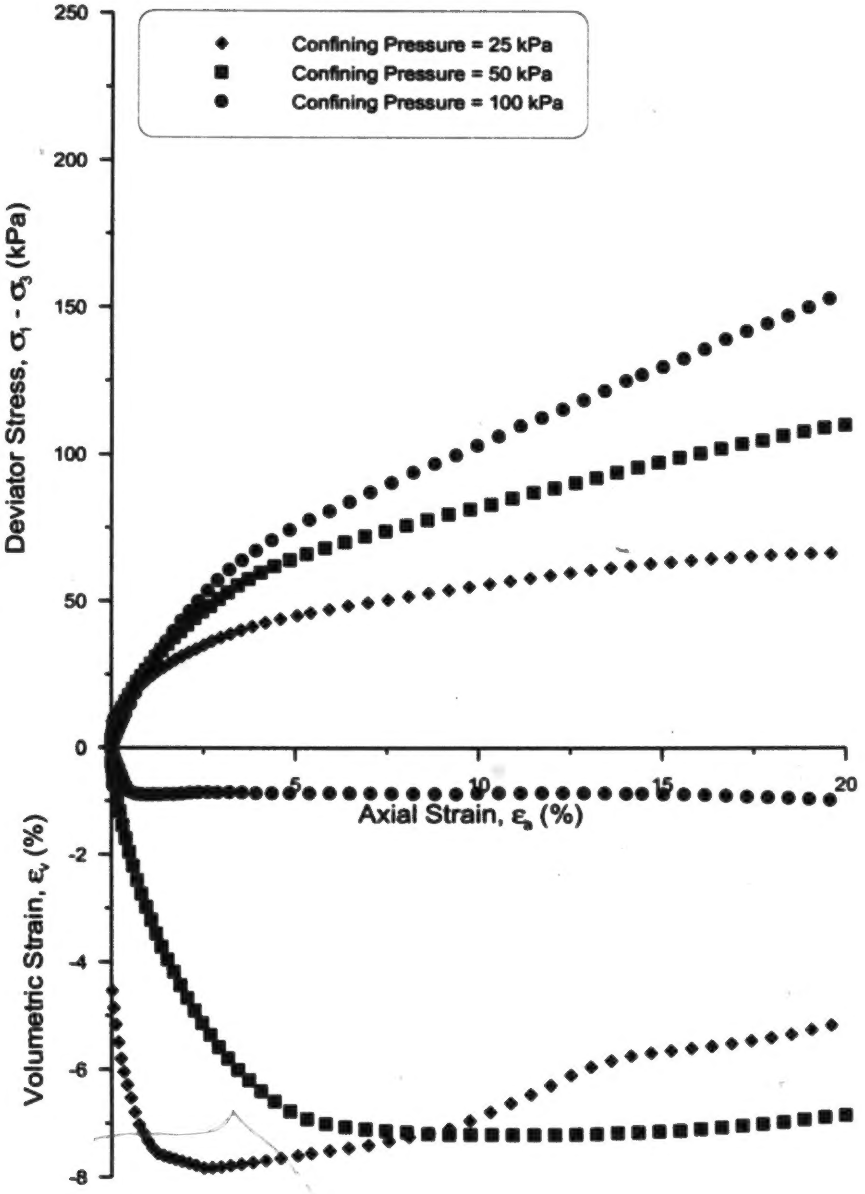

Figure G. 12 Deviatoric stress and volumetric strain versus axial strain, No. 10 - No. 20 (Tire Recyclers of Calgary)

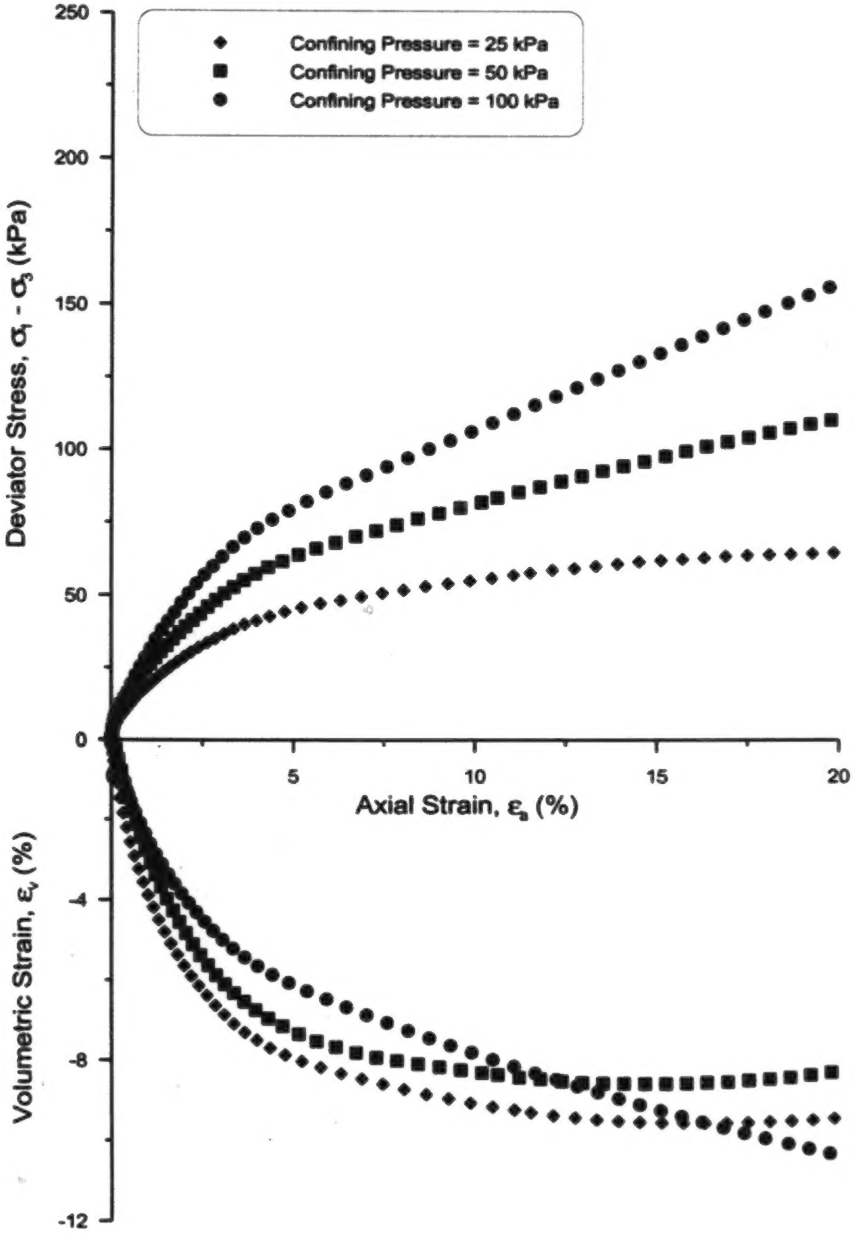

Figure G. 13 Deviatoric stress and volumetric strain versus axial strain, No. 10 (Midwest Tire Processors of Vulcan)

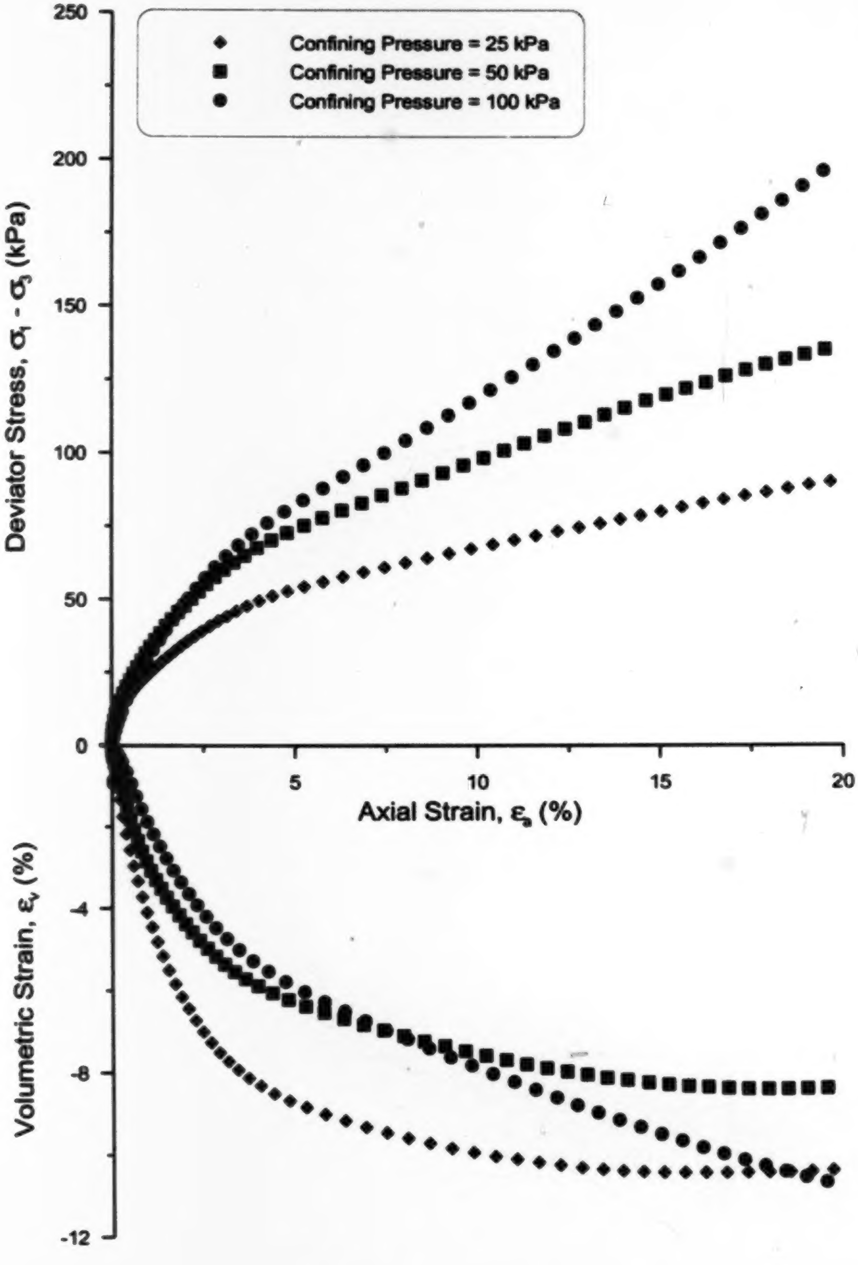

Figure G. 14 Deviatoric stress and volumetric strain versus axial strain, No. 8 - No. 14 (Tire Recyclers of Calgary)

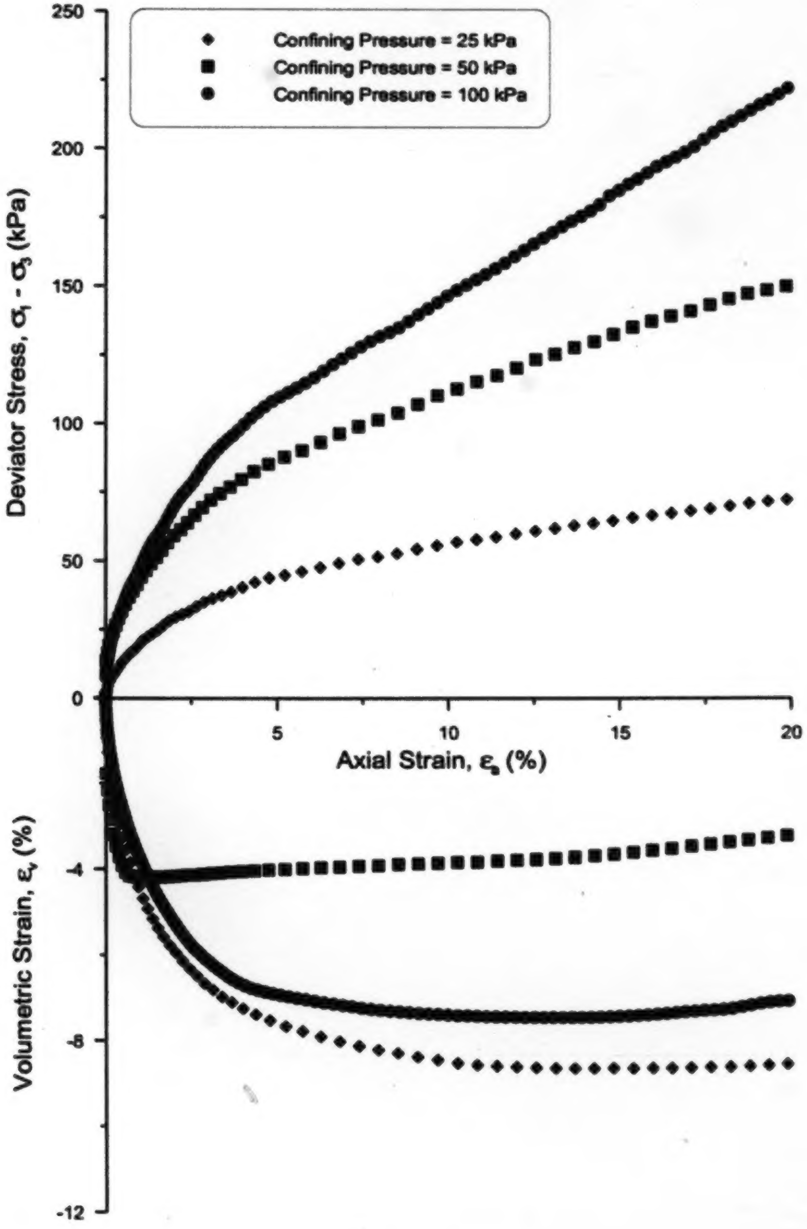

Figure G. 15 Deviatoric stress and volumetric strain versus axial strain, No. 4 - No. 8 (Tire Recyclers of Calgary)

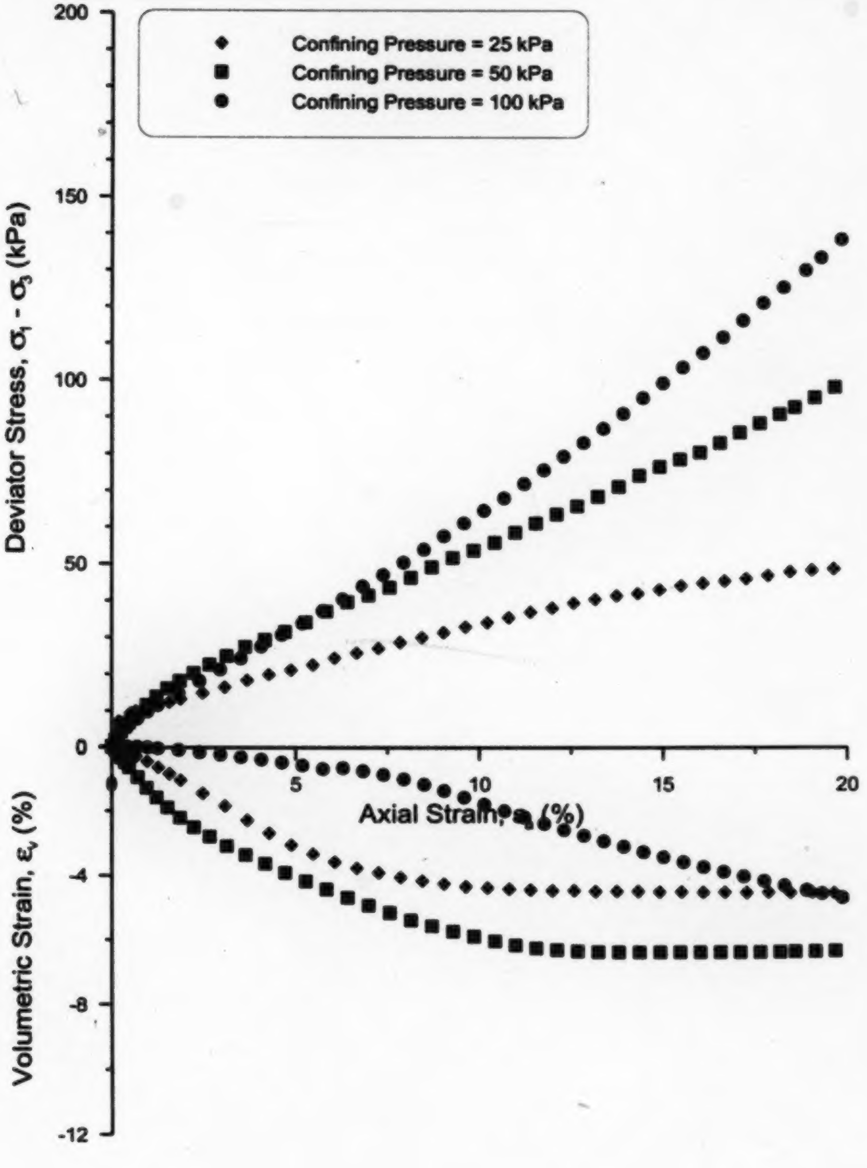

Figure G. 16 Deviatoric stress and volumetric strain versus axial strain, 1/4 in (Midwest Tire Processors of Vulcan)

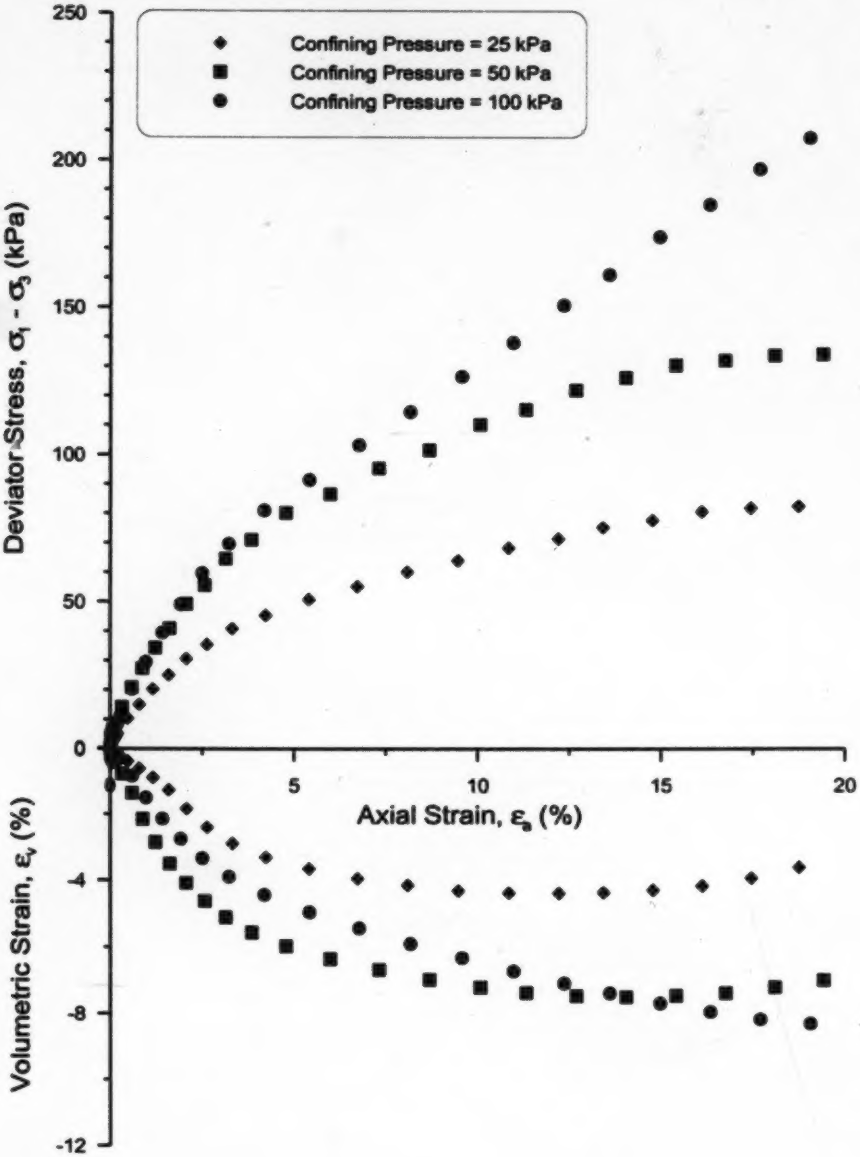

Figure G. 17 Deviatoric stress and volumetric strain versus axial strain, 1/4 in (Alberta Environmental Rubber Products)

Table G. 6 Shear strength parameters, triaxial compression, Method A' ($c \neq 0$)

Size	Supplier	ε_a (%)	$\tan\alpha$	a	ϕ (°)	c (kPa)	R^2
No. 20 minus	Tire Recyclers of Calgary	5	0.263	0	15	0	0.996
		10	0.324	1	19	1	0.998
		15	0.379	2	22	3	0.998
		20	0.425	3	25	4	0.999
No. 10 - No. 20	Tire Recyclers of Calgary	5	0.161	16	9	17	0.911
		10	0.235	17	14	17	0.961
		15	0.302	16	18	17	0.980
		20	0.366	14	21	15	0.987
No. 10	Midwest Tire Processors of Vulcan	5	0.183	15	11	15	0.968
		10	0.248	16	14	16	0.976
		15	0.317	15	19	15	0.985
		20	0.377	12	22	13	0.987
No. 8 - No. 14	Tire Recyclers of Calgary	5	0.145	20	8	20	0.871
		10	0.229	19	13	20	0.957
		15	0.300	18	17	19	0.982
		20	0.367	15	22	16	0.997
No. 4 - No. 8	Tire Recyclers of Calgary	5	0.286	11	17	11	0.937
		10	0.346	11	20	11	0.957
		15	0.399	9	24	10	0.973
		20	0.442	7	26	8	0.986
1/4 in	Midwest Tire Processors of Vulcan	5	0.062	9	4	9	0.644
		10	0.146	11	8	11	0.889
		15	0.234	10	14	10	0.946
		20	0.320	8	19	8	0.967
1/4 in	Alberta Environmental Rubber Products	5	0.190	17	11	17	0.817
		10	0.271	18	16	18	0.917
		15	0.346	15	20	16	0.978
		20	0.412	10	24	11	0.999

Table G. 7 Shear strength parameters, triaxial compression, Method B' (c = 0)

Size	Supplier	ε_a (%)	$\tan\alpha$	a	ϕ (°)	c (kPa)	R^2
No. 20 minus	Tire Recyclers of Calgary	5	0.264	0	15	0	0.999
		10	0.337	0	20	0	0.999
		15	0.398	0	23	0	0.999
		20	0.449	0	27	0	0.999
No. 10 - No. 20	Tire Recyclers of Calgary	5	0.317	0	19	0	0.956
		10	0.382	0	22	0	0.973
		15	0.430	0	25	0	0.983
		20	0.467	0	28	0	0.990
No. 10	Midwest Tire Processors of Vulcan	5	0.324	0	19	0	0.965
		10	0.385	0	23	0	0.977
		15	0.433	0	26	0	0.986
		20	0.469	0	28	0	0.991
No. 8 - No. 14	Tire Recyclers of Calgary	5	0.332	0	19	0	0.949
		10	0.395	0	23	0	0.970
		15	0.440	0	26	0	0.982
		20	0.475	0	28	0	0.990
No. 4 - No. 8	Tire Recyclers of Calgary	5	0.377	0	22	0	0.982
		10	0.430	0	25	0	0.988
		15	0.468	0	28	0	0.992
		20	0.494	0	30	0	0.996
1/4 in	Midwest Tire Processors of Vulcan	5	0.168	0	10	0	0.911
		10	0.257	0	15	0	0.957
		15	0.328	0	19	0	0.979
		20	0.384	0	23	0	0.990
1/4 in	Alberta Environmental Rubber Products	5	0.346	0	20	0	0.958
		10	0.416	0	25	0	0.975
		15	0.460	0	27	0	0.987
		20	0.482	0	29	0	0.996

Table G. 8 Shear strength parameters, triaxial compression, Method C'

Size	Supplier	ε_a (%)	m	ln(b)	b	R^2	Secant Tangent					
							25 to 50 kPa			50 to 100 kPa		
							tanϕ	ϕ (°)	c (kPa)	tanϕ	ϕ (°)	c (kPa)
No. 20 Minus	Tire Recyclers of Calgary	5	0.955	-1.135	0	0.993	0.261	15	0	0.253	14	1
		10	0.916	-0.692	1	0.994	0.338	19	1	0.319	18	2
		15	0.904	-0.459	1	0.995	0.404	22	1	0.378	21	3
		20	0.902	-0.321	1	0.996	0.460	25	2	0.430	23	3
No. 10 - No. 20	Tire Recyclers of Calgary	5	0.485	1.269	4	0.955	0.271	15	10	0.189	11	14
		10	0.591	0.997	3	0.983	0.369	20	9	0.278	16	14
		15	0.677	0.738	2	0.991	0.442	24	7	0.353	19	12
		20	0.764	0.414	2	0.994	0.494	26	5	0.419	23	9
No. 10	Midwest Tire Processors of Vulcan	5	0.529	1.090	3	0.988	0.289	16	9	0.208	12	13
		10	0.613	0.904	2	0.991	0.377	21	8	0.288	16	13
		15	0.705	0.611	2	0.994	0.448	24	7	0.365	20	11
		20	0.786	0.309	1	0.994	0.496	26	5	0.428	23	8
No. 8 - No. 14	Tire Recyclers of Calgary	5	0.422	1.611	5	0.930	0.265	15	13	0.178	10	17
		10	0.554	1.215	3	0.980	0.376	21	11	0.276	15	16
		15	0.653	0.879	2	0.993	0.451	24	8	0.355	20	13
		20	0.738	0.561	2	1.000	0.502	27	6	0.419	23	10

Table G. 8 Continued

Size	Supplier	ε_a (%)	m	ln(b)	b	R^2	Secant Tangent					
							25 to 50 kPa			50 to 100 kPa		
							tanϕ	ϕ (°)	c (kPa)	tanϕ	ϕ (°)	c (kPa)
No. 4 - No. 8	Tire Recyclers of Calgary	5	0.768	0.150	1	0.965	0.387	21	4	0.330	18	7
		10	0.814	0.077	1	0.976	0.450	24	4	0.396	22	6
		15	0.865	-0.079	1	0.985	0.492	26	3	0.449	24	5
		20	0.906	-0.224	1	0.992	0.517	27	2	0.484	26	3
1/4 in	Midwest Tire Processors of Vulcan	5	0.368	1.070	3	0.789	0.111	6	7	0.072	4	9
		10	0.553	0.714	2	0.942	0.227	13	6	0.166	9	9
		15	0.706	0.285	1	0.971	0.326	18	5	0.266	15	8
		20	0.847	-0.207	1	0.981	0.397	22	2	0.358	20	4
1/4 in	Alberta Environmental Rubber Products	5	0.554	1.054	3	0.898	0.320	18	9	0.235	13	13
		10	0.649	0.831	2	0.956	0.420	23	8	0.329	18	13
		15	0.734	0.544	2	0.990	0.485	26	6	0.403	22	10
		20	0.826	0.144	1	1.000	0.508	27	4	0.450	24	7

APPENDIX H - DYNAMIC PROPERTIES

Table H. 1 Dynamic property testing of Ottawa sand, large-strain apparatus and bender elements

From amplitude-frequency curve

A_{max} (mV)	A (mV)		f_o (Hz)	f_1 (Hz)	f_2 (Hz)	δ	D (%)
1.525	$0.5A_{max}$	0.762	3518	3115	4935	1.07	16.8
1.525	-	0.901	3518	3355	3908	0.37	5.9
1.525	$0.707A_{max}$	1.075	3518	3395	3807	0.37	5.9
1.525	-	1.339	3518	3463	3640	0.29	4.7

Sample Ht: 28.167 mm
Mass Sand: 427.710 g
ρ_d: 1889.324 kg/m^3
γ_d: 18.534 kg/m^3
G_s: 2.70
e: 0.43

From amplitude-decay curve

Cycles of Oscillation, n	Amplitude (mV)	δ	D (%)
0	7.7	0.39	6.2
1	8.9		
2	4.0		
0	8.2	0.25	4.0
1	8.9		
2	5.3		
3	3.6		
4	2.9		
5	1.5		
6	-0.7		
7	0.4		
10	0.6		
11	1.2		
12	-0.2		
13	-0.4		
14	-0.5		
15	0.2		

Table H. 2 Dynamic property testing of Ottawa sand, triaxial cell apparatus and bender elements, amplitude-frequency curve

σ_v (kPa)	A_{max} (mV)	A (mV)		f_o (Hz)	f_1 (Hz)	f_2 (Hz)	D (%)	δ
0	1.019	$0.707A_{max}$	0.721	3508	3233	3640	5.7	0.36
20	0.903	$0.707A_{max}$	0.639	2930	2752	3082	5.6	0.35
40	0.986	$0.707A_{max}$	0.697	7619	7295	7939	4.2	0.27
60	1.407	$0.707A_{max}$	0.995	8007	7810	8320	3.2	0.20
80	1.339	-	1.222	7030	6927	7223	4.7	0.30
100	1.616	-	1.160	7030	6960	7233	2.0	0.13

Sample Mass:

$(M_{rubber + glass\ beaker})_{initial}$ =343.750 g
$(M_{rubber + glass\ beaker})_{final}$ =123.820 g

Sample Dimensions:

Ht. =42.837 g
Diam. =63.817 mm
ρ_d =1605.1 kg/m3
γ_d =15.7 kN/m3
Gs =2.7
e =0.68

Table H. 3 Dynamic property testing of tire crumbs, large-strain apparatus and bender elements, No. 20 minus (Tire Recyclers of Calgary)

σ_v (kPa)	f_o (Hz)	A_{max} (mV)	A (mV)		f_1 (Hz)	f_2 (Hz)	D (%)	δ
10	684	0.500	$0.707A_{max}$	0.354	303	1045	45.9	3.2
			$0.5A_{max}$	0.250	259	1373	47.3	3.4
20	878	0.545	$0.707A_{max}$	0.385	333	1133	35.2	2.4
			$0.5A_{max}$	0.273	278	1368	31.7	2.1
50	586	0.555	-	0.422	471	781	31.2	2.1
			$0.707A_{max}$	0.392	459	1207	~~60.0~~	~~4.7~~
			$0.5A_{max}$	0.278	417	1397	~~55.6~~	~~4.2~~
100	683	0.470	$0.707A_{max}$	0.332	614	940	26.1	1.7
			$0.5A_{max}$	0.235	552	1450	~~47.1~~	~~3.4~~

Sample Ht @ 0 kPa = 50 g
$M_{rubber+cell}$ = 3586.83 g
M_{cell} = 3339.05 g
Reciever Bender = 8.51 mm
Transmitter Bender = 8.33 mm

Table H. 4 Dynamic property testing of tire crumbs, large-strain apparatus and bender elements, No. 10 - No. 20 (Tire Recyclers of Calgary)

σ_v (kPa)	f_o (Hz)	A_{max} (mV)	A (mV)		f_1 (Hz)	f_2 (Hz)	D (%)	δ
10	293	0.219	$0.707A_{max}$	0.155	249	346	16.6	1.0
	293	0.219	$0.5A_{max}$	0.110	221	383	16.3	1.0
20	437	0.084	-	0.054	338	558	21.1	1.3
50	679	0.215	-	0.152	560	780	15.6	1.0
100	830	0.286	-	0.202	635	1045	14.1	0.9

Sample Ht @ 0 kPa =98.0 mm
$M_{rubber+cell}$=3663.66 g
M_{cell}=3339.05 g
Reciever Bender =8.51 mm
Transmitter Bender =8.33 mm

Table H. 5 Dynamic property testing of tire crumbs, large-strain apparatus and bender elements, No. 10 (Midwest Tire Processors of Vulcan)

σ_v (kPa)	f_o (Hz)	A_{max} (mV)	A (mV)		f_1 (Hz)	f_2 (Hz)	D (%)	δ
10	293	0.433	-	0.381	275	391	38.0	2.4
20	391	0.508	-	0.359	342	586	39.0	2.5
50	585	0.369	-	0.302	463	682	25.2	1.6
100	1953	1.625	$0.707A_{max}$	1.149	1650	2745	30.3	1.9

Sample Ht @ 0 kPa = 51.7 mm
$M_{rubber + cell}$ = 3579.29 g
M_{cell} = 3339.05 g
Reciever Bender = 8.51 mm
Transmitter Bender = 8.33 mm

Table H. 6 Dynamic property testing of tire crumbs, large-strain apparatus and bender elements, 1/4 in (Midwest Tire Processors of Vulcan)

σ_v (kPa)	f_o (Hz)	A_{max} (mV)	A (mV)		f_1 (Hz)	f_2 (Hz)	D (%)	δ
10	293	0.485	$0.707A_{max}$	0.343	228	480	44.9	2.8
	293	0.485	$0.5A_{max}$	0.243	176	627	49.9	3.1
20	584	0.374	-	0.329	488	655	25.0	1.6
	584	0.374	$0.707A_{max}$	0.264	249	792	37.7	2.4
50	585	0.278	$0.707A_{max}$	0.197	328	990	51.3	3.2
	585	0.278	$0.5A_{max}$	0.139	222	1118	44.1	2.8
100	778	0.231	$0.707A_{max}$	0.163	499	874	20.7	1.3
	778	0.231	$0.5A_{max}$	0.116	334	1110	25.9	1.6

Sample Ht @ 0 kPa = 53.0 mm
$M_{rubber+cell}$ = 3593.42 g
M_{cell} = 3339.05 g
Reciever Bender = 8.51 mm
Transmitter Bender = 8.33 mm

Table H. 7 Dynamic property testing of tire crumbs, large-strain apparatus and bender elements, 1/4 in (Alberta Environmental Rubber Products)

σ_v (kPa)	f_o (Hz)	A_{max} (mV)	A (mV)		f_1 (Hz)	f_2 (Hz)	D (%)	δ
0	391	0.291	-	0.241	195	434	33.9	2.1
20	391	0.850	$0.707A_{max}$	0.601	257	546	35.1	2.2
	391	0.850	$0.5A_{max}$	0.425	27	848	~~53.0~~	~~3.3~~
50	586	0.798	$0.707A_{max}$	0.564	380	768	30.7	1.9
	586	0.798	$0.5A_{max}$	0.399	306	1047	~~38.3~~	~~2.4~~
100	586	0.370	$0.707A_{max}$	0.262	485	789	27.1	1.7
	586	0.370	$0.5A_{max}$	0.185	411	909	26.6	1.7

Sample Ht @ 0 kPa = 51.2 mm
$M_{rubber+cell}$ = 3586.32 g
M_{cell} = 3339.05 g
Reciever Bender = 8.51 mm
Transmitter Bender = 8.33 mm